



HAL
open science

Study of the activation of hydrogen peroxide by the copper(II)-phenanthroline complex for the color-stripping of recovered cellulosic fibers

Elsa Walger

► **To cite this version:**

Elsa Walger. Study of the activation of hydrogen peroxide by the copper(II)-phenanthroline complex for the color-stripping of recovered cellulosic fibers. Reactive fluid environment. Université Grenoble Alpes, 2016. English. NNT : 2016GREAI040 . tel-01533315

HAL Id: tel-01533315

<https://theses.hal.science/tel-01533315>

Submitted on 16 Mar 2018

HAL is a multi-disciplinary open access archive for the deposit and dissemination of scientific research documents, whether they are published or not. The documents may come from teaching and research institutions in France or abroad, or from public or private research centers.

L'archive ouverte pluridisciplinaire **HAL**, est destinée au dépôt et à la diffusion de documents scientifiques de niveau recherche, publiés ou non, émanant des établissements d'enseignement et de recherche français ou étrangers, des laboratoires publics ou privés.

THÈSE

Pour obtenir le grade de

DOCTEUR DE LA COMMUNAUTE UNIVERSITE GRENOBLE ALPES

Spécialité : **Mécanique des fluides, Procédés, Énergétique**

Arrêté ministériel : 7 août 2006

Présentée par

Elsa WALGER

Thèse dirigée par **Gérard MORTHA** et
co-encadrée par **Nathalie MARLIN**

préparée au sein du **Laboratoire Génie des Procédés Papetiers**
dans **l'École Doctorale I-MEP2 : Ingénierie - Matériaux**
Mécanique Énergétique Environnement Procédés Production

Etude de l'activation du peroxyde d'hydrogène par le complexe cuivre(II)- phénanthroline pour la décoloration de fibres cellulosiques récupérées

Thèse soutenue publiquement le **22 juillet 2016**,
devant le jury composé de :

Mme Carole DUBOC

Directeur de Recherche CNRS, Université Joseph Fourier, Présidente

M. Stéphane GRELIER

Professeur, Université de Bordeaux, Rapporteur

M. Bodo SAAKE

Professeur, Université de Hambourg, Rapporteur

Mme Béatrice TUCCIO-LAURICELLA

Maître de Conférences, Aix-Marseille Université, Examinatrice

M. Gérard MORTHA

Professeur, Grenoble INP, Directeur de thèse

Mme Nathalie MARLIN

Maître de Conférences, Grenoble INP, Co-encadrante



**STUDY OF THE ACTIVATION OF HYDROGEN PEROXIDE
BY THE COPPER(II)-PHENANTHROLINE COMPLEX FOR
THE COLOR-STRIPPING OF RECOVERED CELLULOSIC
FIBERS**

ACKNOWLEDGEMENTS

I would like to thank everyone who contributed to this thesis. First of all, Nathalie, I would like to thank you again for believing in me from the beginning until the last days and for your understanding. Gérard, thanks for being so full of ideas and still letting me make my own decisions. I learned so much doing this thesis under the supervision of you two.

It was a great pleasure and chance to have Carole as president of the jury, merci Carole. Thanks to Béatrice Tuccio for being part of this jury, it was an honor to be evaluated by a spin-trapping expert. Many thanks to my thesis reviewers, Pr Stéphane Grelier and Pr Bodo Saake. I was very happy to hear that you accepted to be part of this examination and truly appreciated our discussions.

Thanks to all who directly contributed to this research work: Patrice Nortier for the kind and patient introduction to PHREEQC, Laure Fort and Yves Gimbert for the advice and access to mass spectrometry, Marie-Christine Brochier-Salon for the NMR experiments, but also lots of discussions and analysis work, Carole Duboc for the great "EPR" collaboration, and of course Florian Molton for his patience as I always had more samples and questions. By the way, thanks Carole for inviting Jennifer and I to the MRM (magnetism and magnetic resonance) school to learn more about EPR and NMR, and thanks Florian and Jennifer for the memorable "course d'orientation" in the forest! Thanks to Karine Janel and David Dallérac who were so precious, not only helping me in my work with some experiments, but also taking very good care of lab life and "Biochip" life. Merci Karine pour avoir fait des mesures pour moi quand je n'avais plus le temps, pour avoir toujours pris soin de nous et du labo, merci David pour ta patience avec l'HPLC, pour avoir supporté mes ultrasons en B14 et pour tous les gâteaux! I would like to thank Frédéric Pouyet and the group of students he assisted at Pagora during their preliminary study of dyed pulp color-stripping carried out in the very beginning of my thesis: Laure Dechambenoy, Valentin Guigon, François Leleu, Lucas Quinet, Déborah Quinot, and Luc Syty. I am proud that one of them, Valentin, is now a brilliant PhD candidate working at LGP2. Finally, many thanks to the two master students who joined me in this project and contributed tremendously to the "dyed pulp color-stripping" study: Camille Rivollier, who worked with the yellow pulp and some UV-vis analysis of his effluents, and Muhammad Khairumuzdaniel, who played around with the red (pink!) pulp and mechanical characterizations.

Obviously, a thesis requires some paper work and organization, for this I would like to thank Monique Rousset and Augustine Alessio from the I-MEP2 doctoral school.

There are so many people I would like to thank... I am grateful for having worked at Pagora and LGP2 for almost four years. Thanks to all the departments. The administration, with Nathalie Agopian, Isabelle Dufreney on the school side, Sylvie on the lab side, Manuel. Thanks to Anne-Marie for her help and her "joie de vivre", thanks to Stéphane Vernac for his support in all HR matters, especially when I applied for the ATER position and then when I left! Thanks to the communication department, to the school directors, Bernard Pineaux and then Naceur Belgacem, thanks to our librarians, Emmanuelle, Coralie and especially Laurent. This makes me think I would like to thank the "English lunch" group! Special thanks to Beth for that, and thanks to John. Thanks to the directors of LGP2, Evelyne with the assistance of Marc, and later Didier. Thanks for your work for

Acknowledgements

the lab and for your support to the PhD students. Didier, I loved your teaching methods already as a student, and these were inspiring for me as a teacher. Thanks for your kindness and support.

Thanks to everyone who took care of cleaning the buildings, especially those who had to clean the office, thanks for their work and patience, as our office was probably the one with the highest concentration of students, desks, chairs, bins and... other things on the floor.

Of course I would like to thank everyone from « Service technique »: Philippe, Xavier, Momo, Olivier (pour toutes les fois où tu m'as jetée dehors !), et bien sûr mes chouchous Chu et Charlotte. Je n'oublie pas Stéphane Dufreney, merci de m'avoir sauvée en TP de pdp et merci pour ta patience (oui j'ai bien écrit patience !). And I would like to give special thanks to the IT service. Franck who saves you whatever happens, and Lydia for her friendship, the nice cake tastings ☺, etc.

During this PhD, I was not only a young researcher, but also a young teacher. I would like to thank all the professors in Pagora for welcoming me in their world. Thanks to everyone. Marc, sorry for letting you down with the fluid mechanics. But I'm sure you were happy to work with Chamseddine after all! Thanks to my main teaching colleagues: Nathalie, who proposed me to become "monitrice" and taught me everything in a very short time as I started the chemistry labs on the 3rd day of my PhD. Thanks to Aurélie, best "TP" partner, merci Lilie, but also Alain Maréchal, who taught me how to measure dryness as no one does but also many other things, Sandrine, who proved it was possible to follow five student groups working on five different topics at the same time, Gérard who gave me the great chance to give a lecture, which was not the easiest one but clearly was one of my best (most difficult!) teaching experiences.

I would like to thank the paper physics team: Jean-Francis, José, Evelyne and Raphaël, and thanks to my ATER colleague, Chamseddine, for sharing experiences and for his motivation. I would also like to thank Didier and Naceur who let me be responsible of practical works on surface phenomena, to Mikael who was there with me and repeated the same thing to the students so many times. Thanks to Lionel who trusted me for evaluating the students on "numerical methods". My area of teaching was so wide that I even had the chance to work together with Mazen on Visual Basic programming. I loved it, merci Mazen pour ta patience et ta confiance.

We have not all been working together but thanks to everyone else, especially Nadège who is always full of energy, Aurore, Pierre, Fred Munoz, other professors from the Biochip group such as Agnès, Martine, Dominique, and of course our head, Christine, who supports me until now in my research and for finding new opportunities. Finally, I would like to thank Isabelle Desloges. Thank you for accepting me as a teaching assistant from the beginning of my thesis, and for your support from the beginning until my application to become "ATER".

Special thanks to everyone who participated in the life of the lab with coffee breaks, lunch breaks and the events organized by the PhD students. Je pense par exemple à Guillaume et Karim, qui ne rentrent pas facilement dans les autres "cases" de ces remerciements, mais aussi à Nevin, Mathilde, Bertine, Maxime.

As all know, young researchers are essential to research. It is now time to thank all of them, including those I will forget in the following list.

My office, B125, was definitely the best one in LGP2: « le bureau des filles » ! Elsa, Karima, Kenza, Lorenzo, Awatef, Sudha, Jenny, Flavien, and all others: Yohanes, Lisias, Beatriz, Giulio... You were the best officemates and I miss you. Lollo, if you say « in bocca al lupo », I reply « crepi il lupo ». You are the kindest Italian basketball player I will ever meet. Thanks for your friendship, for always

saying you are tired but actually always being ready to work, eat, go out, help... Thank you Attoufa, tu as été ma grande sœur de thèse, qui a fait deux bébés en moins de trois ans et qui m'a toujours soutenue (en échange de nombreux services informatiques :)), merci merci ! Jenny, I knew from the first day that I would like you. Thanks for everything we shared as colleagues and officemates, it was great to brainstorm and help each other, to share the A206 lab with you, you even did some experiments for me... I am very grateful for all that and of course for everything we shared as friends. Sudha, you are the sweetest officemate, I wish you started earlier to share more with you.

I would like to thank some other great friends: Claire, Farfadette, Carolina, Victoria, Megan. Thanks Clairou for teaching me the basics of pulping and especially how to make « boulettes » out of paper pulp, thanks for your unconditional friendship and for many things such as taking care of printing my thesis when I was already in Finland! Fanny, Farfadette, thank you for your friendship and support, thanks for making me happy everytime you were coming to Grenoble during your PhD, and thanks for everything we shared. Carolina, you are my "little sister" from Pagora. Thanks for your love and generosity to Nicolas and I, thanks for your support. Victoria, I am grateful to have a friend like you as well. Thanks for your energy and motivation, thanks for coming to sing with me, for the too rare hikes and paragliding events, the gym sessions... Megan, you are the kindest, I loved the time spent together and the time spent with Xabi (who is the cutest cat even though it's impossible to work when he's around!). Thanks for everything.

Jordan, you were my favorite lindy hop partner, thanks for having the idea to propose me to join! I would like to thank you for scientific advice but also great support especially in the last year. I hope I can support you as much. Thanks for your friendship. I would like to thank one of my best friends in the first year of this PhD: Satyajit. Thanks for the great discussions during experiments in A206. It was not easy to do a titration in your presence as I am easily distracted, but it was definitely worth the challenge.

Thanks also to sweet Ahlem aka Halouma for sharing good time together at the lab, during PhD courses and outside. Thanks to Fred for his support and... crazy ideas, to Jérémy for his smile, for coming to the office to say it's time for "pausa", to Alexandre for his generosity and humor, to sweet Lamia, Fufu, Raphaël, Marion, Maëlle, thanks to Peter, Javier, Thomas, Oussama! Please don't think I thank you only for one or two things: these are just examples! Thanks to my great « grande marraine » Nathalie Lavoine who is for me an example of hardworking successful young researcher. Thanks to the PhD students who started with me, Bobby, Benoît, Sasha, Seema, Claire, Marion. Always having fun with Bobby and Benoît, always eating some good chocolate and laughing when Marion was visiting! Thanks also to Jalila who always visited us when she had a meeting or workshop at CTP. And thanks to those who started their PhD not long after me: Fanny Tricot (Farfadette), Fanny Bardot, also good classmates from Pagora, Fanny B aka the F of "B&F", we always have something to chat about, and this is precious! By the way thanks to you and Benoît for the great gatherings at your place, the "galette" parties, etc. Let's not forget those who started a year later and joined our breaks and lunch expeditions, especially the great trio: Fanny Hoeng (thanks for your patience and for always sharing good chocolate and saucisson, not to mention everything), Jordan, Jennifer.

Thanks to Sébastien, aka « mon fillot ». It was great to have you around. Thanks to Laure and to Martin as well! And this reminds me of Jean! Thanks to you and Alina for welcoming me in Finland. Thanks for being my first audience when preparing my thesis presentation. Thanks to Naveen, to the group of Iranian girls who supported me when I was preparing the defense: Pegah, Ghazaleh, and Shirin. I also thank Herbert Sixta who encouraged me to finalize my thesis when I had already

Acknowledgements

started a postdoc in his group (I like that this is now in the middle of thanks to “young researchers”), and Michael, Sanna, Jiaqi, Gerardo, Saija, Heidi.

I would like to thank Lucas who was also my classmate at Pagora. I wish I was more present in the last year, but it was a pleasure to see you back in Grenoble! Thanks to Luis and Ara for their kindness, thanks Ara for your support and for teaching me how to make nanocellulose (crystals and fibers!). I would like to thank so many other people who were all nice to collaborate with as well as to chat or hang out with. Thanks to Marie-Alix for her kind advice and support, to Lakshman, to Marcos, Daniele, to Besma Ben Fadel, to Karthik, thanks to Ying, Arnaud, Laëtitia, Fedia, Ramzi, Besma Berrima, Virginie, Etzaël, Maxime, Erwan, Victor, Louis, Vivien, Vincent and Charlène who did a great work as PhD student representatives, to my students who soon became PhD students, Fleur, Valentin, Hélène, Johanna, Hippolyte, Flavien...

I am almost done. I would like to thank all my friends from Marseille (especially the group from Thiers: Johanne, Justine, Audrey, Mathilde, Loïc, Michaël, but also Mélanie, and Julien, who came to Grenoble at the same time as me, started a PhD at the same time, and unfortunately was not available to attend my defense) and from Pagora. All of you. Thanks to my former flatmates, to François, Juju, Bob, to Valentine, to Marjory who visited us when Carolina was working for her, Manu, to Aude, Sophie Sophou, for your joy and optimism, for everything we shared when you were in Grenoble and for everything we still share now that we are away, and all the other “mamies”: Miaou (Laëtitia), Farfadette, Flora, Steff, Marylou, Roro, Laure. Merci les filles !

I would like to thank the Rainbow swingers and Grenoble swing, and special thanks to my favorite paragliding club, l'aile et la cuisse (en particulier Vincent pour les parties d'échecs à la maison, pendant lesquelles ma rédaction avançait à une vitesse imbattable, mais aussi Phiphi, J-C et tous les autres). Thanks to Jeremy, Claire and Jordan for starting the paragliding lessons with me. Paragliding makes you happy. The best moments of these “thesis years” were probably in the air, alone and with Nicolas, especially during the writing period.

Finally, I wish to thank my family: those who came to the defense and those who could not. Thanks to everyone. Merci à Lucy, Margot, Marilynne et Xavier pour leurs encouragements, désolée d'avoir soutenu en plein mois de juillet... Un grand merci à François, merci à la famille de Nicolas, en particulier Serge, Martine et François, merci à tous de vous être déplacés pour l'événement et d'avoir supporté les heures de présentation et discussions en anglais. Thanks to my family in Iran and the US, thanks to my loving grandparents, aunts and uncle. Special thanks to khaleh Yekta for the tea breaks when I was writing at home in Tehran. And of course thanks to my parents. Merci pour tout, du soutien depuis le début de mes études à l'assistance technique pour compiler les pdf à des heures inavouables, merci maman pour tous tes efforts et pour avoir préparé un délicieux buffet iranien pour mon pot de thèse, merci d'ailleurs également à Awatef et Claire pour t'avoir aidée à l'installer. Thanks to my little brother, Thomas Thomou (best brother ever) who read lots of abstracts and pieces of thesis even though my research was so far from his field. Merci Thomas pour ton soutien inconditionnel.

And I would like to thank those who were next to me every day: my plants (aka my babies), coffee, and Nicolas. Merci de m'avoir fait voler bien sûr, mais aussi de m'avoir soutenue et supportée chaque jour jusqu'à maintenant. Tu mérites toi aussi un diplôme pour ta patience.

TABLE OF CONTENTS

INTRODUCTION.....	1
LIST OF ABBREVIATIONS.....	5
I - BIBLIOGRAPHIC STUDY	7
TABLE OF CONTENTS.....	8
LIST OF FIGURES.....	9
LIST OF TABLES.....	11
LIST OF EQUATIONS.....	11
I.1 INTRODUCTION	13
I.2 VIRGIN FIBERS.....	13
<i>I.2.1 Wood constituents.....</i>	<i>13</i>
I.2.1.1 Carbohydrates.....	14
I.2.1.2 Lignin	14
I.2.1.3 Other wood constituents.....	15
<i>I.2.2 Pulping.....</i>	<i>15</i>
I.2.2.1 Chemical pulping	16
I.2.2.2 Mechanical pulping.....	16
<i>I.2.3 Bleaching.....</i>	<i>17</i>
I.2.3.1 Overview.....	17
I.2.3.2 Chemical pulp bleaching.....	17
I.2.3.3 Mechanical pulp bleaching	19
<i>I.2.4 Hydrogen peroxide.....</i>	<i>20</i>
I.2.4.1 General aspects.....	20
I.2.4.1.i History and production.....	20
I.2.4.1.ii Chemical properties	21
I.2.4.1.iii Decomposition	21
I.2.4.1.iv Stabilization of hydrogen peroxide	23

Table of contents

I.2.4.2 Virgin fiber bleaching.....	23
I.2.4.2.i Bleaching conditions	23
I.2.4.2.ii Reactions during an ECF-P stage: hydrogen peroxide brightening.....	25
I.2.4.2.iii Reactions during a TCF-P stage: delignification	27
I.3 RECOVERED FIBERS.....	34
<i>I.3.1 Generalities</i>	<i>34</i>
I.3.1.1 Overview.....	34
I.3.1.1.i Legislation.....	35
I.3.1.1.ii Paper recycling in Europe: some figures	35
I.3.1.1.iii Prices.....	38
I.3.1.1.iv Recovered paper grades.....	38
I.3.1.2 The recycling process	39
I.3.1.3 DIP's fibers.....	40
I.3.1.4 DIP's chromophores	41
I.3.1.5 Paper dyes.....	41
I.3.1.5.i Structure.....	41
I.3.1.5.ii Classification	42
<i>I.3.2 Recovered fiber bleaching</i>	<i>43</i>
I.3.2.1 Overview.....	43
I.3.2.2 Use of H ₂ O ₂ in deinking lines	44
I.3.2.3 Reductive stages: FAS and Y	44
I.3.2.3.i Sodium dithionite	44
I.3.2.3.ii FAS.....	45
I.3.2.1 Conclusion.....	45
<i>I.3.3 Limits of paper recycling.....</i>	<i>45</i>
I.4 ACTIVATION OF HYDROGEN PEROXIDE BLEACHING THANKS TO A COPPER-PHENANTHROLINE COMPLEX.....	46
<i>I.4.1 Introduction to hydrogen peroxide delignification catalysis/activation</i>	<i>46</i>
<i>I.4.2 Copper-phenanthroline.....</i>	<i>48</i>
I.4.2.1 Overview.....	48
I.4.2.2 Copper	50
I.4.2.3 Phenanthroline	51
I.4.2.4 Copper-phenanthroline complex.....	52
<i>I.4.3 Oxygen delignification catalysis/activation.....</i>	<i>54</i>
<i>I.4.4 Hydrogen peroxide delignification activation/catalysis.....</i>	<i>56</i>

<i>I.4.5 On recovered fibers</i>	58
I.4.5.1 Native lignin brightening.....	58
I.4.5.2 Residual lignin degradation	59
I.4.5.3 Paper dye degradation	59
I.5 CONCLUSION	59
I.6 REFERENCES	60
II - MATERIALS AND METHODS	71
TABLE OF CONTENTS	72
LIST OF FIGURES	73
LIST OF TABLES	74
LIST OF EQUATIONS	74
II.1 RAW MATERIALS	75
<i>II.1.1 Dyes and other chemicals</i>	75
<i>II.1.2 Copper-phenanthroline complexes</i>	75
<i>II.1.3 Bleached kraft pulp</i>	75
<i>II.1.4 Dyed pulp</i>	76
II.2 METHODS	76
<i>II.2.1 To characterize the dyes</i>	76
II.2.1.1 UV-visible spectroscopy.....	76
II.2.1.2 HPLC	76
II.2.1.3 FTIR spectroscopy	78
II.2.1.4 NMR spectroscopy	79
II.2.1.4.i General principle of NMR spectroscopy.....	79
II.2.1.4.ii Principle of ¹³ C NMR.....	80
II.2.1.4.iii Conditions of analysis.....	81
II.2.1.5 Elemental analysis	82
<i>II.2.2 To characterize the copper-phenanthroline complex</i>	82
II.2.2.1 UV-visible analysis.....	82
II.2.2.2 EPR spectroscopic analysis.....	82
II.2.2.2.i General principle of EPR spectroscopy	82
II.2.2.2.ii EPR spectroscopy for copper complexation study	84

Table of contents

II.2.2.2.iii Conditions of copper complexation analysis.....	84
II.2.2.3 Speciation calculation (PHREEQC simulations).....	85
II.2.3 <i>To characterize the pulps</i>	85
II.2.3.1 Optical characterization.....	85
II.2.3.2 Physico-chemical characterization.....	87
II.2.3.3 Physical characterization.....	88
II.2.4 <i>To characterize dye solutions</i>	88
II.2.4.1 UV-vis spectroscopy.....	88
II.2.4.2 Electrospray Ionization-Mass Spectrometry	89
II.2.5 <i>To follow the formation of radicals</i>	89
II.2.5.1 Chemiluminescence method	89
II.2.5.1.i Principle	89
II.2.5.1.ii Analysis conditions	90
II.2.5.2 UV-vis method using DMNA	90
II.2.5.3 EPR/spin-trapping method	91
II.2.5.3.i Principle	91
II.2.5.3.ii Analysis conditions	93
II.2.5.3.iii Result analysis: integration and simulations	94
II.3 CU-PHEN-ACTIVATED H ₂ O ₂ TREATMENTS	94
II.3.1 <i>Preparation of the complex</i>	94
II.3.2 <i>Pulp bleaching or color-stripping</i>	95
II.3.3 <i>Dye solution color-stripping</i>	96
II.4 REFERENCES	96

III - CHARACTERIZATION OF THE DYES AND INTERACTIONS WITH COPPER-PHENANTHROLINE	101
TABLE OF CONTENTS	102
LIST OF FIGURES	103
LIST OF TABLES.....	106
III.1 INTRODUCTION.....	107
III.2 CHARACTERIZATION OF THE DYES.....	107
III.2.1 <i>UV-visible analysis</i>	107
III.2.2 <i>Acidimetric titrations</i>	110

III.2.2.1 DR81L	110
III.2.2.2 DY11L.....	112
III.2.3 FTIR spectroscopic analyses	115
III.2.4 ESI-MS analysis.....	117
III.2.5 NMR spectroscopic analyses.....	120
III.2.5.1 Analysis of DR81L.....	120
III.2.5.2 Analysis of DY11L.....	127
III.2.5.3 Conclusions.....	132
III.2.6 Conclusion.....	132
III.3 COPPER-PHENANTHROLINE SPECIATION	132
III.4 ANALYSIS OF THE CU-PHEN COMPLEX.....	138
III.4.1 $CuSO_4$	138
III.4.2 Phenanthroline	138
III.4.3 Cu-Phen.....	140
III.4.4 Evidence of coordination by EPR.....	140
III.5 ANALYSIS OF THE DR81L DYE/CU-PHEN SYSTEM	142
III.5.1 Dye/ $CuSO_4$	142
III.5.2 Dye/Phenanthroline.....	143
III.5.3 Dye/Cu-Phen.....	143
III.5.3.1 Alkaline pH: variation of Cu:Phen ratio.....	144
III.5.3.2 Alkaline pH: variation of the dye/Cu ratio.....	146
III.5.3.3 Neutral pH.....	148
III.5.3.4 Supplementary evidence for complexation.....	150
III.5.3.4.i Evidence by HPLC.....	151
III.5.3.4.ii Evidence by MS.....	151
III.5.3.4.iii Evidence by EPR.....	155
III.5.3.5 Conclusions.....	161
III.6 CONCLUSIONS	161
III.7 REFERENCES.....	163

IV – DYED PULP COLOR-STRIPPING BY ACTIVATED HYDROGEN PEROXIDE	165
TABLE OF CONTENTS	166
LIST OF FIGURES	167
LIST OF TABLES.....	167
IV.1 INTRODUCTION.....	169
IV.2 PRELIMINARY STUDY ON A DY11L-COLORED PULP	169
<i>IV.2.1 Introduction</i>	<i>169</i>
<i>IV.2.2 Experimental.....</i>	<i>170</i>
<i>IV.2.3 Activating effect of Cu-Phen and Phen</i>	<i>170</i>
IV.2.3.1 Color-stripping results.....	170
IV.2.3.2 Results on pulp optical properties	171
IV.2.3.3 Results on cellulose viscosity.....	172
IV.2.3.4 General view.....	173
IV.2.3.5 Conclusion.....	176
<i>IV.2.4 Design of experiments: influence of time, temperature, and NaOH dose</i>	<i>176</i>
<i>IV.2.5 Conclusions</i>	<i>180</i>
IV.3 COLOR-STRIPPING OF A DR81L-COLORED PULP	181
<i>IV.3.1 Introduction</i>	<i>181</i>
<i>IV.3.2 Experimental.....</i>	<i>181</i>
<i>IV.3.3 White pulp bleaching</i>	<i>182</i>
<i>IV.3.4 Dyed pulp color-stripping.....</i>	<i>186</i>
IV.3.4.1 Decolorizing effect.....	187
IV.3.4.1.i Color-stripping results.....	187
IV.3.4.1.ii At low alkalinity (0.2% NaOH).....	188
IV.3.4.1.iii Under conventional alkaline conditions (2% NaOH)	189
IV.3.4.2 Cellulose degradation.....	190
IV.3.4.3 Impact of the color-stripping treatments on the mechanical properties of the dyed pulp	191
IV.3.4.4 Conclusions.....	192
<i>IV.3.5 Comparison with the color-stripping of a DY11L-dyed pulp</i>	<i>192</i>
<i>IV.3.6 Conclusions</i>	<i>193</i>
IV.4 CONCLUSION	194
IV.5 REFERENCES	194

V – MECHANISTIC STUDY OF THE H ₂ O ₂ /CU-PHEN SYSTEM.....	197
TABLE OF CONTENTS	198
LIST OF FIGURES	199
LIST OF TABLES.....	202
LIST OF EQUATIONS.....	203
V.1 INTRODUCTION	204
V.2 EXAMINATION OF THE CATALYTIC ROUTE.....	204
<i>V.2.1 Introduction.....</i>	<i>204</i>
<i>V.2.2 Assessment of a possible catalytic cycle.....</i>	<i>205</i>
V.2.2.1 Influence of the cellulosic substrate in the possible reduction of Cu ^{II}	206
V.2.2.1.i Cellulosic fibers	206
V.2.2.1.ii Avicel	206
V.2.2.1.iii Soluble cellulose: cellobiose.....	208
V.2.2.1.iv Conclusions.....	209
V.2.2.2 Influence of dyes on the possible reduction of Cu ^{II}	210
V.2.2.3 Possible reduction of Cu ^{II} in the absence of substrate.....	211
V.2.2.4 Conclusion	212
V.3 EXAMINATION OF DYE DEGRADATION IN AQUEOUS SOLUTION	212
<i>V.3.1 Introduction.....</i>	<i>212</i>
<i>V.3.2 UV-vis spectroscopic study.....</i>	<i>214</i>
<i>V.3.3 Analysis of the dye degradation products by ESI-MS</i>	<i>217</i>
V.4 INVESTIGATION OF A RADICAL MECHANISM.....	219
<i>V.4.1 Studies using chemiluminescence and UV-vis spectroscopy.....</i>	<i>220</i>
V.4.1.1 Radical detection by chemiluminescence	220
V.4.1.2 Radical detection by UV-visible spectroscopy	222
<i>V.4.2 EPR/Spin-trapping.....</i>	<i>226</i>
V.4.2.1 Experimental	226
V.4.2.2 Results at near-neutral/weak alkaline pH.....	227
V.4.2.2.i EPR/spin-trapping results and qualitative interpretation.....	227
V.4.2.2.ii Simulation of the EPR/spin-trapping results and semi-quantitative interpretation	240
V.4.2.2.iii Conclusions.....	243

Table of contents

V.4.2.3 Results at alkaline pH	244
V.4.2.3.i Results without H ₂ O ₂	244
V.4.2.3.ii Introduction of H ₂ O ₂	247
V.4.2.3.iii Conclusions.....	249
V.4.2.4 The H ₂ O ₂ /Cu-Phen system with substrate	249
V.4.2.4.i With dyes	249
V.4.2.4.ii With cellulosic fibers	251
V.4.2.5 Conclusions	251
V.5 PROPOSITION OF A FENTON-LIKE MECHANISM	252
V.6 REFERENCES.....	255
CONCLUSION	261
ANNEXES	265
TABLE OF CONTENTS	266
LIST OF FIGURES	266
LIST OF TABLES.....	266
ANNEX 1	268
ANNEX 2	271

INTRODUCTION

Today, cellulosic fibers from recovered paper and board represent more than 50% of the fibrous sources used by the European paper and board industry. However, the utilization of high grades of recovered fibers such as office papers is very low, around 10%, since the production of high grade paper by recycling this fiber sort is difficult and expensive. Indeed, to obtain high quality and white fibers from this raw material, several operations are necessary, the major ones being deinking and bleaching. Usually, deinking is conducted using physicochemical processes such as flotation. Bleaching consists in decolorizing all the colored components brought by or attached to fibers (chromophores). These are typically brown kraft pulp lignin from envelopes (wood lignin that was highly modified by the kraft alkaline pulping process), lignin from mechanical pulp fibers (close to wood native lignin), and paper dyes from colored papers.

The removal of paper dyes is an important issue. Indeed, it is rather difficult to obtain perfect color-stripping when a variety of dyes exists and none of them have the same sensitivity to bleaching agents. Usually, the bleaching process starts with an alkaline hydrogen peroxide stage which decolorizes native lignin and also partly degrades or bleaches kraft lignin. However, the color-stripping effect of hydrogen peroxide on paper dyes is often limited: hydrogen peroxide has a poor reactivity towards azo groups, which are often present in paper dyes. Therefore, the peroxide stage is generally combined with a reductive stage able to decolorize azo dyes, either with formamidine sulfonic acid (FAS) or with sodium dithionite. Unlike hydrogen peroxide, these chemicals are quite effective for dye color-stripping. Unfortunately, they are more expensive than hydrogen peroxide, and also more polluting, whereas hydrogen peroxide is environmentally friendly, since its decomposition products are water and oxygen.

The goal of this thesis project was to improve deinked pulp bleaching to encourage the utilization of high quality recovered fibers in printing and writing papers, using environmentally friendly processes. The idea was to enhance the efficacy of hydrogen peroxide and therefore reduce the use of reducing agents. Hydrogen peroxide can be introduced during recovered paper disintegration at near neutral pH at the beginning of the recycling line to partly bleach fibers, or in the bleaching step in alkaline medium after deinking. Hence, the improvement of hydrogen peroxide's efficacy will be investigated at both neutral and alkaline pHs.

In previous works, the improvement of hydrogen peroxide bleaching has been thoroughly studied in the context of chemical pulp delignification. In particular, the activation or catalysis of alkaline hydrogen peroxide by copper-phenanthroline complexes was found to be very effective, with strong enhancement of delignification. However, cellulose was also severely depolymerized. This inspired a preliminary bleaching study on deinked pulp and dyed pulp, and resulted in significant improvement of dye removal, which gave birth to our project.

Several effects may be hypothesized to explain the improvement of peroxide color-stripping in the presence of copper-phenanthroline complexes: (1) first, one or several complexes may have a particular chemical action on the dye even in the absence of hydrogen peroxide, (2) copper-phenanthroline complexes may catalyze the oxidation of the dye by hydrogen peroxide, (3) copper-phenanthroline complexes may activate the decomposition of hydrogen peroxide into highly oxidative free radicals, which would be responsible for dye oxidation, but also for cellulose fiber oxidation.

The purpose of this work was to determine to what extent copper-phenanthroline could improve the H_2O_2 color-stripping of dyed cellulosic fibers, depending on the applied conditions, especially the effect of pH and copper-to-ligand ratio, and also how. To answer these questions, three issues were addressed successively:

1. Does copper-phenanthroline have an effect on the dye alone?
2. Does copper-phenanthroline improve the color-stripping of a dyed pulp by H_2O_2 ?
3. By which mechanism does the H_2O_2 /copper-phenanthroline system improve dye color-stripping?

Consequently, this thesis is organized as follows:

In the first chapter, a literature review will highlight the importance of paper recycling and present the last developments concerning hydrogen peroxide activation using copper-phenanthroline complexes. Such systems have already been studied in biological medium (neutral pH), but also on chemical pulps to improve alkaline H_2O_2 delignification. It will be shown that the mechanism involved is not clear and that further investigations are required to successfully apply the H_2O_2 /Cu-Phen system to the color-stripping of recovered cellulosic fibers under neutral and alkaline conditions. This review inspired our first approach, which consisted in selecting hydrogen peroxide-resistant azo dyes, and conducting H_2O_2 color-stripping trials on these dyes with and without cellulosic fibers (dyed fiber suspensions and aqueous dye solutions).

In a second chapter, the methodology used to achieve this work will be presented through a comprehensive description of the materials and methods chosen to characterize the system, to perform the different kinds of color-stripping trials, but also to investigate the mechanism involved.

After this, the results and discussions will be divided into three chapters, which correspond to the three questions mentioned earlier: (1) first, the dye and the Cu-Phen complex were characterized in the absence of any oxidant in neutral and alkaline medium and the interactions between the dye and the Cu-Phen complex were examined, (2) then, the hydrogen peroxide/copper-phenanthroline system was applied on dyed pulp to assess its color-stripping potential at neutral and alkaline pHs and to attempt to optimize it, and (3) finally, the oxidation mechanism was investigated mainly via trials in aqueous solution, in the absence of fibers. Two routes were investigated: a catalytic cycle and a radical mechanism.

Lastly, a conclusion will synthesize the main findings, suggest chemical routes for the color-stripping of direct azo dyes and paper colored with those dyes, and finally propose some perspectives in the fields of deinked pulp bleaching as well as wastewater treatment.

LIST OF ABBREVIATIONS

A	Acid stage
AOP	Advanced Oxidation Process
AOX	Adsorbable Organic Halogen (here, chlorinated organic compounds)
BKP	Bleached kraft pulp
BL ₀	Zero-span breaking length
CEPI	Confederation of European Paper Industries
CIE	International Commission on Illumination (from French : Commission internationale de l'éclairage)
COD	Chemical oxygen demand
COPACEL	Association of French Paper Industries
CTMP	Chemi-thermomechanical pulp
Cu-Phen	Copper-phenanthroline complex
D	Chlorine dioxide stage
dBKP	Dyed bleached kraft pulp
DIP	Deinked pulp
DMNA	N,N-dimethyl-4-nitrosoaniline
DMPO	5,5-dimethylpyrroline-N-oxyl
DMSO	Dimethylsulfoxide
DNA	Deoxyribonucleic acid
DP	Degree of polymerization
DP _v	Viscosity-average degree of polymerization
DR81	Direct Red 81
DR81S	Solid Direct Red 81 dye (powder)
DRI	Dye removal index
DY11	Direct Yellow 11
DY11L	Liquid Direct Yellow 11 dye
E	Alkaline extraction stage
ECF	Elemental-chlorine free
ERPA	European Recovered Paper Association
ERPC	European Recovered Paper Council

List of abbreviations

FAS	Formamidine sulfinic acid
HexA	Hexenuronic Acid
HPLC	High Performance Liquid Chromatography
ISO	International Organization for Standardization
MCC	Microcrystalline Cellulose
MS	Mass Spectrometry
O	Oxygen stage
odp	Oven-dried pulp
P	Hydrogen peroxide bleaching stage
POM	Polyoxometalate
Q	Chelating stage
RCF	Recovered cellulosic fibers
RNA	Ribonucleic acid
TCF	Totally chlorine-free
TMP	Thermomechanical pulp
Z	Ozone bleaching stage

I. BIBLIOGRAPHIC STUDY

TABLE OF CONTENTS

LIST OF FIGURES	9
LIST OF TABLES.....	11
LIST OF EQUATIONS.....	11
I.1 INTRODUCTION	13
I.2 VIRGIN FIBERS.....	13
<i>I.2.1 Wood constituents</i>	13
I.2.1.1 Carbohydrates	14
I.2.1.2 Lignin.....	14
I.2.1.3 Other wood constituents.....	15
<i>I.2.2 Pulping</i>	15
I.2.2.1 Chemical pulping.....	16
I.2.2.2 Mechanical pulping.....	16
<i>I.2.3 Bleaching</i>	17
I.2.3.1 Overview.....	17
I.2.3.2 Chemical pulp bleaching	17
I.2.3.3 Mechanical pulp bleaching.....	19
<i>I.2.4 Hydrogen peroxide</i>	20
I.2.4.1 General aspects	20
I.2.4.1.i History and production	20
I.2.4.1.ii Chemical properties	20
I.2.4.1.iii Decomposition.....	21
I.2.4.1.iv Stabilization of hydrogen peroxide	23
I.2.4.2 Virgin fiber bleaching	23
I.2.4.2.i Bleaching conditions	23
I.2.4.2.ii Reactions during an ECF-P stage: hydrogen peroxide brightening	25
I.2.4.2.iii Reactions during a TCF-P stage: delignification	27
I.3 RECOVERED FIBERS.....	34
<i>I.3.1 Generalities</i>	34
I.3.1.1 Overview.....	34
I.3.1.1.i Legislation	35
I.3.1.1.ii Paper recycling in Europe: some figures	35
I.3.1.1.iii Prices	38
I.3.1.1.iv Recovered paper grades.....	38
I.3.1.2 The recycling process	39
I.3.1.3 DIP's fibers	40
I.3.1.4 DIP's chromophores.....	41
I.3.1.5 Paper dyes.....	41
I.3.1.5.i Structure	41
I.3.1.5.ii Classification.....	42
<i>I.3.2 Recovered fiber bleaching</i>	43
I.3.2.1 Overview.....	43
I.3.2.2 Use of H ₂ O ₂ in deinking lines.....	44
I.3.2.3 Reductive stages: FAS and Y.....	44
I.3.2.3.i Sodium dithionite	44

I.3.2.3.ii FAS.....	45
I.3.2.1 Conclusion.....	45
I.3.3 <i>Limits of paper recycling</i>	45
I.4 ACTIVATION OF HYDROGEN PEROXIDE BLEACHING THANKS TO A COPPER-PHENANTHROLINE COMPLEX	46
I.4.1 <i>Introduction to hydrogen peroxide delignification catalysis/activation</i>	46
I.4.2 <i>Copper-phenanthroline</i>	48
I.4.2.1 Overview.....	48
I.4.2.2 Copper.....	50
I.4.2.3 Phenanthroline.....	51
I.4.2.4 Copper-phenanthroline complex.....	52
I.4.3 <i>Oxygen delignification catalysis/activation</i>	54
I.4.4 <i>Hydrogen peroxide delignification activation/catalysis</i>	56
I.4.5 <i>On recovered fibers</i>	58
I.4.5.1 Native lignin brightening	58
I.4.5.2 Residual lignin degradation.....	58
I.4.5.3 Paper dye degradation.....	59
I.5 CONCLUSION	59
I.6 REFERENCES.....	59

LIST OF FIGURES

Figure I-1. Scheme of the hierarchical structure of wood, from fiber to molecular composition, as illustrated by Per Hoffmann [1].....	13
Figure I-2. Structure of cellulose.....	14
Figure I-3. Polymer model for lignin from poplar, as estimated from NMR analysis of isolated lignin from wild poplar [4].....	15
Figure I-4 Generic medium consistency bleaching stage [12].....	17
Figure I-5. Outline of a fiberline for the production of bleached kraft pulp [9].....	19
Figure I-6. Relationship between time, temperature and alkalinity for hydrogen peroxide bleaching of mechanical pulp [34]	25
Figure I-7. Reaction of the perhydroxyl anion with enal or enone side chain structures [23].....	26
Figure I-8. Reaction of the perhydroxyl anion with ortho- and para- (o- and p-) quinonoid structures [37]	27
Figure I-9. Initial addition of the hydroxyl radical on a lignin aromatic ring under alkaline conditions, as described by Gierer [39].....	28

Figure I-10. Subsequent reactions on phenoxy radicals under alkaline conditions, adapted from Gierer [39].....	29
Figure I-11. Subsequent reactions on cyclohexadienyl radicals under alkaline conditions, from structure 3: hydroxylation and dealkoxylation, from structure 4: C α -C β cleavage, and from structure 5: hydrogen abstraction from C α	30
Figure I-12. Effect of hydroxyl radicals on carbohydrates: cleavage of the C4 glycosidic bond by β -elimination, after H-abstraction from the 2-position carbon atom, adapted from Gierer [42], Sues [16], and Hon and Shiraishi [44]	31
Figure I-13. Effect of hydroxyl radicals on carbohydrates: cleavage of the glycosidic bond of 1,4-anhydrocellobitol, according to Guay [48].....	32
Figure I-14. Initiation of radical bleaching reactions with $HO \bullet$, $HOO \bullet$, $ClO_2 \bullet$, $Cl \bullet$ depending on the pH, as summarized by Gierer [39]	33
Figure I-15. Reaction of the hydroxyl anion with quinonoid structures [23]	34
Figure I-16. CEPI utilization of paper for recycling by sector and by grade in 2014 [52]	37
Figure I-17. CEPI utilization of paper for recycling by grade, from 1991 to 2014 [52].....	37
Figure I-18. Contaminants in recovered paper [22].....	39
Figure I-19. Deinking line to produce magazine or writing and printing paper from sorted recovered papers. Source: CTP	40
Figure I-20. Molecular structure of Direct Red 81	42
Figure I-21. Molecular structure of Direct Yellow 11	43
Figure I-22. Molecular structure of formamidine sulfinic acid	45
Figure I-23. Molecular structure of the Mn-complex used to catalyze hydrogen peroxide bleaching by Patt and coworkers [79], [80]	47
Figure I-24. Molecular structure of 1,10-phenanthroline	51
Figure I-25. Geometry of $[Cu(bpy)_2]^{2+}$ in water according to Garribba et al. [129].....	52
Figure I-26. Geometry of the $Cu(Phen)_2CO_3$ complex according to Korpi [131]	52
Figure I-27. Copper-phenanthrolines used in Gueneau's and Elder's studies	53
Figure I-28. Scheme of the catalytic mechanism proposed by Ma et al. for the oxidation of veratryl alcohol by Cu-Phen [146].....	55
Figure I-29. Catalytic cycle proposed by Korpi et al. for the oxidation of veratryl alcohol in alkaline medium with oxygen and a copper-phenanthroline catalyst [93]	57
Figure I-30. Scheme of the pathway proposed by Perez-Benito for hydrogen peroxide decomposition in the presence of Cu^{II} at low copper concentration [151].....	58

LIST OF TABLES

Table I-1. Average wood composition of scots pine (softwood) and silver birch (hardwood). Contents are given in % of dry solids.....	13
Table I-2. Main chemical-pulp bleaching oxidants.....	18
Table I-3. Other stages commonly found in bleaching sequences	19
Table I-4. Mechanical pulp bleaching agents.....	20
Table I-5. Operating conditions of a chemical pulp bleaching peroxide stage [9], [21]	24
Table I-6. Operating conditions of a (chemi)mechanical pulp bleaching peroxide stage [21]	24
Table I-7. Paper and board recycling in France in 2014.....	36
Table I-8. Price watch in Europe for recovered paper grades to produce DIP [57].....	38
Table I-9. Main chemical agents used for wood-containing deinked pulp bleaching [22]	43
Table I-10. Overview of the occurrence, uses and main properties of copper.....	50
Table I-11. Properties and uses of CuSO_4	51

LIST OF EQUATIONS

Equation I-1	21
Equation I-2	21
Equation I-3	21
Equation I-4	21
Equation I-5	21
Equation I-6	21
Equation I-7	21
Equation I-8	21
Equation I-9	22
Equation I-10	22
Equation I-11	22
Equation I-12	22
Equation I-13	22

I. Bibliographic study

Equation I-14	22
Equation I-15	22
Equation I-16	22
Equation I-17	22
Equation I-18	22
Equation I-19	22
Equation I-20	23
Equation I-21	44
Equation I-22	45
Equation I-23	45
Equation I-24	49
Equation I-25	51
Equation I-26	51
Equation I-27	53
Equation I-28	53
Equation I-29	53
Equation I-30	53
Equation I-31	53
Equation I-32	54
Equation I-33	54
Equation I-34	54
Equation I-35	57

I.1 INTRODUCTION

As mentioned in the thesis introduction, the objective of this work was to activate hydrogen peroxide for dye color-stripping in the context of recovered cellulosic fiber bleaching.

This chapter presents this chemical system and various aspects of its actions. It starts with an overview on virgin cellulosic fibers and their bleaching, followed by the description of recovered fibers, and finally the activation of hydrogen peroxide with copper-phenanthroline.

I.2 VIRGIN FIBERS

Virgin fibers come from either annual plants or wood. Our focus will be on wood fibers. Figure I-1 illustrates the multiscale structure of wood, from tree to fibers, fibrils and chemical composition.

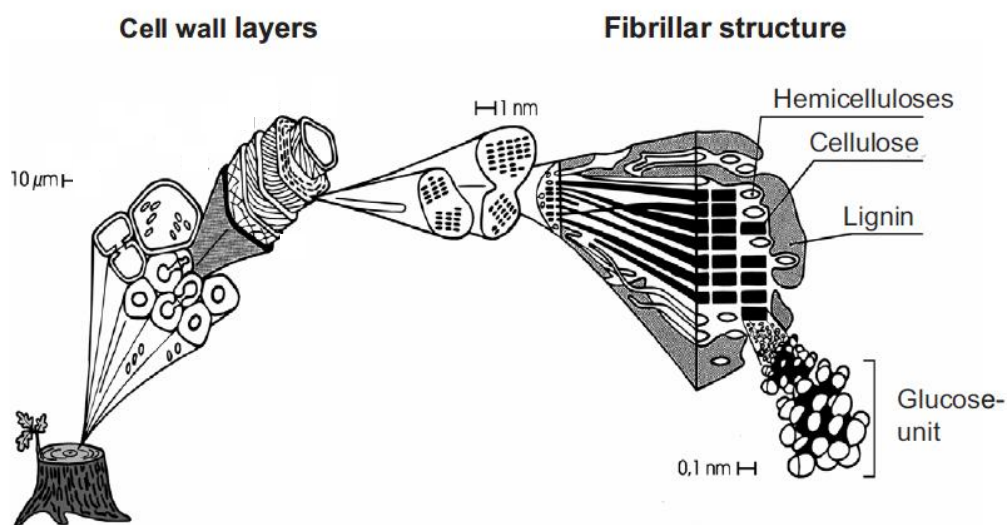


Figure I-1. Scheme of the hierarchical structure of wood, from fiber to molecular composition, as illustrated by Per Hoffmann [1]

I.2.1 Wood constituents

The main chemical constituents of wood are three polymers: cellulose, hemicelluloses and lignin. Minor compounds are various types of extractives, mostly organic ones. The content of minerals is generally below 1% in the wood species used for pulping. Typical compositions are presented in Table I-1, as reported by Willför *et al.* [2].

Table I-1. Average wood composition of scots pine (softwood) and silver birch (hardwood). Contents are given in % of dry solids.

	Scots pine	Silver birch
Cellulose	40	40
Hemicelluloses	25-30	30-35
Lignin	25-30	20-25
Others	<5	<5

I.2.1.1 Carbohydrates

Carbohydrates (cellulose and hemicelluloses) are the major constituents of wood. Cellulose is present in both amorphous and crystalline forms, whereas hemicelluloses are only amorphous. Carbohydrates are subject to intra- and inter-molecular bonding via hydrogen bonds. These contribute to the strength of the fiber network during papermaking.

Cellulose is a polymer of β -D-glucopyranose units linked by $\beta(1\rightarrow4)$ -glycosidic bonds, as presented in Figure I-2. Its degree of polymerization (DP) reaches 10,000 in native wood and decreases down to 500-2,000 in chemical pulps [3].

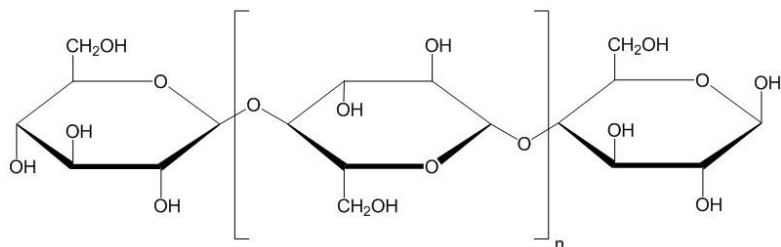


Figure I-2. Structure of cellulose

Hemicelluloses are heteropolysaccharides with building units composed of neutral sugars (hexoses, pentoses), partially methylated and acetylated, and uronic acids. Elemental sugars in wood hemicellulose chains are xylose, arabinose, mannose, glucose, and galactose. They have average DPs of 50 to 300 [1], [3].

I.2.1.2 Lignin

Lignin is an amorphous polymer made of phenylpropane (C₉) building units without any systematic structuration. It is a polyphenolic molecule, with different types of free or etherified phenolic structures. The building blocks are p-hydroxycinnamyl alcohols mainly linked by ether bonds, but also by C-C bonds [3]. They are trans-coniferyl alcohol (guaiacyl), trans-sinapyl alcohol (syringyl) and trans-p-coumaryl alcohol. Hardwood lignins consist of both guaiacyl and syringyl-type units (see an example in Figure I-3), whereas softwood lignins are made of more than 90% guaiacyl units.

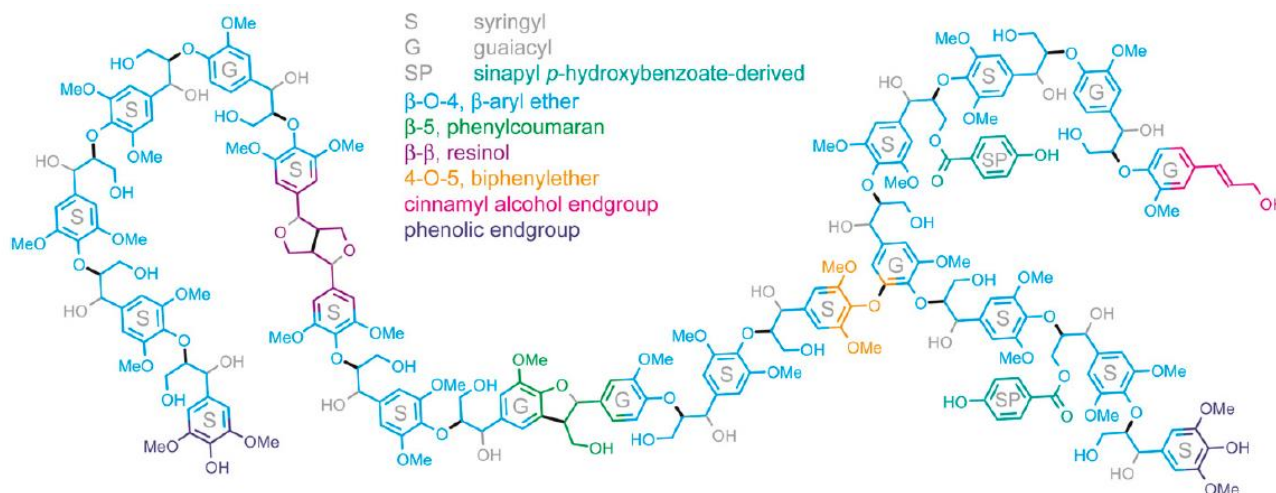


Figure I-3. Polymer model for lignin from poplar, as estimated from NMR analysis of isolated lignin from wild poplar [4]

In wood, lignin (also called native lignin) acts as a natural glue for fibers and is responsible for the structure and mechanical resistance of wood, as well as for its color. Therefore, lignin has to be removed or bleached in order to produce white fibers.

I.2.1.3 Other wood constituents

Other wood constituents are organic and inorganic compounds with varying contents depending on the wood species, geographical origin (different environmental conditions: soil, climate, etc.), and location within the tree [1], [3].

Some organic compounds can be extracted by hot water and some organic solvents. They are thus called “extractives” and can be divided into three classes: volatile oils, wood resins, and fats and acids [1]. Their content and nature vary among wood species and also depend on the season and geographical origin as they are related to environmental conditions.

Inorganic compounds are contained in the ash obtained after wood burning. Various minerals are found in the ash: calcium (main component), potassium, magnesium, manganese, iron, sodium, etc. [1]

The processing of wood into cellulosic fibers (pulp) requires a good knowledge of the structure and composition of wood. In mechanical processes, the overall chemical composition is not changed; however, chemical pulping removes some components such as lignin.

I.2.2 Pulping

Pulping consists in the separation of wood fibers with minimum morphological degradation. Two main methods are used: chemical pulping and mechanical pulping. A general description of these pulping methods is relevant to our state of the art as recovered fibers are made of mixtures of chemical and mechanical pulps. However, this study focused on the color-stripping of dyed chemical pulps. This is why chemical pulps and their bleaching are particularly detailed in this first chapter.

I.2.2.1 Chemical pulping

During chemical pulping, most of the lignin present in the fiber walls is dissolved, allowing fiber separation. Pulping processes are divided into acidic processes (acid-sulfite and bisulfite pulping) and alkaline processes (soda-AQ and kraft pulping). The acidic pulping processes are dedicated to specialty pulps while the alkaline processes mainly produce paper and board pulps. Soda cooking was developed in 1851 by Hugh Burgess and Charles Watt in England. In 1857, acid sulfite pulping was invented by Benjamin Tilghman in the United States. Kraft pulping was patented in 1884 by Dahl: caustic soda was replaced by sodium sulfate, which led to a cooking liquor made of sodium hydroxide and sodium sulfide and resulted in stronger pulps [5].

Nowadays, the kraft process is the primary chemical pulping process: approximately 90% of chemical pulps are kraft pulps [5]. Wood chips are cooked with a liquor made of sodium hydroxide and sodium sulfide, called “white liquor”, with a liquor-to-wood ratio of 3.5:1 to 5:1 [6], for 3-4 hours at 155-175°C [3]. Kraft pulping removes the majority of the lignin present in the wood, although 3-5% of highly colored residues are found in the pulp after cooking [3]. The resulting pulp is thus called wood-free pulp (i.e. lignin-free), and its integrity is preserved, which leads to a pulp with good mechanical properties.

During kraft cooking, two competing phenomena occur. The first one is lignin fragmentation into soluble products; the second one is re-condensation of these fragments, either with other lignin fragments or with carbohydrates [3]. The lignin remaining in the pulp after kraft cooking is called residual lignin, as it is different from native lignin in wood. Residual lignin is one of the main colored residues in kraft pulp. In addition, the cleavage of phenolic structures from lignin can lead to the formation of colored quinones and the reaction of hydrosulfide ions with lignin methoxy groups tends to form malodorous sulfur compounds (methyl mercaptans). The main chemical structures responsible for the brown color of kraft pulp are quinones [7] and other highly conjugated structures containing carbonyls and carbon-carbon double bonds [3], [8].

After pulping, softwood pulps reach a kappa number (index measuring the lignin content) of 25–30, and hardwood kraft pulps have a kappa number of 15–20 [5]. This corresponds to an ISO brightness of 20-30%, which is far from the standards for white paper production, i.e. typically 88-91% [3]. This is why these brown pulps require bleaching. For this purpose, residual lignin has to be degraded and removed or at least brightened.

Besides, part of the hemicelluloses contained in wood are also extracted during kraft pulping, which explains why the pulp yield reaches only 45 to 55% [5]. These “strong pulps” are used for brown paper and board applications such as brown envelopes or packaging if unbleached, and for all kinds of white papers if bleached.

One major advantage of kraft pulping over the sulfite process is its very efficient recovery process. Through the concentration and incineration of the cooking liquor (so-called black liquor), it produces a great amount of energy and regenerates the cooking chemicals, i.e. sodium sulfide and sodium hydroxide, after caustification of the carbonates.

I.2.2.2 Mechanical pulping

To produce mechanical pulp, the wood fibers are separated mechanically, either by grinding wood logs with a revolving pulpstone or by refining wood chips with a disc refiner [9]. These treatments, conducted under moist atmosphere at a temperature of 100 – 120°C, are able to soften lignin, which allows the fibers to be separated. However, mechanical pulping degrades the fibers. Its

efficiency can be improved by reinforcing the temperature and/or the pressure, or it can be complemented with a preliminary chemical treatment.

The specificity of mechanical pulping is its high pulp yield, in the range of 85 – 95% [10] (up to 98% for thermomechanical pulp from debarked spruce [9]), leading to a pulp containing all the components of wood, especially native lignin. This is why it is also called “wood-containing pulp”. Heat, moisture and oxygen are responsible for the formation of colored structures during mechanical pulping. Consequently, mechanical pulps do not reach high brightness levels: their initial brightness is usually around 55-65% ISO (softwood from forest thinning or wood chips from saw mills) [11]. This brightness level allows their use in newspaper without bleaching; however, bleaching is required for higher white grades. Moreover, with or without bleaching, mechanical pulps are subject to yellowing when exposed to heat or sunlight, as their large amount of lignin contributes to the poor brightness stability of the pulp.

Due to the mechanical treatment, mechanical pulps contain fines, which bring opacity and bulk to the final paper. However, the fibers being short, partly degraded and aggregated, these pulps do not have high mechanical properties. They are used in newspapers and magazine papers, but also in paperboard and in the composition of some fine papers and soft tissue [9].

I.2.3 Bleaching

The aim of pulp bleaching is to remove the color that remains after pulping. It can be either by removing the dark brown residual lignin remaining in kraft pulps after cooking, or by decolorizing the chromophores brought by native lignin in mechanical pulps. For high quality paper grades, the desired brightness can be up to 90 – 95% ISO brightness and good brightness stability is required. At the same time, for all paper applications, cellulose degradation has to be limited since it generally impairs the strength properties of the pulps.

I.2.3.1 Overview

Pulp bleaching, depending on the type of pulp, requires multi-stage sequences. Generally, oxidative stages are followed by washing steps and sometimes alkaline extraction (E stage), to remove the dissolved products.

I.2.3.2 Chemical pulp bleaching

The set-up of a bleaching stage consists of specific equipment and can be generalized as the scheme presented in Figure I-4.

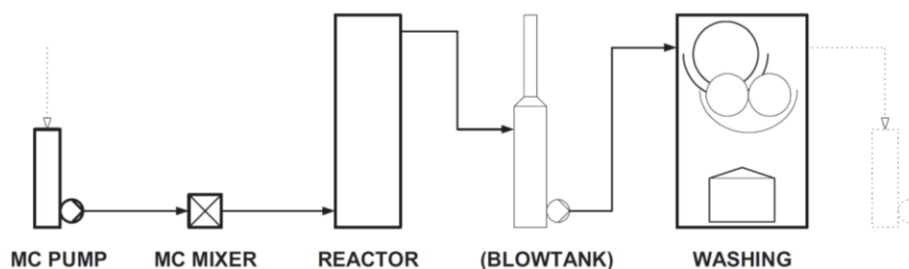


Figure I-4 Generic medium consistency bleaching stage [12]

Although most stages use chemical agents, biotechnological solutions also exist. Enzymatic treatments have been studied as pre-bleaching stages to reduce chemical consumption [13] and even to replace some stages, since enzymes such as xylanases, laccases, or lignin peroxidases are able to delignify chemical pulps [14], [15].

Since the early 1990's, the chlorine delignification stage, which used to be largely implemented at the beginning of the sequence, was gradually suppressed. Indeed, it generated high amounts of toxic organochlorinated compounds (AOX, as for Adsorbable Organic Halogen). Therefore, chlorine dioxide soon became the most important delignification and bleaching chemical.

Besides, new developments appeared to reduce chlorine dioxide consumption. First, the use of an oxygen delignification stage prior to the bleaching sequence allowed substantial reductions. Other developments consisted in the reinforcement of alkaline extraction with oxygen and/or hydrogen peroxide, the use of a final P stage, and also the implementation of ozone (Z stage), although developed in a limited number of mills [16].

Bleaching sequences using chlorine dioxide instead of molecular chlorine are called elemental chlorine-free sequences (ECF). They became prevalent in the last two decades: while only 5% of bleached pulps were ECF-bleached in 1990, they represented more than 75% of bleached pulps in 2002 (64 million tons worldwide) [14], and reached 93% in 2012 [17]. When no chlorinated chemical is used in a bleaching sequence, it is called totally chlorine-free (TCF). These sequences have been developed for ecological reasons as they avoid any AOX generation. They remain minor because they are considered as less effective than ECF sequences for complete delignification and not as selective, with typical commercial pulps having lower viscosity at the same brightness level [12].

The main oxidants used in chemical-pulp bleaching sequences are presented in Table I-2 and other common stages are listed in Table I-3.

Table I-2. Main chemical-pulp bleaching oxidants

Oxidant	Stage symbol
Chlorine dioxide, ClO ₂	D
Molecular oxygen, O ₂	O
Hydrogen peroxide, H ₂ O ₂	P
Ozone, O ₃	Z

The primary bleaching agent used in the industry is chlorine dioxide, used in acidic medium [18]. Its success is due to its high selectivity and relatively low environmental impact. Its action results mainly in lignin fragmentation and formation of acidic moieties that require further extraction from the fiber matrix by a subsequent alkaline extraction stage E, see Table I-3 [18]. In most mills, alkaline extraction is reinforced by the addition of hydrogen peroxide and/or molecular oxygen under pressure, in (EP), (EO) and (EOP) stages. Stages in parentheses are not subject to intermediate washing.

As they are chlorine-free, oxygen-based bleaching effluents can be recovered. These can be mixed with the kraft cooking effluent, concentrated, and burnt in the recovery furnace of the kraft cooking cycle. However, oxygen-based bleaching agents are generally not as effective and selective as chlorine dioxide [19]. While oxygen and ozone are also able to oxidize and solubilize lignin, hydrogen peroxide usually only decolorizes lignin, unless high temperatures are used (above 80°C [16]). Such conditions also favor carbohydrate degradation. Non-oxidative stages such as Q (chelating stage) and A (acid stage) allow to remove transition metals, which are detrimental to pulp quality, especially as they catalyze the decomposition of H₂O₂ into highly oxidative radicals. Acid stages using hot H₂SO₄ are also used in some modern hardwood pulp mills to remove hexenuronic acids (HexA), which are hemicellulose components born by pulp xylans, and consume a significant amount of chlorine dioxide if they are not eliminated before the D stages.

Table I-3. Other stages commonly found in bleaching sequences

Stage/Chemical	Stage symbol	Action
Chelating stage (EDTA, DTPA)	Q	Removal of transition metal ions at acidic pH (5-6.5) [16]
Acid stage (generally with H ₂ SO ₄)	A	Removal of transition metal ions at low temperature (40-60°C) or hexenuronic acid at high temperature (hydrolysis, above 90°C) [16]
Alkaline extraction (NaOH)	E	Solubilization of oxidized lignin at alkaline pH (9.5-11) [16]

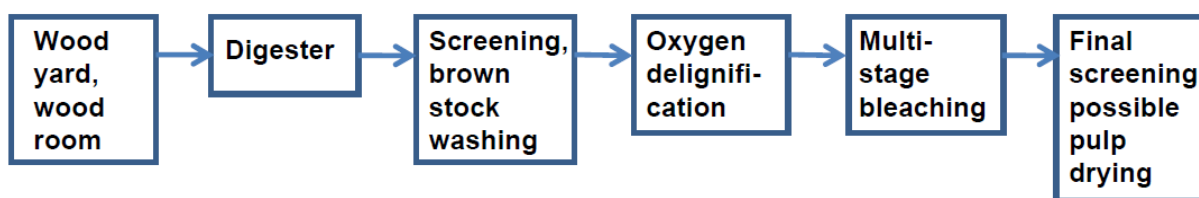
Typical chemical pulp bleaching sequences used to be D(EO)D, DEDED (where (EO) can be replaced by (EOP) and E can be replaced by (EO)), before the O delignification stage was developed to give sequences such as OD(EO)D [12]. (EOP) can also be written Eop.

Moreover, some differences are observed between softwood and hardwood kraft pulps. Generally, softwood kraft pulps require longer bleaching sequences than hardwood kraft pulps. For instance, a typical ECF sequence for softwood pulp bleaching would be ODEopDEpD, whereas ODEpD may be enough for hardwood kraft pulps, as their delignification is easier [16].

Since hardwood pulps typically contain relatively high amounts of hexenuronic acid (HexA), an acidic hydrolysis stage (A) usually follows oxygen delignification to eliminate them and reduce their consumption of bleaching chemicals [20]. This leads to sequences such as OADP or OAZDP (in which ozone enables to reduce the ClO₂ charge even more) [16]. The A stage may also be combined with ClO₂.

Some typical TCF sequences are OQPZP, O(ZQ)P(ZQ)P, OAP(ZQ)P [9]. They usually require to increase the intensity of the O delignification stage [16] and use ozone to replace chlorine dioxide. However, some sequences run without ozone: they use peracetic acid [20] or only oxygen and peroxide (bleaching of hardwood kraft pulps with OQOPP) [16].

Figure I-5 gives an example of a fiberline producing bleached virgin kraft fibers. After wood processing into chips, the cooking takes place in a batch or continuous digester. The resulting pulp is screened and washed, then sent to an O stage tower. Oxygen delignification is applied in all modern mills to reduce the ClO₂ charge in the full bleaching sequence.

**Figure I-5. Outline of a fiberline for the production of bleached kraft pulp [9]**

I.2.3.3 Mechanical pulp bleaching

In mechanical pulp bleaching, the main objective is to reach high selectivity in order to remove chromophores while maintaining the high pulp yield. For this purpose, lignin is retained and only decolorized. This is called brightening or lignin-retaining bleaching. It is usually performed by the application of an oxidative P stage at limited temperature (below 70°C), and sometimes by the application sodium dithionite (reductive Y stage), see Table I-4. Both hydrogen peroxide and sodium dithionite are able to react with the carbonyl chromophores of lignin to decolorize them

without extracting them out of the pulp. The drawback of the presence of lignin is the occurrence of color reversion with time. Factors like UV light, humidity and heat accelerate this yellowing effect [12], [21].

Table I-4. Mechanical pulp bleaching agents

Stage/ Chemical	Stage symbol	Action	Advantages	Drawbacks
Hydrogen peroxide H_2O_2	P	Decolorization of native lignin by oxidation [21], [22] (brightening effect)	Easy to handle (liquid), low capital costs [19] Lignin-retaining bleaching	Expensive [19] (chemical cost: 500€/t in 2012-2013, source: Arkema)
Sodium dithionite $Na_2S_2O_3$	Y	Color-stripping [22] Reduction and decolorization of native lignin [21]	Low capital costs [19]	Expensive (chemical cost: 1150 €/t in 2016, source: Norske Skog Golbey) Polluting [22] Fast decomposition [21] Limited brightness gain [18]

With sodium dithionite (also called hydrosulfite), at slightly acidic pH (4-6), the dithionite ion is decomposed into sulfur dioxide radical ions, which are thought to be the active species. They would be able to react on quinones and also remove coniferaldehyde-type structures [23]. Sulfur dioxide SO_2 , another reductant, is also present and complementary. Nevertheless, sodium dithionite is a polluting chemical that inhibits further aerobic biological treatments of wastewaters [22], [24].

The peroxide stage will be presented in details in the following paragraph (I.2.4).

I.2.4 Hydrogen peroxide

I.2.4.1 General aspects

I.2.4.1.i History and production

Hydrogen peroxide was discovered in 1818 by Louis-Jacques Thénard [25]. It is commercially available at concentrations ranging from 30 to 70%. Peroxide solutions are stabilized to limit the natural decomposition of H_2O_2 in the presence of metals, alkali, or heat.

Hydrogen peroxide is mostly used by the pulp and paper industries for the bleaching of pulp. Other applications are the production of detergents, wastewater treatment via advanced oxidation processes, disinfection, or cosmetic applications.

The production of hydrogen peroxide by direct combination of molecular hydrogen and oxygen is not implemented in pulp mills for operating and safety reasons [26]. Hence, it is mostly manufactured by chemicals suppliers via the anthraquinone auto-oxidation cyclic process: alkyl anthraquinone is hydrogenated via catalysis and oxidized to form hydrogen peroxide [21], [26]. In bleaching plants, it is stored in well-controlled tanks at a concentration of approximately 50% and diluted prior to introduction into the pulp [21].

I.2.4.1.ii Chemical properties

Hydrogen peroxide (H-O-O-H) is a strong oxidant with an oxygen-atom oxidation number of I. Its dissociation in aqueous solution follows Equation I-1.



H₂O₂ is a very weak acid with a pK_A of 11.75 at 20°C [27] and 11.6 at 25°C [9]: its dissociation is easier as the temperature rises.

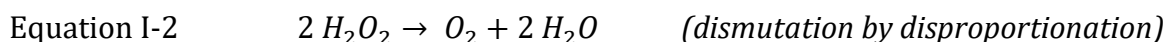
HOO⁻, the perhydroxyl anion, is a strong nucleophile. It is considered as the main species involved in peroxide bleaching reactions, and also participates to delignification as a complement to other oxygenated species, at high temperature.

I.2.4.1.iii Decomposition

I.2.4.1.iii.a Overview

Hydrogen peroxide is easily decomposed, and this phenomenon is catalyzed by metals or alkali. This decomposition forms intermediate oxidative free radicals that can degrade cellulose. Therefore, in most P stages, two types of additives are used to prevent decomposition: chelating agents (EDTA, DTPA) and sodium silicate. This will be detailed in paragraphs I.2.4.2.ii and I.3.2.2. Nevertheless, the decomposition of H₂O₂ is desired in some cases, as it can improve peroxide bleaching [28].

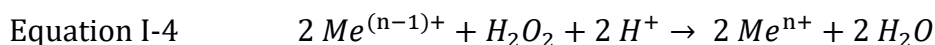
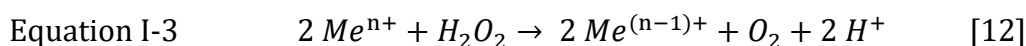
The overall H₂O₂ decomposition reaction is presented in Equation I-2.



Equation I-2 illustrates one major advantage of hydrogen peroxide: its decomposition produces water and dioxygen. It is thus an environmentally friendly substance. Different types of H₂O₂ decomposition will be described in the following paragraphs, starting with the influence of metal ions.

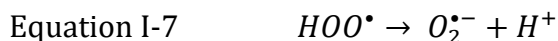
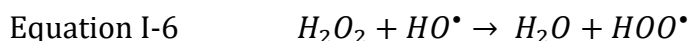
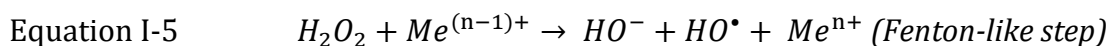
I.2.4.1.iii.b Hydrogen peroxide decomposition by metal ions

Metal ions, which are naturally present in wood and remain partly in pulps, are able to either oxidize or reduce H₂O₂, as illustrated in Equation I-3 and Equation I-4.

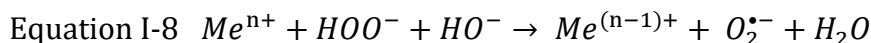


where Me is the abbreviation for metal and Meⁿ⁺ and Me⁽ⁿ⁻¹⁾⁺ are metal ions

Equation I-5, Equation I-6 and Equation I-7 show the formation of three possible radical species (hydroxyl, hydroperoxy or perhydroxyl, and superoxide), initiated by a Fenton-like reaction.



Another route for superoxide generation is presented in Equation I-8.



(metal-induced O₂^{•-} formation at alkaline pH) [9]

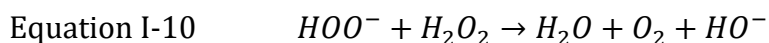
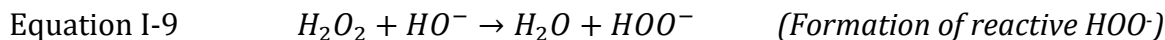
HO[•] is a very strong electrophile and oxidant, which is why it is able to react with lignin as well as carbohydrates. O₂^{•-} is a strong nucleophile and a moderate reductant. In aqueous solution, it is in equilibrium with the hydroperoxy (or perhydroxyl) radical HOO[•], its protonated form, as shown

in Equation I-7, with an equilibrium pKa of 4.88 at 25°C [29]. Unlike $O_2^{\bullet-}$, HOO^{\bullet} can act as an oxidant.

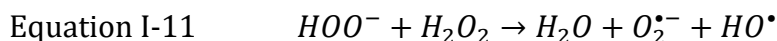
Note that a Fenton-like reaction is defined by Equation I-5. The classical Fenton system is made of the H_2O_2/Fe^{II} couple which forms hydroxyl radicals at acidic pH (around 3). At acidic pH, in the presence of metal ions, hydrogen peroxide is easily decomposed via Fenton-like mechanisms.

I.2.4.1.iii.c Alkaline decomposition

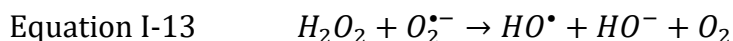
H_2O_2 also decomposes (disproportionation) in the presence of alkali, as shown in Equation I-9 and Equation I-10 below [12].



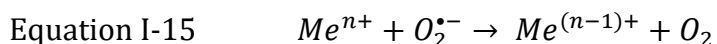
Equation I-10 involves radical intermediates. A route for this radical mechanism involves Equation I-11 and Equation I-12 [27].



Equation I-12 would thus represent the end of the decomposition chain reaction. Various alternate reactions might occur, such as those described in Equation I-13 and Equation I-14 [27].



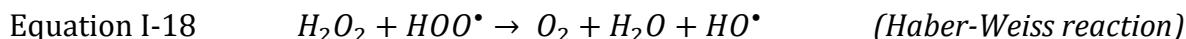
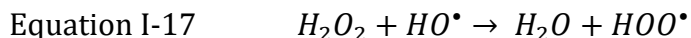
Finally, under alkaline conditions, Colodette and collaborators proposed the following reaction sequence for metal-catalyzed decomposition of H_2O_2 [30]: HO^{\bullet} and $O_2^{\bullet-}$ generation via Fenton-like mechanisms corresponding to Equation I-5 and Equation I-8, followed by O_2 generation via reduction of Me^{n+} by $O_2^{\bullet-}$ (Equation I-15), and Equation I-12 as a terminating step.



Of course, factors other than alkali and metal ions lead to H_2O_2 decomposition.

I.2.4.1.iii.d Other factors influencing hydrogen peroxide decomposition

In a review on photo-initiated reactions of aqueous H_2O_2 , Luňák and Sedlák [31] reported that the products of H_2O_2 photolysis (Equation I-16) are the same as those for thermal decomposition, i.e. H_2O and O_2 . Indeed, the photolysis of hydrogen peroxide is followed by Equation I-17 and Equation I-18, which give the overall reaction Equation I-2.



Hydrogen peroxide can also encounter thermal cleavage, as illustrated in Equation I-19 [12].



The various decomposition ways described here reveal the relatively low stability of hydrogen peroxide regarding light, metal impurities, temperature, alkali, etc. Therefore, it requires stabilization.

I.2.4.1.iv Stabilization of hydrogen peroxide

To avoid decomposition during storage, hydrogen peroxide is kept cool and away from light in stainless steel tanks. It is usually stabilized by addition of phosphoric acid (as it is very stable below pH 3), stannate and low amounts of chelating compounds [12].

Hydrogen peroxide has been used as a bleaching agent for virgin wood chemical pulps since the 80's. Peroxide bleaching of virgin fibers is detailed in the next chapter.

I.2.4.2 Virgin fiber bleaching

The P stage is considered as a complementary stage in ECF bleaching. However, it is a major bleaching stage in TCF sequences.

Hydrogen peroxide has three possible actions during bleaching:

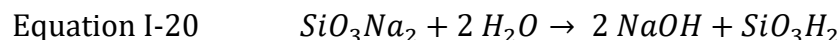
- Brightening (lignin-retaining bleaching) via the action of HOO^- during classical P stage
- Delignification via the reinforcement of O (O_P stage) or via HO^\bullet , $\text{O}_2^{\bullet-}$ and O_2 generation
- Extraction via the reinforcement of E (E_P and E_{OP} stages)

I.2.4.2.i Bleaching conditions

Peroxide stages are usually preceded by chelating stages (Q), owing to H_2O_2 's sensitivity to metal ions. These stages generally last 30 min at 60-70°C [22], with for instance an addition of 0.2% DTPA (diethylene triamine pentaacetic acid) on odp. The pulp consistency can vary from 4 to 35% depending on the type of pulp and on the possible combination with oxygen bleaching under pressure.

To avoid cellulose degradation and thus enhance the bleaching efficiency, sodium silicate and magnesium sulfate are added. The former is only used for mechanical pulp bleaching.

Sodium silicate is used to stabilize H_2O_2 . It is hydrolyzed in aqueous solution according to Equation I-20.



Silicic acid SiO_3H_2 is partially colloidal and able to adsorb some metal ions, thus preventing H_2O_2 decomposition and radical-induced oxidation. The hydrolysis of silicate also releases hydroxide ions, thus contributing to raising and buffering the pH of the medium.

Magnesium sulfate is also used as a cellulose protecting agent, during either mechanical or chemical pulp bleaching. Different actions are cited to explain its benefit: in alkaline medium, Mg^{2+} ions form semi-colloidal $\text{Mg}(\text{OH})_2$ complexes which might co-precipitate with transition metal ions, thus stabilizing hydrogen peroxide [32]; or partially hydroxylated Mg^{2+} ions would form direct complexes with the carbonyl functions present on some oxidized spots of the cellulose chain, inhibiting further alkaline depolymerization of the cellulose chain; or by directly complexing the partially dissociated hydroxyl groups of cellulose, Mg^{2+} would protect them from the electrophilic attacks of hydroxyl radical [33].

In terms of alkali, an optimum dosage of sodium hydroxide can be set for a given dose of H_2O_2 . Generally, 2% H_2O_2 are applied with 1 to 2% NaOH. However, the bleaching conditions vary depending on the type of pulp, especially whether these are chemical or mechanical pulps.

I.2.4.2.i.a Bleaching of chemical pulps

Hydrogen peroxide does not have the same role in ECF and TCF bleaching sequences. In ECF sequences, the bleaching of chemical pulps usually includes a P stage as a final brightening stage to enhance brightness and brightness stability. It is also applied in the alkaline extraction stages to avoid yellowing induced by sodium hydroxide and to reinforce delignification after the action of chlorine dioxide. In TCF sequences, P stages are included as regular bleaching stages, thanks to the delignification properties of HOO^- and of the reaction by-products, i.e. molecular oxygen and oxygenated radicals.

P stages are typically performed in retention towers at medium pulp consistency (10%), or they are performed under oxygen pressure ((PO) or (OP) stages) at medium or high pulp consistency (up to 35%). Table I-5 lists the normal operating conditions for P bleaching of chemical pulps.

Table I-5. Operating conditions of a chemical pulp bleaching peroxide stage [9], [21]

	Pressure (bars)	Pulp consistency (%)	Temperature (°C)	Time (min)	NaOH charge (% on odp)	pH	H ₂ O ₂ charge (% on odp)
“Classical” P stage at atmospheric pressure	1	10-15	60-90	30-240			
(PO) or (OP) stage under pressure	3-8	10-35	80-120	30-180	0.2-4	10-12	0.2-4

According to Dence and Reeve [21], the total peroxide charge in a sequence can range from 1.5 to 4.5% on odp for TCF bleaching. Yet, in a single stage, it should not exceed 2.5%. At atmospheric pressure, the maximum temperature operated is 90°C, whereas it can be increased when the P stage is pressurized, as soon as it does not exceed 130°C, to avoid excessive thermal cleavage of H₂O₂.

I.2.4.2.i.b Bleaching of mechanical pulps

The conditions of mechanical-pulp bleaching differ from those used for chemical pulps. Table I-6 presents the operating conditions found in various (chemi)mechanical-pulp bleaching sequences. These P stages are carried out at atmospheric pressure.

Table I-6. Operating conditions of a (chemi)mechanical pulp bleaching peroxide stage [21]

Pulp consistency (%)	Temperature (°C)	Time (min)	NaOH charge (% on odp)	Silicate charge (% on odp)	H ₂ O ₂ charge (% on odp)
4-35 (15-20 for TMP and CTMP)	35-98	30-240 (generally 120 for TMP and CTMP)	1.4-2.5	2-3	2-3

To choose the operating conditions, the relationship between time, temperature and alkalinity has to be taken into account, as illustrated in Figure I-6.

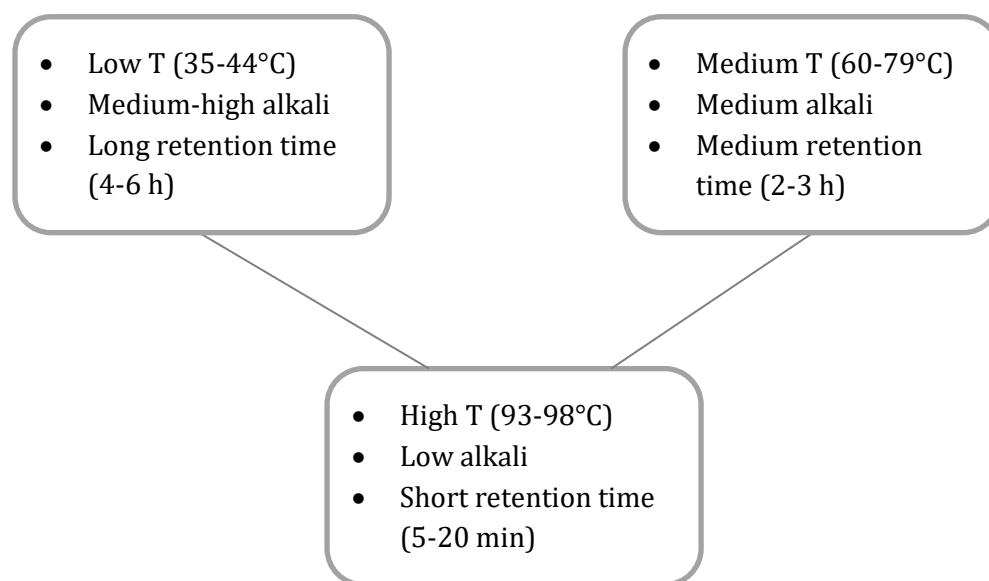


Figure I-6. Relationship between time, temperature and alkalinity for hydrogen peroxide bleaching of mechanical pulp [34]

Hydrogen peroxide is used under alkaline conditions, so that the active species is the perhydroxyl anion (also called hydroperoxide anion), which is able to oxidize lignin carbonyl groups into carboxylic groups, thus decreasing lignin conjugation and brightening the pulp [34]. The bleaching of mechanical pulps aims at increasing brightness while preserving the high pulp yield, which is a major advantage of peroxide bleaching as opposed to delignification stages. To avoid delignification, the bleaching temperature must be kept below 80°C. Indeed, as shown in Figure I-6, hydrogen peroxide can act as a brightening or delignifying agent depending on the temperature, both cases resulting in a bleaching action on the pulp.

I.2.4.2.ii Reactions during an ECF-P stage: hydrogen peroxide brightening

The classical chemistry of hydrogen peroxide bleaching at medium temperature involves the action of the perhydroxyl anion HOO^- . It is not able to attack the aromatic rings directly, but it oxidizes carbonyl groups, thus brightening lignin, as described in I.2.4.2.i.

Some authors proposed that hydroxyl radicals formed by decomposition of H_2O_2 at medium temperature would enable the cleavage of cross-links in the lignin matrix, thus facilitating the penetration of HOO^- [12], [35]. At the same time, these radicals degrade carbohydrates, leading to DP drops.

Although the brightening effect of HOO^- is predominant, at medium temperature, side-chains of free phenolic units can be degraded via Dakin and Dakin-like reactions, so that lignin is eventually partly depolymerized [12].

The reactions of HOO^- on enone side chain chromophore structures are detailed in Figure I-7. Type A-enone structures (see Figure I-7) are from coniferaldehyde units. They are found in native softwood lignin. Type B-enones (see Figure I-7) are not present in native lignin, they are thought to be formed after alkaline treatment of the pulp [23], [36]. With the conjugate addition of HOO^- , the $\text{C}_\alpha\text{-C}_\beta$ bond in the side chain is broken and aromatic aldehydes or carboxylic acids are formed, for type A- and type B- enal/enone structures, respectively. However, these products, which absorb in the UV range, can be converted to new chromophores.

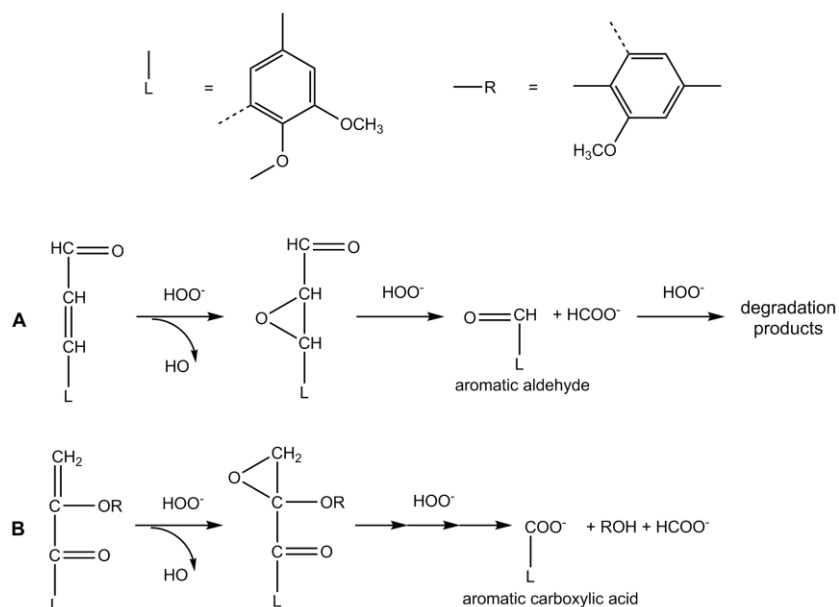


Figure I-7. Reaction of the perhydroxyl anion with enal or enone side chain structures [23]

Quinonoid rings (ortho- and para- types) can be attacked on different sites. Some possible routes are detailed in Figure I-8. Whatever the mechanism, the reaction of HOO^- always leads to the formation of carboxylic acids. If these remain attached to lignin, the carboxyl content of the pulp increases. Most of these routes lead to ring opening via the formation of muconic acid derivatives.

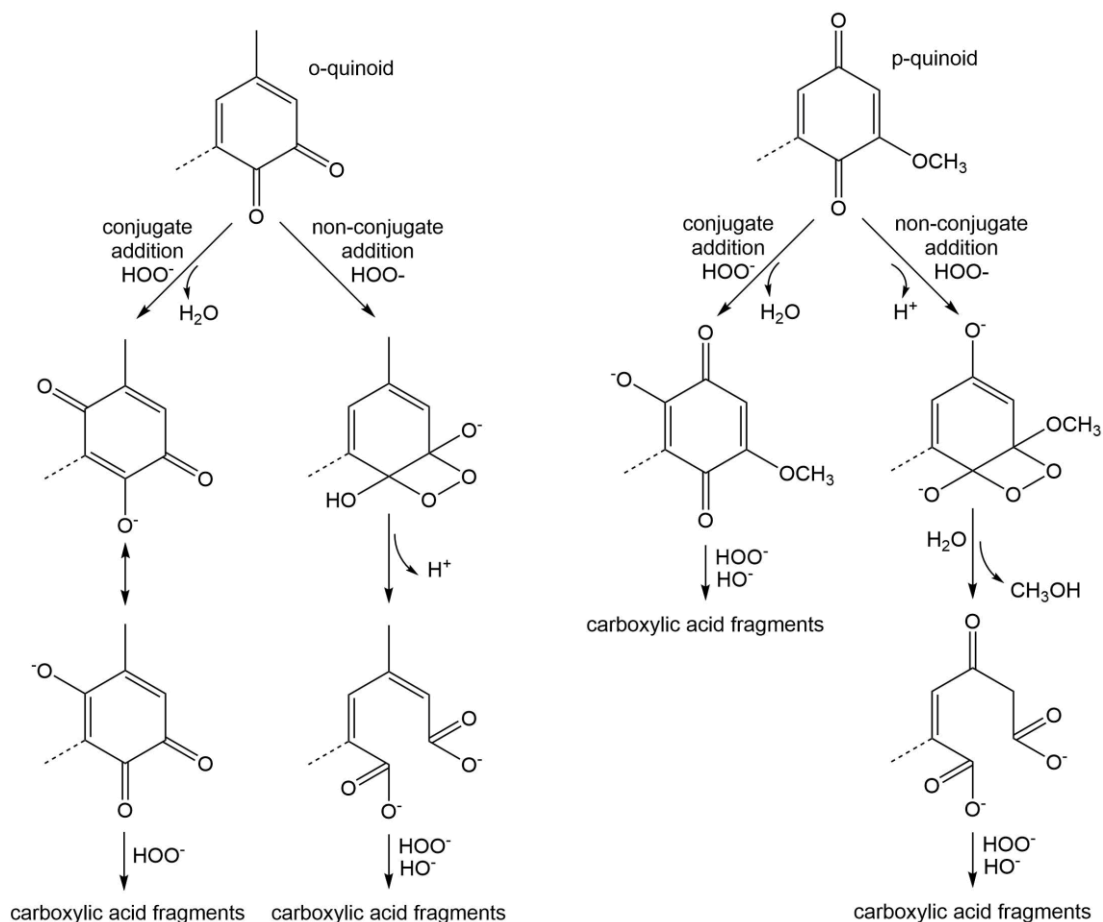


Figure I-8. Reaction of the perhydroxyl anion with ortho- and para- (o- and p-) quinonoid structures [37]

These reactions become more active at high temperatures. The reinforcement of the Dakin reaction makes HOO^- less specific and some attack of non-phenolic structures can take place. However, more radicals being produced at high temperature, the radical route becomes predominant. With oxidative intermediates such as the superoxide radical, molecular oxygen, the hydroxyl ion and the hydroxyl radical, P stages thus become lignin-degrading stages.

I.2.4.2.iii Reactions during a TCF-P stage: delignification

As mentioned previously, hydrogen peroxide-induced delignification is avoided during mechanical pulp bleaching. This is why this part focuses on hydrogen peroxide reactions during chemical pulp bleaching. Delignification during a P stage is possible at high temperature, when hydrogen peroxide decomposes into radicals.

These oxygenated radicals formed during alkaline hydrogen peroxide bleaching are electrophilic compounds whose actions enable lignin-degrading bleaching rather than only brightening [37].

Delignification during a hydrogen peroxide stage is due to both free radicals and hydroperoxide anions [16], [28]. Gierer [38] proposed to rationalize the general mechanisms of bleaching by dividing them into two steps: initial electrophilic reactions (via cationic or radical processes) and subsequent nucleophilic reactions. In the case of alkaline hydrogen peroxide bleaching, the first one involves radical processes, and the second one involves reactions of hydroperoxide and superoxide anions. As the electrophilic reactions form carbonyl and conjugated carbonyl

structures, which are the substrates for lignin-degrading HOO^\cdot bleaching, these initial reactions cooperate with HOO^\cdot to allow it to degrade lignin.

In particular, the action of hydroxyl radicals on pulp is well documented [35], [37], [39]–[43]. Their action on lignin depends on its type. Under alkaline conditions, phenolic structures are turned into phenoxy radicals (2 in Figure I-9), whereas non-phenolic structures give hydroxyl-cyclohexadienyl radicals (3 in Figure I-9). These structures face various subsequent reactions, such as hydroxylation, dealkoxylation or $\text{C}_\alpha\text{-C}_\beta$ bond cleavage. Then, delignification can be pursued via nucleophilic reactions such as those presented in I.2.4.2.ii.

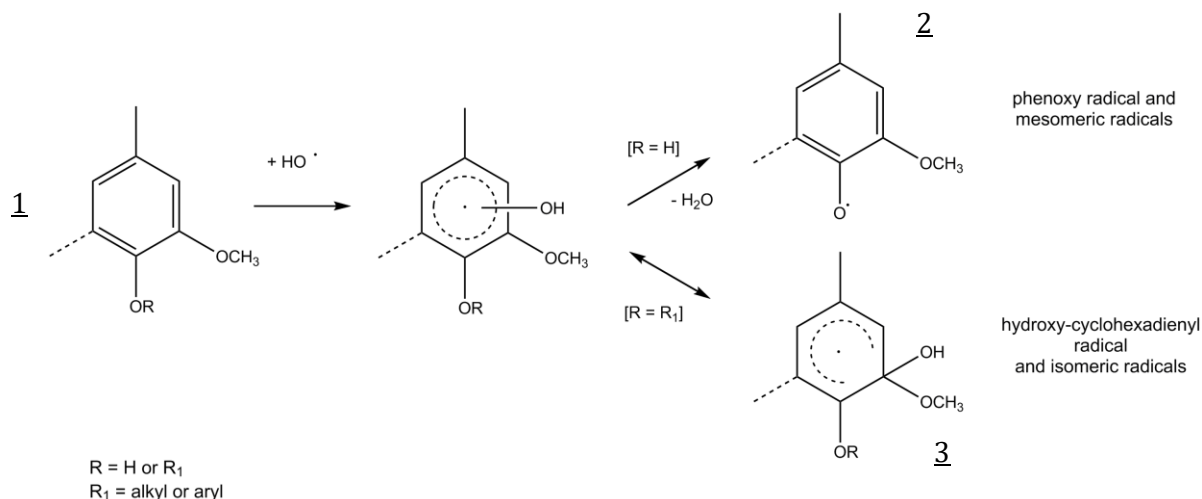


Figure I-9. Initial addition of the hydroxyl radical on a lignin aromatic ring under alkaline conditions, as described by Gierer [39]

Subsequent reactions of phenoxy radicals start with coupling reactions between the phenoxy radical and HO^\cdot . The main possible reactions [39] are presented in Figure I-10. The resulting hydroxyl-cyclohexadienones are subject to different reactions. The first one in Figure I-10 is hydrolysis of aryl ether bonds, forming a quinonoid structure. The second one is simple hydroxylation, and the third one, with structure 2', allows C1-C_α bond cleavage via proton elimination.

Obviously, phenoxy radicals are subject to coupling with other radical species as well, especially with other phenoxy radicals (dimerization), which is detrimental to bleaching and competes with effective lignin-degrading reactions.

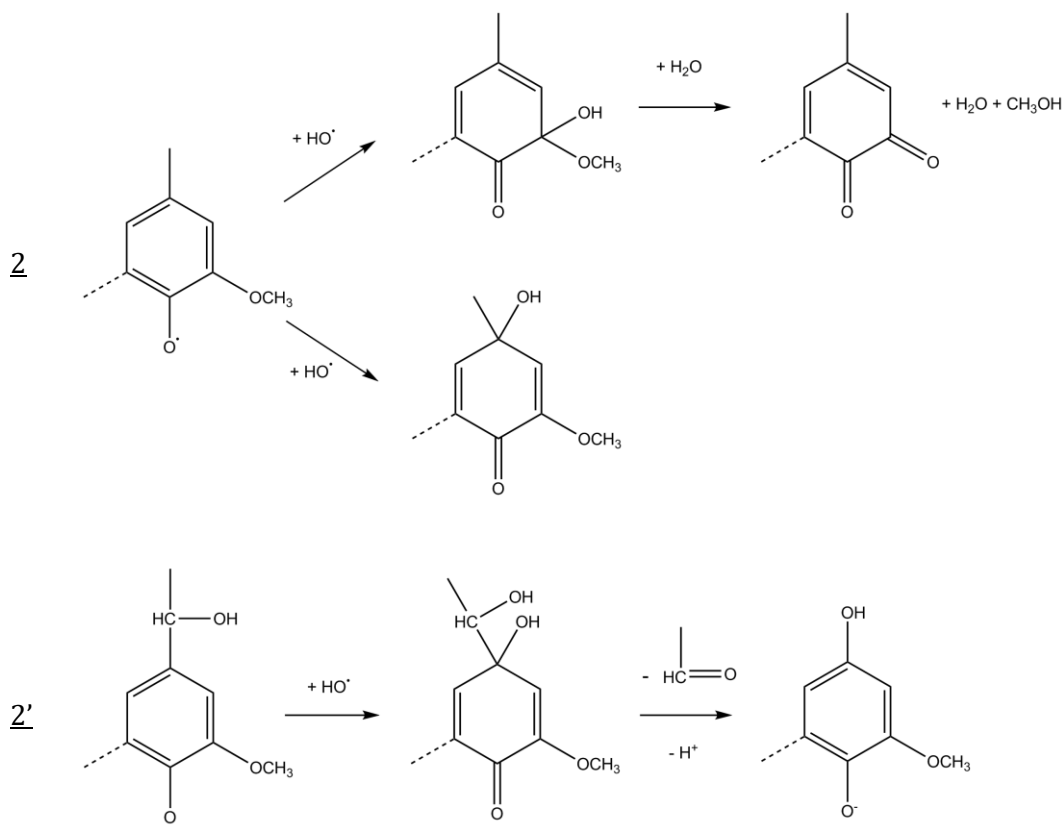


Figure I-10. Subsequent reactions on phenoxy radicals under alkaline conditions, adapted from Gierer [39]

As presented in Figure I-11, subsequent reactions on hydroxy-cyclohexadienyl radicals also include hydroxylation and dealkoxylation, starting from structure 3. Yet, other reactions are observed. Some particular structures (4 in Figure I-11) are subject to C_{α} - C_{β} bond cleavage, owing to a homolytic rearrangement and contributing to further solubilization of lignin. This reaction competes with a hydrogen abstraction from the benzylic carbon from 5, forming an α -carbonyl structure.

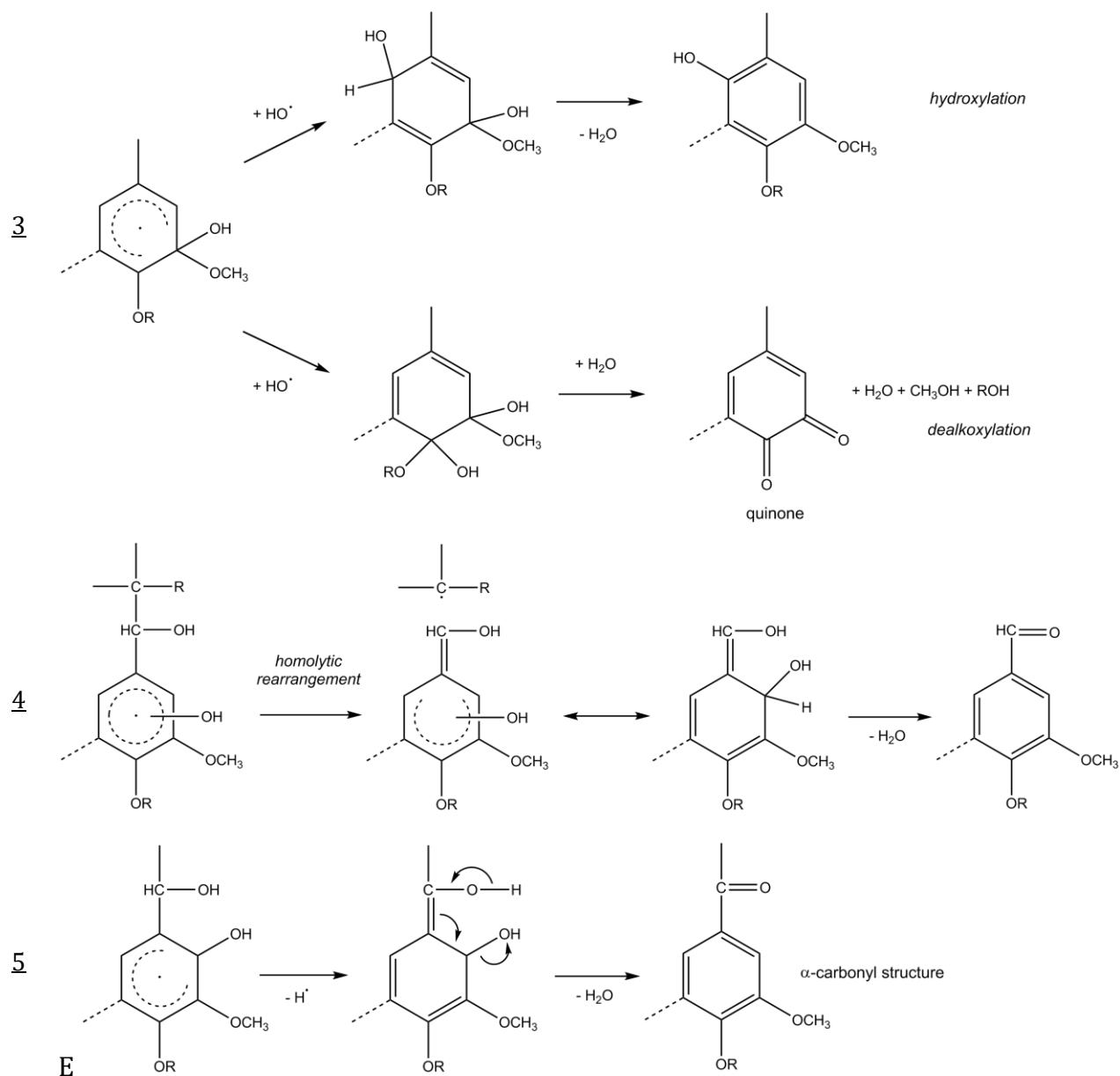


Figure I-11. Subsequent reactions on cyclohexadienyl radicals under alkaline conditions, from structure 3: hydroxylation and dealkoxylation, from structure 4: C_α - C_β cleavage, and from structure 5: hydrogen abstraction from C_α

Radicals also attack olefinic structures in lignin. Therefore, some studies were conducted on stilbenes for instance [40], [41]. The high electron density at the olefinic carbon would make it a preferred radical site and an electrophilic attack center. Gierer et al. [41] proved that olefinic hydroxylation, hydration and oxidation are predominant over aromatic hydroxylation, dealkoxylation but also intra- and intermolecular phenolic coupling (more important at acidic pH).

Unfortunately, under delignifying conditions (i.e. at higher temperatures), carbohydrates are also subject to degradation. This will be described in the following paragraphs. Carbohydrates can be attacked by hydroxyl radicals, which abstract a hydrogen atom from the C_2 , C_3 or C_4 carbon atom, then forming a carbonyl group by oxidation of the carbon, leading to the cleavage of glycosidic bonds by β -elimination [16], [27], [38]. The mechanism in Figure I-12 illustrates this reaction

pattern, starting with hydrogen abstraction from the C2 position. The same result is obtained after H-abstraction from C3 or C6 [44].

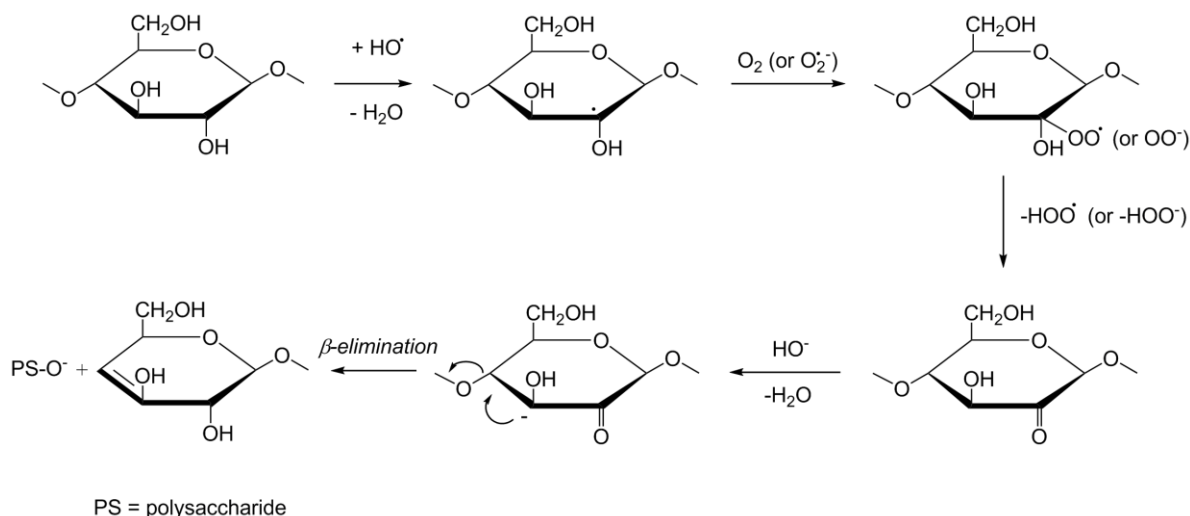


Figure I-12. Effect of hydroxyl radicals on carbohydrates: cleavage of the C4 glycosidic bond by β -elimination, after H-abstraction from the 2-position carbon atom, adapted from Gierer [42], Suess [16], and Hon and Shiraishi [44]

In a study on ozone bleaching, Chirat and Lachenal [45] proposed another mechanism involving hydrogen abstraction from the C2 atom. In this case, a dicarbonyl structure would be formed.

Guay and collaborators studied the action of hydroxyl radicals on different cellulose model compounds: methyl β -D-glucopyranoside [46], methyl β -cellobioside [47], and finally cellulose [48]. The authors proposed a mechanism that consists in substitution reactions on the C1 position, which would cleave the glycosidic linkage C1-O, as presented in Figure I-13 with the example of 1,4-anhydrocellobitol fragmentation. Then, the cellulose fragment with a reducing end would be subject to diverse reactions forming aldonic acids and lower order aldoses [47], [48].

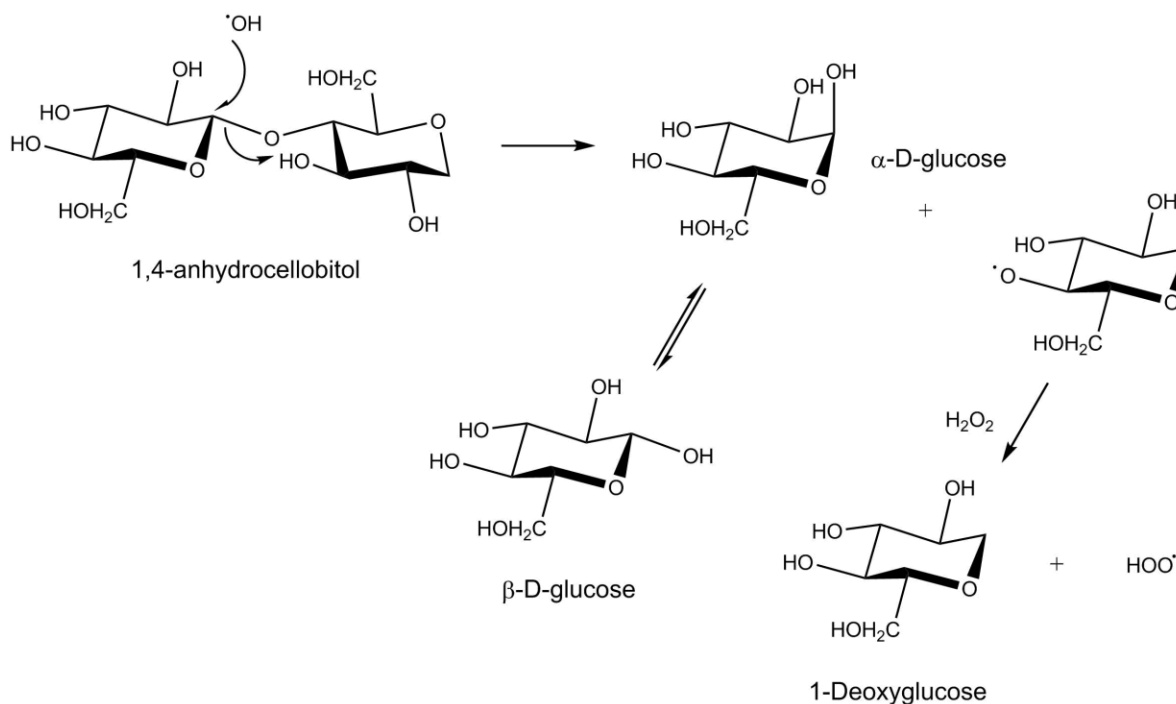


Figure I-13. Effect of hydroxyl radicals on carbohydrates: cleavage of the glycosidic bond of 1,4-anhydrocellobitol, according to Guay [48]

The authors found that the same mechanism occurred for the hydroxylation of 2-methoxytetrahydropyran, i.e. without any hydroxyl group on C2, C3, C4 and C6. This means that hydroxyl radicals would be able to cleave any glycosidic bond. Experiments on cellulosic compounds, MCC (microcrystalline cellulose) and filter paper, tended to confirm this conclusion [48].

According to studies conducted on model compounds, the selectivity of hydroxyl radicals is 5 to 6 times higher towards lignin than towards carbohydrates during pulp bleaching [49], [50]. This “selectivity factor” was calculated as the ratio of the rate constants for the reaction of hydroxyl radicals with lignin and with carbohydrate models. According to Gierer [38], the selectivity of bleaching is mainly due to the fact that the initial addition of radicals to aromatic rings and olefinic groups occurs faster than the abstraction of hydrogen from carbohydrates.

In a study on radical formation during oxygen delignification, it was found that the oxyl radical anions ($\text{O}^{\cdot-}$), more reactive towards carbohydrates than hydroxyl radicals, were predominant at pH above 11.8, thus reducing the selectivity of the oxidation [43].

Hydroxyl radicals are not the only radicals involved and even collaborate with other radical species during bleaching [38], [39], [51]. In particular, the cleavage of hydrogen peroxide under alkaline conditions gives two radicals: the hydroxyl radical and the superoxide anion radical. The latter, contrarily to the hydroxyl radical, is able to cleave C-C bonds. This leads to ring opening in the case of non-conjugated structures and to the scission of conjugated C=C bonds between two lignin units (after prior addition of a hydroxyl radical on a phenolic unit, producing a primary substrate radical) in the case of conjugated structures [40].

Finally, the general course of radical bleaching proposed by Gierer [39] generalizes the main initial actions of radicals on lignin, from acidic to alkaline pH, for oxygen-derived as well as chlorine-derived radicals, see Figure I-14. Indeed, hydrogen peroxide may be applied at neutral and acidic

pHs, although our focus in this paragraph remained on alkaline pH, the latter corresponding to classical peroxide bleaching conditions.

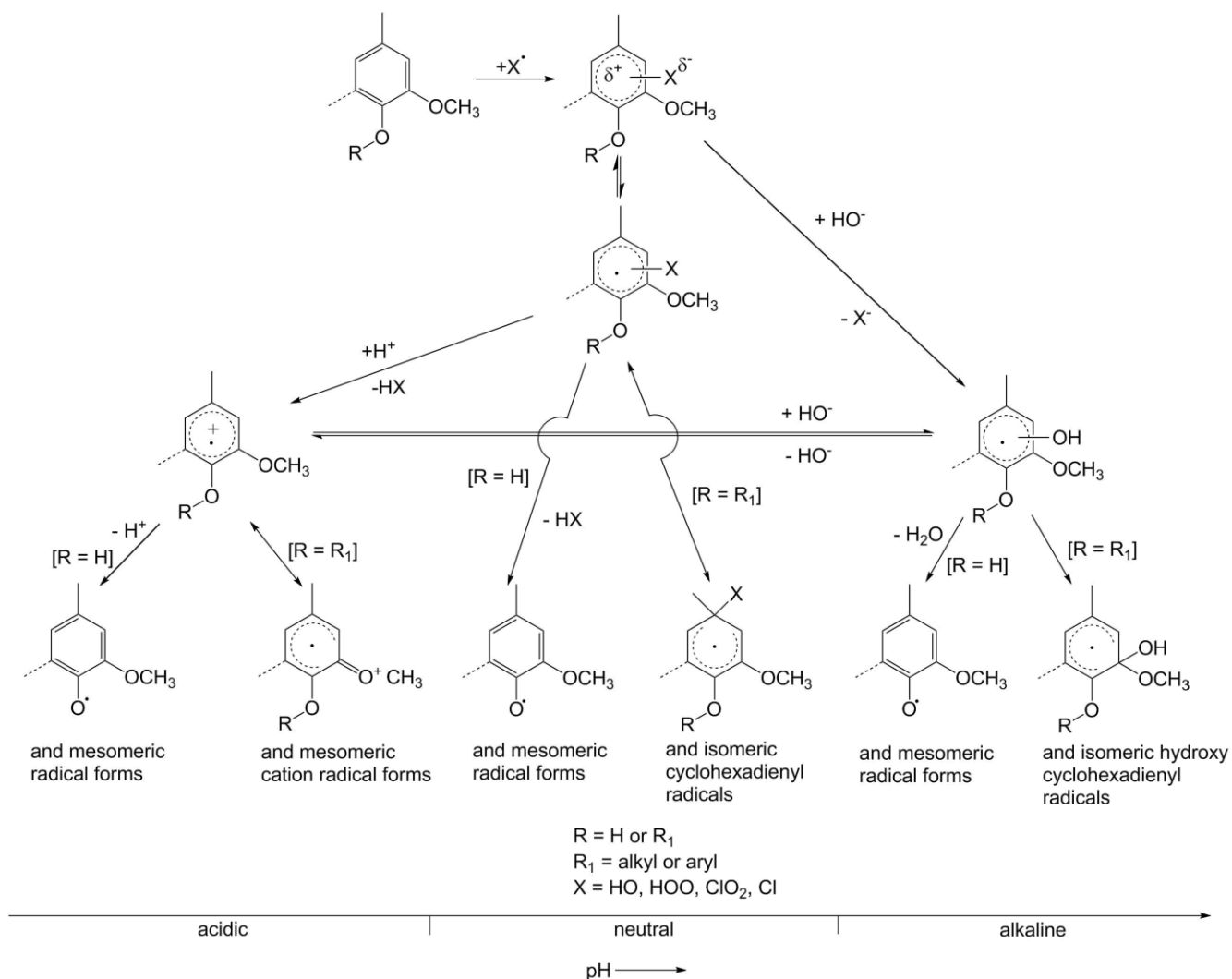


Figure I-14. Initiation of radical bleaching reactions with HO^\bullet , HOO^\bullet , ClO_2^\bullet , Cl^\bullet depending on the pH, as summarized by Gierer [39]

As introduced in the previous part about lignin brightening, above 80-90°C, the perhydroxyl anion reacts with different structures from pulp, especially enones and quinonoid structures, leading to lignin degradation. To some extent, these quinonoid chromophores are also eliminated after reaction with hydroxide ions, as illustrated in Figure I-15. On the left, a hydroxylated catechol dianion is formed after conjugate addition of HO^- , although it is weaker than HOO^- . This molecule is not colored but can be further reoxidized to produce a colored hydroxyquinone structure. On the right, a ring contraction by benzylic rearrangement allows partial discoloration [23].

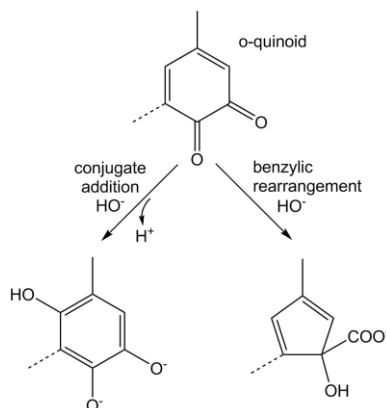


Figure I-15. Reaction of the hydroxyl anion with quinonoid structures [23]

Finally, quinone-methide structures can also be eliminated thanks to HO^\bullet . Conjugate addition of HO^\bullet to the methide group yields p-quinonoid structures, which can be eliminated via the previous mechanisms described in Figure I-8, and addition to stilbene quinone units leads to aromatic aldehydes that may be converted to p-quinonoids as well, via Dakin-like reaction (the aryl aldehyde is transformed into a p-hydroxybenzyl alcohol, the oxidation of which gives a p-benzoquinone).

In conclusion, alkaline hydrogen peroxide bleaching involves different active species. At moderate temperatures, the effect is mostly brightening and retains lignin in the pulp. At high temperatures, delignification is possible: free radical processes are essential to this lignin-degrading bleaching and cooperate with hydroperoxide anion to selectively react with lignin rather than with carbohydrates.

After this description of virgin fiber bleaching, it seems important to explain some key features about recovered fibers and their requirements in terms of bleaching, since the specific context of our project is the bleaching of high quality recovered fibers.

I.3 RECOVERED FIBERS

I.3.1 Generalities

I.3.1.1 Overview

To make paper and board, one of the major fiber sources is recovered paper and board. It represents more than 50% of the total fibrous sources in Europe, with 47.5 Mt utilization vs 41.1 Mt consumption for virgin pulp fibers in 2014 [52]. Recovered papers and boards have two origins: pre-consumer (industrial broke, rejects, unsold products) and post-consumer (waste from household, offices). They contain numerous contaminants: inks, dyes, coating agents, rubber, staples, adhesives, etc. In order to be reused, they have to be treated to remove impurities and obtain a high content of cellulosic fibers [53].

Why recycling? It is firstly for economic reasons: the raw material can be cheaper and the water consumption is lower. However, in some cases the energy consumption can be higher. The raising environmental concern in our society has also had a significant impact on recycling. The idea of

preserving natural resources and valorizing waste has been supported with legal and financial regulations encouraging recycling.

The utilization rate (recovered paper consumption/total production, see Table I-7) is high for board since board grades do not need to have a high brightness and the fibers are not much affected by the recycling process. It is also high for newspaper and magazine grades as low brightness is accepted (60-70% ISO brightness) and high mechanical properties are not expected [22].

However, the utilization rate of printing and writing papers is very low [52], as it is difficult and expensive to produce white paper for high grades with good mechanical properties comparable to those of virgin fibers. One objective of this thesis is to enhance the recycling of these printing and writing papers to produce bright fibers for printing and writing paper or tissue. For this purpose, the high quality recovered fibers have to be deinked but also bleached while preserving the mechanical strength of both fibers and the fiber network.

I.3.1.1.i Legislation

In Europe, Germany was a pioneer in developing a waste strategy (prevention of waste, re-use or recycling of used paper products, disposal or incineration of waste). It inspired the European Waste Guideline 91/156 EWG (1991), which is part of the EU's waste management directives [22]. The European Recovered Paper Council (ERPC) was created after the First European Declaration on Paper Recovery in November 2000 to monitor the progress of this European Declaration, which sets recycling targets for Europe.

I.3.1.1.ii Paper recycling in Europe: some figures

In its annual monitoring report [54], the ERPC reported a recycling rate (amount of recovered paper and board used as raw material in the paper and board industry/total paper and board consumption) of 72% in Europe in 2013. It is higher than the target of 70% set in 2011 in the third European Declaration on Paper Recycling, although some European countries are still below 60%.

In its recent statistic report [55], COPACEL, the Association of French Paper Industries, listed some information about recovered fibers in France. In 2014, the recovered paper utilization rate seemed to be slowly increasing as it reached 66%, compared to 58% in 2004. The recovery rate, or collection rate (amount of recovered paper and board for all material recycling/total paper and board consumption, see Table I-7) reached 82% vs. 58% ten years before. The data reported by COPACEL is presented in Table I-7.

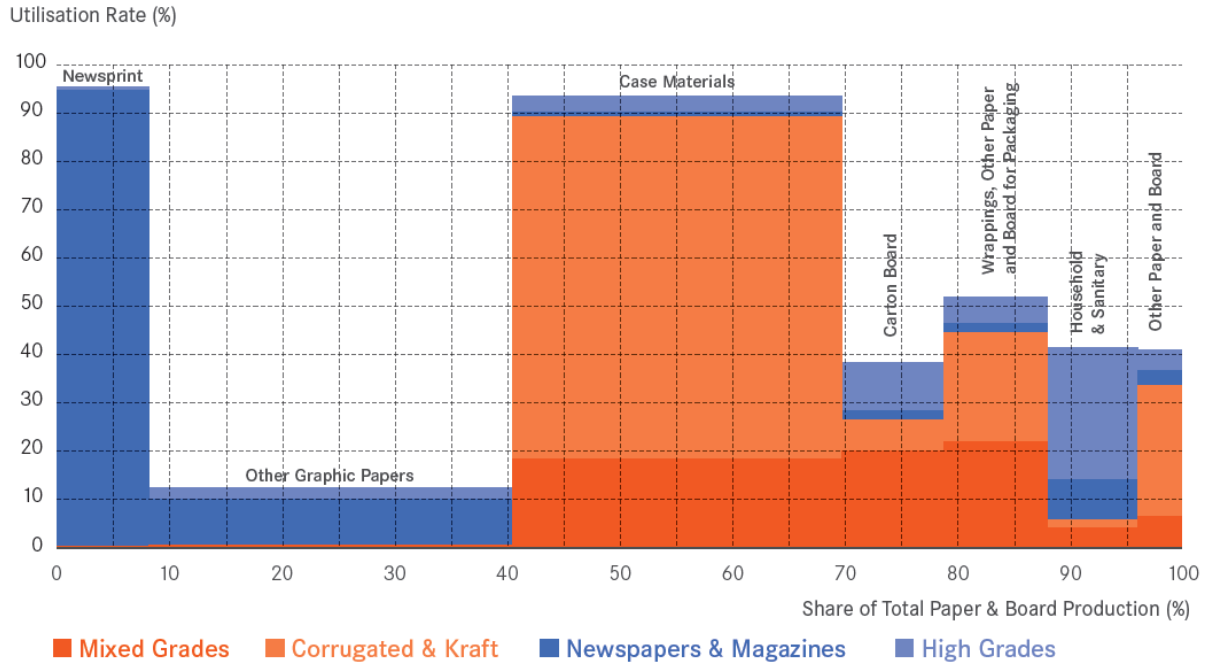
Table I-7. Paper and board recycling in France in 2014

		<i>Assignment or calculation formula</i>	<i>2014 figures</i>
<i>2014 figures Source: Copacel [55]</i>	Recovered paper and board consumption (kt)	A	5400
	Apparent recovery, for all material recycling (kt)	B	7319
	Total paper and board consumption (kt)	C	8903
	Total paper and board production (kt)	D	8191
<i>Corresponding indices</i>	Recycling rate (%)	A/C	60.7
	Recovery rate (%)	B/C	82.2
	Utilization rate (%)	A/D	65.9

According to our calculation, the recycling rate in France was actually lower than 61% in 2014, which is below the European average.

However, as mentioned earlier, according to CEPI (Confederation of European Paper Industries) statistics, the utilization rate of graphic papers other than newsprint is much lower than the overall paper and board utilization rate, with only 12.4% in 2014 [52]. Among these, high-grade papers represented 19.4% of the utilized grades (the major one being newspapers and magazines), meaning that the utilization rate of high grades among graphic papers other than newsprint was only 2.4%. This is due to the difficulty to recycle « white papers » at acceptable costs.

As shown in Figure I-16, high-grade papers for recycling are used to produce household and sanitary papers, paperboard, and graphic papers other than newsprint. They represent 10.5% of the total “paper for recycling”, see Figure I-17. In addition, Figure I-16 shows that the utilization rates of RCFs for newsprint and case materials (paper and board for corrugated board production) are very high, with 96% and 93% respectively.



For instance: case materials represent 29% of total paper and board production, have an utilisation rate of 93% and use 51.5% of total paper for recycling volumes used by the industry.

Important Note: Paper for recycling is composed of fibres but also unusable materials – non-paper components as well as paper and board detrimental to production. The share of unusable materials depends on the actual sorting and collection of used paper. It varies according to grades of paper for recycling and countries. The volume of recycled fibres actually used to produce new paper is therefore lower than the volume of paper for recycling considered. The utilisation rate compares utilisation of paper for recycling to paper & board production.

Figure I-16. CEPI utilization of paper for recycling by sector and by grade in 2014 [52]

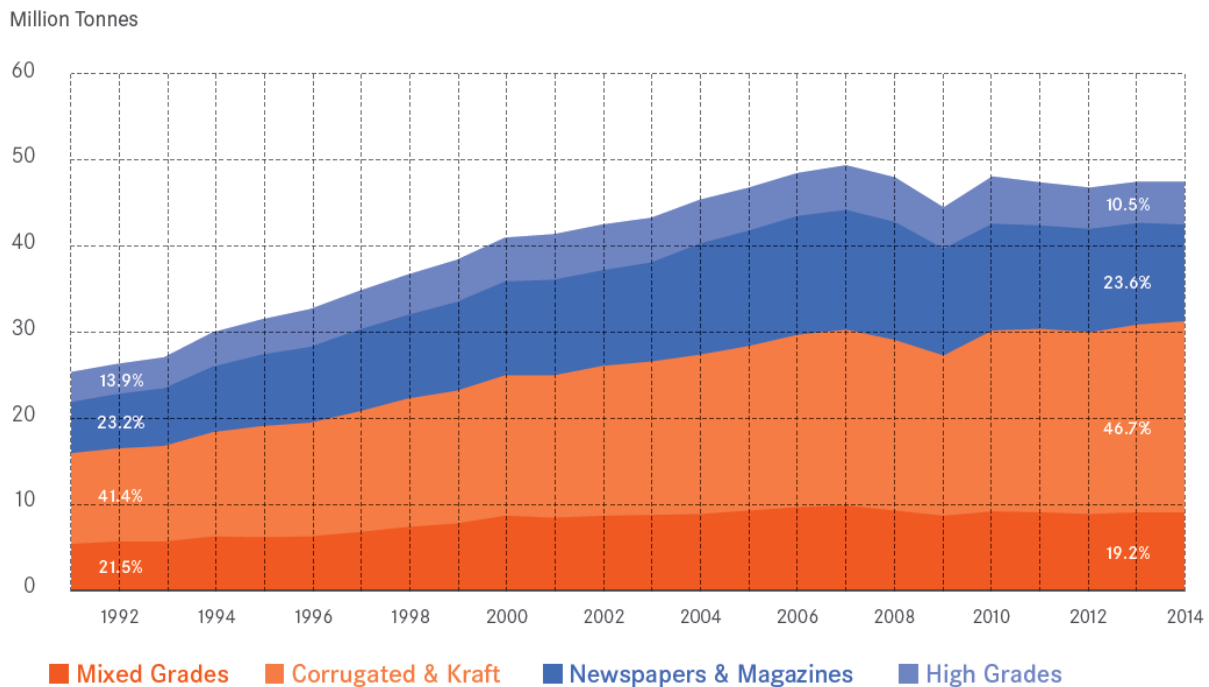


Figure I-17. CEPI utilization of paper for recycling by grade, from 1991 to 2014 [52]

I.3.1.1.iii Prices

The prices of recovered papers and DIPs are very variable [56]. The objective for deinked pulp producers is to compete with equivalent virgin pulp grades, with comparable properties and prices. In Europe, in June 2015, deinked market pulp was cheaper than virgin eucalyptus pulp, with 680-700\$/t vs. 790-800\$/t for similar properties [57].

In terms of final paper, in June 2015 in France, the price of offset rolls of 80g (80 g/m²) uncoated wood-free paper was between 725 and 780€/t vs. 670-680€/t for the equivalent grade made of 100% recycled fibers [57]. These figures illustrate the competitiveness of deinked pulp and of the paper made out of it.

I.3.1.1.iv Recovered paper grades

The European list of standard grades of paper and board for recycling EN 643 [58] classifies recovered paper and board into five groups:

- Group 1: Ordinary grades
- Group 2: Medium grades
- Group 3: High grades
- Group 4: Kraft grades
- Group 5: Special grades

They are numbered following a numerical code system where the first number corresponds to the group, the second one to the grade and the third one to the subgrade. For example, 1.06 corresponds to unsold magazines, 2.05.00 is for ordinary sorted office paper (containing a minimum of 60% wood-free paper), 2.05.01 for sorted office paper (minimum of 80% wood-free paper), and 3.01 stands for mixed lightly colored printer shavings.

RISI (Resource Information Systems Inc.) provides information such as market data, prices, forecasts, etc. for the global forest products industry. According to their price watch dated from July 2015, the prices of recovered paper have had a tendency to decrease for newspapers and sorted graphic papers and a tendency to increase for white grades [59]. Pap'argus is a French journal focusing on the French and European markets. Some selected data from their price watch of June 2015 [57] are presented in Table I-8. It shows that before deinking, recovered papers cost between 70 and 360€/t, depending on their grade.

Table I-8. Price watch in Europe for recovered paper grades to produce DIP [57]

Grades	Ordinary and medium grade papers			High grade printing and writing papers			
	Subgrades	Sorted graphic paper for deinking	Newspapers	Colored woodfree magazines	Mixed lightly colored printer shavings	White woodfree letters	White woodfree shavings
	(1.06)	(1.11)	(2.01)	(2.08)	(3.01)	(3.05)	(3.18.00)
Price in June 2015 (€/t)	87-97	70-70	125-145	150-165	135-155	235-255	335-360
Variation/ June 2014 (%)	-20	-16	0	10	-3	4	6

I.3.1.2 The recycling process

The paper recycling process consists in the removal of all contaminants and impurities found in recovered papers, in order to obtain only fibers.

Besides dyes, inks and fillers, recovered papers contain various external contaminants (sand, glass, wires, styrofoam, etc.) which should not be present, but also contaminants coming from converting, such as adhesives, metals, plastics, etc. Thermoplastic compounds such as wax, adhesives, plastics and latex are considered as stickies. Their presence has a detrimental effect on paper production and quality, as stickies deposit on wires and rolls and induce web breaks [22].

Figure I-18 presents a list of contaminants found in recovered paper, classified according to their size. Indeed, particle size is one of the main distinguishing characteristics used to remove contaminants, along with density, surface properties and shape [22].

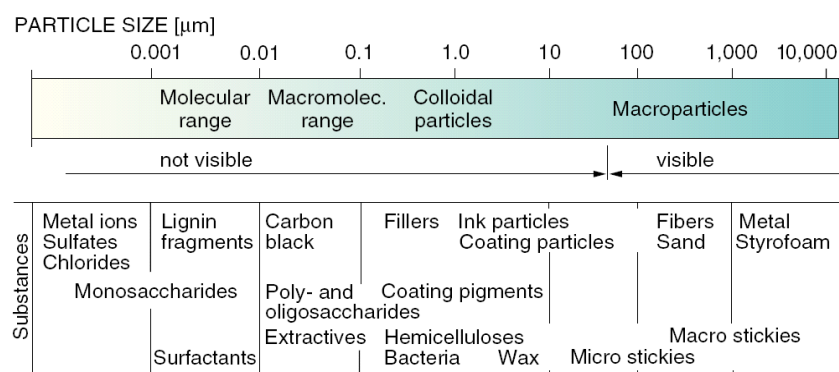


Figure I-18. Contaminants in recovered paper [22]

In order to remove these numerous contaminants and due to their wide variety, the recycling process consists of a sequence of different unit operations:

- Pulping: defibering and separation of some contaminants
- Screening: contaminant removal by retention on a screen
- Cleaning: particle separation thanks to a centrifugal flow of the fiber suspension
- Flotation: removal of hydrophobic particles (especially from ink): they coalesce with air bubbles and are floated up on the surface of the fiber suspension to be collected
- Washing: removal of small hydrophilic particles through a fine screen, with water
- Thickening: dewatering by thickening and pressing
- Kneading: dispersion of residual contaminants
- Bleaching: oxidation or reduction of residual color (mainly dyes and lignin)

The recycling line in Figure I-19 is intended to produce deinked pulp for printing and writing or magazine paper, with ordinary and medium grade recovered papers as raw material. It uses the unit operations described above and ends with bleaching to improve the pulp's brightness.

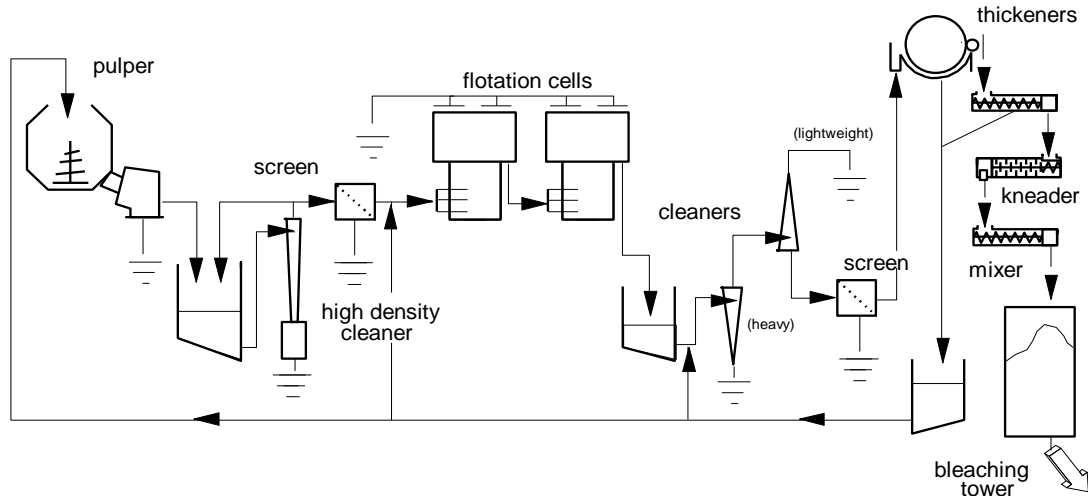


Figure I-19. Deinking line to produce magazine or writing and printing paper from sorted recovered papers. Source: CTP

The successive operations also affect the cellulosic fibers, so that DIP fibers' characteristics are different from those of virgin fibers. This is described in I.3.1.3.

I.3.1.3 DIP's fibers

Recycled fibers are more fibrillated and their fine content is higher than before recycling. Their overall mechanical properties are generally worse than those of virgin fibers, especially in terms of flexibility and inter-fiber bonding [21], leading to lower pulp strength.

In a review, Howard reported the effect of recycling on chemical pulp fibers [60]. Their tensile and burst indices dropped dramatically during recycling but the tear index increased. The author suggested that recycled fibers are more brittle and break easily when beaten. Some attempts were made to upgrade recycled fibers by refining. Despite the dramatic increase of breaking length by 70%, the fine content was then so high that drainage was too long and therefore not applicable.

In a laboratory study, Howard and Bichard investigated the effects of recycling on the physical properties of different pulps [61]. In particular, notable differences were found between beaten chemical pulps, mechanical pulps, and unbeaten bleached chemical pulps. The first suffered hornification, whereas mechanical fibers were flattened and more flexible (which would be due to enhanced internal fibrillation), and finally unbeaten bleached chemical fibers, which were initially curved, were discovered to be de-curved by the recycling process.

Fiber flexibility is the wet plasticity of fibers. Many studies have shown that drying causes loss of swelling capacity and that the swelling properties of the fibers are irreversible. This is called loss in flexibility of wet pulp fibers or hornification. This phenomenon appears for chemical pulp fibers but is very low for mechanical pulp fibers. The mechanism explaining hornification is still on debate.

Overall, the reason why the physical properties of recycled fibers are generally lower than those of the original fibers may be that recycled fibers are usually a mixture of chemical and mechanical fibers, the loss of bond strength of chemical fibers gaining over improvements in mechanical fiber strength.

In 1994, Nazhad and Paszner published a review on the causes of strength loss in recycled papers [62], mostly focusing on chemical pulp fibers since mechanical pulp fibers, as pointed out by

Howard and Bichard in 1992 [61], actually form stronger sheets after recycling. The main hypothesis to explain the loss of strength during recycling is a loss of bonding, which would be a function of fiber flexibility and surface condition.

Nazhad and Paszner concluded that drying may create new and perfectly aligned lamellae through hydrogen bonds (as in crystalline cellulose) in the cell wall of chemical pulp fibers. The authors concluded that fiber structural evolution, fiber surface inactivation and fiber-water interactions have to be taken into account to understand the loss of strength during recycling [62].

In a more recent review [63], the importance of the fibers' history was highlighted and the author reported recent results in favor of the hypothesis that strength loss (in particular tensile strength loss) is mainly due to surface bond strength loss rather than fiber hornification. The modification of surface chemistry also has an impact on mechanical fibers, although flattening is still believed to be a factor. The importance of fiber surface over fiber swelling was confirmed by pre-treatments with either cationic starch or sodium hydroxide, showing good strength development with the first (which corresponds to fiber surface treatment) compared to the second (which causes fiber swelling).

On top of their specificity in terms of mechanical properties, DIP's fibers contain various chromophores. These influence the bleachability of the fibers.

I.3.1.4 DIP's chromophores

The bleachability of DIPs depends on the sorting. Most recovered fibers are mixtures of chemical pulps and mechanical pulps, thus containing both native and residual lignin. Depending on their origin, the mechanical fibers may have been subjected to yellowing. Moreover, some fibers are printed and some are dyed. If the deinking operation prior to bleaching is effective, the inks should not affect the bleachability. Consequently, the main chromophores of DIPs are wood native lignin, residual lignin and paper dyes, although some residual printing ink and other impurities may be found.

I.3.1.5 Paper dyes

Our project focused on the bleaching of colored fibers. These are colored by dyes that are attached to them and absorb light in specific wavelengths among the visible range. When the wavelengths that are not absorbed are reflected to an observer's eye, the corresponding specific color is perceived.

Dyes are commonly used in paper manufacturing to produce colored papers. The structure and classification of paper dyes is detailed in the following paragraphs.

I.3.1.5.i Structure

Dyes absorb the visible light because of their highly conjugated structures, which contain several groups with π -electron clouds, such as azo groups, ethylene groups, carbonyl groups and aromatic rings. When combined, these structures constitute the chromophore part of the molecule.

The other properties of the dye, i.e. solubility, charge, and affinity to cellulose, are provided by auxochrome groups. Auxochrome groups are ionizable groups that can modify the absorption wavelength of a chromophore by increasing its electronic delocalization [64]. When the absorption wavelength is increased, the auxochrome group has a bathochromic effect (red shift), whereas when it is reduced, it is called a hypsochromic effect (blue shift). Auxochrome groups can be either acidic (hydroxyl, sulfonic, and carboxyl groups) or basic (amines).

I.3.1.5.ii Classification

The great majority of paper dyes are synthetic organic dyes. They are classified according to their affinity with fibers.

Acid dyes are anionic molecules with very low affinity to bleached pulp and lignin-containing pulp. Fixing agents (usually alum) are thus necessary and a better dyeing is obtained with sizing¹. Despite their brilliant color, with low light-fastness² and the necessity of fixative and sizing, other groups of dyes are generally preferred.

Basic dyes are cationic molecules. Most of them are chloride or zinc double salts of organic dyes, e.g. rhodamine or triphenylmethane derivatives. The auxochrome groups of basic dyes are ionized in aqueous medium, thus getting positively charged. This is why they have a good affinity with anionic molecules such as lignin, and they attach to lignin-containing pulp (mechanical pulp, unbleached chemical pulp) without any fixative. Basic dyes have a clear color shade, good bleeding-fastness³ but low light-fastness.

Direct dyes represent more than half of the dyes present in the pulp and textile industries [65]. They have a good affinity to fully bleached chemical pulp and are also used with semi-bleached and unbleached chemical pulps. However, they are usually not applied on wood-containing pulp, as it would induce uneven coloring. Their light-fastness is better than basic dyes, but their color intensity is lower. Direct dyes are found in wood-free writing papers, napkins, sanitary papers, etc. Most of them are anionic, but they can also be cationic. They usually contain one or several azo group(s) and sulfonic acid groups that provide solubility.

Direct azo dyes are the most common dyes found in high grades of recovered paper. This is why our study focused on this type of dye, with two models: Direct Red 81, a di-azo molecule (Figure I-20), and Direct Yellow 11, a mono-azo dye (Figure I-21).

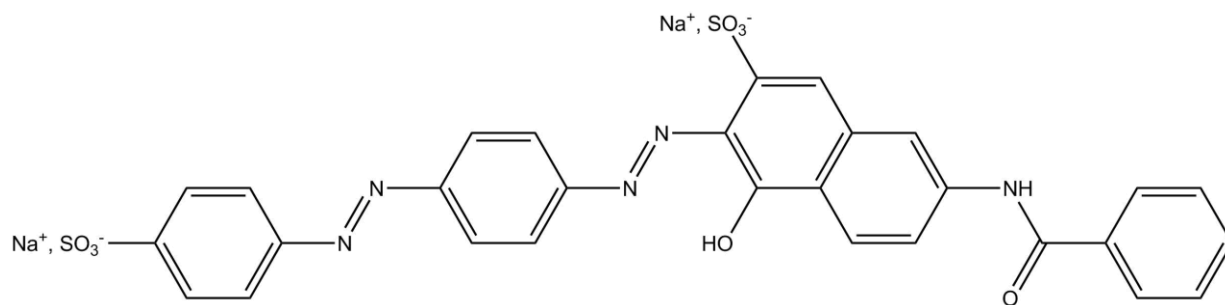


Figure I-20. Molecular structure of Direct Red 81

¹ Sizing: papermaking additives used to improve the wet strength of paper

² Light-fastness: resistance of a dye to fading during light exposure

³ Bleeding-fastness: resistance of a dye to migration from a colored paper to a substrate moistened with e.g. water

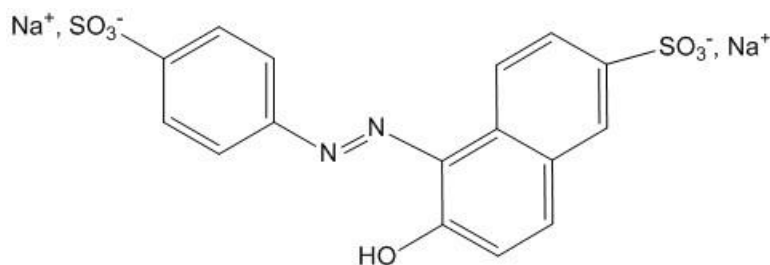


Figure I-21. Molecular structure of Direct Yellow 11

I.3.2 Recovered fiber bleaching

I.3.2.1 Overview

Recovered office papers are used to produce market DIPs and high quality papers such as printing papers and tissue papers [22]. Therefore, these recovered fibers have to be treated to reach a high brightness. They are first deinked, usually by a flotation process, and then bleached. The bleaching of deinked pulps (DIPs) is a complex process, due to the variability of the chromophores present.

In North America, most deinked pulps are wood-free pulps. These pulps are mainly used for tissue paper making [22]. Wood-free pulps used to be treated with chlorinated bleaching agents, which are more and more replaced by oxygenated compounds, although it implies some drawbacks: O stages are not very effective, Z stages are expensive and affect cellulose.

On the contrary, in Europe, which is our region of interest, recovered fibers are mainly wood-containing. Owing to the presence of native lignin in these pulps, the main bleaching agents used for DIP bleaching are hydrogen peroxide (oxidant), sodium dithionite, and formamidine sulfinic acid (reductive agents), which can degrade the dyes and decolorize native lignin without solubilizing it, so that a high yield is maintained. These bleaching agents are presented in Table I-9.

Table I-9. Main chemical agents used for wood-containing deinked pulp bleaching [22]

Bleaching agent	Stage	Action
Hydrogen peroxide H_2O_2	P	Mechanical fiber brightening (native lignin brightening)
Sodium dithionite $Na_2S_2O_4$	Y	Dye color-stripping (reduction) + mechanical fiber brightening
Formamidine sulfinic acid $(NH)(NH_2)CSO_2H$	FAS	Dye color-stripping (reduction) + mechanical fiber brightening

According to Göttsching and Pakarinen [22] pulps containing more than 0.5% residual lignin cannot be bleached without lignin-degrading agents such as oxygen or chlorine dioxide. In 1995, Air Liquid and Ponderosa Fibres developed an ozone-peroxide bleaching sequence for recovered fiber bleaching, as ozone is very effective for dye removal and allows to gain around 15 points brightness [66]. However, ozone is rarely used nowadays in RCF bleaching.

Wood containing pulps are usually bleached with lignin-preserving agents, and so are mechanical pulps. The main issue with wood-containing pulp is yellowing, which occurs during ageing but also during alkaline pulping. Hydrogen peroxide is an appropriate bleaching agent for wood-containing DIP. Its use as a recovered-paper bleaching agent has developed in the 1980's. 1-2% are applied on odp, under alkaline conditions, similarly to mechanical pulp bleaching. If high final brightness is expected, the P stage is followed by an additional step with sodium dithionite or FAS, because

I. Bibliographic study

hydrogen peroxide could not remove all the DIP chromophores (H_2O_2 reacts on lignin but not on azo dyes)

I.3.2.2 Use of H_2O_2 in deinking lines

Hydrogen peroxide can be applied to the pulper, in a disperser or as a post-bleaching stage.

Addition of H_2O_2 in the pulper is the oldest peroxide application in recycling lines [22]. It is classical for preventing yellowing of wood-containing fibers, as alkali is needed to re-pulp the furnish and H_2O_2 can prevent or compensate alkaline yellowing. For recovered graphic papers, the consistency has been brought up to 15-18% to be more favorable to H_2O_2 . The retention time is about 15 minutes, pH is adjusted to 10-10.5 with NaOH and/or sodium silicate [21], and a charge of 0.3-1% H_2O_2 is applied [21], with a temperature of 40-50°C. 1% H_2O_2 is used in case no further bleaching is to be applied [22].

Application of H_2O_2 during dispersing has been developed to avoid graying of the pulp by dispersion of residual ink [22]. Classical dispersion is carried out at high consistency (25-30%) and 60-95°C for a few minutes. This is too short and the conditions are not fully suitable for peroxide action. Therefore, dispersion bleaching is usually performed as follows: H_2O_2 and NaOH are added during dispersing at high temperature, then the pulp is diluted down to 12% and pumped into a bleaching pipe or tower to bleach for 30-60 min at 60°C. The peroxide charge is usually set between 1-2%.

Finally, “real” bleaching in deinking lines is called post-bleaching, as it is performed at the end of stock processing. It is usually performed at 60°C in a bleaching tower with a pulp consistency of around 15% during 1-3 h. Rarely, H_2O_2 is applied at ultra-high consistency (up to 40%) in order to reduce alkaline demand, COD (chemical oxygen demand) loads in the effluents and reaction time. Common chemical doses are 1-2.5% H_2O_2 and 0.5-1.5% NaOH, with the addition of 1-2% sodium silicate.

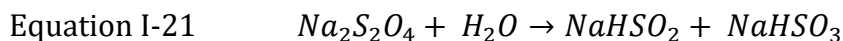
I.3.2.3 Reductive stages: FAS and Y

Reductive chemicals are able to reduce both carbonyl and azo groups. Hence, they can brighten native lignin and reduce azo dyes. Two options are commonly used for deinked pulp bleaching, mostly following an oxidative stage (generally a P stage): sodium dithionite bleaching (Y stage) and FAS bleaching.

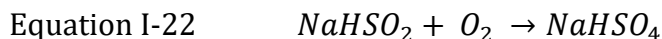
Both chemicals are approximately twice as expensive as hydrogen peroxide, with 1000-1200€/t for FAS and dithionite vs. 480-500€/t for H_2O_2 (source: Arkema).

I.3.2.3.i Sodium dithionite

Sodium dithionite $Na_2S_2O_4$, also called sodium hydrosulfite, has been used in mechanical pulp bleaching for the first time in the 1930's. In aqueous solution, it dissociates into $NaHSO_3$ and $NaHSO_2$ (Equation I-21), where $NaHSO_2$ would be the active species involved in bleaching.



At neutral pH, $NaHSO_2$ is able to reduce carbonyl groups from lignin and azo groups from dyes. It can degrade simple quinonoid structures (ortho-quinone, semi-quinone, coniferaldehyde) and reacts with others to form less colored substances, e.g. flavones are transformed into chalcones [22]. Sodium dithionite is sensitive to oxygen (Equation I-22: oxidation into acid bisulfate). Therefore, the presence of O_2 in the medium must be limited, which is made possible thanks to pumps that evacuate the air from the pulp while mixing the chemicals.



Some authors reported that the reactive species is actually a sulfur dioxide radical ion originated from dithionite ion dissociation [23], see Equation I-23.



The reaction time ranges between 15 and 60 min for a temperature of 60°C, and shorter times should be used for higher temperatures. An initial pH of 6-7 gives optimal results with 1% dithionite. Usually, the applied dose is 0.5-1% and the ISO brightness gain is of 4-7% on wood-containing DIPs [22].

Nevertheless, as mentioned earlier, sodium dithionite is a polluting compound.

I.3.2.3.ii FAS

Formamidine sulfinic acid (Figure I-22) is a more recent bleaching agent that has been used since the 1980's. It has partly replaced dithionite, since it has a similar action on both native lignin and azo dyes: it is less polluting and has a higher reducing power [22]. Moreover, it is also more stable in the presence of oxygen.

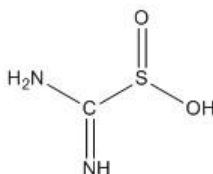


Figure I-22. Molecular structure of formamidine sulfinic acid

FAS is used under alkaline conditions (pH 8-11). Daneault and Leduc [67] found a relationship between final brightness and the different process parameters in the case of mechanical pulp bleaching with FAS. Temperature (generally not below 80°C) appeared to be a key parameter to improve bleaching efficacy, as well as the amount of FAS (from 0.25 to 2% on odp). However, high pulp consistency was detrimental to bleaching and reaction time was of little importance.

I.3.2.1 Conclusion

Finally, recovered fiber bleaching is a complex process. It requires a good knowledge of the pulp composition, so that the process can be adapted depending on the chromophores. In particular, dye removal is usually performed with FAS or sodium dithionite rather than with hydrogen peroxide.

I.3.3 Limits of paper recycling

One limit of the recycling process is that it generates new waste through rejects such as deinking sludge (containing fillers, inks, adhesive particles, coating pigments, fibers), rejects from screening, effluents from thickening, etc. The amount and composition of the rejects depends on the recovered paper grades used at the beginning of the line and on the quality of the final paper to be produced [22]. Generally, solid rejects are incinerated or landfilled and the effluents are treated and reused in the recycling line. Unfortunately, the amount of fibers in deinking sludges is too low to allow full conversion of organic compounds into energy via incineration.

One other difficulty for the production of paper from recovered fibers is that the quality of DIP varies much more than that of virgin pulps [68] making it difficult to produce paper with constant

quality. Moreover, despite the advances in deinking and bleaching technologies, recycling still uses a lot of energy and comes along with quality loss.

Improving the collection and sorting of recovered paper and board would certainly help reducing the negative impact of recycling. With specific raw material selection for each paper to be produced, the energy consumption and waste production would be reduced, and the quality of the fibers would be preserved. Collection in Europe can be improved with a correct implementation of the European standard EN 643 and thanks to European projects such as EcoPaperLoop, which aims at enhancing paper recycling in Europe, partly via exhaustive recommendations on collection strategies [69]. At the same time, CEPI and ERPA (European Recovered Paper Association) members are investing to improve automated sorting [54].

The production of high quality fibers for printing and writing from recovered office papers is all the more difficult, since it requires a complex treatment to obtain fibers that are both bright and strong. This is why the utilization rate of high paper grades is low. The production of printing and writing papers uses a lot of resources and creates much pollution as compared to other paper grades. Therefore, to reduce its cost and environmental impact, it is all the more important to increase the recycled content in this type of paper.

In fact, the bleaching processes that are currently applied to produce high quality fibers for printing and writing paper from recovered office papers do not match society's environmental expectations. To produce high grade market DIP, reductive chemicals such as dithionite and FAS are required, but these are polluting chemicals. For this reason, research in process improvement is necessary. Enhancing the bleaching efficacy of hydrogen peroxide (especially on dye removal) could be a solution to reduce the use of these bleaching agents.

In this research work, hydrogen peroxide was activated thanks to a copper(II)-phenanthroline complex, which was recently found to make P stages more active for delignification. The state of the art on this subject is presented in the next part.

I.4 ACTIVATION OF HYDROGEN PEROXIDE BLEACHING THANKS TO A COPPER-PHENANTHROLINE COMPLEX

Various solutions are possible to activate the action of hydrogen peroxide. Several authors have proposed the use of a copper-phenanthroline complex to catalyze oxygen delignification and, more recently, hydrogen peroxide delignification. This chapter proposes an overview of the results found in the literature in order to highlight the potential of hydrogen peroxide activation for color-stripping applications.

I.4.1 Introduction to hydrogen peroxide delignification catalysis/activation

Several catalysts or activators of hydrogen peroxide have been developed in the fields of biology, chemistry, or pulp and paper science. In the paper industry, few applications exist at an industrial scale, for several reasons: price of the activator, difficulty of implementation, low selectivity of the catalyzed bleaching, etc. Some of these catalysts or activators will be presented in this part. Note that most of them were only studied at a laboratory scale.

In 1992, Eckert patented a delignification process based on acidic hydrogen peroxide activated by transition metals [70]. The author hypothesized the formation of peroxo complexes, which are stronger oxidants than hydrogen peroxide.

Molybdenum oxides and other molybdenum compounds have also been studied for their ability to activate hydrogen peroxide. Kubelka proved the activation of peroxide delignification of kraft pulps in acidic medium by molybdenum oxides [71]. As proposed by Eckert, diperoxo complexes formed with H_2O_2 could explain this activation phenomenon. In 2011, Azevedo described the use of a peroxide stage catalyzed by molybdenum as a first stage of an ECF sequence for the bleaching of eucalyptus kraft pulp [72]. Some authors studied the catalysis of hydrogen peroxide with molybdate under acidic conditions [73], [74], in which case the catalyst would be the peroxomolybdate formed in the presence of H_2O_2 . Today, this treatment is used in a Scandinavian mill producing ECF and TCF-bleached softwood and hardwood pulps [74].

According to Lange *et al.* [75], organometallic compounds are widely used to catalyze lignin oxidation by hydrogen peroxide or oxygen. For instance, methyltrioxo rhenium (MTO) is a very effective catalyst for lignin oxidation, and salen complexes of metals such as cobalt are known to activate oxygen or hydrogen peroxide for the oxidation of organic species including lignin model compounds. In some cases, this oxidation does not lead to delignification. As an example, the aerobic oxidation of lignin model phenols catalyzed by $\text{Co}(\text{salen})$ led to the synthesis of para benzoquinones [76], which would be an interesting conversion of lignin to high value chemicals in the context of a biorefinery.

Polyoxometalates (POMs) have also been proved to activate oxygen [77] and hydrogen peroxide [78] under acidic conditions for lignin oxidation, but they are not used due to their high cost and toxicity.

An interesting catalyst mimicking laccase-mediator systems (see Figure I-23) has been developed in the 90's by Patt and coworkers for the alkaline hydrogen peroxide bleaching of kraft and sulfite pulps [79], [80]. Odermatt *et al.* studied the possibility of catalyzing hydrogen peroxide to develop a new TCF sequence for the bleaching of various pulps and found that it was particularly effective on softwood kraft pulps. The catalytic mechanism was studied with lignin model compounds [81], [82], but the synthesis of the manganese complex was complicated and therefore too expensive for implementation.

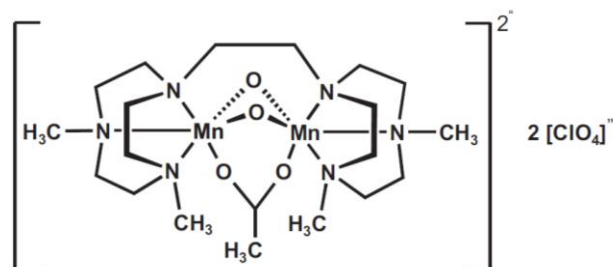


Figure I-23. Molecular structure of the Mn-complex used to catalyze hydrogen peroxide bleaching by Patt and coworkers [79], [80]

The development of tetraamido macrocyclic ligand (TAML) activators has brought various possibilities in the field of biology and is also interesting for industrial applications. Collins and coworkers studied the catalytic effect of iron-TAML complexes on hydrogen peroxide oxidation for various applications, including pulp bleaching [83]. In this case, it was proposed that such an

activated P stage could replace the D stage to develop TCF bleaching. However, the selectivity obtained with this new P stage was lower than that of a D stage.

Other nitrogen-based catalysts have been developed. The use of cyanamide to improve alkaline peroxide bleaching and delignification was patented in the 1990's [84], [85]. Kadla and coworkers evidenced the production of radical intermediates with the addition of cyanamide [86], [87] and proposed that the superoxide radical may be the predominant radical species involved in improved oxidation of phenolic lignin model compounds [86]. Chen [88] and Coucharrière [89] demonstrated that the dimer of cyanamide, dicyandiamide, could give even better results.

A well-known activator for textile bleaching, developed in the 1970's, is the tetraacetylenediamine (TAED), which was also shown to activate alkaline hydrogen peroxide bleaching of cellulosic pulps [89], [90]. The active species is the peracetate anion formed in alkaline medium, i.e. the conjugate base of peracetic acid (pKa of 8.2 at 25°C). Acidic pH was also suggested since peracetic acid would then be prevalent, but it was not as effective nor as selective as a simple peracetic acid bleaching stage. Coucharrière proposed to combine an acidic step with a subsequent alkaline step allowing a peroxide-reinforced alkaline extraction stage, and obtained interesting results [89]. However, no pilot scale or industrial trials were carried out to go further.

Finally, polypyridines have been investigated as peroxide catalysts. Argyropoulos and coworkers [91] improved oxygen delignification by introducing hydrogen peroxide and phenanthroline or bipyridine (both are polypyridines) during an O stage. They found that the addition of copper to the system enabled to reach an even higher delignification rate, confirming Coucharrière's hypothesis that the real catalyst in 1,10-phenanthroline activation was actually a copper-phenanthroline complex formed with copper ions present in the pulp. Halma et al. investigated the action of Cu-Phen on the oxidation of lignin model compounds by alkaline hydrogen peroxide [92]. The dimeric models containing β -O-4 linkages were subject to different activated peroxide treatments and the products were analyzed by HPLC. The results on non-phenolic lignin models suggested a catalytic mechanism similar to that proposed by Korpi *et al.* with oxygen [93]. On phenolic model compounds, the authors observed the production of vanillin, which is usually not possible with H₂O₂ alone. This mechanism, which involves Cu-Phen, is unknown.

The alkaline H₂O₂/Cu-Phen system was then tested on recovered fibers and gave interesting preliminary results [94], [95]. However, the mechanism was not explained.

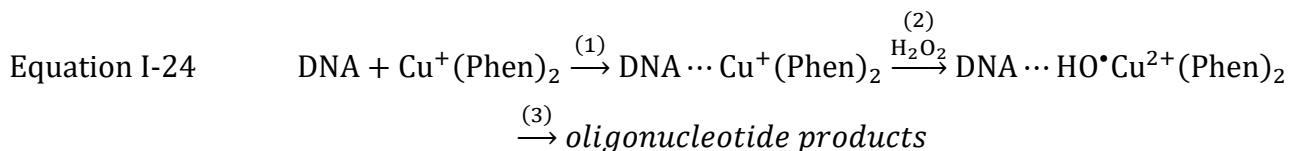
These results on the activation of H₂O₂ by Cu-Phen rose our interest towards this complex, particularly in view of testing its efficacy to enhance the color-stripping of dyes and dyed pulps. This is why this thesis focused on the copper-phenanthroline complex, which is introduced in the next chapter.

I.4.2 Copper-phenanthroline

I.4.2.1 Overview

2,2'-bipyridine was synthesized by Fritz Blau in 1888 and discovered to form intense red ferrous salts. In 1898, he synthesized 1,10-phenanthroline and showed that its properties were similar to those of 2,2'-bipyridine. He prepared iron, nickel, cobalt and copper(II) complex salts of 2,2'-bipyridine and 1,10-phenanthroline and was able to recognize them as Werner coordination compounds, with an octahedral configuration and so classed them as hexaammines [96].

Copper-phenanthroline complexes were first applied at neutral pH in biology. In 1979, $\text{Cu}^+(\text{phenanthroline})_2$ was discovered to have a nuclease activity [97], meaning that it is able to cleave the phosphodiester bonds between DNA or RNA nucleotides. The scission of DNA was proposed to occur in the presence of two co-reactants: $\text{Cu}^+(\text{phenanthroline})_2$ and H_2O_2 [98], [99]. According to Sigman [98], as presented in Equation I-24, $\text{Cu}^+(\text{phenanthroline})_2$ would bind to DNA (1) and the oxidation of this coordinate by H_2O_2 would form a cupric hydroxyl radical-like coordinate (2), responsible for the scission of DNA (3).



Hence, copper-phenanthroline coordinates (Cu-Phen) were the first artificial nucleases studied in biology. Generally, they consist of bis(1,10-phenanthroline)copper complexes, as described by Sigman and his collaborators [97]–[99] and more recently Oyoshi [100] and Chikira [101], although a mono(1,10-phenanthroline)copper complex was found to have better nuclease activity by Lu and colleagues [102].

The species described as a nuclease was generally a cuprous complex of phenanthroline: $\text{Cu}^+(\text{phenanthroline})_2$. However, Chikira and coworkers evidenced the intercalative binding of the cupric complex $\text{Cu}^{2+}(\text{phenanthroline})_2$ with DNA, and attributed the cleavage of DNA to the bonding between DNA and this cupric complex. This had been described by Liu and colleagues with cupric complexes that would cleave DNA in the presence of H_2O_2 and a reductant, via a mechanism including the binding between copper and DNA [103]. Moreover, while reviewing nucleases, Sigman mentioned the possibility of a mechanism involving oxidized states of copper: Cu^{II} and even Cu^{III} [104].

This complex has been proved to have anti-inflammatory properties [105] but also antimicrobial [106] and anticancer [107]–[109] properties due to its cytotoxicity (toxicity towards cells). Therefore, many authors have investigated the cytotoxic properties of $\text{Cu}(\text{Phen})_2$.

Prisecaru *et al.* managed to enhance Cu-Phen's binding to DNA by replacing $\text{Cu}(\text{Phen})_2^{2+}$ with $\text{Cu}(\text{Phen})_2(\text{RCOO})^+$, where R was $-\text{H}$, $-\text{CH}_3$, $-\text{C}_2\text{H}_5$, $-\text{CH}(\text{CH}_3)_2$, and $-\text{C}(\text{CH}_3)_3$ [110]. The coordination of these carboxylate ligands to Cu-Phen aimed at modulating the biological profile of Cu-Phen in terms of selectivity, cytotoxicity, interaction with hydrogen peroxide, etc. and generally increased DNA binding while reducing protein binding.

Owing to ongoing research on copper(II)-phenanthroline-based drugs, the interaction between the complex and human serum was recently investigated [106]. Human serum albumin (HSA) was shown to bind to phenanthroline, thus forming different coordinate species in aqueous solution, the binding constants of which were determined under the study's conditions.

Besides, Cu^{II} and Ni^{II} complexes of a phenanthroline derivative (phenanthroline linked to a pyridine group via a thioether bond) were found to have nucleic acid recognition properties. They were able to bind to G-quadruplexes (also G-4, which is a particular DNA arrangement), which could be used as an anticancer drug [111]. This study was partly based on a previous work on G-4 recognition and binding properties of Cu^{II} complexes of phenanthroline and phenanthroline derivatives containing one or two N,N-dimethylaminoethylamino side-chains [112].

Wu *et al.* studied the cytophysiological mechanism of HepG2 (a human liver carcinoma cell line) treatment with $\text{Cu}(\text{Phen})_2$, which causes apoptosis⁴ of this cancer cell line. They evidenced that the copper complex induces reactive oxygen species (ROS: peroxides or superoxide) generation in the cells, thus damaging DNA and proteins and leading, through a complex mechanism, to apoptosis of HepG2. Once again Cu-Phen's action was related to oxygenated species.

Numerous studies focused on multi-ligand coordinates containing copper and phenanthroline. Interestingly, Lakshmipraba *et al.* monitored the interactions between DNA and a $\text{Cu}(\text{II})$ -phenanthroline-polymer complex by UV-vis titration [113]. If the binding was through intercalation, a hypochromic and bathochromic shift was observed, whereas hyperchromism would happen in case of electrostatic binding (external contact).

The oxidative action of Cu-Phen complexes in the presence of H_2O_2 [98], [114] has been the starting point of oxidation studies of lignin compounds using copper(II)-phenanthroline coordinates under alkaline conditions. This $\text{H}_2\text{O}_2/\text{Cu-Phen}$ system was also used for the decolorization of colored cellulosic fibers [115]. Under neutral conditions (without the addition of alkali), the treatment led to 50% color-stripping. However, it was accompanied by strong cellulose degradation. The main hypothesis to explain this phenomenon was a radical mechanism: the presence of Cu-Phen would activate H_2O_2 's decomposition into highly oxidative hydroxyl radicals.

I.4.2.2 Copper

Copper is a reddish-brown metal with high electrical and thermal conductivity. Although it is one of the essential micronutrients, it becomes toxic at high concentration, which is why its levels in soil and aquatic environments are widely documented [116]. Its uses and general properties are described in Table I-10.

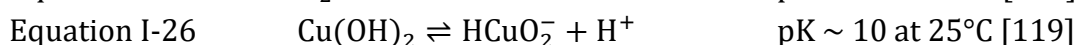
Table I-10. Overview of the occurrence, uses and main properties of copper

General description	Applications [117]	Copper compounds	Minerals	Reactions	In aqueous solution
Atomic number: 29	Coinages	Oxides	Cuprite Cu_2O	Stable	+2 state is more stable
Atomic weight: 63.546	Alloys	Sulfates	Chalcopyrite	compounds: +1 and +2	than +1, unless
Electron configuration: $[\text{Ar}]3d^{10}4s^1$	Electric wiring	Chlorides	CuFeS_2	valence states (cuprous and cupric forms)	complexes with ammonia, cyanide ion, chloride ion
Cu^+ : $[\text{Ar}]3d^{10}$	Electrodes	Sulfides	Azurite		Most water-soluble Cu compounds: cupric
Cu^{2+} : $[\text{Ar}]3d^9$	Plumbing	Arsenides	$2\text{CuCO}_3, \text{Cu}(\text{OH})_2$		$2\text{Cu}^+ \rightarrow \text{Cu}^0 + \text{Cu}^{2+}$
[117]	Piping	Carbonates	Tenorite CuO		$K = 1.2 \times 10^6$ at 25°C
	Roofing	Arsenosulfides	Chalcocite Cu_2S		($\text{Cu}^0 = \text{metallic Cu}$)
	Cooking utensils	Etc.	Bornite Cu_5FeS_4		[117]
			Etc.		

The cupric ion Cu^{II} has a d^9 electron configuration (see Table I-10), it is a paramagnetic ion. It is thus subject to distortions such as axial elongation (Jahn-Teller effect) [118]. In aqueous solution, it usually forms the $[\text{Cu}(\text{H}_2\text{O})_6]^{2+}$ complex. Added ligands then replace some of these water molecules. The geometry of Cu^{II} coordinates is often square-planar and ligands are weakly attached in the axial position, forming tetragonally distorted octahedral structures, although trigonal-bipyramidal geometries also occur.

⁴ Apoptosis: programmed death of cells

Some dissociation constants for copper(II) hydroxylated compounds are reported in the literature, see Equation I-25 and Equation I-26.



A well-known and often used Cu^{II} compound is copper sulfate. This chemical has been chosen to provide cupric ions in our study. Copper sulfate's molecular formula is CuSO_4 , although it also exists in a pentahydrate form: $\text{CuSO}_4 \cdot 5 \text{H}_2\text{O}$. It is often reported as the most important of all copper compounds. Its main properties and uses are described in Table I-11.

Table I-11. Properties and uses of CuSO_4

Physical properties [117]	Reactions (aqueous solution)	Applications [117], [120]
<u>Anhydrous salt</u>	Thermal decomposition	Fungicide
- Greenish-white	products: copper(II) oxide and	Feed additive (poultry and
- Hygroscopic	sulfur trioxide	swine industries)
- Soluble in water	When heated with NaOH:	Plant nutrition
<u>Pentahydrate</u>	formation of copper(II)	Mordant in textiles, Pigments
- Blue	hydroxide [117]	Electric batteries
- Very soluble in water, moderately		Copper plating
soluble in methanol		Wood preservative (against
- Loses water on heating		decay and termite infestation)
(2 molecules at 30°C vs 5 at room		Lithography
temperature)		Medicine
		Dehydrating agent
		Manufacture of catalysts
		Manufacture of other copper
		compounds

I.4.2.3 Phenanthroline

After its first synthesis by Fritz Blau in 1898, phenanthroline (Figure I-24) has been used as a metal ligand, especially with iron. In 1931, Walden *et al.* reported the use of "ferroin", the phenanthroline-ferrous ion, as a redox indicator, its oxidation turning it from intense red to light blue. This represented a great advance in the field of analytical chemistry [121] and rose the interest in the phenanthroline molecule.

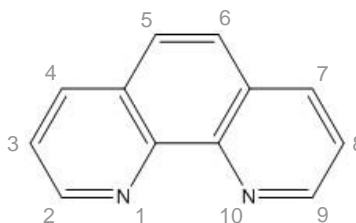


Figure I-24. Molecular structure of 1,10-phenanthroline

In 1935, Smith and Getz [122] proposed some improvements to the synthesis of phenanthroline monohydrate via two "Skraup syntheses" (to prepare quinoline derivatives from *o*-nitroaniline) following Knueppel's improved method with the addition of arsenic rather than nitrobenzene [123].

Metal-phenanthroline complexes have been studied until today, e.g. with the recent development of a potentiometric titration method to determine the speciation of iron in aqueous solution, thanks to Ce and Co ions and their redox potential modulations with phenanthroline [124].

The coordination of phenanthroline with copper(II) was first studied by Pfeiffer and Tappermann in 1933 [125], before further works on copper(I)-phenanthroline complexes [126], for applications in the colorimetric determination of copper.

1,10-phenanthroline is also known to have strong antimicrobial activity [127], thus exhibiting interesting antibacterial properties. Yet, until today, it has mainly been used as a metal ion ligand for numerous applications in biology, analytical chemistry or process chemistry.

I.4.2.4 Copper-phenanthroline complex

In aqueous solution, copper(II)-phenanthroline complexes are generally reported to exhibit a tetragonally distorted octahedral geometry [128], as well as copper(II)-bipyridine coordinates [129]. Anitha *et al.* reported a distorted trigonal bipyramidal geometry for $[\text{Cu}(\text{bpy})_2\text{Cl}]^+$ and $[\text{Cu}(\text{phen})_2\text{Cl}]^+$, while $[\text{Cu}(\text{bpy})_2(\text{H}_2\text{O})\text{Cl}]^+$ and $[\text{Cu}(\text{phen})_2(\text{H}_2\text{O})\text{Cl}]^+$ would display a tetragonally distorted octahedral geometry [128]. Garribba and collaborators also found the tetragonally distorted octahedral geometry to be preferred by $[\text{Cu}(\text{bpy})_2]^{2+}$ in water, as in Figure I-25.

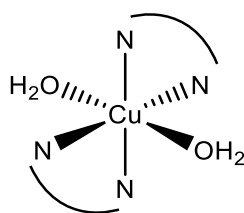


Figure I-25. Geometry of $[\text{Cu}(\text{bpy})_2]^{2+}$ in water according to Garribba *et al.* [129]

The same configuration was reported by Oladipo *et al.* for $\text{Cu}(\text{Phen})_2\text{SO}_4$ [127] and by Zhou *et al.* with a mono-phenanthroline complex $\text{Cu}(\text{Phen})(\text{SO}_4)(\text{H}_2\text{O})_2$ [130] (solid state structures).

In his thesis, Korpi performed slow evaporation of alkaline aqueous solutions of catalysts to analyse their solid state structure [131]. For bis(phenanthroline)copper(II), the author found a distorted square pyramidal geometry around the copper atom in $\text{Cu}(\text{Phen})_2\text{CO}_3 \cdot 7 \text{H}_2\text{O}$ where the carbonate group came from CO_2 dissolution from air. This geometry is illustrated in Figure I-26.

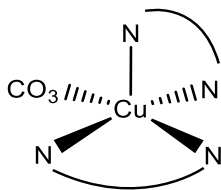


Figure I-26. Geometry of the $\text{Cu}(\text{Phen})_2\text{CO}_3$ complex according to Korpi [131]

Density functional theory (DFT) calculations recently allowed Elder and Rudie [132] to assess the catalytic activity of different copper-phenanthrolines used in the ligand screening conducted by Gueneau *et al.* in a pulp oxygen delignification study [133]. The studied complexes were dihydroxy-copper(II) mono-phenanthrolines with substituted phenanthrolines, as presented in Figure I-27.

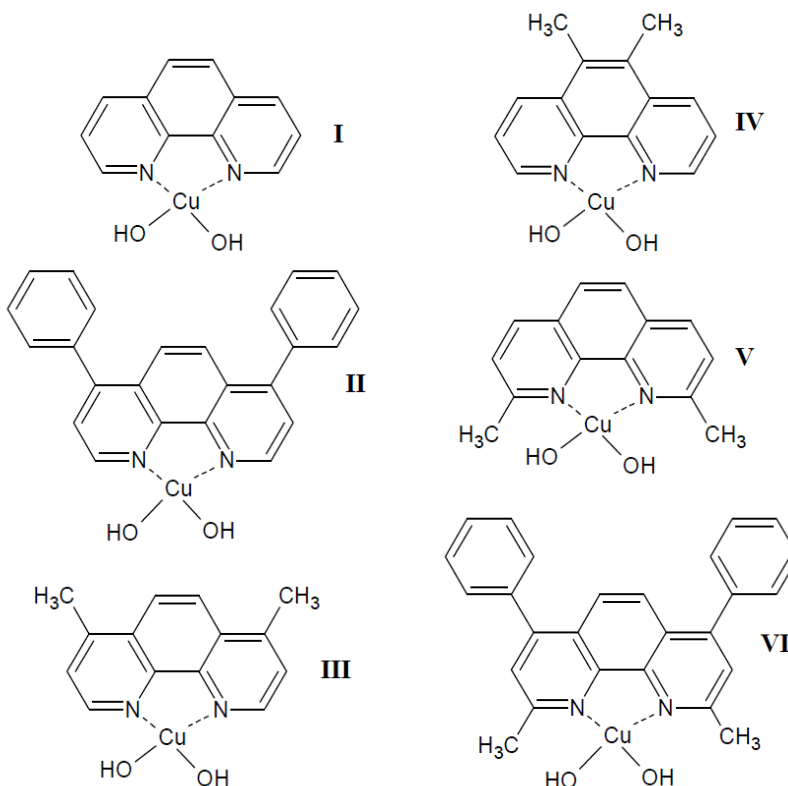
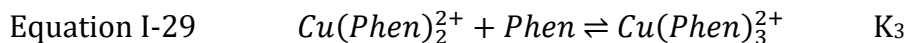
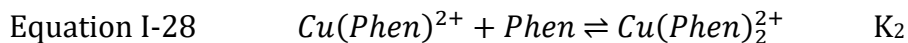
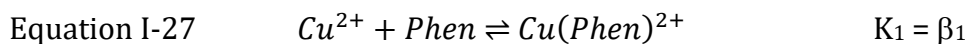


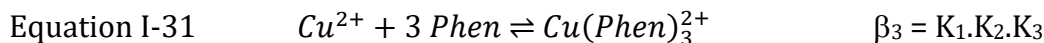
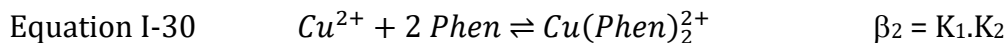
Figure I-27. Copper-phenanthrolines used in Gueneau's and Elder's studies

According to the DFT calculations performed on these complexes, only those with 2,9-substituted phenanthrolines (V and VI) were not planar, with $\text{Cu}(\text{OH})_2$ twisted out of the plane of the ligand [132]. The authors proposed that this may explain the lower delignification observed with these complexes in Gueneau's study.

Three copper(II)-phenanthroline coordinates can be found: mono-phenanthroline, bis-phenanthroline and tris-phenanthroline cupric ions. Their formation reactions are listed in Equation I-27, Equation I-28, and Equation I-29 with the corresponding stability constants at 25°C.



These equilibria can also be represented by n phenanthroline ligands associated to Cu^{2+} to form the $\text{Cu}(\text{Phen})_n^{2+}$ complex, see Equation I-27, Equation I-30, and Equation I-31.



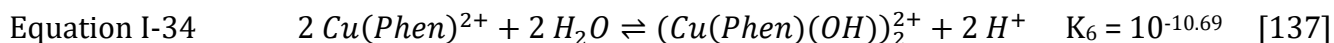
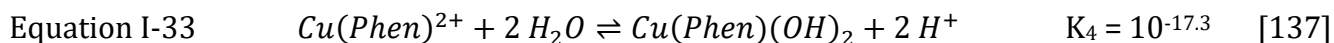
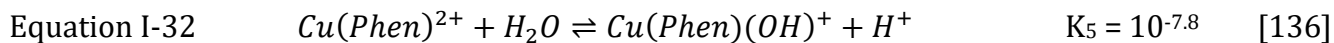
Where
$$\beta_n = \frac{[\text{Cu}^{2+}][\text{Phen}]^n}{[\text{Cu}(\text{Phen})_n^{2+}]} \quad (\text{dissociation constant})$$

According to Ringbom [134], $\beta_1 = 10^{-9.1}$, $\beta_2 = 10^{-15.8}$, and $\beta_3 = 10^{-21.0}$, from which the K constants can be calculated: $K_1 = 10^{-9.1}$, $K_2 = 10^{-6.7}$, and $K_3 = 10^{-5.2}$.

I. Bibliographic study

According to Schilt [135], $K_1 = 10^{-9.30}$ to $10^{-8.82}$, $K_2 = 10^{-6.75}$ to $10^{-6.42}$, and $K_3 = 10^{-5.35}$ to $10^{-4.63}$. Both authors agreeing on these figures, we randomly chose to use Ringbom's constants in our study.

Under alkaline conditions, hydroxylated species are also formed. Their formation reactions are detailed below:



In the context of lignin oxidation via catalytic mechanisms involving Cu-Phen, the distribution of different copper-phenanthroline-hydroxyl complexes, depending on the pH and initial concentrations of copper sulfate and phenanthroline, was studied by Korpi and collaborators [93]. The authors calculated a distribution under the conditions of their study, via the HySS program [138], which is based on stability constants from the NIST Standard Reference Database 46.

The present work also took into account these distributions and similar calculations were performed to be aware of the copper-phenanthroline-hydroxyl speciation depending on the chosen operating conditions.

As presented in I.3.3, our aim was to enhance the action of hydrogen peroxide thanks to copper-phenanthroline. This complex was first used in the field of pulp and paper for the activation of oxygen cooking of wood or oxygen delignification of pulp. The catalysis of oxygen has been investigated to reduce the costs by improving the efficiency of delignification. As the oxidation mechanisms of oxygen involve H_2O_2 , the catalysis of oxygen is strongly related to hydrogen peroxide catalysis. This is why the activation of oxygen is presented before developing the state of the art concerning hydrogen peroxide activation.

I.4.3 Oxygen delignification catalysis/activation

Cu-Phen complexes were first applied in oxygen-alkaline pulping by Germer and coworkers. In the 1980's, they patented a method to improve oxygen-alkaline cooking of spruce and aspen wood thanks to the addition of phenanthroline, with or without Mn^{II} or Cu^{II} . The inventors proposed that phenanthroline would form active coordinates with these transition metals. This method would increase the pulp yield while avoiding polysaccharide degradation [139]. In the 1990's, Germer studied the catalytic action of phenanthroline on oxygen-alkaline delignification and evidenced the involvement of phenanthroline as a ligand for transition metals, especially the cupric ion [140]–[142].

The catalysis of oxygen during cooking inspired many authors for bleaching applications. Korpi and collaborators showed that oxygen's delignification efficiency could be improved thanks to metal-phenanthroline complexes, yet cellulose underwent extensive depolymerization [143]. Several authors have then shown that the catalytic action of Cu-Phen for the alkaline oxidation of lignin was improved by oxygen [93], [131], [133], [143]–[145]. In particular, some studies focused on lignin model compounds, such as veratryl alcohol, and proposed a catalytic mechanism involving a reduction of $\text{Cu}^{\text{II}}(\text{Phen})(\text{OH})_2$ into $\text{Cu}^{\text{I}}(\text{Phen})(\text{OH})$, while the former would act as a catalyst.

Density functional theory (DFT) studies were recently conducted on the aerobic oxidation of veratryl alcohol in the presence of Cu-Phen [146]. These calculations evidenced a binuclear

mechanism for the oxidation of veratryl alcohol to veratraldehyde by copper(II)-phenanthroline-dihydroxide, which is followed by the reduction of molecular oxygen as described in Figure I-28.

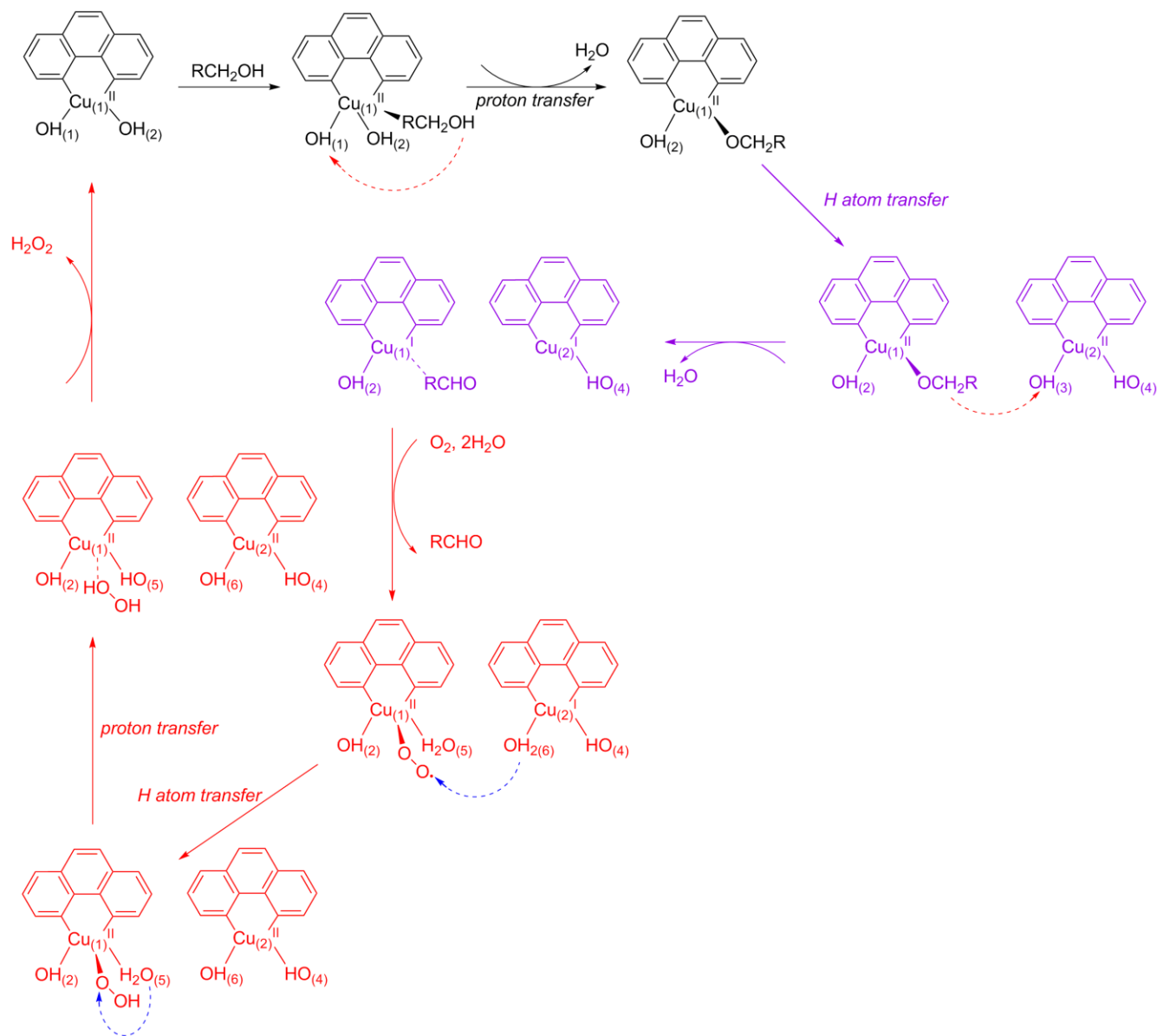


Figure I-28. Scheme of the catalytic mechanism proposed by Ma *et al.* for the oxidation of veratryl alcohol by Cu-Phen [146].

Coucharrière [89] observed that a Cu-Phen activated P stage was not very effective after an O delignification stage, which seemed logical as the author hypothesized that copper-phenanthroline-lignin complexes were responsible for peroxide activation. Therefore, a peroxide-reinforced oxygen delignification stage was developed as a combination of the advantages of both O and activated P. This may be considered as a start for hydrogen peroxide activation with Cu-Phen.

I.4.4 Hydrogen peroxide delignification activation/catalysis

Hydrogen peroxide is an interesting bleaching agent because of its low environmental impact, as well as oxygen. However, its delignification efficacy is limited and its cost is not as low as that of oxygen. Yet, compared to the latter, it exhibits higher brightening properties. This is why some attempts have been made to activate the action of H_2O_2 in order to reduce its consumption or to make it more effective in delignification and to reduce the consumption of other chemicals. It has been particularly studied in the frame of the development of TCF bleaching sequences.

Cu-Phen complexes have been shown to activate H_2O_2 for chemical pulp delignification under alkaline conditions [89], [94], [147]; see also the patents [148], [149]. The quoted authors demonstrated that the action of H_2O_2 could be enhanced by means of copper-phenanthroline complexes, leading to the improvement of lignin oxidation in alkaline medium.

The activated P delignification stage of Coucharrière (2 hours at $90^\circ C$, 10% consistency, 2% H_2O_2 and 2% NaOH with 0.15% $Cu(Phen)_2$) allowed to reach a kappa number of 12.6, as compared to 17.0 after a non-activated P stage, knowing that the initial unbleached kraft pulp had a kappa number of 22.5. The pulp viscosity was imparted by the activated treatment, with initial DP_v values of 1170, 1120 after P and 1070 after activated P [89], [94].

Vladut *et al.* applied P and activated P stages on oxygen-delignified softwood kraft pulps. The conditions were close to those of a brightening P stage, with 3 hours at $50^\circ C$, 10% consistency, 2% H_2O_2 and 2% NaOH with 0.05% Cu-Phen (1:2). With an initial kappa number of 11.3, the pulp reached a kappa number of 8.9 after P and 6.5 after activated P. However, a rather high level of cellulose degradation was observed. The DP_v dropped from 1280 for the initial pulp to 1000 after the activated P stage [147].

As discussed before, the use of copper(II)-phenanthroline complexes as hydrogen peroxide or oxygen activators has been the subject of several studies for delignification improvement. Trials conducted in alkaline aqueous medium on lignin model compounds showed that oxidation could be catalyzed by such complexes [93], [143]–[145], [150]. During the reaction, H_2O_2 generated or already present in the medium played a major role in lignin oxidation [93], [145]. This could happen via a catalytic cycle as proposed by Korpi [93], see Figure I-29.

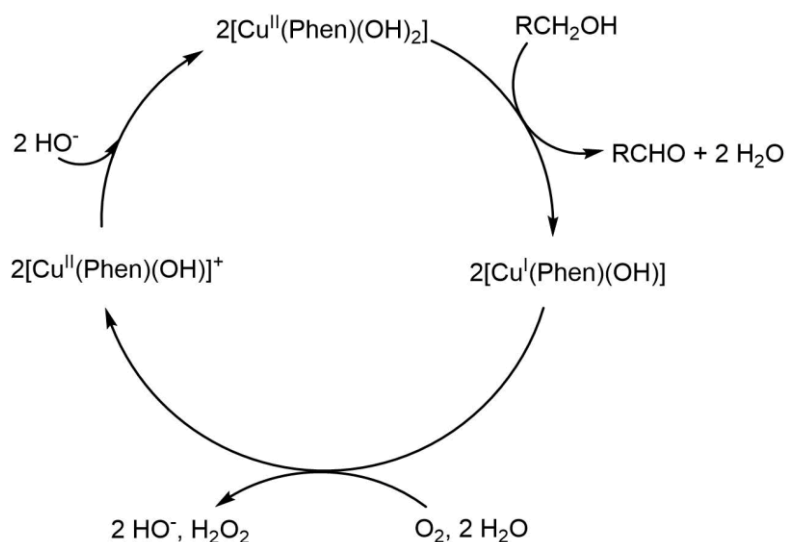
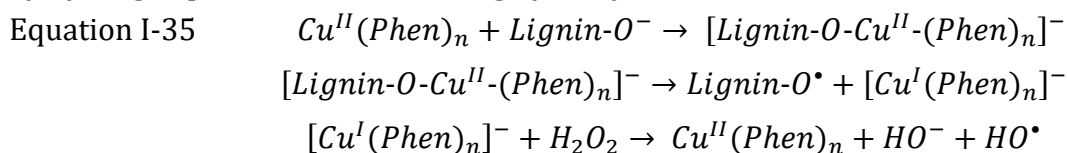


Figure I-29. Catalytic cycle proposed by Korpi et al. for the oxidation of veratryl alcohol in alkaline medium with oxygen and a copper-phenanthroline catalyst [93]

Korpi's cycle starts with the reduction of $\text{Cu}^{\text{II}}\text{Phen}(\text{OH})_2$ into $\text{Cu}^{\text{I}}\text{Phen}(\text{OH})$ by veratryl alcohol, which forms veratraldehyde. Molecular oxygen allows the reoxidation of Cu^{I} into Cu^{II} while forming H_2O_2 .

Coucharrière proposed a catalytic mechanism for copper-phenanthroline-activated P stages, as detailed in Equation I-35 [89]. This mechanism involves the formation of lignin-copper-phenanthroline complexes as evidenced by EPR spectroscopy. First, copper binds to lignin phenolic groups. A homolytic cleavage of the resulting lignin-copper-phenanthroline complex forms a phenoxy radical and the reduced form of the copper complex, which is further reoxidized by hydrogen peroxide while forming hydroxyl radicals.



On the contrary, Vladut *et al.* suggested that the predominant mechanism in this activated peroxide stage would be a radical mechanism involving hydroxyl radicals [147]. The authors proved that Cu-Phen-lignin complexes existed but were no delignifying species. This radical mechanism would require the initial reduction of Cu^{II} into Cu^{I} , further reoxidized in the presence of H_2O_2 to form hydroxyl radicals via a Fenton-like mechanism, as proposed by Perez-Benito at near-neutral pH [151], see Figure I-30.

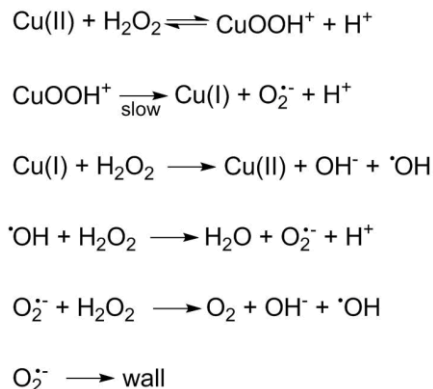


Figure I-30. Scheme of the pathway proposed by Perez-Benito for hydrogen peroxide decomposition in the presence of Cu^{II} at low copper concentration [151]

Finally, two hypotheses have been brought out to explain the activation of hydrogen peroxide by copper-phenanthroline: a catalytic route and a radical mechanism.

After these interesting results on virgin fibers, and due to our interest in the color-stripping of recovered cellulosic fibers, the next part will deal with the application of Cu-Phen to activate the hydrogen peroxide bleaching of recovered fibers.

I.4.5 On recovered fibers

In view of the application of a Cu-Phen-activated or catalyzed P stage for recovered fiber bleaching, some preliminary trials with deinked pulps and dyed pulps were conducted under alkaline conditions [94], [95].

To bleach recovered fibers, the three main chromophore categories have to be brightened or removed: native lignin, residual lignin, and paper dyes. Therefore, Marlin and coworkers performed several bleaching trials to assess the bleaching-enhancing ability of Cu-Phen-activated hydrogen peroxide on deinked pulps. Mild conditions were applied on a DIP model made of 50% newsprint and 50% magazine with an initial brightness of 63.9%: 1 hour at 60°C, 2% H₂O₂ and 1% NaOH, with 0.15% Cu-Phen in the case of the activated stage [94]. While the P stage brightened the pulp with a brightness gain of 8 points, the activated P stage actually reduced the pulp's brightness by one point. It is difficult to explain this result as DIPs contain various chromophores. Hence, the authors assessed the activating-ability of copper-phenanthroline on different pulps: wood-free and wood-containing pulp models, and a colored pulp (bleached chemical pulp colored with a red H₂O₂-resistant dye). The bleaching conditions were the following: 2 hours at 90°C, 2% H₂O₂ and 2% NaOH with 0.15% Cu-Phen in the case of the activated stages.

I.4.5.1 Native lignin brightening

Marlin's activated P stage applied on a model wood-containing pulp of initial ISO brightness 64.7% did not improve the brightening effect of hydrogen peroxide which allowed reaching 72.8% brightness. It even had a negative effect, as the brightness dropped down to 59.4%. The authors assumed that this was due to the formation of colored copper-lignin complexes [94].

I.4.5.2 Residual lignin degradation

The effect of activated hydrogen peroxide on the residual lignin present in deinked pulp should be the same as that of activated hydrogen peroxide applied on chemical pulps. In Marlin's work, the P

stage applied on wood-free pulp already allowed to gain 13 points of brightness, and the activated P stage led to a pulp with only slightly higher brightness (0.4-point gain as compared to the P stage). This might be due to the low amount of residual lignin in that model pulp, which was made of 90% bleached chemical pulp and 10% unbleached chemical pulp (initial ISO brightness of 67.2%) [94].

I.4.5.3 Paper dye degradation

In the same study, however, the color-stripping effect of activated H₂O₂ was obvious: the brightness improved from 51.3% for the “red pulp” to 59.5% after P and up to 72.6% after activated P [94]. This finding indicates that in the case of H₂O₂-resistant dyes, this compound can make H₂O₂ more effective in dye removal or destruction.

The color-stripping effect should be evaluated by other means than brightness measurement, as proposed by Marlin *et al.* in another study on the improvement of peroxide stages for deinked pulp color-stripping [95]. In this paper, the authors assessed the decolorizing effect by calculating a dye removal index, defined by Sharpe and Lowe as the percentage of discoloration in the CIE L*a*b* color system [152].

Besides, the mechanism of the color-stripping activation discovered by Marlin *et al.* has not been studied yet. Hence, the aim of our work was to investigate the effect of the copper-phenanthroline complex during the H₂O₂ treatment of a dyed pulp.

I.5 CONCLUSION

In conclusion, high quality recovered fibers constitute a very complex mixture and further deinked pulps contain various contaminants. Therefore, they cannot be easily modelled. Since H₂O₂ is known to have a limited effect on paper dye oxidation, the present study proposes to apply an activated P stage on a dyed chemical pulp to improve hydrogen peroxide’s color-stripping ability using copper-phenanthroline complexes as activators.

The state of the art concerning hydrogen peroxide activation by copper-phenanthroline in the context of pulp delignification revealed two possible chemical mechanisms: a catalytic action and a radical route. These will be confronted in this thesis, which will evaluate the activating effect of copper-phenanthroline on the hydrogen peroxide-induced color-stripping of a dyed pulp. Indeed, very little is known on the mechanisms involved in this system.

Now that the different constituents of our raw material have been defined and that previous studies on hydrogen peroxide activation have been described, the next chapter will present the materials and experimental methods used in this work, before focusing on the characterization of the dyes and complex, and on the interactions between the two.

I.6 REFERENCES

- [1] G. Koch, “Raw material for pulp,” in *Handbook of pulp - Part I: Chemical pulping*, vol. 1, 2 vols., Weinheim: Wiley, 2006, pp. 21–68.
- [2] S. Willför, “Raw materials,” in *Chemical pulping Part 1, Fibre chemistry and technology*, 2e édition., Helsinki (Finlande): Fapet Oy, 2011, pp. 12–186.

- [3] P. Fardim, *Chemical pulping Part 1, Fibre chemistry and technology*, 2nd ed. Helsinki (Finland): Fapet Oy, 2011.
- [4] R. Vanholme, B. Demedts, K. Morreel, J. Ralph, and W. Boerjan, "Lignin Biosynthesis and Structure," *Plant physiology*, vol. 153, no. 3, pp. 895–905, Jul. 2010.
- [5] H. Sixta, A. Potthast, and A. W. Krotschek, "Chemical pulping processes," in *Handbook of pulp - Part I: Chemical pulping*, vol. 1, 2 vols., Weinheim: Wiley, 2006, pp. 109–510.
- [6] J. Gullichsen and C.-J. Fogelholm, *Chemical pulping*. Helsinki (Finland): Fapet Oy, 1999.
- [7] D. Lachenal, N. Benattar, M. Allix, N. Marlin, and C. Chirat, "Bleachability of Alkaline Pulps: Effect of Quinones Present in Residual Lignin," in *Proceedings of the 13th International Symposium on Wood Fibre and Pulping Chemistry*, Auckland, New Zealand, 2005, pp. 23–27.
- [8] J. Gierer, "The Reactions of Lignin during Pulping. A Description and Comparison of Conventional Pulping Processes," *Svensk Papperstidning*, vol. 73, no. 18, pp. 571–599, Sep. 1970.
- [9] J. Sundholm, J. A. Kurdin, and P. Y. Suomen, *Mechanical pulping*. Helsinki: Fapet Oy - published in cooperation with the Finnish Paper Engineers' Association and TAPPI, 1999.
- [10] J. Blechschmidt and S. Heinemann, "Introduction," in *Handbook of pulp - Part II: Mechanical pulping*, vol. 2, 2 vols., Weinheim: Wiley, 2006, pp. 1071–1072.
- [11] H.-U. Süss, "Bleaching of mechanical pulp," in *Handbook of pulp - Part II: Mechanical pulping*, vol. 2, 2 vols., Weinheim: Wiley, 2006, pp. 1123–1136.
- [12] H. Sixta, "Pulp properties and applications," in *Handbook of pulp - Part I: Chemical pulping*, vol. 2, 2 vols., Weinheim: Wiley, 2006, pp. 1009–1068.
- [13] A. R. Esteghlalian, M. M. Kazaoka, B. A. Lowery, A. Varvak, B. Hancock, T. Woodward, J. O. Turner, D. L. Blum, D. Weiner, and G. P. Hazlewood, "Prebleaching of softwood and hardwood pulps by a high performance xylanase belonging to a novel clade of glycosyl hydrolase family 11," *Enzyme and Microbial Technology*, vol. 42, no. 5, pp. 395–403, Apr. 2008.
- [14] B. Gysin and T. Griessmann, "Bleaching wood pulp with enzymes," EP0418201 (A2), 20-Mar-1991.
- [15] P. Dwivedi, V. Vivekanand, N. Pareek, A. Sharma, and R. P. Singh, "Bleach Enhancement of Mixed Wood Pulp by Xylanase–Laccase Concoction Derived Through Co-culture Strategy," *Appl Biochem Biotechnol*, vol. 160, no. 1, pp. 255–268, May 2009.
- [16] H. U. Suess, *Pulp Bleaching Today*, Walter de Gruyter. Berlin, New York, 2010.
- [17] "Trends in world bleached chemical pulp production: 1990-2012," The Alliance for Environmental Technology, 2013.
- [18] D. W. Reeve, "IV 3: Chlorine dioxide in delignification," in *Pulp bleaching: principles and practice*, Atlanta (Ga.): TAPPI Press, 1996, pp. 261–290.
- [19] D. W. Reeve, "I 1: Introduction to the principles and practice of pulp bleaching," in *Pulp bleaching: principles and practice*, Atlanta (Ga.): TAPPI Press, 1996, pp. 1–24.
- [20] P. W. Hart and A. W. Rudie, *The bleaching of pulp*, 5th ed. Norcross, USA: Tappi Press, 2012.
- [21] C. W. Dence and D. W. Reeve, *Pulp bleaching: principles and practice*. Atlanta (Ga.): TAPPI Press, 1996.

- [22] L. Göttsching and H. Pakarinen, *Recycled fiber and deinking*. Helsinki: Fapet Oy, 2000.
- [23] C. W. Dence, "III 4: Chemistry of mechanical pulp bleaching," in *Pulp bleaching : principles and practice*, Atlanta (Ga.): TAPPI Press, 1996, pp. 161–182.
- [24] P. Huber and B. Carré, "Decolorization of process waters in deinking mills and similar applications: A review," *BioResources*, vol. 7, no. 1, pp. 1366–1382, 2012.
- [25] L.-J. Thénard, "Observations sur des combinaisons nouvelles entre l'oxygène et divers acides," *Annales de Chimie et de Physique*, vol. 8, pp. 306–313, 1818.
- [26] J. M. Campos-Martin, G. Blanco-Brieva, and J. L. G. Fierro, "Hydrogen peroxide synthesis: an outlook beyond the anthraquinone process," *Angewandte Chemie International Edition*, vol. 45, no. 42, pp. 6962–6984, Oct. 2006.
- [27] S. H. Zeronian and M. K. Inglesby, "Bleaching of cellulose by hydrogen peroxide," *Cellulose*, vol. 2, no. 4, pp. 265–272, Dec. 1995.
- [28] G. C. Hobbs and J. Abbot, "The role of the hydroxyl radical in peroxide bleaching processes," *Journal of Wood Chemistry and Technology*, vol. 14, no. 2, pp. 195–225, May 1994.
- [29] D. Behar, G. Czapski, J. Rabani, L. M. Dorfman, and H. A. Schwarz, "Acid dissociation constant and decay kinetics of the perhydroxyl radical," *The Journal of Physical Chemistry*, vol. 74, no. 17, pp. 3209–3213, 1970.
- [30] J. L. Colodette, S. Rothenberg, and C. W. Dence, "Factors affecting hydrogen peroxide stability in the brightening of mechanical and chemimechanical pulps. Part I. Hydrogen peroxide stability in the absence of stabilizing systems," *Journal of Pulp and Paper Science*, vol. 14, no. 6, pp. J126–J132, 1988.
- [31] S. Luňák and P. Sedlák, "Photoinitiated reactions of hydrogen peroxide in the liquid phase," *Journal of Photochemistry and Photobiology A: Chemistry*, vol. 68, no. 1, pp. 1–33, Aug. 1992.
- [32] A. F. Gilbert, E. Pavlovova, and W. H. Rapson, "Mechanism of magnesium retardation of cellulose degradation during oxygen bleaching," *Tappi Journal*, vol. 56, no. 6, pp. 95–99, Jun. 1973.
- [33] J. Defaye and A. Gadelle, "Magnesium salts in the alkaline-oxygen degradation of cellulose," *Pulp & Paper Canada*, vol. 75, no. 11, pp. 50–53, 1974.
- [34] J. R. Presley and R. T. Hill, "V 1: Peroxide bleaching of (chemi)mechanical pulps," in *Pulp bleaching : principles and practice*, Atlanta (Ga.): TAPPI Press, 1996, pp. 457–489.
- [35] J. Gierer, K. Jansbo, and T. Reitberger, "Formation of hydroxyl radicals from hydrogen peroxide and their effect on bleaching of mechanical pulps," *Journal of Wood Chemistry and Technology*, vol. 13, no. 4, pp. 561–581, Dec. 1993.
- [36] S. Omori and C. W. Dence, "The reactions of alkaline hydrogen peroxide with lignin model dimers: Part 1: Phenacyl α -aryl ethers," *Wood Science and Technology*, vol. 15, no. 1, pp. 67–79, 1981.
- [37] J. Gierer, "Chemistry of delignification: Part 2: Reactions of lignins during bleaching," *Wood Science and Technology*, vol. 20, no. 1, pp. 1–33, 1986.
- [38] J. Gierer, "Basic principles of bleaching. Part 2. Anionic processes," *Holzforschung*, vol. 44, no. 6, pp. 395–400, 1990.

- [39] J. Gierer, "Basic principles of bleaching. Part 1: Cationic and radical processes," *Holzforschung*, vol. 44, no. 5, pp. 387–94, 1990.
- [40] J. Gierer, E. Yang, and T. Reitberger, "The reactions of chromophores of the stilbene type with hydroxyl radical (HO·) and superoxide radical (O₂⁻/HO₂·). Part I. The cleavage of the conjugated double bond," *Holzforschung*, vol. 50, no. 4, pp. 342–352, Jan. 1996.
- [41] J. Gierer, E. Yang, and T. Reitberger, "The reactions of chromophores of the stilbene type with hydroxyl radical (HO·) and superoxide radical (O₂⁻/HO₂·). Part II. Reactions other than cleavage of the conjugated double bond," *Holzforschung*, vol. 50, no. 4, pp. 353–359, Jan. 1996.
- [42] J. Gierer, "Formation and involvement of superoxide (O₂⁻/HO₂·) and hydroxyl (OH·) radicals in TCF Bleaching Processes: A Review," *Holzforschung*, vol. 51, no. 1, pp. 34–46, Jan. 1997.
- [43] J. Bouchard, J. Wang, and R. Berry, "The role of hydroxyl and oxyl anion radicals in selectivity of oxygen delignification," *Holzforschung*, vol. 64, no. 2, pp. 153–159, Feb. 2010.
- [44] D. N. S. Hon and N. Shiraishi, *Wood and cellulosic chemistry*. New York: M. Dekker, 1991.
- [45] C. Chirat and D. Lachenal, "Effect of hydroxyl radicals on cellulose and pulp and their occurrence during ozone bleaching," *Holzforschung*, vol. 51, no. 2, pp. 147–154, Jan. 1997.
- [46] D. F. Guay, B. J. W. Cole, R. C. Fort Jr, J. M. Genco, and M. C. Hausman, "Mechanisms of oxidative degradation of carbohydrates during oxygen delignification. Part I. Reaction of methyl β-D-glucopyranoside with photochemically generated hydroxyl radicals," *Journal of Wood Chemistry and Technology*, vol. 20, no. 4, pp. 375–394, 2000.
- [47] D. F. Guay, B. J. W. Cole, R. C. Fort Jr, M. C. Hausman, J. M. Genco, T. J. Elder, and K. R. Overly, "Mechanisms of oxidative degradation of carbohydrates during oxygen delignification. Part II. Reaction of photochemically generated hydroxyl radicals with methyl β-cellobioside," *Journal of wood chemistry and technology*, vol. 21, no. 1, pp. 67–79, 2001.
- [48] D. F. Guay, B. J. W. Cole, R. C. Fort Jr., M. C. Hausman, J. M. Genco, and T. J. Elder, "Mechanisms of oxidative degradation of carbohydrates during oxygen delignification. Part III. Reaction of photochemically generated hydroxyl radicals with 1,5-anhydrocellobitol and cellulose.," *J. Pulp Pap. Sci.*, vol. 28, no. 7, pp. 217–221, 2002.
- [49] M. Ek, J. Gierer, K. Jansbo, and T. Reitberger, "Study on the selectivity of bleaching with oxygen-containing species," *Holzforschung*, vol. 43, no. 6, pp. 391–396, Jan. 1989.
- [50] C. W. Dence, "III 3: Chemistry of chemical pulp bleaching," in *Pulp bleaching : principles and practice*, Atlanta (Ga.): TAPPI Press, 1996, pp. 125–159.
- [51] J. Gierer, "The interplay between oxygen-derived radical species in the delignification during oxygen and hydrogen peroxide bleaching," in *Lignin: Historical, Biological, and Materials Perspectives*, vol. 742, W. G. Glasser, R. A. Northey, and T. P. Schultz, Eds. Washington, DC: American Chemical Society, 1999, pp. 422–446.
- [52] "CEPI Key Statistics 2014," Jun. 2015.
- [53] H.-J. Putz, "Chapter 3: Collection systems, sources, and sorting of recovered paper," in *Recycled fiber and deinking*, Helsinki: Fapet Oy, 2000, pp. 47–59.
- [54] "Paper Recycling - ERPC's Monitoring Report 2013," European Recovered Paper Council, Brussels, 2014.

- [55] COPACEL, "Rapport statistique 2014 de l'industrie papetière française," Jul. 2015.
- [56] E. D. Clark, *Les fibres secondaires*. Cégep De Trois-Rivières.
- [57] J. Poncet, "L'observatoire des prix," *PAP'ARGUS*, no. 314, pp. 12–20, Jun. 2015.
- [58] European Committee for Standardization, *EN 643:2014 - Paper and board - European list of standard grades of paper and board for recycling*. 2014.
- [59] "RISI - Pulp and Paper - Price Watch (Global)," Jul. 2015.
- [60] R. C. Howard, "The effects of recycling on paper quality," *Paper Technology (Bury, United Kingdom)*, vol. 32, no. 4, pp. 20–25, 1991.
- [61] R. C. Howard and W. Bichard, "The basic effects of recycling on pulp properties," *Journal of Pulp and Paper Science*, vol. 18, no. 4, pp. J151–J159, Jul. 1992.
- [62] M. M. Nazhad and L. Paszner, "Fundamentals of strength loss in recycled paper," *Tappi Journal*, vol. 77, no. 9, pp. 171–179, 1994.
- [63] M. M. Nazhad, "Recycled Fiber Quality- A Review," *J. Ind. Eng. Chem.*, vol. 11, no. 3, pp. 314–329, 2005.
- [64] C. R. Bury, "Auxochromes and resonance," *Journal of the American Chemical Society*, vol. 57, no. 11, pp. 2115–2117, 1935.
- [65] R. Alén, "Papermaking additives," in *Papermaking Chemistry*, 2nd ed., Helsinki: Fapet Oy, 2007.
- [66] M. Muguet and M. Sundar, "New ozone technology provides cost-effective secondary fiber bleaching," *Pulp and paper magazine*, vol. 70, no. 6, p. 77, Jun. 1996.
- [67] C. Daneault and C. Leduc, "Bleaching of mechanical pulp with formamidine sulfinic acid.," *Cellul. Chem. Technol.*, vol. 28, pp. 205–17, 1994.
- [68] C. Ackermann, L. Göttching, and H. Pakarinen, "Chapter 10: Papermaking potential of recycled fibers," in *Recycled fiber and deinking*, Helsinki: Fapet Oy, 2000, pp. 359–438.
- [69] EcoPaperLoop, "III - Guideline Document: Recommendations on collection strategies," in *EcoPaperLoop Project - Optimising Paper Products, Packaging and Collection Systems*, 2014, p. 34.
- [70] R. C. Eckert, "Delignification and bleaching process and solution for lignocellulosic pulp with peroxide in the presence of metal additives," CA1129161 A1, 10-Aug-1982.
- [71] V. Kubelka, R. C. Francis, and C. W. Dence, "Delignification with acidic hydrogen peroxide activated by molybdate," *Journal of Pulp and Paper Science*, vol. 18, no. 3, pp. J108–J114, 1992.
- [72] M. A. Bandeira Azevedo, V. M. Duarte Pasa, H. Hämäläinen, A. H. Munteer, R. C. de Oliveira, and J. L. Colodette, "ECF bleaching with molybdenum activated acid peroxide and its impact on eucalyptus pulp properties and effluent quality," *Natural Resources*, vol. 2, no. 1, pp. 61–70, 2011.
- [73] J. Jakara, A. Paren, and J. Patola, "Peroxide activation - a key to high brightness in TCF bleaching of softwood kraft pulp," in *Proceedings of the 8th International Symposium on Wood Pulping Chemistry*, Helsinki, 1995, vol. 1, pp. 377–382.
- [74] H. Hamalainen, A. Paren, J. Jakara, B. Brogdon, and T. Fant, "Mill-scale application of a molybdate-activated peroxide delignification process in ECF and TCF production of softwood and

hardwood kraft pulps," presented at the TAPPI Fall Technical Conference: Engineering, Pulping & PCE&I, Chicago, 2003, pp. 468–473.

[75] H. Lange, S. Decina, and C. Crestini, "Oxidative upgrade of lignin – Recent routes reviewed," *European Polymer Journal*, vol. 49, no. 6, pp. 1151–1173, Jun. 2013.

[76] J. J. Bozell, T. Elder, B. Biannic, D. Cedeno, S. Chatterjee, K. Cheng, and C. Njiojob, "Catalysis for conversion of biorefinery lignin to high value chemicals - structural and computational analysis for improved catalyst design," in *ISWFPC 2015 Proceedings*, Vienna, 2015, vol. 1, pp. 66–68.

[77] D. V. Evtuguin, C. Pascoal Neto, and J. D. Pedrosa de Jesus, "Bleaching of kraft pulp by oxygen in the presence of polyoxometalates," *Journal of Pulp and Paper Science*, vol. 24, no. 4, pp. 133–140, 1998.

[78] M. L. Bianchi, R. Crisol, and U. Schuchardt, "Bleaching of commercial pulps with H₂O₂ catalyzed by heteropolyacids," *Bioresource Technology*, vol. 68, no. 1, pp. 17–21, Apr. 1999.

[79] R. Patt and H. J. Mielisch, "Application of a catalyst in TCF pulp bleaching," in *Proceedings*, Curitiba, 1997, vol. 6, pp. 44–58.

[80] H. J. Mielisch, O. Kordsachia, and R. Patt, "Catalyzed hydrogen peroxide bleaching," *Papier*, vol. 50, no. 10A, pp. V13–V23, 1996.

[81] Y. Cui, C.-L. Chen, J. S. Gratzl, and R. Patt, "A Mn(IV)-Me₄DTNE complex catalyzed oxidation of lignin model compounds with hydrogen peroxide," *Journal of Molecular Catalysis A: Chemical*, vol. 144, no. 3, pp. 411–417, Aug. 1999.

[82] J. Odermatt, O. Kordsachia, R. Patt, L. Kühne, C.-L. Chen, and J. S. Gratzl, "A manganese-based catalyst for alkaline peroxide bleaching," in *Oxidative Delignification Chemistry*, vol. 785, D. S. Argyropoulos, Ed. Washington, DC: American Chemical Society, 2001, pp. 235–254.

[83] T. J. Collins, "TAML oxidant activators: a new approach to the activation of hydrogen peroxide for environmentally significant problems," *Accounts of Chemical Research*, vol. 35, no. 9, pp. 782–790, Sep. 2002.

[84] B. Hammer, H. Michaud, and S. Weiss, "Process for bleaching and delignifying cellulose-containing products," US5034096 A, 23-Jul-1991.

[85] W. Sturm, "Process for the chlorine-free bleaching and delignification of cellulose," CA2036173 C, 23-Jan-1996.

[86] J. F. Kadla, H. Chang, C. L. Chen, and J. S. Gratzl, "Reactions of lignin with cyanamide activated hydrogen peroxide. Part 1. The degradation of lignin model compounds," *Holzforschung*, vol. 52, no. 5, pp. 506–512, Jan. 1998.

[87] J. F. Kadla, H. Chang, C. L. Chen, and J. S. Gratzl, "Reactions of lignin with cyanamide activated hydrogen peroxide. Part 2. The degradation mechanism of phenolic lignin model compounds," *Holzforschung*, vol. 52, no. 5, pp. 513–520, Jan. 1998.

[88] J. Chen, "Process for delignification and bleaching of chemical wood pulps with hydrogen peroxide and a dicyandiamide activator," US5620563 A, 15-Apr-1997.

[89] C. Coucharriere, "Mise au point et étude d'un système d'activation du peroxyde d'hydrogène en délignification et blanchiment des pâtes chimiques.," PhD thesis, University of Grenoble, France, 2000.

- [90] B. Coles, N. Turner, A. Mathews, C. Baum, and I. Chadwick, "Recycled Fibre Bleaching," WO2003048450 A1, 12-Jun-2003.
- [91] D. S. Argyropoulos, M. Suchy, and L. Akim, "Nitrogen-Centered Activators of Peroxide-Reinforced Oxygen Delignification," *Industrial & Engineering Chemistry Research*, vol. 43, no. 5, pp. 1200–1205, Mar. 2004.
- [92] M. Halma, D. Lachenal, N. Marlin, A. Deronzier, M. C. Brochier, and M. Zarubin, "H₂O₂ oxidation of lignin model dimers catalyzed by copper(II)-phenanthroline," *Industrial Crops and Products*, vol. 74, pp. 514–522, Nov. 2015.
- [93] H. Korpi, P. J. Figiel, E. Lankinen, P. Ryan, M. Leskelä, and T. Repo, "On in situ prepared Cu-Phenanthroline complexes in aqueous alkaline solutions and their use in the catalytic oxidation of veratryl alcohol," *European Journal of Inorganic Chemistry*, vol. 2007, no. 17, pp. 2465–2471, Jun. 2007.
- [94] N. Marlin, C. Coucharriere, G. Mortha, D. Lachenal, P. Larnicol, and J. C. Hostachy, "Use of o-phenanthroline as a catalyst in hydrogen peroxide stages," in *Proceedings of the 13th International Symposium on Wood Fibre and Pulp Chemistry*, Auckland, New Zealand, 2005, pp. 29–34.
- [95] N. Marlin, J. Fernandes, and N. Benattar, "New ways to improve color-stripping of deinked pulps and dyed effluents," in *Proceedings of the 14th International Symposium on Wood Fibre and Pulp Chemistry*, Durban, South Africa, 2007.
- [96] F. Blau, "Über neue organische Metallverbindungen," *Monatshefte für Chemie und verwandte Teile anderer Wissenschaften*, vol. 19, no. 1, pp. 647–689, 1898.
- [97] D. S. Sigman, D. R. Graham, V. D'Aurora, and A. M. Stern, "Oxygen-dependent cleavage of DNA by the 1,10-phenanthroline cuprous complex. Inhibition of Escherichia coli DNA polymerase I," *J. Biol. Chem.*, vol. 254, no. 24, pp. 12269–12272, Dec. 1979.
- [98] D. S. Sigman, "Nuclease activity of 1,10-phenanthroline-copper ion," *Accounts of Chemical Research*, vol. 19, no. 6, pp. 180–186, Jun. 1986.
- [99] T. B. Thederahn, M. D. Kuwabara, T. A. Larsen, and D. S. Sigman, "Nuclease activity of 1,10-phenanthroline-copper: kinetic mechanism," *Journal of the American Chemical Society*, vol. 111, no. 13, pp. 4941–4946, Jun. 1989.
- [100] T. Oyoshi and H. Sugiyama, "Mechanism of DNA Strand Scission Induced by (1,10-Phenanthroline)copper Complex: Major Direct DNA Cleavage Is Not through 1',2'-Dehydronucleotide Intermediate nor β -Elimination of Forming Ribonolactone," *Journal of the American Chemical Society*, vol. 122, no. 26, pp. 6313–6314, Jul. 2000.
- [101] M. Chikira, Y. Tomizawa, D. Fukita, T. Sugizaki, N. Sugawara, T. Yamazaki, A. Sasano, H. Shindo, M. Palaniandavar, and W. E. Antholine, "DNA-fiber EPR study of the orientation of Cu(II) complexes of 1,10-phenanthroline and its derivatives bound to DNA: mono(phenanthroline)-copper(II) and its ternary complexes with amino acids," *Journal of Inorganic Biochemistry*, vol. 89, no. 3–4, pp. 163–173, Apr. 2002.
- [102] L.-P. Lu, M.-L. Zhu, and P. Yang, "Crystal structure and nuclease activity of mono(1,10-phenanthroline) copper complex," *Journal of Inorganic Biochemistry*, vol. 95, no. 1, pp. 31–36, May 2003.

- [103] C. Liu, J. Zhou, Q. Li, L. Wang, Z. Liao, and H. Xu, "DNA damage by copper(II) complexes: coordination-structural dependence of reactivities," *Journal of Inorganic Biochemistry*, vol. 75, no. 3, pp. 233–240, Jun. 1999.
- [104] D. S. Sigman, A. Mazumder, and D. M. Perrin, "Chemical nucleases," *Chemical Reviews*, vol. 93, no. 6, pp. 2295–2316, 1993.
- [105] F. Dimiza, S. Fountoulaki, A. N. Papadopoulos, C. A. Kontogiorgis, V. Tangoulis, C. P. Raptopoulou, V. Psycharis, A. Terzis, D. P. Kessissoglou, and G. Psomas, "Non-steroidal antiinflammatory drug–copper(ii) complexes: Structure and biological perspectives," *Dalton Transactions*, vol. 40, no. 34, p. 8555, 2011.
- [106] D. Sanna, P. Buglyó, A. I. Tomaz, J. C. Pessoa, S. Borović, G. Micera, and E. Garribba, "VIVO and CuII complexation by ligands based on pyridine nitrogen donors," *Dalton Transactions*, vol. 41, no. 41, p. 12824, 2012.
- [107] A. Kellett, M. McCann, O. Howe, M. O'Connor, and M. Devereux, "DNA cleavage reactions of the dinuclear chemotherapeutic agent copper(II) bis-1,10-phenanthroline terephthalate," *Int. Journal of Clinical Pharmacology and Therapeutics*, vol. 50, no. 01, pp. 79–81, Jan. 2012.
- [108] A. Kellett, M. O'Connor, M. McCann, M. McNamara, P. Lynch, G. Rosair, V. McKee, B. Creaven, M. Walsh, S. McClean, A. Foltyn, D. O'Shea, O. Howe, and M. Devereux, "Bis-phenanthroline copper(ii) phthalate complexes are potent in vitro antitumour agents with 'self-activating' metallo-nuclease and DNA binding properties," *Dalton Trans.*, vol. 40, no. 5, pp. 1024–1027, 2011.
- [109] M. Devereux, D. O Shea, A. Kellett, M. McCann, M. Walsh, D. Egan, C. Deegan, K. Kędziora, G. Rosair, and H. Müller-Bunz, "Synthesis, X-ray crystal structures and biomimetic and anticancer activities of novel copper(II)benzoate complexes incorporating 2-(4'-thiazolyl)benzimidazole (thiabenzazole), 2-(2-pyridyl)benzimidazole and 1,10-phenanthroline as chelating nitrogen donor ligands," *Journal of Inorganic Biochemistry*, vol. 101, no. 6, pp. 881–892, Jun. 2007.
- [110] A. Prisecaru, V. McKee, O. Howe, G. Rochford, M. McCann, J. Colleran, M. Pour, N. Barron, N. Gathergood, and A. Kellett, "Regulating Bioactivity of Cu²⁺ Bis-1,10-phenanthroline Artificial Metallonucleases with Sterically Functionalized Pendant Carboxylates," *Journal of Medicinal Chemistry*, vol. 56, no. 21, pp. 8599–8615, Nov. 2013.
- [111] S. Bianco, C. Musetti, A. P. Krapcho, M. Palumbo, and C. Sissi, "Ni²⁺ and Cu²⁺ complexes of a phenanthroline-based ligand bind to G-quadruplexes at non-overlapping sites," *Chemical Communications*, vol. 49, no. 73, p. 8057, 2013.
- [112] C. Musetti, L. Lucatello, S. Bianco, A. P. Krapcho, S. A. Cadamuro, M. Palumbo, and C. Sissi, "Metal ion-mediated assembly of effective phenanthroline-based G-quadruplex ligands," *Dalton Transactions*, no. 19, p. 3657, 2009.
- [113] J. Lakshmipraba, S. Arunachalam, A. Riyasdeen, R. Dhivya, S. Vignesh, M. A. Akbarsha, and R. A. James, "DNA/RNA binding and anticancer/antimicrobial activities of polymer–copper(II) complexes," *Spectrochimica Acta Part A: Molecular and Biomolecular Spectroscopy*, vol. 109, pp. 23–31, May 2013.
- [114] W. K. Pogozelski and T. D. Tullius, "Oxidative Strand Scission of Nucleic Acids: Routes Initiated by Hydrogen Abstraction from the Sugar Moiety," *Chemical Reviews*, vol. 98, no. 3, pp. 1089–1108, May 1998.

- [115] E. Walger, C. Rivollier, N. Marlin, and G. Mortha, "Activated hydrogen peroxide decolorization of a model azo dye-colored pulp," *Holzforschung*, vol. 69, no. 6, pp. 677–683, 2015.
- [116] C. A. Flemming and J. T. Trevors, "Copper toxicity and chemistry in the environment: a review," *Water Air Soil Pollut*, vol. 44, no. 1–2, pp. 143–158, Mar. 1989.
- [117] P. Patnaik, *Handbook of inorganic chemicals*, McGraw Hill, 2003.
- [118] B. J. Hathaway, "A new look at the stereochemistry and electronic properties of complexes of the copper (II) ion," in *Complex Chemistry*, Springer, 1984, pp. 55–118.
- [119] D. D. Perrin, *Constantes de dissociation des acides et des bases inorganiques en solution aqueuse: Dissociation constants of inorganic acids and bases in aqueous solution*. London: Butterworths, 1969.
- [120] H. W. Richardson, *Handbook of Copper Compounds and Applications*. CRC Press, 1997.
- [121] G. H. Walden, L. P. Hammett, and R. P. Chapman, "A reversible oxidation indicator of high potential especially adapted to oxidimetric titrations," *Journal of the American Chemical Society*, vol. 53, no. 10, pp. 3908–3908, 1931.
- [122] G. F. Smith and C. A. Getz, "The improved synthesis of o-phenanthroline.," *Chem. Rev.*, vol. 16, no. 1, pp. 113–120, Feb. 1935.
- [123] Knueppel, Chr. A., "Improvement of Skraup's quinoline synthesis," *Berichte der Deutschen Chemischen Gesellschaft*, vol. 29, pp. 703–9, 1896.
- [124] M. A. Rizvi, N. Teshima, and G. M. Peerzada, "1,10-phenanthroline modulated redox potentials explored for benign iron speciation analysis," *Croatica Chemica Acta*, vol. 86, no. 3, pp. 345–350, 2013.
- [125] P. Pfeiffer and F. Tappermann, "Dipyridyl- and phenanthroline-containing complex salts of bivalent metals," *Z. Anorg. Chem.*, vol. 215, pp. 273–287, 1933.
- [126] J. Hoste, "On a new copper specific group," *Analytica Chimica Acta*, vol. 4, pp. 23–37, Feb. 1950.
- [127] M. A. Oladipo, O. A. Olayiwola, and D. O. Adeoye, "Synthesis, characterization and antibacterial studies of some copper (II) complexes of 2,2'-bipyridine and 1,10-phenanthroline.," *J. Chem. Pharm. Res.*, vol. 5, no. 8, pp. 69–73, 2013.
- [128] N. Anitha, R. Balamurugan, and M. Palaniandavar, "Spectral and electrochemical studies of bis(diimine)copper(II) complexes in anionic, cationic and nonionic micelles," *Journal of Colloid and Interface Science*, vol. 362, no. 2, pp. 243–252, Oct. 2011.
- [129] E. Garribba, G. Micera, D. Sanna, and L. Strinna-Erre, "The Cu(II)-2,2'-bipyridine system revisited," *Inorganica Chimica Acta*, vol. 299, no. 2, pp. 253–261, Mar. 2000.
- [130] J. Zhou, M. Wang, Y. Huo, Y. Wang, H. Yang, K. Zhong, and S. Zhang, "Synthesis, crystal structures, and magnetic properties of two supramolecular coordination complexes constructed by sulfonate groups," *Journal of Coordination Chemistry*, vol. 66, no. 5, pp. 772–779, Mar. 2013.
- [131] H. Korpi, "Copper di-imine complexes: Structures and catalytic activity in the oxidation of alcohols by dioxygen," PhD thesis, University of Helsinki, 2005.

- [132] T. Elder and A. Rudie, "Computational study of copper-phenanthrolines as pulping catalysts," in *ISWFPC 2015 Proceedings*, Vienna, 2015, vol. 1, pp. 136–137.
- [133] B. Gueneau, N. Marlin, A. Deronzier, and D. Lachenal, "Pulp delignification with oxygen and copper(II)-polyimine complexes," *Holzforschung*, vol. 68, no. 4, Jan. 2014.
- [134] A. Ringbom, *Les complexes en chimie analytique: comment choisir rationnellement les meilleures méthodes d'analyse complexométrique*. Paris: Dunod, 1967.
- [135] A. A. Schilt, *Analytical applications of 1,10-phenanthroline and related compounds*, 1st ed., vol. 32. Oxford London Edinburgh: Pergamon Press, 1969.
- [136] W. A. E. McBryde, *A Critical review of equilibrium data for proton and metal complexes of 1,10-phenanthroline, 2,2'-bipyridyl and related compounds*. Oxford New York Toronto Rushcutters Bay Paris Kronberg-Taunus: Pergamon press, 1978.
- [137] R. M. Smith and A. E. Martell, *Critical stability constants*. New York London: Plenum Press, 1975.
- [138] L. Alderighi, P. Gans, A. Ienco, D. Peters, A. Sabatini, and A. Vacca, "Hyperquad simulation and speciation (HySS): a utility program for the investigation of equilibria involving soluble and partially soluble species," *Coordination Chemistry Reviews*, vol. 184, no. 1, pp. 311–318, Apr. 1999.
- [139] S. A. Onokhin, E. I. Germer, and Y. G. Butko, "Method of preparing cellulose pulp semifinished product," SU910897 (A1), 07-Mar-1982.
- [140] E. I. Germer, "pH effect on the catalysis of oxygen-alkaline delignification by 1,10-phenanthroline," in *Ligno-Cellul. [Cellucon 90]*, 1992, pp. 371–83.
- [141] E. I. Germer, "Catalysis of the oxygen-alkaline wood delignifications: conditions and ways of its realization," presented at the 8th International Symposium on Wood and Pulping Chemistry, Helsinki, 1995.
- [142] E. I. Germer, "Chemistry and mechanism of catalysis of oxygen-alkaline delignification by some complex compounds," presented at the 5th European Workshop on Lignocellulosics and Pulp, Aveiro, 1998, pp. 33–38.
- [143] H. Korpi, P. Lahtinen, V. Sippola, O. Krause, M. Leskelä, and T. Repo, "An efficient method to investigate metal-ligand combinations for oxygen bleaching," *Applied Catalysis A: General*, vol. 268, no. 1–2, pp. 199–206, Aug. 2004.
- [144] P. Lahtinen, H. Korpi, E. Haavisto, M. Leskelä, and T. Repo, "Parallel screening of homogeneous copper catalysts for the oxidation of benzylic alcohols with molecular oxygen in aqueous solutions," *Journal of Combinatorial Chemistry*, vol. 6, no. 6, pp. 967–973, Nov. 2004.
- [145] V. O. Sippola and A. O. I. Krause, "Bis(o-phenanthroline)copper-catalysed oxidation of lignin model compounds for oxygen bleaching of pulp," *Catalysis Today*, vol. 100, no. 3–4, pp. 237–242, Feb. 2005.
- [146] L. Ma, Q. Zhang, L. Cheng, Z. Wu, and J. Yang, "DFT studies on the mechanism of veratryl alcohol oxidation catalyzed by Cu-phen complexes," *RSC Advances*, vol. 4, no. 58, p. 30558, Jun. 2014.

- [147] N. I. Vladut, V. Durrieu, J. Albet, J. Blanc, C. Calais, and G. Mortha, "Novel investigations on hydrogen peroxide bleaching catalysis by copper-phenanthroline complex," in *Proceedings*, Tianjin, China, 2011, vol. 2, pp. 715–720.
- [148] L. Cabanne, P. Larnicol, and C. Coucharriere, "Hydrogen peroxide activation in delignification and bleaching of wood pulp using a phenanthroline-copper complex," WO03080925 (A2), 02-Oct-2003.
- [149] J. Blanc, C. Calais, and J. L. Dubois, "Process for delignification and bleaching of paper pulp using activated hydrogen peroxide," WO2012028800 (A1), 29-Jun-2012.
- [150] H. Korpi, V. Sippola, I. Filpponen, J. Sipilä, O. Krause, M. Leskelä, and T. Repo, "Copper-2,2'-bipyridines: Catalytic performance and structures in aqueous alkaline solutions," *Applied Catalysis A: General*, vol. 302, no. 2, pp. 250–256, Apr. 2006.
- [151] J. F. Perez-Benito, "Reaction pathways in the decomposition of hydrogen peroxide catalyzed by copper(II)," *Journal of Inorganic Biochemistry*, vol. 98, no. 3, pp. 430–438, Mar. 2004.
- [152] P. E. Sharpe and R. W. Lowe, "The bleaching of colored recycled fibers," in *Proceedings of the 1993 Pulping Conference*, Boston, 1993, vol. 3, pp. 1205–1217.

II. MATERIALS AND METHODS

TABLE OF CONTENTS

LIST OF FIGURES	73
LIST OF TABLES	74
LIST OF EQUATIONS.....	74
II.1 RAW MATERIALS.....	75
<i>II.1.1 Dyes and other chemicals.....</i>	75
<i>II.1.2 Copper-phenanthroline complexes</i>	75
<i>II.1.3 Bleached kraft pulp</i>	75
<i>II.1.4 Dyed pulp</i>	75
II.2 METHODS	76
<i>II.2.1 To characterize the dyes</i>	76
II.2.1.1 UV-visible spectroscopy.....	76
II.2.1.2 HPLC.....	76
II.2.1.3 FTIR spectroscopy.....	78
II.2.1.4 NMR spectroscopy	78
II.2.1.4.i General principle of NMR spectroscopy	79
II.2.1.4.ii Principle of ¹³ C NMR.....	80
II.2.1.4.iii Conditions of analysis.....	81
II.2.1.5 Elemental analysis.....	82
<i>II.2.2 To characterize the copper-phenanthroline complex</i>	82
II.2.2.1 UV-visible analysis	82
II.2.2.2 EPR spectroscopic analysis	82
II.2.2.2.i General principle of EPR spectroscopy.....	82
II.2.2.2.ii EPR spectroscopy for copper complexation study	84
II.2.2.2.iii Conditions of copper complexation analysis.....	84
II.2.2.3 Speciation calculation (PHREEQC simulations).....	85
<i>II.2.3 To characterize the pulps</i>	85
II.2.3.1 Optical characterization.....	85
II.2.3.2 Physico-chemical characterization	87
II.2.3.3 Physical characterization	88
<i>II.2.4 To characterize dye solutions</i>	88
II.2.4.1 UV-vis spectroscopy	88
II.2.4.2 Electrospray Ionization-Mass Spectrometry	89

<i>II.2.5 To follow the formation of radicals</i>	89
II.2.5.1 Chemiluminescence method.....	89
II.2.5.1.i Principle.....	89
II.2.5.1.ii Analysis conditions	90
II.2.5.2 UV-vis method using DMNA.....	90
II.2.5.3 EPR/spin-trapping method.....	91
II.2.5.3.i Principle.....	91
II.2.5.3.ii Analysis conditions	93
II.2.5.3.iii Result analysis: integration and simulations	94
II.3 CU-PHEN-ACTIVATED H ₂ O ₂ TREATMENTS.....	95
<i>II.3.1 Preparation of the complex</i>	95
<i>II.3.2 Pulp bleaching or color-stripping</i>	95
<i>II.3.3 Dye solution color-stripping</i>	96
II.4 REFERENCES	96

LIST OF FIGURES

Figure II-1. Scheme of the energy transition which leads to an EPR signal in the case of one unpaired electron	83
Figure II-2. Typical signal of a Cu(II) compound [7]	84
Figure II-3. Representation of the CIE L*a*b* color space at three different L* levels. Source: www.fulviiovilla.com/category/tutorial/	86
Figure II-4. Scheme representing the principle of DRI calculation. R ₁ is the distance from P ₁ to perfect white and R ₂ is the distance from P ₂ to the perfect white, the “color removal” is calculated as R ₁ - R ₂	86
Figure II-5. Oxidation of luminol.....	90
Figure II-6. Reaction path revealing the hydroxylation of phtalhydrazide by chemiluminescence	90
Figure II-7. Molecular structure of DMNA (N,N-dimethyl-4-nitrosoaniline).....	91
Figure II-8. Hydroxylation of DMPO into DMPO-OH and typical DMPO-OH signal [19], [21], [22].....	92
Figure II-9. Typical DMPO-OH signal [19]	92
Figure II-10. Typical DMPO-CH ₃ signal [19] (a) and DMPO-COO ⁻ signal (simulated based on constants given by Buettner [22] (b).....	93

LIST OF TABLES

Table II-1. HPLC separation of dyes in the literature.....	77
Table II-2. HPLC conditions for the separation of the dye solutions with or without Cu-Phen complex by ion-pairing.....	78
Table II-3. NMR vs. EPR.....	83

LIST OF EQUATIONS

Equation II-1	83
Equation II-2	83
Equation II-3	87
Equation II-4	87
Equation II-5	87
Equation II-6	88
Equation II-7	93
Equation II-8	93
Equation II-9	95
Equation II-10	95
Equation II-11	96
Equation II-12	96
Equation II-13	96

II.1 RAW MATERIALS

II.1.1 Dyes and other chemicals

The dyes used to colorize the pulp were paper and textile dyes provided by Archroma (previously Clariant). The following data were given by the dye supplier. The red dye, giving a pink pulp, was DR81 (C.I. Direct Red 81), 16% w/w, 675.60 g/mol, and the yellow dye was DY11 (C.I. Direct Yellow 11), 23% w/w, 452.37 g/mol. The chemical composition of these commercial paper dyes was unknown as the dye producer was not authorized to divulgate the nature of possible additives. They will be referred to as DR81L and DY11L.

In the search for different dyes to perform this study, a pure powder (no additives) of DR81 was found: DR81S (50% w/w, Sigma Aldrich). Its exact composition was unknown and the purity of 50% had been calculated by the supplier after elemental analysis, considering that the product of DR81's synthesis was pure. This dye was not used to colorize the pulp but only to study the color-stripping reactions in the absence of fibers.

Apart from the dyes, commercial chemical products of analytical grade were used: NaOH (99%, Carl Roth), H₂O₂ (35%, Carl Roth), CuSO₄ · 5 H₂O (98.0%, Sigma Aldrich), 1,10-phenanthroline (99.0%, Acros Organics).

II.1.2 Copper-phenanthroline complexes

The copper-phenanthroline complex (also named "activator") was prepared using copper sulfate, CuSO₄ · 5 H₂O (98%, 249.69 g/mol, from Sigma-Aldrich) and 1,10-phenanthroline (99%, 180.21 g/mol, from Acros Organics). The complex was prepared in aqueous solution by dissolving phenanthroline and adding CuSO₄, using 1 to 3 moles of phenanthroline for 1 mole of CuSO₄. It will be referred to as Cu-Phen.

II.1.3 Bleached kraft pulp

Eucalyptus fibers were chosen to model cellulosic recovered fibers because of their low strength properties compared to softwood fibers. An ECF-bleached eucalyptus kraft pulp, provided by Fibria (Brasil), was thus used in this study. The initial properties of this pulp were: cellulose DP_v = 1191, ISO brightness = 89.2%, and CIE L*a*b* coordinates in the color system (L*, a*, b*) = (97.14 ± 0.08, -0.55 ± 0.01, 2.76 ± 0.05).

Elemental analysis of the pulp showed that it contained less than 1 ppm Cu, 2.8 ppm Fe and 0.6 ppm Mn.

This pulp was not beaten before use. Since the objective was to observe the impact of the oxidative system on the resistance of the fiber matrix, it was decided that studying homogeneous pulp batches was more important than producing a pulp that would be comparable to conventional paper pulps. Therefore, the strength properties of the pulp were quite low compared to usual. Indeed, beating – or refining – consists in treating the pulp mechanically to hydrate the fibers and to create fibrils, microfibrils, and fines, especially in order to improve its bonding properties.

II.1.4 Dyed pulp

The whole batch of pulp was mixed with the desired amount of dye without any fixative agent, at room temperature, 4% consistency, and within a contact time of 30 min. After dyeing, the fibers

II. Materials and methods

were centrifuged and stored in a big plastic bag, to homogenize the pulp's humidity before measuring its dryness.

In the preliminary trials, the pulp was dyed with 0.1% DY11L (commercial product) on odp, to get a standard color depth of 1/25, according to the supplier. Spectroscopic analysis of the draining water after filtration (results not shown) revealed that 65% of the dye was actually fixed to the fibers. The dyed pulp was designated as dBKP. Elemental analysis of the dBKP gave the following results: Cu = 3.7 ppm, Fe = 3.3 ppm, Mn < 0.50 ppm. Since almost no Cu was present in the BKP, most of the Cu element originated from the dye solution. Hence, the molar ratio Cu:dye in the dye solution was estimated to be 1:22.

Most of the pulp color-stripping trials were conducted on the pink pulp (dyed with DR81L). In the case of this pulp, the dye and complex charges applied were calculated in order to work with 1 mole of dye for 1.5 mole of complex, considering that 100% of the dye remained attached to the pulp (the red dye was not found in the draining water after dyeing) and that the dye purity given by the supplier (16% for DR81L) was right. For all the trials, 0.02% copper-phenanthroline complex on odp were used when the activator was present. Although it is well known that various complexes are present in a copper-phenanthroline solution, it was considered that 1 mole of Cu combines with 2 moles of Phen to form 1 mole of $[\text{Cu}(\text{Phen})_2]^{2+}$. This enables to calculate a theoretical molecular weight of the complex, which would be 423.966 g/mol. For 1 kg of pulp, the equivalent Cu-Phen charge would be 0.2 g, i.e. 472 μmol . The quantity of dye would thus be of 314.5 μmol . Knowing the concentration and molecular weight of the dye, 1.328 g of DR81L were added per kg of pulp.

A new batch of DY11L dyed pulp was also prepared using the same molar ratio, in order to make comparisons with results obtained on the DR81L-dyed pulp. With similar calculation, the dose of DY11L to be applied on the pulp was estimated at 0.0619% on odp.

II.2 METHODS

II.2.1 To characterize the dyes

II.2.1.1 UV-visible spectroscopy

UV-visible spectroscopy was used to study dye modifications (complexation, ionization, degradation) in aqueous solution. Since they are used to give color to paper or textile, dyes absorb in the visible range.

The absorbance spectra of the dye solutions were recorded from 200 to 800 nm on a Shimadzu UV-1800 UV-vis spectrophotometer, after the introduction of the sample to be analyzed in a quartz cell, at room temperature.

II.2.1.2 HPLC

HPLC (High Performance Liquid Chromatography) is often used to characterize or separate mixtures of chemicals. In the present work, it was first used to analyze the dye formulation since some additives are generally present to stabilize the dye. Moreover, HPLC was also used in an attempt to separate the dye components and the copper-phenanthroline complex after oxidation by the $\text{H}_2\text{O}_2/\text{Cu-Phen}$ system. Table II-1 below presents some HPLC conditions used to characterize DR81, DY11 or similar dyes in the literature. All these authors used C18 columns.

Table II-1. HPLC separation of dyes in the literature

Reference	Dye	Mobile phase	Modifier/ ion-pairing agent	λ (nm)	Flow rate (mL/ min)	t_R (min)	Remarks
Sahasrabudhe <i>et al.</i> 2014 [1]	DR81	MeOH	n/a	511	/	1.71	Detection of degradation products
Wegener <i>et al.</i> 1987 [2]	DR81	MeOH: H ₂ O gradient elution	TBA (tetrabutylammonium) 5 mM in the MeOH phase (adjusted to pH 7)	/	1.0	/	Injection volume: 10 μ L
Chen <i>et al.</i> 1998 [3]	Various sulfonated azo dyes	MeOH	Ammonium acetate 0.05 M in MeOH (electrolyte)	254	0.9	/	Electrolyte: for a better separation of ionizable species
Ansorgova <i>et al.</i> 2003 [4]	Various sulfonated azo dyes	MeOH: H ₂ O isocratic mode	TEEA (triethylammonium acetate) 2.5 mM in both MeOH and H ₂ O phases	254	1.0	3.3 to 13.0	HPLC/ESI- MS with gradient elution
Van Bommel <i>et al.</i> 2007 [5]	Various dyes, including 2 direct dyes: DY4; DR28	2 gradient methods with MeOH and H ₂ O	(1) phosphoric acid (5% in water, 0 to 10% of the total mobile phase concentration (v/v) or (2) TBA 5 mM in the whole mobile phase	/	0.2	(1) DY4: 21 min DR28: 29 min (2) DY4: 21 min DR28: 22 min	65 dyes tested
Kagalkar <i>et al.</i> 2009 [6]	DR81	MeOH:ACN gradient (75:25)	n/a	254	1.0	10 min	/

The first separation trials were conducted using water/acetonitrile gradients. Unfortunately, the phenanthroline molecule was not correctly separated and identified in the HPLC diagrams. Other analysis conditions were then tested using TBA in water/methanol mobile phase as proposed in the literature for the study of dye formulations (see Wegener *et al.* and Van Bommel *et al.*, second and fifth references in Table II-1). TBA is an ion-pair reagent (also called a modifier) which allows to improve the quality of HPLC with reversed-phase columns such as C18 silica columns, and to avoid peak tailing with molecules such as our dyes and phenanthroline (containing nitrogen). TBA coordinates with the sulfonic groups of the dyes to form an electrically neutral ion-pair, which is

II. Materials and methods

retained by the column. Wegener and collaborators [2] separated DR81, using a methanol/water mobile phase with TBA 0.005 M in methanol, on gradient mode, with a C18 column. More recently, Van Bommel *et al.* [5] used TBA in a methanol-water mobile phase and a C18 column to analyze numerous dyes including DY4 and DR28, also on gradient mode.

The preparation of the mobile phase was done as follows: 250 mL of an equimolar solution of tetrabutylammonium (TBA-OH) and potassium hydroxide (KOH) 50 mM was prepared and adjusted to pH 7 with phosphoric acid. The chemicals were: TBA-OH, 30 H₂O: 799.93 g/mol, 98%; KOH: 56.11 g/mol, 90%; phosphoric acid 10%; ultrapure water. 10.20 g of TBA-OH, 30 H₂O (12.5 mmol) were dissolved into 100 mL of ultrapure water. 779 mg of KOH (12.5 mmol) were dissolved into 80 mL of water and introduced in the TBA solution. The pH was adjusted (acidification) with phosphoric acid and the total volume was adjusted to 250 mL.

Two solutions were prepared for the mobile phase:

- A – 100 mL TBA 50 mM + 900 mL ultrapure water → TBA 5 mM in water
- B – 100 mL TBA 50 mM + 900 mL HPLC-grade methanol → TBA 5 mM in methanol:water (90:10 v/v)

The chosen HPLC conditions are listed in Table II-2.

Table II-2. HPLC conditions for the separation of the dye solutions with or without Cu-Phen complex by ion-pairing

Dye (mM)	phase A	phase B	Injection volume (μL)	Flow rate (mL/min)	λ (nm)	Column	mode	A:B
0.5	TBA-OH 5 mM in water	TBA-OH 5 mM in methanol:water = 90:10 (v/v) buffered pH 7	20	0.7	254	Reverse-phase C18 Hypersil ODS (250 x 4.6 mm, 5μ)	isocratic	50:50

II.2.1.3 FTIR spectroscopy

Fourier Transform Infra-Red spectroscopy was used to analyze the commercial dyes. FTIR is based on the electric component interaction of the IR radiation with the molecule dipole moment. Each functional group has its specific vibrational signal characteristic of the chemical linkages. The analysis provides a FTIR spectrum giving only qualitative information on the structure of the studied molecule.

KBr pellets containing 1% w/w lyophilized or powdered dye were analyzed on a Perkin Elmer spectrum 65 spectrometer. The Fourier-Transformed Infrared (FTIR) spectra were collected with a resolution of 1 cm⁻¹ in the range of 4000-600 cm⁻¹.

II.2.1.4 NMR spectroscopy

¹H- and ¹³C-NMR were used to characterize the dyes and additives present in the commercial dye solutions: DR81L and DY11L.

To reach high dye concentrations, the commercial dye solutions were lyophilized. The resulting products had very different aspects: DY11L formed thin layers of dry “plasticized” dye, whereas DR81L was not as dry and had the aspect of a paste. 1 g of each resulting product was diluted in 4

mL D₂O. The corresponding pHs (measured in water at the same concentration) were 7.3 for DR81L and 8.6 for DY11L.

The principle of NMR spectroscopy and the methods used in this work are presented in a first part, before detailing the parameters used in this specific study.

II.2.1.4.i General principle of NMR spectroscopy

Nuclear magnetic resonance is one of the most commonly used tools for chemical structure analysis. NMR spectroscopy exploits the magnetic properties of certain atomic nuclei. Only spin-possessing atom nuclei are detected by NMR. The interaction energy of the nuclear magnetic moments ($\Sigma\mu_i$) of a substance with a magnetic field B is made of several characteristic discrete levels of energy (E_i). Using a high frequency emitter, transitions between these energy levels are induced, $\Delta E = h\nu$ where $\nu = \gamma \cdot B_0$, γ being the gyromagnetic factor of the particle, characteristic of each nucleus. The resulting energy absorption is recorded as a spectral line or **nuclear magnetic resonance spectrum** (NMR signal). Only atoms having a magnetic moment can give magnetic resonance, among them the proton ¹H, fluorine ¹⁹F, nitrogen isotopes ¹⁴N and ¹⁵N, phosphorus ³¹P. Hence, carbon ¹²C, one of the most abundant elements in organic compounds, as well as nuclei having even mass and atomic number (i.e. having no magnetic moment), does not give any resonance signal. This is why the NMR signal of C is limited to its ¹³C isotope which has a natural abundance of only 1.1%.

Current NMR instruments are Fourier Transform (FT) devices. The nucleus excitation is generated by a high frequency pulse which is a high-power field (around 50 W) with a short duration (around 10-50 μ s). The macroscopic magnetic vector M, resulting from individual nuclear moments μ_z , is deviated in the y direction and is no longer subject to the action of B after the pulse. This vector rises around the z axis with a Larmor frequency ($\gamma \cdot B_0$), characteristic of the isotope. The temporal signal S(t) induced onto the receiver coil by the M component in the xy plane, weakens due to the relaxation. The observed response is a decreasing exponential function with time (Free Induction Decay, FID), giving the evolution of M during its return path to equilibrium. Its Fourier transform provides the frequency signal S(ν).

With this technique, all the spectral signals can be excited simultaneously by only one pulse. Moreover, data may be recorded with a fast measuring time (some s) and accumulated before carrying out Fourier transformation to get access to the frequencies. More the number of FIDs are recorded to improve the better signal-to-noise ratio. The FT technique is thus useful for the NMR study of low sensitivity nuclei such as ¹³C. In addition, pulse spectroscopy enables to carry out plenty of experiments to solve problems related to signal assignment, sensitivity and resonance frequency correlations between different nuclei (2D NMR).

Three main pieces of information could be extracted from the spectra: the chemical shift, the signal integral and the coupling constant (in the case of hyperfine structures). The chemical shift (δ in ppm) is characteristic of a chemical group. The signal integral is the area under the peaks. If NMR is used in a quantitative mode, the signal integral is proportional to the number of nuclei responsible for the signal. Finally, the coupling constant (J-coupling or scalar coupling) provides details on the linkages between atoms in the studied molecule.

II.2.1.4.ii Principle of ^{13}C NMR

II.2.1.4.ii.a 1D ^{13}C NMR

NMR analysis is based on three successive time intervals: preparation, evolution and detection. During preparation, the system is prepared for the experiment on one hand and on the other hand, some time is preserved to get back to the equilibrium. This delay, d_1 , depends on the relaxation time T_1 of the system. The delay is in the range of several seconds. During evolution, the system is evolving under the influence of several factors depending on the pulse sequence. The average evolution time is in the range of the second. Finally, the signal is recorded during the detection time, also called acquisition time. This time depends on the desired signal resolution.

To detect ^{13}C by NMR (except some particular cases where H-C couplings are studied), couplings resulting from scalar interaction with protons should be removed. Indeed, couplings lead to hyperfine structures for each carbon, which on the one hand complicates the spectrum with overlapping areas, and on the other, causes the decrease of the signal-to-noise ratio because the signal intensity is dispersed on several components.

To perform quantitative measurements, first, all carbon nuclei should have enough time to go back to the equilibrium before each new pulse scan, so longer d_1 (relaxation delay) must be used. Moreover, the nOe effect (nuclear Overhauser effect), which is responsible for variations of signal intensity with respect of the carbon multiplicity, should be avoided. The nOe effect is due to proton decoupling double resonance. The proton decoupling is switched off during preparation and evolution time in order to suppress the nOe effect. Then it is switched on during acquisition to suppress the proton coupling only. This sequence is named the inversed-gate sequence. This sequence is time consuming and is generally not applied when the quantity of the material to be analyzed is too low. In that case, only a qualitative analysis is performed.

For qualitative NMR, proton decoupling is carried out using a broad band decoupling coil during all the sequence and the number of acquisitions is increased. The d_1 could be decreased. But in that case, quaternary carbons are discriminated against the other carbons since they have longer relaxation times and the nOe effect is not as beneficial as for the other protonated carbons.

II.2.1.4.ii.b ^{13}C NMR for multiplicity discrimination: DEPT sequence

The DEPT technique (Distortionless Enhancement by Polarization Transfer: polarization transfer from a sensitive nucleus to a less sensitive nucleus, i.e. from ^1H to ^{13}C) uses a sequence generating pulses in parallel on ^1H and ^{13}C nuclei, x and y being the directions of the pulse.

d_1 = required time for the proton relaxation. It is fixed to 3.0 seconds.

d_2 = delay of the polarization transfer. It is equal to $1/(2J)$ where J is the mean value of the coupling constant $^1J_{\text{HC}}$, usually 145 Hz for molecules bearing aliphatic and aromatic groups.

The variation of the last pulse θ_y , allows the access to the different carbon multiplicities. The full experiment requires the acquisition of 4 sub-spectra with different values of θ_y and is time consuming. In our case, using 135° for the angle of the last pulse, the CH and CH_3 signals appear with positive intensities on the spectrum and the CH_2 signal with negative intensity. This way, CH_2 signals are easily differentiated.

II.2.1.4.ii.c 2D ^{13}C NMR

Two-dimensional NMR methods allow to plot data on two frequency axes instead of one. The evolution time t_1 is regularly varying by addition of time increments Δt_1 . After a first Fourier transform compared to t_2 , a series of spectra in the frequencies F_2 is obtained. The signal amplitude or the signal phase of the spectra is modulated. A second Fourier transform compared to t_1 is then possible and the frequency F_1 axis is accessible. It contains the frequencies of the mechanisms operating during the evolution time t_1 and which produced the modulation of the observed signal (amplitude or phase). Correlation maps are obtained. This method enables for example to make correlations between X – Y nuclei which are involved either in scalar couplings through chemical bond, or dipolar couplings through the space. Correlation peaks with $\delta(X) / \delta(Y)$ coordinates, obtained on a 2D spectra, allow to detect linkages between X and Y atoms.

- *COSY ^1H - ^1H : correlation spectroscopy*

One of the most useful 2D-NMR experiments is the homonuclear correlation spectroscopy (COSY) sequence. It allows to identify coupled spins. The 2D spectrum resulting from the COSY experiment gives the frequencies for a single nucleus, here ^1H along both axes. With this sequence, $^n\text{J}_{\text{HH}}$ scalar couplings are detected: each coupling gives two symmetrical cross peaks, above and below the diagonal of the 2D spectrum.

In a standard COSY sequence, the preparation and mixing periods both consist of a single 90° pulse. They are separated by the evolution time, and the sample's resonance signal is detected during the measurement period.

- *HSQC: Hetero Single Quantum Coherence, and HMBC: Hetero Multiple Bond Correlation*

HSQC detects correlations between two different nuclei separated by one bond (^1J). This method displays one peak for each pair of coupled nuclei, and the two coordinates of a peak correspond to the chemical shifts of the coupled nuclei. With this method, the detection of a low sensitive nucleus is made via the detection of a more sensitive nucleus by polarization transfer. For example, correlations between single-coupling ^1H and ^{13}C ($^1\text{J}_{\text{CH}}$) could be obtained.

The HMBC method also detects heteronuclear correlations, but over longer ranges of bonds, usually 2 to 4 ($^n\text{J}_{\text{CH}}$).

II.2.1.4.iii Conditions of analysis

All NMR analyses have been performed at the « Institut Nanoscience et Cryogénie (INAC) » in the « Commissariat à l'Energie Atomique et aux Energies Alternatives (CEA) », Grenoble.

The NMR spectroscopic measurements were conducted on a Bruker AVANCE400 spectrometer equipped with a 10 mm BB/1H/D Z-GRD probe operating at 100.612 MHz for ^{13}C and 400.130 MHz for ^1H . Acquisition and data treatment were done using the LINUX TopSpin 3.2 software. Sample tubes were prepared with D_2O and pH was controlled.

Direct ^{13}C : the Bruker *invgate* sequence was used. The experiments were conducted in D_2O at 298K, with 1.1 s acquisition time, 20 s relaxation delay and a 60° pulse using a 25000 Hz spectral width. Proton broad band decoupling was applied only during acquisition time. 32k data points were used for data acquisition on a spectral width of 240 ppm for ^{13}C . Prior to Fourier transformation, zero-filling at 64 K was applied, followed by apodization with a 8 Hz exponential. Chemical shifts are

II. Materials and methods

given relative to TMS (tetramethylsilane, $\delta = 0$ ppm). The positions of the peaks were referred to the internal reference tube containing TSP-d₄ (trimethylsilyl propionic acid salt d₄).

¹³C DEPT: the Bruker *dept* sequence was used. The experiments were conducted in DMSO-d₆ at 323K, with 1.1 s acquisition time, 3.0 s relaxation delay, a last pulse at 135° to select CH₂ carbons reversed compared to CH and CH₃, with a 145 Hz coupling constant.

²D: the Bruker *hsqcetgpsi2* and *hmbcgplpndqf* sequences were used for HSQC and HMBC, respectively. The experiments were conducted at 298K, with 0.21 s acquisition time, 1.5 s relaxation delay, a spectral window of 10 ppm for ¹H and 220 ppm for ¹³C, 2048 data points for acquisition, 256 FIDs, and delays optimized for the coupling constant ¹J_{CH} = 145 Hz and ⁿJ_{CH} = 5 Hz. Prior to the Fourier transformation, zero-filling at 2 K was applied in both dimensions and it was followed by apodization with sine multiplication.

The Bruker *cosygpppqf* sequence was used for COSY. The experiments were conducted at 298K, with 0.22 s acquisition time, 2 s relaxation delay, a spectral window of 10 ppm for ¹H, 2048 data points for acquisition, 256 FIDs. Prior to the Fourier transformation, zero-filling at 4 K was applied in both dimensions and it was followed by apodization with sine multiplication and symetrization.

II.2.1.5 Elemental analysis

Traces of metal ions in the dye formulations and pulps (dyed or not) were analyzed by ICP-EAS, i.e. inductively coupled plasma atomic emission spectroscopy. C, H, N and S contents in dye formulations were measured by classical elemental analysis, after combustion of the sample in pure oxygen, and separation and detection of the corresponding CO₂, H₂O, N₂ and SO₂ produced. These analyses were subcontracted to FILAB SAS, Dijon, France.

II.2.2 To characterize the copper-phenanthroline complex

II.2.2.1 UV-visible analysis

UV-visible spectroscopy was used to determine the concentration of copper-phenanthroline complex in a solution. Copper-phenanthroline complexes absorb in the UV range as well as phenanthroline (two peaks at 228.5 and 264 nm, see more details in III.3.2 and III.3.3), which is quite convenient as it does not overlap the dyes' main absorbance signals.

The absorbance spectra were recorded from 200 to 800 nm on a Shimadzu UV-1800 UV-vis spectrophotometer, after the introduction of the sample to be analyzed in a quartz cell, at room temperature.

II.2.2.2 EPR spectroscopic analysis

Electron Paramagnetic Resonance (EPR), also called Electron Spin Resonance (ESR) was discovered in 1945 by Zavoisky. It is an absorption technique used to study materials with unpaired electrons, especially metal complexes or organic radicals.

II.2.2.2.i General principle of EPR spectroscopy

Contrarily to NMR, EPR is based on the spin of electrons and the resonance is obtained with a constant frequency and varying magnetic field, see Table II-3.

Table II-3. NMR vs. EPR

NMR	EPR
Nuclear spin	Electron spin
Constant field B, varying frequency ν	Constant ν (9 GHz, X band), varying B

Every electron has a magnetic moment μ_e and a spin quantum number $s=1/2$, with magnetic components $m_s=+1/2$ and $m_s=-1/2$. In the presence of an external magnetic field B_0 , the electron's magnetic moment aligns itself either parallel ($m_s=-1/2$) or antiparallel ($m_s=+1/2$) to the field, each alignment having a specific energy. The energy is equal to $\mu_e \times B_0$. Hence, the energy required to create a transition state is given by Equation II-1.

$$\text{Equation II-1} \quad E = g \times \beta \times m_s \times B_0 \text{ with } m_s = \pm 1/2$$

where g is the Landé factor ($g = 2.0023$ for free electron), β the Bohr magneton ($9.2740 \times 10^{27} \text{ J.T}^{-1}$)

Therefore, the separation between the lower and the upper state is $\Delta E = g \times \beta \times B_0$ for unpaired free electrons. The energy level splitting is directly proportional to the B_0 strength, as shown in Figure II-1.

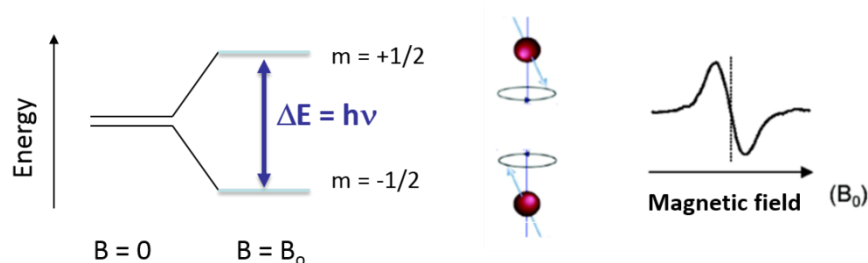


Figure II-1. Scheme of the energy transition which leads to an EPR signal in the case of one unpaired electron

The unpaired electron can move between the two energy levels by either absorbing or emitting a photon of $h\nu$ energy, where $h\nu = \Delta E$. This leads to Equation II-2:

$$\text{Equation II-2} \quad h\nu = \Delta E = g \times \beta \times B_0$$

The resulting electron excitation provokes the formation of a line on the absorption spectrum. The detection of resonance signal is an evidence of the presence of unpaired electrons. The intensity of the signal, proportional to the number of unpaired electrons, may be used for quantitative studies in comparison with a standard. However, the success of EPR is mainly due to the existence of hyperfine structures resulting from the interaction between unpaired electrons and magnetic nuclei in paramagnetic substances. In many cases, such structures enable to identify chemical species unambiguously. The isotropic hyperfine splitting pattern for a radical freely tumbling in a solution can be predicted. The magnetic moment of a nucleus with a spin number s may adopt $2s+1$ orientations in the B_0 field. Hence, there are $2s+1$ energy sub-levels associated to each orientations of the unpaired electron. Consequently, $2s+1$ transitions are allowed and hyperfine structure spectra exhibit $2s+1$ lines with equivalent spacing and same intensity. The spectral line spacing is measured by the isotropic hyperfine coupling constants.

II.2.2.2.ii EPR spectroscopy for copper complexation study

Copper compounds are widely applied in catalytic chemistry using the Cu(I)/Cu(II) redox cycle. Cu(II) is the most stable state. Since it exhibits a d^9 configuration, Cu(II) is a paramagnetic species as all Cu(II) complexes. Cu(II) containing species thus give a typical EPR signal. On the contrary, Cu(I), less stable than Cu(II), has a d^{10} electronic configuration with no unpaired electrons, making it undetectable by EPR.

Cu(II) species' spectra are anisotropic and give a typical signal depending on the coordination geometry. The typical spectrum for a Cu(II) compound is given in Figure II-2.

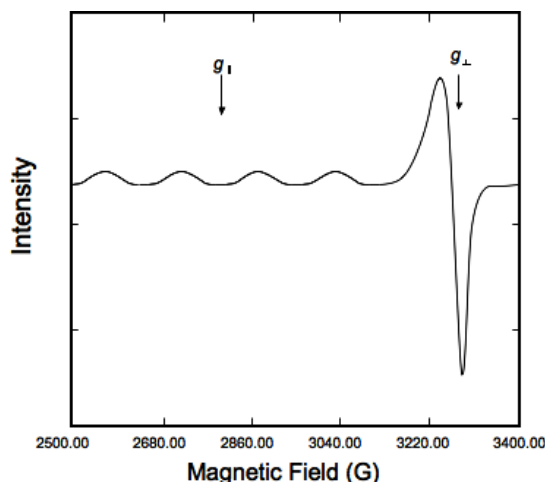


Figure II-2. Typical signal of a Cu(II) compound [7]

If Cu(II) coordinates with other molecules, the copper signal will be modified ($g_{||}$ and g_{\perp} values modification). In Figure II-2, the four small absorption-like peaks correspond to $g_{||}$ and indicate that Cu(II) is coordinated to four identical atoms. The intense asymmetric derivative peak at higher magnetic field corresponds to g_{\perp} and indicates elongation along the z axis. Moreover, if all Cu(II) species are reduced into Cu(I), a decrease in the signal intensity should be observed.

In this work, EPR was used (1) to study the complexation of copper with phenanthroline and substrates (dyes and cellulose) and (2) to characterize copper's state during the color-stripping trials conducted on the dye solution with the H_2O_2 /Cu-Phen system. These EPR analyses were conducted on frozen samples. This allows to obtain a random collection of paramagnets and to improve the spectrum resolution.

II.2.2.2.iii Conditions of copper complexation analysis

X-band EPR spectra were recorded at 100 K with a Bruker EMX Plus spectrometer equipped with an ER-4131 VT Bruker cavity for the liquid nitrogen experiments. The instrument settings were the following: receiver gain 30 dB, modulation amplitude 4 G, attenuation 10 dB.

The tested samples were aqueous solutions of $CuSO_4$ and Cu-Phen, with or without dyes and cellulose model compounds, and with or without sodium hydroxide, leading to different pH values. The concentrations were the following: 0.1 or 1 mM dyes, 1.5 mM $CuSO_4$, and Cu:Phen molar ratio = 1:1, 1:2 or 1:3. Sample volumes of 300 μ L were introduced in EPR quartz cells of 4 mm outer diameter and 0.5 mm wall thickness. The different experimental details will be presented before the corresponding results in Chapter III and Chapter V.

II.2.2.3 Speciation calculation (PHREEQC simulations)

The concentration of each copper-phenanthroline complex was calculated using the open-source software PHREEQC. A preliminary work consisted in database validation, and introduction of the stability constants of the different possible copper complexes with phenanthroline and hydroxide [8]–[11]. The software enabled the calculation of the species concentration vs. pH profiles for each species.

The PHREEQC software was used with the inclusion of the stability constants of copper-phenanthroline-hydroxide complexes in the database, based on selected published data [8]–[11]. The considered reactions and constants were presented in Chapter I (I.3.2.4).

Besides, in some cases, the software proposed the production of Cu^{I} , which was not supposed to occur in the absence of a reductant. Hence, all Cu^{I} species were removed from the database used in the simulations.

II.2.3 To characterize the pulps

II.2.3.1 Optical characterization

The efficiency of color removal was determined by measuring the color and/or the brightness of the fibers on handsheets before and after treatment. The handsheets dedicated to optical property determination were formed using deionized water to avoid the presence of any colored impurities such as additional metal ions.

2.0 grams of odp were diluted into 1 L of deionized water and mixed for 10 seconds using a mixer until a defibered suspension was obtained. The suspension was then introduced into a handsheet machine, following the ISO 5269/1 standard. The handsheet was dried at 80°C for five minutes under vacuum using a Franck dryer.

The reflectometer used for the optical measurements was the ELREPHO 2000 Datacolor spectrophotometer. Eight measurements were performed per handsheet (4 on each side).

For white pulps, free of dye, brightness was the main optical characterization. It was measured following the ISO 2470-1 standard. For dyed pulps, color is evaluated through the determination of a triplet of coordinates in the CIE 1976 $L^*a^*b^*$ (CIELAB) color space, according to the ISO 5631-2:2008 standard, with CIE illuminant D65 and the CIE 10° observer. L^* , a^* , and b^* are the rectangular coordinates of a color in the uniform CIELAB color space, meaning that equal distances in this space are perceived as equal color differences. L^* measures the lightness and varies from 0 for black to 100 for white (perfect diffuser). a^* represents the red-green axis: positive values (up to +299) indicate redness and negative values (down to -300) indicate greenness. b^* represents the yellow-blue axis: positive values (up to +299) indicate yellowness and negative ones (down to -300) indicate blueness.

The CIE $L^*a^*b^*$ color space is represented in Figure II-3.

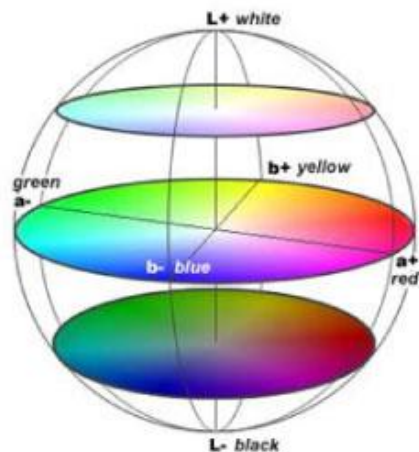


Figure II-3. Representation of the CIE L*a*b* color space at three different L* levels.
 Source: www.fulviovilla.com/category/tutorial/

To estimate the percentage of color removal, a Dye Removal Index (DRI) was calculated using a formula inspired from Sharpe and Lowe’s work [12]. The DRI indicates the percentage of discoloration in the CIE L*a*b* color system. The initial pulp is represented by point P₁ with coordinates L*₁, a*₁, b*₁. After color-stripping, the pulp is represented by point P₂ (L*₂, a*₂, b*₂). Inspired from Sharpe and Lowe’s definition, the amount of color removed was considered to be the reduction in the distance from perfect white (L*=100, a*=b*=0) when moving from point P₁ to P₂, as illustrated in Figure II-4.

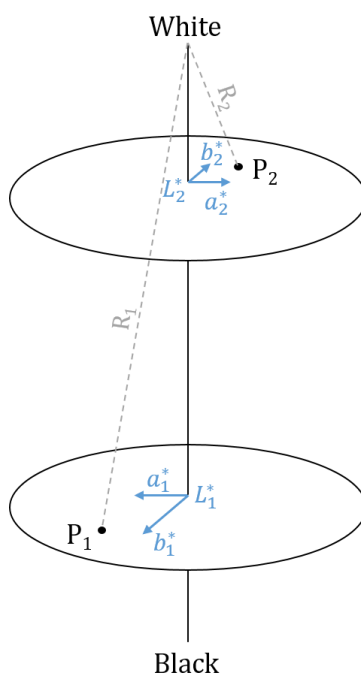


Figure II-4. Scheme representing the principle of DRI calculation. R₁ is the distance from P₁ to perfect white and R₂ is the distance from P₂ to the perfect white, the “color removal” is calculated as R₁ - R₂.

The DRI (Equation II-3) was thus calculated as the ratio between this distance reduction and the initial distance from white.

$$\text{Equation II-3} \quad \text{DRI (\%)} = -100 \times \frac{\sqrt{a_2^{*2} + b_2^{*2} + (100 - L_2^*)^2} - \sqrt{a_1^{*2} + b_1^{*2} + (100 - L_1^*)^2}}{\sqrt{a_1^{*2} + b_1^{*2} + (100 - L_1^*)^2}}$$

The DRI's standard deviation was calculated based on the propagation of the respective standard deviations of L_1^* , a_1^* , b_1^* , L_2^* , a_2^* , and b_2^* . These variables were considered independent, so that the common variance formula (Equation II-4) could be used.

$$\text{Equation II-4} \quad s_f = \sqrt{\left(\frac{\partial f}{\partial x}\right)^2 s_x^2 + \left(\frac{\partial f}{\partial y}\right)^2 s_y^2 + \left(\frac{\partial f}{\partial z}\right)^2 s_z^2}$$

where s_f is the standard deviation of $f(x,y,z)$ and s_x , s_y , and s_z are the standard deviations of x , y , and z

This formula was applied to the DRI function thanks to the Mathematica software. The resulting standard deviation of the DRI, based on the uncertainty of the $L^*a^*b^*$ measurements, was calculated systematically. In the following chapters, it will appear in the result tables as standard deviation and in charts through the error bars. However, the standard deviation due to the repeatability of the trials may be higher. When trials were repeated more than twice, this other standard deviation was also presented.

II.2.3.2 Physico-chemical characterization

Cellulose DP_v indicates the polymerization degree of cellulose. Therefore, high DP_v drops reveal strong cellulose degradation. The viscosity-average cellulose DP_v was determined by measuring the viscosity of cellulose dissolved into 0.5 M cupriethylene diamine (CED, a cellulose solvent) at a concentration of 5 g/L. This method is adapted from TAPPI standard T 230 om-13. Its accuracy was estimated to be ± 25 .

The equivalent of exactly 250.0 mg of oven-dried pulp is weighed and inserted into a bottle along with seven glass beads. Exactly 25.00 mL of distilled water are inserted into the bottle before it is let to agitate on a mechanical shaker for one night. The next day, 25.00 mL of 1 M CED are added into the fiber suspension, and the surface is purged with nitrogen gas for 10 seconds in order to de-oxygenate the air on the top of the bottle. The bottle is closed and covered with aluminum foil before being shaken again for two hours. After two hours, the cellulose should be dissolved.

Using a capillary viscometer, the solution is sucked until it reaches a certain level. The viscometer is immersed in a water bath at $25.00 \pm 0.05^\circ\text{C}$. The time needed for the liquid to pass between two lines is measured thanks to a chronometer. These lines are the limits of a calibrated volume. Knowing the relationship between cellulose DP_v and the solution viscosity [13], a calculation gives access to the cellulose DP_v .

The TAPPI viscosity V (mPa.s) is calculated as follows:

$$\text{Equation II-5} \quad V = C \times t \times d$$

where C is the calibration constant of the capillary ($\times 10^{-6} \text{ m}^2 \cdot \text{s}^{-2}$), t the flow time (s), and d the density of the solution, i.e. 1.052 g/cm^3 .

II. Materials and methods

The equation used to calculate the DP_v is Equation II-6 below:

$$\text{Equation II-6} \quad DP_v = (0.75 \times (\log(C \times t \times d) \times 954 - 325))^{1.105}$$

II.2.3.3 Physical characterization

To appraise the papermaking ability of the treated pulps, 65 g/m² paper handsheets were prepared following the ISO 5259-2:2004(E) standard, and two main strength properties were tested: (1) the wet zero-span tensile strength (or breaking length) of pulp, BL_0 , expressed in km, which is known to give the intrinsic strength of the fiber, and (2) the burst index, expressed in kPa.m²/g, giving access to the strength of the whole fiber web.

After bleaching/color-stripping, the pulp was mixed for one minute in a Lhomargy mixer to separate the fibers perfectly, before the suspension was added into the handsheet former. At least 5 handsheets were made from each pulp sample. The handsheets were then dried according to the same protocol as before but for seven minutes and stored in a conditioned room (23-24°C, 50% RH) before measuring their weight and thickness in order to calculate their grammage.

The physical properties were then measured in the same conditioned room.

The wet zero-span breaking length BL_0 was measured according to ISO standard ISO 15361:2000(E). The test was performed with a tensile testing machine with “zero-span” clamping jaws, meaning that the grip separation was of 0.00 mm. The sample was immersed into water for 30 seconds to break hydrogen bonds. It was then dewatered by gently pressing a light roll on the sample placed in between two blotting papers. The sample was readily tested. The results were calculated from the average of 10 values for each pulp sample, i.e. two measurements per handsheet.

The burst index, expressed in kPa.m²/g, was measured according to ISO 2758:2001(E), thanks to a burst-test meter. The bursting strength is described as the maximum uniformly distributed pressure that a single sheet of paper can withstand. The burst index is defined as the bursting strength of a handsheet divided by its grammage. As for zero-span breaking length, the results were calculated from the average of 10 values for each pulp sample, i.e. two measurements per handsheet.

II.2.4 To characterize dye solutions

After treatment, the dye solutions were characterized to determine the percentage of dye removal or degradation but also to identify the degradation products. In addition, some analyses were performed to follow the generation of radicals when hydrogen peroxide was present.

II.2.4.1 UV-vis spectroscopy

UV-visible spectroscopy was used to study the dye modification (complexation, ionization, degradation) in aqueous solutions. The absorbance spectra were recorded from 200 to 800 nm on a Shimadzu UV-1800 UV-vis spectrophotometer, after the introduction of the sample to be analyzed in a quartz cell, at room temperature.

In case of precipitation, the samples were centrifuged beforehand. In accordance with Beer-Lambert law, the dye concentration was proportional to its absorbance at its maximum absorption wavelength in the visible range.

Several replicates were analyzed to verify the reproducibility of the measurements, which was useful to evaluate whether the difference between two results was significant.

II.2.4.2 Electrospray Ionization-Mass Spectrometry

Liquid chromatography–mass spectrometry is an analytical chemistry technique combining the physical separation of molecules through liquid chromatography (HPLC) with the mass analysis of these molecules using mass spectrometry (MS). This technique allows the separation, general detection and potential identification of chemicals of particular masses in the presence of other chemicals (i.e. in complex mixtures).

In this work, electrospray ionization-mass spectrometry (ESI-MS) was used. In that case MS is applied on the analyte molecules after their conversion into ions using an electrospray (high voltage) to create an aerosol. The molecules are first introduced into the ionization source of the mass spectrometer, where they are ionized to acquire positive or negative charges. Then the ions travel through the mass analyzer and arrive at different parts of the detector according to their mass/charge (m/z) ratio. After ion detection, signals are generated and recorded by a computer system. The computer displays the signals graphically as a mass spectrum showing the relative abundance of the signals according to their m/z ratio [14], [15].

ESI-MS is especially useful for macromolecule studies because no molecule fragmentation occurs when ionized.

ESI-MS was performed after direct infusion of solutions of DR81S, DR81L and DY11L (50 μM), with and without sodium hydroxide (0.02 M), thanks to a Bruker Daltonics Esquire 3000+ iontrap mass detector equipped with an ESI source. Data acquisition was processed using the Bruker DataAnalysis 2.0 software.

The analyses were performed under both positive and negative mode, and the main parameters were the following: dry temperature 300°C, dry gas flow 5 L/min, nebulizer pressure 11 psi, capillary voltage 4000 V, skimmer voltage 40 or -40 V (for positive and negative mode, respectively). Nitrogen was used as nebulization and desolvation gas.

II.2.5 To follow the formation of radicals

Radical detection during a reaction could be made using several techniques. Molecules reacting with the radicals and forming more stable species enable indirect detection. In this work, three methods were tested to detect the generation of radicals, especially hydroxyl radicals: a chemiluminescence method, a UV-vis method and the EPR/spin-trapping method with DMPO as a spin trap.

II.2.5.1 Chemiluminescence method

A simple and economic method for the detection of hydroxyl radicals is based on the chemiluminescence of 3-hydroxy-phthalhydrazide which is formed by oxidation of phthalhydrazide by hydroxyl radical.

II.2.5.1.i Principle

Reitberger and Gierer [16] developed a method to study the role of hydroxyl radicals in oxidative processes. 3-aminophthalic hydrazide (luminol) is a chemiluminescent substance. Its oxidation leads to the very exothermic expulsion of nitrogen, which excites the resulting 3-aminophthalate. Hence, the emitted energy results in light emission (Figure II-5).

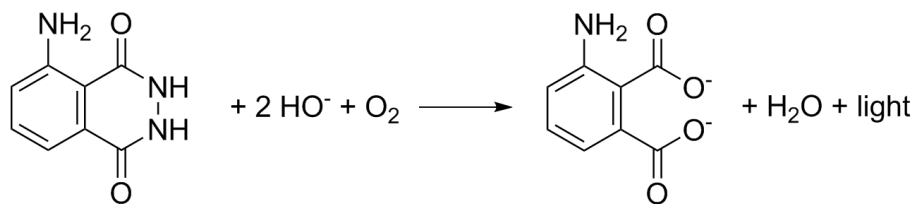


Figure II-5. Oxidation of luminol

Phtalhydrazide (luminol without the amino-group), when oxidized by hydroxyl radicals, forms 3-hydroxy-phtalhydrazide, a chemiluminescent substance comparable to luminol. The addition of Na_2CO_3 , $(\text{NH}_4)_2\text{S}_2\text{O}_8$ and hydrogen peroxide to 3-hydroxy-phtalhydrazide results in the formation of 3-hydroxyphtalic acid (3-hydroxyphtalate) and light emission at a wavelength 415 nm, as illustrated by Figure II-6.

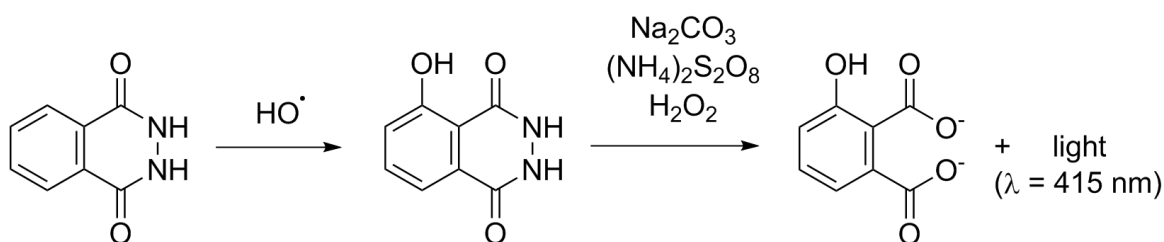


Figure II-6. Reaction path revealing the hydroxylation of phtalhydrazide by chemiluminescence

II.2.5.1.ii Analysis conditions

A BioOrbit 1250 luminometer was equipped with a plotter and graph paper.

Trace amounts of phtalhydrazide ($C = 0.5$ to 5 mM) were introduced in the studied solution. The scavenging of HO^\bullet was thus negligible compared to the overall HO^\bullet generation.

Two solutions were prepared in advance:

- Solution A: Na_2CO_3 1M, EDTA 25 mM
- Solution B: H_2O_2 50 mM, $(\text{NH}_4)_2\text{S}_2\text{O}_8$ 50 mM

These solutions should be stored at low temperature (4 to 10°C), away from light, and kept no more than one week.

At a given time after starting the reaction, an aliquot (0.1 mL) of solution was introduced in 1 mL of solution A previously introduced in a vial. 0.2 mL of solution B was finally added to reveal the chemiluminescence and the signal was recorded.

II.2.5.2 UV-vis method using DMNA

Among the available trapping techniques, another simple one is the UV-visible method based on the discoloration of N,N-dimethyl-4-nitrosoaniline (DMNA) when it reacts with hydroxyl radicals.

DMNA (Figure II-7) was discovered to be a good hydroxyl radical-probe by Kraljic and Trumbore [17]. Their experiments were based on pulse radiolysis and allowed them to determine relative rate constants for hydroxyl radicals and other species such as Br^- , I^- , NO_2^- , CH_3COO^- , CH_3OH .

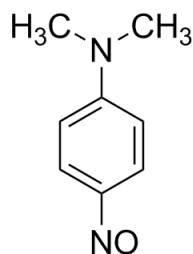


Figure II-7. Molecular structure of DMNA (N,N-dimethyl-4-nitrosoaniline)

DMNA absorbs light at 440 nm, yielding a bright yellow color. When oxidized by hydroxyl radicals, the absorbance intensity decreases. This phenomenon is also called “bleaching”. DMNA was shown to be very selective towards hydroxyl radicals in comparison with other oxygenated radical species. The objective of this UV-vis method is to detect the generation of hydroxyl radicals by reduction of DMNA’s absorbance intensity. Yet, it is not a quantitative method since the reaction of two moles of DMNA with hydroxyl radicals may yield only one mole of oxidized DMNA [18].

The measurements were conducted with a DMNA concentration of 1 to $2 \cdot 10^{-4}$ mol/L. This concentration was close to those found in the literature and allowed the DMNA:H₂O₂:metal ion molar ratio to remain similar to those generally used in similar studies. The UV-vis analyses were performed on the same spectrophotometer (Shimadzu UV-1800) as usual.

II.2.5.3 EPR/spin-trapping method

II.2.5.3.i Principle

Because radicals contain one unpaired electron, they could be analyzed by EPR spectroscopy. Unfortunately, lots of radicals have a short life-time, not allowing them to reach a sufficient stationary concentration for their direct detection by EPR in conventional conditions. To detect these radicals, the spin-trapping method is thus applied.

This method uses a “diamagnetic trap molecule”, T, which reacts with the R• radical to form a more stable adduct with paramagnetic spin, (TR)•. The EPR spectrum analysis of the adduct enables to get information on the radical R• species, initially trapped by the spin-trap molecule. In the most favorable cases, R• can be identified on the basis of information extracted from the adduct spectrum (values of g and hyperfine coupling constants) [19]. However, some adducts formed after entrapment of different radicals, may lead to similar spectra. To discriminate the radicals, scavengers may be used in parallel of the spin trap. EPR spin-trapping with and without scavenger was used in this study to detect hydroxyl radicals HO•. The spin-trap was 5,5-dimethylpyrroline-N-oxide (DMPO).

In the presence of hydroxyl radicals, DMPO forms a stable paramagnetic nitroxide radical adduct, DMPO-OH [20]. DMPO-OH is a good example of a radical adduct. The unpaired electron of the oxygen atom interacts with the circled nitrogen ($s = 1$) and hydrogen ($s = \frac{1}{2}$) atoms of the nitrene in Figure II-8. Their hyperfine coupling constants are $a_N = a_H = 14.9$ G. Therefore, instead of 6 lines $((2 \times 1 + 1) \times (2 \times 0.5 + 1))$, the spectrum consists of 4 peaks, two of which are more intense (Figure II-8 and Figure II-9).

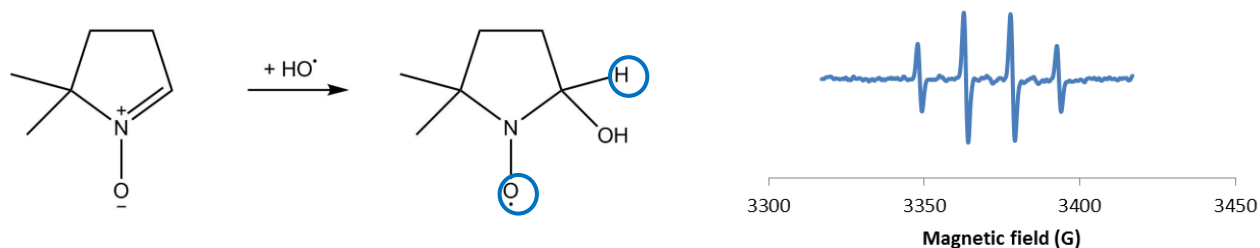


Figure II-8. Hydroxylation of DMPO into DMPO-OH and typical DMPO-OH signal [19], [21], [22]

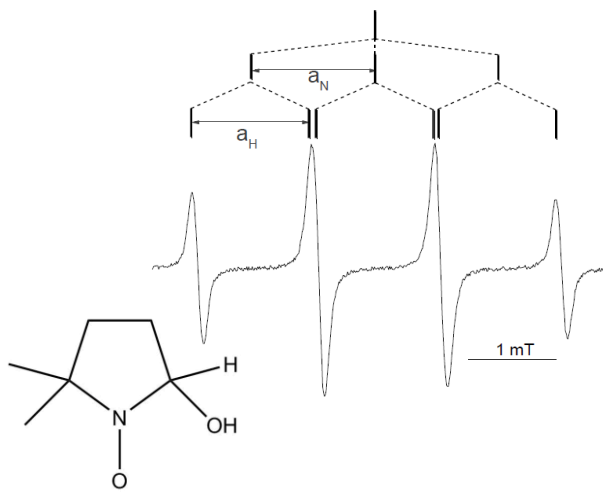
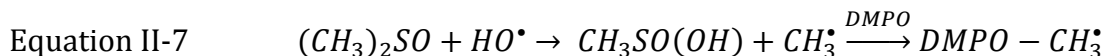


Figure II-9. Typical DMPO-OH signal [19]

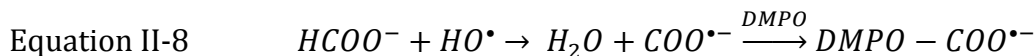
However, obtaining DMPO-OH does not necessarily mean that HO^\bullet radicals were formed. Indeed, several phenomena lead to the DMPO-OH adduct, such as superoxide radical spin-trapping and decomposition of the corresponding DMPO-OOH adduct into DMPO-OH, the oxidation of DMPO by very strong oxidants (called inverted spin-trapping) [23], or the nucleophilic addition of water onto the DMPO spin-trap (Forrester-Hepburn reaction [24]). The nucleophilic addition of water is quite usual in aqueous solution and has been proved to be catalyzed by copper ions [25]–[27].

To confirm that the DMPO-OH adduct originates from HO^\bullet addition and not from side reactions with DMPO (e.g. nucleophilic addition reactions) or other radical entrapment, an indirect method using scavengers was also applied. The selected scavengers are more reactive towards hydroxyl radicals than DMPO, as their rate constants are higher than that of the spin-trap, $k(\text{DMPO}/\text{HO}^\bullet)$, and they can be added at higher concentrations. Depending on the method and conditions used to measure the rate constants, $k(\text{DMPO}/\text{HO}^\bullet)$ ranges from 1.9×10^9 to $4.3 \times 10^9 \text{ M}^{-1}\text{s}^{-1}$ ($1.93 \times 10^9 \text{ M}^{-1}\text{s}^{-1}$ according to Villamena and colleagues, obtained by UV photolysis and competition with ethanol, in the presence of hydrogen peroxide and a phosphate buffer [28]; $2.8 \times 10^9 \text{ M}^{-1}\text{s}^{-1}$ according to Eberson [23]; $4.3 \times 10^9 \text{ M}^{-1}\text{s}^{-1}$ according to Hanna and Mason [25]).

Among the scavengers, dimethyl sulfoxide (DMSO) and formate (HCOO^-) are often used. Their scavenging reactions are the following:



Where $k(\text{DMSO}/\text{HO}^\bullet) = 4.2 \times 10^9$ [29] to $7.1 \times 10^9 \text{ M}^{-1}\text{s}^{-1}$ [30], knowing that Cederbaum and collaborators reported $7 \times 10^9 \text{ M}^{-1}\text{s}^{-1}$ (obtained via the pulse radiolysis method based on the competition between HO^\bullet and CNS^- , in neutral aqueous solution at room temperature) [31].



Where $k(\text{HCOO}^-/\text{HO}^\bullet) = 2.5 \times 10^9$ [32] (obtained by pulse radiolysis and comparison with I $^-$) to $2.9 \times 10^9 \text{ M}^{-1}\text{s}^{-1}$ [23]. The rate constants of formic acid vary with pH: in neutral aqueous solution at room temperature, $k(\text{HCOOH}/\text{HO}^\bullet) = 2.45 \times 10^9$ to $3.1 \times 10^9 \text{ M}^{-1}\text{s}^{-1}$ (depending on the method used to determine the rate constant – pulse radiolysis or steady irradiation) [30]; at acidic pH, $k(\text{HCOOH}/\text{HO}^\bullet) = 5 \times 10^9$ to $6.8 \times 10^9 \text{ M}^{-1}\text{s}^{-1}$ [32]. A pH below 7 would thus induce faster scavenging of HO^\bullet radicals.

To summarize, HO^\bullet reacts with DMSO or HCOO^- to form respectively $^\bullet\text{CH}_3$ and $\text{COO}^{\bullet-}$, further trapped by DMPO. The resulting adducts are $\text{DMPO}-\text{CH}_3^\bullet$ with a typical 6-line signal ($a_N=16.1 \text{ G}$, $a_H=23 \text{ G}$), and $\text{DMPO}-\text{COO}^{\bullet-}$ with another 6-line pattern ($a_N=15.75 \text{ G}$, $a_H=19.09 \text{ G}$), see Figure II-10.

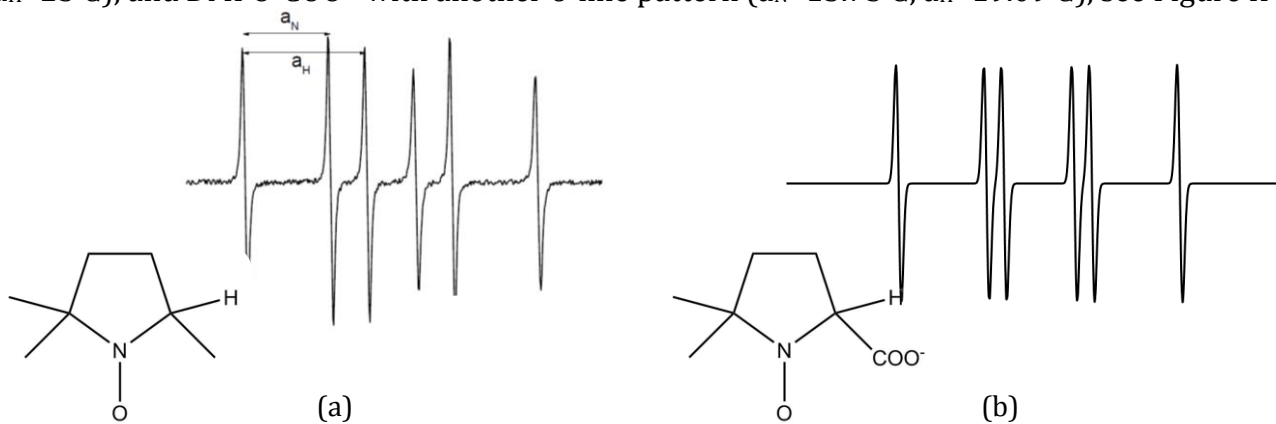


Figure II-10. Typical DMPO- CH_3 signal [19] (a) and DMPO- COO^- signal (simulated based on constants given by Buettner [22] (b))

II.2.5.3.ii Analysis conditions

All the spin-trapping trials were carried out in aqueous solution at room temperature, except some exceptional assays with heating.

- *EPR experiments*

X-band EPR spectra were recorded with a Bruker EMX Plus spectrometer, either at room temperature or after heating. The instrument settings were the following: receiver gain 30 dB, modulation amplitude 1 G, microwave power 0.02 W. The tested samples were aqueous solutions of CuSO_4 , Phen and Cu-Phen (called activators) with or without hydrogen peroxide, in the presence of DMPO as a spin-trap and DMSO or sodium formate as hydroxyl radical scavengers.

Three complementary methods were used: simple spin-trapping (DMPO), spin-trapping after scavenging with DMSO (DMSO+DMPO), and after scavenging with HCOO^- (HCOO^- +DMPO).

II. Materials and methods

- *Solution preparation*

The commercial chemical products of analytical grade were 5,5-dimethyl-1-pyrroline N-oxide (99%, Sigma Aldrich), dimethyl sulfoxide (99.9%, Sigma Aldrich), sodium formate HCOONa (99%, Carl Roth).

The reactants were introduced in a total volume of 300 μL , in the following order: ultrapure water, alkali or acid, scavenger, spin-trap, activator, H_2O_2 . Whatever the method, the following concentrations were respected: 5.6 M DMSO, approximately 5 M sodium formate, $6.0 \cdot 10^{-2}$ M DMPO, $1.5 \cdot 10^{-5}$ M CuSO_4 , $3.0 \cdot 10^{-2}$ M Phen, $1.0 \cdot 10^{-4}$ M H_2O_2 , $6.0 \cdot 10^{-2}$ M NaOH.

With formate, the pH was around 9 in the absence of NaOH and it was equal to 12.5 with NaOH. With DMSO, the pH was around 9 alone, around 8 with Cu-Phen, 7.6 with CuPhen+ H_2O_2 , and 14 with CuPhen+ H_2O_2 +NaOH.

The solution was then transferred to a bottom-sealed Pasteur pipette and immediately analyzed. For the trials requiring heating, a heat gun was used to heat the pipette for approximately 15 seconds, then the pipette was placed in the EPR cavity.

II.2.5.3.iii Result analysis: integration and simulations

The EPR simulations were conducted using the SimEPR software, which is a free isotropic simulation program provided by the (US) National Institute of Environmental Health Sciences' Public Electron Paramagnetic Resonance Software Tools [33], [34]. It was useful to confirm the assignment of the experimental constants to the most probable radical species.

To operate a simulation, the experimental spectrum's data was first modified to obtain a 1024-data point file. Then, on the SimEPR software, several parameters were indicated, mainly:

- the scan range
- the number of species to be simulated
- the "g-shift" (distance from the center of the scan, to have the spectrum centered)
- For each species:
 - hyperfine coupling constants for N ($S=1$) and other spins, e.g. 3 H ($S=1/2$): a_N , a_H
 - linewidths L_w
 - lineshapes (percentage of Lorentzian in a mix of Lorentzian and Gaussian lineshapes)
 - relative percentage of the species if more than one

Then, the experimental spectrum was superimposed with the simulated one and the parameters were adjusted until the two spectra were close to fitting. Finally, last adjustments were made automatically thanks to the program's optimization tools, in order to improve the fitting of the simulated spectrum.

II.3 CU-PHEN-ACTIVATED H₂O₂ TREATMENTS

II.3.1 Preparation of the complex

The complex was prepared as described in II.1.2.

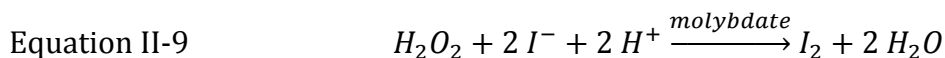
II.3.2 Pulp bleaching or color-stripping

Pulp bleaching stages were carried out at 10 % consistency in polyethylene (PE) bags in a thermostated water bath. The pulp (20 or 30 g odp) was rehydrated with 1.5-2 L of distilled water and defibrated in a Lhomargy mixer during one minute. The suspension was then filtered on a filter crucible. The rehydrated pulp was weighed inside the PE bag. Chemicals were added in the following order: sodium hydroxide, Cu-Phen or CuSO₄ or Phen, and finally hydrogen peroxide. Water was added to reach a consistency of 10%. The reactor was sealed and softly kneaded by hand to ensure a well-homogenized suspension. It was then introduced into a water bath set 5°C above the desired pulp temperature, for the desired bleaching time. During the reaction, the suspension was kneaded every 10 to 15 minutes to ensure a well-mixed suspension and homogeneous bleaching.

At the end of the bleaching time, the reactor (PE bag) was removed from the water bath and placed under cold running tap water for five minutes, to cool down the suspension, thus stopping the bleaching reaction. It was then cut open and the fiber suspension was filtered using a clean and dry filter crucible. The filtrate was collected for final pH measurement and hydrogen peroxide consumption determination. The treated fibers were then washed three times on the filter crucible using 500 or 750 mL of distilled water each time (4% consistency).

The operating conditions of the treatments are detailed in the respective result paragraphs in Chapter IV.

After pulp bleaching or color-stripping, the efficacy of the treatment was evaluated in terms of optical properties (brightness or residual color) and fiber strength properties as described in II.5.3. The pH was also checked and residual hydrogen peroxide was titrated in order to calculate its consumption. The iodometric method was used for this titration: H₂O₂ oxidizes the excess of iodide (Equation II-9) and the produced molecular iodine is titrated by sodium thiosulfate (Equation II-10). Ammonium molybdate was used to catalyze this reaction. The chemicals used were potassium iodate KI 10% w/w, sulfuric acid H₂SO₄ 2M, ammonium molybdate (supernatant of a saturated solution), and sodium thiosulfate Na₂S₂O₃ 0.1 M.



Approximately 100 mL water, 10 mL KI, 20 mL sulfuric acid and 5 mL ammonium molybdate were mixed together in an erlenmeyer. A precise volume of the solution to titrate (V_s) was then introduced and left to react for 5 minutes in a closed Erlenmeyer (in this acidic medium, the oxygen from air oxidizes the iodide ions) while mixing by magnetic stirring. The produced iodine was then titrated by Na₂S₂O₃ 0.1 M (accurate concentration), the equivalence point (V_{eq}) corresponding to the disappearance of iodine's brown/yellow color.

The resulting concentration was calculated as follows:

Equation II-11
$$[H_2O_2] = \frac{M(H_2O_2) \times C(S_2O_3^{2-}) \times V_{eq}}{2 \times V_s}$$

$[H_2O_2]$ is a concentration in weight (g/L), M is the molecular weight of H_2O_2 (34.0 g/mol), and C is a molar concentration (mol/L).

Hence,

Equation II-12
$$[H_2O_2] = \frac{17 \times C(S_2O_3^{2-}) \times V_{eq}}{V_s}$$

This titration allowed the calculation of H_2O_2 's consumption during a bleaching stage knowing the initial quantity of H_2O_2 (in mol or g) applied and residual H_2O_2 (in mole or g). The consumption of H_2O_2 can be calculated as follows:

Equation II-13
$$Consumption (\%) = \frac{100 \times (nH_2O_{2i} - nH_2O_{2f})}{nH_2O_{2i}}$$

Where nH_2O_{2i} and nH_2O_{2f} are the initial and final quantities of H_2O_2 in the pulp (in mol or g).

II.3.3 Dye solution color-stripping

Aqueous dye solutions were treated with hydrogen peroxide alone and in the presence of activator. Some treatments were carried out during 1 hour at alkaline pH and at 25 or 80°C in a double envelope reactor heated with water from a thermostated water bath. Controls without H_2O_2 and activator were also performed. The pH of the solution was checked before and after each reaction.

Other treatments were performed at smaller scale in 10 mL vials in a water bath, during 30 min at 60°C. These reactions were carried out at higher concentrations, allowing further analysis by ESI-MS.

The color-stripping effect was followed by UV-vis spectroscopy and ESI-MS was used in the second case (trials at 60°C) to analyze the dye degradation products as described in II.2.4.

II.4 REFERENCES

- [1] M. M. Sahasrabudhe, R. G. Saratale, G. D. Saratale, and G. R. Pathade, "Decolorization and detoxification of sulfonated toxic diazo dye C.I. Direct Red 81 by *Enterococcus faecalis* YZ 66," *Journal of Environmental Health Science and Engineering*, vol. 12, no. 1, p. 151, Dec. 2014.
- [2] J. W. Wegener, J. C. Klamer, H. Govers, and U. A. T. Brinkman, "Determination of organic colorants in cosmetic products by high-performance liquid chromatography," *Chromatographia*, vol. 24, no. 1, pp. 865–875, Dec. 1987.
- [3] M. Chen, D. Moir, F. M. Benoit, and C. Kubwabo, "Purification and identification of several sulphonated azo dyes using reversed-phase preparative high-performance liquid chromatography," *Journal of Chromatography A*, vol. 825, no. 1, pp. 37–44, Oct. 1998.
- [4] D. Ansorgová, M. Holčapek, and P. Jandera, "Ion-pairing high-performance liquid chromatography-mass spectrometry of impurities and reduction products of sulphonated azodyes," *J. Sep. Science*, vol. 26, no. 11, pp. 1017–1027, Jul. 2003.

- [5] M. R. van Bommel, I. V. Berghe, A. M. Wallert, R. Boitelle, and J. Wouters, "High-performance liquid chromatography and non-destructive three-dimensional fluorescence analysis of early synthetic dyes," *Journal of Chromatography A*, vol. 1157, no. 1–2, pp. 260–272, Jul. 2007.
- [6] A. N. Kagalkar, U. B. Jagtap, J. P. Jadhav, V. A. Bapat, and S. P. Govindwar, "Biotechnological strategies for phytoremediation of the sulfonated azo dye Direct Red 5B using *Blumea malcolmii* Hook," *Bioresource Technology*, vol. 100, no. 18, pp. 4104–4110, Sep. 2009.
- [7] C. Bovet and A. R. Barron, "Electron Paramagnetic Resonance Spectroscopy of Copper(II) Compounds - OpenStax CNX." [Online]. Available: <http://cnx.org/contents/NB5XiHcn@2/Electron-Paramagnetic-Resonanc>. [Accessed: 17-May-2016].
- [8] W. A. E. McBryde, *A Critical review of equilibrium data for proton and metal complexes of 1,10-phenanthroline, 2,2'-bipyridyl and related compounds*. Oxford New York Toronto Rushcutters Bay Paris Kronberg-Taunus: Pergamon press, 1978.
- [9] A. Ringbom, *Les complexes en chimie analytique: comment choisir rationnellement les meilleures méthodes d'analyse complexométrique*. Paris: Dunod, 1967.
- [10] A. A. Schilt, *Analytical applications of 1,10-phenanthroline and related compounds*, 1st ed., vol. 32. Oxford London Edinburgh: Pergamon Press, 1969.
- [11] R. M. Smith and A. E. Martell, *Critical stability constants*. New York London: Plenum Press, 1975.
- [12] P. E. Sharpe and R. W. Lowe, "The bleaching of colored recycled fibers," in *Proceedings of the 1993 Pulping Conference*, Boston, 1993, vol. 3, pp. 1205–1217.
- [13] TAPPI Standard, *T 230 om-13 Viscosity of pulp (capillary viscometer method)*. 2013.
- [14] C. Ho, C. Lam, M. Chan, R. Cheung, L. Law, L. Lit, K. Ng, M. Suen, and H. Tai, "Electrospray Ionisation Mass Spectrometry: Principles and Clinical Applications," *Clin Biochem Rev*, vol. 24, no. 1, pp. 3–12, Feb. 2003.
- [15] S. Banerjee, S. Mazumdar, S. Banerjee, and S. Mazumdar, "Electrospray Ionization Mass Spectrometry: A Technique to Access the Information beyond the Molecular Weight of the Analyte, Electrospray Ionization Mass Spectrometry: A Technique to Access the Information beyond the Molecular Weight of the Analyte," *International Journal of Analytical Chemistry, International Journal of Analytical Chemistry*, vol. 2012, 2012, p. e282574, Mar. 2012.
- [16] T. Reitberger and J. Gierer, "Chemiluminescence as a means to study the role of hydroxyl radicals in oxidative processes," *Holzforschung*, vol. 42, no. 6, pp. 351–356, 1988.
- [17] I. Kraljić and C. N. Trumbore, "p-nitrosodimethylaniline as an OH radical scavenger in radiation chemistry," *Journal of the American Chemical Society*, vol. 87, no. 12, pp. 2547–2550, Jun. 1965.
- [18] W. Bors, C. Michel, and M. Saran, "On the Nature of Biochemically Generated Hydroxyl Radicals Studies using the Bleaching of p-Nitrosodimethylaniline as a Direct Assay Method," *European Journal of Biochemistry*, vol. 95, no. 3, pp. 621–627, 1979.
- [19] R. Lauricella and B. Tuccio, "Détection et caractérisation de radicaux libres après piégeage de spins," in *La spectroscopie de résonance paramagnétique électronique: Applications*, 2014th ed., EDP Sciences, 2014, pp. 49–78.

- [20] G. R. Buettner and L. W. Oberley, "Considerations in the spin trapping of superoxide and hydroxyl radical in aqueous systems using 5,5-dimethyl-1-pyrroline-1-oxide," *Biochemical and Biophysical Research Communications*, vol. 83, no. 1, pp. 69–74, Jul. 1978.
- [21] E. Finkelstein, G. M. Rosen, and E. J. Rauckman, "Spin trapping of superoxide and hydroxyl radical: Practical aspects," *Archives of Biochemistry and Biophysics*, vol. 200, no. 1, pp. 1–16, Mar. 1980.
- [22] G. R. Buettner, "Spin Trapping: ESR parameters of spin adducts 1474 1528V," *Free Radical Biology and Medicine*, vol. 3, no. 4, pp. 259–303, 1987.
- [23] L. Ebersson, B. Balinov, G. Hagelin, H. Dugstad, T. Thomassen, B. H. Forngren, T. Forngren, P. Hartvig, K. Markides, U. Yngve, and M. Ögren, "Formation of Hydroxyl Spin Adducts via Nucleophilic Addition--Oxidation to 5,5-Dimethyl-1-pyrroline N-Oxide (DMPO)," *Acta Chemica Scandinavica*, vol. 53, pp. 584–593, 1999.
- [24] A. R. Forrester and S. P. Hepburn, "Spin traps. A cautionary note," *Journal of the Chemical Society C: Organic*, p. 701, 1971.
- [25] P. M. Hanna and R. P. Mason, "Direct evidence for inhibition of free radical formation from Cu(I) and hydrogen peroxide by glutathione and other potential ligands using the EPR spin-trapping technique," *Archives of Biochemistry and Biophysics*, vol. 295, no. 1, pp. 205–213, May 1992.
- [26] P. M. Hanna, W. Chamulitrat, and R. P. Mason, "When are metal ion-dependent hydroxyl and alkoxyl radical adducts of 5,5-dimethyl-1-pyrroline N-oxide artifacts?," *Archives of Biochemistry and Biophysics*, vol. 296, no. 2, pp. 640–644, Aug. 1992.
- [27] M. J. Burkitt, S. Ying Tsang, S. Ching Tam, and I. Bremner, "Generation of 5,5-Dimethyl-1-pyrrolineN-Oxide Hydroxyl and Scavenger Radical Adducts from Copper/H₂O₂Mixtures: Effects of Metal Ion Chelation and the Search for High-Valent Metal–Oxygen Intermediates," *Archives of Biochemistry and Biophysics*, vol. 323, no. 1, pp. 63–70, Oct. 1995.
- [28] F. A. Villamena, C. M. Hadad, and J. L. Zweier, "Kinetic Study and Theoretical Analysis of Hydroxyl Radical Trapping and Spin Adduct Decay of Alkoxy carbonyl and Dialkoxyphosphoryl Nitrones in Aqueous Media," *The Journal of Physical Chemistry A*, vol. 107, no. 22, pp. 4407–4414, Jun. 2003.
- [29] G. Meissner, A. Henglein, and G. Beck, "Pulsradiolytische Untersuchung von Dimethylthioäther und Dimethylsulfoxid in wässriger Lösung," *Zeitschrift für Naturforschung B*, vol. 22, no. 1, pp. 13–19, Jan. 1967.
- [30] L. M. Dorfman and G. E. Adams, *Reactivity of the Hydroxyl Radical in Aqueous Solutions*, U.S. Department of Commerce-National Bureau of Standards., vol. 46. 1973.
- [31] A. I. Cederbaum, E. Dicker, E. Rubin, and G. Cohen, "The effect of dimethylsulfoxide and other hydroxyl radical scavengers on the oxidation of ethanol by rat liver microsomes," *Biochemical and Biophysical Research Communications*, vol. 78, no. 4, pp. 1254–1262, Oct. 1977.
- [32] M. Anbar and P. Neta, "A compilation of specific bimolecular rate constants for the reactions of hydrated electrons, hydrogen atoms and hydroxyl radicals with inorganic and organic compounds in aqueous solution," *The International Journal of Applied Radiation and Isotopes*, vol. 18, no. 7, pp. 493–523, Jul. 1967.

[33] D. R. Duling, "Simulation of multiple isotropic spin-trap EPR spectra," *J Magn Reson B*, vol. 104, no. 2, pp. 105–110, Jun. 1994.

[34] "SimEPR Manual." [Online]. Available: <http://www.niehs.nih.gov/research/resources/software/tox-pharm/tools/simepr/index.cfm>. [Accessed: 23-May-2016].

III. CHARACTERIZATION OF THE DYES AND INTERACTIONS WITH COPPER-PHENANTHROLINE

TABLE OF CONTENTS

LIST OF FIGURES	103
LIST OF TABLES	106
III.1 INTRODUCTION.....	107
III.2 CHARACTERIZATION OF THE DYES.....	107
<i>III.2.1 UV-visible analysis.....</i>	<i>107</i>
<i>III.2.2 Acidimetric titrations.....</i>	<i>110</i>
III.2.2.1 DR81L	110
III.2.2.2 DY11L.....	112
<i>III.2.3 FTIR spectroscopic analyses.....</i>	<i>115</i>
<i>III.2.4 ESI-MS analysis.....</i>	<i>117</i>
<i>III.2.5 NMR spectroscopic analyses</i>	<i>120</i>
III.2.5.1 Analysis of DR81L.....	120
III.2.5.2 Analysis of DY11L	127
III.2.5.3 Conclusions.....	132
<i>III.2.6 Conclusion.....</i>	<i>132</i>
III.3 COPPER-PHENANTHROLINE SPECIATION	132
III.4 ANALYSIS OF THE CU-PHEN COMPLEX.....	138
<i>III.4.1 CuSO₄.....</i>	<i>138</i>
<i>III.4.2 Phenanthroline</i>	<i>138</i>
<i>III.4.3 Cu-Phen</i>	<i>140</i>
<i>III.4.4 Evidence of coordination by EPR</i>	<i>140</i>
III.5 ANALYSIS OF THE DR81L DYE/CU-PHEN SYSTEM	142
<i>III.5.1 Dye/CuSO₄.....</i>	<i>142</i>
<i>III.5.2 Dye/Phenanthroline</i>	<i>143</i>
<i>III.5.3 Dye/Cu-Phen</i>	<i>143</i>
III.5.3.1 Alkaline pH: variation of Cu:Phen ratio	144
III.5.3.2 Alkaline pH: variation of the dye/Cu ratio	146
III.5.3.3 Neutral pH.....	148
III.5.3.4 Supplementary evidence for complexation	150
III.5.3.4.i Evidence by HPLC.....	151
III.5.3.4.ii Evidence by MS.....	151

III.5.3.4.iii Evidence by EPR.....	155
III.5.3.5 Conclusions.....	161
III.6 CONCLUSIONS.....	161
III.7 REFERENCES.....	163

LIST OF FIGURES

Figure III-1. Molecular structure of Direct Red 81.....	107
Figure III-2. Molecular structure of Direct Yellow 11.....	107
Figure III-3. UV-vis spectra of DR81L at 10 μ M and at different pHs	108
Figure III-4. UV-vis spectra of DR81S and DR81L at a theoretical concentration of 20 μ M, at pH 10.7	109
Figure III-5. UV-vis spectra of DY11L at 10 μ M and at different pHs.....	110
Figure III-6. Acidimetric titration of DR81L (a) whole spectrum, (b) focus on the pH jump	111
Figure III-7. UV-vis spectra of DR81L while successively adding small volumes of HCl. The corresponding pHs are presented in the legend.....	112
Figure III-8. Acidimetric titration of DY11L (a) whole spectrum, (b) focus on the pH jump	113
Figure III-9. UV-vis spectra of DY11L while successively adding small volumes of HCl. The corresponding pHs are presented in the legend.....	114
Figure III-10. FTIR spectra of DR81S, DR81L and DY11L	115
Figure III-11. Negative-ion scan ESI mass spectra of alkaline solutions of DR81L and DR81S.....	118
Figure III-12. Negative-ion scan ESI mass spectrum of an alkaline solution of DY11L.....	119
Figure III-13. Quantitative ^1H NMR spectrum of DR81L.....	121
Figure III-14. Quantitative ^1H NMR spectrum of the additive (3.0 to 4.2 ppm).....	121
Figure III-15. Quantitative ^{13}C NMR spectrum (top) and DEPT 135 (bottom) of DR81L	122
Figure III-16. Quantitative ^{13}C spectrum of the additive (50 to 75 ppm)	122
Figure III-17. 2D HSQC of the dye (lower threshold level)	123
Figure III-18. 2D HSQC of the additive (higher threshold level).....	124
Figure III-19. 2D HSQC enlargement of the additive	124
Figure III-20. 2D HSQC enlargement of the additive (55 ppm ^{13}C area)	125
Figure III-21. 2D COSY enlargement of the additive (alkyl area)	125

III. Characterization of the dyes and interactions with copper-phenanthroline

Figure III-22. 2D HMBC of the additive	126
Figure III-23. 2D HMBC enlargement of the additive (alkyl area)	126
Figure III-24. Conclusions of the NMR analyses and proposition of a structure for DR81L's main additive	127
Figure III-25. Quantitative ^1H NMR spectrum of DY11L.....	128
Figure III-26. Quantitative ^1H NMR enlargement spectrum of additive (2.7 to 4.0 ppm)	128
Figure III-27. Quantitative ^{13}C NMR and DEPT 135 spectra of DY11L.....	129
Figure III-28. Quantitative ^{13}C NMR enlargement spectrum for the additive	129
Figure III-29. HSQC experiment of additive.....	130
Figure III-30. HMBC ^{13}C NMR experiment of additive	131
Figure III-31. Conclusions of the NMR analyses and proposition of a structure for DY11L's main additive	131
Figure III-32. Calculated distributions of different species in CuSO_4 and Cu-Phen solutions as a function of pH. CuSO_4 alone, Cu:Phen = 1:1; initial CuSO_4 concentration $[\text{Cu}] = 15 \mu\text{M}$ at 25°C , with or without the occurrence of precipitation.....	133
Figure III-33. Calculated distributions of different species in Cu-Phen solutions as a function of pH. Cu:Phen = 1:2 and 1:3; initial CuSO_4 concentration $[\text{Cu}] = 15 \mu\text{M}$ at 25°C , with or without the occurrence of precipitation.....	134
Figure III-34. Absorbance spectra of copper sulfate solutions at pH 10.7 and 12.3, with $[\text{CuSO}_4] = 15 \mu\text{M}$	138
Figure III-35. Absorbance spectra of 1,10-phenanthroline at pH 10.7 and 12.3, with $[\text{Phen}] = 30 \mu\text{M}$ (equivalent to the amount of phenanthroline with DR81L:Cu = 1:1.5, Cu:Phen = 1:2, and $[\text{Cu}] = 15 \mu\text{M}$).....	139
Figure III-36. Absorbance spectra of the Cu-Phen solutions at (a) pH 10.7 and (b) pH 12.3, with Cu:Phen = 1:1, 1:2 and 1:3, and $[\text{Cu}] = 15 \mu\text{M}$	140
Figure III-37. Typical X-band EPR spectrum of copper(II) compounds [20].....	141
Figure III-38. Experimental X-band EPR spectra recorded at 100 K in frozen aqueous solutions of CuSO_4 and Cu-Phen at pH 12.3, with Cu:Phen = 1:2 and $[\text{Cu}] = 1.5 \text{ mM}$	141
Figure III-39. Absorbance spectra of the dye/copper sulfate system at pH 10.7 and 12.3, with DR81L: $\text{CuSO}_4 = 1:1.5$ and $[\text{DR81L}] = 10 \mu\text{M}$, compared to the dye alone at the same pHs.....	142
Figure III-40. Absorbance spectra of the dye/phenanthroline system at pH 10.7 and 12.3, with DR81L:Phen = 1:3 and $[\text{DR81L}] = 10 \mu\text{M}$ (equivalent to the amount of phenanthroline with DR81L:Cu = 1:1.5, Cu:Phen = 1:2, and $[\text{Cu}] = 15 \mu\text{M}$), compared to the dye alone at the same pHs	143
Figure III-41. Absorbance spectra of the dye/copper-phenanthroline system at pH 10.7, with Cu:Phen = 1:1, 1:2 and 1:3, DR81L:Cu= 1:1.5, and $[\text{DR81L}] = 10 \mu\text{M}$, compared to the dye alone at the same pH.....	144

Figure III-42. Absorbance spectra of the dye/copper-phenanthroline system at pH 12.3, with Cu:Phen = 1:1, 1:2 and 1:3, DR81L:Cu = 1:1.5, and [DR81L] = 10 μ M, compared to the dye alone at pH 10.7 and 12.3..... 145

Figure III-43. Absorbance spectra of the dye/copper-phenanthroline system at pH 10.7, with Cu:Phen = 1:2 and [DR81L] = 10 μ M, for different DR81L:Cu ratios147

Figure III-44. Absorbance spectra of the dye/copper-phenanthroline system at pH 12.3, with Cu:Phen = 1:2 and [DR81L] = 10 μ M, for different DR81L:Cu ratios 148

Figure III-45. Experimental X-band EPR spectra recorded at 100 K in frozen aqueous solutions of CuSO₄ and Cu-Phen at pH 6.5, with Cu:Phen = 1:1 and 1:2 and [Cu] = 1.5 mM 149

Figure III-46. Absorbance spectrum of the dye/copper-phenanthroline system at pH 6.5, with Cu:Phen = 1:2 and DR81L:Cu = 1:1.5, compared to the dye alone and copper-phenanthroline alone 150

Figure III-47. Chromatograms of DR81S and DR81S+Cu-Phen, elution by a gradient of TBA-OH 5 mM in methanol/TBA-OH 5 mM in water, flow of 0.7 mL/min, UV detection at 254 nm 151

Figure III-48. Molecular structure of BPS 152

Figure III-49. Negative-ion scan ESI-MS spectrum of Cu-BPS (1:3) at 2.5 mM in water 152

Figure III-50. Negative-ion scan ESI-MS spectrum of DR81S+Cu-BPS (1:3) with DR81S 50 μ M and Cu-BPS 75 μ M 153

Figure III-51. Negative-ion scan ESI-MS spectrum of DR81S+Cu-BPS (1:3) with DR81S, enlargement from 700 to 1000 m/z 154

Figure III-52. Comparison between experimental peaks (top) and simulated peaks (bottom) at 591 m/z (a) and 860 m/z (b) 155

Figure III-53. Experimental X-band EPR spectra recorded at 100 K in frozen aqueous solutions of (a) CuSO₄ and CuSO₄+DR81L (b) Cu-Phen and Cu-Phen+DR81L (c) CuSO₄+DR81L and Cu-Phen+DR81L, at pH 12.3, with Cu:Phen = 1:2, DR81L:Cu = 1:1.5 and [Cu] = 1.5 mM 156

Figure III-54. Experimental X-band EPR spectra recorded at 100 K in frozen aqueous solutions of (a) CuSO₄ and CuSO₄+DR81L (b) Cu-Phen and Cu-Phen+ DR81L (c) CuSO₄+ DR81L and Cu-Phen+ DR81L, at pH 6.5, with Cu:Phen = 1:2, DR81L:Cu = 1:1.5 and [Cu] = 1.5 mM 157

Figure III-55 Experimental X-band EPR spectra recorded at 100 K in frozen aqueous solutions of Cu-Phen and Cu-Phen+DR81L at pH 10.7, with Cu:Phen = 1:2, DR81L:Cu = 1:1.5 and [Cu] = 1.5 mM 158

Figure III-56. Experimental X-band EPR spectra recorded at 100 K in frozen aqueous solutions of (a) CuSO₄ and CuSO₄+DR81L (b) Cu-Phen and Cu-Phen+ DR81L (c) CuSO₄+ DR81L and Cu-Phen+ DR81L, at pH 12.3, with Cu:Phen = 1:2, DR81L:Cu = 10:1.5 and [Cu] = 1.5 mM 159

Figure III-57. Experimental X-band EPR spectra recorded at 100 K in frozen aqueous solutions of (a) CuSO₄ and CuSO₄+DR81L (b) Cu-Phen and Cu-Phen+ DR81L (c) CuSO₄+ DR81L and Cu-Phen+ DR81L, at pH 6.5, with Cu:Phen = 1:2, DR81L:Cu = 10:1.5 and [Cu] = 1.5 mM 160

LIST OF TABLES

Table III-1. Potential chemical groups corresponding to the peaks of both dyes.....	116
Table III-2. Proposed molecular structures depending on the peaks observed in the ESI mass spectra of DR81L and DR81S.....	118
Table III-3. Predicted concentrations of the different species at pH 6.5, 10.7 and 12.3, for Cu:Phen = 1:0, 1:1, 1:2 and 1:3, with an initial CuSO ₄ concentration of 15 μM at 25°C, assuming no precipitation occurrence. The results are given as molar percentages of total [Cu].....	136
Table III-4. Predicted concentrations of the different species at pH 6.5, 10.7 and 12.3, for Cu:Phen = 1:0, 1:1, 1:2 and 1:3, with an initial CuSO ₄ concentration of 15 μM at 25°C, assuming the occurrence of precipitation. The results are given as molar percentages of total [Cu].....	137
Table III-5. Assignments of the mass peaks obtained after ESI-MS analysis of the Cu-BPS solution	153
Table III-6. Assignments of the mass peaks obtained after ESI-MS analysis of the DR81S+Cu-BPS solution	154

III.1 INTRODUCTION

The objective of this chapter was to characterize the dyes selected in this project and to analyze their interactions with the Cu-Phen complex in aqueous solution, before adding any oxidant and in the absence of fibers.

III.2 CHARACTERIZATION OF THE DYES

First of all, the selected dyes were characterized via different techniques, especially UV-visible, mass spectrometry and NMR spectroscopy. The objective was to check the data given by the dye supplier, especially the structures of the dyes: Direct Red 81 for DR81L (Figure III-1) and Direct Yellow 11 for DY11L (Figure III-2).

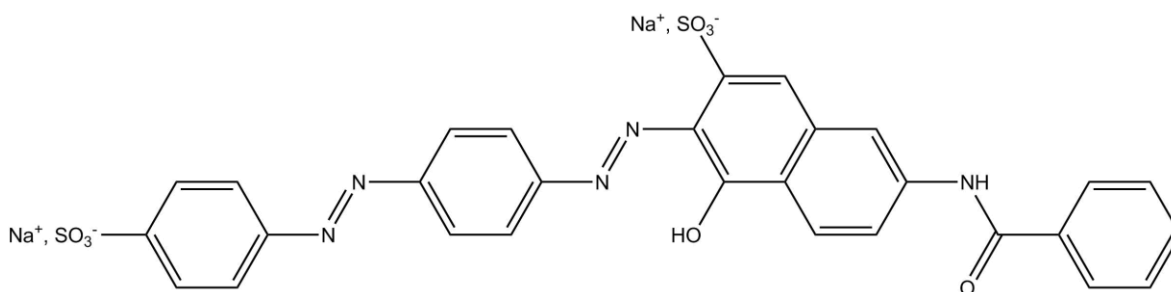


Figure III-1. Molecular structure of Direct Red 81

The DR81 molecule (Figure III-1) bears two azo groups and five aromatic nuclei, which are conjugated and constitute the chromophore part, while the auxochrome groups consist of one hydroxyl group (of the naphthol group) and two sulfonic acid groups that allow the dissolution of DR81 into water and its fixation to cellulose fibers.

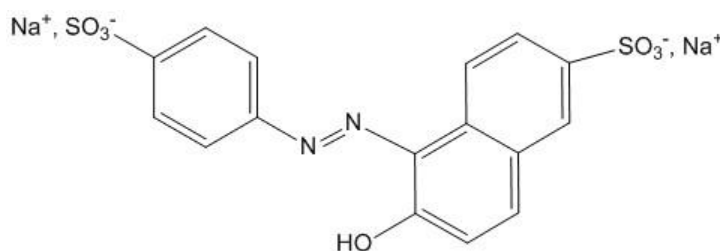


Figure III-2. Molecular structure of Direct Yellow 11

The structure of the DY11 molecule (Figure III-2) is simpler than that of DR81. It is almost a substructure of the DR81 molecule. The chromophore part is ensured by the presence of three aromatic rings conjugated with one azo function. As in the DR81 molecule, the auxochrome groups of DY11 consist of one hydroxyl group (of the naphthol group) and two sulfonic acid groups.

III.2.1 UV-visible analysis

UV-visible spectroscopy is a convenient method to characterize the dyes. It allows to analyze dye structures and their possible modifications, due to the variation of physical and chemical properties of the medium, or due to reactions. In particular, UV-vis spectroscopy allowed to determine the molar extinction coefficients and maximum absorbance wavelengths of the studied dyes at different pHs. Thanks to these results, the concentration of a dye solution could be verified

systematically. In addition, it was verified that both dyes were thermally stable since their absorbance after heating during 1 h at 80°C was unchanged.

Figure III-3 shows the UV-vis spectra of the DR81L dye at different pHs from 4.5 to 12.3, obtained with the addition of 1 M NaOH or diluted H₂SO₄.

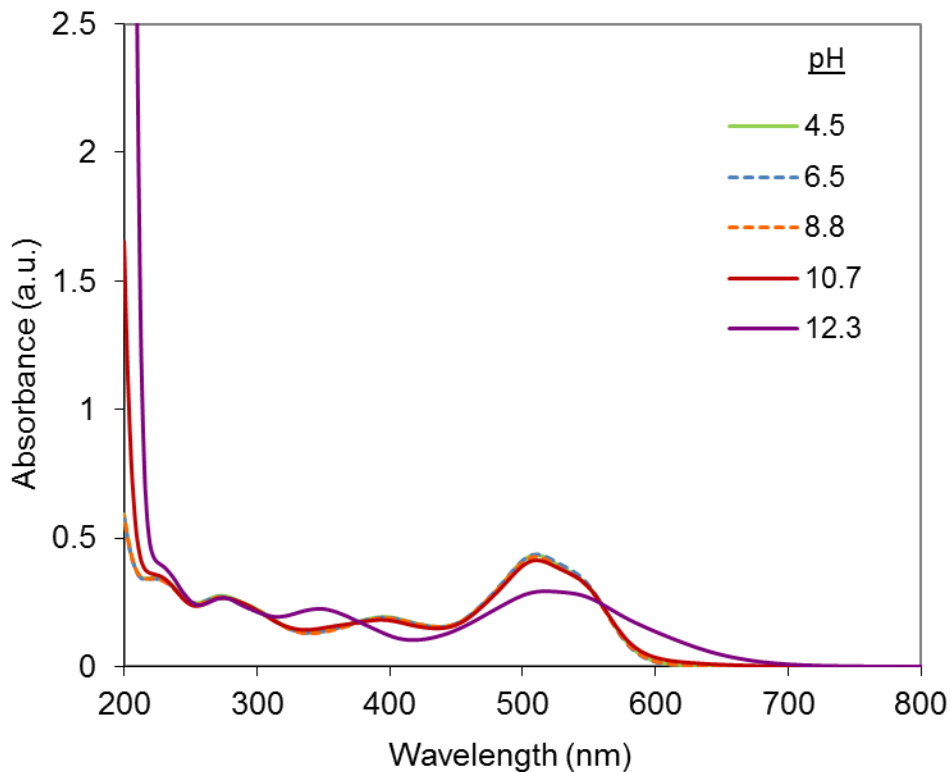


Figure III-3. UV-vis spectra of DR81L at 10 μM and at different pHs

In the visible range, the dye solution exhibited a maximal absorbance at around 510-518 nm depending on the pH. It was red from pH 4.5 to pH 10.7 (λ_{max} around 510 nm) and red-purple at strong alkaline pH (12.3) ($\lambda_{\text{max}} = 517.5$ nm). This is illustrated in Figure III-3 by the bathochromic and hypochromic absorbance shift observed from pH 10.7 to pH 12.3.

The bathochromic shift between pH 10.7 and 12.3 is attributed to the ionization of the free naphthol group of the dye in the presence of hydroxyl anions. Since the acid dissociation constants of the naphthol groups in dyes are typically above 10, lower pHs were tested in order to determine whether the dye was already ionized at pH 10.7. According to Figure III-3, there is almost no change of the spectrum between pH 4.5 and 10.7, which shows that the dye was not ionized in this pH range.

In the study of dye interactions with Cu-Phen, it was thus decided to focus on these two pH values (10.7 and 12.3), representative of the non-ionized and ionized forms of the DR81 molecule.

Besides, the DR81L dye being a commercial paper dye, it was compared with the same dye without additives: DR81S, supplied by Sigma Aldrich and supposed purer than DR81L (see II.1.1) (Figure III-4). The comparison was made using the same theoretical dye concentration, taking into account the purity given by both dye suppliers.

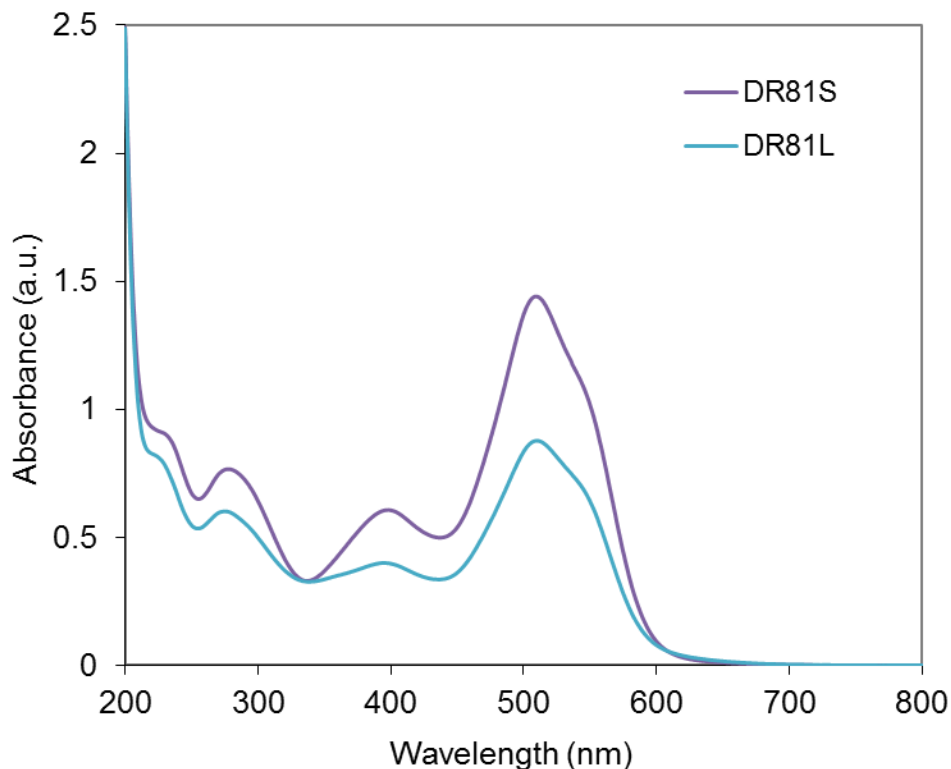


Figure III-4. UV-vis spectra of DR81S and DR81L at a theoretical concentration of 20 μM , at pH 10.7

Figure III-4 reveals that the concentrations given by the suppliers may not be perfectly right, since the dye appeared to be at a higher concentration in DR81S than in DR81L, for a same theoretical concentration. The absorbance at 510 nm reached 1.4417 and 0.8774 a.u. for DR81S and DR81L respectively, meaning that the concentration of DR81L represented 60.9% of that of DR81S.

Figure III-5 below presents the UV-vis spectra of the DY11L dye at different pHs.

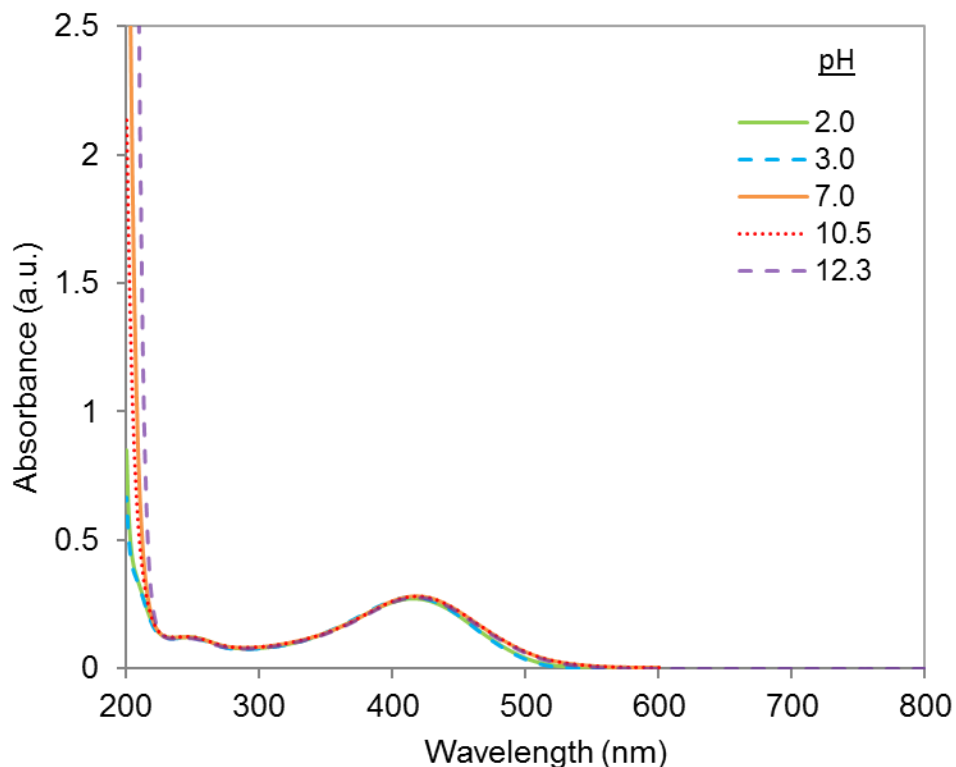


Figure III-5. UV-vis spectra of DY11L at 10 μ M and at different pHs

Contrarily to DR81L, the absorbance of the DY11L dye did not vary in the 7-12.3 pH interval. Yet, a slight bathochromic shift occurs between pH 3 and 7 when increasing the pH.

After the UV-vis study of the dyes, acidimetric titration was performed to characterize the different acidic functions present in the dye structures.

III.2.2 Acidimetric titrations

Acid/base titration was performed on both dyes in order to better understand their chemical behaviors and try to find the acid dissociation constants of their acidic functions.

III.2.2.1 DR81L

A 100 mL solution of DR81L 2×10^{-4} M was prepared with 1.3 mL NaOH 1M and titrated by HCl 0.1 M. The HCl solution was added slowly and both pH and UV-vis absorbance were measured all along the dosage. The acidimetric titration is illustrated in Figure III-6 with the pH vs. HCl volume plot.

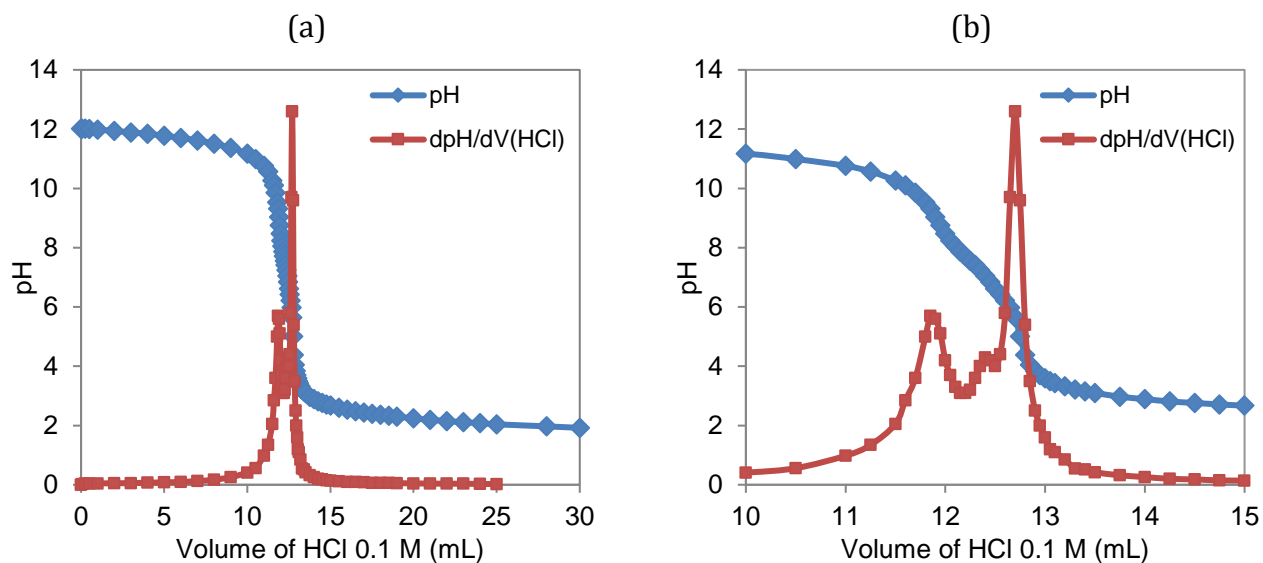


Figure III-6. Acidimetric titration of DR81L (a) whole spectrum, (b) focus on the pH jump

Figure III-6a shows that an important pH drop occurred after the addition of around 13 mL HCl 0.1 M, which corresponds to the titration of the hydroxide ions present in the medium (1.3 mL NaOH 1 M). Figure III-6b reveals that there were actually three equivalence points: the first one at pH 9.2, a very small one at pH 7.0 and the major one at pH 5.6.

To find whether these pH drops were related to color changes depending on pH, the UV-vis spectra obtained after incremented addition of HCl are presented in Figure III-7.

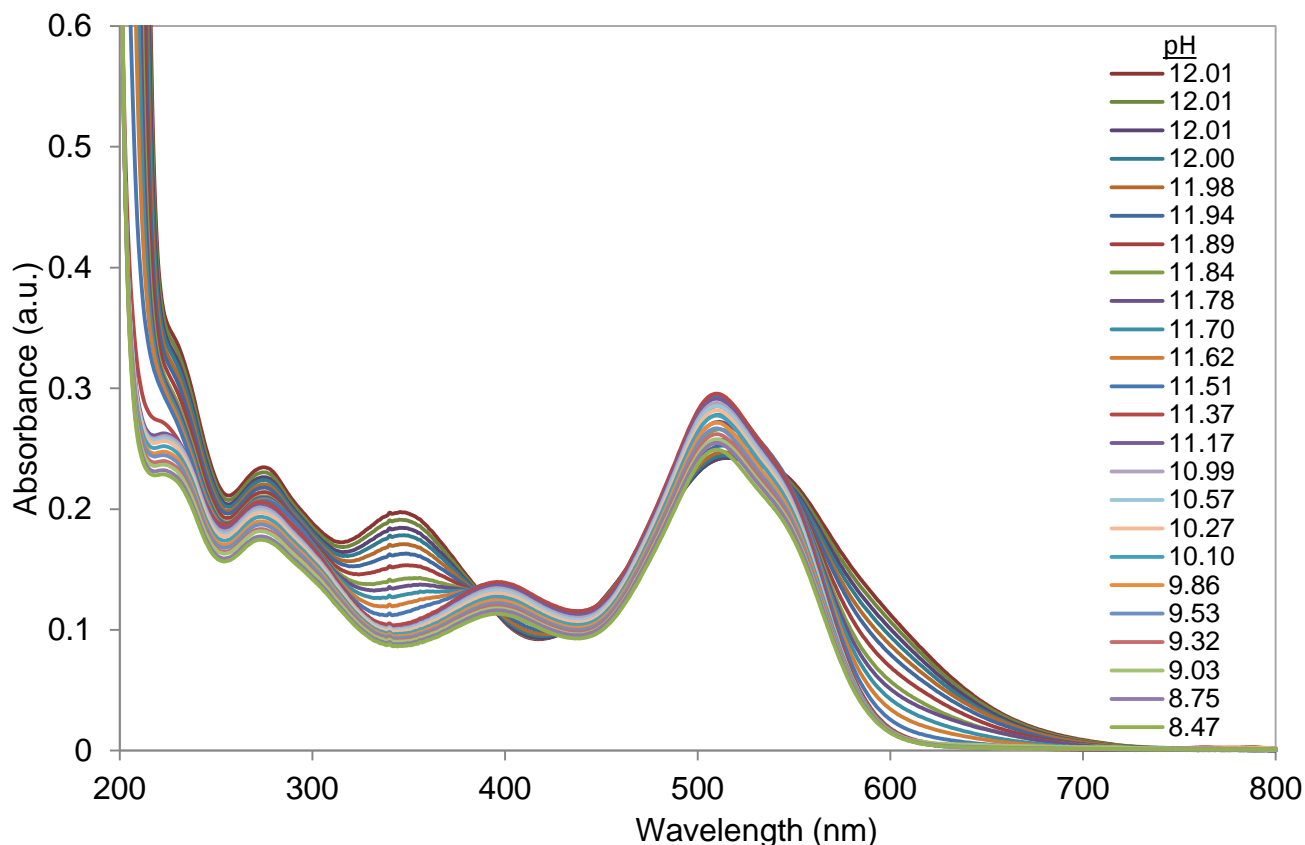


Figure III-7. UV-vis spectra of DR81L while successively adding small volumes of HCl. The corresponding pHs are presented in the legend.

First, after the addition of an excess of NaOH and before beginning the titration by HCl, the DR81 dye was in its ionized form. Then the addition of acid induced slight dilution of the dye and explains the slowly decreasing absorbance observed in Figure III-7. However, a hypsochromic shift is clearly visible. In addition, this study allowed to measure the maximum absorbance wavelength at each pH and to know more precisely how it evolved. It was found to be 510 nm from pH 1.9 to pH 11.5 and to start increasing afterwards, from 510.5 at pH 11.6 to 517.5 nm at pH 12.3.

Therefore, the DR81 dye structure seems to contain a weak acid/base function of pKa between 11.5 and 12.3, i.e. around 11.9. Since at this pH, the spectrum is intermediary, between the shape of the ionized dye spectrum and the unionized dye spectrum (Figure III-7), the color shift with pH may be attributed to the ionization of the naphthol group. Consequently, the pKa of 11.9 seems to be that of the dye's naphthol group, which was actually titrated at high pH, before the first observed pH drop in Figure III-6. This high pKa is consistent with the findings of Oakes and Gratton, who observed that the pKa was higher for azo dyes with the hydroxyl group of the naphthol in ortho position to the azo group [1]. The other equivalence points found between pH 9.2 and 5.6 probably correspond to some functions originated from the additives present in the dye solution.

III.2.2.2 DY11L

A 100 mL solution of DY11L 2×10^{-4} M was prepared with 2 mL NaOH 1M and titrated by HCl 0.1 M. HCl was added slowly and both pH and UV-vis absorbance were measured. The acidimetric titration is illustrated in Figure III-8 with the pH vs. HCl volume plot.

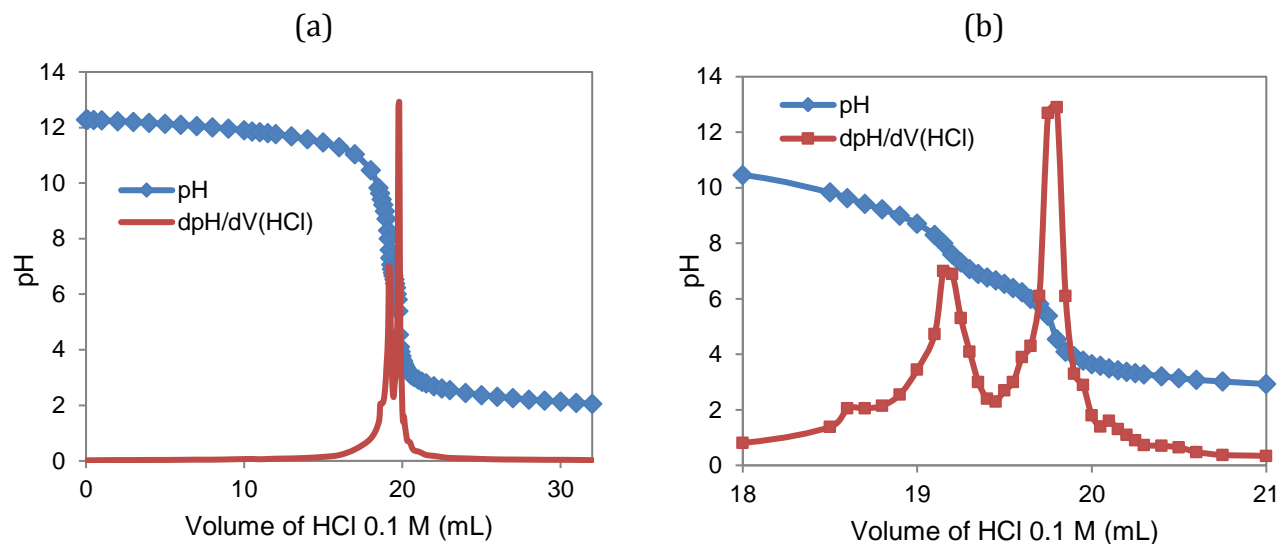


Figure III-8. Acidimetric titration of DY11L (a) whole spectrum, (b) focus on the pH jump

Figure III-8a shows that as expected, the pH dropped after the addition of around 20 mL HCl 0.1M, due to the neutralization of the NaOH excess by HCl. Figure III-8b, with a narrower pH range displays two pH jumps: the first equivalence point is at pH 7.8 and the second one at pH 4.8.

Again, to correlate the titration curve to color changes, the UV-vis spectra obtained after incremented addition of 0.1 M HCl are presented in Figure III-9.

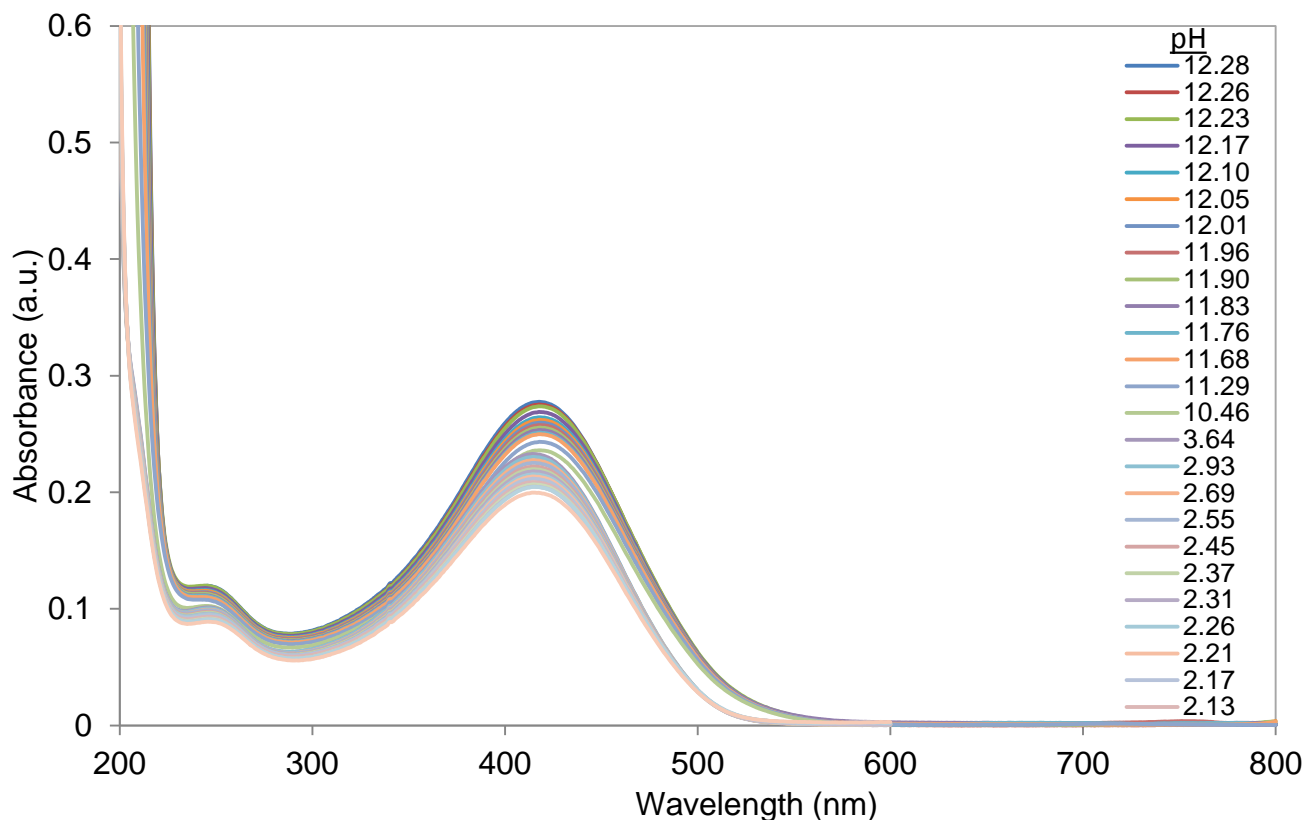


Figure III-9. UV-vis spectra of DY11L while successively adding small volumes of HCl. The corresponding pHs are presented in the legend.

As already observed with the DR81 dye molecule, the absorbance slightly decreased because of the low dilution during titration. However, here, the UV-vis spectra were quite similar although a little hypsochromic shift was observed when moving towards acidic pH. Indeed, the maximum absorbance wavelength between pH 10.5 and 12.3 was 418 nm, whereas it was 414.5 nm between pH 2 and 3.6. If this modification when acidifying is due to the naphthol group's deionization as in the case of the DR81 dye, it means (1) that the pKa of the naphthol is lower than that of the DR81 molecule and (2) that this function is actually titrated in the range of the observed pH drops. It should thus correspond to one of the two drops, the other one probably owing to one additive in DY11L.

The pKa of the naphthol group was certainly influenced by mesomeric and inductive effects of the conjugated structure and the sulfonated groups at the extremities of the molecule, making the hydrogen of the hydroxyl group more or less labile. In the case of DY11, the environment of the naphthol group has a stronger electron withdrawing effect than in DR81, since the molecule is shorter. This can explain why its pKa is more acidic than that of the naphthol group in DR81.

III.2.3 FTIR spectroscopic analyses

As a simple way to check the structures of the dyes and the main functional groups they contain, FTIR spectra of the dyes were recorded as described in II.2.1.3.

The Fourier-Transformed Infra-Red spectra of the three available dyes (DR81S, DR81L and DY11L) are presented in Figure III-10. DR81S was analyzed directly as a powder and DR81L and DY11L after lyophilization.

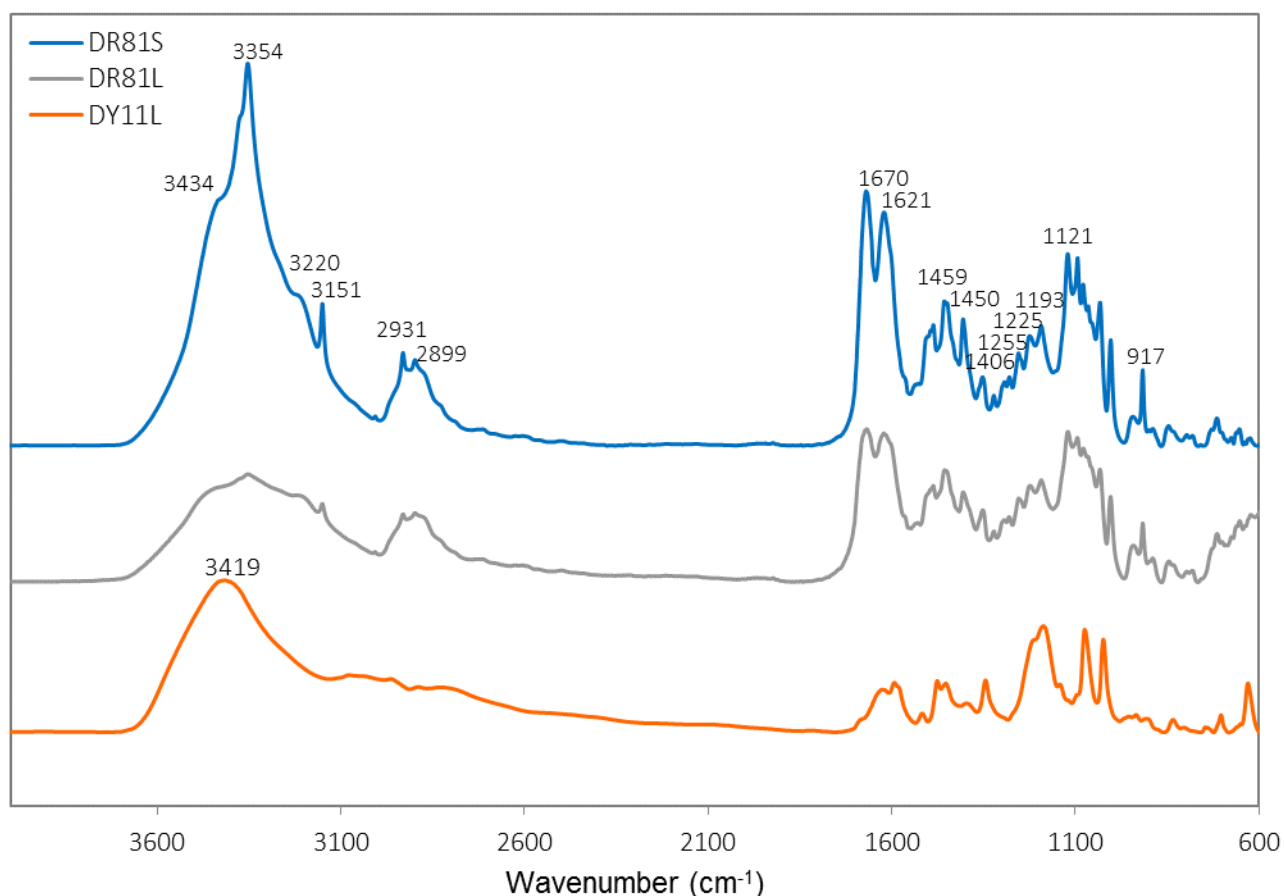


Figure III-10. FTIR spectra of DR81S, DR81L and DY11L

The spectra of DR81S/DR81L and DY11L are close, confirming very similar structures between these dyes. The main differences consist in supplementary peaks for DR81, which is logical since the DR81 molecule's structure is longer and contains more chemical functions than DY11's. The peaks attributed to DR81 and DY11 are thus listed in Table III-1 and some corresponding groups are proposed.

Table III-1. Potential chemical groups corresponding to the peaks of both dyes

Wavenumber (cm ⁻¹)	DR81	DY11	Potential corresponding groups [2]
3434	x	x	OH
3354	x	x	SO ₃
3151	x		NH
2931	x		benzene/naphthalene
2899	x		benzene/naphthalene
1670	x		CO-NH-R
1621	x	x	N=N
1459	x	x	α-naphthalene
1450	x	x	α-naphthalene
1406	x	x	Aromatic alcohol
1255	x	x	ar-NH-R or RSO ₃ ⁻
1225	x	x	RSO ₃ ⁻
1193	x	x	?
1121	x		?
917	x		O-H deformation

The main differences are visible in Figure III-10 with the peaks that appear only or mostly with DR81: amine, benzene/naphthalene, CO-NH-R, etc. Looking at its structure (Figure III-2), DY11 does not contain any amine group and has only one benzene vs. 3 in DR81. Moreover, the carbonyl group CO-NH-R appears in the structure of DR81 only. Consequently, the FTIR spectra are in accordance with the dye structures given by the suppliers.

Since DR81S and DR81L exhibit almost identical FTIR spectra, it seems that the additives present in DR81L cannot be detected by FTIR in this wavenumber range. It may be the case with DY11L's additives as well, but this could not be verified experimentally since no "pure" DY11 molecule was found to proceed to the comparison.

However, the experimental dye spectra were compared with those presented in the literature for the same dye molecules.

In a study on the microbial decolorization of DR81, Sahasrabudhe and collaborators [3] analyzed the dye and its degradation by FTIR and found a spectrum for DR81 which was quite similar to those obtained in the present work. A broad peak corresponded to hydroxyl groups at 3491 cm^{-1} and some peaks were found with the exact same wavenumbers, i.e. the naphthalene peak at 1450 cm^{-1} , the sulfonate peak at 1225 cm^{-1} and the peak at 1121 cm^{-1} . Other spectra in chemistry databases corroborated these results, even though some differences could be observed from one spectrum to another [4]–[6]. Kagalkar *et al.* [7] also analyzed the Direct Red 81 dye in the frame of a decolorization study. The peaks for the azo bonds and the bonded NH group were found at 1599 cm^{-1} and 3065 cm^{-1} , respectively, i.e. not at the exact same frequencies as in our experimental results, but still in the write ranges to be assigned to the same chemical groups. Similarly, the O-H stretching was also found at the highest wavenumbers (3622 cm^{-1}).

The spectrum obtained with the commercial DY11L dye was very similar to those found in the literature [8], [9], especially spectrum NIDA15442. This suggests that the additives present in DY11L do not have a significant influence on its FTIR spectrum.

As FTIR could not give any detailed information on the dyes' structures and on the additives present in the dye formulations, further characterizations were required. Mass spectroscopy was used for that purpose. The results are presented in the next part.

III.2.4 ESI-MS analysis

ESI-MS combines the separation of the chemicals present in a complex mixture, i.e. the commercial dye formulation in the present case, and their identification through the measurement of their molar masses. The electrospray technique ionizes the separated molecules before mass analysis. The resulting mass spectrum gives the relative abundance of the negatively or positively charged molecule signals depending on their m/z ratios. The ESI-MS method was introduced in detail in II.2.4.2.

The objective of these analyses was to measure the molar masses of the molecules present in the commercial dyes, in order to identify the additives present and to confirm the dye formula given by the supplier. The peaks were attributed to different molecules thanks to the Bruker Daltonics DataAnalysis 3.3 software, which allowed to find the exact m/z values and charges corresponding to each peak.

Figure III-11 presents the mass spectra obtained for DR81L and DR81S at $50\text{ }\mu\text{M}$, at strong alkaline pH (conditions of a conventional H_2O_2 bleaching stage), under negative mode (to see the negatively charged molecules).

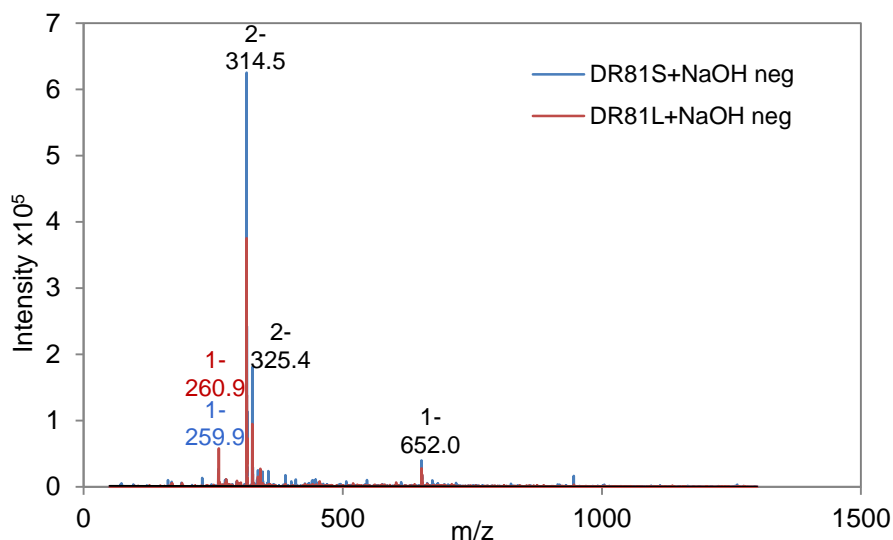
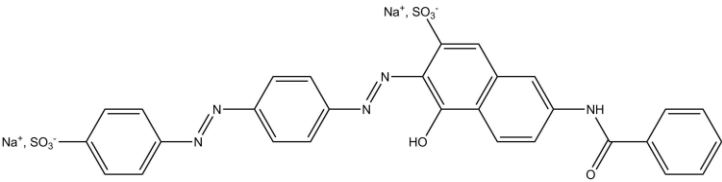
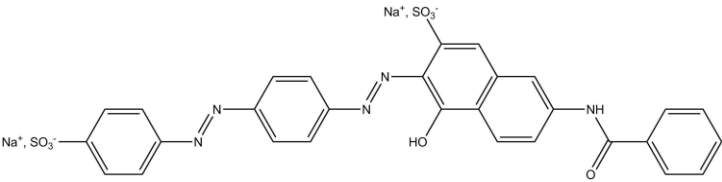
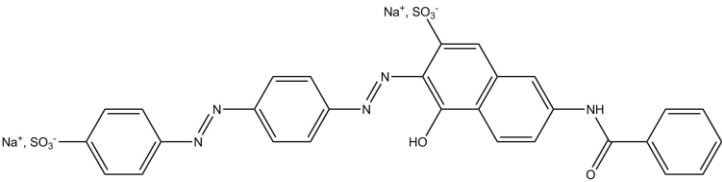
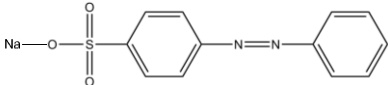
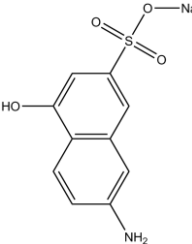


Figure III-11. Negative-ion scan ESI mass spectra of alkaline solutions of DR81L and DR81S

Table III-2 lists the main peaks observed in Figure III-11, their corresponding ion structures and initial compounds.

Table III-2. Proposed molecular structures depending on the peaks observed in the ESI mass spectra of DR81L and DR81S

Compound	Molar mass	m/z ratios	Corresponding ion structure
	675	314.5	$[M-2Na]^{2-}$ *
	675	325.4	$[M-H-Na]^{2-}$
	675	652.0	$[M-Na]^{-}$
	284	260.9	$[M-Na]^{-}$
	261	259.9	$[M-H]^{-}$

* M symbolizes the compound represented in the first column, $[M-2Na]^{2-}$ means that the peak observed at 314.5 m/z corresponds to M after removal of 2 sodium atoms, which makes it a dianion

Under negative mode, DR81's molecular structure (Figure III-1) was found in both DR81S and DR81L alkaline solutions (Figure III-11). Indeed, the major detected peak at 314.5 m/z corresponds to a dianion of the DR81 molecule without its sodium atoms. Moreover, the peak at 325.4 m/z corresponds to the dianion formed by deprotonation of the naphthol and removal of one Na. Finally, the anion at 652.0 m/z corresponds to DR81 without one of the two Na. Besides,

two fragments also appeared in solution, probably originating from the commercial dye synthesis: one with an m/z ratio of 260 in DR81S, with an intensity representing around 3% of that of the main peak, and one with m/z 261 in DR81L, with an intensity representing around 15% of that of the main peak. Therefore, DR81S can be considered as purer compared to DR81L, even without taking additives into account. Indeed, some additives were found in DR81L under positive mode ionization: numerous peaks with a regular space of 44 m/z (m/z of 173.1, 217.1, 261.1, 305.2, 349.2, 393.2, 437.3) suggest a polymer such as polyethylene glycol (ethylene glycol has a molecular weight of 44 g/mol). It was not possible to go further on the additive characterization of the DR81L or DR81S dye formulation with the ESI-MS analysis.

The same analysis was performed on the DY11L dye. The ESI-MS spectrum is presented in Figure III-12.

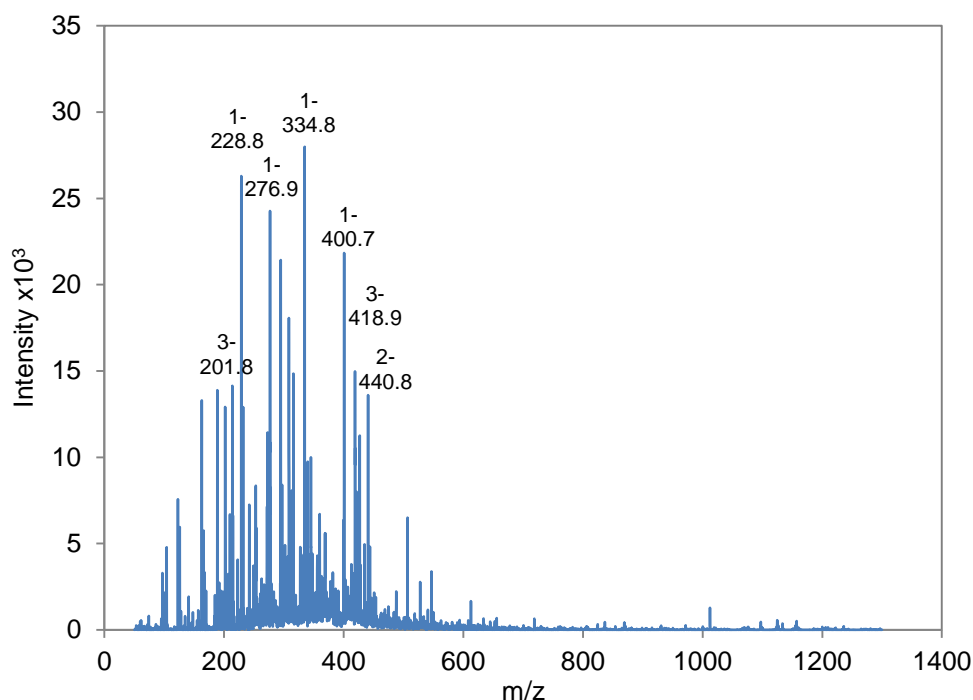


Figure III-12. Negative-ion scan ESI mass spectrum of an alkaline solution of DY11L

Using the same theoretical concentration as for the DR81S and DR81L analysis, 50 μM , the spectrum of DY11L was less intense and did not exhibit any of the expected peaks. With a molecular weight of 452 g/mol, the removal of one sodium would give 429 m/z and the removal of two would give 203 m/z . In spite of this, the highest of the numerous peaks exhibited in Figure III-12 were at m/z ratios of 228.8, 276.9, 294.8, 334.8, 400.7. It is therefore difficult to conclude on the dye's molecular structure, all the more as some of the peaks may come from additives present in this commercial dye solution. The same analysis was performed with a more concentrated solution and the resulting spectrum was more intense but as complicated as this one.

Hence, the DY11 molecular structure as given by the dye supplier (Figure III-2) could not be detected. There are three possible explanations: (1) the dye molecule may be diluted so that additives are in majority; (2) the dye molecular structure given by the supplier may not be right, or (3) the dye molecule was fragmented during the ionization by electrospray.

To evaluate these possibilities and in an attempt to go further in the commercial dyes characterization, NMR spectroscopy was used. This study is presented in the next part.

III.2.5 NMR spectroscopic analyses

Liquid nuclear magnetic resonance spectroscopy allowed further analysis, especially to supplement previous results on the composition and concentration of the commercial dye solutions, the NMR technique providing structural information concerning the object of interest. The methodology was presented in II.2.1.4.

Some preliminary studies were carried out to know the NMR possibilities and the solution concentrations required to obtain reasonable-quality spectra:

- working with a 10 mm probe for spins detected by increasing the coil,
- working with a dye concentration of 3.5 mM, corresponding to the dye:Cu:Phen ratio of 1:1.5:3 to get the highest phenanthroline concentration possible (for it to be soluble), i.e. around 10.5 mM,
- 2 pH values were tested (ionized and unionized dye),
- ^{15}N , ^{13}C and ^1H were tested.

First of all, ^{15}N experiments were carried out. With the conditions optimized to detect the NH amidic one (so *INEPT* sequence with proton decoupling corresponding to $^1J = 90$ Hz and selectivity on NH Nitrogen atom), no signal was detected over 24 hours of acquisition: only a flat baseline. Consequently, ^{15}N -enriched products would have been necessary to provide exploitable spectra.

Some tests were undertaken at the same concentration for ^{13}C experiments: some signals were detected, but the S/N ratio was very low, even over 24 hours of acquisition. It was the same for ^1H : the S/N ratio was lower than expected, and some aliphatic "impurities" were observed, mainly triethanolamine for DY11L.

For each compound, similar spectra were obtained with the two different pH values. No differences were observed.

In the further studies, the commercial dyes were lyophilized and re-solubilized in deuterated solvent, giving more concentrated solutions for structural analysis of impurities.

III.2.5.1 Analysis of DR81L

The quantitative ^1H NMR spectrum full scale of DR81L is given in Figure III-13.

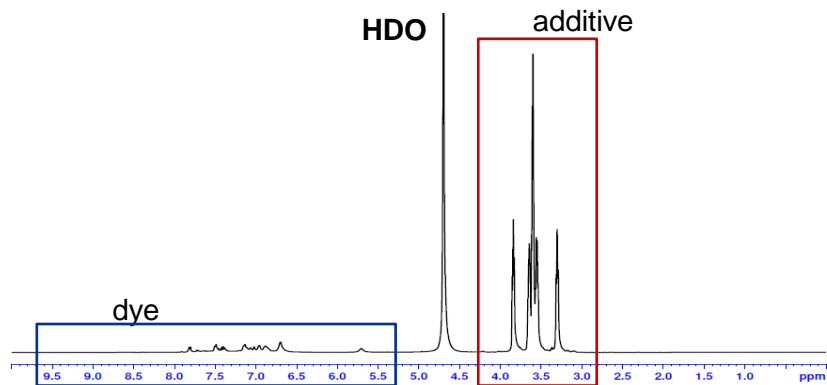


Figure III-13. Quantitative ^1H NMR spectrum of DR81L

Only protons in the 8.0 to 6.5 ppm area corresponding to aromatic structures were expected for DR81L. The additive was predominant around the 3.5 ppm area. The ^1H NMR spectrum enlargement in the range between 3.0 and 4.2 ppm corresponding to the additive is given in Figure III-14. Hyperfine structures corresponding to ^1H - ^1H coupling were observed. The chemical shifts indicate the neighboring of hetero atoms for the alkyl groups. Five different multiplets could be distinguished labelled from a to e with the corresponding integrals: 2 / 2 / 4 / 2 / 2.

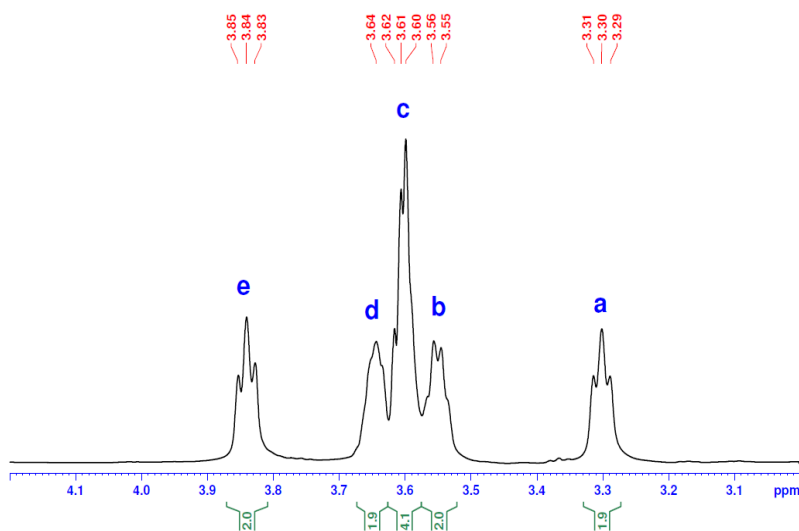


Figure III-14. Quantitative ^1H NMR spectrum of the additive (3.0 to 4.2 ppm)

The quantitative ^{13}C NMR spectrum of DR81L is given in Figure III-15 (top) with the corresponding DEPT 135 spectrum (bottom).

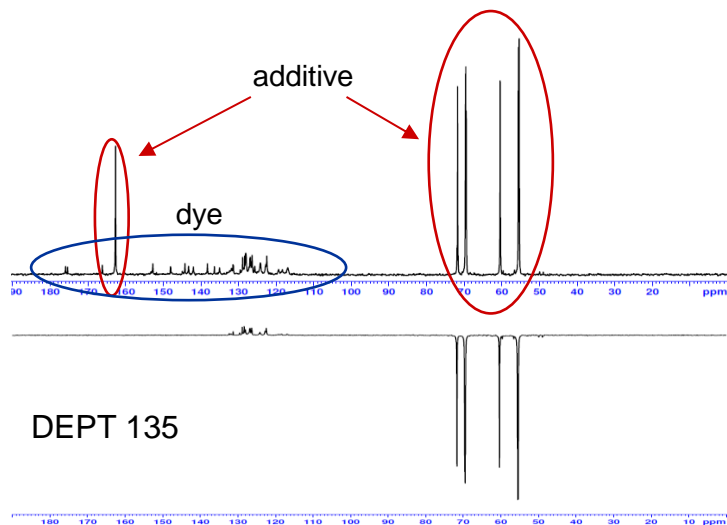


Figure III-15. Quantitative ^{13}C NMR spectrum (top) and DEPT 135 (bottom) of DR81L

Small peaks in the aromatic region 180 – 110 ppm correspond to the dye structure. Figure III-15 mainly exhibits very high fine supplementary signals from the additive(s). From the DEPT 135 spectrum, CH_3 and CH peaks should be positive and CH_2 peaks have an inverse negative phase. Hence, we could deduce that only CH_2 carbons were present (54-73 ppm), plus a quaternary carbon C at 163 ppm (no signal for quaternary carbons with the DEPT 135 experiment). Once again, the CH_2 chemical shifts confirm the neighboring of hetero atoms.

Figure III-16 below gives the enlargement of the aliphatic part ^{13}C NMR spectrum of the additive. No coupling (except with ^2D and ^{19}F or some nuclei) exists for usual ^{13}C spectra, so the two different signals at 55.5 and 55.4 ppm correspond to two different carbon atoms. As the spectrum was registered with quantitative conditions (respecting a long relaxation delay, and with ^1H broad band decoupling during acquisition time only, to avoid nOe enhancement), integrals of the signals could be measured. These are in agreement with 6 CH_2 and 1 quaternary C .

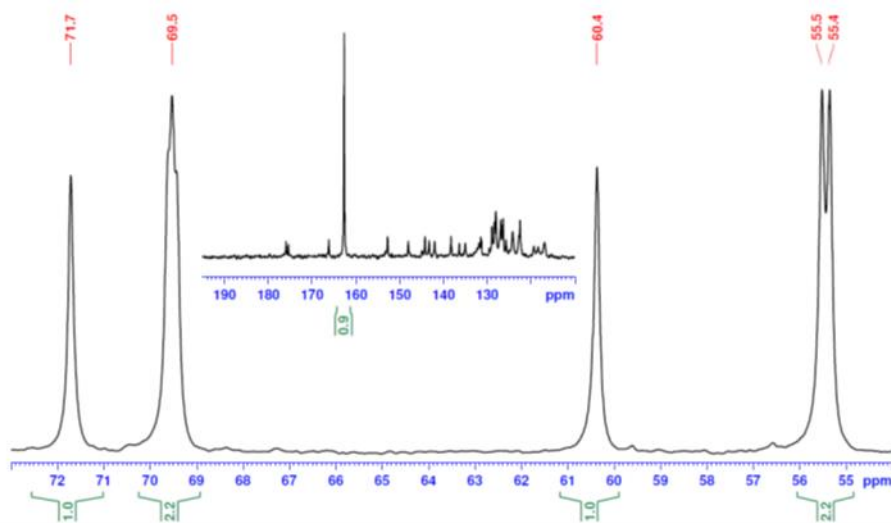


Figure III-16. Quantitative ^{13}C spectrum of the additive (50 to 75 ppm)

To allow peak assignment, some 2D experiments - showing the correlations between protons and carbons – were used.

HSQC informed us about $^1\text{H} - ^{13}\text{C}$ close correlations corresponding to $^1J_{\text{HC}}$ coupling constants, i.e. which carbon is directly bonded to which proton. Due to the heterogeneity of the peak intensities, it was not possible to obtain all the correlations with only one 2D map. Therefore, it was necessary to work with several threshold levels, and several enlargements. The main map is shown in Figure III-17. The dye correlation cross peaks are detectable, and allow the structural confirmation; yet the intensity enhancement induces a lot of spikes or baseline deformations impeding any adequate additive assignment.

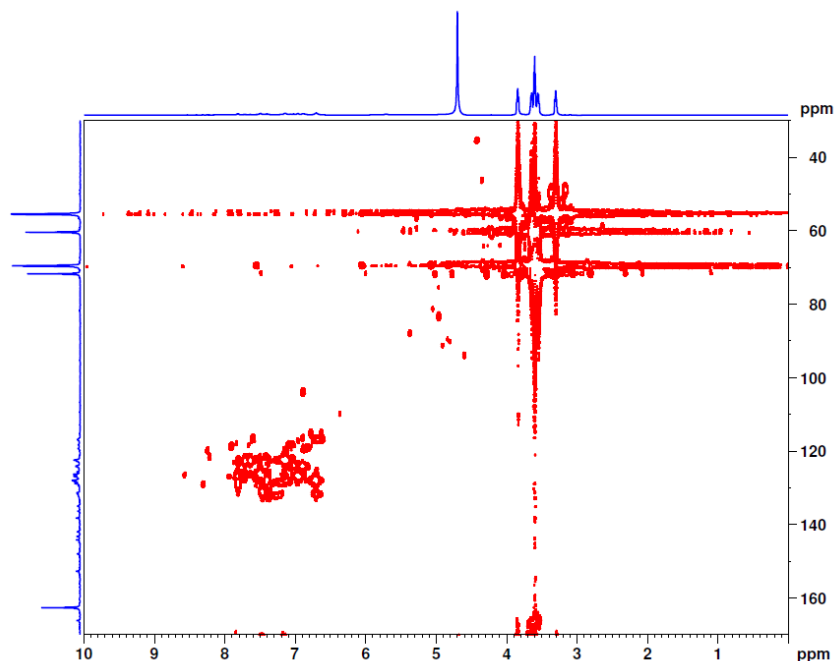


Figure III-17. 2D HSQC of the dye (lower threshold level)

Hence, a higher threshold level was then used.

On the main map (Figure III-18), the only visible correlation cross peaks are those of the additive. In accordance with the previous observations with the DEPT experiment, the carbon at 163 ppm exhibits no correlation, which was expected due to its quaternary multiplicity.

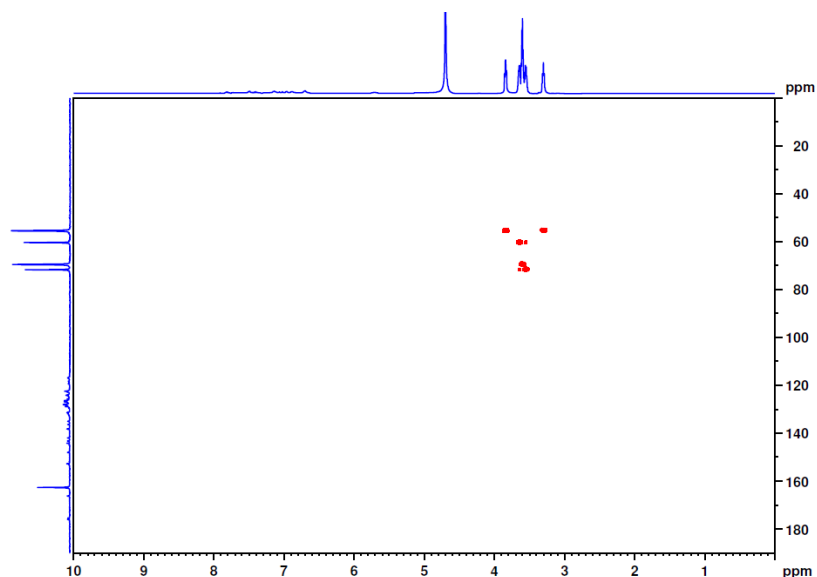


Figure III-18. 2D HSQC of the additive (higher threshold level)

The enlargement of the alkyl area (see Figure III-19) allowed the assignment of the carbon atoms.

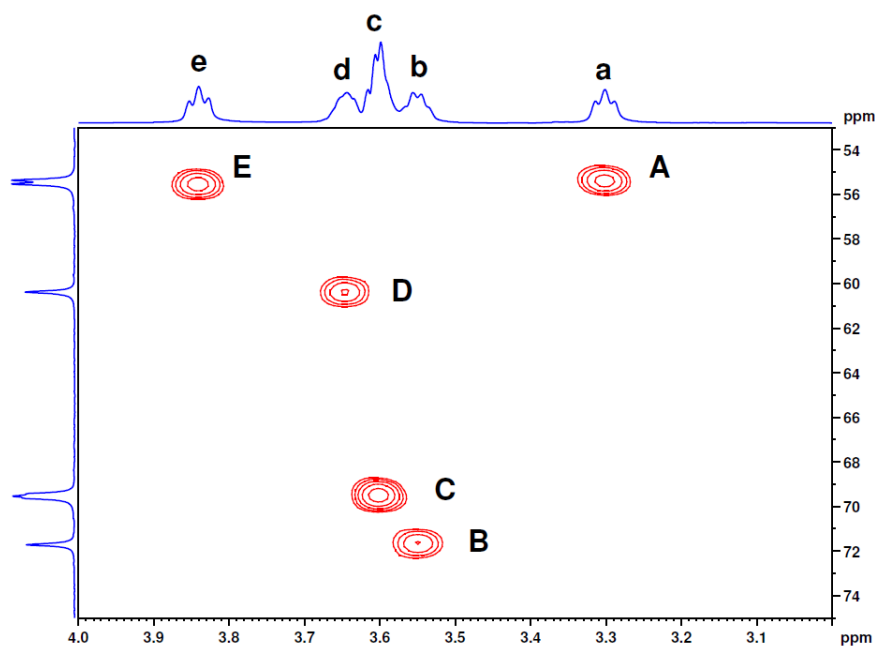


Figure III-19. 2D HSQC enlargement of the additive

To distinguish between A and E, the enlargement must be higher (see Figure III-20). Figure III-20 suggests that the carbon atom at 55.4 ppm is directly bonded to the protons at 3.30 ppm, and that the carbon atom at 55.5 ppm is directly bonded with the protons at 3.84 ppm.

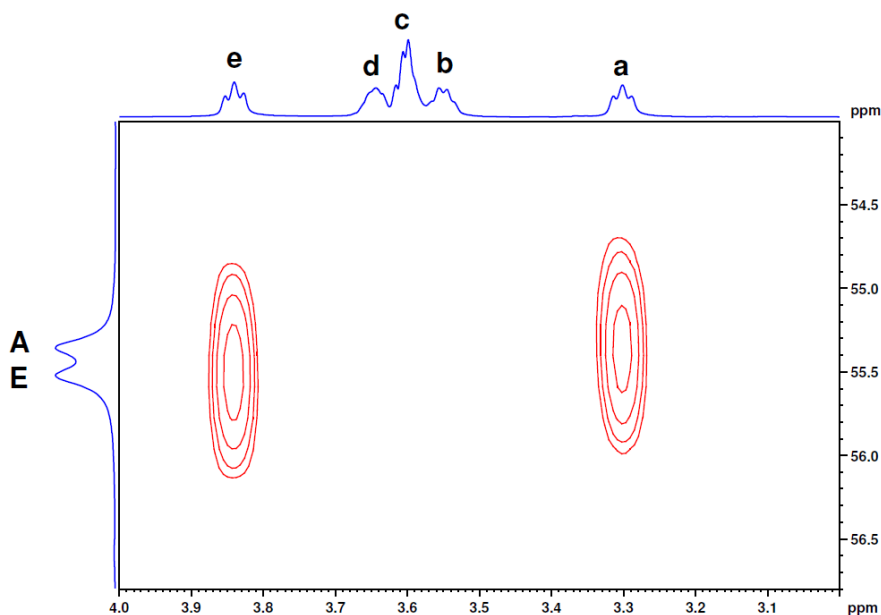


Figure III-20. 2D HSQC enlargement of the additive (55 ppm ^{13}C area)

Some other 2D NMR experiments could help to get access to more information, showing the long-range correlations *i.e.* 2, 3, even 4 (in the case of conjugated system) bond correlations either between protons (COSY), or between carbons and protons (HMBC).

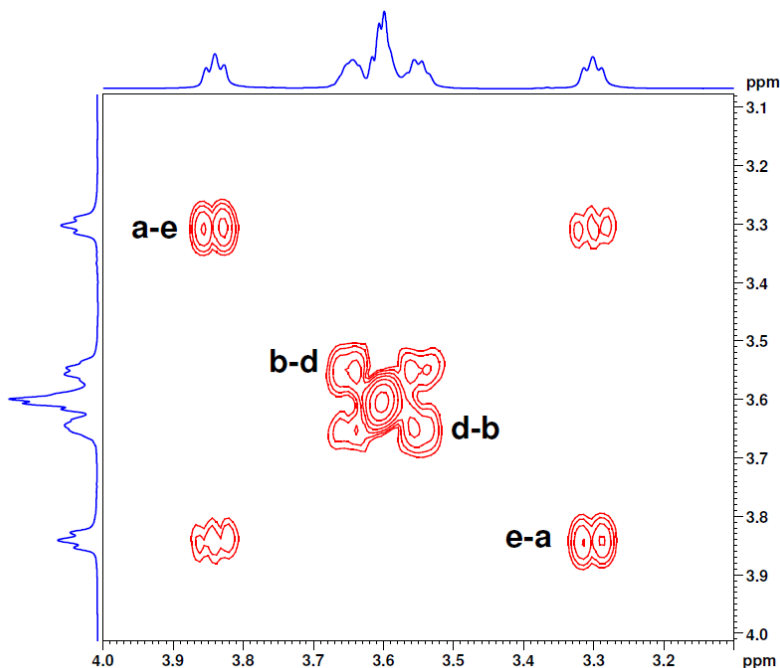


Figure III-21. 2D COSY enlargement of the additive (alkyl area)

As shown in Figure III-21 representing the additive region only of a COSY experiment, the CH_2 protons **a** and **e** appear to be correlated, CH_2 protons **b** and **d** also, and CH_2 protons **c** with themselves. We must keep in mind that there are 2 CH_2 protons **c** (as indicated by protons and carbons integrals).

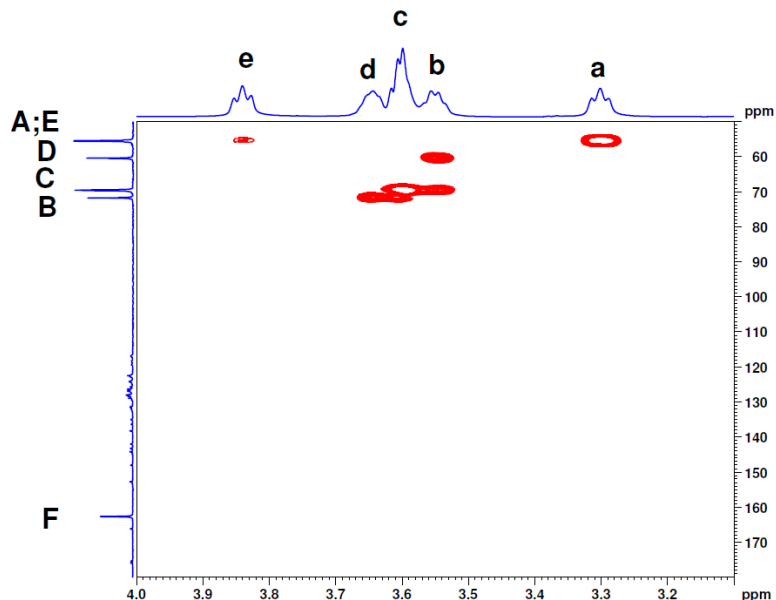


Figure III-22. 2D HMBC of the additive

HMBC (Figure III-22) informed us about $^1\text{H} - ^{13}\text{C}$ “long range” correlations ($^n\text{J}_{\text{HC}}$, mainly $^3\text{J}_{\text{HC}}$). First of all, the **F** carbon exhibits no correlation. It is a quaternary carbon, and since there is no proton correlation cross peak, it was certainly linked to 2 heteroatoms (O and/or N).

For the alkyl part of the additive on the enlargement proposed in Figure III-23, the correlations between the carbons and the protons are shown.

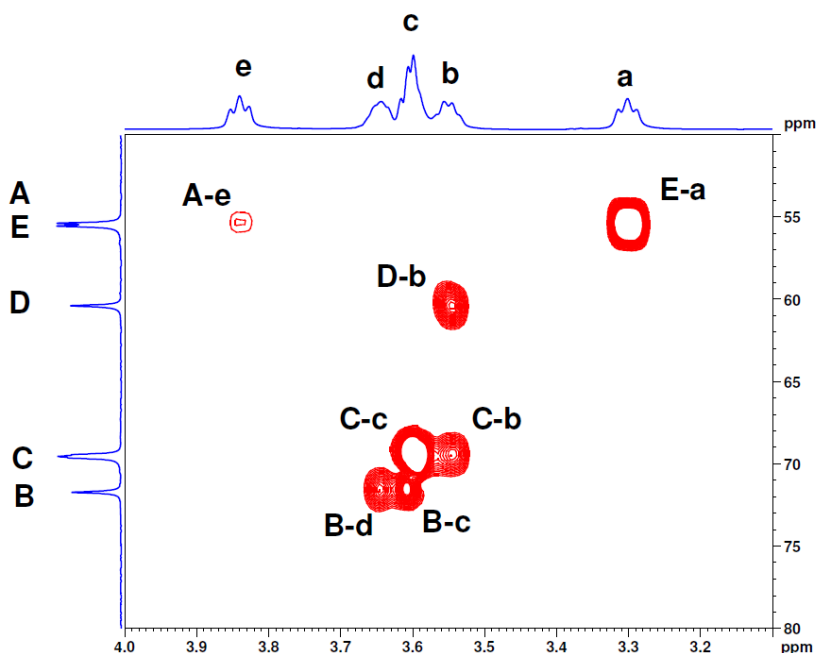


Figure III-23. 2D HMBC enlargement of the additive (alkyl area)

These analyses, combined with the chemical shift values, led to the proposal of a structure for the prominent additive in DR81L, with a diethylene glycol chain, see Figure III-24.

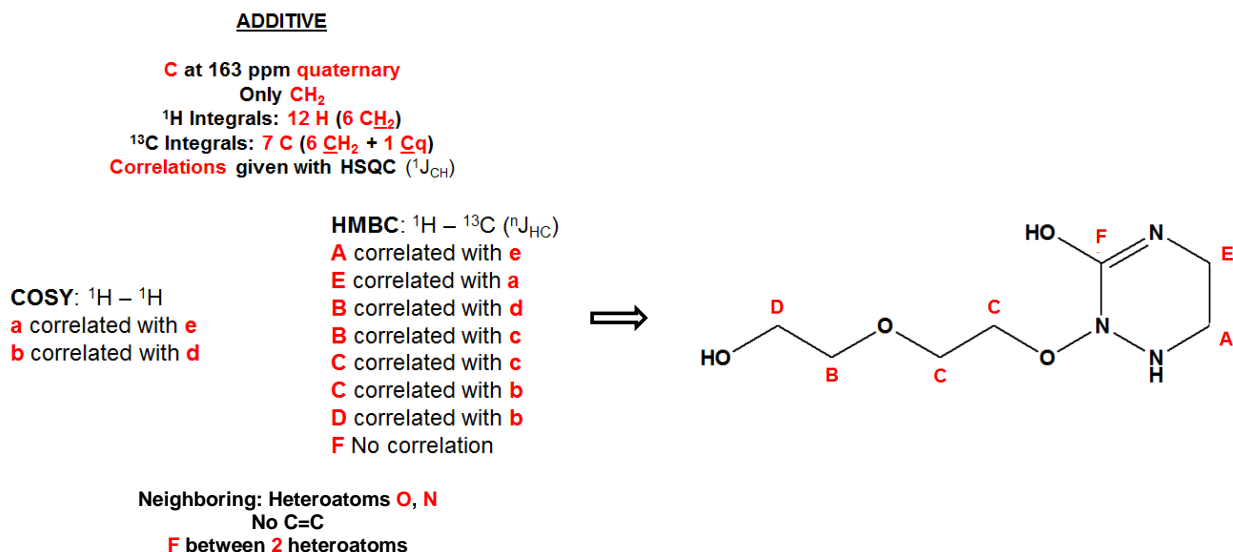


Figure III-24. Conclusions of the NMR analyses and proposition of a structure for DR81L's main additive

For all the other small peaks detected with carbon and proton NMR, the 2D correlations are consistent with the DR81L structure. On the basis of our proposal, the integration values reveal that 1 molecule of additive (structure as proposed) is present for 0.125 molecule of DR81. The ratios would be different in the case of another chemical structure.

Diethylene glycol is often used as a solvent to improve the solubility of organic products into water. This might be its role in DR81L. The other part of the proposed molecule is also very soluble.

III.2.5.2 Analysis of DY11L

The same method was applied to lyophilized DY11L, and similar NMR experiments were conducted. On the quantitative ¹H spectrum proposed in

Figure III-25, larger signals of weak intensities correspond to the dye's chemical structure, whereas supplementary higher and very well defined signals were attributed to the additive in the aliphatic area below 4 ppm.

Once again, the signals corresponding to additives were much more intense than those of the dye, which is in accordance with the MS results: DY11 was not detected and other molecules seemed to be predominant.

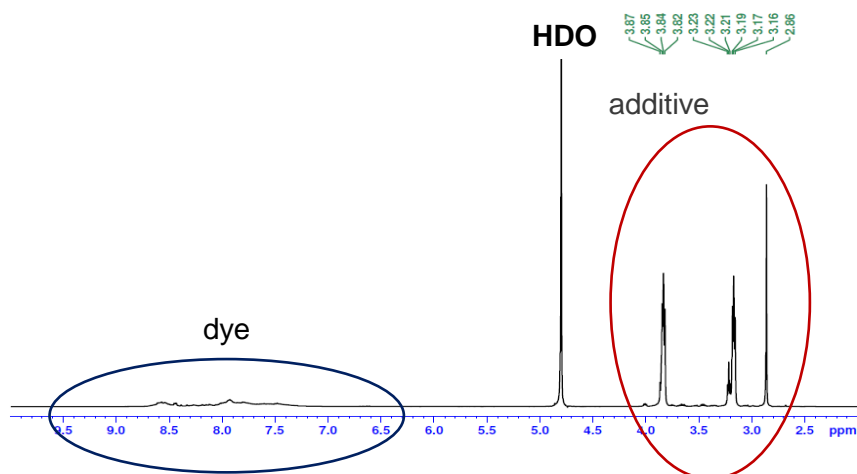


Figure III-25. Quantitative ^1H NMR spectrum of DY11L

With the enlargement of the additive part (Figure III-26), the hyperfine structure gives some information: a singlet at 2.81 ppm may correspond to methyl groups bonded to a heteroatom, more probably to nitrogen than oxygen in relation with its chemical shift. Then a series of triplets may correspond to some CH_2 coupled with each other. The differences of chemical shifts (3.2 and 3.8 ppm) indicate that the neighborings were different. The integrals (which are proportional only) were 6, 14 and 14 for the protons a, b + c, and d + e respectively.

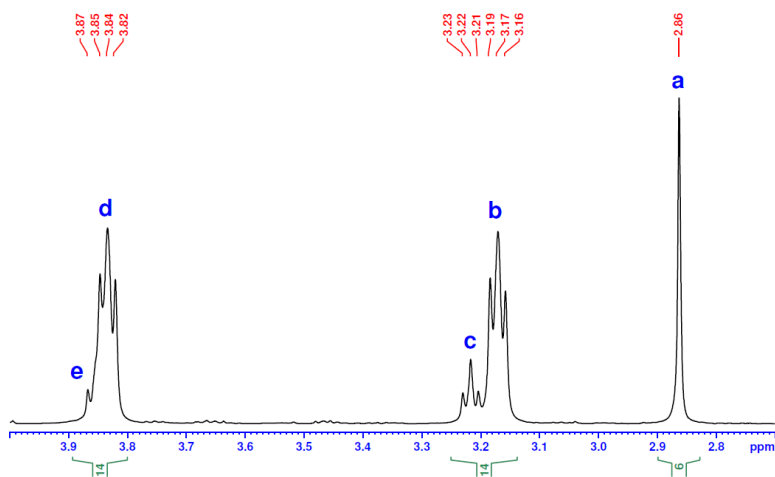


Figure III-26. Quantitative ^1H NMR enlargement spectrum of additive (2.7 to 4.0 ppm)

The quantitative ^{13}C NMR spectrum of DY11L is given in Figure III-27 (top) with the corresponding DEPT 135 spectrum (bottom). As for DR81L, small peaks in the aromatic region 180 – 110 ppm correspond to the dye structure. Figure III-27 mainly exhibits very high fine supplementary signals from the additive(s). No additive peaks in the aromatic region were detected. In the aromatic area, the peaks were larger, too numerous, and there were not only the signals which could be assigned to the dye, but also some small “impurities”, not belonging to the additive. The comparison of the areas shows that about 70% of the total aromatic signals area could be assigned to the dye structure.

Due to overlapping with the dye signals, no detailed studies were undertaken about them. Only the additive part was studied.

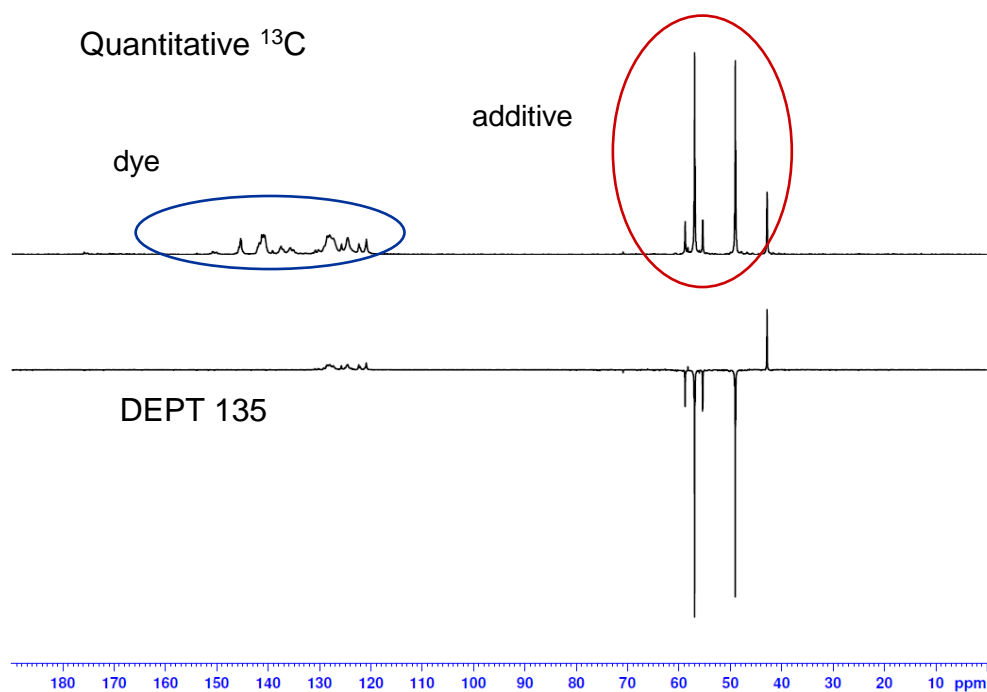


Figure III-27. Quantitative ^{13}C NMR and DEPT 135 spectra of DY11L

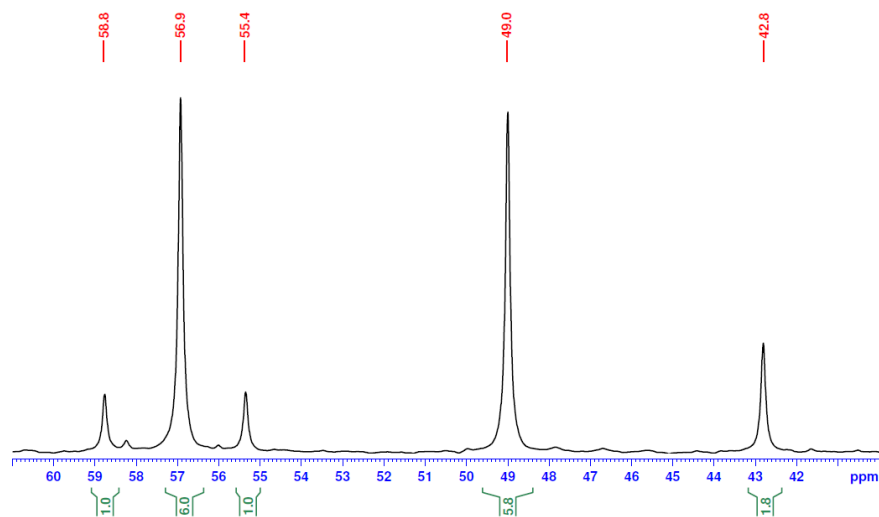


Figure III-28. Quantitative ^{13}C NMR enlargement spectrum for the additive

Figure III-28 mainly exhibits signals from the additive(s). DEPT 135 proved that only CH_2 were present except the C atom at 43 ppm which could be either CH or CH_3 . DEPT 90 (not shown) allowed the differentiation between CH and CH_3 , and confirmed the CH_3 multiplicity expected to be in agreement with ^1H results. The integration confirms also the proton results with 2 CH_3 , 6 CH_2 at 49 ppm, 1 CH_2 at 55.4 ppm, 6 CH_2 at 56.9 ppm and 1 CH_2 at 58.8 ppm. All the carbon chemical shifts led to the same conclusions: different nitrogen (N and/or NH) neighboring, more probably than oxygen one.

Full carbon assignment was performed with the HSQC experiment (see Figure III-29), which gives information about $^1\text{H} - ^{13}\text{C}$ close correlations ($^1J_{\text{HC}}$). All the carbons could be assigned. There was concordance with all the protons' and carbons' integrals.

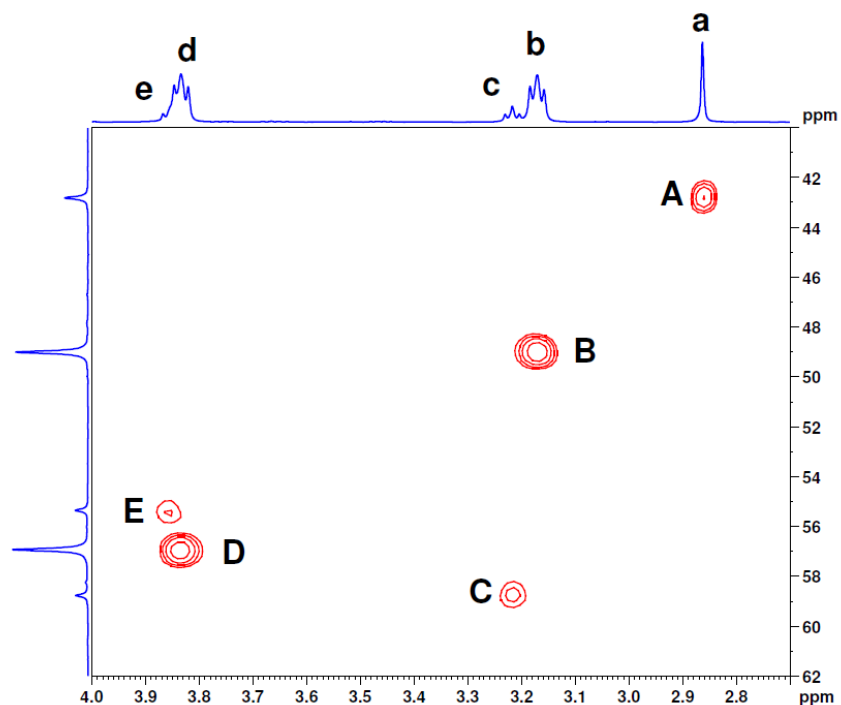


Figure III-29. HSQC experiment of additive

HMBC (see Figure III-30) was used to study $^1\text{H} - ^{13}\text{C}$ “long range” correlations ($^nJ_{\text{HC}}$, mainly $^3J_{\text{HC}}$) and provided more information about the chemical structure. The assignments were labelled on the map.

Due to the heterogeneity for the carbons' and protons' intensities, the threshold level must be lowered to observe the correlations involving the weak intensity of carbons and protons C and E. At this level, some residual 1J signal (HSQC correlations) could appear on the map: therefore, we could measure the residual $^1J_{\text{CH}} = 143 \text{ Hz}$ between **C_A** and **H_a**.

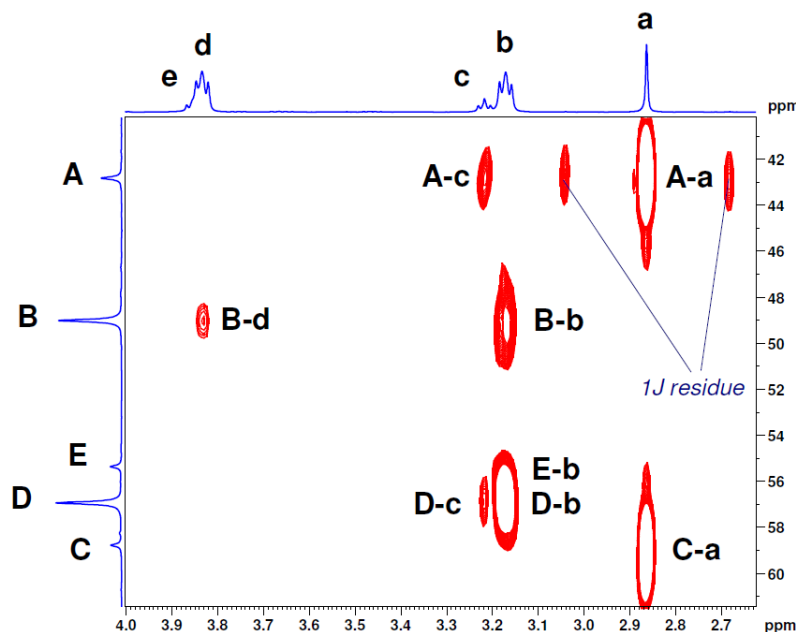


Figure III-30. HMBC ^{13}C NMR experiment of additive

All the NMR results allowed to finally propose a chemical structure for the detected additive, see Figure III-31.

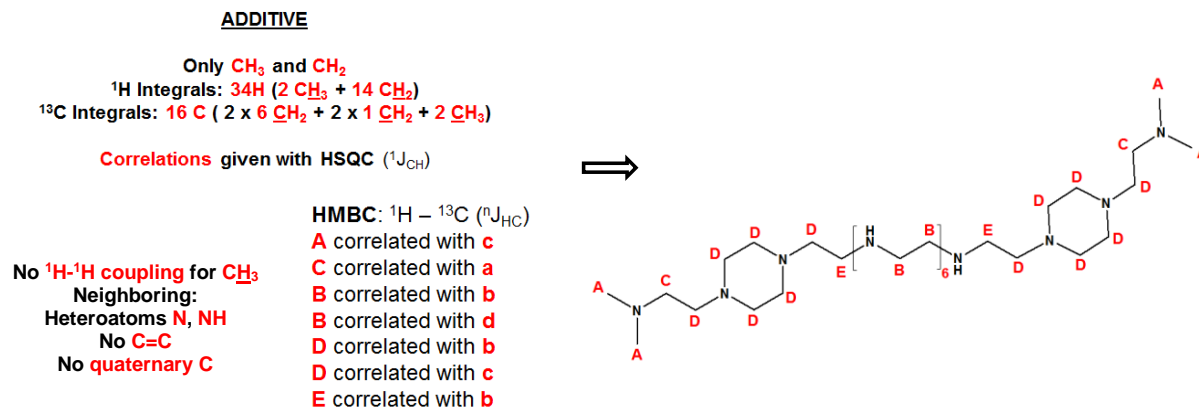


Figure III-31. Conclusions of the NMR analyses and proposition of a structure for DY11L's main additive

The proposed additive structure is similar to those of many surfactants and dispersants. Hence, this additive is probably used either to reduce the surface tension or as a dispersing agent in the liquid dye solution.

Based on this structure proposal, it can be concluded from the integration values of the aromatic and aliphatic areas, that 1 additive molecule is present for 2.5 molecules of DY11L. Taking into account the fact that only 70% of the aromatic area really corresponded to the dye, the ratio decreases to 1 additive molecule for 1.75 dye molecule DY11L. The ratios would be different in the case of another chemical structure for the additive.

III.2.5.3 Conclusions

The first NMR analyses enabled to confirm the molecular structure of the DR81L dye given by the dye supplier, whereas the DY11L dye structure could not be verified. Moreover, for both DR81L and DY11L dye formulations, additives were detected in significant amounts and the NMR experiments allowed to propose possible structures. These structures suggest that they are used as dispersants in the commercial dye solutions. Unfortunately, the NMR study did not give sufficient information to calculate the real concentrations of the dye molecules in the dye formulations. Therefore, in all the following experiments, the purities of the dyes were considered to be those given by the dye supplier.

III.2.6 Conclusion

To conclude on the characterization of the selected dyes, it allowed to determine their UV-vis signatures, their behavior depending on pH and approximative pKas. The commercial dyes were found to include significant amounts of additives and 2D-NMR allowed to propose some structures for these in both DR81L and DY11L. However, the structure of DY11 itself was not recognized by ESI-MS in the DY11L dye solution, and NMR spectroscopy could not confirm it either. Therefore, the study of dye/copper-phenanthroline interactions will rather be conducted on the DR81L dye.

III.3 COPPER-PHENANTHROLINE SPECIATION

The following part is devoted to the characterization of the “activator”, i.e. copper-phenanthroline species.

When copper is introduced in a 1,10-phenanthroline solution, various species are formed, depending on the Cu:Phen stoichiometric ratio (1:1, 1:2, 1:3). It is reported in the literature that such mixtures may contain free and hydroxylated copper, free phenanthroline (Phen) and hydroxylated or non-hydroxylated complexes such as CuPhen(OH)_2 , Cu(Phen)_3^{2+} , CuPhenOH^+ , Cu(Phen)_2^{2+} , etc. [10]–[13]. Indeed, it is well known that the composition of a metal ion-ligand solution at thermodynamic equilibrium depends on the initial reagent concentrations, temperature and pH [14].

Modeling with the PHREEQC software allowed the calculation of concentration-pH profiles for each Cu-Phen species including free copper and free phenanthroline at an equilibrium state, with or without considering the occurrence of precipitation. Indeed, some complexes may precipitate. The predicted results are shown in Figure III-32 and Figure III-33. These were calculated for Cu:Phen = 1:1, 1:2 and 1:3 with an initial CuSO_4 concentration of 15 μM at 25°C, from pH 6.5 to pH 12.5. In the case “with solid phase”, the solids are represented by one profile gathering every copper-based precipitate theoretically present.

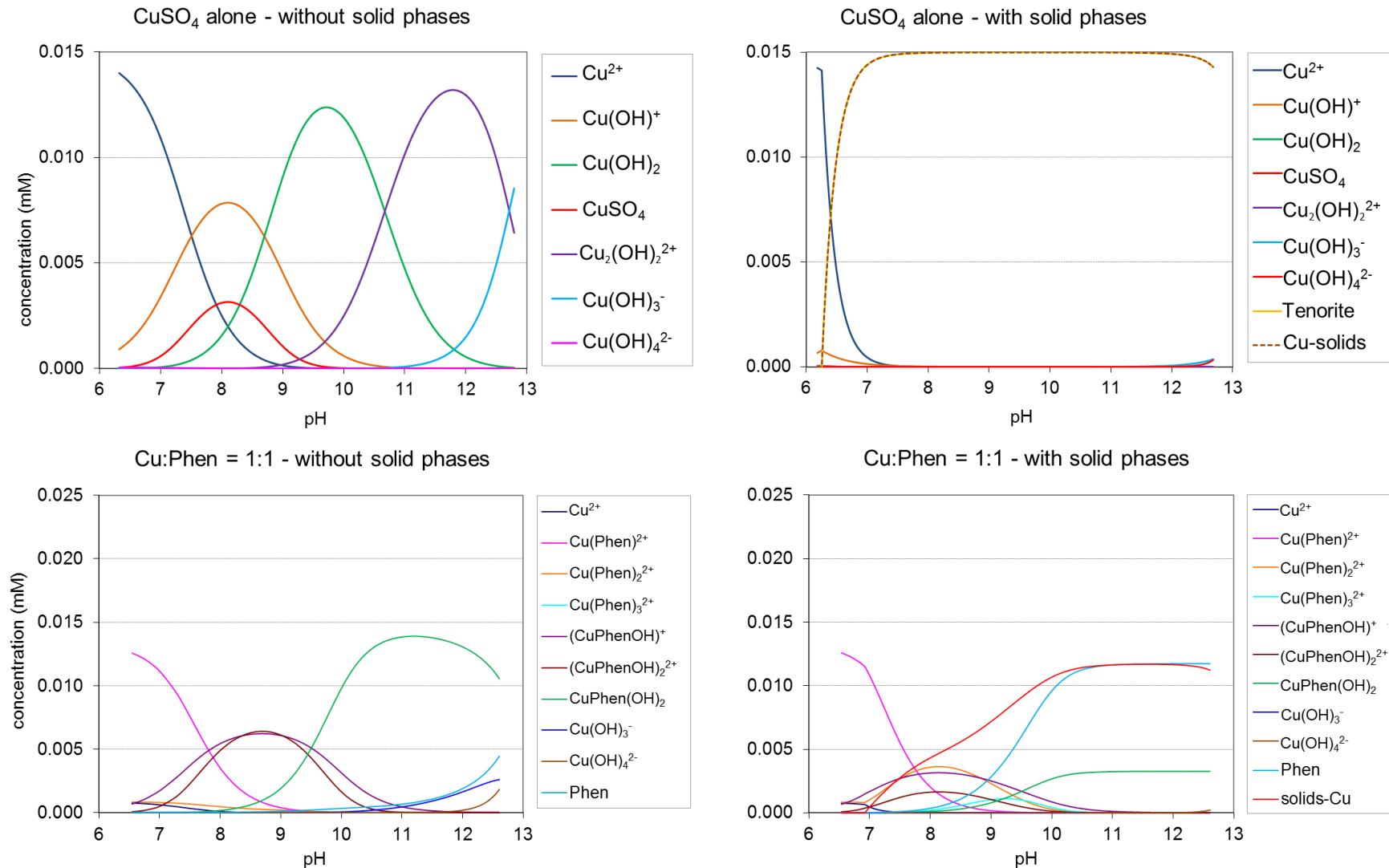


Figure III-32. Calculated distributions of different species in CuSO₄ and Cu-Phen solutions as a function of pH. CuSO₄ alone, Cu:Phen = 1:1; initial CuSO₄ concentration [Cu] = 15 μM at 25°C, with or without the occurrence of precipitation.

III. Characterization of the dyes and interactions with copper-phenanthroline

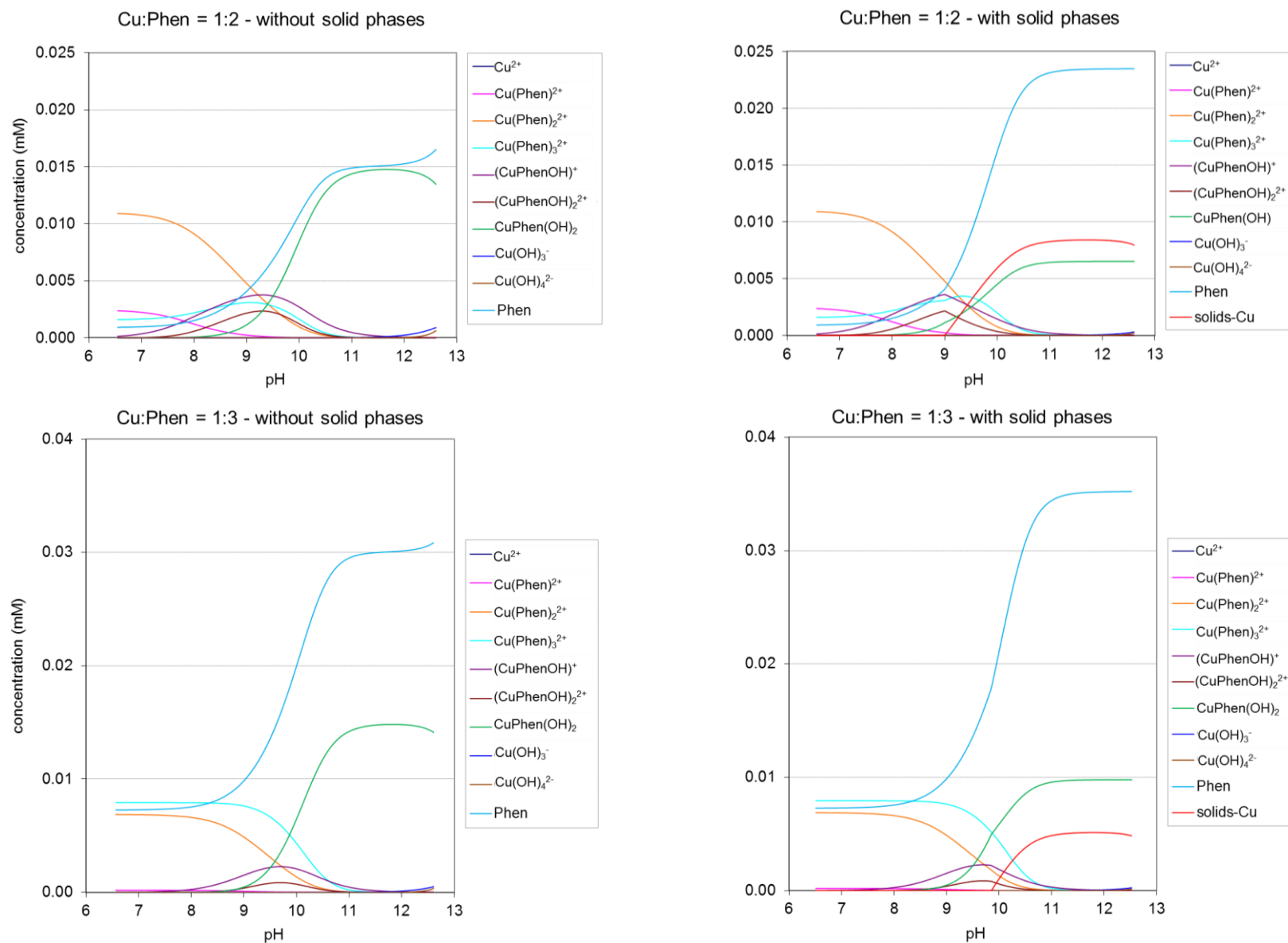


Figure III-33. Calculated distributions of different species in Cu-Phen solutions as a function of pH. Cu:Phen = 1:2 and 1:3; initial CuSO_4 concentration $[\text{Cu}] = 15 \mu\text{M}$ at 25°C , with or without the occurrence of precipitation.

Without solid phase, under the conditions of this simulation, copper sulfate gave rise to a majority of free cupric ions from pH 6 to 7.5. Increasing the pH raised the degree of hydroxylation of copper, reaching a majority of $\text{Cu}(\text{OH})_4^{2-}$ above pH 12.7. With the occurrence of precipitation, cupric ions appeared to be replaced by tenorite (CuO) from pH 6 to 7.4. Above 7.4, tenorite should be the only copper species present until pH 12.

In the case of Cu:Phen = 1:1, the calculated distributions were much different with or without solid phase. In the case “with solid phase”, a high proportion of copper precipitates, starting at pH 7 and reaching a maximum (0.012 mM) above pH 10, leading to a high amount of free phenanthroline. The experimental observation of the prepared mixtures confirmed this statement, since the Cu-Phen (1:1) stock solution was actually not quite stable and precipitates were visible after some days or weeks at rest.

Concerning the other Cu:Phen ratios (1:2 and 1:3), the modeling “with solid phase” resulted in lower concentrations of precipitates (around 0.008 mM above pH 10.5 and 0.005 mM above pH 11, respectively, compared to 0.012 mM at a ratio of 1:1). Indeed, these solutions were found more stable since no precipitate was visible after several weeks. Therefore, it appears that higher Phen:Cu ratios favor soluble complexes between copper and phenanthroline, rather than precipitated complexes.

The distributions presented in Figure III-32 and Figure III-33 differ from those described in the literature by Korpi *et al.* [15] since the initial concentrations (chosen to fit our experimental range) were much lower: $[\text{Cu}] = 15 \mu\text{M}$ vs. 10 mM. The conditions of Korpi *et al.* were also tested for comparison and a good fit was found when the calculations did not account for precipitation phenomena.

For further use in the investigation of Cu-Phen interaction with the dye at different pHs, three pH values: 6.5, 10.7 and 12.3 were chosen. The abundances of the species at these specific pHs are gathered in Table III-3 (without precipitation) and Table III-4 (with precipitation) as a function of the initial Cu:Phen molar ratio.

Table III-3. Predicted concentrations of the different species at pH 6.5, 10.7 and 12.3, for Cu:Phen = 1:0, 1:1, 1:2 and 1:3, with an initial CuSO₄ concentration of 15 μM at 25°C, assuming no precipitation occurrence.

The results are given as molar percentages of total [Cu].

Cu:Phen	1:0			1:1			1:2			1:3			
	pH	6.5	10.7	12.3	6.5	10.7	12.3	6.5	10.7	12.3	6.5	10.7	12.3
Cu ²⁺	90.2	ε	ε	5.1	ε	ε	ε	ε	ε	ε	ε	ε	ε
CuOH ⁺	8.8	0.5	ε	0.5	ε	ε	ε	ε	ε	ε	ε	ε	ε
Cu(OH) ₂	0.1	48.1	1.6	ε	1.7	0.3	ε	0.1	0.1	ε	ε	ε	ε
CuSO ₄	0.3	ε	ε	ε	ε	ε	ε	ε	ε	ε	ε	ε	ε
Cu ₂ (OH) ₂ ²⁺	0.6	ε	ε	ε	ε	ε	ε	ε	ε	ε	ε	ε	ε
Cu(OH) ₃ ⁻	ε	51.2	77.4	ε	1.8	14.5	ε	0.1	3.1	ε	ε	1.6	ε
Cu(OH) ₄ ²⁻	ε	0.2	21.0	ε	ε	3.9	ε	ε	0.8	ε	ε	0.4	ε
Cu(Phen) ²⁺	/	/	/	84.3	ε	ε	15.9	ε	ε	1.3	ε	ε	ε
Cu(Phen) ₂ ²⁺	/	/	/	5.5	ε	ε	72.8	0.6	ε	45.8	1.1	ε	ε
Cu(Phen) ₃ ²⁺	/	/	/	ε	ε	ε	10.6	1.4	ε	52.8	4.9	ε	ε
(CuPhenOH) ⁺	/	/	/	4.1	5.8	0.2	0.8	5.9	0.2	0.1	5.7	0.2	ε
(CuPhenOH) ₂ ²⁺	/	/	/	0.4	0.9	ε	ε	0.9	ε	ε	0.8	ε	ε
CuPhen(OH) ₂	/	/	/	ε	89.7	81.2	ε	91.1	95.9	ε	87.4	97.7	ε
Phen	/	/	/	0.1	3.5	18.7	6.1	96.8	104.0	48	189	202	ε

^a ε represents a negligible value (below 0.1%)

Table III-4. Predicted concentrations of the different species at pH 6.5, 10.7 and 12.3, for Cu:Phen = 1:0, 1:1, 1:2 and 1:3, with an initial CuSO₄ concentration of 15 μM at 25°C, assuming the occurrence of precipitation.

The results are given as molar percentages of total [Cu].

Cu:Phen	1:0			1:1			1:2			1:3		
	6.5	10.7	12.3	6.5	10.7	12.3	6.5	10.7	12.3	6.5	10.7	12.3
Cu ²⁺	29.9	ε	ε	5.1	ε	ε	ε	ε	ε	ε	ε	ε
CuOH ⁺	3.0	ε	ε	0.5	ε	ε	ε	ε	ε	ε	ε	ε
Cu(OH) ₂	ε	ε	ε	ε	ε	ε	ε	ε	ε	ε	ε	ε
CuSO ₄	0.1	ε	ε	ε	ε	ε	ε	ε	ε	ε	ε	ε
Cu ₂ (OH) ₂ ²⁺	0.1	ε	ε	ε	ε	ε	ε	ε	ε	ε	ε	ε
Cu(OH) ₃ ⁻	ε	ε	0.9	ε	ε	0.9	ε	ε	0.9	ε	ε	0.9
Cu(OH) ₄ ²⁻	ε	ε	0.3	ε	ε	0.3	ε	ε	0.3	ε	ε	0.3
Cu(Phen) ²⁺	/	/	/	84.3	ε	ε	15.9	ε	ε	1.3	ε	ε
Cu(Phen) ₂ ²⁺	/	/	/	5.5	0.1	ε	72.8	0.4	ε	45.8	0.9	ε
Cu(Phen) ₃ ²⁺	/	/	/	ε	0.2	ε	10.6	1.5	ε	52.8	4.6	ε
(CuPhenOH) ⁺	/	/	/	4.1	1.4	ε	0.8	2.7	0.1	0.1	4.0	0.1
(CuPhenOH) ₂ ²⁺	/	/	/	0.4	ε	ε	ε	0.2	ε	ε	0.4	ε
CuPhen(OH) ₂	/	/	/	ε	21.3	21.7	ε	41.7	43.5	ε	60.9	65.2
Phen	/	/	/	ε	76.5	78.2	6.1	150.1	156.5	48.5	219.1	234.7
Tenorite	66.9	100.0	98.8	ε	77.0	77.0	ε	53.4	55.3	ε	29.2	33.5
Solids-Cu	66.9	100.0	98.8	ε	77.0	77.0	ε	53.4	55.3	ε	29.2	33.5

^a ε represents a negligible value (below 0.1%)

According to Figure III-32, Figure III-33, Table III-3 and Table III-4, CuPhen(OH)₂ appears to be the major species at alkaline pH (81 to 98% of total Cu in the case without precipitation). Moreover, the amount of free phenanthroline (last row in Table III-3) increases significantly when the Cu:Phen ratio varies from 1:1 to 1:3. Besides, more hydroxylated species are found at pH 12.3. Whatever the pH, Cu(Phen)²⁺ is almost inexistent, and the other non-hydroxylated species Cu(Phen)₂²⁺ and Cu(Phen)₃²⁺ are only present at pH 10.7, at low concentrations.

At near neutral pH (6.5), copper and phenanthroline mainly form Cu(Phen)²⁺, Cu(Phen)₂²⁺ and Cu(Phen)₃²⁺, the relative percentage depending on the Cu:Phen molar ratio.

As explained before, when the Cu-Phen stock solutions at a ratio of 1:1 were stored for several days, the solution eventually precipitated. Therefore, all experiments were performed with freshly prepared solutions whatever the Cu:Phen ratio, and no precipitation was observed at initial time. In the following part (dealing with the analysis of Cu-Phen coordination), all explanations will be based on the modeling case “without solid”.

III.4 ANALYSIS OF THE CU-PHEN COMPLEX

The Cu-Phen complexation was mainly analyzed by UV-visible spectroscopy. In a first part, the contribution of CuSO_4 and Phen alone to the UV-vis absorbance was analyzed.

III.4.1 CuSO_4

Copper sulfate alone was first studied (Figure III-34).

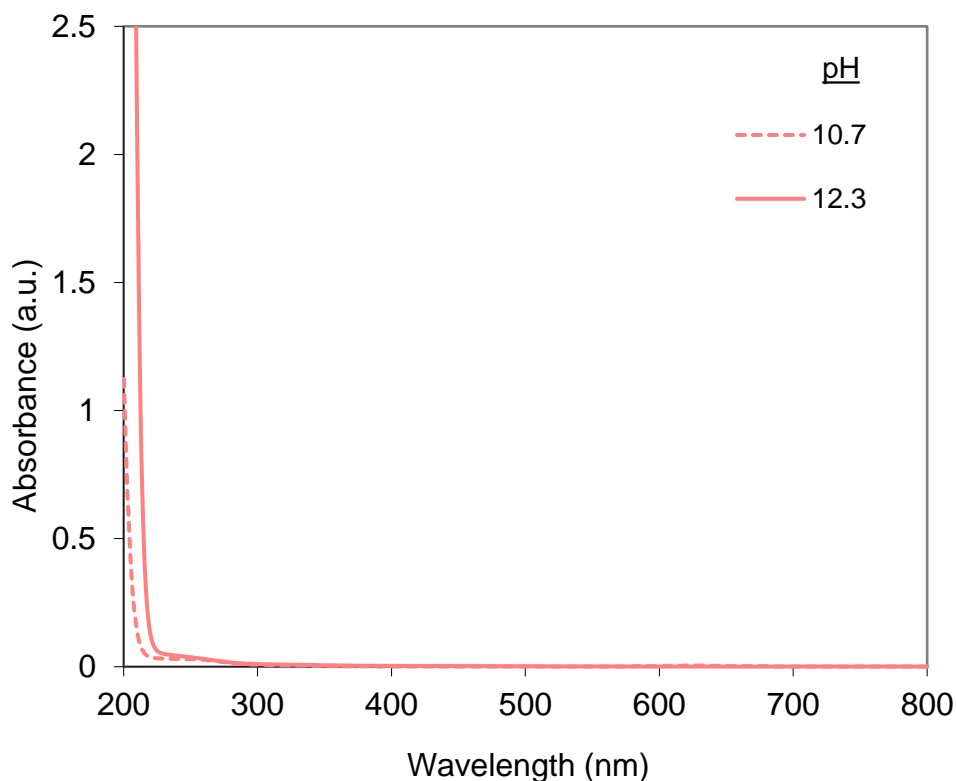


Figure III-34. Absorbance spectra of copper sulfate solutions at pH 10.7 and 12.3, with $[\text{CuSO}_4] = 15 \mu\text{M}$

At the concentration used in this study, a slight absorption contribution was noticed in the UV range and nothing absorbed in the visible range.

Yet, the blue shade of copper(II) is visible at higher concentrations.

III.4.2 Phenanthroline

The UV-vis absorbance spectra of pure phenanthroline at alkaline pH (10.7 and 12.3) are presented in Figure III-35.

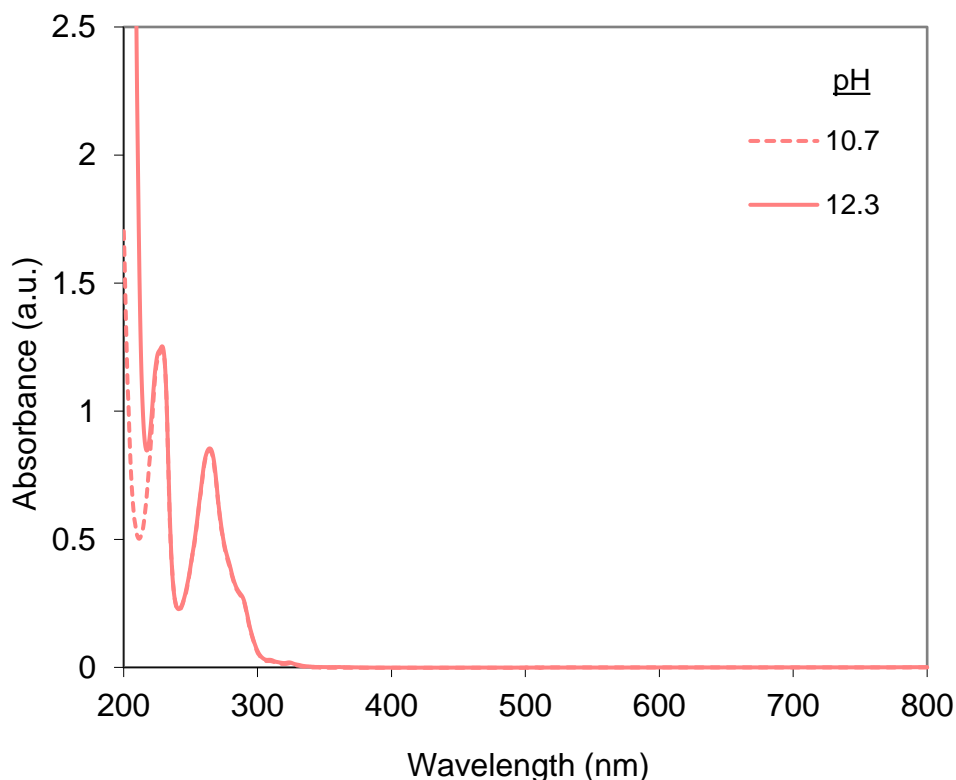


Figure III-35. Absorbance spectra of 1,10-phenanthroline at pH 10.7 and 12.3, with [Phen] = 30 μ M (equivalent to the amount of phenanthroline with DR81L:Cu = 1:1.5, Cu:Phen = 1:2, and [Cu] = 15 μ M)

Two peaks are observed at 228.5-229 nm and 264 nm. Nothing appears in the visible range at the concentrations used in our experiments. This is in accordance with previous results from Yamazaki et al. [16], who reported the first peak at 228 and 227 nm, respectively, and the second peak at 263 nm, at near-neutral pH in solutions containing hexane. Therefore, since phenanthroline only absorbs light at wavelengths, its signal will not disturb the dye's signal in the visible range.

Yamazaki et al. calculated molar extinction coefficients at various wavelengths: $\log \epsilon_{\max}$ (227 nm) = 5.3; $\log \epsilon_{\max}$ (263 nm) = 5.2. In the present work, slightly different values were found: $\log \epsilon_{\max}$ (228.5 nm) = 4.6, and $\log \epsilon_{\max}$ (264 nm) = 4.5, probably attributable to differences of analytical conditions (different solvents and pHs). However, the result for the second peak is very close to that of Armaroli et al. [17] in a CH_2Cl_2 solution ($\log \epsilon_{\max}$ (264 nm) = 4.5), and to that of Vallée et al. [18] with crystalline dihydrochloride phenanthroline ($\log \epsilon_{\max}$ (265 nm) = 4.5).

It can also be noticed that the phenanthroline spectra presented in Figure III-35 were identical at both pHs except from 200 to 220 nm, where the absorbance of sodium hydroxide interfered.

III.4.3 Cu-Phen

The absorbance spectra of Cu-Phen solutions at pH 10.7 and pH 12.3 are presented in Figure III-36 with Cu:Phen ratios varying from 1:1 to 1:3.

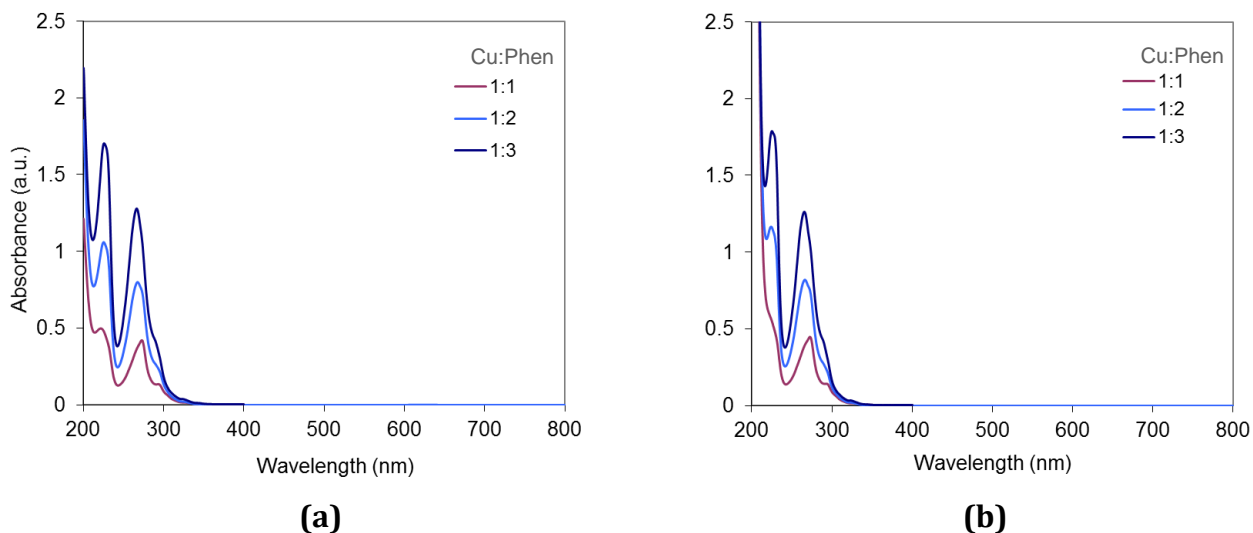


Figure III-36. Absorbance spectra of the Cu-Phen solutions at (a) pH 10.7 and (b) pH 12.3, with Cu:Phen = 1:1, 1:2 and 1:3, and [Cu] = 15 μ M.

The Cu-Phen solution spectra are very close to those of Phen alone (Figure III-35). This was expected since Ni *et al.* reported two peaks at 227 nm and 264.5 nm for $\text{Cu}(\text{Phen})_2^{2+}$ prepared with $\text{Cu}(\text{NO}_3)_2$ and 1,10-phenanthroline monohydrate in a tris-HCl buffer (pH 7.4) [19].

Figure III-36 indicates that at each pH, the absorbance of copper-phenanthroline increases almost proportionally to the initial concentration of phenanthroline in the complex, in accordance with Beer-Lambert's law. As observed with Phen alone, at the concentrations used in the present study, Cu-Phen solutions did not exhibit any signal in the visible range.

However, at given pH and Cu:Phen ratio, some slight differences between Phen and Cu-Phen can be observed in terms of maximum absorption wavelengths. This proves that coordination between copper ions and phenanthroline occurs. Moreover, no clear difference was observed between pH 10.7 and 12.3, suggesting that the coordination was not influenced by the pH, probably because at these pHs, the major copper species is the same ($\text{CuPhen}(\text{OH})_2$).

The Cu-Phen coordination was examined using EPR spectroscopy in the following paragraph.

III.4.4 Evidence of coordination by EPR

Paramagnetic species such as copper(II) are detectable by EPR, especially at very low temperature, in which case their hyperfine structure can be observed. An example of this hyperfine structure is shown in Figure III-37. The technique and experimental conditions were presented in II.2.2.2.

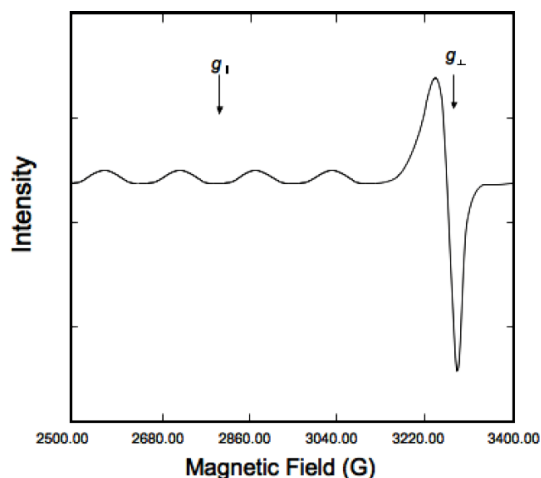


Figure III-37. Typical X-band EPR spectrum of copper(II) compounds [20]

X-band EPR spectra of the Cu salt (CuSO_4) and of Cu-Phen were recorded at 100 K and at pH 12.3 (Figure III-38). EPR detection of copper(II) requiring millimolar concentration, these analyses were performed with 100 times higher concentrations as before, i.e. $[\text{Cu}] = 1.5 \text{ mM}$.

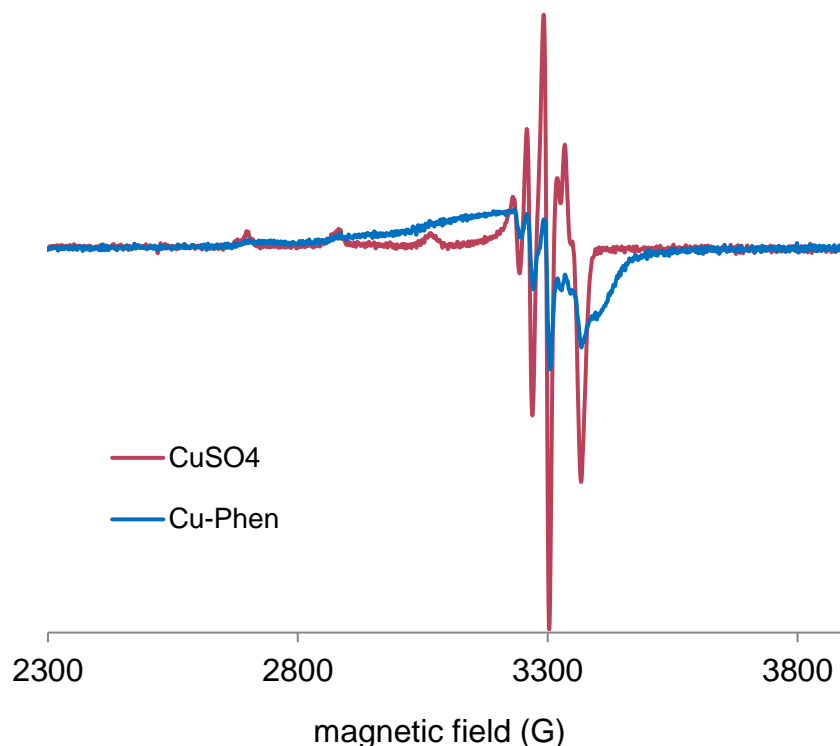


Figure III-38. Experimental X-band EPR spectra recorded at 100 K in frozen aqueous solutions of CuSO_4 and Cu-Phen at pH 12.3, with Cu:Phen = 1:2 and $[\text{Cu}] = 1.5 \text{ mM}$

Both spectra are characteristic of $S = \frac{1}{2}$ systems. They are consistent with mononuclear paramagnetic Cu(II) (a d^9 ion) since Cu^I (a d^{10} ion) is diamagnetic. It is therefore proven that Cu is present in solution in its oxidized state, Cu^{2+} , in both cases. However, when phenanthroline is

present in solution, the EPR spectrum is significantly modified, which evidences the coordination between Cu^{2+} and phenanthroline.

III.5 ANALYSIS OF THE DR81L DYE/CU-PHEN SYSTEM

As done with CuSO_4 and phenanthroline, the possibility of dye complexation with CuSO_4 and Cu-Phen was examined using UV-vis spectroscopy. Before studying the Direct Red 81 (DR81L)/copper-phenanthroline system by UV-vis analysis, some controls were performed.

III.5.1 Dye/ CuSO_4

Dye and copper sulfate alone were first investigated as a control. CuSO_4 was introduced at alkaline pH in the dye solution at a DR81L:Cu molar ratio of 1:1.5, which corresponds to the highest copper dose applied in the following experiments. The results are gathered in Figure III-39.

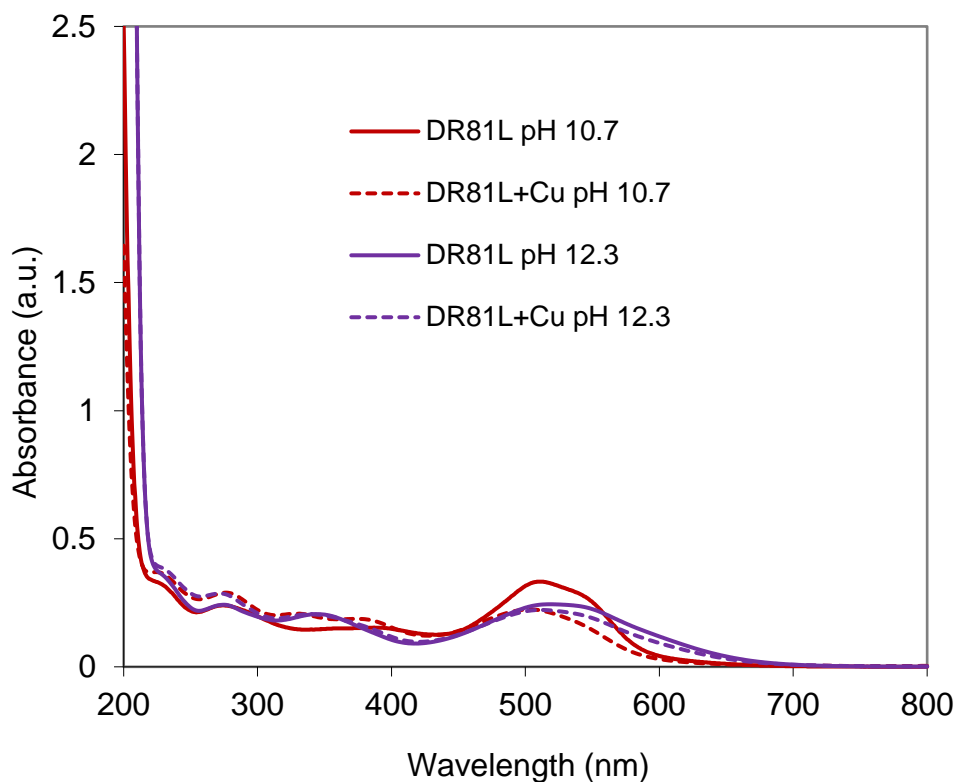


Figure III-39. Absorbance spectra of the dye/copper sulfate system at pH 10.7 and 12.3, with DR81L:CuSO₄ = 1:1.5 and [DR81L] = 10 μM, compared to the dye alone at the same pHs

Figure III-39 shows that adding CuSO_4 to the dye solution modifies the absorbance in the visible range, especially at pH 10.7. Indeed, a strong hypochromic effect was observed (33% decrease of absorbance at 510 nm), suggesting a modification of the chromophore in the presence of copper, most likely due to coordination between copper and the dye molecule.

III.5.2 Dye/Phenanthroline

As a second control, phenanthroline alone was added to the dye solution. The resulting spectrum is given in Figure III-40.

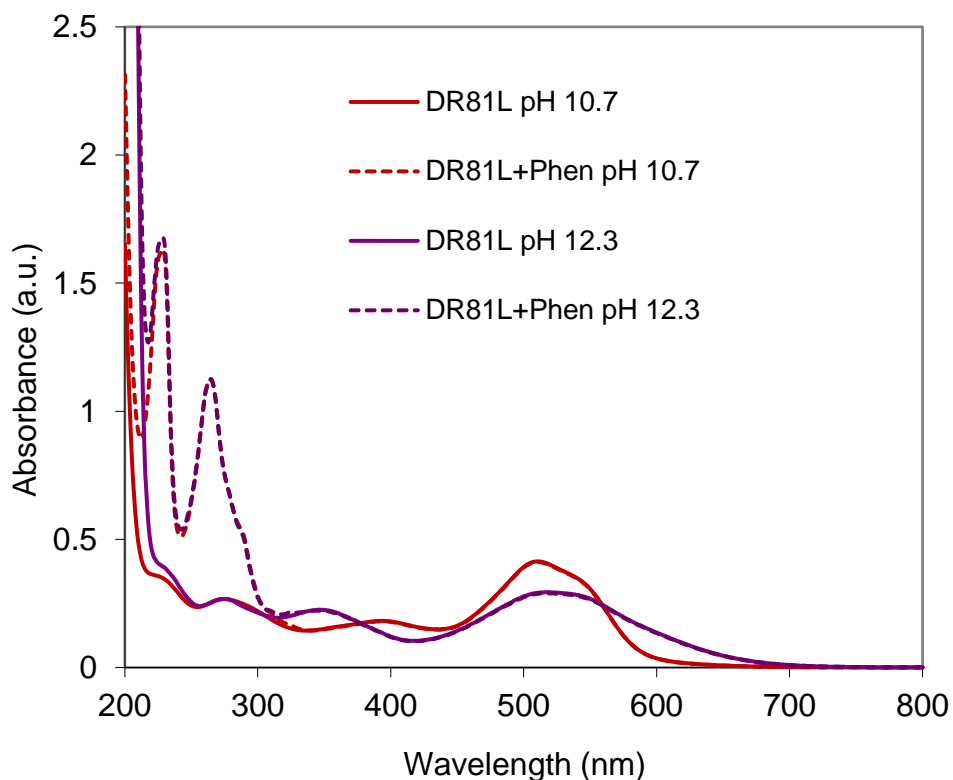


Figure III-40. Absorbance spectra of the dye/phenanthroline system at pH 10.7 and 12.3, with DR81L:Phen = 1:3 and [DR81L] = 10 μ M (equivalent to the amount of phenanthroline with DR81L:Cu = 1:1.5, Cu:Phen = 1:2, and [Cu] = 15 μ M), compared to the dye alone at the same pHs

The spectrum of the dye/phenanthroline solution was equal to the addition of phenanthroline's and DR81L's spectra. The chromophore part of the dye was unchanged with or without phenanthroline. Hence, no interaction between phenanthroline and the dye was evidenced.

III.5.3 Dye/Cu-Phen

Finally, the dye/Cu-Phen system was examined. The objective was to study the possible coordination between the dye, copper and Phen.

First, the system was studied at alkaline pHs. pH 10.7 and 12.3 were analyzed to check the possible differences depending on the ionization of the dye and copper-phenanthroline distributions presented earlier. Three Cu:Phen ratios were compared.

III.5.3.1 Alkaline pH: variation of Cu:Phen ratio

Figure III-41 displays the absorbance spectra obtained with Cu:Phen molar ratios of 1:1, 1:2 and 1:3, and a DR81L:Cu ratio of 1:1.5, at pH 10.7. At this pH, the dye is not ionized.

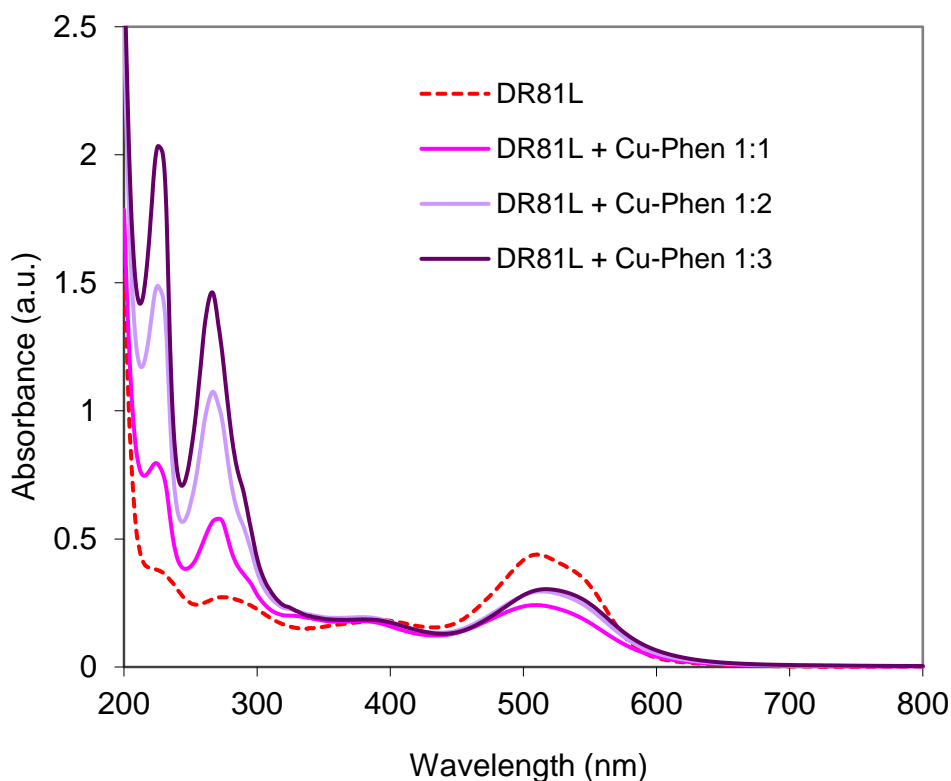


Figure III-41. Absorbance spectra of the dye/copper-phenanthroline system at pH 10.7, with Cu:Phen = 1:1, 1:2 and 1:3, DR81L:Cu= 1:1.5, and [DR81L] = 10 μ M, compared to the dye alone at the same pH

The spectrum of the Cu-Phen/dye solution was different from that of the dye alone, especially in the visible range (Figure III-41). The addition of Cu-Phen into the dye solution led to a hypochromic effect similar to that observed with addition of CuSO_4 alone in the dye solution (Figure III-39): the hypochromic effect was the same for Cu:Phen = 1:2 and 1:3 and CuSO_4 (33% decrease of the absorbance intensity), whereas the addition of Cu:Phen = 1:1 to the dye solution had a more pronounced hypochromic effect, with a 45% decrease. Since almost 50% of color was removed in the visible range, the introduction of Cu-Phen, even without any oxidative agent, is already responsible for partial “color-stripping”.

The maximum absorption wavelength of the dye at 510 nm was shifted to 513.5 nm for Cu:Phen = 1:2 and to 517 nm for Cu:Phen = 1:3 (bathochromic shift), which evidences coordination between the dye and copper, even in the presence of phenanthroline. Copper phenanthroline and copper dye coordination were probably in competition. Copper binds most likely to nitrogen atoms of the dye, as it is observed on common blue dyes such as Direct Blue 86 or Reactive Blue 163. Consequently, the π -conjugation structure of the dye is modified, leading to a hypochromic effect in the visible range (decrease of the molar extinction coefficient), resulting in partial color-stripping.

In addition, the signal of Cu:Phen = 1:1 in Figure III-41 differed from those of the 1:2 and 1:3 ratios, which were almost identical. An explanation may arise from the data of Table III-3, in which the only important difference appears in the amount of free phenanthroline in solution: 3.5% for the 1:1 system vs. 96.8 and 189% for the 1:2 and 1:3 systems, respectively. Free phenanthroline in solution would thus compete and limit copper coordination with the dye molecule, although a minimum amount of Phen would be required to stabilize copper in solution and thus make it available for the formation of a Cu-dye complex. Yet, the hypochromic effect was equal for copper alone (no free phenanthroline to compete) and Cu:Phen = 1:2 and 1:3, with 33% decrease, whereas it reached 45% with the 1:1 ratio. Consequently, this hypothesis may be wrong. Another hypothesis would be that Phen is ejected from Cu's environment in the cases when Cu:Phen = 1:2 and 1:3, which would explain why CuSO₄ had the same effect than Cu-Phen at these ratios.

In conclusion, at pH 10.7, one or several Cu-Phen species would coordinate to the dye molecule via the Cu atom, since the latter can bind to the nitrogen lone pairs of an azo group. For instance, if Cu(Phen)(OH)₂ (major species determined by PHREEQC) coordinates to the dye molecule, it would form a DR81-Cu-Phen co-coordinate with total or partial release of the hydroxyl groups.

The same trials were conducted at pH 12.3, with the ionized dye. The results are given in Figure III-42.

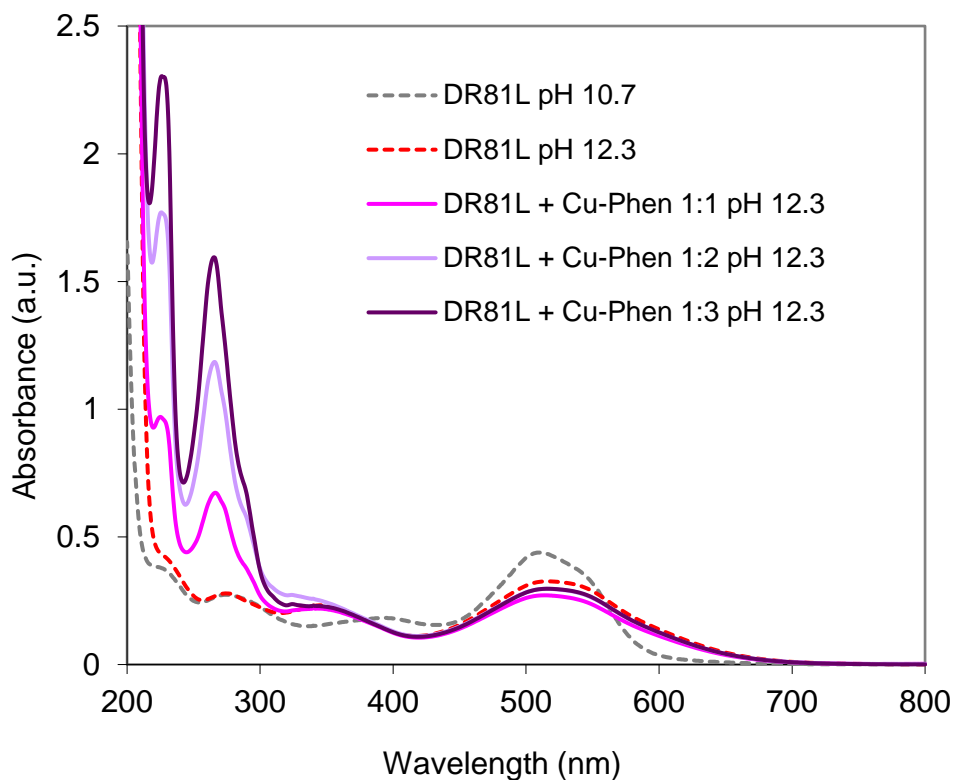


Figure III-42. Absorbance spectra of the dye/copper-phenanthroline system at pH 12.3, with Cu:Phen = 1:1, 1:2 and 1:3, DR81L:Cu = 1:1.5, and [DR81L] = 10 μ M, compared to the dye alone at pH 10.7 and 12.3

At pH 12.3, a hypochromic effect was also observed with the addition of Cu-Phen in the dye solution, but it appeared to be of very low magnitude (comparison between Figure III-41 and

Figure III-42). Again, this effect could be attributed to the complexation of copper with the dye in its ionized form. The weakest effect was observed for 1:2 and 1:3 Cu:Phen ratios (superimposed curves), and was equal to that of copper alone: 9% intensity decrease. At a ratio of 1:1, the complexation appeared to be more effective (17% decrease), possibly because of the lower excess of free phenanthroline in solution, or due to the ejection of Phen from Cu's environment at the 1:2 and 1:3 ratios, as discussed earlier for pH 10.7.

Figure III-41 and Figure III-42 also show that, compared to the dye's spectrum at pH 10.7, the decrease of absorbance was slightly higher at pH 12.3 (about 10% higher). Dye color-stripping by Cu-Phen addition would thus be more efficient when the dye remains unionized. Again, these results may be explained by the speciation calculations presented in Table III-3. At pH 12.3, more hydroxylated copper species ($\text{Cu}(\text{OH})_3^-$, $\text{Cu}(\text{OH})_4^{2-}$, non-coordinated to phenanthroline) and more free Phen are found, compared to pH 10.7, especially at a Cu:Phen ratio of 1:1. For the other Cu:Phen ratios, the amount of $\text{Cu}(\text{Phen})(\text{OH})_2$ increases more significantly.

Overall, the results revealed better "color-stripping" results at pH 10.7 than at pH 12.3. This may be related to the fact that at pH 10.7, DR81 is not ionized, or to the lower hydroxylation of Cu, inducing less competition between the dye and hydroxyl groups around the copper atom. More, CuSO_4 was found to be as effective as Cu-Phen to "decolorize" the dye solution, for Cu:Phen molar ratios of 1:2 and 1:3. Yet, as Phen allows to stabilize copper in alkaline medium, it seems preferable to use Cu-Phen rather than CuSO_4 alone. A Cu:Phen ratio of 1:1 appeared to enable the "best" color-stripping. If this decolorization is directly related to Cu-dye coordination, then it is probably because less phenanthroline was left free to compete with the dye. However, owing to the low stability of 1:1 solutions, a compromise can be found with the 1:2 ratio.

III.5.3.2 Alkaline pH: variation of the dye/Cu ratio

Increasing the amount of Cu-Phen was also tested on the same quantity of dye. The chosen Cu:Phen ratio was 1:2, so that the complex solution could be stable. The DR81L:Cu molar ratio varied from 1:0.5 to 1:1.5; pH 10.7 and 12.3 were tested. The results are gathered in Figure III-43 and Figure III-44.

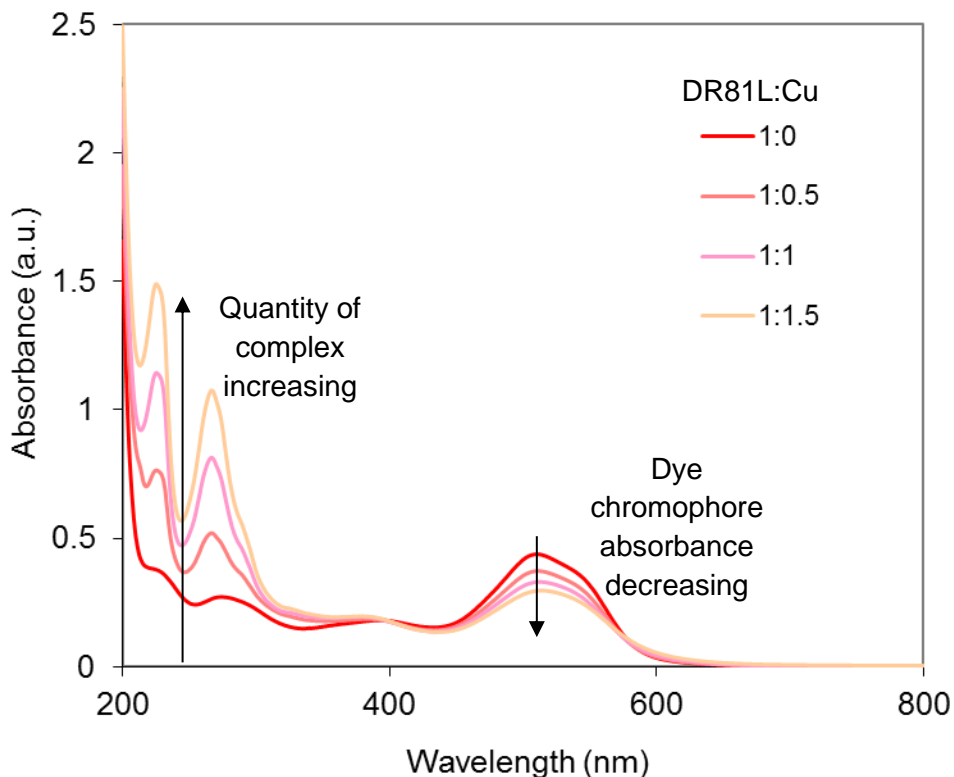


Figure III-43. Absorbance spectra of the dye/copper-phenanthroline system at pH 10.7, with Cu:Phen = 1:2 and [DR81L] = 10 μ M, for different DR81L:Cu ratios

At pH 10.7 (Figure III-43), increasing the amount of Cu-Phen significantly reduced the absorbance intensity in the visible absorption range of the dye. This is probably caused by a higher complexation of the dye but possibly also by modification of its chromophore electronic structure (molar extinction coefficient). However, even with the highest amount of Cu-Phen, the discoloration was far from being fully effective, since the absorbance reduction was below 50%.

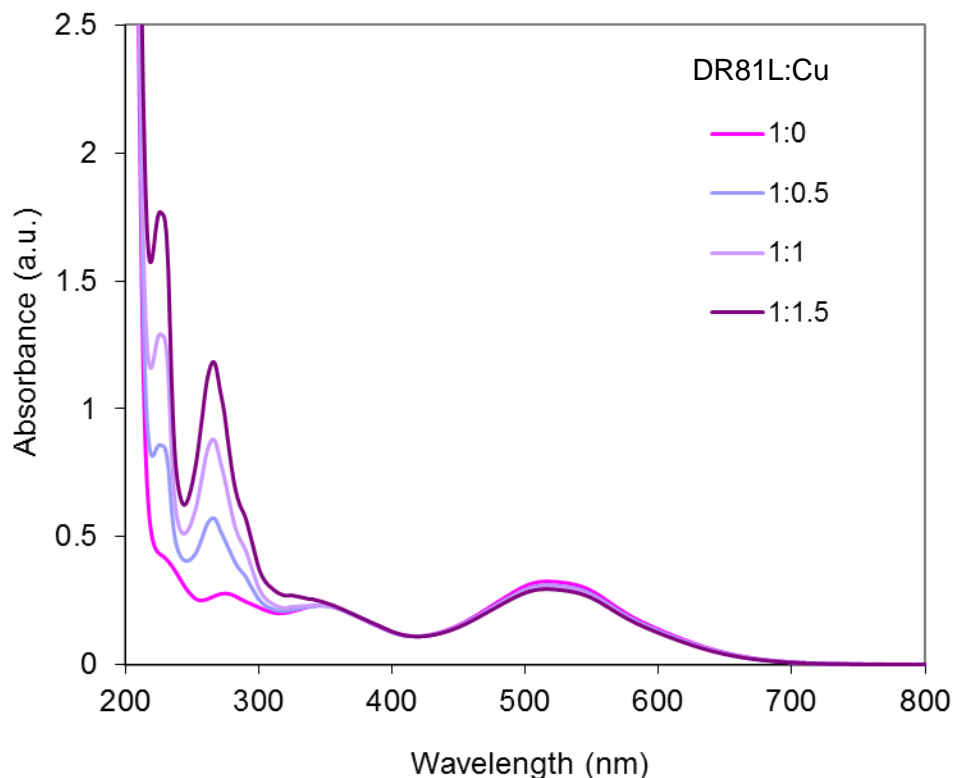


Figure III-44. Absorbance spectra of the dye/copper-phenanthroline system at pH 12.3, with Cu:Phen = 1:2 and [DR81L] = 10 μ M, for different DR81L:Cu ratios

At pH 12.3 (Figure III-44), the decrease of absorbance by increasing the amount of complex was far less pronounced (almost inexistent). A Cu:Phen ratio of 1:3 led to similar results (results not shown).

As a summary, at pH 12.3, the only significant color variation of the dye in the presence of Cu-Phen would be the bathochromic and hypochromic effect from pure unionized initial dye to the ionized dye at pH 12.3. Indeed, copper complexation had almost no effect (Figure III-44). An opposite case was observed at pH 10.7: a color-stripping effect was observed due to the coordination between Cu and DR81. This difference may be due to a lower complexation at pH 12.3, or to the fact that the dye is unionized at pH 10.7, or both.

Since a lower pH increased the color-stripping in the presence of Cu-Phen, some trials were performed at a near neutral pH of 6.5 using the same chemical concentrations as for the previous experiments.

III.5.3.3 Neutral pH

The first control test was a mixture of the dye and CuSO_4 , in which case no precipitation occurred. Comparison with DR81L alone (results not presented) showed a very limited interaction between copper and DR81L, as evidenced by a slight decrease of absorbance in the visible range in the presence of a small excess of copper sulfate.

The second control was performed with pure phenanthroline. No interaction between the dye and phenanthroline occurred, as it was already seen at higher pHs.

Before studying the effect of Cu-Phen on the dye at pH 6.5, the coordination between copper and phenanthroline at this pH was verified. The EPR spectra obtained from frozen solutions of CuSO_4 and Cu-Phen at pH 6.5 are presented in Figure III-45.

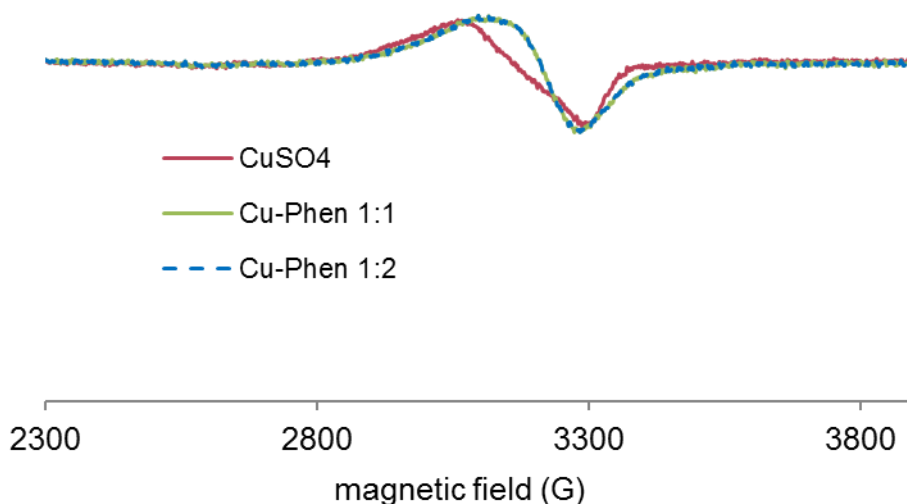


Figure III-45. Experimental X-band EPR spectra recorded at 100 K in frozen aqueous solutions of CuSO_4 and Cu-Phen at pH 6.5, with Cu:Phen = 1:1 and 1:2 and $[\text{Cu}] = 1.5 \text{ mM}$

At pH 6.5, the Cu-Phen signal (1:1 or 1:2 ratio) was clearly different from CuSO_4 alone, thus evidencing the copper-phenanthroline coordination. Besides, both Cu-Phen solutions exhibited the same signal, which seems to show a mixture of copper species with difference hyperfine coupling constants that are not visible, contrarily to the Cu-Phen signal observed at pH 12.3 in Figure III-38. The fact that both Cu:Phen ratios gave identical signals suggests that the major coordinate may be the same in both cases. According to the speciation calculations by PHREEQC, with $[\text{Cu}] = 1.5 \text{ mM}$, $\text{Cu}(\text{Phen})^{2+}$ would be the major species when Cu:Phen = 1:1 and $\text{Cu}(\text{Phen})_2^{2+}$ would replace most of it when Cu:Phen = 1:2. Consequently, it is more probable that the EPR signature of copper is not much modified whether one or two phenanthroline ligands are attached to the copper atom.

Besides, the CuSO_4 signal in Figure III-45 was different from that observed at alkaline pH (Figure III-38), as it did not exhibit the multiple peaks around 3300 G attributed to copper hydroxylation.

Figure III-46 shows the effect of adding Cu-Phen (1:2) to the dye solution at pH 6.5 in terms of UV-visible absorbance.

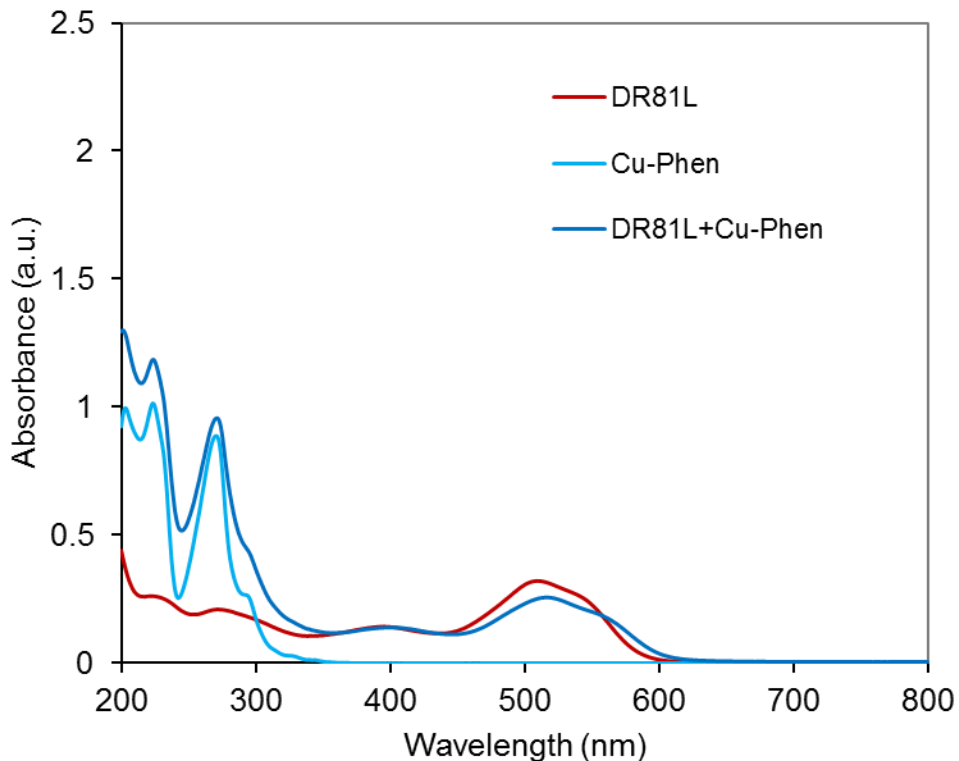


Figure III-46. Absorbance spectrum of the dye/copper-phenanthroline system at pH 6.5, with Cu:Phen = 1:2 and DR81L:Cu = 1:1.5, compared to the dye alone and copper-phenanthroline alone

At neutral pH, the introduction of Cu-Phen in the dye solution modified the absorbance spectrum. The pronounced red shift (from 510 to 516.5 nm) and hypochromic effect (20% intensity decrease) observed when adding Cu-Phen suggest that the dye was coordinated to copper. It could have been expected that no difference would appear compared to pH 10.7, because the dye was in the same unionized state. Yet, the change of pH induced little spectrum modification compared to pH 10.7. The difference is thus probably due to the copper environment at pH 6.5.

Finally, the sharpest decrease of color was obtained at pH 10.7, which seems to gather the best conditions for copper-dye coordination. To confirm the actual coordination of copper to the dye, and attempt to relate it to the UV-visible modifications observed in this part, further studies were implemented, as described in III.5.3.4.

III.5.3.4 Supplementary evidence for complexation

Our experiments based on UV-visible spectroscopy led to the conclusion that DR81 alone would be subjected to bathochromic/hypochromic shift due to its ionization between pH 10.7 and 12.3, and that DR81 and Cu-Phen (possibly partly hydroxylated) would form a co-coordinate, since the addition of CuSO₄ and Cu-Phen induced some color variations in the visible range. Yet, the complexation evidence brought by UV-visible spectroscopy is rather limited, since the electronic structures of chromophores might be more or less affected by coordination, depending on the molecular structure and solution environment. This is why supplementary analyses were performed to prove the occurrence of complexation.

III.5.3.4.i Evidence by HPLC

Copper-phenanthroline was introduced in a DR81S solution and analyzed under the conditions described in II.2.1.2 by ion-pair chromatography, at neutral pH (buffered eluent). DR81S was at a theoretical concentration of 0.5 mM and Cu-Phen at 0.75 mM. The resulting chromatogram is presented in Figure III-47 and compared to that of DR81S alone.

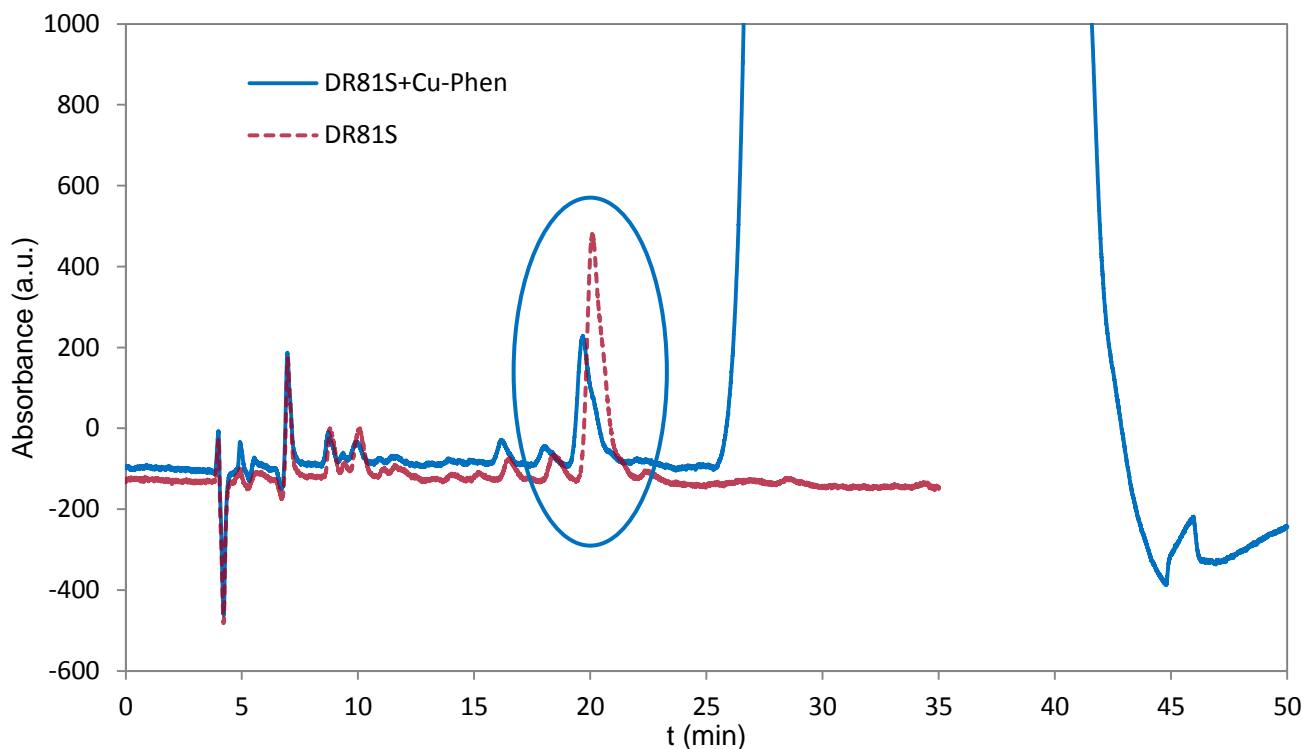


Figure III-47. Chromatograms of DR81S and DR81S+Cu-Phen, elution by a gradient of TBA-OH 5 mM in methanol/TBA-OH 5 mM in water, flow of 0.7 mL/min, UV detection at 254 nm

The very large peak from 25 to 45 min in Figure III-47 corresponds to Cu-Phen. As circled on the Figure, a specific peak of DR81S at around 20 min had a slightly shorter retention time in the presence of Cu-Phen. The coordination between Cu and the dye could explain this slight modification of retention time.

It would have been interesting to verify this coordination by MS analysis. Unfortunately, TBA and methanol were not compatible with this analysis. Therefore, two other methods were tested prior to ESI-MS analysis: either another separation by HPLC, or direct injection.

III.5.3.4.ii Evidence by MS

Two methods were tested: LC/MS by using a water:acetonitrile gradient (0:100 to 50:50 within 5 min) prior to injection, or direct injection.

The preliminary results were the following:

- In negative mode, the dye was detected only after HPLC separation, with a peak at 314 m/z (dianionic DR81, 2 Na removed) and a peak at 630 m/z (monoanionic DR81, 1 Na removed).

III. Characterization of the dyes and interactions with copper-phenanthroline

- In positive mode, Phen and Cu-Phen were detected in the case of direct injection, with a peak at 181 m/z for Phen, and a peak at 423 m/z for $\text{Cu}^+(\text{Phen})_2$, which shows that copper was reduced during the ionization.
- Mixing the dye with Cu-Phen (50 and 75 μM respectively) did not change the results: they were the same as with the dye alone after HPLC separation in negative mode, and the same as Cu-Phen alone after direct injection in positive mode (since in that case the dye was not visible).

In fact, since the phenanthroline molecule is not charged, the coordination between Cu and the dye probably gives a neutral complex, not detectable by MS. The idea was to replace the unionized phenanthroline by a similar charged ligand for ESI-MS analysis. The 4,7-diphenyl-1,10-phenanthroline disulfonic acid (BPS Figure III-48) was found to match these requirements.

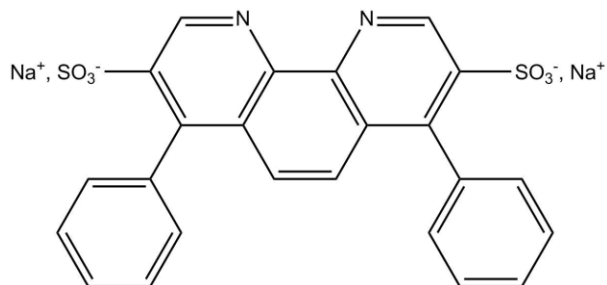


Figure III-48. Molecular structure of BPS

First of all, the Cu-BPS complex was analyzed alone at 2.5 mM in water. It was prepared with 1 mole of CuSO_4 for 3 moles of BPS. The resulting MS spectrum is presented in Figure III-49.

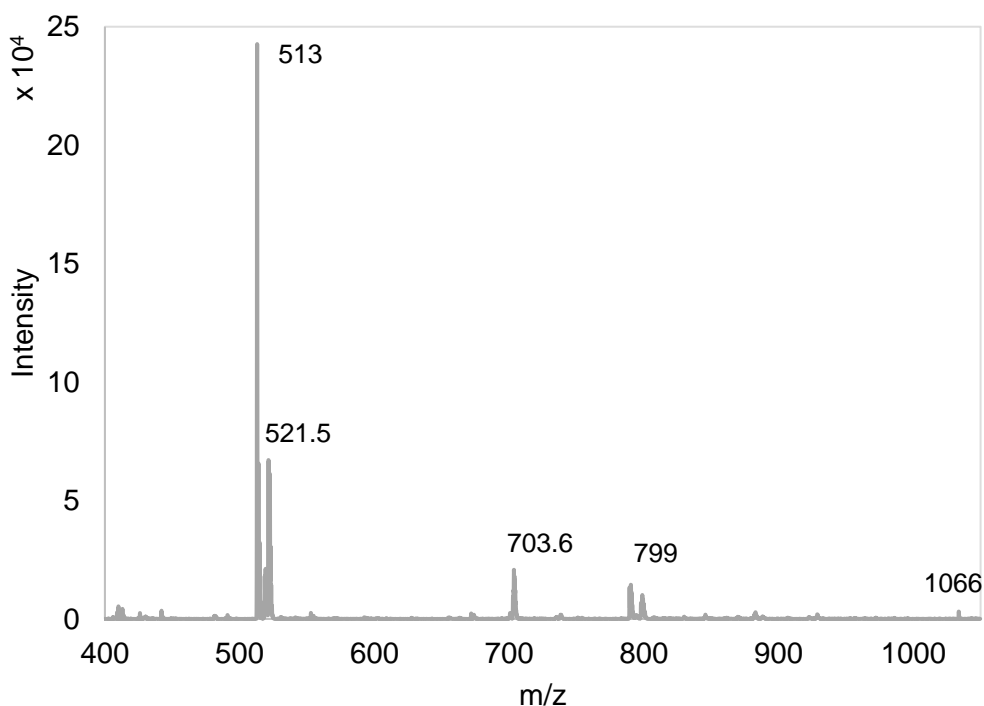


Figure III-49. Negative-ion scan ESI-MS spectrum of Cu-BPS (1:3) at 2.5 mM in water

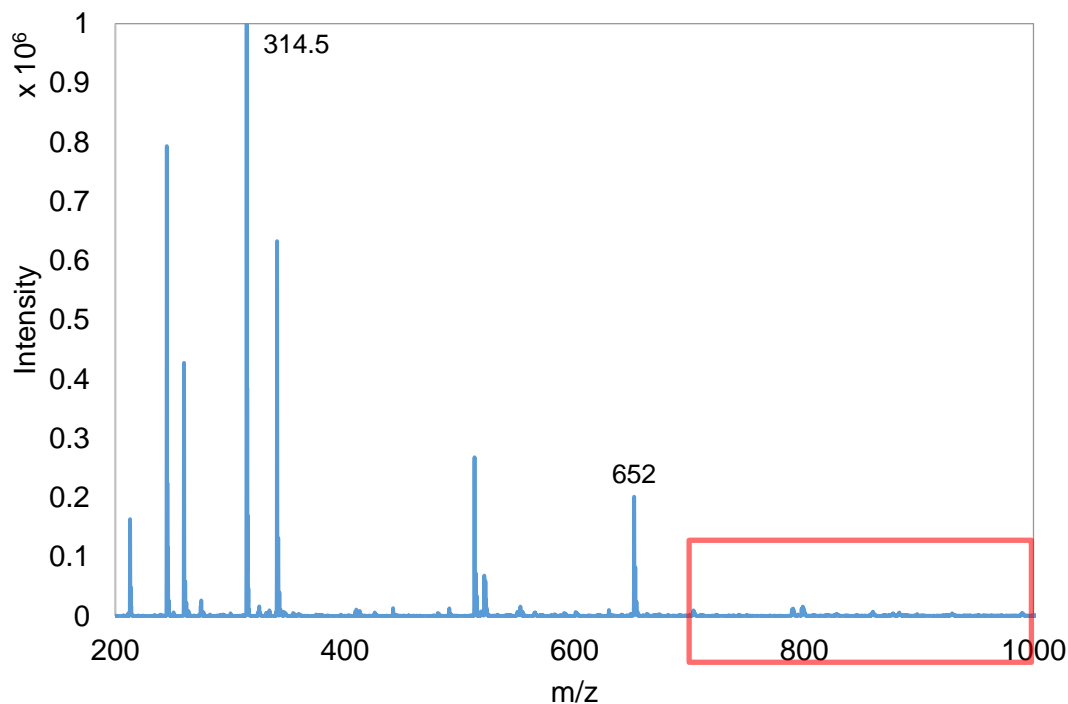
In negative mode, the following peaks were assigned to Cu-BPS compounds (Table III-5).

Table III-5. Assignments of the mass peaks obtained after ESI-MS analysis of the Cu-BPS solution

m/z	Corresponding complex	Number of removed Na atoms
513	$\text{Cu}(\text{BPS})^-$	1
521.5	$\text{Cu}(\text{BPS})_2^{2-}$	2
703.6	$\text{Cu}_2(\text{BPS})_4^{3-}$	7
799	$\text{Cu}_2(\text{BPS})_3^{2-}$	6
1066	$\text{Cu}(\text{BPS})_2^-$	1

The Cu-BPS complex was thus easily detected by negative-ion scan ESI-MS, and some “binuclear” complexes were found. These probably originate from rearrangements by dimerization of two complexes during the ionization.

Then, the Cu-BPS complex was mixed to the DR81S dye, with concentrations of 50 μM dye and 75 μM Cu-BPS. The mass spectrum obtained under negative mode is given in Figure III-50.

**Figure III-50. Negative-ion scan ESI-MS spectrum of DR81S+Cu-BPS (1:3) with DR81S 50 μM and Cu-BPS 75 μM**

As previously shown in the dye characterization section (III.2.4), the main peaks (314.5 m/z, 652 m/z) are attributed to the dye alone. However, some new peaks appeared above 700 nm. These other detectable peaks are focused on in Figure III-51, with an enlargement of the ESI-MS spectrum between 700 and 1000 m/z.

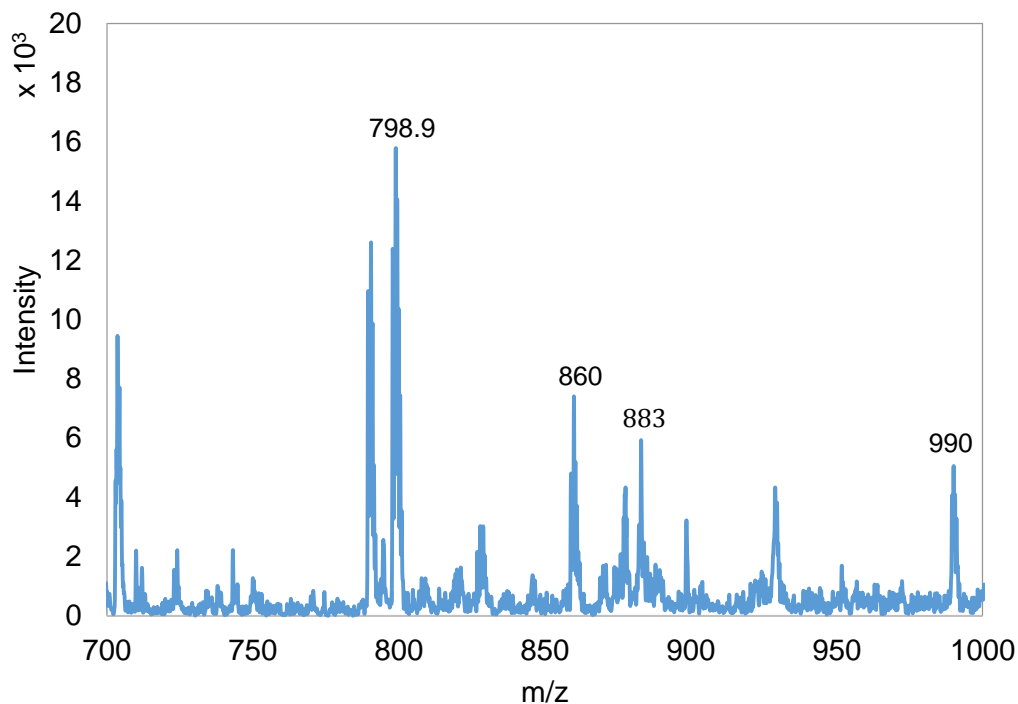


Figure III-51. Negative-ion scan ESI-MS spectrum of DR81S+Cu-BPS (1:3) with DR81S, enlargement from 700 to 1000 m/z

These peaks have been assigned and the results are gathered in Table III-6.

Table III-6. Assignments of the mass peaks obtained after ESI-MS analysis of the DR81S+Cu-BPS solution

m/z	Corresponding complex	Number of removed Na atoms
565	$\text{Cu}(\text{BPS})_2(\text{DR81})^{3-}$	5
591	$\text{Cu}(\text{BPS})(\text{DR81})^{2-}$	4
799	$\text{Cu}_2(\text{BPS})_3^{2-}$	6
860	$\text{Cu}(\text{BPS})_2(\text{DR81})^{2-}$	4

To verify that the assignments for 591 and 860 m/z were right, MS spectrum simulations were performed for the proposed complexes. Figure III-52 presents the comparison between the experimental spectra and the corresponding simulated spectra at both 591 m/z and 860 m/z.

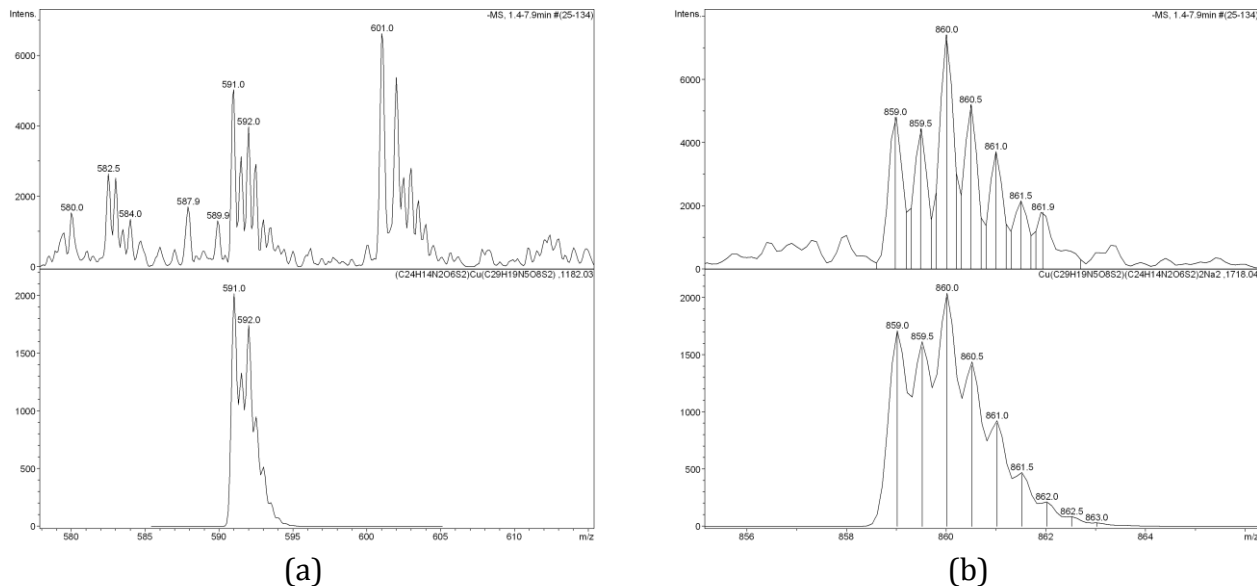


Figure III-52. Comparison between experimental peaks (top) and simulated peaks (bottom) at 591 m/z (a) and 860 m/z (b)

Figure III-52 shows that the simulated peaks have the same shape as the experimental signals, thus validating the proposed assignments. Consequently, although they were detected in a small amount compared to free dye, ESI-MS proved the presence of Cu-BPS-DR81 complexes. This novel result suggests that similar Cu-Phen-DR81 co-coordinates could be formed in the studied system.

To complement this result, EPR analyses were implemented at low temperature in order to follow the hyperfine structure of copper(II) depending on the molecules it coordinates with (dye or phenanthroline). The results are presented in the next part.

III.5.3.4.iii Evidence by EPR

EPR spectroscopy was used to study the chemical environment of copper(II) depending on the medium conditions. EPR spectra of CuSO_4 with and without phenanthroline ($\text{Cu}:\text{Phen} = 1:2$), and in the presence of DR81L or not, were recorded at high pH (12.3) and near-neutral pH (6.5) (Figure III-53 and Figure III-54, respectively).

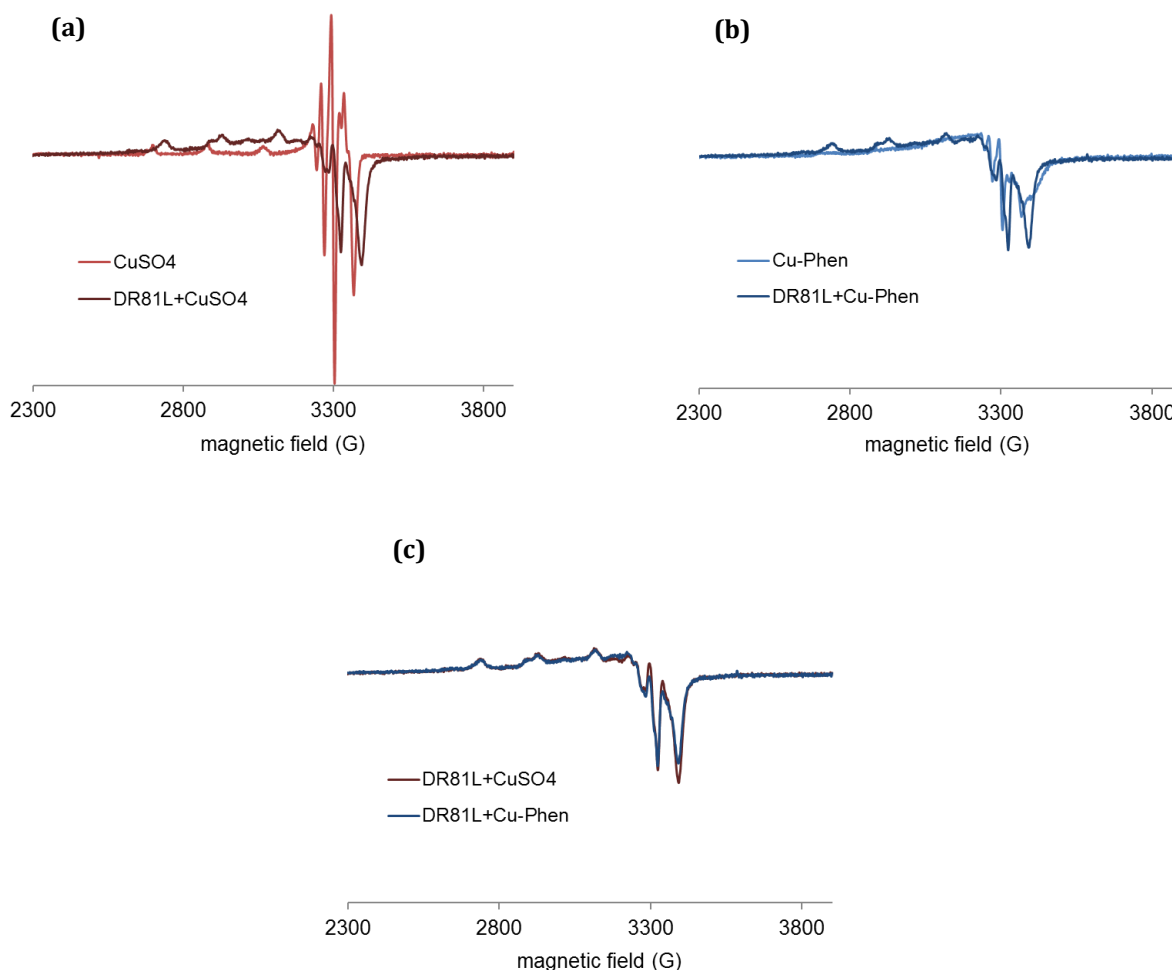


Figure III-53. Experimental X-band EPR spectra recorded at 100 K in frozen aqueous solutions of (a) CuSO₄ and CuSO₄+DR81L (b) Cu-Phen and Cu-Phen+DR81L (c) CuSO₄+DR81L and Cu-Phen+DR81L, at pH 12.3, with Cu:Phen = 1:2, DR81L:Cu = 1:1.5 and [Cu] = 1.5 mM

At pH 12.3, the addition of DR81L notably modified the EPR spectrum of CuSO₄ (Figure III-53a), displaying different coupling constants and thus confirming the Cu-dye coordination. In the same manner, Figure III-53b shows the Cu-dye coordination in the case of Cu-Phen. However, the spectra recorded in the presence of DR81L were absolutely similar and superimposed with or without phenanthroline (Figure III-53c). This observation implies that the phenanthroline ligand has been fully eliminated and replaced by the dye in the coordination sphere of the copper ion. The affinity of copper towards the dye is thus higher than that towards phenanthroline.

According to the PHREEQC simulations, under these conditions, the major species in a 1:2 complex solution would be Cu(Phen)(OH)₂, which means that one phenanthroline would be ejected to leave some space for the dye. In the case of copper alone, the major species would be Cu(OH)₃⁻, one hydroxyl group of which can easily be exchanged with the dye molecule. However, such a modification of the copper environment hardly affected the dye chromophore structure, as it was seen in the corresponding UV-visible spectrum of Figure III-39.

The same copper EPR analyses were conducted at near neutral pH, i.e. 6.5. Results are given in Figure III-54.

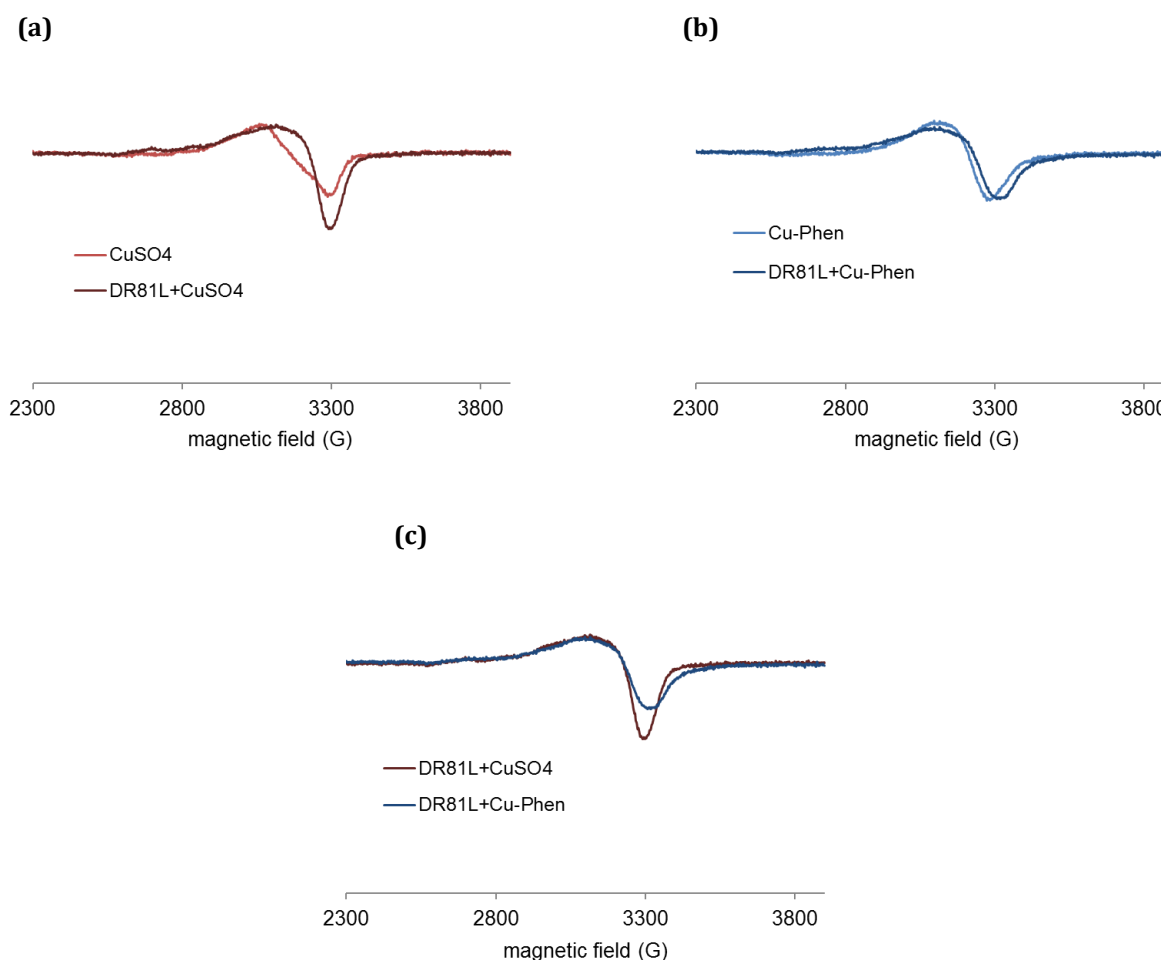


Figure III-54. Experimental X-band EPR spectra recorded at 100 K in frozen aqueous solutions of (a) CuSO_4 and CuSO_4 +DR81L (b) Cu-Phen and Cu-Phen+ DR81L (c) CuSO_4 +DR81L and Cu-Phen+ DR81L , at pH 6.5, with $\text{Cu:Phen} = 1:2$, $\text{DR81L:Cu} = 1:1.5$ and $[\text{Cu}] = 1.5 \text{ mM}$

At neutral pH (Figure III-54), CuSO_4 and Cu-Phen solutions displayed different EPR spectra. These spectra also differed from those recorded in alkaline medium. This evidences the presence of different complexes as a function of pH, as predicted by PHREEQC. In the case of CuSO_4 (Figure III-54a), the addition of DR81L led to the appearance of a new EPR signature. This signature probably corresponds to a mixture of a majority of CuSO_4 and some Cu-dye complex, as the hyperfine structure was not quite visible. A similar effect was observed in the case of Cu-Phen (Figure III-54b), with a new signature probably due to a mixture of Cu-Phen and some Cu-dye complex.

Although rather comparable, the signals of Figure III-54c are not fully superimposed, contrarily to the equivalent signals at pH 12.3 (Figure III-53c). Again, it is shown that the dye interacts strongly with Cu(II) . The small difference between the signals of Figure III-54c is attributed to the presence of some phenanthroline in the coordination sphere of the copper ion (with Cu-Phen), which differs

from the case observed at pH 12.3. At pH 6.5, the speciation should be much different from pH 12.3. According to our calculations, the major species in the presence of 1:2 Cu-Phen would be $\text{Cu}(\text{Phen})_2^{2+}$, as compared to $\text{Cu}(\text{Phen})(\text{OH})_2$ at pH 12.3. Therefore, an average of 2 phenanthroline ligands should be present around the copper atom in a Cu-Phen solution of 1.5 mM at pH 6.5. It seems unlikely that both ligands would be ejected to be replaced by the dye, which would easily explain the differences between the DR81L+CuSO₄ and DR81L+Cu-Phen spectra.

When mixing DR81L to Cu-Phen, the best “color-stripping” results were obtained at pH 10.7. Therefore, it was interesting to perform a few EPR analyses at this pH, in order to check whether the dye-Cu-Phen coordination was enhanced. If so, it could be owing to speciation differences or to the non-ionized state of the dye at that pH.

Frozen solutions of Cu-Phen and Cu-Phen+DR81L were thus analyzed at pH 10.7, as shown in Figure III-55.

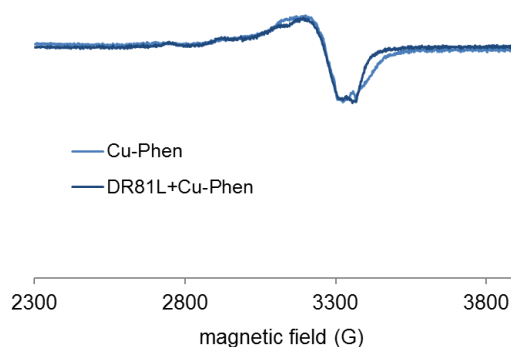


Figure III-55 Experimental X-band EPR spectra recorded at 100 K in frozen aqueous solutions of Cu-Phen and Cu-Phen+DR81L at pH 10.7, with Cu:Phen = 1:2, DR81L:Cu = 1:1.5 and [Cu] = 1.5 mM

Figure III-55 shows that coordination also occurs at pH 10.7. The signals were different from those at pH 12.3 and 6.5, suggesting again a different mixture of coordinates. This is quite logical since the PHREEQC simulation gave the $\text{Cu}(\text{Phen})_3$ complex as the major species at pH 10.7 (45% of total Cu), with a relatively high amount of $\text{Cu}(\text{Phen})(\text{OH})_2$ as well (34%).

In order to better understand the effect of dye addition to the copper sulfate or copper-phenanthroline solution, an excess of dye was tested: DR81L:Cu = 10:1.5 instead of 1:1.5. The results at pH 12.3 are presented in Figure III-56.

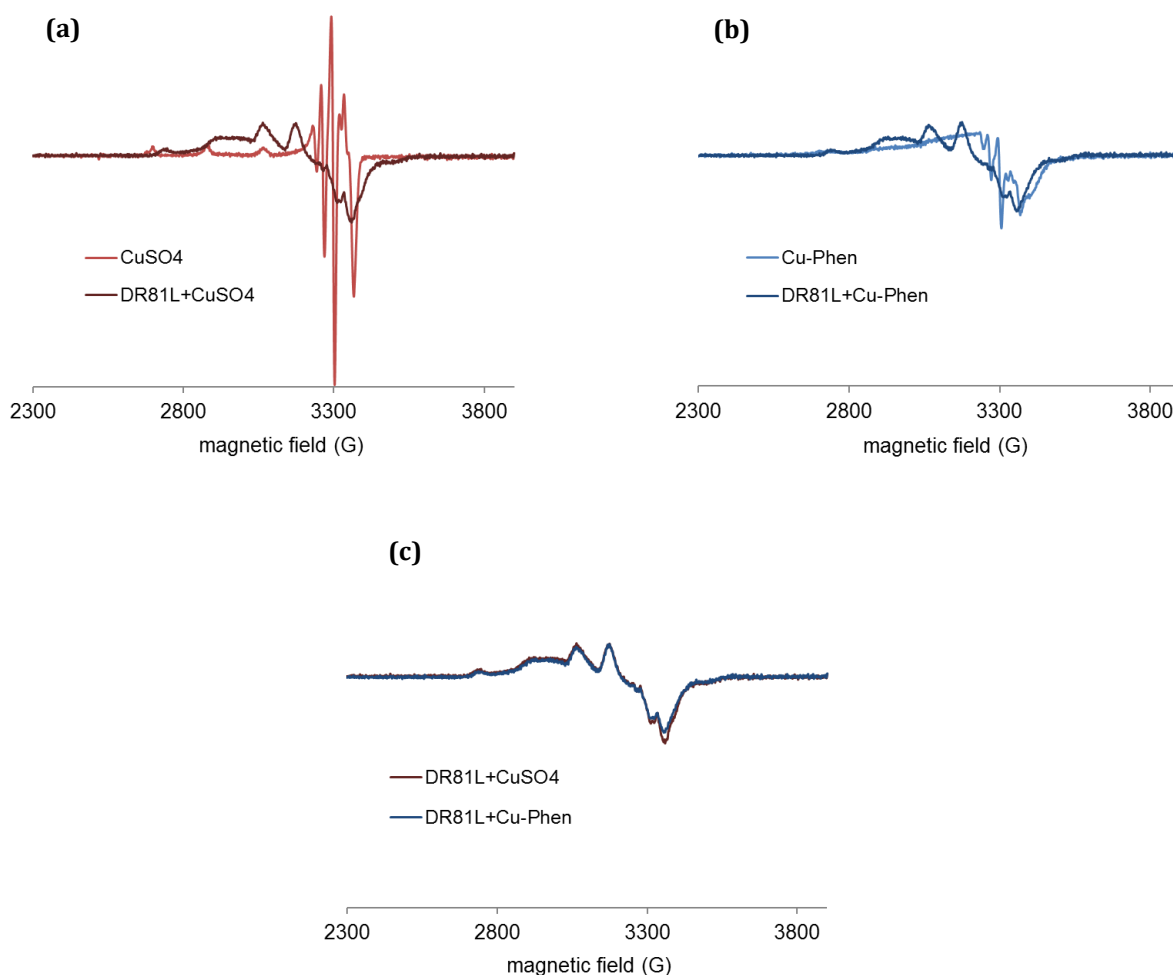


Figure III-56. Experimental X-band EPR spectra recorded at 100 K in frozen aqueous solutions of (a) CuSO₄ and CuSO₄+DR81L (b) Cu-Phen and Cu-Phen+ DR81L (c) CuSO₄+DR81L and Cu-Phen+ DR81L, at pH 12.3, with Cu:Phen = 1:2, DR81L:Cu = 10:1.5 and [Cu] = 1.5 mM

Using an excess of dye, the addition of DR81L clearly structured copper's environment, as the hyperfine structure is markedly visible in both cases (Cu in Figure III-56a and Cu-Phen in Figure III-56b). However, as well as with a lower amount of dye, Figure III-56c shows that phenanthroline was ejected from copper's environment in the presence of DR81L: the same Cu-dye coordinate was formed in both cases. According to the signature, it was certainly a mixture of coordinates. However, this signature does not seem to exhibit the hyperfine coupling constants of CuSO₄ or Cu-Phen. Therefore, most of the copper was probably bonded to the dye.

The same experiment was repeated at pH 6.5 with an excess of DR81L (Figure III-57).

III. Characterization of the dyes and interactions with copper-phenanthroline

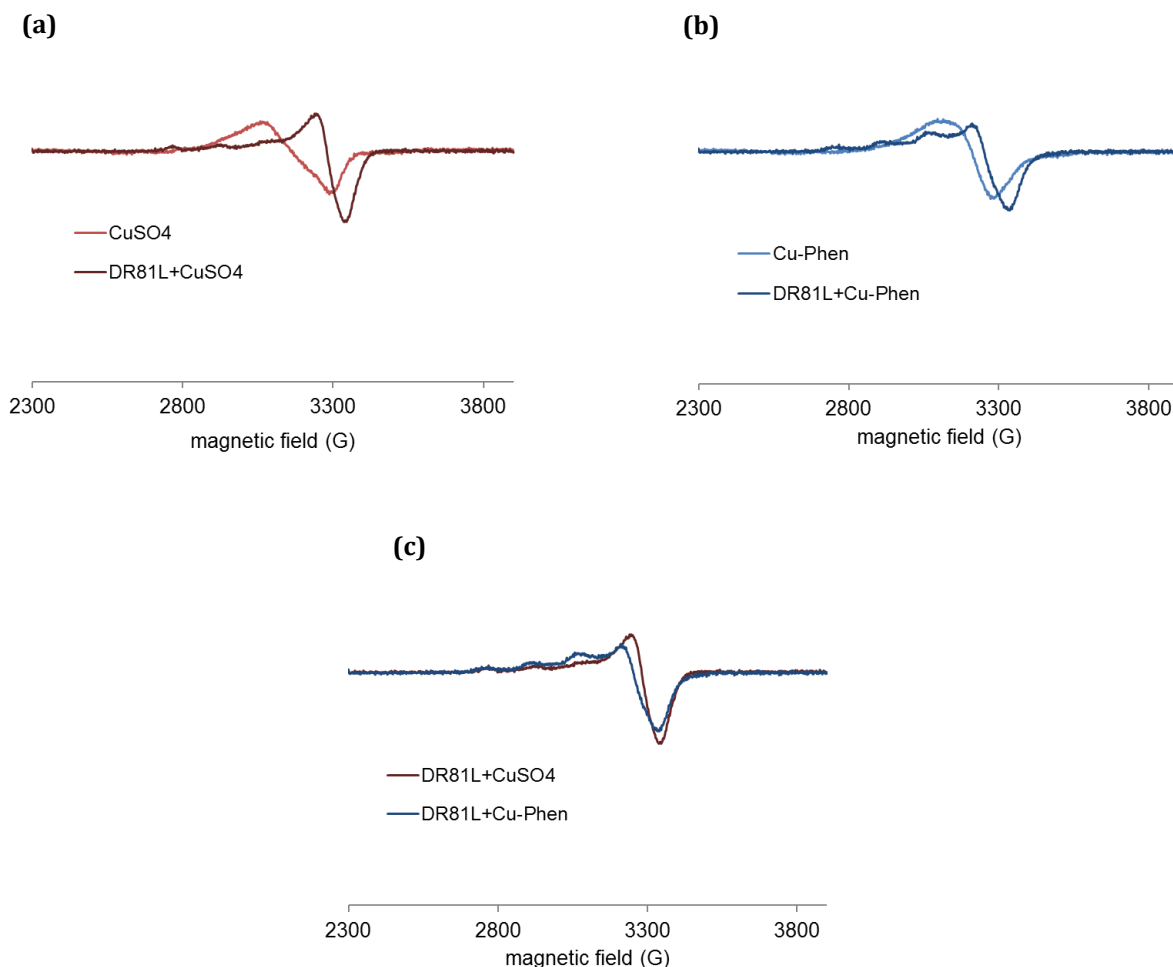


Figure III-57. Experimental X-band EPR spectra recorded at 100 K in frozen aqueous solutions of (a) CuSO₄ and CuSO₄+DR81L (b) Cu-Phen and Cu-Phen+ DR81L (c) CuSO₄+DR81L and Cu-Phen+ DR81L, at pH 6.5, with Cu:Phen = 1:2, DR81L:Cu = 10:1.5 and [Cu] = 1.5 mM

At pH 6.5, again, the structuration of copper when adding DR81L was more noticeable than with a lower amount of dye. This confirms the coordinating effect between copper and DR81L also in near-neutral medium. Besides, as well as with DR81L:Cu = 1:1.5, Figure III-57c exhibits two different spectra. The DR81L/CuSO₄ mixture was thus different from the DR81L/Cu-Phen mixture: phenanthroline was not fully replaced by the dye in copper's coordination sphere in the second case. Finally, the coordination effect was more important with an excess of dye but the differences depending on the pH did not vary.

All these results, in which phenanthroline would not or only partly be coordinated to the copper-dye complex, corroborate the previous UV-visible spectroscopic observation, as similar "color-stripping" was observed with either CuSO₄ or Cu-Phen, at both pH 10.7 (strong effect) and pH 12.3 (weak effect). At pH 6.5, however, Cu-Phen seemed to have a more intense hypochromic effect on the dye than CuSO₄ alone. This is most likely due to the formation of a Phen-Cu-dye co-coordinate in the first case.

As the “color-stripping” effect was much higher at pH 10.7, it can be assumed that complexation has more or less influence on the chromophore structure of the dye. Moreover, it probably also depends on the involved coordinates and on the pH.

Actually, two cases can be distinguished:

- 1) In the strong alkaline case (ionized dye at pH 12.3) and the near neutral case (unionized dye, pH 6.5), with or without phenanthroline, the chromophore’s electronic structure was hardly affected by copper complexation.
- 2) In the alkaline case at pH 10.7 (unionized dye), with or without phenanthroline, the chromophore structure was partly modified.

The EPR results also showed that the geometry around the cupric ion varied as a function of pH for all three species, i.e. CuSO₄, Cu-Phen and Cu-DR81. Besides, at near-neutral pH, some phenanthroline remained in the coordination sphere of copper, probably owing to the presence of some Phen-Cu-DR81 complex.

As seen in III.1, NMR and MS analyses of the commercial dye solution of DR81 (DR81L) showed that it contained not only the dye molecule, but also some additives. Therefore, a complexation between copper and an additive or the influence of some additives on the complexation between copper and the dye are not excluded.

III.5.3.5 Conclusions

The purpose of this study was to ascertain the effect of copper-phenanthroline complexes on the Direct Red 81 dye in aqueous solution.

The results showed that whatever the pH, Cu-Phen can reduce the color of a Direct Red 81 solution. This apparent color-stripping effect would be due to the coordination of copper with the dye after total or partial release of the phenanthroline ligand, which was evidenced by EPR spectroscopy. Interestingly, at pH 6.5, some phenanthroline remained in the coordination sphere of copper, whereas at alkaline pH, it seemed to be ejected.

The complexation of copper with Direct Red 81 is certainly responsible for the decrease of its absorbance in the visible range, although this absorbance could not be totally cancelled. This phenomenon was more effective at medium alkalinity (pH 10.7) with a Cu:Phen molar ratio between 1:1 and 1:2.

III.6 CONCLUSIONS

In conclusion, the results presented in this Chapter allowed to characterize the dye/Cu-Phen system in aqueous solution and in the absence of any oxidant.

First, the selected dyes (DR81L and DY11L) were characterized as well as the copper-phenanthroline complex. The DR81 dye structure given by the dye supplier was confirmed, whereas the DY11 structure was not. The dye concentration could not be verified by NMR but some major additives were detected and corresponding molecular structures were proposed. However, the dye formulation remains still secretive. Since the DY11L dye structure could not be confirmed, the present study focused on the DR81L dye.

Second, speciation calculations allowed to list the different possible copper-phenanthroline depending on pH. In alkaline medium, the major species are hydroxylated Cu-Phen complexes, whereas cationic Cu-Phen complexes are dominant a near-neutral pH. The Cu-Phen complexation was also proved by EPR analysis at 100 K.

Then, the interactions between the DR81L dye and the Cu-Phen complexes were investigated at different pHs. It was proved that DR81L formed coordinates with copper-phenanthroline with possible ejection of phenanthroline at alkaline pH. Several complexes were formed. The complexation of DR81L with Cu-Phen led to almost 50% “decolorization”, depending on the dye solution’s pH. The best results were obtained at pH 10.7, in which case the red dye was unionized and the Cu-dye complex hydroxylated, with possibly a minority of Phen-Cu-dye complex. At near-neutral pH (6.5), the dye was also unionized, but copper could not be hydroxylated, and phenanthroline was clearly present in the complex, thus forming Phen-Cu-dye coordinates.

Combining all these results together:

At neutral pH:

1) CuSO_4 is found as Cu^{2+} , and some precipitation into tenorite is already possible. After dye introduction, at a dye:Cu molar ratio of 1:1.5, the solution would be composed of a mixture of free Cu^{2+} and Cu-dye complex, in which Cu^{2+} would be the major species. It is only with an excess of dye that the Cu-dye complex becomes predominant. The coordination between Cu and the dye occurs most certainly with at least one nitrogen atom of the dye.

2) A solution of CuSO_4 and Phen leads to a mixture of Cu-Phen complexes: $\text{Cu}(\text{Phen})^{2+}$, $\text{Cu}(\text{Phen})_2^{2+}$ and $\text{Cu}(\text{Phen})_3^{2+}$, with different speciations depending on the initial Cu:Phen molar ratio. After dye introduction, as observed with CuSO_4 alone, some Cu-Phen complexes would still be present, but some co-coordinates would also appear, with two types of ligands around the copper atom: phenanthroline and the dye. The coordinating sites are probably nitrogen atoms of Phen and of the dye, and possibly one oxygen atom from the naphthol group of the dye.

At alkaline pH:

1) CuSO_4 is mainly present as $\text{Cu}(\text{OH})_3^-$ and $\text{Cu}(\text{OH})_4^{2-}$; after dye introduction, a mixture of $\text{Cu}(\text{OH})_3^-$, $\text{Cu}(\text{OH})_4^{2-}$ and Cu-dye complex would be in solution. To form the Cu-dye complex, the dye replaced at least one hydroxyl group around copper. The coordination site is again nitrogen and possibly an oxygen atom.

2) A solution of CuSO_4 and Phen results in a majority of $\text{CuPhen}(\text{OH})_2$. After dye introduction, one or several complex(es) of Cu and the dye would be formed, with total replacement of phenanthroline.

This Cu-Phen complexing system would be very interesting to apply for dyed effluent treatment. It might be used as an alternative to physicochemical techniques, such as chemical oxidation, chemical reduction, or adsorption, to decolorize colored wastewaters. Indeed, a simple addition of copper and phenanthroline is enough to reduce the color significantly. This is not sufficient to reduce the impact of the effluent, but might allow its recycling in the process. This complexation could also be used to provoke the precipitation of Cu-dye or Phen-Cu-dye complexes on purpose, to recover the dye, copper (and phenanthroline) in a solid state.

Another application may be in deinked pulp bleaching (after deinking, residual color due to recovered dyed papers is generally removed by reductive bleaching). However, the application of

such a system to colored cellulosic fibers would require further experimentation and testing, due to the strong fixation of the dyes on fibers. Color-stripping by dye complexation only is probably not efficient in that case. In the next Chapter, hydrogen peroxide will be used as an oxidant and Cu-Phen as an activator to decolorize the dyes in the presence of fibers. These color-stripping trials will be performed on both DY11L- and DR81L-dyed pulps.

III.7 REFERENCES

- [1] J. Oakes and P. Gratton, "Kinetic investigations of azo dye oxidation in aqueous media," *Journal of the Chemical Society, Perkin Transactions 2*, no. 9, pp. 1857–1864, 1998.
- [2] H. M. Randall, *Infrared determination of organic structures*. New York: Van Nostrand Co, 1949.
- [3] M. M. Sahasrabudhe, R. G. Saratale, G. D. Saratale, and G. R. Pathade, "Decolorization and detoxification of sulfonated toxic diazo dye C.I. Direct Red 81 by *Enterococcus faecalis* YZ 66," *Journal of Environmental Health Science and Engineering*, vol. 12, no. 1, p. 151, Dec. 2014.
- [4] "Integrated Spectral Database System of Organic Compounds," National Institute of Advanced Industrial Science and Technology, Japan, Spectrum ID: NIDA28107.
- [5] "Bio-Rad/Sadtler IR Data Collection," Bio-Rad Laboratories, Philadelphia, PA (US), Spectrum ID: BR149792.
- [6] Wiley Subscription Services, Inc., US, Spectrum ID: MPCC-25316-766Z.
- [7] A. N. Kagalkar, U. B. Jagtap, J. P. Jadhav, V. A. Bapat, and S. P. Govindwar, "Biotechnological strategies for phytoremediation of the sulfonated azo dye Direct Red 5B using *Blumea malcolmii* Hook," *Bioresource Technology*, vol. 100, no. 18, pp. 4104–4110, Sep. 2009.
- [8] "Integrated Spectral Database System of Organic Compounds," National Institute of Advanced Industrial Science and Technology, Japan, Spectrum ID: NIDA15442.
- [9] "Integrated Spectral Database System of Organic Compounds," National Institute of Advanced Industrial Science and Technology, Japan, Spectrum ID: NIDA18400.
- [10] A. Ringbom, *Les complexes en chimie analytique: comment choisir rationnellement les meilleures méthodes d'analyse complexométrique*. Paris: Dunod, 1967.
- [11] A. A. Schilt, *Analytical applications of 1,10-phenanthroline and related compounds*, 1st ed., vol. 32. Oxford London Edinburgh: Pergamon Press, 1969.
- [12] R. M. Smith and A. E. Martell, *Critical stability constants*. New York London: Plenum Press, 1975.
- [13] W. A. E. McBryde, *A Critical review of equilibrium data for proton and metal complexes of 1,10-phenanthroline, 2,2'-bipyridyl and related compounds*. Oxford New York Toronto Rushcutters Bay Paris Kronberg-Taunus: Pergamon press, 1978.
- [14] T. Moeller, *Inorganic chemistry: an advanced textbook*. New York: Wiley, 1952.
- [15] H. Korpi, P. J. Figiel, E. Lankinen, P. Ryan, M. Leskelä, and T. Repo, "On in situ prepared Cu-Phenanthroline complexes in aqueous alkaline solutions and their use in the catalytic oxidation of veratryl alcohol," *European Journal of Inorganic Chemistry*, vol. 2007, no. 17, pp. 2465–2471, Jun. 2007.

III. Characterization of the dyes and interactions with copper-phenanthroline

- [16] K. Yamazaki, H. Yokoi, and K. Sone, "Spectrochemical studies on o-phenanthroline complex salts," vol. 69, pp. 137–140, 1948.
- [17] N. Armaroli, L. De Cola, V. Balzani, J.-P. Sauvage, C. O. Dietrich-Buchecker, and J.-M. Kern, "Absorption and luminescence properties of 1,10-phenanthroline, 2,9-diphenyl-1,10-phenanthroline, 2,9-dianisyl-1,10-phenanthroline and their protonated forms in dichloromethane solution," *Journal of the Chemical Society, Faraday Transactions*, vol. 88, no. 4, pp. 553–556, 1992.
- [18] B. L. Vallee, J. A. Rupley, T. L. Coombs, and H. Neurath, "The Role of Zinc in Carboxypeptidase," *J. Biol. Chem.*, vol. 235, no. 1, pp. 64–69, Jan. 1960.
- [19] Y. Ni, D. Lin, and S. Kokot, "Synchronous fluorescence, UV–visible spectrophotometric, and voltammetric studies of the competitive interaction of bis(1,10-phenanthroline)copper(II) complex and neutral red with DNA," *Analytical Biochemistry*, vol. 352, no. 2, pp. 231–242, May 2006.
- [20] C. Bovet and A. R. Barron, "Electron Paramagnetic Resonance Spectroscopy of Copper(II) Compounds - OpenStax CNX." [Online]. Available: <http://cnx.org/contents/NB5XiHcn@2/Electron-Paramagnetic-Resonanc>. [Accessed: 17-May-2016].

IV. DYED PULP COLOR-STRIPPING BY ACTIVATED HYDROGEN PEROXIDE

TABLE OF CONTENTS

LIST OF FIGURES	167
LIST OF TABLES	167
IV.1 INTRODUCTION.....	169
IV.2 PRELIMINARY STUDY ON A DY11L-COLORED PULP.....	169
<i>IV.2.1 Introduction.....</i>	<i>169</i>
<i>IV.2.2 Experimental.....</i>	<i>170</i>
<i>IV.2.3 Activating effect of Cu-Phen and Phen.....</i>	<i>170</i>
IV.2.3.1 Color-stripping results.....	170
IV.2.3.2 Results on pulp optical properties	171
IV.2.3.3 Results on cellulose viscosity	172
IV.2.3.4 General view.....	173
IV.2.3.5 Conclusion.....	176
<i>IV.2.4 Design of experiments: influence of time, temperature, and NaOH dose.....</i>	<i>176</i>
<i>IV.2.5 Conclusions</i>	<i>180</i>
IV.3 COLOR-STRIPPING OF A DR81L-COLORED PULP	181
<i>IV.3.1 Introduction.....</i>	<i>181</i>
<i>IV.3.2 Experimental.....</i>	<i>181</i>
<i>IV.3.3 White pulp bleaching.....</i>	<i>182</i>
<i>IV.3.4 Dyed pulp color-stripping.....</i>	<i>186</i>
IV.3.4.1 Decolorizing effect	187
IV.3.4.1.i Color-stripping results.....	187
IV.3.4.1.ii At low alkalinity (0.2% NaOH)	188
IV.3.4.1.iii Under conventional alkaline conditions (2% NaOH).....	189
IV.3.4.2 Cellulose degradation.....	190
IV.3.4.3 Impact of the color-stripping treatments on the mechanical properties of the dyed pulp	191
IV.3.4.4 Conclusions.....	192
<i>IV.3.5 Comparison with the color-stripping of a DY11L-dyed pulp.....</i>	<i>192</i>
<i>IV.3.6 Conclusions</i>	<i>193</i>
IV.4 CONCLUSION	194
IV.5 REFERENCES.....	194

LIST OF FIGURES

Figure IV-1. DRI vs DP_v after color-stripping of the DY11L-dyed pulp	174
Figure IV-2. Predicted concentrations of the different possible species in a copper-phenanthroline solution, depending on pH, at 25°C. The initial concentrations were $[CuSO_4] = 1.66 \times 10^{-4} M$ and $[Phen] = 5.22 \times 10^{-4} M$	175
Figure IV-3. ISO brightness after treatment of the BKP	183
Figure IV-4. Cellulose DP_v after treatment of the BKP	184
Figure IV-5. Wet zero-span breaking length after treatment of the BKP	185
Figure IV-6. Burst index after treatment of the BKP	186
Figure IV-7. DRI after color-stripping of the DR81L-dyed pulp	188
Figure IV-8. a^* value after color-stripping of the DR81L-dyed pulp	188
Figure IV-9. Cellulose DP_v after color-stripping of the DR81L-dyed pulp	190
Figure IV-10. Wet zero-span breaking length after color-stripping of the DR81L-dyed pulp	191
Figure IV-11. Burst index after color-stripping of the DR81L-dyed pulp	192

LIST OF TABLES

Table IV-1. Amounts of $CuSO_4$ and Phen introduced in the pulp (30 g odp)	170
Table IV-2 Color-stripping results for P and activated P stages, compared with control samples (BKP and dBKP)	171
Table IV-3. Predicted distributions of the different possible species at pH 4.7 and 10.5, presented as percentage rates compared to the initial concentration of Cu, when considering no precipitation phenomena	175
Table IV-4. Levels of the DOE variables	177
Table IV-5. Box-Behnken DOE	177
Table IV-6. Results of the DOE	178
Table IV-7. Results of the tested optimal conditions on the DY11L-dyed pulp	179
Table IV-8. Predicted distributions of the different possible species at pH 7.3, 10.6 and 11.4, presented as percentage rates compared to the initial concentration of Cu, when considering no precipitation phenomena	180
Table IV-9. Amounts of $CuSO_4$ and Phen introduced in the pulp (20 g odp)	182

IV. Dyed pulp color-stripping by activated hydrogen peroxide

Table IV-10. Bleaching results for P, activated P stages and controls performed on the original bleached pulp with 2% or 0.2% NaOH	182
Table IV-11. Detailed results of the color-stripping trials performed on the DR81L-dyed pulp..	187
Table IV-12. Results of some key color-stripping treatments performed on the DY11L-dyed pulp compared to the same treatments on the DR81L-dyed pulp, with 2% NaOH.....	193

IV.1 INTRODUCTION

In the context of high-grade recovered-fiber bleaching, the color-stripping of DIPs focuses on the removal or degradation of paper dyes. The most common dyes present in those recovered pulps are direct azo dyes (see I.2.1.5). Since azo bonds are not oxidizable by HOO^- , direct azo dyes are not degraded by conventional alkaline peroxide treatment. As mentioned in Chapter I (see I.2.3), improving the effectiveness of peroxide bleaching by activation or catalysis would be helpful to minimize the amount of sodium dithionite and FAS needed in deinking lines.

As detailed in I.3.5.3, previous studies already reported the improvement of DIP color-stripping during Cu-Phen-activated peroxide stages [1], [2]. However, the activation mechanism has never been presented.

A first objective was to validate the results reported in the literature. For this purpose, some trials were performed on dyed pulps to optimize their discoloration using the $\text{H}_2\text{O}_2/\text{Cu-Phen}$ system. Then, other tests were conducted on the dye in the absence of fiber, see Chapter V. The purpose of these aqueous trials was to better understand the action of the activated system on the dye.

In this chapter, color-stripping treatments were carried out on a bleached chemical pulp dyed with commercial dyes: either DY11L (containing Direct Yellow 11, see Figure I-23) or DR81L (containing Direct Red 81, Figure I-22). These direct azo dyes were chosen for their resistance to peroxide bleaching and their complementary structures: the chromophore part of DY11 is present in DR81, which is a longer molecule with two azo bonds. The color-stripping trials were performed under conventional and weak alkaline conditions. The former corresponded to typical peroxide bleaching conditions for either virgin or deinked pulp; the latter were tested with the idea of (1) reducing the environmental impact of the bleaching stage by using a lower pH, and (2) assessing the possible activation of H_2O_2 at another step of the deinking line, i.e. during pulping. The performance of these treatments was evaluated in terms of pulp optical properties and mechanical strength, in order to optimize the bleaching conditions and to propose some hypotheses to explain the action of the activated system on dyed fiber suspensions.

The first part of this chapter will present a preliminary study on a DY11L-colored pulp, leading to the choice of some optimal bleaching conditions. Then, the color-stripping of a DR81L-colored pulp will be analyzed, as well as its impact on the pulp's strength properties.

IV.2 PRELIMINARY STUDY ON A DY11L-COLORED PULP

IV.2.1 Introduction

The objectives of this preliminary study were (1) to confirm the results presented by Marlin et al. [1], [2] concerning the activation of hydrogen peroxide (P stage) by a copper-phenanthroline complex for DIP bleaching, and (2), to compare this activation at two pHs. A pulp colored with DY11L was subjected to color-stripping. The specific conditions of these preliminary trials are presented in IV.2.2.

IV.2.2 Experimental

The activator was prepared as described in II.1.2, using the concentrations given in Table IV-1. This corresponds to approximately 3 moles of Phen for 1 mole of CuSO_4 . Similarly, Coucharrière used 2 to 3 moles of Phen for 1 mole of CuSO_4 to catalyze the peroxide delignification of a softwood kraft pulp [3]. The best delignification results were obtained with Phen:Cu = 3:1 (kappa number of 11.6 vs. 24.8 for the initial pulp, and viscosity of 12.0 vs. 22.6 cP), although these results were very close to the 2:1 ratio (kappa number of 11.8 and viscosity of 11.7 cP). At ratios above 3:1, thanks to elemental analysis, Coucharrière observed a stabilization of the amount of Cu in the pulp. Assuming that $\text{Cu}(\text{Phen})_3^{2+}$ was the major species in that case, the author supposed that this species remained in solution, which would explain lower delignification.

Table IV-1. Amounts of CuSO_4 and Phen introduced in the pulp (30 g odp)

Activator	CuSO_4 (μmol)	Phenanthroline (μmol)
Phen	0	140.9
Cu-Phen	44.9	140.9

The color-stripping stages were carried out during 1 h at 80°C , on 30 g odp. The P and activated P stages were prepared with 2% H_2O_2 and either 0.12% or 1% NaOH (weak or conventional alkaline conditions), with or without the addition of Phen or Cu-Phen solutions. Supposing that the complex is $\text{Cu}(\text{Phen})_3$, its molecular weight would be 604.1 g/mol, which allows to calculate a dose by weight of 0.09% on odp. Controls without H_2O_2 were also performed: 0.12% and 1.0% NaOH with or without activator, also during 1 h at 80°C .

IV.2.3 Activating effect of Cu-Phen and Phen

IV.2.3.1 Color-stripping results

The results of the color-stripping trials on the DY11L-dyed pulp are given in Table IV-2. The pulp's characteristics after treatment are reported: $L^*a^*b^*$ values, calculated dye removal index (using the corrected DRI formula given in II.2.3.1), cellulose DP_v , as well as some process data: final pH and H_2O_2 consumption. This Table also presents the properties of the original bleached kraft pulp (BKP), and that of the untreated dyed bleached kraft pulp (dBKP) for comparison.

Table IV-2 Color-stripping results for P and activated P stages, compared with control samples (BKP and dBKP)

Entry	NaOH (%)	Assay	L*	a*	b*	DRI (%)	Final pH	H ₂ O ₂ cons.(%) ^a	DP _v
1	-	BKP ^b	96.7±0.12	0.9±0.05	0.6±0.05	-	-	-	1156
2	-	dBKP ^c	93.4±0.14	1.3±0.09	24.3±0.30	-	-	-	1191
3		-	94.0±0.12	0.8±0.00	20.7±0.22	14.5±0.2	9.5	-	1208
4		Cu-Phen	93.4±0.12	0.4±0.00	19.7±0.22	17.5±0.2	9.0	-	1122
5	0.12	H ₂ O ₂	93.2±0.14	1.8±0.05	20.5±0.05	13.9±0.1	6.2	89	320
6		H ₂ O ₂ +Phen	95.3±0.12	-0.2±0.04	15.9±0.05	34.4±0.1	6.8	92	815
7		H ₂ O ₂ +Cu-Phen	94.0±0.13	0.6±0.00	16.0±0.05	32.1±0.1	4.7	93	289
8		-	92.0±0.11	4.6±0.04	20.2±0.16	12.0±0.2	11.4	-	1145
9		Cu-Phen	90.5±0.02	6.2±0.04	18.0±0.14	15.7±0.1	11.9	-	1040
10	1.0	H ₂ O ₂	94.8±0.11	0.0±0.05	18.8±0.27	22.8±0.3	11.2	100	779
11		H ₂ O ₂ +Phen	95.8±0.11	-0.6±0.04	12.9±0.11	46.1±0.1	11.0	82	728
12		H ₂ O ₂ +Cu-Phen	95.1±0.10	-0.4±0.04	13.9±0.08	41.5±0.1	10.5	100	676

^a H₂O₂ consumption; ^b original bleached kraft pulp; ^c BKP dyed with Direct Yellow 11L

The discussion of these results will first focus on optical properties and cellulose viscosity separately, before commenting the activating effects more generally.

IV.2.3.2 Results on pulp optical properties

With NaOH alone (0.12% and 1%), a slight color-stripping effect was observed (DRIs of 14.5% and 12.0%, respectively). This can be attributed to partial solubilization of the dye in alkaline medium, since the effluent was slightly yellow. Moreover, with 1 % NaOH (pH = 11.4), the a* value of the dyed pulp was 4.6, while that of the untreated dyed pulp was 1.3. At weak alkalinity (0.12 % NaOH, pH = 9.5), the a* value was almost unchanged (a* = 0.8). The high alkalinity (1% NaOH) certainly induced the ionization of the naphthol group of DY11, which led to bathochromic effects, as shown earlier by UV-vis spectroscopic analysis of the dye in aqueous solution (see III.2.1).

Adding Cu-Phen (without peroxide) slightly improved the color-stripping at both pHs (DRI = 17.5% or 15.7% with 0.12% or 1% NaOH, respectively). At weak alkalinity (0.12% NaOH, pH = 9.0), the a* and b* values decreased. Hence, the addition of Cu-Phen contributed to slightly higher dye removal. The results were somewhat different at higher alkalinity (1% NaOH, pH = 11.9): the improved DRI was accompanied by a more pronounced decrease of b* and an important increase of a*, as observed with NaOH alone. Again, this shows that the chromophore structure was affected. The a* value was even higher than with NaOH alone (a* = 6.2 vs. 4.6). This may be explained by two different effects: (1) a higher dye ionization in the presence of Cu-Phen (pH = 11.9 vs. 11.4 without Cu-Phen), (2) the complexation of Cu-Phen with the dye, thus modifying the electronic structure of the chromophore; or both.

Conventional P stage conditions (2% H₂O₂ and 1% NaOH) allowed partial bleaching of the dyed pulp (the DRI reached 22.8%), despite the resistance of the dye chromophores towards H₂O₂. Since the b* value decreased significantly (from 24.3 to 18.8) and the L* value increased (from 93.4 to 94.8), the dye was certainly chemically degraded, possibly due to a slight generation of highly oxidative radical species (hydroxyl and superoxide radicals), which normally occurs during peroxide bleaching.

IV. Dyed pulp color-stripping by activated hydrogen peroxide

Under weak alkaline conditions (0.12% NaOH), P bleaching was not effective (the DRI of 13.9% was similar to that measured without peroxide, i.e. 14.5%). The observed color-stripping was thus mainly due to dye solubilization. Yet, the presence of radicals is not excluded since the cellulose DP_v was strongly affected (discussed later). However, under weak alkaline conditions, these radicals may have been less active towards the dye.

The addition of Cu-Phen or Phen in a conventional alkaline P stage (1% NaOH) strongly improved the DRI (DRIs of 41.5% and 46.1%, respectively). With 0.12% NaOH, the color-stripping was less effective (DRIs of 32.1% with Cu-Phen and 34.4% with Phen). Under both pH conditions, the variation of L^* , a^* and b^* was more pronounced than without activation (H_2O_2 alone) and the drop of b^* was particularly accentuated.

Interestingly, the activation was more effective with Phen alone. This might be explained by the presence of free copper in the dyed pulp (about 3 ppm, i.e. 3% of the 100 ppm of copper introduced when adding Cu-Phen). This small amount (and possibly traces of other metal ions) might be sufficient to form Cu-Phen and activate peroxide, while an excess of Cu-Phen would accelerate peroxide decomposition rather than contribute to color-stripping. This hypothesis should be confirmed by applying H_2O_2 and Phen after removal of the metal ions present in the pulp by chelation (Q stage).

Besides, with 1% NaOH, all the peroxide was consumed in the cases of H_2O_2 alone and H_2O_2 +Cu-Phen. When peroxide was activated by Phen alone, 18% of residual H_2O_2 remained after treatment, which may explain the higher L^* value in that case. Indeed, it is known that bleached kraft pulp contains residual lignin, which, in the absence of residual peroxide, can lead to alkaline darkening. Yet, this possible bleaching effect was rather negligible and color-stripping should be mainly attributed to dye removal.

IV.2.3.3 Results on cellulose viscosity

Bleaching treatments have an impact on the physico-chemical state of the pulp: cellulose is often depolymerized. This degradation was measured via the viscosity-average degree of polymerization (DP_v). As expected, NaOH alone had almost no effect on cellulose DP_v , whereas Cu-Phen alone induced a slight degradation under both weak and conventional alkaline conditions ($DP_v = 1122$ and 1040 respectively, compared to 1191 for the untreated dyed pulp) (Table IV-2). The addition of Cu-Phen thus favored cellulose oxidation, probably caused by the traces of oxygen in the pulp, also catalyzed by Cu-Phen [4]–[8].

The conventional P treatment (1% NaOH) had a detrimental effect on cellulose ($DP_v = 779$). It was probably mainly due to the well-known decomposition of H_2O_2 into hydroxyl radicals and the absence of any cellulose-protecting agent. To evaluate the stability of H_2O_2 at alkaline pH, the conditions of the conventional P treatment were reproduced without pulp nor dye. 23% of residual peroxide were found after 1 h at 80°C , whereas in the presence of dyed pulp, the peroxide consumption was total (Table IV-2). Indeed, both pulp and dye should contribute to the consumption of hydrogen peroxide. Additional trials were carried out in the absence of pulp, with DY11L alone. After 1 h at 80°C , 49% of residual peroxide were found, evidencing that DY11L actually limits the consumption of H_2O_2 .

The dye may protect H_2O_2 from decomposition by coordinating to metal ion traces present as impurities in solution. This hypothesis seems quite probable, considering the results presented in Chapter III (see III.5) on Cu-dye coordination. Since phenanthroline is known to chelate metal ions as well, the same experiment was carried out with phenanthroline alone (without dye) to

determine whether it had the same effect. Indeed, the results showed a similar protecting effect, with even more residual peroxide (59%). Hence, H_2O_2 decomposition was reduced in the presence of dye or phenanthroline.

With pulp, the metal ions present in the medium probably led to more H_2O_2 decomposition than in pure aqueous solution. Moreover, the presence of cellulose fibers may reduce the accessibility of the dye and phenanthroline to these metal ions. Both effects are likely to explain the faster Fenton-like decomposition of H_2O_2 in the presence of fibers.

Under weak alkaline conditions (0.12% NaOH), cellulose was much more degraded by the P stage ($\text{DP}_v = 320$). This result is not surprising as it is well known (see I.1.4.1.iii) that below pH 7 (final pH = 6.2), H_2O_2 is unstable and rapidly decomposes into hydroxyl radicals.

The addition of Cu-Phen or Phen in a conventional alkaline P stage (1% NaOH) slightly increased cellulose depolymerization ($\text{DP}_v = 676$ or 728 , respectively) compared to the P stage without activator ($\text{DP}_v = 779$). Cu-Phen and Phen probably enhanced the generation of free radicals during the P stage, which may be related to the pH decrease in the presence of activators (pH = 10.5 with Cu-Phen and 11.0 with Phen, vs. 11.9 without activator).

Under weak alkaline conditions, the addition of Cu-Phen also slightly accentuated cellulose degradation ($\text{DP}_v = 289$ vs. 320 without activator). Again, the pH dropped in the presence of Cu-Phen (pH = 4.7 vs. 6.2 without activator), which may be responsible for stronger radical generation. Surprisingly, the addition of Phen alone led to a higher final pH (pH = 6.8) and to a higher DP_v ($\text{DP}_v = 815$). However, 0.6 point of pH difference is not enough to explain such a gap. Phenanthroline is a ligand for Fe as well as for Cu. When free, it may sequester some of the iron present in the pulp (around 3 ppm) and thus protect cellulose against Fenton oxidation.

IV.2.3.4 General view

All the results are gathered in Figure IV-1 to illustrate the relationship between DRI and cellulose DP_v variations. This Figure shows that effective color-stripping generally came along with cellulose degradation.

IV. Dyed pulp color-stripping by activated hydrogen peroxide

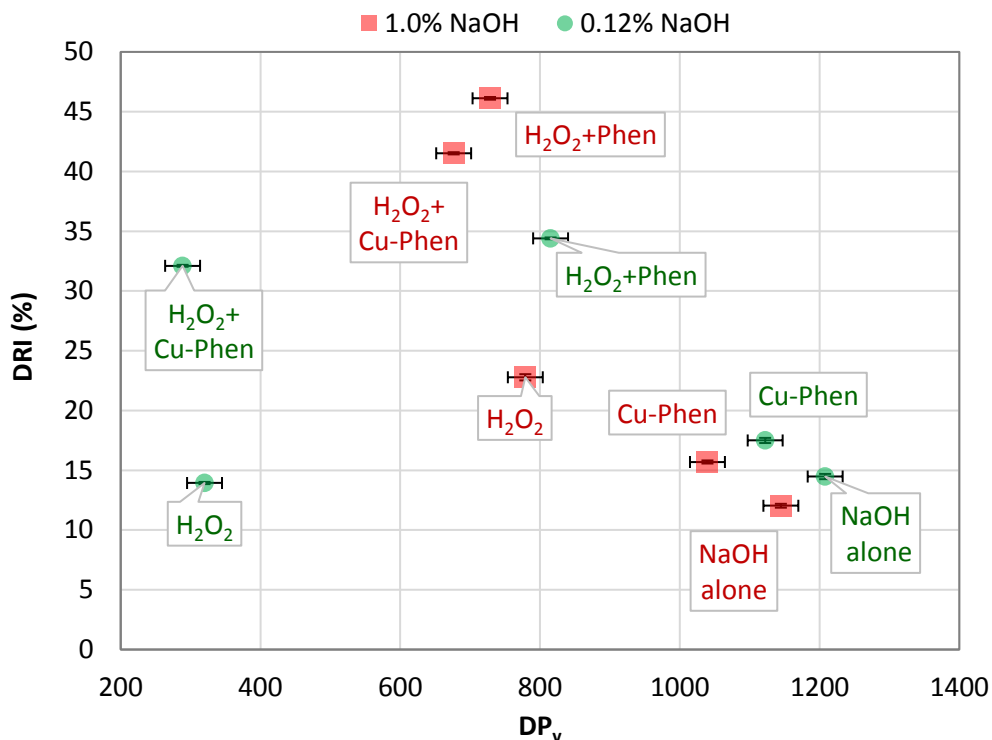


Figure IV-1. DRI vs DP_v after color-stripping of the DY11L-dyed pulp

Peroxide activation by Cu-Phen was different under weak and conventional alkaline conditions (Table IV-2). The mechanism of the H₂O₂/Cu-Phen system was thus pH-dependent. Free radicals produced via the decomposition of H₂O₂ in the presence of the activator are probably responsible for the cellulose degradation observed in all the trials and especially under weak alkaline conditions.

Moreover, the radical route was probably complemented by a chemical action of some particular Cu-Phen species present in the medium. Indeed, the relative abundances of these species are pH-dependent and may explain some of the color-stripping results.

Hence, to go further, the calculation of copper-phenanthroline composition was implemented using the PHREEQC software.

Given the concentrations of the reactants (copper, phenanthroline and sodium hydroxide), PHREEQC allowed the calculation of the equilibrium distributions of free species, soluble complexes and insoluble precipitates in the medium without considering the presence of any dye, fiber or other molecule. Some complementary trials performed in aqueous solution (under the same conditions as on pulp but without fibers) will be presented in Chapter V. No precipitate was observed right after mixing these solutions. Yet, in some cases, precipitates were observed after a certain time at rest. The solid-state species were thus set to zero concentration in the simulations, assuming a retarded precipitation phenomenon.

The relative abundance curves obtained at 25°C under the experimental conditions with Cu-Phen, i.e. [CuSO₄] = 1.66 × 10⁻⁴ M and [Phen] = 5.22 × 10⁻⁴ M, are presented in Figure IV-2.

The concentrations of the possible coordinates are detailed in Table IV-3 as percentage rates compared to the initial copper concentration, for pH 4.7 and 10.5. These correspond to the final pHs of the Cu-Phen-activated P stages.

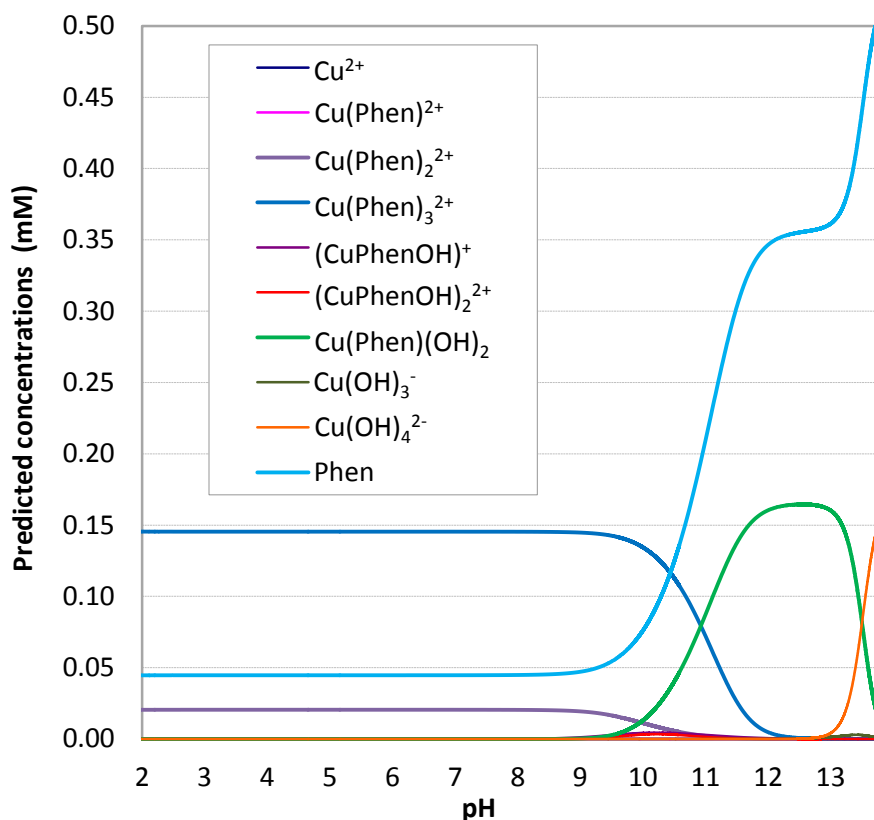


Figure IV-2. Predicted concentrations of the different possible species in a copper-phenanthroline solution, depending on pH, at 25°C. The initial concentrations were $[\text{CuSO}_4] = 1.66 \times 10^{-4} \text{ M}$ and $[\text{Phen}] = 5.22 \times 10^{-4} \text{ M}$

Table IV-3. Predicted distributions of the different possible species at pH 4.7 and 10.5, presented as percentage rates compared to the initial concentration of Cu, when considering no precipitation phenomena

	pH	4.7	10.5
Predicted percentage (%)	Cu^{2+}	ϵ^a	ϵ
	$\text{Cu}(\text{Phen})^{2+}$	ϵ	ϵ
	$\text{Cu}(\text{Phen})_2^{2+}$	12	3.5
	$\text{Cu}(\text{Phen})_3^{2+}$	88	68
	$(\text{CuPhenOH})^+$	ϵ	2.5
	$(\text{CuPhenOH})_2^{2+}$	ϵ	1.8
	$\text{Cu}(\text{Phen})(\text{OH})_2$	ϵ	24
	$\text{Cu}(\text{OH})_3^-$	ϵ	ϵ
	$\text{Cu}(\text{OH})_4^{2-}$	ϵ	ϵ
	Phen	27	75

^a ϵ corresponds to a negligible value (below 0.1%)

At a final pH of 10.5, the predominant copper species were the ionic complex $\text{Cu}(\text{Phen})_3^{2+}$ (68%) and the non-ionic complex $\text{Cu}(\text{Phen})(\text{OH})_2$ (24%). A significant excess of free phenanthroline

IV. Dyed pulp color-stripping by activated hydrogen peroxide

remained in solution. At a final pH of 4.7, the major copper species were $\text{Cu}(\text{Phen})_3^{2+}$ (88%) and $\text{Cu}(\text{Phen})_2^{2+}$ (12%), with a lower excess of phenanthroline.

As the activated P stage was more effective under conventional alkaline conditions (i.e. better DRI and lower DP_v loss), we can assume that in alkaline medium, $\text{Cu}(\text{Phen})(\text{OH})_2$ plays a major role in the mechanism of color-stripping. This hypothesis is in accordance with the conclusions of Korpi and collaborators, who proposed that $\text{Cu}(\text{Phen})(\text{OH})_2$ would be the active species in the catalysis of veratryl alcohol oxidation by oxygen in alkaline medium [5], as detailed in I.3.3 and I.3.4. The authors even proposed a catalytic cycle for veratryl alcohol oxidation by O_2 , initiated by $\text{Cu}(\text{Phen})(\text{OH})_2$ and involving H_2O_2 . A second possibility would be that free Phen (more concentrated at alkaline pH) improves the DRI.

IV.2.3.5 Conclusion

P stage activation by Cu-Phen was quite effective in the color-stripping of the DY11L-dyed pulp. Interestingly, phenanthroline alone also gave good results, even a little better than with Cu-Phen. Moreover, color-stripping was more effective at conventional alkaline pH: the DRIs obtained with 1% NaOH were about 10 points above those with 0.12% NaOH.

However, cellulose depolymerization also occurred during pulp treatment, especially when the final pH was acidic. At both pHs, the drop of DP_v was already significant after a classical P stage and the introduction of the Cu-Phen complex hardly affected it. Therefore, whatever the conditions, color-stripping with H_2O_2 resulted in some cellulose degradation.

The use of the PHREEQC software showed that the relative abundances of these Cu-Phen species were largely pH- and concentration-dependent. From these model calculations and the experimental results obtained on the dyed pulps (color-stripping and DP_v measurements), it can be proposed that (1) the involvement of free radicals may be dominant at acidic pH and that (2) another mechanism appears in alkaline medium, involving $\text{Cu}(\text{Phen})(\text{OH})_2$ as an activating agent. In addition, this mechanism is likely to involve a coordination of the dye with Cu-Phen (see Chapter III). These hypotheses will be further discussed in Chapter V.

To conclude, the addition of Cu-Phen in a conventional P stage using 2% H_2O_2 and 1% NaOH on odp improved dye removal, with a DRI of about 45% vs. 23% without activator. Different behaviors were found depending on pH, and in all cases cellulose was degraded.

Yet, only two pH conditions were tested in the results presented above and the bleaching time and temperature were not changed. Therefore, a design of experiments (DOE) was implemented to explore the optimal conditions for a Cu-Phen-activated P stage applied on the DY11L-dyed kraft pulp.

IV.2.4 Design of experiments: influence of time, temperature, and NaOH dose

The optimization was performed by using a Box-Behnken DOE, as recently used in the optimization of linen ozone bleaching by Perincek [9]. The variables were reaction time, temperature and percentage of alkali (NaOH, %). The design responses were the dye removal index (DRI, %) and cellulose DP_v . Minitab statistical software was used to analyze the results. The levels of each variable (X_1 , X_2 , X_3) are presented in Table IV-4 and the Box-Behnken design is detailed in Table IV-5.

Table IV-4. Levels of the DOE variables

Level	X ₁ : t (min)	X ₂ : T (°C)	X ₃ : NaOH (%)
-1	20	40	0.050
0	40	55	0.525
1	60	70	1.000

The conditions were chosen with the aim of reaching high color-stripping while preserving cellulose. The highest variable levels were thus below or equal to the time, temperature and highest NaOH dose used in the previous study.

Although 1% NaOH gave the best results in the preliminary study, the goal of the project being to reduce the environmental impact of color-stripping, it was decided to optimize the treatment in a wide range and to examine the possibility of near-neutral/acidic treatments as well.

The maximum temperature was set to 70°C as a conventional P stage for DIP bleaching. With the idea of reducing energy consumption, it was decided to explore lower temperatures only. The chosen minimum temperature was 40°C, which corresponds to pulping temperature in a deinking line (see I.2.2.2).

The bleaching time range also represented possible retention times in a bleaching tower (60 min) or in the pulper (20 min).

Table IV-5. Box-Behnken DOE

Trial no.	X ₁ : t	X ₂ : T	X ₃ : NaOH
1	1	0	-1
2	0	0	0
3	0	1	-1
4	0	1	1
5	0	-1	-1
6	0	0	0
7	-1	1	0
8	1	0	1
9	-1	-1	0
10	-1	0	1
11	1	-1	0
12	-1	0	-1
13	0	-1	1
14	0	0	0
15	1	1	0
16	0	0	0
17	0	0	0
18	0	0	0

IV. Dyed pulp color-stripping by activated hydrogen peroxide

The DOE results are presented in Table IV-6, including final pH and H₂O₂ consumption.

Table IV-6. Results of the DOE

Trial no.	t (min)	T (°C)	NaOH (%)	DRI (%)	Final pH	H ₂ O ₂ cons. ^a (%)	DP _v
1	60	55	0.050	14.5±1.5	7.2	77	679
2	40	55	0.525	21.1±1.3	10.5	92	855
3	40	70	0.050	7.0±1.7	6.9	71	616
4	40	70	1.000	19.1±1.4	11.7	98	785
5	40	40	0.050	7.0±1.6	7.3	58	858
6	40	55	0.525	20.4±1.6	10.6	95	776
7	20	70	0.525	21.5±1.4	10.7	92	901
8	60	55	1.000	28.0±1.4	11.4	91	861
9	20	40	0.525	6.9±1.6	10.4	66	956
10	20	55	1.000	11.6±1.6	11.3	83	924
11	60	40	0.525	14.5±1.5	10.4	75	869
12	20	55	0.050	4.7±1.4	7.4	69	968
13	40	40	1.000	15.9±1.5	11.2	70	906
14	40	55	0.525	19.7±1.4	10.8	88	766
15	60	70	0.525	31.4±1.3	10.6	99	744
16	40	55	0.525	14.7±1.4	10.7	90	874
17	40	55	0.525	16.6±1.6	10.8	90	941
18	40	55	0.525	13.6±1.7	10.8	92	838

^a H₂O₂ consumption

The results show that the DRI increased with reaction time (e.g.: trial 12 vs. 1; trial 9 vs. 11). The minimum temperature (40°C) did not allow to exceed 20% DRI. Increasing the temperature to 55 and 70°C improved the DRI, yet the impact of this parameter was rather limited. As seen earlier, increasing the pH improved the DRI (e.g.: trial 3 vs. 4; trial 1 vs. 8). As for the DP_v, it generally decreased when reducing the NaOH dosage to 0.05% (e.g.: trial 3 vs. 4; trial 1 vs. 8).

Therefore, keeping a sufficiently high alkalinity appears to be of primary importance, probably for several reasons: (1) the relation between pH and the generation of hydroxyl radicals, which are likely to be major reacting species, (2) the possible dye extraction by alkali, and (3) the effect of pH on the relative abundances of the different complexes: Cu(Phen)²⁺, Cu(Phen)₂²⁺, Cu(Phen)₃²⁺, Cu(Phen)(OH)₂, etc.

An attempt of optimization was made using the Minitab software. The objective was to reach a maximal DRI with a minimum DP_v target at 800. The predicted optimal conditions were 60 min, 70°C, 0.83% NaOH, resulting in a DRI of 29.3% and a DP_v of 808. This result suggests that the optimal bleaching is not necessarily obtained with the highest NaOH dose. Yet, the five center points (40 min, 55°C, 0.525% NaOH) gave a mean DRI of 17.7% with a standard deviation of 3.2%, i.e. 17.9% variation among the results. Therefore, the DOE as such was not valid since the variance was too high.

Still, the “optimal conditions” predicted by Minitab were applied on the dyed pulp. The treatments were repeated five times to examine their repeatability. The results are presented in Table IV-7.

Table IV-7. Results of the tested optimal conditions on the DY11L-dyed pulp

Trial no.	t (min)	T (°C)	NaOH (%)	H ₂ O ₂ (%)	DRI (%)	Final pH	H ₂ O ₂ cons. ^a (%)	DP _v
19	60	70	0.83	2	17.3±1.4	11.3	99	760
20	60	70	0.83	2	20.1±1.5	11.5	99	827
21	60	70	0.83	2	22.1±1.1	11.3	100	779
22	60	70	0.83	2	24.0±1.2	11.3	100	760
23	60	70	0.83	2	27.5±1.3	11.2	99	788
Mean value					22.2			783
Standard deviation					3.9			28
Variation coefficient (%)					17.4			3.5

^a H₂O₂ consumption

Table IV-7 indicates that the deviation due to trial repeatability was higher than that due to the measurements. For instance, the standard deviation due to measurement was around 1.3% for the DRI (6.0% variation), whereas when comparing the five trials to test their repeatability, the standard deviation reached 3.9% (17.4% variation). Therefore, the experimental results (mean DRI of 22.2%, mean DP_v of 783) can be considered rather close to the predicted results (DRI = 29.3% and DP_v = 808).

An additional trial was performed under the predicted optimal conditions with Phen instead of Cu-Phen. The color-stripping result was close to that obtained with Cu-Phen (DRI of 20.1%); however, the peroxide consumption was noticeably lower (74%) and the DP_v much higher (1013). This is consistent with the results of the preliminary study, which had shown that Phen was almost as effective for color-stripping activation as Cu-Phen, while minimizing cellulose degradation.

To complete the study, the Cu-Phen dosage was varied, with half the dose, twice more and four times more. Considering the variations due to the repeatability of the trials, the results did not show obvious improvement nor negative impact.

Some controls were also performed to examine the possible extraction of the dye by washing (removal by water and possibly some alkaline extraction). The DRI reached 9.0±1.7% after 40 min at 55°C with 1% NaOH, and 10.3±1.5% after 1 h at 70°C with 0.83% NaOH. Consequently, under the predicted optimal conditions, almost half of dye removal (mean DRI of 22.2±3.9%) could be imparted to this washing effect.

In conclusion, although the addition of Cu-Phen improved the color-stripping of the P stage, a DRI below 30% with significant cellulose DP_v degradation remain rather limited results. The DRI values obtained in this DOE were lower than those given by the previous study, probably due to milder operating conditions: in the DOE, the maximum temperature was 70°C vs. 80°C in the preliminary study, and the most severe conditions (1% NaOH, 70°C, 60 min) were not tested.

Therefore, the activated P stage optimization requires some improvement, which will be further discussed in the conclusion of this paragraph.

As discussed above, pH was a key parameter in the P stage. The three NaOH doses applied in the DOE led to final pHs of 7.3±0.2 (0.05% NaOH), 10.6±0.2 (0.525% NaOH) and 11.4±0.2 (1% NaOH). To evaluate the possible influence of some particular Cu-Phen species, Table IV-8 presents the predicted species concentrations at these pHs, as given by PHREEQC.

Table IV-8. Predicted distributions of the different possible species at pH 7.3, 10.6 and 11.4, presented as percentage rates compared to the initial concentration of Cu, when considering no precipitation phenomena

		pH	7.3	10.6	11.4
Predicted percentage (%)	Cu ²⁺		ε ^a	ε	ε
	Cu(Phen) ²⁺		11	ε	ε
	Cu(Phen) ₂ ²⁺		70	2.1	0.1
	Cu(Phen) ₃ ²⁺		14	13	0.9
	(CuPhenOH) ⁺		3.4	6.1	1.3
	(CuPhenOH) ₂ ⁺		1.1	3.6	0.2
	Cu(Phen)(OH) ₂		ε	75	97
	Cu(OH) ₃ ⁻		ε	ε	0.1
	Cu(OH) ₄ ²⁻		ε	ε	ε
	Phen		2.2	72	98

^a ε corresponds to a negligible value (below 0.1%)

According to this simulation, free Phen and Cu(Phen)(OH)₂ were equally predominant in alkaline medium at pH 10.6 and 11.4, while the major species at neutral pH was Cu(Phen)₂²⁺. Again, the reaction mechanisms of the activated P stage were probably different in alkaline and neutral media. Since the color-stripping efficacy was higher under alkaline conditions, Cu(Phen)(OH)₂ and/or Phen might be the activating species. Besides, the presence of Cu(Phen)₂²⁺ under neutral conditions could be unfavorable to peroxide bleaching. As mentioned with the previous simulation, these results are consistent with the calculations of Korpi [5].

To conclude on this part, we attempted to optimize the bleaching of a dyed pulp with the H₂O₂/Cu-Phen system using a DOE. Due to high variance of the design response, no clear optimum was found. The results showed that the DRI could not exceed 30% in the studied domain while preserving the cellulose DP_v (minimum target of 800). The best results were obtained at high temperature, with high NaOH doses and long reaction time. Above all, alkalinity was confirmed to play a major role in color-stripping. It probably favors active Cu-Phen species and contributes to extracting the dye from the fibers. The analysis of the PHREEQC software simulations suggested again that the Cu(Phen)(OH)₂ complex, predominant in alkaline medium, may be the active species in the alkaline H₂O₂/Cu-Phen system. At near-neutral pH, different Cu-Phen species would be present, meaning that another mechanism is probably involved. Hence, it would be interesting to explore higher NaOH doses in order to perform strong alkaline color-stripping treatments and to find whether these could have a higher decolorizing effect.

IV.2.5 Conclusions

The activated P treatments conducted on a DY11L-dyed pulp (yellow dye) using Phen and Cu-Phen did not result in very effective color-stripping (best DRI of 46%). Several parameters were examined in a DOE, i.e. pH, temperature, and treatment time. The results were completed by PHREEQC simulations, which allowed to specify the species that should be present at different pHs. It is likely that acid-base reactions, complexation and free radical generation are gathered to form a complex oxidation mechanism, with some governing parameters such as medium alkalinity. Actually, better results might be found with higher amounts of NaOH. Moreover, the addition of

CuSO₄ alone as an activator was not tested. It would be interesting to measure its effect compared to Cu-Phen and Phen.

The next study (section IV.3) deals with the decolorization of a DR81L-colored pulp (red dye). Among other conditions, higher alkali doses were applied and CuSO₄-activated P treatments were carried out, in addition to Cu-Phen- and Phen-activated treatments.

IV.3 COLOR-STRIPPING OF A DR81L-COLORED PULP

IV.3.1 Introduction

This part proposes to examine the effect of the H₂O₂/Cu-Phen system on another peroxide-resistant azo dye: DR81L. Contrarily to the DY11L dye, whose structure was not fully confirmed (see III.2.4), the structure of DR81L was verified. This will facilitate further mechanistic investigations by analyzing some reaction products, see Chapter V.

The color-stripping trials were first conducted on a DR81L-dyed pulp under weak (0.2% NaOH) and strong (2% NaOH) alkaline conditions. The color-stripping efficacy was evaluated as well as the impact on pulp strength properties.

Preliminary bleaching trials were performed on the white pulp (BKP) in order to examine the possible bleaching effect of traces of residual lignin remaining in the BKP. Similar trials were then applied on the DR81L-dyed pulp. Some of these treatments (the most significant ones) were finally applied on the DY11L-dyed pulp (yellow pulp) for comparison. The conditions applied in this part are presented in IV.3.2.

IV.3.2 Experimental

The color-stripping treatments were carried out for 1 h at 70°C, on 20 g odp, using 2% H₂O₂ and 0.2% or 2% NaOH. These alkali charges were chosen based on the preliminary study. 0.2% NaOH allowed to work closer to pH 9 at the end of the P stage and 2% NaOH was a high dose to reach strong alkaline conditions (pH above 12).

This time, a Cu:Phen molar ratio of 1:2 was chosen. Indeed, some assays on pulp showed that 1:2 and 1:3 did not yield much different results. More, PHREEQC simulations proved that the major species were the same and that the distribution did not vary much from one ratio to another. The concentration of Cu-Phen was set to 0.02% on odp, using the “theoretical molecular weight” of Cu(Phen)₂ to represent Cu-Phen, i.e. 424.0 g/mol.

The activated P treatments were performed by adding either CuSO₄ alone, Phen alone, or Cu-Phen (previously dissolved in water), under the same operating conditions as for P treatments. The corresponding activator concentrations are given in Table IV-9. Controls without H₂O₂ were also performed. Final pH and H₂O₂ consumption were measured.

Table IV-9. Amounts of CuSO₄ and Phen introduced in the pulp (20 g odp)

Activator	CuSO ₄ (μmol)	Phenanthroline (μmol)
Phen	0	18.87
Cu	9.435	0
Cu-Phen	9.435	18.87

The results of the control bleaching trials will be presented first, after what the color-stripping results will be given and discussed.

IV.3.3 White pulp bleaching

As mentioned earlier, two phenomena may occur simultaneously during the color-stripping of a dyed pulp (dBKP): pulp bleaching and dye removal (extraction and/or oxidation). The former was assumed negligible although this was not proven in our previous work. Here, to evaluate the possible bleaching effect, the original uncolored bleached pulp (BKP) was bleached in the absence of dye. The results are gathered in Table IV-10.

Table IV-10. Bleaching results for P, activated P stages and controls performed on the original bleached pulp with 2% or 0.2% NaOH

Entry	NaOH (%)	Assay	L*	a*	b*	ISO Brightness (%)	Final pH	H ₂ O ₂ cons. (%) ^a
1	-	BKP	97.1±0.08	- 0.6±0.01	2.8±0.05	89.2±0.13	/	/
2		-	97.2±0.04	- 0.6±0.01	2.8±0.04	89.3±0.06	11.0	/
3		Phen	97.2±0.06	- 0.6±0.01	2.8±0.03	89.4±0.11	10.7	/
4		Cu-Phen	96.8±0.12	- 0.8±0.01	2.8±0.06	88.5±0.22	11.1	/
5	0.2	H ₂ O ₂	97.5±0.05	- 0.5±0.01	1.6±0.01	91.7±0.11	9.1	77
6		H ₂ O ₂ +Phen	97.4±0.10	- 0.4±0.01	1.3±0.04	91.6±0.19	9.4	48
7		H ₂ O ₂ +Cu-Phen	97.4±0.05	- 0.5±0.01	1.6±0.03	91.3±0.12	7.1	95
8		-	97.1±0.02	- 0.6±0.01	2.7±0.01	89.5±0.10	12.4	/
9		Phen	97.1±0.13	- 0.5±0.01	2.6±0.03	89.6±0.02	11.0	/
10		Cu-Phen	96.5±0.13	- 0.7±0.01	2.7±0.04	89.0±0.13	12.5	/
11	2	H ₂ O ₂	97.4±0.13	- 0.5±0.01	1.7±0.02	91.2±0.07	12.4	80
12		H ₂ O ₂ +Phen	97.6±0.09	- 0.4±0.01	1.3±0.03	91.8±0.19	12.3	75
13		H ₂ O ₂ +Cu-Phen	97.0±0.07	- 0.5±0.01	1.2±0.02	92.0±0.08	12.5	98

^a H₂O₂ consumption

Table IV-10 shows that the L^* value did not vary significantly in the absence of H_2O_2 , except with Cu-Phen, which seemed to impart L^* (96.8 and 96.5 respectively, see entries 4 and 10, compared to 97.1 for the BKP). Meanwhile, the a^* value was also slightly modified (from -0.6 to -0.8 with 0.2% NaOH and to -0.7 with 2% NaOH), i.e. towards a greener shade. This modification of L^* and a^* reveals that Cu-Phen brought some color to the pulp, which may reduce its brightness (see Figure IV-3).

With H_2O_2 , the most significant effect was a reduction of the b^* value corresponding to the yellow shade of the BKP ($b^* = 2.8$). At weak alkaline pH, H_2O_2 +Cu-Phen was as effective as H_2O_2 alone ($b^* = 1.6$ for both) whereas H_2O_2 /Phen led to $b^* = 1.3$. At strong alkaline pH (entries 11 to 13), b^* reached 1.7 with P and down to 1.2 in the best case (H_2O_2 +Cu-Phen). The effect of the H_2O_2 /Cu-Phen system seems to vary depending on pH.

For a better visualization, the brightness results after treatment of the BKP are presented in Figure IV-3. Trials without H_2O_2 (in blue) can be compared to those with H_2O_2 (in red).

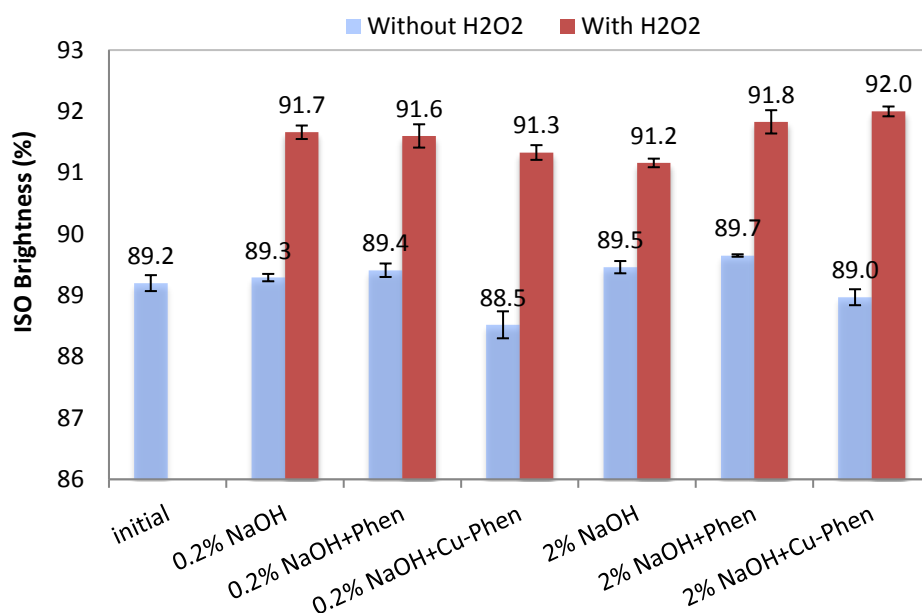


Figure IV-3. ISO brightness after treatment of the BKP

With an initial brightness of 89.2% and controls without H_2O_2 varying between 88.5 and 89.7%, the absence of H_2O_2 did not improve the brightness. Secondly, the addition of Cu-Phen without H_2O_2 slightly reduced the brightness. This negative impact might be due to the blue color of the Cu-Phen complex. However, this is almost negligible since the brightness reduction was below one point.

When adding H_2O_2 , whatever the pH, activators, etc., the brightness rose to reach 91.2 – 92.0%. Therefore, H_2O_2 acted as a bleaching agent. This suggests that the white pulp still contained some residual lignin, which would have been brightened or decolorized by H_2O_2 .

With H_2O_2 , the addition of Phen alone or Cu-Phen slightly improved the brightness under strong alkaline conditions (2% NaOH), whereas no effect was observed at low alkaline pH (0.2% NaOH). Cu-Phen was thus able to activate the action of H_2O_2 on residual lignin under strong alkaline conditions. Moreover, Phen alone was probably partly coordinated to copper traces present in the

pulp, explaining its activation effect as well. Finally, as observed with the b^* value, the H_2O_2 /Cu-Phen system seemed to act differently at low or stronger alkalinity.

The DP_v results presented in Figure IV-4 provide information on cellulose degradation.

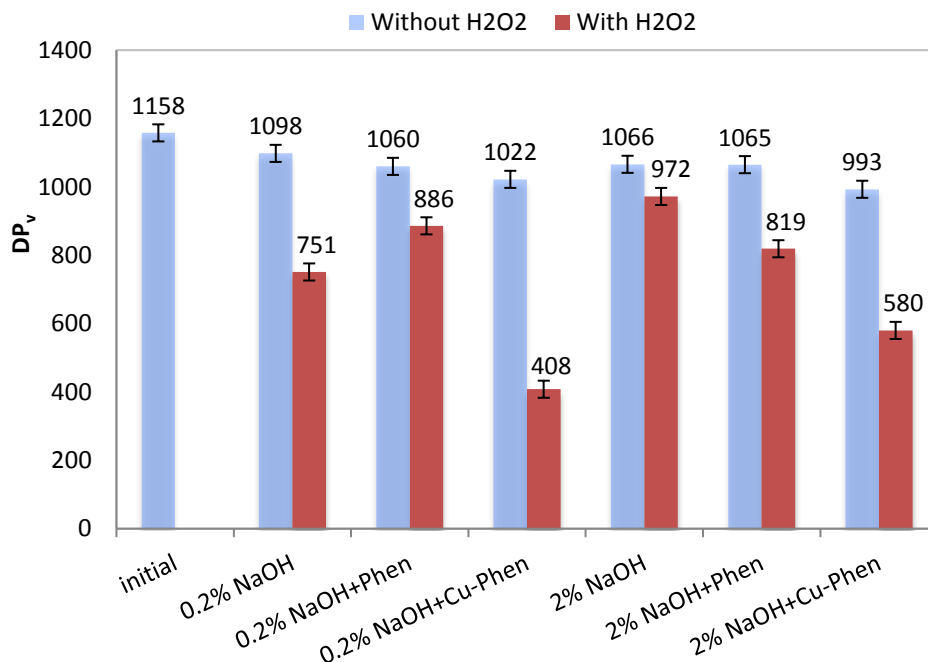


Figure IV-4. Cellulose DP_v after treatment of the BKP

Without H_2O_2 , a minor DP_v decrease was detected, which probably came from the reaction of dissolved oxygen traces with carbohydrates at alkaline pH. Indeed, the addition of Cu-Phen led to slightly stronger degradation compared to NaOH alone and NaOH with Phen. Again, this could be imparted to the simultaneous presence of oxygen and free metal ions in solution, Phen playing the role of a complexing agent.

In the presence of H_2O_2 , an important drop of DP_v was observed. Cellulose was thus oxidized. With the H_2O_2 /Cu-Phen system, the cellulose DP_v was divided by two at alkaline pH and was even lower with low alkali content. Compared to the DP_v s obtained after treatment of the yellow pulp, these were generally higher, which can be related to higher final pHs with both NaOH doses.

To evaluate the paper-making potential of the pulp, two characteristics were tested: the wet zero-span breaking length (BL_0) and the burst index.

The wet zero-span breaking length indicates the intrinsic strength of fibers. The handsheet being saturated with water, no H-bonds should keep the fibers together: the calculated breaking length should only depend on the average tensile strength of the tested fibers. Hence, a reduction in this value indicates that the fibers have been degraded, which can be more or less related to the drop of cellulose DP_v .

Figure IV-5 gives the BL_0 results depending on the bleaching conditions.

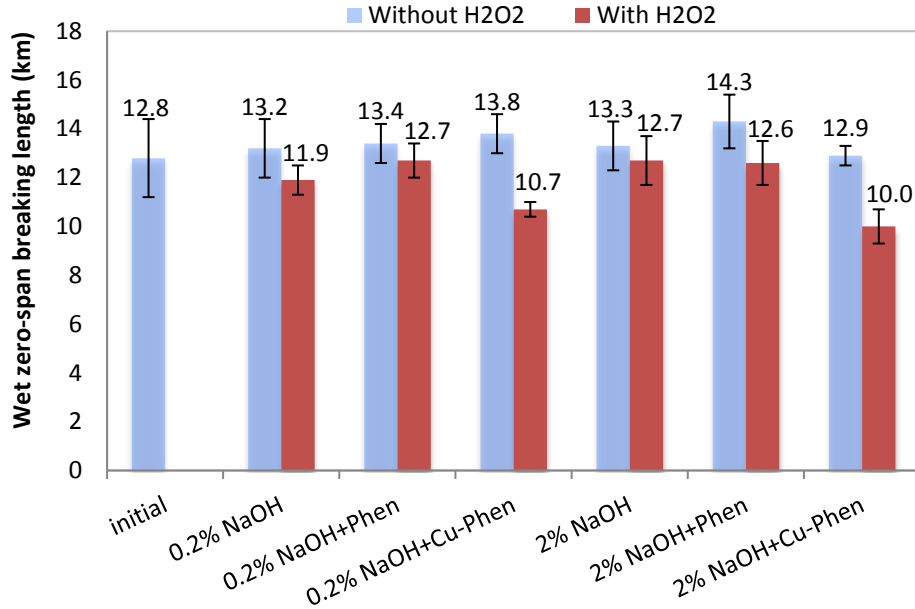


Figure IV-5. Wet zero-span breaking length after treatment of the BKP

The observed variations show a tendency for strength reduction in the presence of H₂O₂. However, these variations were generally not significant since the values were in the range of standard deviations, except for the H₂O₂/Cu-Phen system. In this latter case, the BL₀ values were significantly reduced compared to the initial pulp: around 16% diminution with 0.2% NaOH and 22% with 2% NaOH.

The burst indices presented in Figure IV-6 indicate the strength of the fiber network. The initial index of 1.27±0.06 kPa.m²/g is quite low for a hardwood chemical pulp, probably because the pulp was not refined. The results suggest that the sample's resistance to burst was not affected by the treatments: all the results were either included in the standard deviation of the initial pulp, or even reached higher values.

IV. Dyed pulp color-stripping by activated hydrogen peroxide

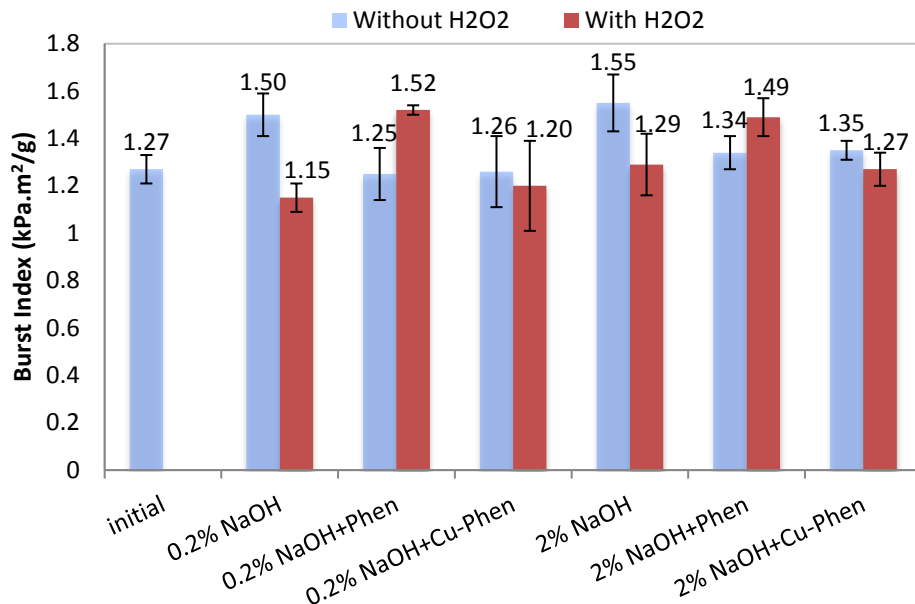


Figure IV-6. Burst index after treatment of the BKP

According to Howard and Bichard [10], the recycling of unbeaten chemical pulp is able to drastically improve the burst index, due to a de-curling effect on the fibers. Our repulping of the treated pulp followed by handsheet manufacture is comparable to the authors' recycling procedure. Hence, if the pulp had not been chemically treated, one could expect the burst index to have increased.

One explanation to the stability of the burst index – and to its rise in some cases – may be that the treatments degraded the fibers, but that the repulping also de-curled them, thus compensating the detrimental effect of the color-stripping treatments on the bursting strength.

Finally, although some degradation occurred at cellulose and fiber scales, these weaknesses did not deteriorate the strength of the fiber network. To extend this conclusion to regular chemical pulps, these characteristics should be tested on refined chemical pulps.

As a summary, this bleaching study showed the effects of the treatments on the original BKP in the absence of dye. It revealed that these treatments are able to bleach the pulp to some extent and that they contribute to cellulose depolymerization, although the final fiber web was not weakened according to burst index evaluation.

After this work, identical treatments were applied on the same BKP after dyeing. The contribution of the bleaching effect observed in this preliminary work will be evaluated by comparison to the intensity of dye removal in the following part.

IV.3.4 Dyed pulp color-stripping

As in the study conducted on the DY11L-dyed pulp, the performance of the activated P stage on the DR81L-dyed pulp was assessed in terms of optical and mechanical fiber properties.

The operating conditions were identical to those used on the white pulp in IV.3.3, except that the H₂O₂/CuSO₄ system was also tested.

The detailed results are presented in Table IV-11. However, for a better comprehension, these results were analyzed first in terms of pulp decolorization, then of cellulose DP_v and finally in terms of fiber and fiber web strength.

Table IV-11. Detailed results of the color-stripping trials performed on the DR81L-dyed pulp

Entry	NaOH (%)	Assay	L*	a*	b*	DRI (%)	Final pH	H ₂ O ₂ cons. (%) ^a	DP _v	BL ₀ (km)	Burst index (kPa.m ² /g)
1	-	BKP	97.1±0.08	-0.6±0.01	2.8±0.05	/	/	/	1158	12.8±0.2	1.27±0.06
2		dBKP ^b	83.4±0.01	22.3±0.03	-1.6±0.01	/	/	/	1118	12.7±0.6	1.06±0.05
3	0	-	85.9±0.02	18.0±0.04	-1.5±0.01	16.8±0.12	/	/	/	12.7±0.6	1.06±0.05
4		-	85.9±0.01	18.4±0.02	-1.8±0.01	16.4±0.08	11.4	/	1132	13.1±0.6	1.14±0.04
5		Phen	86.0±0.01	18.4±0.03	-1.7±0.01	16.5±0.10	11.1	/	1153	12.6±0.3	1.11±0.03
6		CuSO ₄	86.4±0.02	14.7±0.03	-2.4±0.02	27.6±0.14	11.1	/	1130	13.0±0.7	1.00±0.04
7	0.2	Cu-Phen	86.7±0.04	16.3±0.07	-1.8±0.02	24.1±0.22	10.9	/	1083	12.6±0.5	1.13±0.05
8		H ₂ O ₂	89.6±0.03	9.0±0.03	-3.0±0.02	49.3±0.11	9.7	57.8	913	11.5±0.6	1.07±0.06
9		H ₂ O ₂ +Phen	86.6±0.02	16.0±0.02	-2.7±0.01	24.2±0.09	9.7	53.4	938	12.2±1.0	1.10±0.05
10		H ₂ O ₂ +CuSO ₄	90.8±0.02	2.2±0.02	-4.1±0.02	62.8±0.08	8.1	97.4	655	11.1±0.4	1.20±0.03
11		H ₂ O ₂ +Cu-Phen	88.0±0.03	3.5±0.02	-6.2±0.05	49.9±0.13	7.2	92.5	446	10.5±0.6	1.13±0.04
12		-	86.1±0.04	18.2±0.06	-1.6±0.06	17.6±0.21	12.6	/	1164	13.0±0.7	1.18±0.05
13		Phen	86.0±0.02	18.0±0.04	-1.7±0.02	17.6±0.13	12.7	/	1137	13.3±1.0	1.15±0.03
14		CuSO ₄	87.0±0.02	15.8±0.02	-1.5±0.02	26.3±0.16	12.6	/	1092	11.1±0.4	1.07±0.16
15	2	Cu-Phen	86.4±0.02	16.6±0.03	-2.0±0.01	22.5±0.12	12.5	/	1068	13.3±1.0	1.27±0.03
16		H ₂ O ₂	88.0±0.02	14.0±0.04	-2.4±0.02	33.2±0.12	12.3	69.6	1030	12.8±0.5	1.23±0.17
17		H ₂ O ₂ +Phen	87.6±0.02	14.3±0.03	-2.7±0.01	31.3±0.09	12.4	68.3	956	12.3±0.9	1.21±0.06
18		H ₂ O ₂ +CuSO ₄	90.8±0.01	4.1±0.02	-3.2±0.02	61.8±0.05	12.6	94.6	794	11.1±0.4	1.21±0.14
19		H ₂ O ₂ +Cu-Phen	91.4±0.01	3.4±0.01	-3.3±0.02	64.6±0.05	12.5	99.6	657	9.8±0.6	1.33±0.09

^a H₂O₂ consumption; ^b BKP dyed with DR81L

IV.3.4.1 Decolorizing effect

IV.3.4.1.i Color-stripping results

The color-stripping results are presented in Figure IV-7, giving the DRI, and in Figure IV-8, presenting the red shade of the pulp via the a* value.

IV. Dyed pulp color-stripping by activated hydrogen peroxide

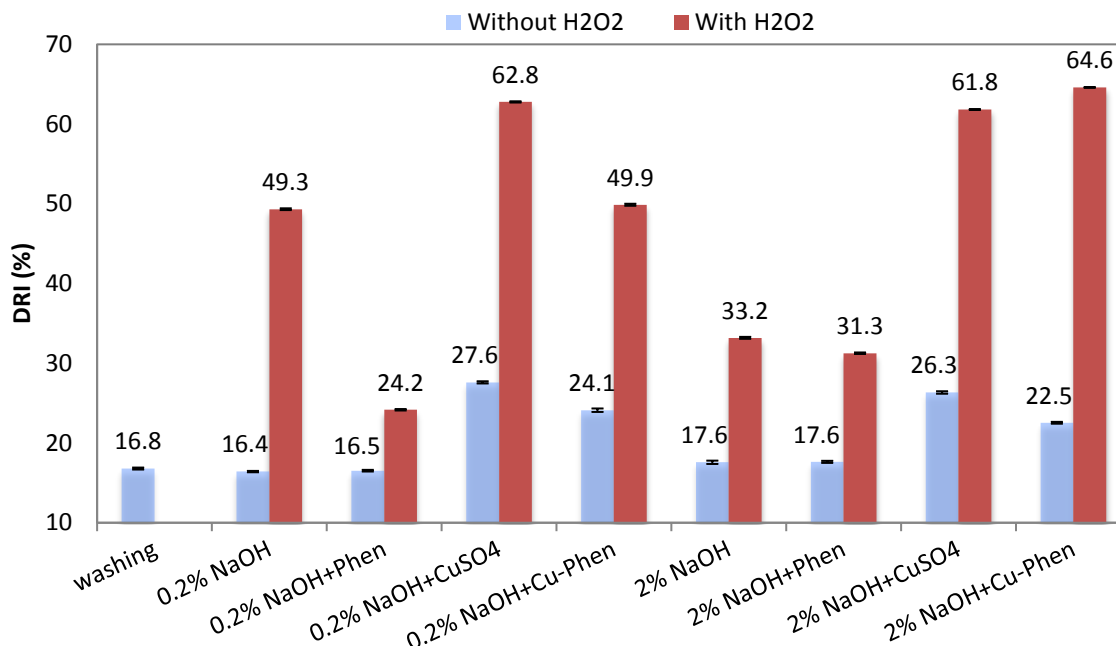


Figure IV-7. DRI after color-stripping of the DR81L-dyed pulp

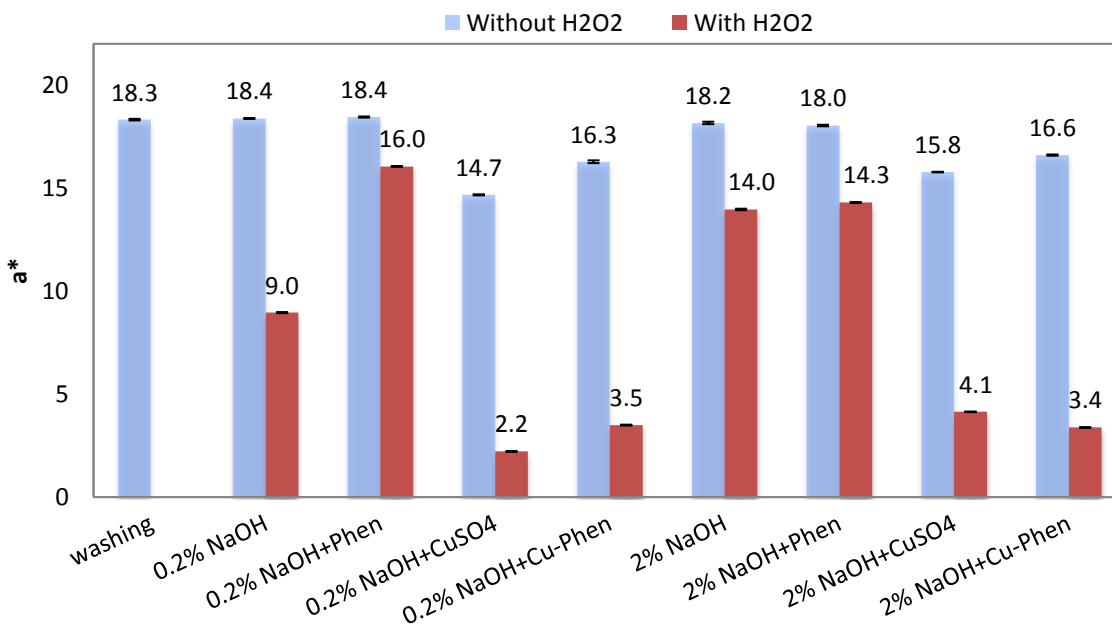


Figure IV-8. a* value after color-stripping of the DR81L-dyed pulp

IV.3.4.1.ii At low alkalinity (0.2% NaOH)

Without peroxide, about 17% of color were removed with or without Phen (Figure IV-7). Moreover, the a* value was not modified (18.4, see Figure IV-8), meaning that the dye was not degraded. This proves that the color removal originated from dye washing,

as shown by the control trial, denoted by “washing”, where the pulp was submitted to a blank bleaching (same conditions as for the other trials, without any chemical).

With CuSO_4 and Cu-Phen, a slight increase of DRI was observed as well as a small decrease of a^* : the dye was partly attacked. Soluble oxygen present in the fiber suspension may contribute to dye degradation after activation by Cu-Phen. A similar effect may occur with CuSO_4 alone. However, the color-stripping remained rather low (DRI = 27.6% and $a^* = 14.7$ with CuSO_4 ; DRI = 24.1% and $a^* = 16.3$ with Cu-Phen).

When peroxide was added, the DRI always increased. H_2O_2 partly removed the red color of the pulp, as confirmed by a^* decrease. High color-stripping was obtained with Cu-Phen: 49.9% DRI and $a^* = 3.5$. The dye was certainly degraded. With Phen, the dye removal was low (24.2%) although some activation occurred. This result is different from that observed on the DY11L-dyed pulp, where H_2O_2 +Phen was as effective as H_2O_2 +Cu-Phen, at both pHs. Yet, Phen is likely to complex the Cu or other metal ions traces originally present in the dyed pulp (approximately 3 ppm of Cu), thus slightly enhancing peroxide decolorization.

Unexpectedly, H_2O_2 alone at low alkali (pH around 9) also partly degraded the dye since the DRI reached 49.3%. This was not observed in the preliminary study on the yellow pulp (the final pH was 6.2). However, the a^* value was higher than that observed with Cu-Phen (9.0 vs 3.5). The H_2O_2 /Cu-Phen system was thus more effective to degrade the dye. Besides, the presence of residual Cu-Phen in the pulp after treatment negatively affected the pulp's color, possibly due to the blue shade of Cu. This was confirmed by the b^* value (see Table IV-11). Consequently, the effect of the H_2O_2 /Cu-Phen system on color-removal may have been under-estimated since Cu-Phen gave a bluish residual color to the pulp.

The H_2O_2 / CuSO_4 treatment was also quite effective, leading to a DRI of 62.8% and an a^* value of 2.2. The absence of Phen seems to promote better brightening, possibly related to the blue color of Cu-Phen solutions as compared to CuSO_4 solutions (not shown). The b^* value decreased in the presence of CuSO_4 only when peroxide was present. This interesting observation is difficult to explain without supplementary information.

IV.3.4.1.iii Under conventional alkaline conditions (2% NaOH)

Again in the absence of H_2O_2 , part of the color was removed by dye solubilization (washing).

As already observed, a slight beneficial effect occurred with Cu-Phen alone. A similar effect was observed with CuSO_4 .

With peroxide, the color-stripping was always improved, particularly with the addition of Cu-Phen, which resulted in 64.6% of color removal. With the addition of Phen only, the color-stripping was a little reduced compared to H_2O_2 alone (DRI = 31.3% and $a^* = 14.3$). Hence, at higher alkalinity, Phen alone was not able to activate H_2O_2 : copper appeared to be required to form the active Cu-Phen complex.

Nevertheless, the H_2O_2 / CuSO_4 system also gave good results with a DRI of 61.8%, which is almost as high as with Cu-Phen. Therefore, color-stripping by the H_2O_2 /Cu-Phen system actually seems to rely on the action of free Cu rather than on that of the Cu-Phen complex. Actually, both free and complexed copper (as $\text{Cu}(\text{Phen})(\text{OH})_2$) may be responsible for the generation of the real active species, which are likely to be free hydroxyl radicals. The nature of the predominating complex formed, in close relation with pH conditions, would play a key role in this radical generation mechanism.

IV.3.4.2 Cellulose degradation

Figure IV-9 presents the cellulose DP_v measured after color-stripping.

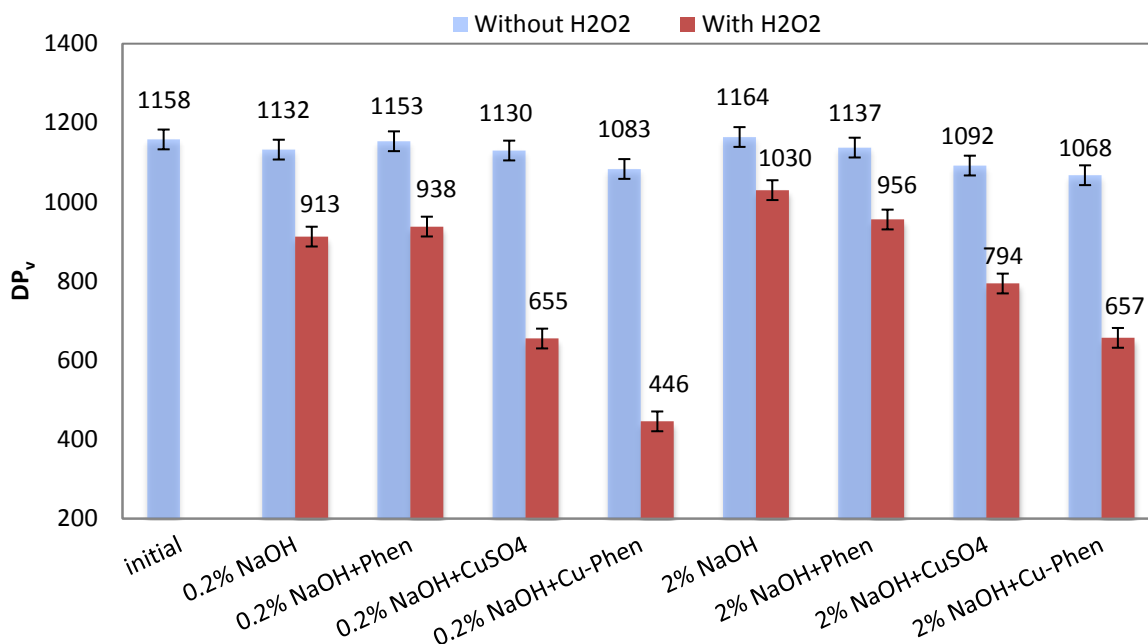


Figure IV-9. Cellulose DP_v after color-stripping of the DR81L-dyed pulp

Without peroxide, whatever the treatment, the cellulose DP_v was logically not affected, except in the presence of Cu-Phen, as already observed on the white pulp.

With peroxide alone, using 0.2 or 2% NaOH, the cellulose DP_v slightly decreased. This well-known degradation is due to partial H_2O_2 decomposition into radicals (mainly $HO\cdot$). Free metal ions and acidic pH catalyze this reaction.

Interestingly, at low NaOH charge, the addition of Phen slightly decreased the aggressiveness of the P stage towards cellulose. The complexation of metal ions by Phen at this pH (final pH of 9.7) probably partially inhibited peroxide decomposition. Indeed, it would lower the amount of free metal ions, and the resulting complexes would not be active, neither directly on cellulose, nor in a free radical generation mechanism.

When $CuSO_4$ or Cu-Phen was added, a significant drop in cellulose DP_v occurred. Cu^{2+} in $CuSO_4$ is less hydroxylated at lower pH, which certainly enhanced cellulose degradation compared to the alkaline case. In the presence of Phen, the contrary was observed, since $Cu(Phen)(OH)_2$ at alkaline pH seemed to enhance peroxide decomposition into free radicals, resulting in stronger cellulose degradation than with $CuSO_4$ alone (in which copper is hydroxylated). At lower pH, Cu-Phen still led to the highest level of cellulose degradation, compared to $CuSO_4$. Even at low alkalinity, the presence of Phen is likely to modify free radical generation induced by copper, here present in large amount. For instance, in a mechanism in which copper would alternate between Cu(I) and Cu(II) while forming hydroxyl radicals (as described by Korpi), the stabilization of Cu in both states varies with the presence of Phen.

Higher oxidation level with $CuSO_4$ or Cu-Phen was accompanied by higher peroxide consumption (above 90% with $CuSO_4$ and Cu-Phen, below 70% for the other trials, see Table IV-11), also evidencing the formation of an intense radical flow in the presence of $CuSO_4$ or Cu-Phen.

Overall, it seems that strong alkaline pH provides the best operating conditions: lower cellulose degradation and better color-stripping. The next part will evaluate whether this cellulose degradation affects the paper-making potential of the fibers, thanks to mechanical characterization of both fiber and fiber network resistance.

IV.3.4.3 Impact of the color-stripping treatments on the mechanical properties of the dyed pulp

The tested mechanical properties were the same as on the white pulp. The wet zero-span tensile strength results are presented in Figure IV-10 as breaking lengths (BL_0).

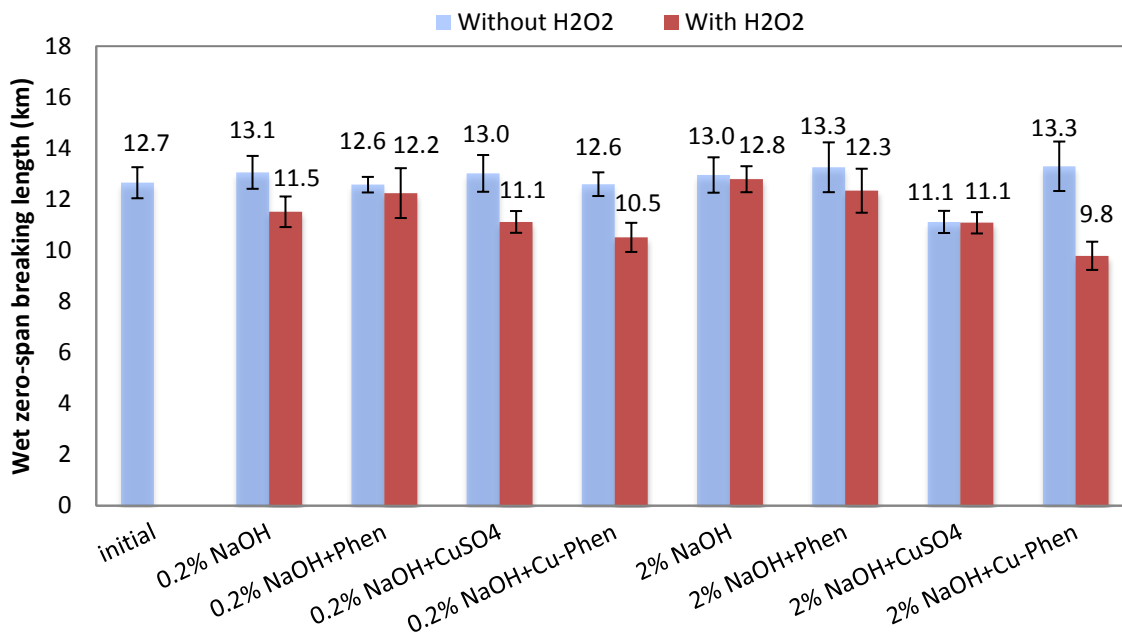


Figure IV-10. Wet zero-span breaking length after color-stripping of the DR81L-dyed pulp

The BL_0 results were very close to those of the white pulp. Logically, the presence of the dye did not influence the fiber strength. Significant variations only occurred in the presence of H_2O_2 , especially in the presence of $CuSO_4$ or $Cu-Phen$. Hence, through the generation of radicals, copper activation directly affected the intrinsic strength of the fibers, although to a rather limited extent. This is consistent with the DP_v results presented earlier. Indeed, when cellulose is strongly depolymerized, the strength of cellulose fibers tends to decrease.

As observed with the white pulp, one interesting fact is that the BL_0 value at 0.2% NaOH with $H_2O_2+Cu-Phen$ was in the same range as at 2% NaOH, although the corresponding DP_v s were significantly different (446 vs. 657). This confirms that cellulose polymerization degree does not have a direct influence on fiber strength. DP_v drops do not seem to strongly affect the wet zero-span breaking length of the pulp, which is favorable to the paper-making ability of our color-stripped pulps.

Contrarily to BL_0 , the burst index (Figure IV-11) did not decrease, taking standard deviations into account. Once again, the repulping and handsheet-making probably acted as a recycling cycle, thus compensating the detrimental action of oxidative treatments via fiber de-curling. Indeed, with 2% NaOH, the $H_2O_2/Cu-Phen$ system even led to the best burst index, above the level of the initial pulp.

IV. Dyed pulp color-stripping by activated hydrogen peroxide

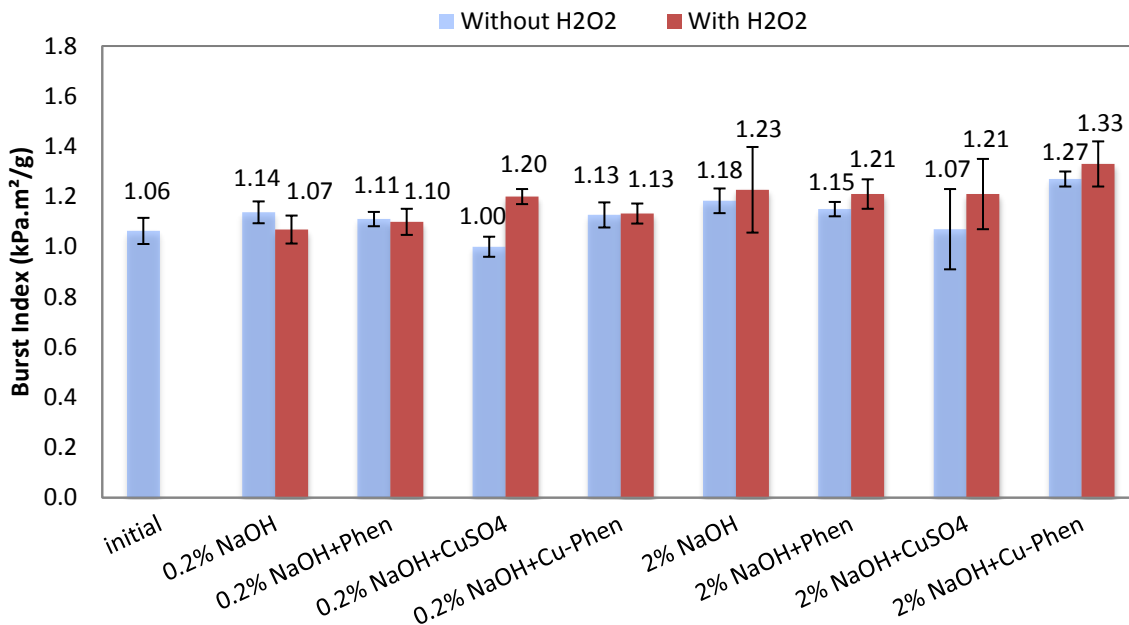


Figure IV-11. Burst index after color-stripping of the DR81L-dyed pulp

IV.3.4.4 Conclusions

The color-stripping of the DR81L-dyed pulp was significantly improved with the activation of H₂O₂ by CuSO₄ or Cu-Phen. The best results were obtained with H₂O₂/Cu-Phen at strong alkaline pH and with H₂O₂/CuSO₄ under both low and strong alkaline conditions. The treatments degraded cellulose and slightly reduced the intrinsic strength of the fibers. Yet, they did not influence the overall strength of the fiber network, which is very promising.

In the next paragraph, the color-stripping of the DR81L-dyed pulp will be compared to that of the DY11L-dyed pulp under the same conditions.

IV.3.5 Comparison with the color-stripping of a DY11L-dyed pulp

A comparison between the red pulp and the yellow pulp in terms of reactivity towards activated hydrogen peroxide will be presented in this part. Supplementary trials were necessary since the operating conditions applied on the red pulp in IV.3.4 were different from those used in the preliminary study on the yellow pulp (IV.2).

The DY11L-dyed pulp was prepared as detailed in II.1.4. The color-stripping trials were performed under the conditions described in IV.3.2, with 2% NaOH and CuSO₄ or Cu-Phen as peroxide activators, as these cases gave rise to the most interesting results on the DR81L-dyed pulp. The experimental results are presented in Table IV-12.

Table IV-12. Results of some key color-stripping treatments performed on the DY11L-dyed pulp compared to the same treatments on the DR81L-dyed pulp, with 2% NaOH

Assay	DY11L					DR81L				
	DRI (%)	b*	Final pH	H ₂ O ₂ cons. (%) ^a	DP _v	DRI (%)	a*	Final pH	H ₂ O ₂ cons. (%) ^a	DP _v
dBKP	/	24	/	/	1191	/	22	/	/	1158
H ₂ O ₂	39.5±0.16	12.1±0.03	12.3	67.5	945	33.2±0.12	14.0±0.04	12.3	69.6	1030
H ₂ O ₂ +CuSO ₄	38.7±0.15	12.2±0.02	12.3	99.4	720	61.8±0.05	4.1±0.02	12.6	94.6	794
H ₂ O ₂ +Cu-Phen	46.0±0.15	10.6±0.02	12.6	99.4	551	64.6±0.05	3.4±0.01	12.5	99.6	657

^a H₂O₂ consumption

The activated P stages applied on the yellow pulp induced little improvement in terms of color-stripping (see DRIs and b* values in the table), with only 46.0% DRI after the most effective treatment, i.e. H₂O₂+Cu-Phen, as compared to 64.6% on the “red pulp”. On both pulps, the dye removal was stronger (DRI increase and b* or a* decrease) using Cu-Phen, but it came along with stronger cellulose depolymerization. If this double oxidation (on cellulose and dyes) results from hydroxyl radicals, it can be assumed that in alkaline medium, Cu-Phen promotes stronger radical generation than CuSO₄.

The final pHs were comparable for both pulps and the peroxide consumptions were also quite similar. Yet, the cellulose DP_v was slightly lower after activated P on the yellow pulp. The color-stripping was less selective on that pulp than on the DR81L-dyed pulp. Indeed, the DP_v after H₂O₂/Cu-Phen treatment was 551 for the yellow pulp, i.e. in the same range as the BKP after the same treatment (580), whereas it was higher in the case of the red pulp (657). This suggests that the presence of the DR81L dye slightly protected cellulose, meaning that it brought some selectivity to the reaction towards cellulose.

IV.3.6 Conclusions

Finally, this part proposed an extensive study on the color-stripping of the DR81L-dyed pulp. The control bleaching trials presented in IV.3.3 evidenced some bleaching effect in the absence of dye and relatively strong resulting cellulose degradation. The fiber strength was also affected but the fiber web resistance was not. Hence, cellulose DP_v drops did not affect the paper-making ability of the pulps.

On the red pulp (IV.3.4) the dye removal was much higher than the bleaching of residual lignin traces in the pulp, which was thus negligible. The color-stripping was improved by both H₂O₂/Cu-Phen and H₂O₂/CuSO₄, and pH effects were noticeable. Overall, the effect of the treatments on cellulose DP_v and fiber strength was quite similar to that obtained on the BKP.

The best conditions for color-stripping using Cu-Phen were generally found at high pHs. However, CuSO₄ alone (without Phen) was also quite effective in terms of decolorization, at both low and high alkalinity. A comparison between DR81L and DY11L (IV.3.5) showed that they did not react the same way: the red pulp was more decolorized than the yellow pulp, with similar or lower cellulose degradation. There could be many reasons for this difference, such as the molecular structure of the dye or its accessibility in the pulp. However, the present investigation does not allow to conclude on this point.

IV.4 CONCLUSION

The Cu-Phen-activated P stage was effective for dyed pulp color-stripping, especially at strong alkaline pH, and the best results were obtained on the DR81L-dyed pulp.

One important result was that CuSO_4 alone was able to activate the action of H_2O_2 on dyed pulp. Adding Phen alone also had an effect, which depended on pH. The most probable assumption is that at low alkalinity, without added copper, Phen complexed some traces of metal ions in the pulp, thus acting as a stabilizer and protecting cellulose from radical oxidation. At higher alkalinity, the Cu(Phen)(OH)_2 complex would be involved, enhancing the generation of radicals, even without copper. When copper is introduced, two different mechanisms would prevail, depending on pH: at low alkalinity, Cu(Phen)(OH)_2 is not predominant and copper alone or a non-hydroxylated copper-phenanthroline complex would be sufficient to promote radical generation; at higher alkalinity, copper alone is more inhibited, but the presence of Cu(Phen)(OH)_2 would enhance radical generation. Overall, as evidenced using PHREEQC, different concentrations and alkalinities lead to various situations for copper species abundances (among which, the presence of free copper ions, the excess of phenanthroline, and the presence of Cu(Phen)(OH)_2) responsible for the generation of free radicals, which would be the actual active species for pulp decolorization.

If the $\text{H}_2\text{O}_2/\text{Cu-Phen}$ or $\text{H}_2\text{O}_2/\text{CuSO}_4$ system was found detrimental for cellulose and for the fiber strength, fortunately no significant impact was found on the fiber web (paper handsheets). Hence, this activated color-stripping treatment would be interesting for recovered paper pulp bleaching, as azo dyes are degraded and the fiber web is preserved. Nevertheless, if our pulps had been refined, the strength of the fiber web might have been deteriorated. Therefore, if adequate pH conditions are chosen, the $\text{H}_2\text{O}_2/\text{CuSO}_4$ system may be preferable, as it tends to induce slightly lower cellulose depolymerization than the $\text{H}_2\text{O}_2/\text{Cu-Phen}$ system, with an equivalent color-stripping effect.

To further understand the activation mechanism, decolorization experiments were conducted in aqueous medium, without fibers. The results were analyzed by UV-visible and ESI-MS, and the generation of radicals was assessed thanks to the EPR/spin-trapping method. This will be the subject of the next chapter (Chapter V).

IV.5 REFERENCES

- [1] N. Marlin, C. Coucharriere, G. Mortha, D. Lachenal, P. Larnicol, and J. C. Hostachy, "Use of o-phenanthroline as a catalyst in hydrogen peroxide stages," in *Proceedings of the 13th International Symposium on Wood Fibre and Pulping Chemistry*, Auckland, New Zealand, 2005, pp. 29–34.
- [2] N. Marlin, J. Fernandes, and N. Benattar, "New ways to improve color-stripping of deinked pulps and dyed effluents," in *Proceedings of the 14th International Symposium on Wood Fibre and Pulping Chemistry*, Durban, South Africa, 2007.
- [3] C. Coucharriere, "Mise au point et étude d'un système d'activation du peroxyde d'hydrogène en délignification et blanchiment des pâtes chimiques," PhD thesis, University of Grenoble, France, 2000.

- [4] H. Korpi, P. Lahtinen, V. Sippola, O. Krause, M. Leskelä, and T. Repo, "An efficient method to investigate metal-ligand combinations for oxygen bleaching," *Applied Catalysis A: General*, vol. 268, no. 1–2, pp. 199–206, Aug. 2004.
- [5] H. Korpi, P. J. Figiel, E. Lankinen, P. Ryan, M. Leskelä, and T. Repo, "On in situ prepared Cu-Phenanthroline complexes in aqueous alkaline solutions and their use in the catalytic oxidation of veratryl alcohol," *European Journal of Inorganic Chemistry*, vol. 2007, no. 17, pp. 2465–2471, Jun. 2007.
- [6] P. Lahtinen, H. Korpi, E. Haavisto, M. Leskelä, and T. Repo, "Parallel screening of homogeneous copper catalysts for the oxidation of benzylic alcohols with molecular oxygen in aqueous solutions," *Journal of Combinatorial Chemistry*, vol. 6, no. 6, pp. 967–973, Nov. 2004.
- [7] H. Korpi, "Copper di-imine complexes: Structures and catalytic activity in the oxidation of alcohols by dioxygen," PhD thesis, University of Helsinki, 2005.
- [8] V. O. Sippola and A. O. I. Krause, "Bis(o-phenanthroline)copper-catalysed oxidation of lignin model compounds for oxygen bleaching of pulp," *Catalysis Today*, vol. 100, no. 3–4, pp. 237–242, Feb. 2005.
- [9] S. Perincek, K. Duran, and A. E. Korlu, "Combination of Ozonation and Hydrogen Peroxide Bleaching for Linen Fabrics: Optimization of the Process Using Experimental Design Technique," *Ozone: Science & Engineering*, vol. 35, no. 4, pp. 316–327, Jul. 2013.
- [10] R. C. Howard and W. Bichard, "The basic effects of recycling on pulp properties," *Journal of Pulp and Paper Science*, vol. 18, no. 4, pp. J151–J159, Jul. 1992.

V. MECHANISTIC STUDY OF THE H₂O₂/CU-PHEN SYSTEM

TABLE OF CONTENTS

LIST OF FIGURES	199
LIST OF TABLES.....	202
LIST OF EQUATIONS.....	203
V.1 INTRODUCTION.....	204
V.2 EXAMINATION OF THE CATALYTIC ROUTE.....	204
<i>V.2.1 Introduction.....</i>	<i>204</i>
<i>V.2.2 Assessment of a possible catalytic cycle.....</i>	<i>205</i>
V.2.2.1 Influence of the cellulosic substrate in the possible reduction of Cu ^{II}	206
V.2.2.1.i Cellulosic fibers	206
V.2.2.1.ii Avicel.....	206
V.2.2.1.iii Soluble cellulose: cellobiose.....	208
V.2.2.1.iv Conclusions	209
V.2.2.2 Influence of dyes on the possible reduction of Cu ^{II}	210
V.2.2.3 Possible reduction of Cu ^{II} in the absence of substrate	211
V.2.2.4 Conclusion.....	212
V.3 EXAMINATION OF DYE DEGRADATION IN AQUEOUS SOLUTION.....	212
<i>V.3.1 Introduction.....</i>	<i>212</i>
<i>V.3.2 UV-vis spectroscopic study.....</i>	<i>214</i>
<i>V.3.3 Analysis of the dye degradation products by ESI-MS.....</i>	<i>217</i>
V.4 INVESTIGATION OF A RADICAL MECHANISM.....	219
<i>V.4.1 Studies using chemiluminescence and UV-vis spectroscopy.....</i>	<i>220</i>
V.4.1.1 Radical detection by chemiluminescence.....	220
V.4.1.2 Radical detection by UV-visible spectroscopy	222
<i>V.4.2 EPR/Spin-trapping</i>	<i>226</i>
V.4.2.1 Experimental	226
V.4.2.2 Results at near-neutral/weak alkaline pH	227
V.4.2.2.i EPR/spin-trapping results and qualitative interpretation.....	227
V.4.2.2.ii Simulation of the EPR/spin-trapping results and semi-quantitative interpretation.....	240
V.4.2.2.iii Conclusions	243
V.4.2.3 Results at alkaline pH.....	244
V.4.2.3.i Results without H ₂ O ₂	244
V.4.2.3.ii Introduction of H ₂ O ₂	247
V.4.2.3.iii Conclusions	249
V.4.2.4 The H ₂ O ₂ /Cu-Phen system with substrate	249
V.4.2.4.i With dyes.....	249
V.4.2.4.ii With cellulosic fibers	251
V.4.2.5 Conclusions	251
V.5 PROPOSITION OF A FENTON-LIKE MECHANISM	252
V.6 REFERENCES	255

LIST OF FIGURES

Figure V-1. Catalytic cycle based on the proposition of Halma et al. (in accordance with the works of Korpi et al. and Coucharrière) for the oxidation of non-phenolic lignin in alkaline medium with hydrogen peroxide and a copper-phenanthroline catalyst [1], [3], [7]	205
Figure V-2. X-band EPR spectra recorded at 100 K in frozen aqueous solutions of Cu-Phen at pH 12.3, with Cu:Phen = 1:2 and [Cu] = 0.15 mM, with and without fibers	206
Figure V-3. X-band EPR spectra recorded at 100 K in frozen aqueous solutions of Cu-Phen at pH 12.3, with Cu:Phen = 1:2 and [Cu] = 1.5 mM, with and without Avicel	207
Figure V-4. X-band EPR spectra recorded at 100 K in frozen aqueous solutions of Cu-Phen at pH 12.3, with Cu:Phen = 1:2 and [Cu] = 1.5 mM, alone, with Avicel and with Avicel and H ₂ O ₂ (Cu:H ₂ O ₂ =1:2 and Avicel in excess)	207
Figure V-5. Structure of cellobiose	208
Figure V-6. X-band EPR spectra recorded at 100 K in frozen aqueous solutions of Cu-Phen at pH 12.3, with Cu:Phen = 1:2 and [Cu] = 1.5 mM, with and without cellobiose (15 mM)	208
Figure V-7. X-band EPR spectra recorded at 100 K in frozen aqueous solutions of Cu-Phen at pH 12.3, with Cu:Phen = 1:2 and [Cu] = 1.5 mM, alone and in the presence of cellobiose and H ₂ O ₂ (Cu:cellobiose:H ₂ O ₂ = 1:1:100).....	209
Figure V-8. X-band EPR spectra recorded at 100 K in frozen aqueous solutions of CuSO ₄ or Cu-Phen, at near-neutral pH and strong alkaline pH, alone, with DR81L, and with DR81L+H ₂ O ₂ , Cu:Phen = 1:2, DR81:Cu:H ₂ O ₂ = 10:1.5:1.5, and [Cu] = 1.5 mM	211
Figure V-9. X-band EPR spectra recorded at 100 K in frozen aqueous solutions of CuSO ₄ at near neutral pH, with and without H ₂ O ₂ , with Cu:H ₂ O ₂ = 1:1, and [Cu] = 1.5 mM	212
Figure V-10. Molecular structure of H-acid.....	214
Figure V-11. UV-vis spectra of the DR81L dye before and after treatment at pH 12.3.....	215
Figure V-12. UV-vis spectra of the DR81S dye before and after treatment at pH 12.3.....	216
Figure V-13. UV-vis spectra of the DY11L dye before and after treatment at pH 12.3	216
Figure V-14. Negative-ion scan ESI mass spectra of alkaline solutions of DR81L alone (a), with H ₂ O ₂ (b), with H ₂ O ₂ and Cu (c), and with H ₂ O ₂ and Cu-Phen (d), after 30 min at 60°C and pH 12.3	218
Figure V-15. Molecular structure of DR81 and possible cleavages	219
Figure V-16. Chemiluminescence signals of different samplings of two heated reactions (80°C): DY11L+H ₂ O ₂ +Cu-Phen and DY11L+H ₂ O ₂ , with 5 mM phthalhydrazide, 65.5 μM DY11L, 61.8 mM H ₂ O ₂ and 63.8 μM Cu-Phen. The values 2 minutes after sampling and immediate chemiluminescence revelation are marked with colored dots.	221
Figure V-17. Typical DMPO-OH signal [38].....	226
Figure V-18. X-band EPR spectrum of DMPO+Phen.....	228
Figure V-19. X-band EPR spectra of DMPO+CuSO ₄ and DMSO+DMPO+CuSO ₄ The simulation revealed the presence of at least three radical species in each case. With DMPO+CuSO ₄ : DMPO-OH,	

$a_N = 15.798$ G, $a_H = 14.928$ G; DMPO-R, $a_N = 15.798$ G, $a_H = 23.237$ G; triplet, $a_N = 14.609$ G; other, $a_N = 16.323$ G, $a_H = 26.653$ G (uncertain). With DMSO+DMPO+CuSO₄: DMPO-OH, $a_N = 14.697$ G, $a_H = 14.015$ G; DMPO-R, $a_N = 15.439$ G, $a_H = 22.586$ G; triplet, $a_N = 14.354$ G Assignments: o=DMPO-OH, |=DMPO-R, +=triplet 228

Figure V-20. Mechanism of nucleophilic addition of water on DMPO in the presence of Cu, leading to the DMPO-OH adduct, as described by Burkitt et al. [45] 229

Figure V-21. X-band EPR spectra of DMPO+Cu-Phen and DMSO+DMPO+Cu-Phen The simulations revealed the presence of three radical species in each case. With DMPO+Cu-Phen: DMPO-OH, $a_N = 15.088$ G, $a_H = 14.943$ G; DMPO-R, $a_N = 15.781$ G, $a_H = 23.27$ G; triplet, $a_N = 14.354$ G. With DMSO+DMPO+Cu-Phen: DMPO-OH, $a_N = 14.697$ G, $a_H = 13.82$ G; DMPO-R, $a_N = 15.488$ G, $a_H = 22.635$ G; triplet, $a_N = 14.305$ G Assignments: o=DMPO-OH, |=DMPO-R, +=triplet..... 230

Figure V-22. X-band EPR spectra of DMPO+Cu-Phen and HCOO⁻+DMPO+Cu-Phen The simulation revealed the presence of four radical species with HCOO⁻+DMPO+Cu-Phen: DMPO-OH, $a_N = 14.843$ G, $a_H = 15.428$ G; DMPO-R, $a_N = 15.644$ G, $a_H = 23.244$ G; triplet, $a_N = 14.593$ G; DMPO-COO⁻, $a_N = 15.683$ G, $a_H = 19.293$ G Assignments: o=DMPO-OH, |=DMPO-R, +=triplet, |=DMPO-COO⁻ 231

Figure V-23. X-band EPR spectra at 100 K of (a) CuSO₄ with and without DMPO (b) Cu-Phen with and without DMPO, [Cu] = 0.15 mM, [DMPO] = 60 mM 231

Figure V-24. X-band EPR spectra of DMPO+Cu-Phen and HCOO⁻+DMPO+Cu-Phen after heating – The simulation revealed the presence of four radical species with HCOO⁻+DMPO+Cu-Phen: DMPO-OH, $a_N = 14.746$ G, $a_H = 15.428$ G; DMPO-R, $a_N = 15.644$ G, $a_H = 23.342$ G; triplet, $a_N = 14.788$ G; DMPO-COO⁻, $a_N = 15.781$ G, $a_H = 19.0$ G Assignments: o=DMPO-OH, |=DMPO-R, +=triplet, |=DMPO-COO⁻ 232

Figure V-25. X-band EPR spectrum of DMPO+H₂O₂ 233

Figure V-26. X-band EPR spectra of DMPO+H₂O₂ at ambient temperature and after heating The simulation revealed the presence of three radical species after heating: DMPO-OH, $a_N = 14.756$ G, $a_H = 15.391$ G; DMPO-R, $a_N = 14.813$ G, $a_H = 21.535$ G; triplet, $a_N = 14.842$ G Assignments: o=DMPO-OH, |=DMPO-R, +=triplet..... 234

Figure V-27. X-band EPR spectra of DMPO+Cu-Phen+H₂O₂ and DMSO+DMPO+Cu-Phen+H₂O₂ - The simulations revealed the presence of three to four radical species. Without DMSO: DMPO-OH, $a_N = 15.0$ G, $a_H = 14.805$ G; DMPO-R, $a_N = 15.781$ G, $a_H = 23.342$ G; triplet, $a_N = 14.549$ G; with DMSO: DMPO-OH, $a_N = 14.7$ G, $a_H = 13.851$ G; DMPO-R, $a_N = 15.7$ G, $a_H = 22.651$ G; triplet, $a_N = 14.349$ G; other, $a_N = 15.786$ G, $a_H = 20.11$ G (minor and uncertain) - Assignments: o=DMPO-OH, |=DMPO-R, +=triplet..... 234

Figure V-28. X-band EPR spectra of DMPO+Cu-Phen+H₂O₂ and HCOO⁻+DMPO+Cu-Phen+H₂O₂ - With HCOO⁻, the simulation revealed the presence of four radical species DMPO-OH, $a_N = 14.902$ G, $a_H = 15.233$ G; DMPO-R, $a_N = 15.64$ G, $a_H = 23.266$ G; triplet, $a_N = 14.593$ G; DMPO-COO⁻, $a_N = 15.749$ G, $a_H = 19.098$ G Assignments: o=DMPO-OH, |=DMPO-R, +=triplet, |=DMPO-COO⁻ 235

Figure V-29. X-band EPR spectra of HCOO⁻+DMPO+Cu-Phen+H₂O₂ at ambient temperature at t=0 and t=10 min and after heating - The simulations revealed the presence of four radical species. At t=10 min: DMPO-OH, $a_N = 15.049$ G, $a_H = 14.976$ G; DMPO-R, $a_N = 15.651$ G, $a_H = 23.872$ G; triplet, $a_N = 14.463$ G; DMPO-COO⁻, $a_N = 15.781$ G, $a_H = 19.098$ G. After heating: DMPO-OH, $a_N = 15.0$ G, $a_H = 14.805$ G; DMPO-R, $a_N = 15.781$ G, $a_H = 23.342$ G; triplet, $a_N = 14.549$ G; other, $a_N = 15.786$ G, $a_H = 20.11$ G (minor and uncertain) - Assignments: o=DMPO-OH, |=DMPO-R, +=triplet..... 234

= 15.074 G; DMPO-R, $a_N = 15.602$ G, $a_H = 23.607$ G; triplet, $a_N = 14.512$ G; DMPO-COO⁻, $a_N = 15.781$ G, $a_H = 19.049$ G Assignments: $|=$ DMPO-COO⁻ 236

Figure V-30. X-band EPR spectra of DMPO+CuSO₄+H₂O₂ and DMSO+DMPO+CuSO₄+H₂O₂ The simulations revealed the presence of three to five radical species. Without DMSO: DMPO-OH, $a_N = 15.244$ G, $a_H = 14.83$ G; DMPO-R, $a_N = 15.70$ G, $a_H = 23.51$ G; triplet, $a_N = 14.598$ G; other, $a_N = 13.975$ G, $a_H = 21.435$ G (minor and uncertain); other, $a_N = 12.195$ G, $a_H = 11.463$ G (3 H, also minor and uncertain). With DMSO: DMPO-OH, $a_N = 14.707$ G, $a_H = 13.951$ G; DMPO-R, $a_N = 15.651$ G, $a_H = 22.658$ G; triplet, $a_N = 14.354$ G Assignments: $o=$ DMPO-OH, $|=$ DMPO-R, $+=$ triplet..... 237

Figure V-31. X-band EPR spectra of DMPO+CuSO₄+H₂O₂ and HCOO⁻+DMPO+CuSO₄+H₂O₂ With HCOO⁻, the simulation revealed the presence of five radical species DMPO-OH, $a_N = 15.269$ G, $a_H = 14.951$ G; DMPO-R, $a_N = 15.749$ G, $a_H = 23.559$ G; DMPO-COO⁻, $a_N = 15.793$ G, $a_H = 18.97$ G; triplet, $a_N = 14.695$ G; other, $a_N = 13.709$ G, $a_H = 7.508$ G (3 H) Assignments: $|=$ DMPO-COO⁻ 238

Figure V-32. Comparison between the X-band EPR spectra of HCOO⁻+DMPO+Cu-Phen+H₂O₂ and HCOO⁻+DMPO+CuSO₄+H₂O₂ - Assignments: $|=$ DMPO-COO⁻ 238

Figure V-33. X-band EPR spectrum of DMPO+Cu-Phen+H₂O₂ at near-neutral pH compared to DMPO+FeSO₄+H₂O₂ at pH 3 (same concentrations of H₂O₂ and [Fe]=[Cu]) With DMPO+FeSO₄+H₂O₂ at pH 3, the simulation revealed the presence of three radical species: DMPO-OH, $a_N = 15.00$ G, $a_H = 14.732$ G; DMPO-R, $a_N = 14.675$ G, $a_H = 21.703$ G; triplet, $a_N = 14.793$ G - Assignments: $o=$ DMPO-OH, $|=$ DMPO-R, $+=$ triplet..... 239

Figure V-34. X-band EPR spectra of DMPO+Fenton and HCOO⁻+DMPO+Fenton Assignments: $o=$ DMPO-OH 240

Figure V-35. Comparison between the experimental and simulated spectra of DMPO+Cu-Phen+H₂O₂ at near-neutral pH..... 241

Figure V-36. X-band EPR spectra of NaOH+DMPO and NaOH+DMPO+Phen Assignments: $+=$ triplet 244

Figure V-37. X-band EPR spectra of NaOH+DMPO+CuSO₄ and NaOH+DMPO+Cu-Phen The simulations revealed the presence of four radical species in both solutions. With CuSO₄: DMPO-OH, $a_N = 15.195$ G, $a_H = 15.294$ G; DMPO-R, $a_N = 15.741$ G, $a_H = 23.488$ G; triplet, $a_N = 14.549$ G; other, $a_H = 17.975$ G (2 H, uncertain). With Cu-Phen: DMPO-OH, $a_N = 15.234$ G, $a_H = 15.623$ G; DMPO-R, $a_N = 15.742$ G, $a_H = 23.83$ G; triplet, $a_N = 14.398$ G; other, $a_N = 14.999$ G, $a_H = 21.246$ G - Assignments: $o=$ DMPO-OH, $|=$ DMPO-R, $+=$ triplet 245

Figure V-38. X-band EPR spectra of NaOH+HCOO⁻+DMPO+Cu-Phen at t=0, t=5 min and t=8 min - The simulations revealed the presence of two radical species: DMPO-R, $a_N = 15.595$ G, $a_H = 22.756$ G; DMPO-COO⁻, $a_N = 15.805$ G, $a_H = 19.00$ G 245

Figure V-39. X-band EPR spectra at 100 K of NaOH+Cu-Phen with and without DMPO - [Cu] = 0.15 mM, [DMPO] = 60 mM 246

Figure V-40. X-band EPR spectra at 100 K of NaOH+CuSO₄ with and without DMPO - [DMPO] = 60 mM 246

Figure V-41. X-band EPR spectra of NaOH+DMPO+Cu-Phen+H₂O₂ and NaOH+DMSO+DMPO+Cu-Phen+H₂O₂ - The simulations revealed the presence of several radical species. Without DMSO: DMPO-OH, $a_N = 15.439$ G, $a_H = 15.049$ G; DMPO-R, $a_N = 15.79$ G, $a_H = 23.488$ G; triplet, $a_N = 14.646$

G. With DMSO: DMPO-OH, a_N = 13.926 G, a_H = 14.072 G; DMPO-CH₃, a_N = 15.937 G, a_H = 22.658 G; triplet, a_N = 14.788 G - Assignments: o=DMPO-OH, |=DMPO-CH₃, +=triplet.....247

Figure V-42. X-band EPR spectra of NaOH+DMPO+Cu-Phen+H₂O₂ and NaOH+HCOO⁻+DMPO+Cu-Phen+H₂O₂ – With HCOO⁻, the simulation revealed the presence of four radical species: DMPO-OH, a_N = 15.342 G, a_H = 15.537 G; DMPO-R, a_N = 15.742 G, a_H = 24.123 G (minor); triplet, a_N = 14.691 G; DMPO-COO⁻, a_N = 15.805 G, a_H = 19.049 G Assignments: o=DMPO-OH, +=triplet, |=DMPO-COO⁻.....248

Figure V-43. X-band EPR spectra of NaOH+DMPO+Cu-Phen+H₂O₂ at t=0 and at t=5 min Assignments: o=DMPO-OH.....248

Figure V-44. X-band EPR spectra of NaOH+DMPO+CuSO₄ and NaOH+DMPO+CuSO₄+H₂O₂249

Figure V-45. X-band EPR spectra of DMPO+Cu-Phen+H₂O₂ with and without the addition of the DR81L dye - Assignments: o=DMPO-OH.....250

Figure V-46. X-band EPR spectra of DMPO+Cu-Phen+H₂O₂ with and without the addition of the DY11L dye - Assignments: o=DMPO-OH.....250

Figure V-47. X-band EPR signal of NaOH+DMPO+Cu-Phen+H₂O₂ with and without cellulosic fibers - Assignments: o=DMPO-OH.....251

Figure V-48. Proposed mechanism for the H₂O₂/Cu-Phen color-stripping system in alkaline medium.....254

Figure V-49. Proposed mechanism for the H₂O₂/Cu-Phen or H₂O₂/CuSO₄ color-stripping system in near-neutral medium255

LIST OF TABLES

Table V-1. Concentrations of the different chemicals used in the UV-vis detection of hydroxyl radicals in the activated H₂O₂ system – DOE conditions223

Table V-2. DMNA decolorization conditions and results in the literature [24]223

Table V-3. First DMNA decolorization in the H₂O₂/Cu-Phen system without alkali – DOE conditions223

Table V-4. DMNA decolorization results at different pHs, for H₂O₂, H₂O₂+Cu-Phen, and H₂O₂+CuSO₄ – DOE conditions224

Table V-5. DMNA decolorization results at different pHs, for H₂O₂+Cu-Phen, with either 1.0×10⁻⁴ or 2.0×10⁻⁴ M DMNA – DOE conditions.....225

Table V-6. EPR hyperfine coupling constants of the observed radical species: experimental and reference values (see Buettner’s spin adduct parameter tables [37]) for comparison.....227

Table V-7. DMPO+Cu-Phen+H₂O₂ – Simulation results.....241

Table V-8. Integration and simulation results: total peak area, and distribution of DMPO adducts and degradation products for some experiments, as relative areas of each radical, in percents.²⁴²

LIST OF EQUATIONS

Equation V-1	204
Equation V-2	252
Equation V-3	252
Equation V-4	252
Equation V-5	252
Equation V-6	252
Equation V-7	252

V.1 INTRODUCTION

To understand the mechanism involved in the color-stripping of the dyed pulps, various analytical techniques were used, and color-stripping trials were performed in aqueous medium with the H₂O₂/Cu-Phen and H₂O₂/CuSO₄ systems.

One of the main explanations found in the literature for the activated action of H₂O₂ in the presence of Cu-Phen is a catalytic mechanism [1]–[3]. Therefore, this chapter starts with the investigation of a possible catalytic route (first hypothesis), which would involve the reduction of Cu^{II} into Cu^I and its reoxidation into Cu^{II} by H₂O₂ (V.2).

The color-stripping experiments in the absence of fibers will be presented in V.3. The degradation of the dye was analyzed to identify some degradation products and attempt to propose a chemical route for decolorization.

The catalytic route being questionable, most of the investigation focused on the second hypothesis, which had been proposed as the major one for H₂O₂/Cu-Phen delignification by Vladut [4] and Das [5], [6], i.e. enhanced H₂O₂ decomposition and radical-induced degradation of dye and cellulose. Therefore, the hypothesis will be assessed in V.4 thanks to radical monitoring techniques.

V.2 EXAMINATION OF THE CATALYTIC ROUTE

V.2.1 Introduction

As mentioned in I.3.4, Korpi and coworkers proposed a catalytic cycle for veratryl alcohol oxidation by oxygen with Cu-Phen under strong alkaline conditions [7], as illustrated in Figure I-33 (first chapter). Korpi's cycle starts with the reduction of Cu^{II}Phen(OH)₂ into Cu^IPhen(OH) by veratryl alcohol, which forms veratraldehyde. Molecular oxygen allows the reoxidation of Cu^I into Cu^{II} while forming H₂O₂.

Two studies attempted to prove that the H₂O₂/Cu-Phen system also involved a catalytic mechanism. In her PhD thesis, Coucharrière examined pulp delignification with H₂O₂ and Cu-Phen under strong alkaline conditions and showed that Cu^{II}-phenanthroline-pulp complexes were formed [1]. The author supposed that these copper complexes were formed via O-bridges on the phenolate extremities of lignin and proposed a catalytic mechanism involving H₂O₂ and these complexes, as presented in Equation V-1.

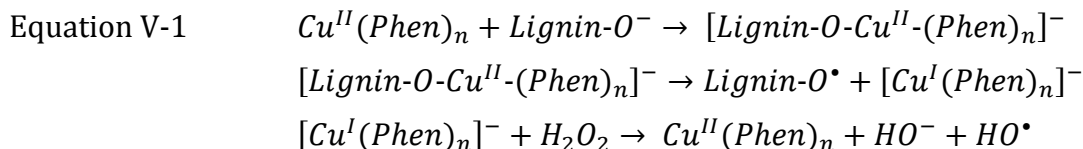


Figure V-1 represents a catalytic cycle that could correspond to Coucharrière's suggestion, as proposed by Halma *et al.* [3].

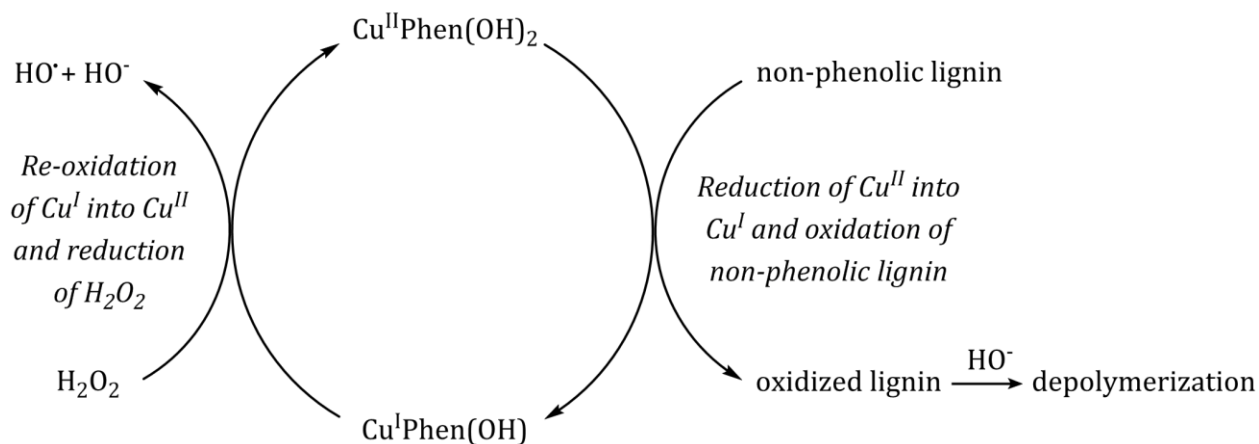


Figure V-1. Catalytic cycle based on the proposition of Halma *et al.* (in accordance with the works of Korpi *et al.* and Coucharrière) for the oxidation of non-phenolic lignin in alkaline medium with hydrogen peroxide and a copper-phenanthroline catalyst [1], [3], [7]

Note that this catalytic cycle involves the production of hydroxyl radicals via a Fenton-like mechanism.

Later, Das and coworkers studied the action of the same system on veratryl alcohol as a non-phenolic lignin model [5], [6]. The authors observed some consumption of veratryl alcohol and the appearance of a small amount of veratraldehyde with the addition of H₂O₂ alone under alkaline conditions, suggesting that radicals that originated from H₂O₂ decomposition were responsible for this oxidation. When adding Cu-Phen, the consumption of veratryl alcohol increased and more veratraldehyde was formed. The authors supposed that veratryl alcohol was oxidized into veratraldehyde via a catalytic cycle similar to that described by Coucharrière. Yet, the part of the cycle with reduction of H₂O₂ and re-oxidation of Cu^I was not investigated, so the catalytic route was not proved. Finally, the hypothesis of a catalytic cycle was not invalidated by Das *et al.*, and they proposed a second possibility: Cu^{II}-Phen would enhance H₂O₂'s decomposition, which would contribute to the oxidation of veratryl alcohol. This second hypothesis was in accordance with the conclusions of Vladut and collaborators [4].

Finally, both studies investigated a catalytic cycle but none of them proved that it was the main route, nor excluded the hypothesis of Vladut *et al.* [4], who proposed that the radical way would be preferred. The possible occurrence of a catalytic cycle will be assessed thanks to EPR spectroscopic analyses in V.2.2, and the radical route will be investigated in V.4.

V.2.2 Assessment of a possible catalytic cycle

In the case of pulp color-stripping, a catalytic cycle similar to that proposed by Coucharrière [1] could be assumed, with cellulose or the dye as a substrate instead of lignin. The substrate would allow the reduction of Cu^{II} into Cu^I and be oxidized, and H₂O₂ would reoxidize Cu^I into Cu^{II} while forming hydroxyl radicals.

If a substrate is able to reduce Cu^{II}, the addition of this substrate to copper-phenanthroline in the absence of hydrogen peroxide should cause the reduction of copper and the disappearance (at least partial) of copper's EPR signal, since Cu^I is diamagnetic and does not give any EPR signal. The first substrate to be tested was cellulose.

V.2.2.1 Influence of the cellulosic substrate in the possible reduction of Cu^{II}

V.2.2.1.i Cellulosic fibers

First of all, Cu-Phen was analyzed in the absence of any substrate under alkaline conditions (pH 12.3-12.5). The addition of a low amount of fully bleached fibers (around 0.3 g/L) at the same pH is illustrated in Figure V-2.

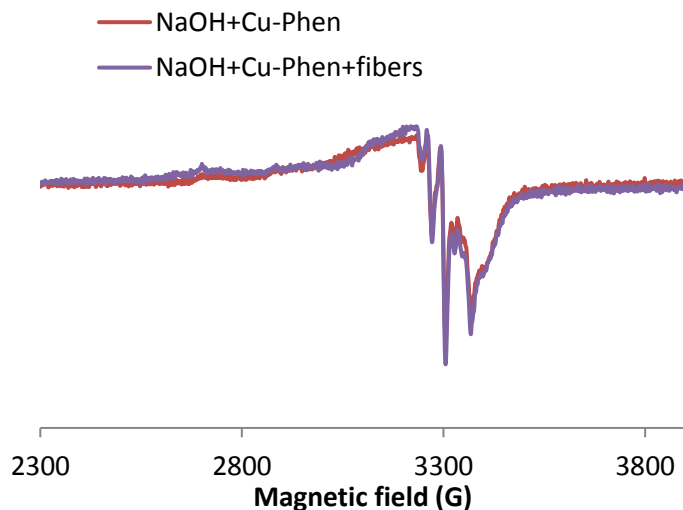


Figure V-2. X-band EPR spectra recorded at 100 K in frozen aqueous solutions of Cu-Phen at pH 12.3, with Cu:Phen = 1:2 and [Cu] = 0.15 mM, with and without fibers

The fibers led to a slightly higher structuration of copper. Yet, no obvious conclusion could be raised. Due to the heterogeneity of the medium with fibers, it was difficult to go further on that study.

Another model for the cellulosic substrate was thus used under similar conditions: the Avicel PH 101 powder from Fluka, which is a microcrystalline cellulose powder.

V.2.2.1.ii Avicel

Microcrystalline cellulose (MCC) is produced by isolating the crystalline regions of cellulose by acid hydrolysis, which hydrolyzes non-crystalline regions preferentially. The physical properties of MCC are better than those of native cellulose, yet its chemical reactivity and swelling are lower [8].

The effect of the addition of Avicel is illustrated in Figure V-3.

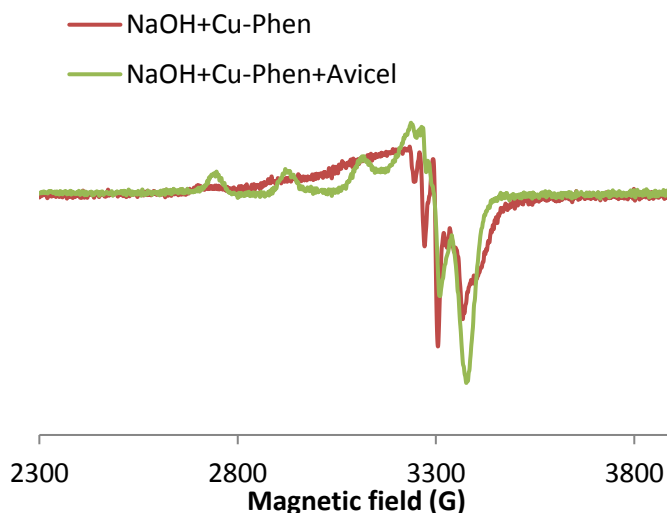


Figure V-3. X-band EPR spectra recorded at 100 K in frozen aqueous solutions of Cu-Phen at pH 12.3, with Cu:Phen = 1:2 and [Cu] = 1.5 mM, with and without Avicel

The EPR signal was drastically modified in the presence of Avicel, more significantly than with fibers (Figure V-2). This difference with the assay with fibers may be due to the homogeneity of the Avicel suspension compared to that of the fiber suspension. The strong structuration of the EPR signal proves that this microcrystalline cellulose powder is able to coordinate with Cu^{II} in Cu-Phen at strong alkaline pH. Besides, the signal exhibited “double peaks”, so it corresponded to a mixture of at least two different complexes with different coupling constants.

When adding H₂O₂ (Cu:H₂O₂ = 1:2) to the same mixture at room temperature (Figure V-4), the signal was identical to that without H₂O₂: no effect of the addition of H₂O₂ was observed.

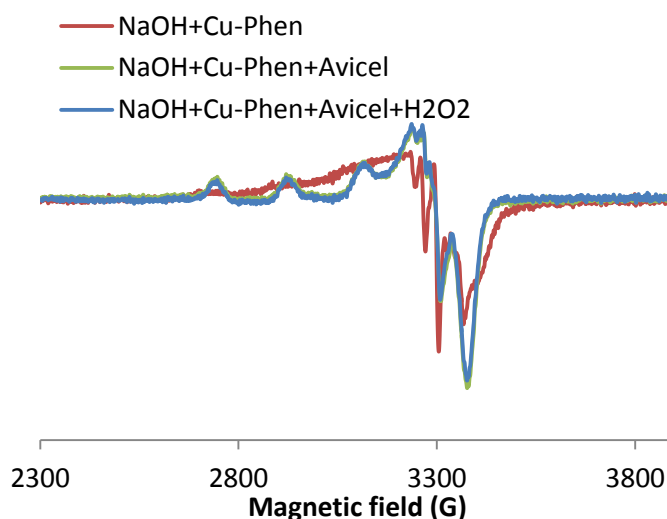


Figure V-4. X-band EPR spectra recorded at 100 K in frozen aqueous solutions of Cu-Phen at pH 12.3, with Cu:Phen = 1:2 and [Cu] = 1.5 mM, alone, with Avicel and with Avicel and H₂O₂ (Cu:H₂O₂=1:2 and Avicel in excess)

V.2.2.1.iii Soluble cellulose: cellobiose

Another trial consisted in adding soluble cellulose in a lower amount, so that it would be equimolar to copper. This way, there would be a sufficient amount of substrate to reduce Cu^{II} but not enough to start a new cycle. H₂O₂ was added to assess whether the supposedly reduced copper could be re-oxidized.

Solid-state cellulose (fibers/Avicel) was thus replaced with a soluble cellulose model species, cellobiose (Figure V-5), which is the (1-4)- β -linked disaccharide of β -D-glucose. Indeed, cellulose can be described as a polymer of cellobiose.

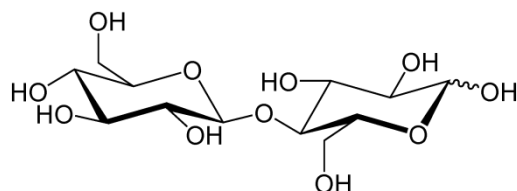


Figure V-5. Structure of cellobiose

First of all, the possible coordination between cellobiose and Cu^{II} was examined with an excess of cellobiose (compared to Cu). The EPR spectra of Cu-Phen with and without cellobiose at alkaline pH are presented in Figure V-6.

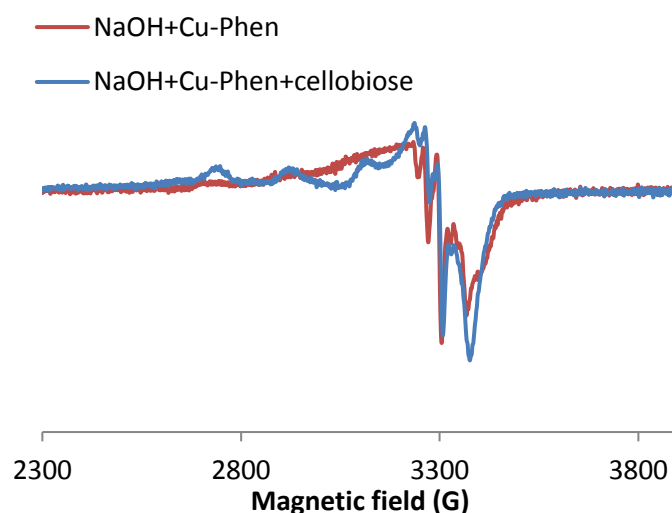


Figure V-6. X-band EPR spectra recorded at 100 K in frozen aqueous solutions of Cu-Phen at pH 12.3, with Cu:Phen = 1:2 and [Cu] = 1.5 mM, with and without cellobiose (15 mM)

An excess quantity of cellobiose led to a drastic modification of the Cu signal (clear hyperfine structure), evidencing strong interaction between Cu^{II} and cellobiose as compared to the interaction observed with fibers. This may be attributed to the homogeneous medium (cellobiose being soluble), which is likely to ensure easier coordination, all the more as cellobiose offers many more coordinating sites for Cu^{II} than cellulose fibers. This coordination seems to be as “effective” as with Avicel, see Figure V-3.

Again, the intensity of the signal did not seem to decrease: the reduction of Cu^{II} was not confirmed.

A second assay was performed by adding hydrogen peroxide, with a cellobiose:Cu ratio of 1:1 (see Figure V-7). As explained earlier, this ratio was chosen to avoid the occurrence of a second cycle in case Cu^{II} would be reduced into Cu^I. Here, the spectrum was again modified although not as much as before. The signal corresponded to a mixture of copper species and no reduction of Cu^{II} seemed to occur.

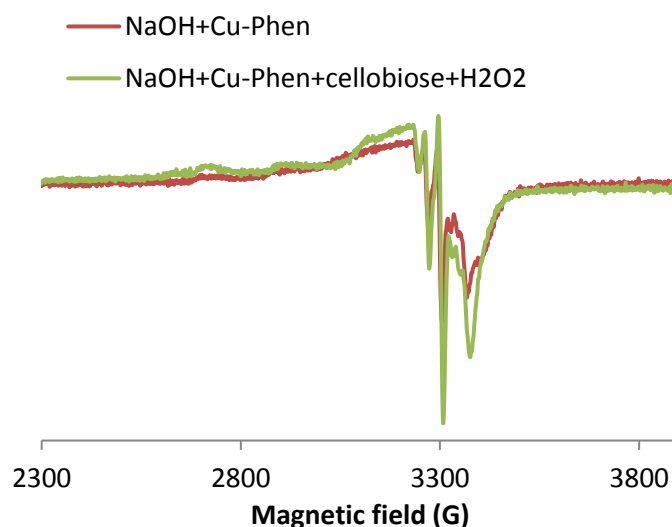


Figure V-7. X-band EPR spectra recorded at 100 K in frozen aqueous solutions of Cu-Phen at pH 12.3, with Cu:Phen = 1:2 and [Cu] = 1.5 mM, alone and in the presence of cellobiose and H₂O₂ (Cu:cellobiose:H₂O₂ = 1:1:100)

The advantage of using Avicel earlier was that it enabled a compromise between fibers and cellobiose monomers. First, cellulose was present as an oligomer (although the DP was lower than in cellulose fibers). In addition, it was possible to prepare a homogeneous suspension (easy to introduce in a quartz EPR cell and more accessible to copper) while the medium was a heterogeneous mixture, therefore closer to reality.

Surprisingly, according to the coupling constants found in the spectra of Figure V-3 and Figure V-7, adding an excess of Avicel to the Cu-Phen solution resulted in the same EPR structure as adding cellobiose. This means that the same Cu complexes were formed with cellobiose and Avicel, which is an interesting result, since cellobiose interacts at a molecular level while the other is in a solid state. Both species are polymers of glucose, but many more terminal units are present in cellobiose. If the complexes were formed on the terminal units, the EPR structures would be different. Therefore, copper was rather coordinated to the cyclic carbons of the anhydroglucose. The C2 and C3 carbons of cellobiose are more probable since C5 is sterically hindered.

V.2.2.1.iv Conclusions

As the signal of Cu^{II} never declined in the presence of cellulosic substrate, the possible reduction of Cu^{II} into Cu^I was not evidenced. Therefore, the supposed catalytic mechanism was not confirmed. However, it cannot be rejected either, since the experimental conditions may have impeded the study. Indeed, due to technical constraints, the trials for EPR analysis could not be performed in an inert atmosphere (nitrogen-degassed solutions but under aerobic conditions). Hence, one explanation for the absence of Cu^I would be that dissolved oxygen in the medium is able to reoxidize Cu^I. Moreover, the trials were performed at room temperature instead of the higher

temperatures used on pulp (40 to 80°C), and followed with slow freezing, which may modify copper's structure and state. Heating the solutions would have been feasible but the much slower freezing afterwards would have enhanced the modification of copper, therefore preventing us from drawing any clear conclusion.

V.2.2.2 Influence of dyes on the possible reduction of Cu^{II}

Another substrate likely to reduce Cu^{II} was the dyes. The Cu/dye system was analyzed by EPR at 100 K, with and without Phen, first in the absence of H₂O₂, and then with the addition of H₂O₂, always at room temperature. The following concentrations were used: NaOH 0 or 0.02 M, DR81L or DY11L 1 mM or 10 mM, CuSO₄ or Cu-Phen 1.5 mM, H₂O₂ 1.5 mM.

The addition of DR81L to Cu-Phen or CuSO₄ was already tested in III.5.3.4.iii. At strong alkaline pH (12.3), Cu-dye coordination was observed and Phen was shown to be replaced by the dye. At near neutral pH, the dye also coordinated to Cu^{II} but some Phen remained in the coordination sphere of Cu^{II}. The intensity of the Cu^{II} signal never varied significantly: Cu^{II} did not seem to be reduced into Cu^I. Here, the addition of H₂O₂ was also tested, and the same trials were actually carried out with the DY11L dye as well, see Annex 1. The main results obtained with DR81L are shown in Figure V-8.

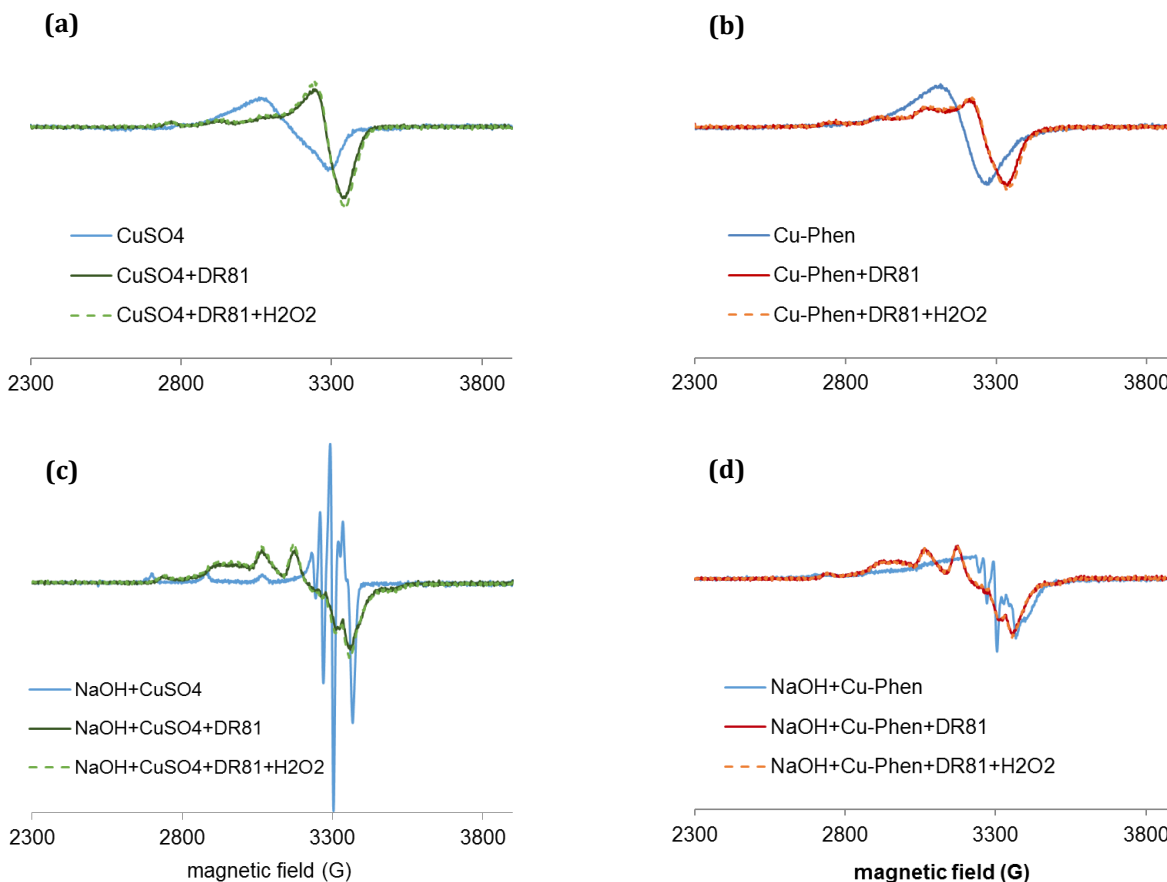


Figure V-8. X-band EPR spectra recorded at 100 K in frozen aqueous solutions of CuSO₄ or Cu-Phen, at near-neutral pH and strong alkaline pH, alone, with DR81L, and with DR81L+H₂O₂, Cu:Phen = 1:2, DR81:Cu:H₂O₂ = 10:1.5:1.5, and [Cu] = 1.5 mM

In the presence of dye, the EPR signal was systematically modified due to coordination. However, the signal never decreased with the addition of H₂O₂: Cu+dye+H₂O₂ gave the same signal as Cu+dye alone (also true with DY11L, see Annex 1). Therefore, Cu^{II} did not seem to be reduced into Cu^I.

V.2.2.3 Possible reduction of Cu^{II} in the absence of substrate

The addition of H₂O₂ to CuSO₄ and Cu-Phen alone was also tested for comparison, at both near-neutral and strong alkaline pH, with Cu:H₂O₂ = 1:1 and [Cu] = 1.5 mM. The spectra were again similar with and without H₂O₂, except in the case of CuSO₄ at near-neutral pH. This only case is thus presented in Figure V-9.

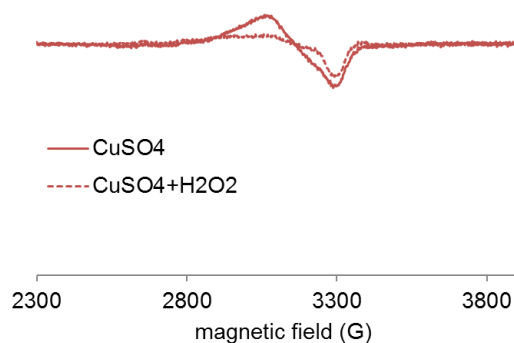


Figure V-9. X-band EPR spectra recorded at 100 K in frozen aqueous solutions of CuSO₄ at near neutral pH, with and without H₂O₂, with Cu:H₂O₂ = 1:1, and [Cu] = 1.5 mM

The signal of Cu^{II} significantly decreased with the addition of H₂O₂. This evidences some reduction into EPR-silent Cu^I. It may be due to the absence of stabilization of Cu^{II} by hydroxyl groups, ligands such as phenanthroline, cellulose or dyes, which would modify the redox potential of copper.

V.2.2.4 Conclusion

In conclusion, comparing both pH conditions, the only case in which Cu reduction was observed was with CuSO₄ and H₂O₂ at near-neutral pH, without any substrate, i.e. when Cu^{II} was not coordinated (neither with hydroxyl groups nor with ligands such as Phen, cellulose or dyes).

With fibers or cellulose model compounds as well as with dyes, the possible reduction of Cu^{II} by the substrate (as a step of a catalytic cycle) was not evidenced, but not rejected either. In their study on the catalytic action of Cu^{II}(Phen)(OH)₂ on the oxidation of veratryl alcohol by oxygen, Korpi and collaborators [7] had the same approach. They observed the EPR spectrum of the complex in the presence of an excess of veratryl alcohol, to validate the hypothesis that the latter was able to reduce Cu^{II}. No reduction was observed under conventional conditions. However, under nitrogen atmosphere, i.e. in the absence of oxygen, Cu^{II} was clearly reduced. In our study, it is likely that oxygen prevented the detection of the cycling by reoxidizing Cu^I into Cu^{II}. Cyclic voltammetry would have been a very interesting method to evidence a redox cycle. Unfortunately, due to time and technical restrictions, this was not tested.

Before any other analysis, aqueous dye solutions were treated with activated hydrogen peroxide using similar conditions as with the DR81L dyed pulp, this time in the absence of fibers. The color-stripping effect was followed by UV-vis spectroscopy before further examination of the involved mechanisms.

V.3 EXAMINATION OF DYE DEGRADATION IN AQUEOUS SOLUTION

V.3.1 Introduction

The color-stripping of dyes in aqueous solution is comparable to paper and textile dye removal during wastewater treatment. Various technologies are currently used and developed for this

purpose: adsorption, membrane technologies, coagulation or flocculation, oxidation, especially advanced oxidation processes (AOPs), etc. [9]

In this context, biotechnologies are widely used, with biosorbents and biocatalysts from fungi, yeast, bacteria, chitosan, algae, peat, etc. [10] In particular, the adsorption method often involves biosorbents, which allow concentrating and removing dyes from solutions. Srinivasan and Viraraghavan wrote a review on different biosorbents that are effective for dye removal [10]. Fungi such as *Aspergillus* 1 were effective on direct yellow dyes, and *Rhizomucor pusillus* or *Rhizopustolonifer* on Direct Red 80, after 24h. Other fungi such as *P. chrysosporium*, applied for 15 days on direct dye solutions, enabled dye removal via a combination of biodegradation and adsorption. Yeast such as *Candida zeylanoides* and *Saccharomyces Cerivisiae* were also effective for adsorption and biodegradation of azo dyes in less than 24 h. The use of bacteria has also been tested. Live bacteria are expensive and mainly act via biodegradation, whereas dead bacteria are good biosorbents. Chitosan, due to its polycationic structure, has a high removal capacity for anionic dyes. Chiou et al. cross-linked chitosan beads to improve their maximum monolayer adsorption capacity, reaching up to 2383 g/kg with Direct Red 81 [11]. Algae have high surface area and high binding affinity, which make them good adsorbents. Depending on cell walls, electrostatic attraction and complexation can occur, so that dyes are efficiently removed. Peat is a partially fossilized plant material formed in areas lacking oxygen. Often pretreated, its high polarity and porosity allow it to adsorb some dyes. According to Srinivasan's review, the most efficient biosorbents are chitosan, fungal biomass, and algal biomass. Even if they are efficient, these treatments are expensive and time consuming. Chemical processes generally require less time. They are described in the next paragraph.

Oxidation by hydrogen peroxide alone was tested on mono-azo dyes such as Acid Orange I and Acid Orange II [12]. In this kinetic and spectroscopic study, the authors found that dye oxidation by hydrogen peroxide proceeded via HOO⁻ ions and hydrazone forms of the dyes (tautomer of the azo structure), and that it was enhanced by ortho-substituents, which had an influence on the dye's pK_a. To improve the degradation of dyes by H₂O₂, a lot of efforts have been put into AOPs. Several studies focused on UV/H₂O₂ for textile wastewater treatment. The kinetics of mono-azo dye degradation was investigated [13] and revealed again the influence of the hydrazone tautomer, as the dye would be slightly more reactive towards hydroxyl radicals when that structure is predominant. Photocatalytic degradation was also investigated. The UV/TiO₂ system was shown to be effective, either with oxygen only or with the addition of H₂O₂ [14]. A UV lamp illuminated the system covered with a catalyst layer made of TiO₂. The flow of wastewater going through the system underwent dye adsorption and degradation by hydroxyl radicals, until complete mineralization into carbon dioxide, water and other non-toxic products. This was tested on different azo and non-azo dyes. Similarly, a UV/Fe₂O₃ system showed good results on Acid Orange II [15]. The iron oxide (hematite) was supported by alumina particles. An aerated aqueous suspension of these particles was mixed with the dye, followed by sintering at 400°C. Thanks to the adsorption of the dye on the catalyst, Acid Orange II was degraded. Instead of UV light, some authors developed solar-driven dye decolorization, with and without catalysis (solar/TiO₂, solar/H₂O₂). This was even applied to photo-Fenton oxidation, with a solar/H₂O₂/Fe²⁺ system. Muruganandham and Swaminathan compared these three solar-driven AOPs for the degradation of an azo dye: Reactive Yellow 14. Solar light was found as effective as UV-light for solar/TiO₂ and solar/Fenton [16]. Fenton's reagent (H₂O₂/Fe²⁺ at pH around 3) has been widely used for wastewater treatment. In 1996, Zhu and coworkers applied it on H-acid wastewater, combined with coagulation [17]. H-acid (see Figure V-10) is a dye intermediate which is responsible for high

COD in the wastewater. This Fenton treatment allowed to oxidize H-acid into inorganic substances (mineralization), thus enhancing its biodegradability.

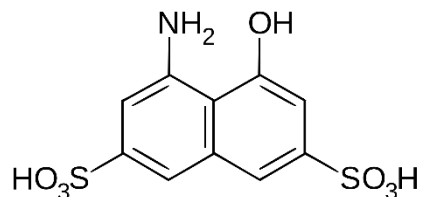


Figure V-10. Molecular structure of H-acid

Later, Swaminathan et al. applied Fenton's reagent on H-acid and other dyes and proposed some optimum parameters: pH 3, hydrogen peroxide 400-500 mg/L, Fe²⁺ 10-25 mg/L, and 120 min contact time, for a dye concentration of 250 mg/L [18]. Another kinetic study compared ferrous hydrogen peroxide to ferric hydrogen peroxide, which is sometimes called "Fenton-like". These were applied on Acid Black 1, a diazo dye, and both were able to degrade it at low temperature and neutral pH, after 100 min treatment. The Fenton system was faster at the beginning but reached maximum degradation at the same time as the "Fenton-like" system. Another AOP is the electro-Fenton system: Fenton's reagent is applied on the dye in aqueous solution in an electrolytic cell with a graphite cathode and an iron anode. Ghosh et al. applied an electro-Fenton treatment on Methylene Blue and Titan Yellow [19]. At pH 3, with 1 mM H₂O₂, 100 mg/L of dye and 4.31 mA/cm² current density, within a reaction time of 60 min, the degradation reached 98 and 96% respectively.

Some attempts were made to replace Fe²⁺ with Cu²⁺, i.e. H₂O₂/Cu²⁺. This system was tested by Cheng et al. on different dyes, and especially Acid Orange II (AOII) [20]. H₂O₂ was catalyzed by Cu²⁺ in the presence of bicarbonate (HCO₃⁻). EPR/spin-trapping revealed the generation of hydroxyl radicals and the degradation products were characterized by ESI-MS. The authors proposed that the azo bond of AOII could get broken, followed with ring opening on the naphthol, and the mechanism may involve the formation of Cu^{III} (e.g. as CuCO₃).

Copper- or copper-phenanthroline-activated H₂O₂ may be comparable to the treatment proposed by Cheng et al. [20], but without bicarbonate. Yet, as shown in Chapter III, the dye can coordinate to copper, leading to precipitation in some cases, which could inspire a physico-chemical process for dye removal.

As mentioned above, the use of Fenton-like systems for direct azo dye degradation has been thoroughly studied. Dye removal was mostly followed by UV-vis spectroscopy and some authors evaluated the effectiveness of their treatments by mass spectrometry. This was the approach of the following study on the color-stripping of Direct Red 81 or Direct Yellow 11 by the H₂O₂/Cu-Phen or H₂O₂/Cu system in aqueous solution.

V.3.2 UV-vis spectroscopic study

To better understand the mechanisms involved in dyed pulp color-stripping, it was necessary to study the activated H₂O₂ system in the absence of fibers.

Aqueous color-stripping trials were performed at weak and strong alkaline pHs on DR81L, DR81S and DY11L. The most significant assays are presented in this part. These correspond to the trials performed at a dye concentration of 0.5 mM, with H₂O₂ 0.2 M, CuSO₄ or Cu-Phen 0.75 mM, 0 or 0.02 M NaOH, during 30 min at 60°C, see II.6.3. These solutions were analyzed by UV-vis spectroscopy

but also by ESI-MS, which is why the dye (and therefore all the chemicals) was more concentrated than in Chapter III. The concentrations were calculated to respect the dye:Cu:H₂O₂ ratios used in the color-stripping trials carried out on the DR81L-dyed pulp and the second batch of DY11L-dyed pulp (see II.1.4 for dye concentration and IV.3.2 for color-stripping conditions). For each dye, the dye solution was treated by H₂O₂ alone and in the presence of Cu-Phen or CuSO₄. Controls without H₂O₂ and Cu-Phen were also performed.

First, the trials in the absence of sodium hydroxide led to precipitation every time Cu (either CuSO₄ or Cu-Phen) was present. The precipitation was more important in the case of CuSO₄ alone, which is consistent with the lower stability and solubility of CuSO₄ in aqueous solution compared to Cu-Phen. The supernatant solutions of H₂O₂+Cu were almost colorless, whereas those with H₂O₂+Cu-Phen were still colored.

Then, the same reactions were conducted at alkaline pH, on the three dyes. Whatever the dye, when Cu was present (either CuSO₄ or Cu-Phen), the addition of H₂O₂ in the medium immediately led to the formation of bubbles, revealing the fast decomposition of H₂O₂ into water and oxygen. In the case of H₂O₂+CuSO₄, the medium became a little turbid.

The DR81L was first tested. The UV-visible spectra obtained after 20-times dilution of the alkaline solutions are presented in Figure V-11.

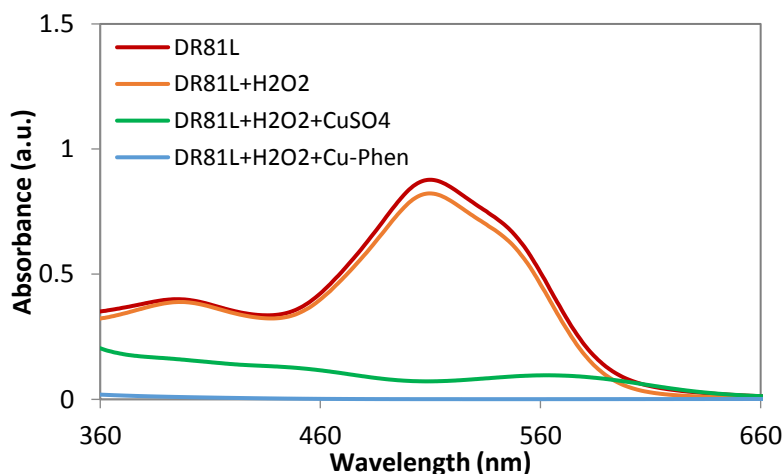


Figure V-11. UV-vis spectra of the DR81L dye before and after treatment at pH 12.3

The dye alone absorbed light at a maximum absorbance wavelength of 515.5 nm. Adding H₂O₂ alone did not modify DR81L's spectrum. This proves that H₂O₂ could not degrade the dye. However, when H₂O₂ was applied in combination with CuSO₄, the intensity of the dye's absorbance at 515.5 nm was reduced by 92%, and with Cu-Phen, the absorbance totally disappeared: both activated systems were thus able to attack the dye in solution, the H₂O₂/Cu-Phen system reaching 100% decolorization.

The same trials were repeated on DR81S. The resulting spectra are given in Figure V-12.

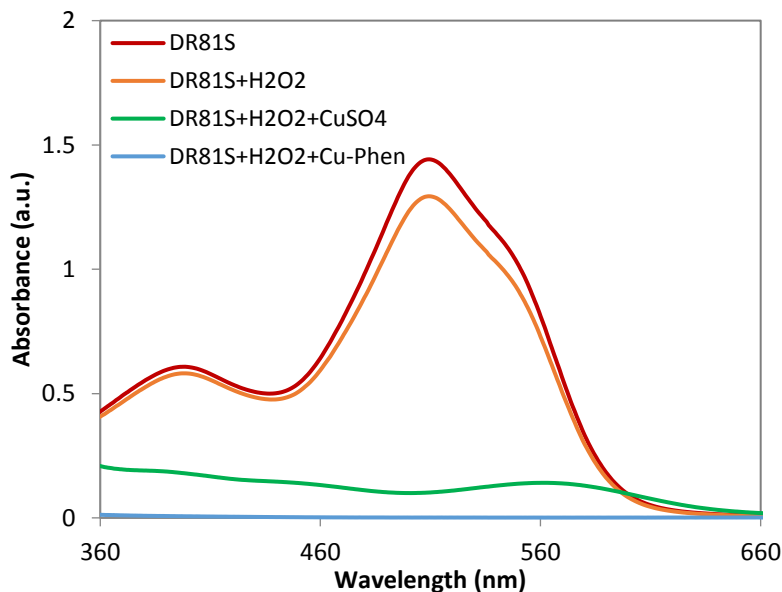


Figure V-12. UV-vis spectra of the DR81S dye before and after treatment at pH 12.3

Figure V-12 displays similar spectra as Figure V-11, but at slightly higher absorbance, since the calculations used to prepare the DR81S and DR81L dye solutions were based on the concentrations given by the suppliers, which were shown earlier not to be perfectly accurate (III.2.1, Figure III.4). The percentages of absorbance decrease observed with DR81S were the same as those with DR81L. This indicates that the additives present in DR81L did not interfere in the color-stripping mechanism, which comforts our previous conclusions and the choice to work with commercial paper dyes in this thesis.

Then, the DY11L dye was also treated by hydrogen peroxide under strong alkaline conditions, with and without activator. The spectra are gathered in Figure V-13.

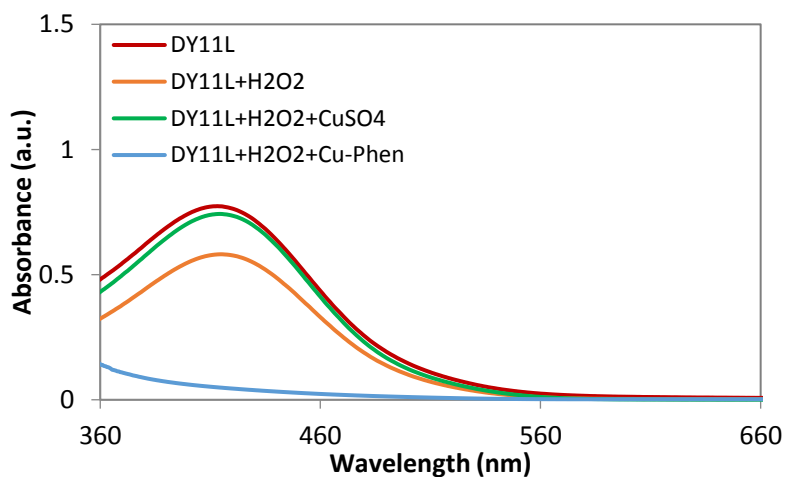


Figure V-13. UV-vis spectra of the DY11L dye before and after treatment at pH 12.3

The DY11L dye alone absorbed light at a maximum absorbance wavelength of 414.5 nm. Adding H₂O₂ alone had little color-stripping effect, with an absorbance decrease of 22% at 414.5 nm. When H₂O₂ was applied in combination with Cu-Phen, the intensity of the dye's absorbance was reduced by 93%.

Here, the addition of H₂O₂ alone was more effective than that of H₂O₂+CuSO₄. Actually, this is in accordance with previous results on pulp. When comparing the effects of these three treatments on the DR81L-dyed pulp and the DY11L-dyed pulp, the addition of CuSO₄ to H₂O₂ resulted in much higher DRI in the case of DR81L (61.8% compared to 33.2%), whereas it led to slightly lower DRI in the case of DY11L (38.7% vs. 39.5%), see Table IV.3.5 in IV.3.5. In the absence of fibers, it seems that CuSO₄ inhibited the action of H₂O₂ on DY11L. One explanation may be that at this high dye and copper concentration, some copper precipitation occurred, thus disturbing the action of H₂O₂ on the dye.

Compared to the trials on pulp, the color-stripping was again more effective with DR81 (L or S), since 100% decolorization was reached with the H₂O₂/Cu-Phen system compared to 93% decolorization on DY11L.

Overall, these experiments proved that the color-stripping of the dyes in aqueous solutions was easier than on pulp. Indeed, up to 100% color removal was obtained, with concentrated dyes treated at only 60°C. This is certainly due to a sort of protection of the dye by cellulose, which acted as a barrier and was also oxidized by the H₂O₂/Cu-Phen system. The selectivity of the system when treating dyed cellulosic fibers was not 100% in favor of dye oxidation, which is why the dye was not totally degraded and cellulose was extensively depolymerized.

Some of the solutions analyzed in this paragraph were further analyzed by ESI-MS in an attempt to observe and identify the degradation products of the dyes.

V.3.3 Analysis of the dye degradation products by ESI-MS

ESI-MS was used to follow the degradation of DR81 (both DR81L and DR81S). The analysis conditions were the same as those applied to characterize the dyes in III.2.4 (see II.2.4.1), but the initial dye concentration was ten times higher (0.5 mM vs. 50 μM). DY11L was not analyzed by ESI-MS after color-stripping since its structure had not been elucidated in Chapter III.

Figure V-14 gathers the mass spectra of DR81L alone and after alkaline treatment with hydrogen peroxide, with and without activation.

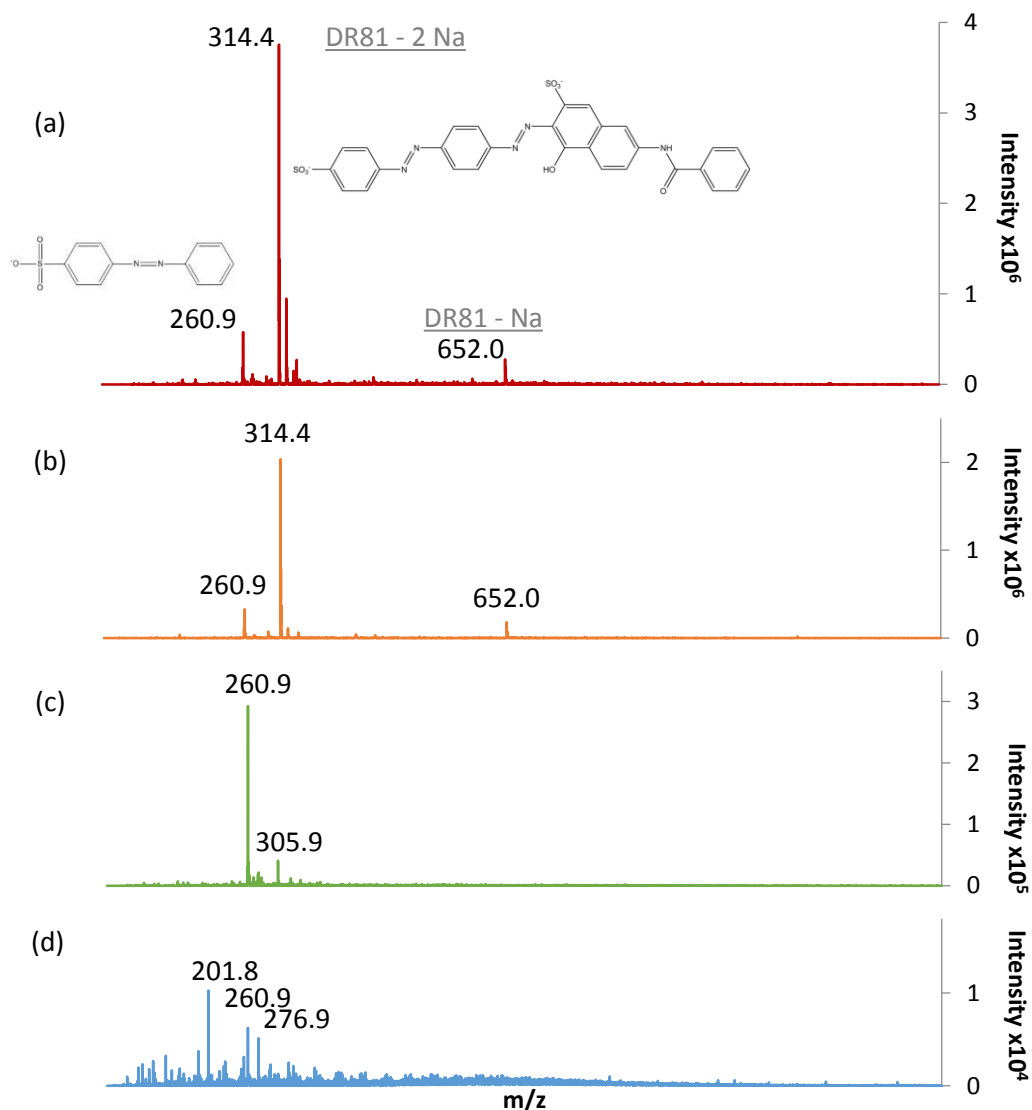


Figure V-14. Negative-ion scan ESI mass spectra of alkaline solutions of DR81L alone (a), with H₂O₂ (b), with H₂O₂ and Cu (c), and with H₂O₂ and Cu-Phen (d), after 30 min at 60°C and pH 12.3

DR81L alone (a) exhibits three main peaks: the most intense one at 314.4 m/z corresponds to the dianion formed after removal of two sodium atoms from DR81. The one at 652.0 m/z is assigned to the anion formed after removal of only one sodium atom. The peak at 260.9 m/z, however, is a sub-structure of the DR81 molecule. This molecule is possibly an impurity originated from the synthesis of the dye, or it may have been produced during electrospray ionization by cleavage (1) represented on Figure V-15, although this technique should be mild and limit this kind of cleavage. DR81L+H₂O₂ resulted in a similar spectrum (b), confirming that H₂O₂ alone, applied in alkaline medium, does not attack the dye molecule.

With the addition of activator (CuSO₄ in (c), Cu-Phen in (d)) the peaks assigned to the dye (at 314.4 and 652.0 m/z) disappeared. Moreover, the intensity of the 260.9 m/z peak also decreased, and even more with Cu-Phen: this fragment seems to be degraded by activated H₂O₂. Finally the H₂O₂/Cu-Phen system, as for dye color-stripping, appears to be more effective than H₂O₂/CuSO₄.

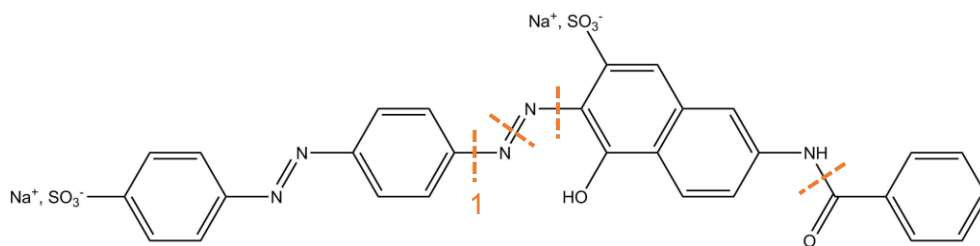


Figure V-15. Molecular structure of DR81 and possible cleavages

The other peaks could not be identified. The corresponding structures are probably due to rearrangements of degradation products, such as those proposed by Cheng et al. after cleavage of the azo bond of Acid Orange II [20], since the molecules resulting from the hypothesized cleavages (Figure V-15) did not match with the observed MS peaks.

As suggested earlier, the dye degradation reported in this part may originate from radical-induced oxidation. The investigation of a radical route will be presented in the next part.

V.4 INVESTIGATION OF A RADICAL MECHANISM

Based on the color-stripping results presented in Chapter IV, dye degradation may be due to radical reactions. Indeed, effective decolorization was accompanied by strong cellulose DP_v drops. This inspired the hypothesis of radical reactions, with different levels of hydrogen peroxide decomposition depending on pH (two ranges were tested: weak alkaline and strong alkaline pH) and on the use of either CuSO₄ or Cu-Phen as activator. The supposed radical route will be explored in this part via radical detection techniques.

Free radicals are involved in many oxidative reactions on pulp, especially during bleaching (see Chapter I). To our knowledge, Gierer's research group was the first one to prove the occurrence of radical reactions during bleaching, thanks to a chemiluminescence method [21]–[23]. During the same period, some authors such as Hobbs and Abbot [24], [25] used a spectroscopic method based on simple UV-visible analysis to detect hydroxyl radicals in peroxide bleaching studies. The radical trapping agent was N,N-dimethyl-4-nitrosoaniline (DMNA), a yellow molecule which is bleached when it reacts with HO•.

Some authors used another UV-visible method based on HO• trapping by N,N'-(5-nitro-1,3-phenylene)-bisglutaramide (NPG), in pulp delignification studies [26] and even in the examination of the H₂O₂/Cu^{II} system causing hair damage during hair coloring [27]. Here, HO• trapping renders the molecule colored. This method was developed by chemists Singh and Hider in the context of their work on the Fenton reaction [28]. It was not used in our work because it required the synthesis of NPG, which made it more difficult to implement.

Chirat and Lachenal used the EPR/spin-trapping method to prove the formation of hydroxyl radicals during ozone bleaching [29], confirmed by Pouyet in a more recent study [30]. This method, developed in the late 60's by the research groups of Lagercrantz [31] and Janzen [32], is well known and often used in the field of biology.

Although much research has been devoted to the EPR/spin-trapping study of hydroxyl radical formation by H₂O₂/Cu systems in biology (biological buffers) [33], little information is available on

this phenomenon in the case of a phenanthroline cupric complex in aqueous solution. The purpose of this work was thus to investigate the decomposition of hydrogen peroxide into radicals in the presence of copper(II)-phenanthroline complexes in aqueous medium.

V.4.1 Studies using chemiluminescence and UV-vis spectroscopy

V.4.1.1 Radical detection by chemiluminescence

The chemiluminescence method described in II.2.5.1 is based on the production of a chemiluminescent substance after the oxidation of phthalhydrazide by hydroxyl radicals. It was tested with H₂O₂ alone and H₂O₂+Cu-Phen on the DY11L dye. Phthalhydrazide (0.25 to 5 mM), Cu-Phen (63.8 μM) and H₂O₂ (61.8 mM) were introduced into a 100 mL DY11L solution at 56.5 μM in a heated double envelope reactor at 80°C. The chemical concentrations corresponded to the theoretical initial concentrations in the liquor during the design of experiments for DY11L-dyed pulp color-stripping (IV.2.4). The concentration of phthalhydrazide was chosen according to previous results in the literature. Many studies used no more than 0.6 mM phthalhydrazide in aqueous solution, as it corresponds to its solubility at near-neutral pH and ambient temperature. Reitberger and Gierer [21] used 0.1 mM phthalhydrazide in aqueous solution and 0.016 mM in pulp liquor (0.01% on odp at a consistency of 2.5%), Gierer *et al.*, Chirat and Lachenal, and Backa *et al.* applied 0.6 mM in aqueous solution [23], [29], [34], whereas higher concentrations were used on the pulp in the study of Gierer *et al.* on the peroxide bleaching of mechanical pulps: 4.8 mM in pulp liquor [23]. More recently, Vladut *et al.* [4] added 50 mM of phthalhydrazide in the pulp liquor during alkaline H₂O₂ and H₂O₂/Cu-Phen bleaching. This is why concentrations from 0.25 mM to 5 mM of phthalhydrazide were tested in this study.

The reaction was started at time t=0 and several samplings were done at different times of the reaction as follows: 0.1 mL aliquots of solution were introduced in solution A (Na₂CO₃, EDTA) and the chemiluminescence was revealed by adding solution B (H₂O₂, (NH₄)₂S₂O₈), as described in II.2.5.1. The chemiluminescence was recorded for a long time, until the next sampling.

Normally, the chemiluminescence signal should stabilize after a few minutes, as a small amount of phthalhydrazide is present in the solution. Therefore, the luminescence should stabilize when all the phthalhydrazide is oxidized or when no more hydroxyl radicals are produced. Usually, a short time after starting the acquisition is chosen and the chemiluminescence values are compared at that same time for each experiment. In this study, the chemiluminescence signal kept increasing even after 30 min. Therefore, Figure V-16, which gathers the results of the experiments described above with a phthalhydrazide concentration of 5 mM, shows the whole recorded signal. Yet, to compare two samplings or two reactions, chemiluminescence values were taken 2 minutes after starting the acquisition.

For the reaction with H₂O₂ alone, the samplings were carried out at t=6 min, 44 min, and 73 min. With H₂O₂+Cu-Phen, they were performed at t=6 min, 25 min, and 265 min.

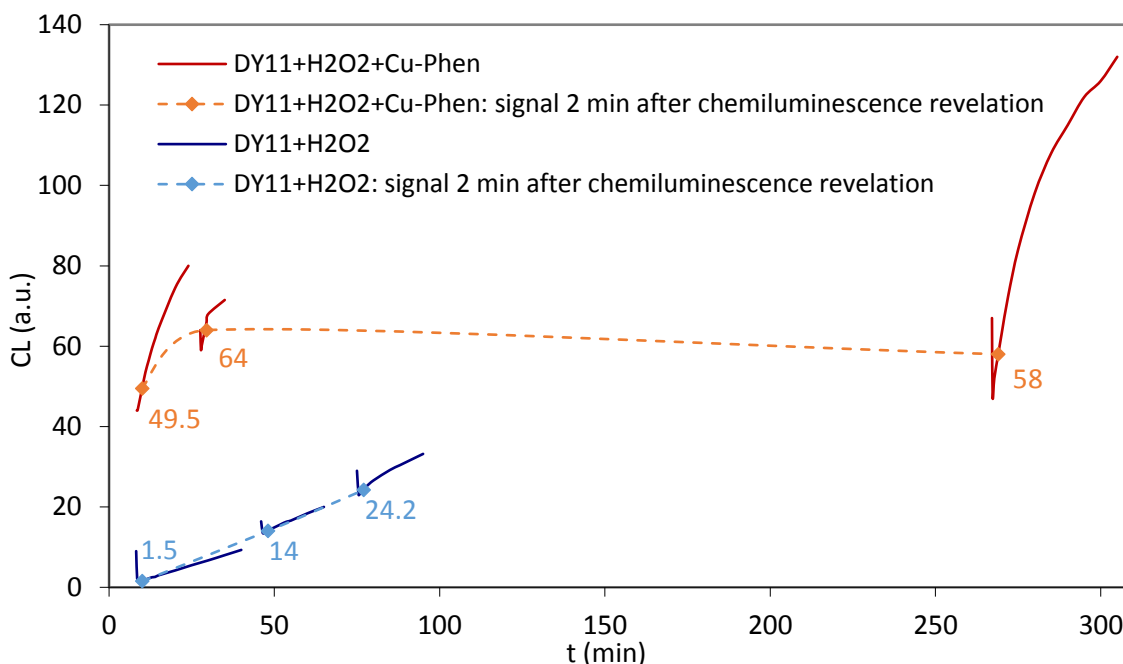


Figure V-16. Chemiluminescence signals of different samplings of two heated reactions (80°C): DY11L+H₂O₂+Cu-Phen and DY11L+H₂O₂, with 5 mM phthalhydrazide, 65.5 μ M DY11L, 61.8 mM H₂O₂ and 63.8 μ M Cu-Phen. The values 2 minutes after sampling and immediate chemiluminescence revelation are marked with colored dots.

In Figure V-16, for both reactions (DY11L+H₂O₂+Cu-Phen in red and DY11L+H₂O₂ in blue), the three samplings gave rise to increasing signals. Yet, these signals increased faster in the presence of activator.

In the case of H₂O₂ alone, when comparing the three samplings, i.e. the chemiluminescence at different times of the color-stripping reaction, the signal 2 minutes after beginning of acquisition appeared to increase linearly (0.34 a.u./min).

In the case of H₂O₂+Cu-Phen, similar results were observed but with higher signal intensity (49.5 a.u. already 2 min after the sampling at t=6 min vs. 1.5 a.u. at the same time in the case of H₂O₂). This shows that H₂O₂+Cu-Phen produced much more HO[•] radicals than H₂O₂ alone. Besides, the chemiluminescence value corresponding to the sampling at t=25 min was 64 a.u., which corresponds to an increase of 0.76 a.u./min between t=6 and t=25 min, i.e. more than twice as fast as with H₂O₂ alone. However, the sampling at t=265 min started at a lower signal intensity. After more than 4 hours, phthalhydrazide might be less stable or less sensitive, but since the signal kept increasing very fast, it is more likely that this value 2 minutes after revelation is rather comparable to that at t=25 min. Consequently, the sampling at t=265 min suggests that the same amount of radicals was detected at that time compared to t=25 min. Either all the phthalhydrazide reacted, thus preventing further detection, or the radical flow stopped after all the hydrogen peroxide was decomposed. Indeed, color-stripping trials on the DY11L-dyed pulp have shown that hydrogen peroxide was consumed quite fast, with 69% consumption after 20 min at only 55°C, at near-neutral pH (see Table IV.6 in IV.2.4).

In addition, the intensity of the signal of the second sampling at t=25 min started at a slightly lower chemiluminescence than the end of the first sampling's signal (18 min after revelation). This

indicates that the revelation of luminescence is not immediate. The origin of this phenomenon is unknown.

A control was performed with solutions A and B alone in the luminometer. It gave a stable signal at 10 a.u., implying that signals below 10 a.u. in our experiments may not be significant. Consequently, at t=6 min when treating the dye with H₂O₂ alone, the presence of hydroxyl radicals is not confirmed. Besides, analyses of the H₂O₂/Cu-Phen system performed with lower amounts of phthalhydrazide (0.25 and 0.5 mM) revealed similar phenomena, only at lower intensity (results not shown).

In conclusion:

- The chemiluminescence signal was much higher with H₂O₂+Cu-Phen than with H₂O₂ alone: hydroxyl radical generation is certainly occurring.
- The chemiluminescence signal kept slowly increasing and never stabilized. This questions the selectivity of the method and may be due to:
 - o The slow formation of the oxidized phthalhydrazide, maybe because HO• are still formed at room temperature after sampling
 - o Other technical limits of the method under our conditions (not identified)
 - o The presence of the dye, which may interfere in the chemiluminescence method
- According to Gierer and coworkers, above pH 9.2, the chemiluminescence signal decreases due to the presence of hydroperoxide ions HOO⁻, which would react with hydroxyl radicals faster than phthalhydrazide [23]. Hence, this chemiluminescence method allows to compare two assays at a same pH but two different pHs would be difficult to compare. This limits the application of this analysis since our study aimed at comparing different pHs.
- The method relies upon the presence of oxygen in the medium, and in our work oxygen was not wanted since it may interfere in the understanding of the reaction involved in H₂O₂ color-stripping. This constitutes another limitation of this analysis in the frame of the mechanism investigations.
- Finally, this method was not quantitative (although other studies were conducted by comparison with γ -irradiation results and considered quantitative [34]).

Consequently, other radical detection methods were tested and will be presented in the next paragraphs.

V.4.1.2 Radical detection by UV-visible spectroscopy

As described in II.2.5.2, the UV-vis method used in this work is based on the discoloration of DMNA when it reacts with hydroxyl radicals. This method was applied to detect hydroxyl radicals in the H₂O₂/Cu-Phen system, without any dye to avoid any interference with DMNA absorption. According to preliminary analyses, the extinction coefficient of DMNA at 440 nm was: $\epsilon_{DMNA}(440 \text{ nm}) = 6816 \text{ L mol}^{-1} \text{ cm}^{-1}$.

The trials were conducted at room temperature in 20 mL flasks by direct addition of H₂O₂ with or without activator in a DMNA solution. In the very first assays, the solution was analyzed after 5 minutes of magnetic stirring, whereas the following experiments were carried out without agitation time: the samples were directly analyzed by UV-vis. DMNA decolorization was calculated based on absorbance decrease at 440 nm.

In the main approach, the chemical concentrations and ratios were chosen based on the conditions of the DOE applied on dyed pulp (IV.2.4). Sodium hydroxide was added in different amounts depending on the desired pH. 1×10^{-4} M, 1×10^{-3} M and 2×10^{-2} M NaOH allowed to reproduce the liquor concentrations of the bleaching stages using 0.05, 0.525 and 1% NaOH on odp respectively. The H₂O₂ and activator concentrations were also those applied in the DOE presented in IV.2.4. The chemical concentration ranges used for this study are gathered in Table V-1.

Table V-1. Concentrations of the different chemicals used in the UV-vis detection of hydroxyl radicals in the activated H₂O₂ system – DOE conditions

NaOH (M)	Cu-Phen, CuSO ₄ or FeSO ₄ (M)	H ₂ O ₂ (M)
0; 1×10^{-4} ; 1×10^{-3} ; 2×10^{-2}	6.4×10^{-5}	6.2×10^{-2}

The DMNA concentration was chosen to get a DMNA/H₂O₂ molar ratio close to that used in the experiments of Hobbs and Abbot on H₂O₂/Cu^{II}, i.e. 0.14% [24]. The experimental data reported by the authors are presented in Table V-2. The DMNA/H₂O₂ and activator/H₂O₂ ratios mentioned in the present study are molar ratios, in percent.

Table V-2. DMNA decolorization conditions and results in the literature [24]

DMNA (M)	H ₂ O ₂ (M)	FeSO ₄ (M)	CuSO ₄ (M)	DMNA/H ₂ O ₂ (%)	Activator/H ₂ O ₂ (%)	DMNA decolorization (%) / 440 nm	Remarks
4.00×10^{-5}	3.53×10^{-2}	/	3.58×10^{-6}	0.14	0.01	6	30 min at 50°C
	3.53×10^{-2}	1.79×10^{-5}	/	0.14	0.05	17	

The first trials were conducted at natural pH (no NaOH) for the H₂O₂/Cu-Phen system and at acidic pH (pH 3) for the Fenton reagent (H₂O₂/Fe^{II}), which was examined for comparison. The solutions were analyzed after 5 minutes of magnetic stirring. The conditions and results are presented in Table V-3.

Table V-3. First DMNA decolorization in the H₂O₂/Cu-Phen system without alkali – DOE conditions

DMNA (M)	H ₂ O ₂ (M)	Cu-Phen (M)	FeSO ₄ (M)	DMNA/H ₂ O ₂ (%)	Activator/H ₂ O ₂ (%)	DMNA decolorization (%) / 440 nm	pH
1.0×10^{-4}	6.18×10^{-2}	/	6.38×10^{-5}	0.16	0.10	85	3.5
1.0×10^{-4}	6.18×10^{-2}	6.38×10^{-5}	/	0.16	0.10	12	4.6

Table V-3 shows that DMNA was able to trap high amounts of radicals (see DMNA decolorization). Moreover, in the chosen conditions, the analyses showed that the H₂O₂/Cu-Phen system formed hydroxyl radicals, but less than the conventional Fenton system (12% reduction of absorbance vs. 85% with the Fenton reagent). Note that the measured pH was higher with the H₂O₂/Cu-Phen system, which may partly influence the generation of radicals.

With the same « liquor concentrations », different pHs were then tested by adding increasing amounts of alkali, see Table V-4. In addition, the effect of Cu-Phen was compared to that of CuSO₄ alone, and to controls without activator. This time, the solution was analyzed immediately after mixing the reactants (no stirring time) in order to avoid additional variations due to the kinetics of HO• generation. The DMNA/H₂O₂ ratio is given as well as the Cu/H₂O₂ ratio (0.10%, see Table

V-4), which was twice as high as that used by Hobbs and Abbot when analyzing a Fenton system (0.05%, see Table V-2).

Table V-4. DMNA decolorization results at different pHs, for H₂O₂, H₂O₂+Cu-Phen, and H₂O₂+CuSO₄ – DOE conditions

DMNA (M)	H ₂ O ₂ (M)	CuPhen (M)	CuSO ₄ (M)	NaOH (% on odp)	Range of pH	DMNA/H ₂ O ₂ (%)	Cu/H ₂ O ₂ (%)	DMNA decolorization (%) /440 nm
				0	5-6			4
				0.05	~9			0
1.0×10 ⁻⁴	6.18×10 ⁻²	/	/	0.525	~11	0.16		4
				0.83	~11-12			2
				1	12-12.5			4
				0	5-6			34
				0.05	~9			60
1.0×10 ⁻⁴	6.18×10 ⁻²	6.38×10 ⁻⁵	/	0.525	~11	0.16	0.10	6
				0.83	~11-12			1
				1	12-12.5			1
				0	5-6			51
				0.05	~9			0
1.0×10 ⁻⁴	6.18×10 ⁻²	/	6.38×10 ⁻⁵	0.525	~11	0.16	0.10	0
				1	12-12.5			0

Controls without H₂O₂ (results no shown) exhibited slight absorbance reductions of no more than 3%. Therefore, the DMNA decolorization observed with peroxide alone (0 to 4%, first line in Table V-4) was not significant and did not prove the presence of hydroxyl radicals.

Table V-4 shows that hydroxyl radicals were trapped by DMNA, preferably at low alkali charges, as soon as CuSO₄ or Cu-Phen were added to hydrogen peroxide. With 1.0×10⁻⁴ M DMNA and no alkali, the absorbance reduction of DMNA reached 34% with the H₂O₂/Cu-Phen system and 51% with H₂O₂/Cu. Yet, with 0.05% NaOH, the reduction was higher with Cu-Phen (60%) whereas no decrease was observed with CuSO₄.

The results obtained with Cu-Phen are quite in accordance with the dyed-pulp color-stripping results observed on pulp in Chapter IV. Indeed, acidic and near-neutral trials were not very effective, whereas with higher alkalinity, better decolorization could be achieved. Here, the detection of hydroxyl radicals was the highest at pH around 9, and it dropped at pH around 11. The first moderate alkaline pH (around 9) may correspond to a peak of activity for hydrogen peroxide decomposition, or this decomposition may be more regular. It is possible that strong hydroxylation of copper above pH 11 inhibits its activating effect. This hypothesis could also be applied to CuSO₄, which would then be inhibited at lower pH than Cu-Phen, possibly due to the absence of competing phenanthroline ligands.

Note that in some cases, the maximum absorbance wavelength of DMNA was different from 440 nm. Yet, the percentage of absorbance reduction was calculated with the absorbance at 440 nm, since the absorbance at the actual λ_{max} was very close and led to the same DMNA decolorization results.

In addition, the concentration of DMNA was doubled to observe whether radicals could be detected at alkaline pH (see Table V-5).

Table V-5. DMNA decolorization results at different pHs, for H₂O₂+Cu-Phen, with either 1.0×10⁻⁴ or 2.0×10⁻⁴ M DMNA – DOE conditions

DMNA (M)	H ₂ O ₂ (M)	CuPhen (M)	NaOH (% on odp)	DMNA/H ₂ O ₂ (%)	Cu/H ₂ O ₂ (%)	DMNA decolorization (%) /440 nm
1.0×10 ⁻⁴	6.18×10 ⁻²	6.38×10 ⁻⁵	0	0.16	0.10	34
			0.05			60
			0.525			6
			0.83			1
			1			1
2.0×10 ⁻⁴	6.18×10 ⁻²	6.38×10 ⁻⁵	0	0.32	0.10	46
			0.05			81
			0.525			23
			1			27

With 2.0×10⁻⁴ M DMNA (line 2), radicals were trapped at all pHs, which may evidence a more accurate detection.

Finally, this method revealed that hydroxyl radicals were formed at room temperature in the presence of hydrogen peroxide and copper activator. However, the concentration of H₂O₂ was quite high, although in the same range as in Hobbs and Abbot's experiments [24]. Some other analyses were performed in solutions modelling the trials conducted in aqueous solution (Chapter III), and with lower H₂O₂ concentration (1×10⁻⁴ M), in the same range as Kraljic and Trumbore [35].

Numerous assays with 1×10⁻⁴ M H₂O₂ exhibited no more than 1% of reduction of the DMNA signal, even with the Fenton reagent.

In conclusion, hydroxyl radicals were detected but only at relatively high peroxide charges. DMNA may not react fast enough as a scavenger, which would explain why this method was not sufficient to draw clear conclusions under the conditions of the present study.

Yet, some interesting results were found. First, strong alkaline pHs did not exhibit any hydroxyl radical trapping or not significantly. It seemed that more radicals were formed at acidic or low alkaline pHs. Besides, the results suggest that more radicals are generated with Cu-Phen. To validate these conclusions, another radical-detection method was tested, the EPR/spin-trapping technique. The results are presented in the next paragraph.

V.4.2 EPR/Spin-trapping

The EPR/spin-trapping method is extensively used in biological studies to follow the formation of oxygenated radicals such as HO•. Some authors studied specifically H₂O₂/Cu systems under physiological (i.e. near-neutral) conditions: Hanna and Mason [36] followed the production of hydroxyl radicals by an H₂O₂/Cu^I system, but also its inhibition by some ligands such as glutathione; Bhattacharjee *et al.* [33] examined the generation of hydroxyl radicals by an H₂O₂/Cu^{II} system involved in DNA damage.

As reported earlier, this method was also used under alkaline conditions in the frame of pulp bleaching studies [29], [30].

V.4.2.1 Experimental

The EPR/spin-trapping method allows to detect short-lived species such as free radicals thanks to the fast reaction of these radicals with “spin-traps” like 5,5-dimethyl-1-pyrroline *N*-oxide (DMPO). This forms DMPO-radical adducts that are much more stable and thus detectable by EPR.

As described in II.2.5.3.i, in the presence of hydroxyl radicals, DMPO forms the DMPO-OH adduct, which gives a typical four-line signal (see Figure V-17), with hyperfine splitting constants $a_N = a_H = 14.9$ G [37].

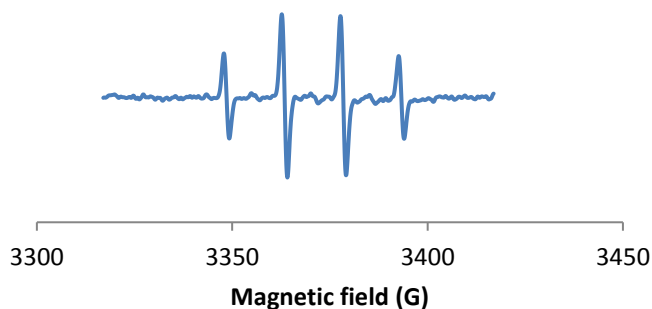


Figure V-17. Typical DMPO-OH signal [38]

However, since DMPO-OH can be formed by other ways than HO• trapping, two scavengers which are specific to HO• radicals were used: dimethyl sulfoxide (DMSO) and sodium formate. The resulting DMPO adducts were the products of their reactions with hydroxyl radicals. Hence, in the presence of HO•, the DMSO scavenger should lead to the DMPO-CH₃ adduct, and with the formate ion, the DMPO-COO⁻ adduct should be formed.

The spin-trapping trials were carried out in aqueous solution following the experimental procedure detailed in II.2.5.3.ii. Most experiments were performed at room temperature due to technical reasons.

The interpretations of the EPR spectra were based on the known hyperfine coupling constants of DMPO adducts such as DMPO-OH, DMPO-R or the DMPO-COO⁻ adduct. The experimental constants found by simulation are gathered in Table V-6 next to reference constants found in the literature. These allowed to assign the experimental constants to the (most probable) corresponding radical species.

Table V-6. EPR hyperfine coupling constants of the observed radical species: experimental and reference values (see Buettner's spin adduct parameter tables [37]) for comparison

		DMPO triplet	DMPO-R	DMPO-OH	DMPO-CH ₃	DMPO-COO ⁻
Number of lines (intensity)		3	6	4 (1:2:2:1)	6	6
Experimental values (from simulation)	a _{Nexp} (G)	14.3-14.8	14.8-15.8	13.9-15.4	15.4-15.9	15.7-15.8
	a _{Hexp} (G)	/	20.1-24.1	13.8-15.6	22.6-23.3	19.0-19.3
Reference values (from the literature)	a _{Nref} (G)	n/a	15.5	14.9	16.1 / 16.4	15.6
	a _{Href} (G)	/	22.0	14.9	23.0 / 23.5	18.7
	Reference	/	[39]	[40], [41]	[40] / [42]	[40], [43]

In the absence of any substrate (dyes or cellulosic fibers), the formation of HO• was first evaluated in the absence of alkali, at pH between 7.5 and 9 (7.5 in the presence of H₂O₂, around 8-8.6 in the absence of H₂O₂, and pH 9 was when adding sodium formate as a HO• scavenger) (V.4.2.2). Then, strong alkaline conditions were also tested with 0.02 M NaOH, at pH 12.5 (V.4.2.3). Lastly, some trials were conducted with dyes and cellulosic fibers in the medium (V.4.2.4).

V.4.2.2 Results at near-neutral/weak alkaline pH

The results obtained on the H₂O₂/Cu-Phen system in the absence of alkali will first be given and interpreted qualitatively (V.4.2.2.i). The hyperfine coupling constants found by simulation will be given to confirm the identification of various radical species. Yet, the precise radical compositions determined by simulation and some integration results will be presented in a second part (V.4.2.2.ii), especially to compare different cases in a more quantitative way.

V.4.2.2.i EPR/spin-trapping results and qualitative interpretation

All the spectra presented in the following part are with the same intensity scale.

V.4.2.2.i.a Results without H₂O₂

First of all, controls in the absence of DMPO (not shown) never exhibited any signal. DMPO alone did not exhibit any signal either. Then, it was analyzed with phenanthroline, copper sulfate and copper-phenanthroline.

- *Phenanthroline*

As expected, no signal was observed with DMPO and phenanthroline, see Figure V-18.

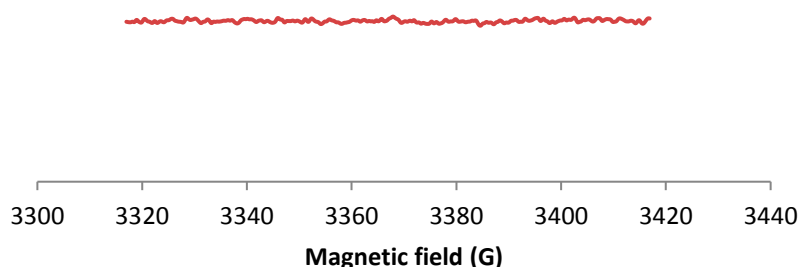


Figure V-18. X-band EPR spectrum of DMPO+Phen

- *Copper sulfate*

A second control was carried out with CuSO₄, with and without DMSO as a HO• scavenger. The resulting EPR spectra are presented in Figure V-19.

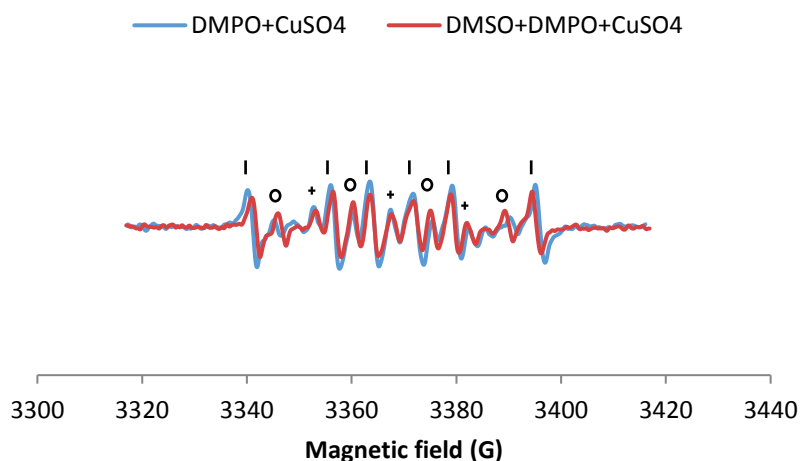


Figure V-19. X-band EPR spectra of DMPO+CuSO₄ and DMSO+DMPO+CuSO₄

The simulation revealed the presence of at least three radical species in each case. With DMPO+CuSO₄: DMPO-OH, $a_N = 15.798$ G, $a_H = 14.928$ G; DMPO-R, $a_N = 15.798$ G, $a_H = 23.237$ G; triplet, $a_N = 14.609$ G; other, $a_N = 16.323$ G, $a_H = 26.653$ G (uncertain). With DMSO+DMPO+CuSO₄: DMPO-OH, $a_N = 14.697$ G, $a_H = 14.015$ G; DMPO-R, $a_N = 15.439$ G, $a_H = 22.586$ G; triplet, $a_N = 14.354$ G

Assignments: o=DMPO-OH, |=DMPO-R, +=triplet

Both spectra in Figure V-19 exhibit three signals: DMPO-OH (o), a carbonated adduct that will be referred to as DMPO-R (|), and a triplet (+).

The addition of DMSO did not decrease the DMPO-OH signal, indicating that the DMPO-OH radical did not originate from the trapping of HO•. Consequently, this adduct was probably formed by nucleophilic addition of water on the spin-trap. Indeed, according to Hanna *et al.* [44] and Burkitt

et al. [45], Cu(II) enhances the nucleophilic addition of water on DMPO. Cu(II) would bind to DMPO (evidenced by Hanna and collaborators by EPR at 77 K), thus polarizing DMPO's double bond and inducing a nucleophilic attack of H₂O on this bond (see Figure V-20).

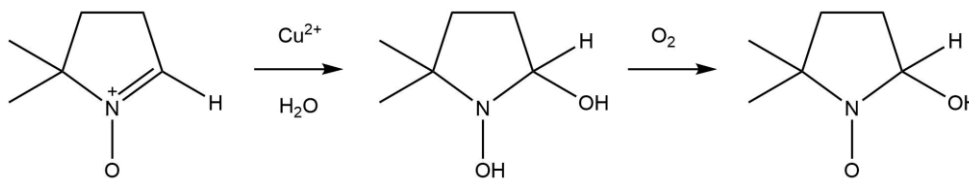


Figure V-20. Mechanism of nucleophilic addition of water on DMPO in the presence of Cu, leading to the DMPO-OH adduct, as described by Burkitt *et al.* [45]

The nucleophilic addition of water on DMPO had already been described by Finkelstein in the presence of iron and copper ion traces in aqueous solutions [38]. Makino *et al.* [46] also reported the formation of a Fe(III)-DMPO complex during spin-trapping experiments with the Fenton reactant, as evidenced by EPR at 77 K. However, the result was not a nucleophilic water addition: the authors found that this Fe(III)-DMPO complex contributed to the degradation of the spin-trap after the addition of hydrogen peroxide (compared to another spin-trap which did not coordinate to iron).

To conclude, the carbonated adduct (DMPO-R) and the triplet observed in Figure V-19 are most likely due to the decomposition of DMPO in the presence of copper, since these radicals did not appear with DMPO and phenanthroline [37].

After copper sulfate, the copper-phenanthroline complex was also analyzed with DMPO.

- *Cu-Phen*

The EPR signals obtained with DMPO and Cu-Phen with and without DMSO are given in Figure V-21.

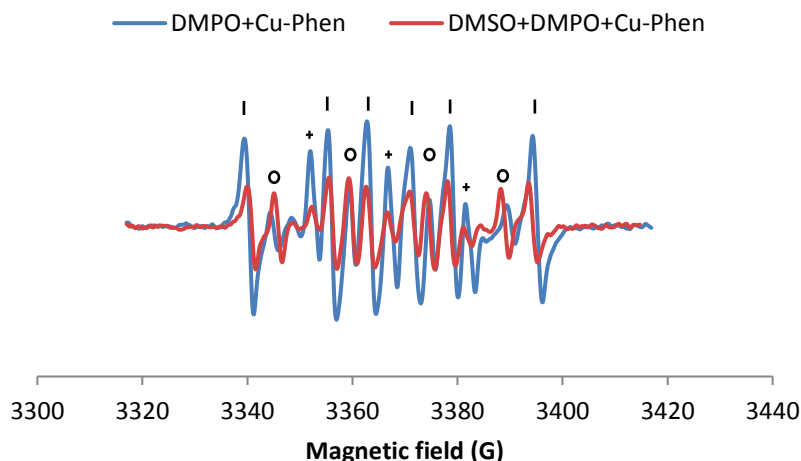


Figure V-21. X-band EPR spectra of DMPO+Cu-Phen and DMSO+DMPO+Cu-Phen

The simulations revealed the presence of three radical species in each case. With DMPO+Cu-Phen: DMPO-OH, $a_N = 15.088$ G, $a_H = 14.943$ G; DMPO-R, $a_N = 15.781$ G, $a_H = 23.27$ G; triplet, $a_N = 14.354$ G. With DMSO+DMPO+Cu-Phen: DMPO-OH, $a_N = 14.697$ G, $a_H = 13.82$ G; DMPO-R, $a_N = 15.488$ G, $a_H = 22.635$ G; triplet, $a_N = 14.305$ G

Assignments: o=DMPO-OH, |=DMPO-R, +=triplet

As well as DMPO+CuSO₄, DMPO+Cu-Phen gave three signals: DMPO-OH, DMPO-R, and a triplet. In addition, the peaks of DMPO-R and the triplet were more intense than with CuSO₄, suggesting that DMPO is degraded faster in the presence of Cu-Phen. Interestingly, the DMPO-R radical formed in the presence of DMSO exhibited different hyperfine coupling constants. The radical was thus different and possibly derived from DMSO.

The addition of DMSO (in red in Figure V-21) did not lower the DMPO-OH signal, proving that once again, this adduct was not due to the presence of hydroxyl radicals but rather to the nucleophilic addition of water onto DMPO in the presence of Cu.

This was confirmed thanks to the other scavenger, HCOO⁻, as illustrated in Figure V-22.

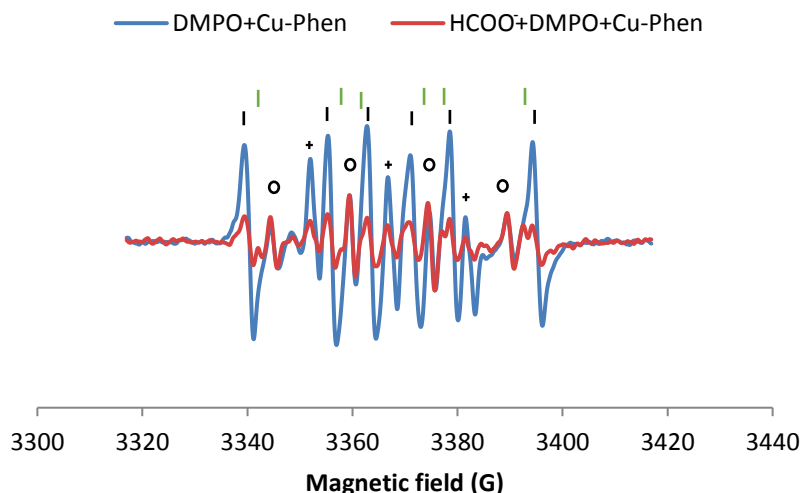


Figure V-22. X-band EPR spectra of DMPO+Cu-Phen and HCOO⁻+DMPO+Cu-Phen
 The simulation revealed the presence of four radical species with HCOO⁻+DMPO+Cu-Phen:
 DMPO-OH, $a_N = 14.843$ G, $a_H = 15.428$ G; DMPO-R, $a_N = 15.644$ G, $a_H = 23.244$ G; triplet, $a_N = 14.593$ G; DMPO-COO⁻, $a_N = 15.683$ G, $a_H = 19.293$ G
 Assignments: o=DMPO-OH, |=DMPO-R, +=triplet, |=DMPO-COO⁻

In the presence of sodium formate, the intensity of the DMPO-OH signal was not reduced, evidencing the absence of hydroxyl radicals and thus confirming that the DMPO-OH signal was due to the nucleophilic addition of water.

As earlier, the carbonated adducts (DMPO-R and triplet) appear to originate from the decomposition of DMPO in the presence of copper. According to Burkitt *et al.* [45], the redox potential of Cu^{II}(Phen)₂/Cu^I(Phen)₂ is slightly higher than that of Cu^{II}/Cu^I (0.17 and 0.16 V, respectively), which could explain the higher degradation of DMPO in the presence of phenanthroline.

In the present work, the binding between DMPO and Cu(II) was evidenced by EPR spectroscopy at 100 K with DMPO 60 mM and Cu(II) 0.15 mM (Figure V-23).

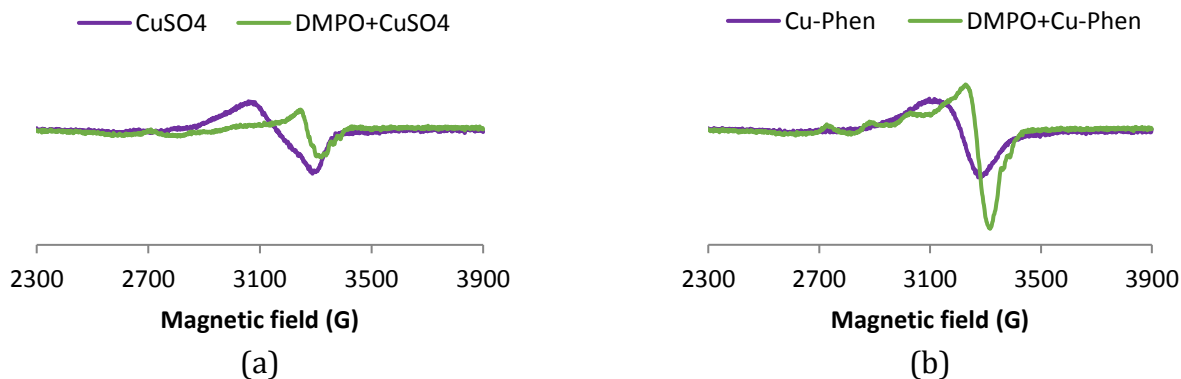


Figure V-23. X-band EPR spectra at 100 K of (a) CuSO₄ with and without DMPO (b) Cu-Phen with and without DMPO, [Cu] = 0.15 mM, [DMPO] = 60 mM

After the addition of DMPO, the Cu(II) spectrum was clearly modified: its hyperfine structure exhibited different constants, attributable to new complexes. A similar experiment by Hanna *et al.*

[44] with DMPO 100 mM and Cu(II) 0.25 mM had shown a visible structuration as well. However, the signals being different, the structuration was not the same with copper sulfate (Figure V-23a) and with copper-phenanthroline (Figure V-23b). In the case of CuSO₄ (a), the addition of DMPO modified the hyperfine structure even though it is not as visible as in the case of Cu-Phen (b). DMPO seems to have more interaction with copper when the latter is coordinated to phenanthroline.

In these trials, DMPO was at the same concentration as in the spin-trapping experiments (60 mM), but in excess compared to CuSO₄. When adding DMPO at the same concentration as copper, i.e. 0.15 mM, the structuration was not visible (results not shown). Therefore, copper is not that reactive towards DMPO. In addition, Cu(II) did not seem to be reduced into Cu(I) (no decrease of signal intensity) in the presence of DMPO. Hence, under the conditions of these trials, Cu(II) may not oxidize DMPO.

- *Cu-Phen at high temperature*

The same experiment was repeated after heating DMPO+Cu-Phen and HCOO⁻+DMPO+Cu-Phen, see Figure V-24.

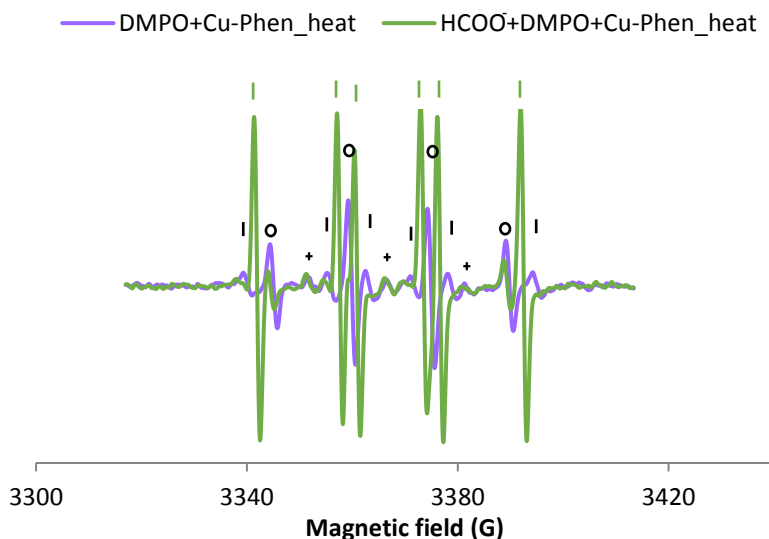


**Figure V-24. X-band EPR spectra of DMPO+Cu-Phen and HCOO⁻+DMPO+Cu-Phen after heating – The simulation revealed the presence of four radical species with HCOO⁻+DMPO+Cu-Phen: DMPO-OH, $a_N = 14.746$ G, $a_H = 15.428$ G; DMPO-R, $a_N = 15.644$ G, $a_H = 23.342$ G; triplet, $a_N = 14.788$ G; DMPO-COO⁻, $a_N = 15.781$ G, $a_H = 19.0$ G
Assignments: o=DMPO-OH, |=DMPO-R, +=triplet, |=DMPO-COO⁻**

After heating in the presence of sodium formate and DMPO, even without H₂O₂, DMPO-COO⁻ was detected, meaning that some HO[•] was formed in the Cu-Phen solution. It is probably owing to the decomposition of soluble oxygen present in the analyzed samples, although the initial solutions had been deoxygenated with nitrogen. Indeed, if we consider that O₂ is present at 2 mg/L in solution, its molar concentration would be 0.6×10^{-4} mol/L, which is close to the H₂O₂ concentration in our experiments, i.e. 1.0×10^{-4} mol/L. This result is in accordance with the slight cellulose depolymerization observed with the Cu-Phen controls during pulp color-stripping trials (Chapter IV). However, how would oxygen be decomposed in the absence of any substrate? DMPO might actually act as an organic substrate: Cu²⁺ would oxidize DMPO and form Cu⁺, which would be able to reduce oxygen, as in the catalytic mechanism proposed by Korpi *et al.* [7]

- *Conclusions*

In conclusion on these control assays at near-neutral pH:

- DMPO was shown to be slightly degraded in the presence of copper (CuSO₄ and Cu-Phen). No interaction is observed with phenanthroline alone.
- Nucleophilic addition of water onto DMPO was evidenced in the presence of copper (CuSO₄ and Cu-Phen), leading to the formation of the DMPO-OH adduct in the absence of hydroxyl radicals.
- With Cu-Phen, when the solution was heated, some hydroxyl radicals were detected, possibly due to the decomposition of soluble oxygen in the medium.
- DMPO was shown to coordinate with copper, possibly more in the case of Cu-Phen. Copper not being inert towards DMPO probably influences the following spin-trapping results.
- No reduction of Cu(II) was observed in the presence of DMPO. Hence, under the conditions of these trials, Cu(II) may not oxidize DMPO.

V.4.2.2.i.b Introduction of H₂O₂

- *H₂O₂ alone*

Before investigating the hydroxyl radical production by the H₂O₂/Cu-Phen and H₂O₂/CuSO₄ systems, controls were conducted with peroxide alone, see Figure V-25. This time, the EPR/spin-trapping method being sensitive, the trials were performed with a low hydrogen peroxide concentration (1.0×10⁻⁴ M).

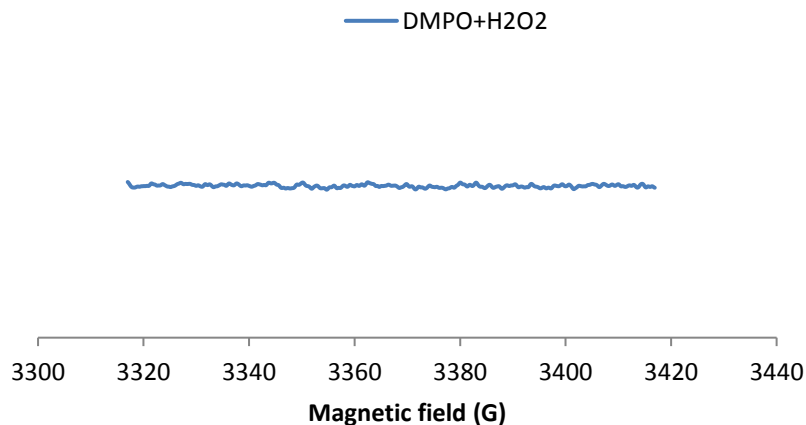


Figure V-25. X-band EPR spectrum of DMPO+H₂O₂

At room temperature, no signal was observed with DMPO and H₂O₂ (Figure V-25). No hydroxyl radicals seemed to be present under these conditions.

However, after heating, a DMPO-OH signal appeared, suggesting that hydrogen peroxide decomposed into hydroxyl radicals at higher temperature, as well known (Figure V-26).

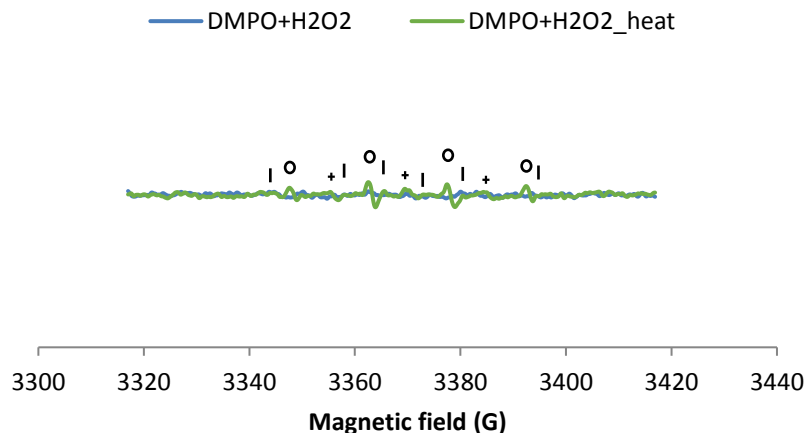


Figure V-26. X-band EPR spectra of DMPO+H₂O₂ at ambient temperature and after heating
The simulation revealed the presence of three radical species after heating: DMPO-OH, a_N = 14.756 G, a_H = 15.391 G; DMPO-R, a_N = 14.813 G, a_H = 21.535 G; triplet, a_N = 14.842 G
Assignments: o=DMPO-OH, |=DMPO-R, +=triplet

- H₂O₂ + Cu-Phen

The H₂O₂/Cu-Phen system was tested with and without DMSO, see Figure V-27.

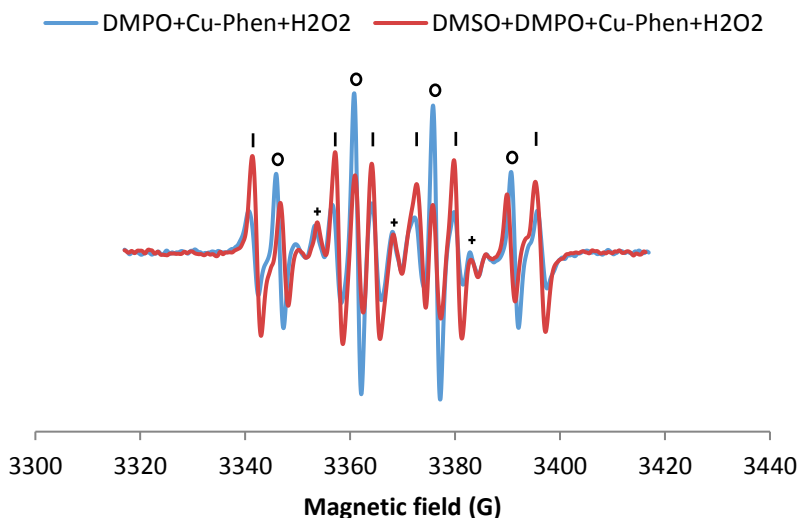
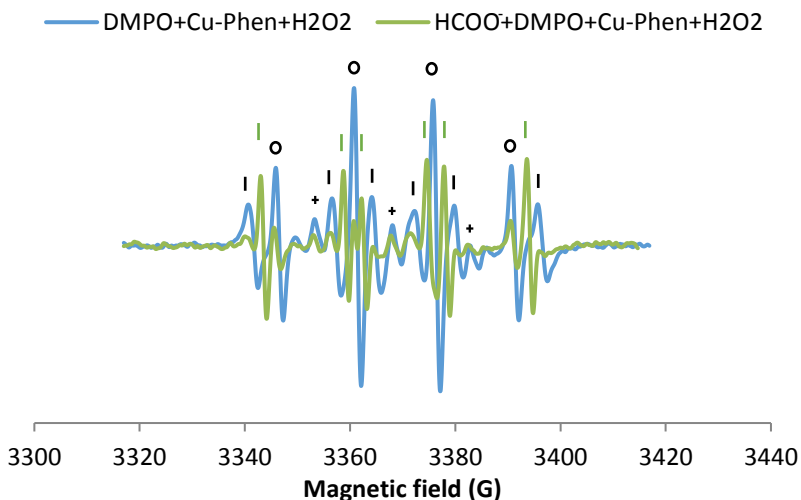


Figure V-27. X-band EPR spectra of DMPO+Cu-Phen+H₂O₂ and DMSO+DMPO+Cu-Phen+H₂O₂ - The simulations revealed the presence of three to four radical species.
Without DMSO: DMPO-OH, a_N = 15.0 G, a_H = 14.805 G; DMPO-R, a_N = 15.781 G, a_H = 23.342 G; triplet, a_N = 14.549 G; with DMSO: DMPO-OH, a_N = 14.7 G, a_H = 13.851 G; DMPO-R, a_N = 15.7 G, a_H = 22.651 G; triplet, a_N = 14.349 G; other, a_N = 15.786 G, a_H = 20.11 G (minor and uncertain) - Assignments: o=DMPO-OH, |=DMPO-R, +=triplet

In the presence of DMPO, the H₂O₂/Cu-Phen system led to intense DMPO-OH peaks and certainly the same carbonated adducts as observed without H₂O₂: DMPO-R and the triplet.

With DMSO, a drop of the DMPO-OH signal was accompanied with the detection of a carbonated DMPO adduct "DMPO-R", which was probably DMPO-CH₃ (a_N = 15.7 G, a_H = 22.651 G). These results

prove that some hydroxyl radicals were produced in solution with H₂O₂ and Cu-Phen. This was confirmed with the other hydroxyl radical scavenger, sodium formate, as shown in Figure V-28.



**Figure V-28. X-band EPR spectra of DMPO+Cu-Phen+H₂O₂ and HCOO⁻+DMPO+Cu-Phen+H₂O₂ - With HCOO⁻, the simulation revealed the presence of four radical species DMPO-OH, $a_N = 14.902$ G, $a_H = 15.233$ G; DMPO-R, $a_N = 15.64$ G, $a_H = 23.266$ G; triplet, $a_N = 14.593$ G; DMPO-COO⁻, $a_N = 15.749$ G, $a_H = 19.098$ G
Assignments: o=DMPO-OH, |=DMPO-R, +=triplet, |=DMPO-COO⁻**

With sodium formate, the DMPO-OH signal dropped and DMPO-COO⁻ (|) was formed (triplet of doublets, $a_{Nexp} = 15.7$ G and $a_{Hexp} = 19.1$ G, see Figure V-28), confirming that DMPO-OH in the absence of scavenger was partly due to hydroxyl radicals.

The apparent disappearance of DMPO-OH in the presence of sodium formate suggests the absence of nucleophilic water addition in this case. This could be explained by either kinetic reasons, due to the low constant rate of the DMPO/H₂O reaction, or by the fact that copper would activate H₂O₂'s decomposition rather than induce the nucleophilic addition of water onto DMPO. However, some DMPO-OH may be present but overlapped by the other peaks.

The solution with HCOO⁻+DMPO+Cu-Phen+H₂O₂ was also analyzed 10 min after the first acquisition to observe the evolution. The same experiment was repeated with heating to compare the intensity of radical generation. The two resulting EPR spectra are shown in Figure V-29.

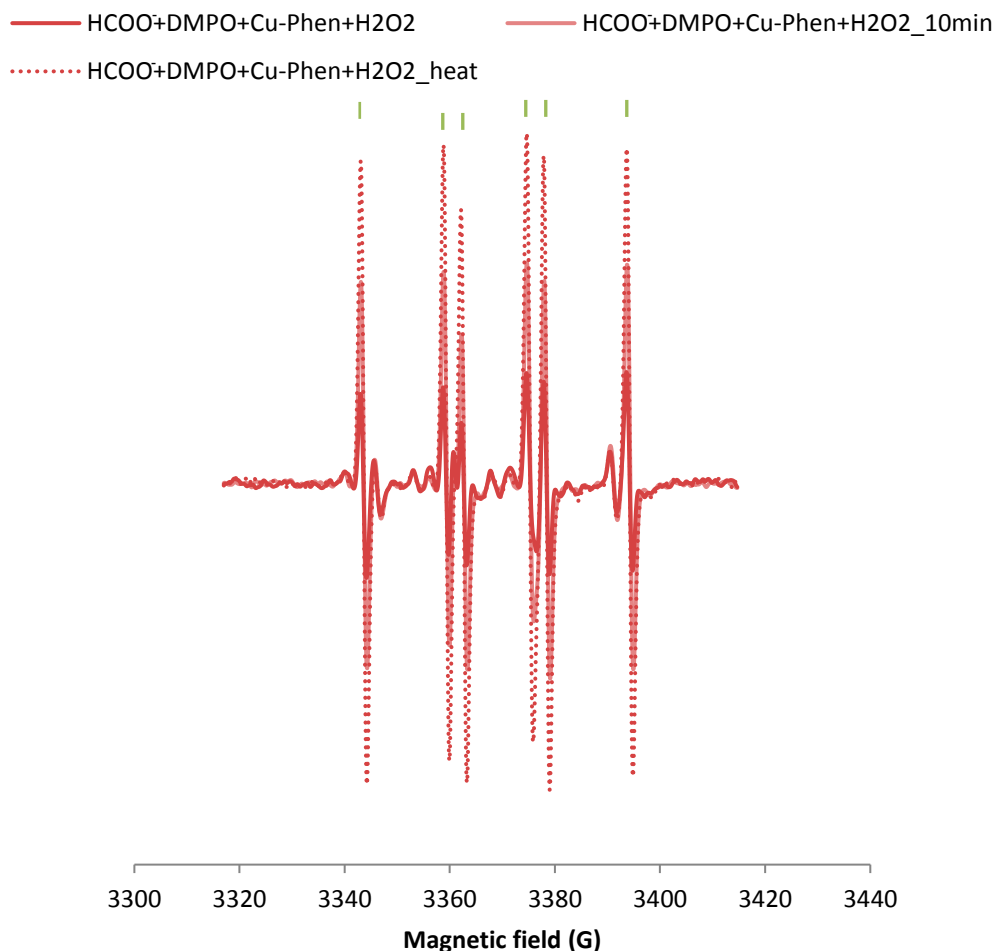


**Figure V-29. X-band EPR spectra of HCOO⁻+DMPO+Cu-Phen+H₂O₂ at ambient temperature at t=0 and t=10 min and after heating - The simulations revealed the presence of four radical species. At t=10 min: DMPO-OH, a_N = 15.049 G, a_H = 14.976 G; DMPO-R, a_N = 15.651 G, a_H = 23.872 G; triplet, a_N = 14.463 G; DMPO-COO⁻, a_N = 15.781 G, a_H = 19.098 G. After heating: DMPO-OH, a_N = 15.0 G, a_H = 15.074G; DMPO-R, a_N = 15.602 G, a_H = 23.607 G; triplet, a_N = 14.512 G; DMPO-COO⁻, a_N = 15.781 G, a_H = 19.049 G
Assignments: | =DMPO-COO⁻**

Figure V-29 shows that after 10 minutes at ambient temperature, hydroxyl radicals were still formed and scavenged by sodium formate, since the DMPO-COO⁻ signal was more intense than after the first analysis. Moreover, the same solution was heated and directly analyzed, giving a very strong signal, even more intense than after 10 minutes at ambient temperature. As observed with H₂O₂ alone, H₂O₂ was thus decomposed faster into HO• after heating the H₂O₂/Cu-Phen solution.

- H₂O₂ + CuSO₄

The H₂O₂/CuSO₄ system was tested with and without scavenging by DMSO. The EPR spectra are shown in Figure V-30.

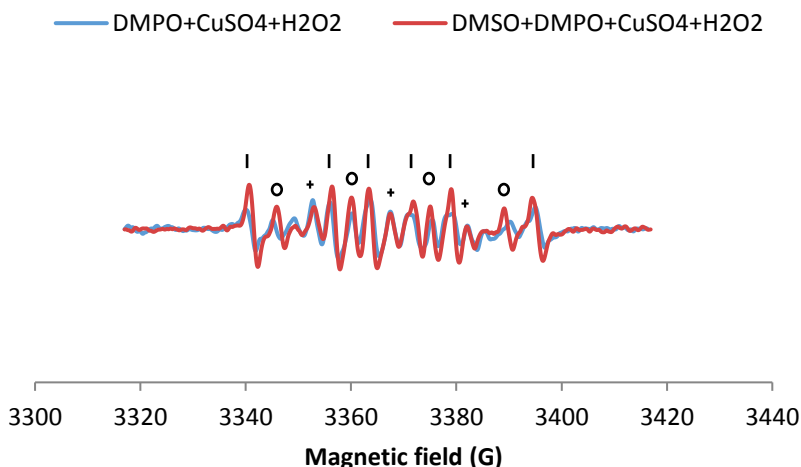


Figure V-30. X-band EPR spectra of DMPO+CuSO₄+H₂O₂ and DMSO+DMPO+CuSO₄+H₂O₂
The simulations revealed the presence of three to five radical species. Without DMSO:
DMPO-OH, $a_N = 15.244$ G, $a_H = 14.83$ G; DMPO-R, $a_N = 15.70$ G, $a_H = 23.51$ G; triplet, $a_N =$
14.598 G; other, $a_N = 13.975$ G, $a_H = 21.435$ G (minor and uncertain); other, $a_N = 12.195$ G,
 $a_H = 11.463$ G (3 H, also minor and uncertain). With DMSO: DMPO-OH, $a_N = 14.707$ G, $a_H =$
13.951G; DMPO-R, $a_N = 15.651$ G, $a_H = 22.658$ G; triplet, $a_N = 14.354$ G
Assignments: o=DMPO-OH, |=DMPO-R, +=triplet

Figure V-30 shows a weak signal of DMPO-OH, DMPO-R and the same triplet as without H₂O₂, with or without DMSO. These spectra are similar to those without H₂O₂, although the amount of DMPO-OH is slightly higher. However, the DMPO-OH signal was very weak compared to that observed earlier with H₂O₂/Cu-Phen.

With DMSO, it was not clear whether DMSO scavenged some hydroxyl radicals or not. Sodium formate was thus used as a potentially more effective hydroxyl radical scavenger (Figure V-31).

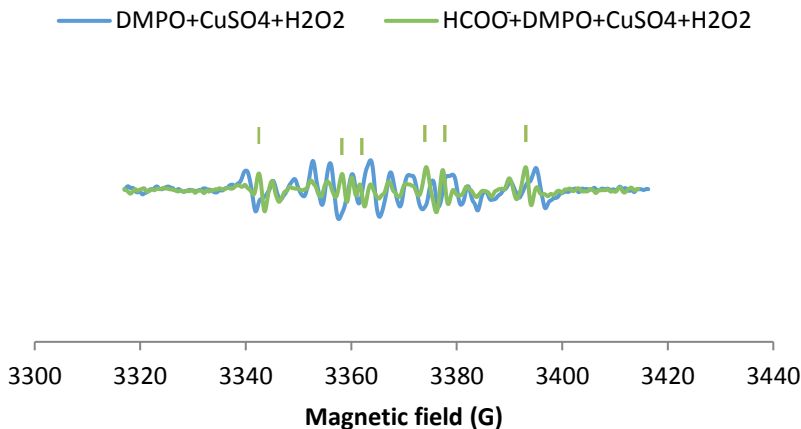


Figure V-31. X-band EPR spectra of DMPO+CuSO₄+H₂O₂ and HCOO⁻+DMPO+CuSO₄+H₂O₂
 With HCOO⁻, the simulation revealed the presence of five radical species DMPO-OH, a_N = 15.269 G, a_H = 14.951 G; DMPO-R, a_N = 15.749 G, a_H = 23.559 G; DMPO-COO⁻, a_N = 15.793 G, a_H = 18.97 G; triplet, a_N = 14.695 G; other, a_N = 13.709 G, a_H = 7.508 G (3 H)
 Assignments: | =DMPO-COO⁻

In the presence of sodium formate, the weak DMPO-OH signal almost disappeared and a weak signal of DMPO-COO⁻ appeared, evidencing the presence of a very low amount of hydroxyl radicals under the studied conditions. This is consistent with the conclusions of Bhattacharjee and collaborators [33], who observed DMPO-OH at physiological pH with DMPO, H₂O₂, and CuCl₂, and concluded that it was due to the presence of hydroxyl radicals (although the authors did not use a scavenger to confirm it).

In Figure V-32, the EPR spectrum obtained after HO[•] scavenging by sodium formate in the case of H₂O₂/CuSO₄ was compared to the equivalent spectrum with H₂O₂/Cu-Phen.

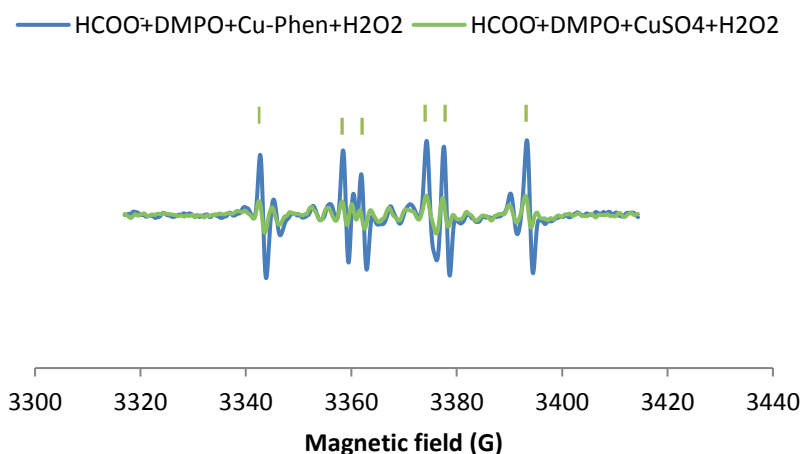


Figure V-32. Comparison between the X-band EPR spectra of HCOO⁻+DMPO+Cu-Phen+H₂O₂ and HCOO⁻+DMPO+CuSO₄+H₂O₂ - Assignments: | =DMPO-COO⁻

Figure V-32 shows that the DMPO-COO⁻ signal with H₂O₂ and CuSO₄ was much lower than with H₂O₂ and Cu-Phen: the H₂O₂/Cu-Phen system generated more HO[•]. Similarly, in the context of dye decolorization, Nerud *et al.* [47] observed that H₂O₂/Cu^{II} was less effective than H₂O₂/Cu^{II}-pyridine

at pH 3 to 9. The authors proposed that hydroxyl radicals were probably involved in the decolorization, since HO• scavengers such as superoxide dismutase inhibited the color-stripping. To conclude, the H₂O₂/Cu-Phen system produced more hydroxyl radicals than H₂O₂/CuSO₄. This new HO• generating system was thus compared to a reference system: Fenton's reagent. The results are given in the next paragraph.

- *Fenton: H₂O₂ + FeSO₄ at pH 3*

Cu-Phen was replaced by FeSO₄ under strong acidic conditions in order to compare the H₂O₂/Cu-Phen system to the Fenton reactant (Figure V-33). The H₂O₂ and metal concentrations were identical.

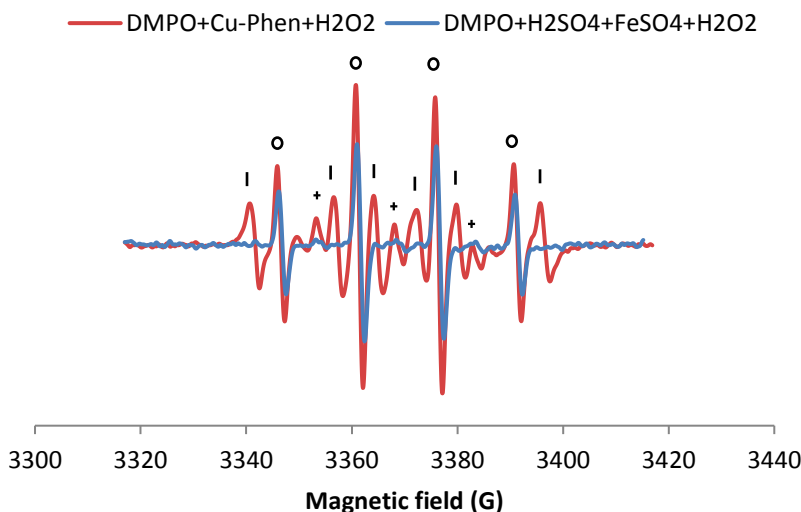


Figure V-33. X-band EPR spectrum of DMPO+Cu-Phen+H₂O₂ at near-neutral pH compared to DMPO+FeSO₄+H₂O₂ at pH 3 (same concentrations of H₂O₂ and [Fe]=[Cu])

With DMPO+FeSO₄+H₂O₂ at pH 3, the simulation revealed the presence of three radical species: DMPO-OH, $a_N = 15.00$ G, $a_H = 14.732$ G; DMPO-R, $a_N = 14.675$ G, $a_H = 21.703$ G; triplet, $a_N = 14.793$ G - Assignments: o=DMPO-OH, |=DMPO-R, +=triplet

As expected, the Fenton control gave a clear four-line signal typical of DMPO-OH. Surprisingly, this signal was not as intense as the one obtained with H₂O₂ and Cu-Phen, suggesting that the H₂O₂/Cu-Phen system may produce more hydroxyl radicals than the Fenton reactant with the same H₂O₂ and “activator” concentrations. Yet, in the case of H₂O₂/Cu-Phen, there was probably a slight contribution from nucleophilic addition of water onto DMPO. Therefore, it can be concluded that the HO• generation of H₂O₂/Cu-Phen was in the same range as that of the Fenton system.

- *Fenton and sodium formate*

Fenton's reagent (H₂O₂+FeSO₄ at pH 3) was tested with and without scavenging by sodium formate. The resulting spectra are shown in Figure V-34.

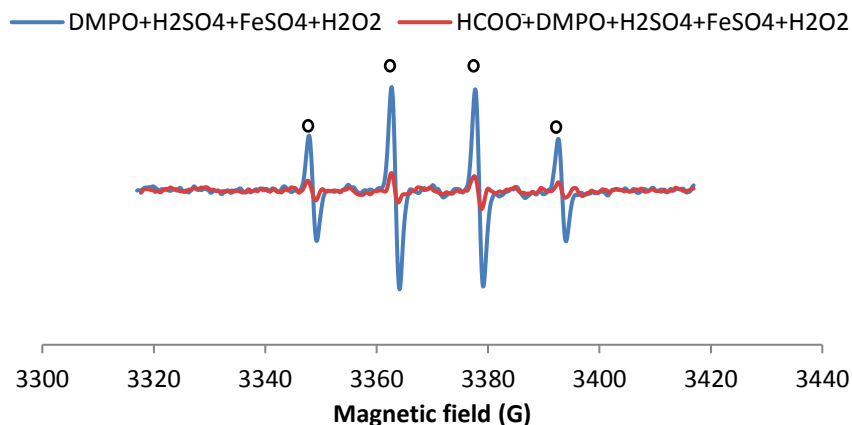


Figure V-34. X-band EPR spectra of DMPO+Fenton and HCOO⁻+DMPO+Fenton
Assignments: o=DMPO-OH

With HCOO⁻, DMPO-OH almost disappeared but DMPO-COO⁻ was not detected. This means that hydroxyl radicals were scavenged but that DMPO-COO⁻ was not formed. The pH of 3 in these trials was a little below HCOOH's pKa, i.e. 3.75. Consequently, HCOOH was the major species, but in equilibrium with a significant amount of HCOO⁻, since pH 3 was close to the pKa. This quantity of HCOO⁻ seems to have been sufficient to scavenge HO[•]. According to Villamena et al. [48], the pKa of DMPO-COOH/DMPO-COO⁻ is 6.8. Hence, even though HCOO⁻ scavenged HO[•] to form the carbon dioxide radical anion COO^{•-}, then the trapping of COO^{•-} by DMPO led to the formation of DMPO-COOH. DMPO-COOH is probably unstable and therefore not visible by EPR, which could explain the decrease of DMPO-OH's signal without detection of another signal.

Yet, note that the introduction of sodium formate may have slightly increased the medium's pH, thus influencing the HO[•] radical generation, since the Fenton system is effective at pH 3. If the alkalinity of sodium formate was able to slow down the radical generation, then it would be another explanation for the DMPO-OH drop, directly due to low HO[•] production.

To conclude, the DMPO-OH signal observed with Fenton's reagent is most certainly due to HO[•] radicals, and sodium formate is not an appropriate scavenger for this acidic system.

V.4.2.2.i.c Conclusion

After these qualitative interpretations, more accurate comparison between different trials required to conduct some integration calculations and radical distribution simulations. These are presented in the next part to confirm the first conclusions and go further in terms of understanding.

V.4.2.2.ii Simulation of the EPR/spin-trapping results and semi-quantitative interpretation

The objective of this part was to quantify the detected radical flows in some significant assays, in order to compare the trials more accurately.

As described in II.2.5.3.iii, some simulations were performed to determine the composition of the radical mixtures giving rise to the recorded signals. The software SimEPR was used to do so: some possible assignments were proposed for each observed EPR signature based on the literature, then the software allowed to simulate the presence of several species and the resulting EPR signal. The

simulated spectra fitted to experimental signals after adjustment of parameters such as the hyperfine coupling constants and the relative ratios of each radical species.

The simulations were based on the known hyperfine coupling constants of DMPO adducts such as DMPO-OH, carbonated adducts of DMPO or the DMPO-COO⁻ adduct. The experimental constants found by simulation are gathered in the beginning of V.4.2.1 in Table V-6, next to reference constants found in the literature. These allowed to assign the experimental constants to the (most probable) corresponding radical species.

For example, Table V-7 and Figure V-35 below display the simulation results for DMPO+Cu-Phen+H₂O₂ at near-neutral pH. The details of the simulation results for DMPO+Cu-Phen+H₂O₂ are given in Table V-7 (hyperfine coupling constants, line widths and relative areas of the different radicals) and the simulated spectrum is compared to the experimental spectrum in Figure V-35.

Table V-7. DMPO+Cu-Phen+H₂O₂ – Simulation results

	DMPO-OH	DMPO-R	Triplet
a _N (G)	15	15.781	14.549
a _H (G)	14.805	23.342	/
L _w (G)	0.609/0.658/0.609	0.988/0.988/1.049	0.854/0.805/0.854
Relative area (%)	38	53	8

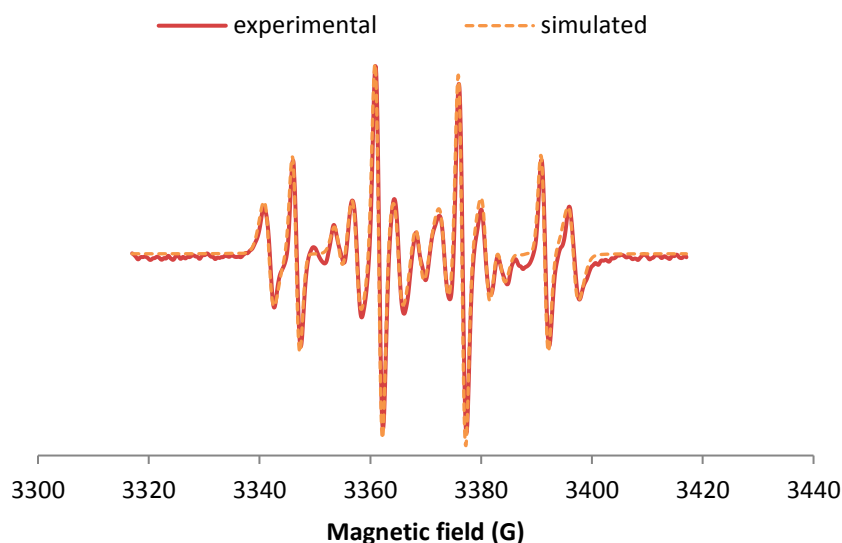


Figure V-35. Comparison between the experimental and simulated spectra of DMPO+Cu-Phen+H₂O₂ at near-neutral pH

The details of some other simulations (Tables similar to Table V-7 and Figures similar to Figure V-35) are presented in Annex 2.

Yet, the main results of the simulations are gathered in Table V-8, as relative areas of the identified radical species. In addition, most spectra were integrated to calculate their total areas (arbitrary units), so that the amounts of each radical species could be roughly compared from one spectrum to another.

Table V-8. Integration and simulation results: total peak area, and distribution of DMPO adducts and degradation products for some experiments, as relative areas of each radical, in percents

Entry	HCOO ⁻	DMSO	H ₂ O ₂	Additive	Details	Total peak area (a.u.)	DMPO-OH (%)	DMPO-CH ₃ (%)	DMPO-COO ⁻ (%)	DMPO-R (%)	Triplet (%)	Other(s) (%)
1				CuSO ₄		1.12	5			74	8	13
2				Cu-Phen		1.46	6			77	17	
3			x	Cu-Phen		1.29	38			54	8	
4		x	x	Cu-Phen		n/a	18	73		4.5	4.5	
5	x		x	Cu-Phen		0.65	18		49	28	5	
6	x		x	Cu-Phen	+10min	0.54	14		70	12	4	
7	x		x	Cu-Phen	heating	0.79	10		79	8	3	
8			x	CuSO ₄		0.89	7			57	16	19
9		x	x	CuSO ₄		n/a	16			76	8	
10	x		x	CuSO ₄		0.21	15		23	34	10	18
11			x	FeSO ₄	pH 3	0.43	86			7	7	

First of all, the controls without H₂O₂ (CuSO₄ and Cu-Phen alone) can be compared quantitatively thanks to Table V-8 (entries 1 and 2). The Cu-Phen spectrum had a relative total peak area (calculated by integration of the spectrum, arbitrary units) of 1.46 vs. 1.12 for CuSO₄. In addition, DMPO-R and the triplet together represented 94% of the radicals vs. 82% for CuSO₄. Consequently, DMPO-R and the triplet were 49% more intense with Cu-Phen than in the case of CuSO₄. This quantification confirms that DMPO is degraded faster in the presence of Cu-Phen.

Then, as seen in Figure V-27, the H₂O₂/Cu-Phen system led to intense DMPO-OH peaks. With 38% DMPO-OH for a total area of 1.29 (entry 3 in Table V-8) vs. 7% for a total area of 1.46 (entry 2), these peaks were actually 4.8 times more intense than without H₂O₂. This already indicates that hydroxyl radicals should be the major contributors to the formation of DMPO-OH with H₂O₂/Cu-Phen. The simulations also confirmed that the other detected adducts were the same as without H₂O₂: DMPO-R and the triplet.

With DMSO (entry 4), a drop of the DMPO-OH signal was accompanied with the detection of a carbonated DMPO adduct, which is DMPO-CH₃, as evidenced by spectrum simulation (see Annex 2). The DMPO-CH₃ radical appeared to be highly predominant as it represented 73% of the detected radicals.

Figure V-28 showed earlier that with the addition of sodium formate, the DMPO-OH signal dropped and DMPO-COO⁻ (II) was formed. The simulation results confirmed that DMPO-OH was partly replaced by DMPO-COO⁻. The latter represented 49% of the detected radicals and a significant amount of DMPO-R was found (28%) compared to the two previous solutions (without scavenger and with DMSO), suggesting stronger DMPO degradation in that case (entry 5 in Table V-8).

The details of the simulations of the H₂O₂/Cu-Phen system, with and without scavenger, are presented in Annex 2.

In addition, after 10 minutes at room temperature, hydroxyl radicals were still formed and scavenged by sodium formate (Figure V-29). According to the simulations (entry 6 in Table V-8), the DMPO-COO⁻ signal was approximately 20% more intense than at the first analysis (70% DMPO-

COO⁻ for a total peak area of 0.54 vs. 49% for a total peak area of 0.65). Moreover, heating an identical solution gave a very strong signal, which was 65% more intense than 10 min after the trial at room temperature, according to the total area of 0.79 with 79% DMPO-COO⁻ (entry 7). This confirms that the H₂O₂/Cu-Phen system produces more radicals at high temperature.

The H₂O₂/CuSO₄ system did not exhibit much difference with CuSO₄ alone, as shown in Figure V-30. Yet, 7.5% more DMPO-OH was found with H₂O₂ and CuSO₄ compared to CuSO₄ alone: from a total area of 1.12 including 5% DMPO-OH to a total area of 0.89 with 7% of DMPO-OH, see entry 8 in Table V-8.

The simulations show that the relative amount of DMPO-OH increased from the assay without scavenger to that with DMSO, and the observed triplet of doublet with DMSO did not seem to originate from DMPO-CH₃ according to its hyperfine coupling constants (see entry 9). This is in accordance with the assumption that DMSO may not have scavenged hydroxyl radicals in the case of H₂O₂+CuSO₄, which is why sodium formate was also tested.

As seen in Figure V-31, when using sodium formate as a scavenger, DMPO-OH partly disappeared. Indeed, although the relative amount of DMPO-OH was lower with formate than without, if the total peak areas are considered, 15% of 0.21 is twice lower than 7% of 0.89. Hence, the amount of DMPO-OH was divided by two while DMPO-COO⁻ appeared. The DMPO-COO⁻ signal with H₂O₂+CuSO₄ was approximately 85% lower than with H₂O₂+Cu-Phen (total area of 0.21 including 23% DMPO-COO⁻ vs. 0.65 including 49% DMPO-COO⁻, see entries 10 and 5 respectively in Table V-8). This calculation confirms the stronger H₂O₂ decomposition with Cu-Phen.

Finally, when analyzing Fenton's reagent without scavenging (Figure V-33), it was found that it only produced DMPO-OH, however the DMPO-OH signal was less intense than that observed with H₂O₂/Cu-Phen at the same H₂O₂ and metal concentrations. The integrations and simulations summarized in Table V-8 (entry 11) indicate that it was approximately 25% lower, since a total area of 0.43 including 86% DMPO-OH was found with H₂O₂/Fe, compared to 1.29 including 38% DMPO-OH with H₂O₂/Cu-Phen. However, assuming that no nucleophilic addition of water occurs in the case of the Fenton system but that it occurs in the case of H₂O₂/Cu-Phen, and with the same intensity as with Cu-Phen alone, then the amount of DMPO-OH due to hydroxyl radicals would be almost identical for both activated systems. Indeed, when removing 7% of a total area of 1.46 a.u. (DMPO+Cu-Phen) from 38% of 1.29 a.u. (DMPO+Cu-Phen+H₂O₂), the total is only 5% higher than 43% of 0.86 a.u. (DMPO+Fenton).

V.4.2.2.iii Conclusions

The addition of Cu-Phen into a hydrogen peroxide solution at near-neutral pH was proved to cause the decomposition of the latter into hydroxyl radicals. Considering that most trials were performed at ambient temperature and that a Fenton control produced similar amounts of radicals, this decomposition effect was quite strong.

The addition of CuSO₄ (without phenanthroline) induced a very low hydroxyl radical production, and the addition of phenanthroline alone led to no radical detection. Therefore, the higher HO[•] production with Cu-Phen was probably due to the modified electronic structure of the copper atom when coordinated to phenanthroline and to the modified resulting redox potential, as this would explain a modified activity.

In terms of method, two scavengers were compared. Under the conditions of this study (excluding the Fenton system), sodium formate was the best scavenger. DMSO may have been less effective because of its coordinating ability with copper [49].

As expected, higher temperatures enhanced H₂O₂'s decomposition into hydroxyl radicals.

The same spin-trapping study was conducted at strong alkaline pH to investigate the radical formation under conventional bleaching conditions. The results are presented in V.4.2.3.

V.4.2.3 Results at alkaline pH

V.4.2.3.i Results without H₂O₂

Controls were performed with DMPO alone and with phenanthroline at strong alkaline pH (12.3-12.5). The EPR spectra are shown in Figure V-36.

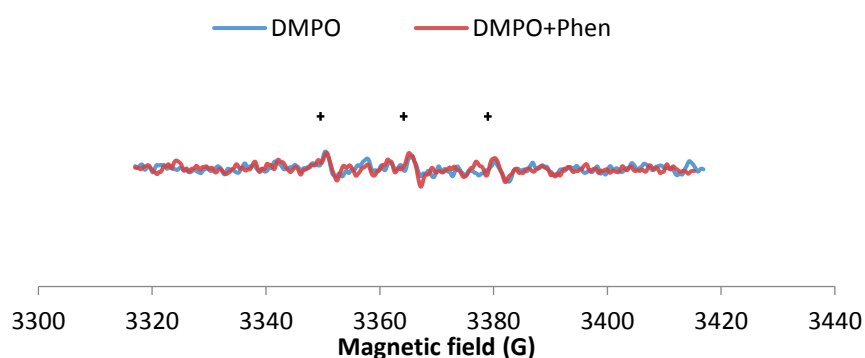


Figure V-36. X-band EPR spectra of NaOH+DMPO and NaOH+DMPO+Phen
Assignments: +=triplet

At strong alkaline pH, DMPO alone was observed to be degraded faster than at near-neutral pH, since the same degradation triplet as before appeared, but this time without any copper or hydrogen peroxide. This is consistent with easier nucleophilic addition at alkaline pH. With the addition of phenanthroline, no difference was detected.

The controls with CuSO₄ and with Cu-Phen are presented in Figure V-37.

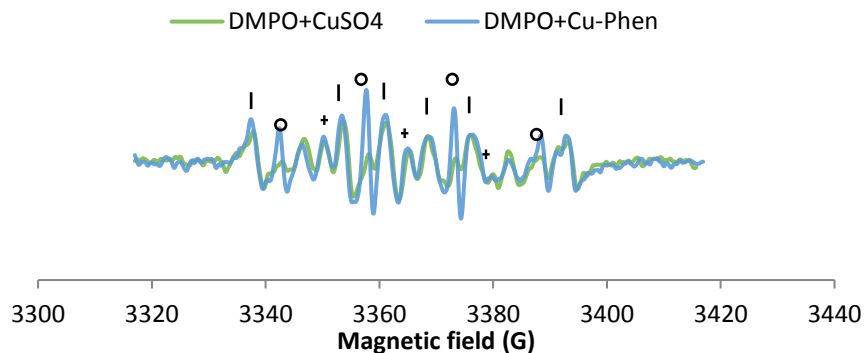


Figure V-37. X-band EPR spectra of NaOH+DMPO+CuSO₄ and NaOH+DMPO+Cu-Phen
 The simulations revealed the presence of four radical species in both solutions. With CuSO₄: DMPO-OH, $a_N = 15.195$ G, $a_H = 15.294$ G; DMPO-R, $a_N = 15.741$ G, $a_H = 23.488$ G; triplet, $a_N = 14.549$ G; other, $a_H = 17.975$ G (2 H, uncertain). With Cu-Phen: DMPO-OH, $a_N = 15.234$ G, $a_H = 15.623$ G; DMPO-R, $a_N = 15.742$ G, $a_H = 23.83$ G; triplet, $a_N = 14.398$ G; other, $a_N = 14.999$ G, $a_H = 21.246$ G - Assignments: o=DMPO-OH, |=DMPO-R, +=triplet

In Figure V-37, the signal with copper sulfate exhibited mostly DMPO degradation products, whereas that with Cu-Phen clearly exhibited some DMPO-OH. Therefore, the Cu-Phen solution was analyzed in the presence of the formate scavenger, see Figure V-38.

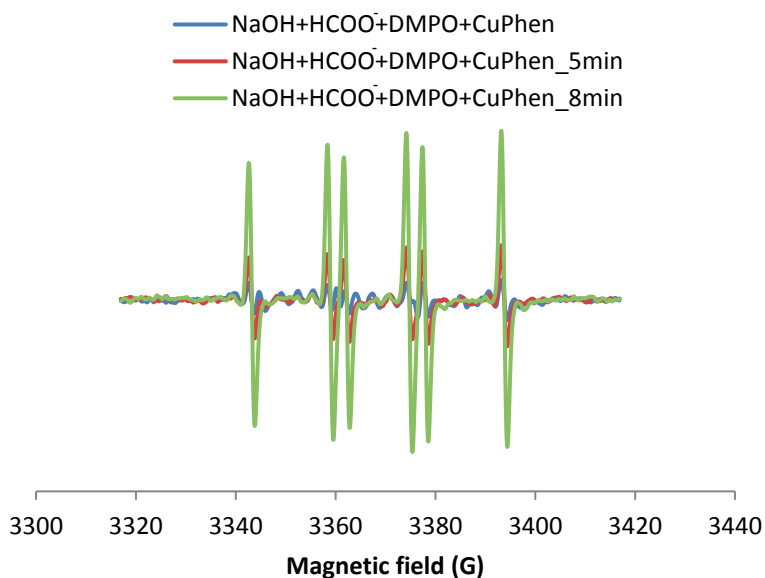


Figure V-38. X-band EPR spectra of NaOH+HCOO⁻+DMPO+Cu-Phen
 at t=0, t=5 min and t=8 min - The simulations revealed the presence of two radical species:
 DMPO-R, $a_N = 15.595$ G, $a_H = 22.756$ G; DMPO-COO⁻, $a_N = 15.805$ G, $a_H = 19.00$ G

Compared to the signal of NaOH+DMPO+Cu-Phen given in Figure V-37, with the addition of sodium formate (Figure V-38), the DMPO-OH signal was replaced with typical DMPO-COO⁻ signal. This confirmed that the DMPO-OH adduct detected in the presence of Cu-Phen originated from hydroxyl radicals. This generation of hydroxyl radicals in the absence of hydrogen peroxide may be due to the catalysis of soluble oxygen by Cu-Phen under alkaline conditions [7], [50], [51]. As mentioned earlier for DMPO+Cu-Phen at near-neutral pH and high temperature, the reduction of oxygen to

give $\text{HO}\cdot$ would be possible due to DMPO. Here, the conditions would be more favorable since the pH was alkaline.

As previously examined under near-neutral conditions, the influence of DMPO on copper's electronic structure was tested at alkaline pH by EPR at 100 K. Both Cu-Phen (Figure V-39) and CuSO_4 (Figure V-40) were analyzed with and without DMPO.

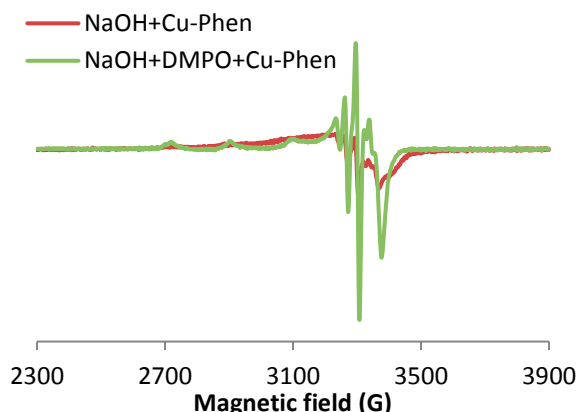


Figure V-39. X-band EPR spectra at 100 K of NaOH+Cu-Phen with and without DMPO - $[\text{Cu}] = 0.15 \text{ mM}$, $[\text{DMPO}] = 60 \text{ mM}$

The addition of DMPO at the same concentration as Cu-Phen (0.15 mM) did not seem to modify the structure of Cu(II) (not shown). When introduced at the concentration of the spin-trapping trials, i.e. 60 mM (Figure V-39), a clear hyperfine structure appeared, evidencing the interaction between Cu and DMPO. Therefore, in the case of Cu-Phen, DMPO and Cu are able to coordinate at alkaline pH as well as at near-neutral pH.

This experiment was repeated with copper sulfate, giving the spectra of Figure V-40.

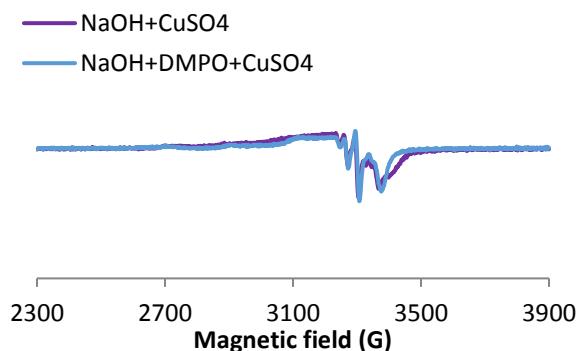


Figure V-40. X-band EPR spectra at 100 K of NaOH+ CuSO_4 with and without DMPO - $[\text{DMPO}] = 60 \text{ mM}$

The addition of DMPO to the alkaline CuSO_4 solution slightly modified the structure of Cu(II). The hyperfine lines were not much more visible but the coupling constants were a little different, thus proving some coordination.

In conclusion on these control assays at alkaline pH:

- DMPO was shown to be degraded at alkaline pH (triplet).

- With Cu-Phen, even at room temperature, some hydroxyl radicals were detected, probably due to the decomposition of soluble oxygen in the medium, favored at alkaline pH and possibly initiated by the oxidation of DMPO. No hydroxyl radicals were detected with CuSO₄.
- As observed at near-neutral pH, some Cu coordinated to DMPO under the conditions of the spin-trapping study, especially in the case of Cu-Phen. Hence, the DMPO spin-trap is not inert towards copper.

Then, H₂O₂ was introduced in the medium to examine its decomposition at alkaline pH.

V.4.2.3.ii Introduction of H₂O₂

As well as at near-neutral pH, no signal was observed with H₂O₂ alone.

- *H₂O₂ + Cu-Phen*

The alkaline H₂O₂/Cu-Phen system was first analyzed, see Figure V-41.

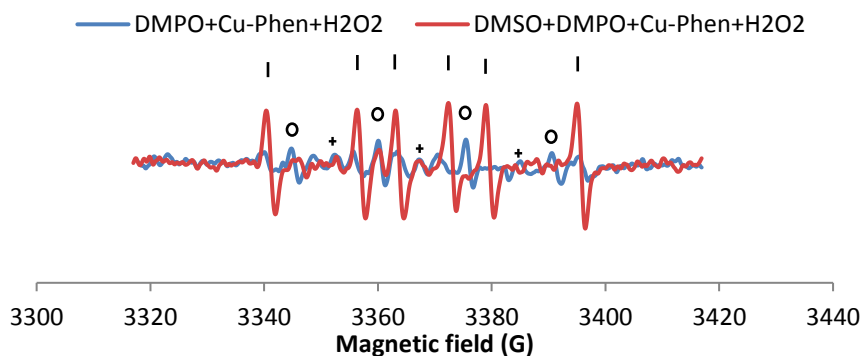
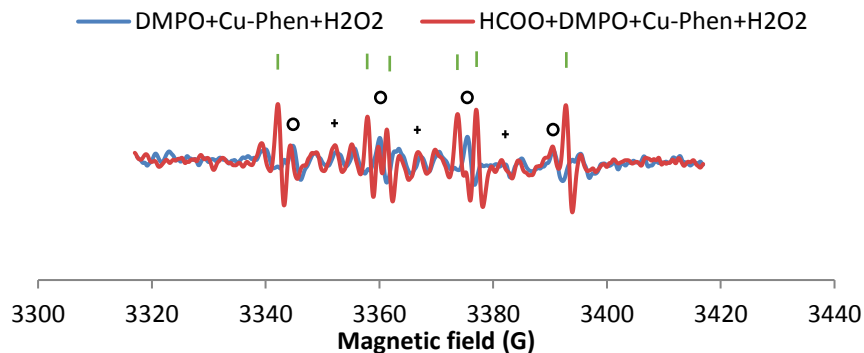


Figure V-41. X-band EPR spectra of NaOH+DMPO+Cu-Phen+H₂O₂ and NaOH+DMSO+DMPO+Cu-Phen+H₂O₂ - The simulations revealed the presence of several radical species. Without DMSO: DMPO-OH, $a_N = 15.439$ G, $a_H = 15.049$ G; DMPO-R, $a_N = 15.79$ G, $a_H = 23.488$ G; triplet, $a_N = 14.646$ G. With DMSO: DMPO-OH, $a_N = 13.926$ G, $a_H = 14.072$ G; DMPO-CH₃, $a_N = 15.937$ G, $a_H = 22.658$ G; triplet, $a_N = 14.788$ G - Assignments: o=DMPO-OH, |=DMPO-CH₃, +=triplet

When adding Cu-Phen to activate H₂O₂, a DMPO-OH signal appeared. HO• scavenging with DMSO led to the disappearance of the DMPO-OH signal and the apparition of DMPO-CH₃, thus confirming that the DMPO-OH signal was due to hydroxyl radicals.

The other scavenger, sodium formate, was also tested, see Figure V-42.



**Figure V-42. X-band EPR spectra of NaOH+DMPO+Cu-Phen+H₂O₂ and NaOH+HCOO⁻+DMPO+Cu-Phen+H₂O₂ – With HCOO⁻, the simulation revealed the presence of four radical species: DMPO-OH, $a_N = 15.342$ G, $a_H = 15.537$ G; DMPO-R, $a_N = 15.742$ G, $a_H = 24.123$ G (minor); triplet, $a_N = 14.691$ G; DMPO-COO⁻, $a_N = 15.805$ G, $a_H = 19.049$ G
Assignments: o=DMPO-OH, +=triplet, |=DMPO-COO⁻**

In Figure V-42, DMPO-OH was replaced by DMPO-COO⁻ when adding the formate scavenger. This result confirms the conclusion raised after DMSO scavenging, i.e. that the H_2O_2/Cu -Phen system produced some hydroxyl radicals at strong alkaline pH.

The generation of hydroxyl radicals at room temperature and alkaline pH with the H_2O_2/Cu -Phen system was less intense than at lower pH. To assess whether it would increase with time, the EPR signal was recorded a few minutes after the first acquisition, see Figure V-43.

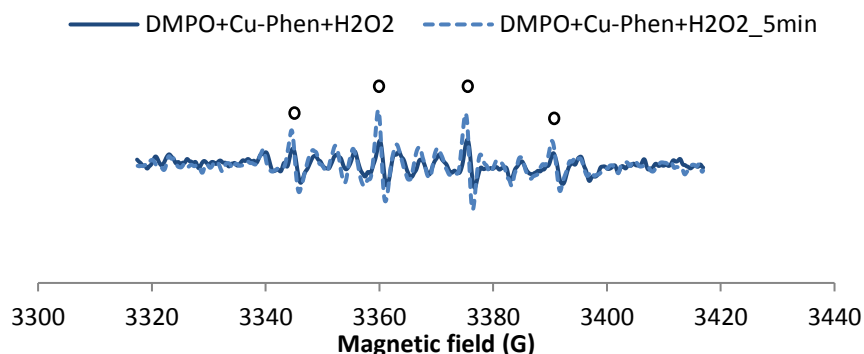


**Figure V-43. X-band EPR spectra of NaOH+DMPO+Cu-Phen+H₂O₂ at t=0 and at t=5 min
Assignments: o=DMPO-OH**

Figure V-43 illustrates the continuous increase of the signal's intensity: the DMPO-OH signal was more intense 5 minutes after the first signal acquisition (the peak heights were doubled), and even after 10 min (not shown). Hence, the radical formation was less intense than at near-neutral pH, but also slower.

This slower radical flow is an interesting observation: under alkaline conditions, Cu-Phen may allow the regulation of H_2O_2 's decomposition, and a slower HO[•] generation may even favor dye color-stripping.

- $H_2O_2 + CuSO_4$

The $H_2O_2/CuSO_4$ system was then tested and compared to $CuSO_4$ alone at alkaline pH, see Figure V-44.

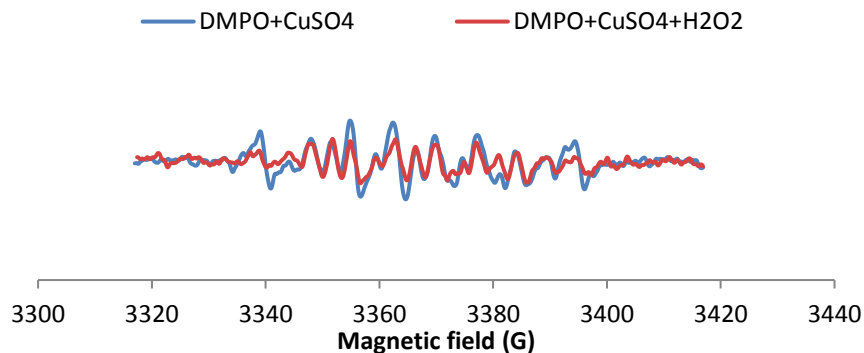


Figure V-44. X-band EPR spectra of NaOH+DMPO+CuSO₄ and NaOH+DMPO+CuSO₄+H₂O₂

As shown in Figure V-44, the spectrum of H₂O₂+CuSO₄ was very close to that of CuSO₄ alone at alkaline pH. Hence, no hydroxyl radicals were detected, as observed at near neutral pH. However, when the solution was heated, a slight hydroxyl radical generation was evidenced. This is likely to be due to H₂O₂ decomposition at high temperature rather than to the presence of Cu.

V.4.2.3.iii Conclusions

Under strong alkaline conditions, DMPO was degraded faster than at near-neutral pH. Kadla and Cornman reported similar signals (a carbonated adduct and a triplet with $a_N = 16.4$ G) when studying alkaline H₂O₂ with cyanamide at pH 13 [52].

The H₂O₂/Cu-Phen system produced hydroxyl radicals at alkaline pH even at room temperature, but not as much as at near-neutral pH: the generation seemed to be lower and slower. On the other hand, H₂O₂/CuSO₄ produced traces of hydroxyl radicals only at high temperature.

Cu-Phen alone induced slight HO• generation at room temperature, probably due to soluble oxygen degradation, as observed at lower pH (but only at high temperature).

Compared to near-neutral pH, DMSO was found to be an effective HO• scavenger at strong alkaline pH.

As seen earlier, at alkaline pH, the copper-phenanthroline-hydroxyl speciation is very different from near-neutral pH. Especially, the Cu-Phen complexes are hydroxylated (CuPhen(OH)₂ being the major compound). It is likely that this hydroxylation of Cu in the presence of Phen stabilizes the complex, which would explain a lower redox potential and therefore a weaker and slower hydroxyl radical generation. In the presence of Phen, hydroxylated Cu is formed, which is probably even harder to reduce into Cu^I to start a redox cycle.

To go further in the modelling of the oxidative system on a dyed pulp, similar experiments were carried out in the presence of substrate: dyes or fibers.

V.4.2.4 The H₂O₂/Cu-Phen system with substrate

V.4.2.4.i With dyes

The first substrate to be tested was dyes. Both near-neutral and strong alkaline pH were studied. Two concentrations were tested: either 10 μM to obtain a dye:Cu ratio of 1:1.5, or 50 μM for an excess of dye.

The addition of DR81L to the H₂O₂/Cu-Phen system was first tested at near-neutral pH. The results are gathered in Figure V-45.

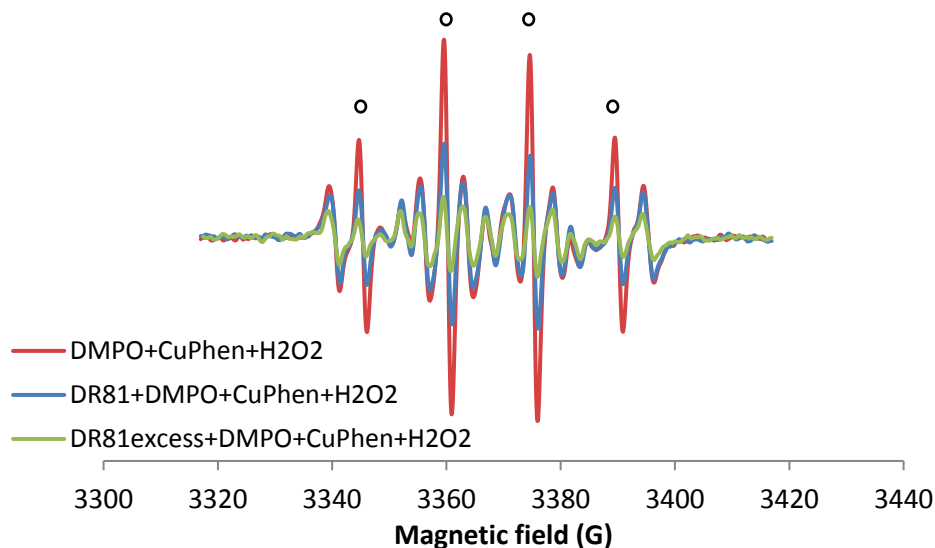


Figure V-45. X-band EPR spectra of DMPO+Cu-Phen+H₂O₂ with and without the addition of the DR81L dye - Assignments: o=DMPO-OH

The addition of the DR81L dye was observed to slow down the apparition of DMPO-OH. Two phenomena may be responsible for this effect: either (1) the inhibition of copper due to the coordination between copper and the dye, thus directly reducing the generation of hydroxyl radicals, or (2) the “scavenging” of HO• by the dye, if hydroxyl radicals are more reactive towards the dye than towards DMPO, thus reducing the spin-trapping but not the generation of radicals.

The same experiment was repeated with the DY11L dye, as shown in Figure V-46.

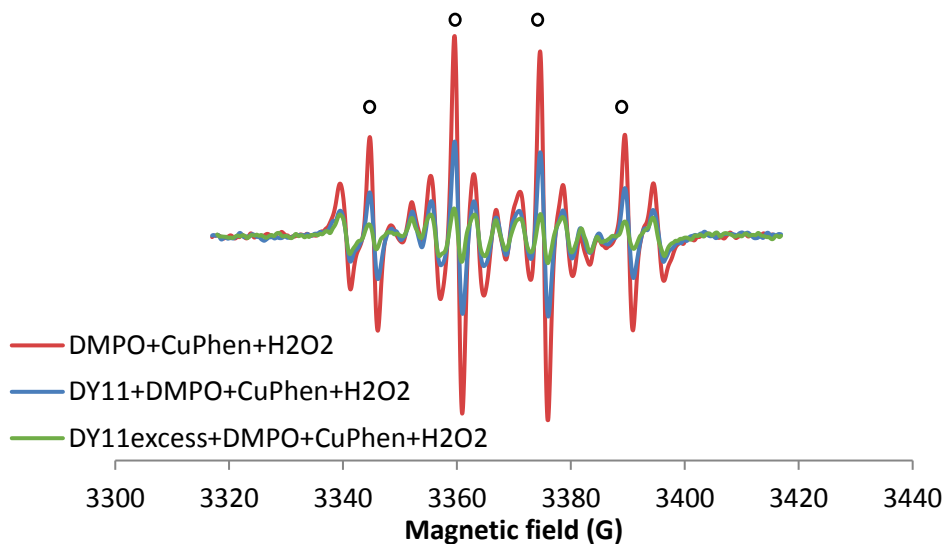


Figure V-46. X-band EPR spectra of DMPO+Cu-Phen+H₂O₂ with and without the addition of the DY11L dye - Assignments: o=DMPO-OH

The DY11L dye had the same slowing effect as DR81L on DMPO-OH formation.

The same experiments conducted at strong alkaline pH on DR81L and DY11L did not exhibit any visible effect (the spectrum was unchanged, results not shown). It might be due to the rather low

and slow hydroxyl radical generation already in the absence of dye. Another explanation would be that the dye inhibits radical formation or HO• spin-trapping only at near-neutral pH.

To conclude, the dye/H₂O₂/Cu-Phen system was confirmed to be difficult to analyze by EPR/spin-trapping. The tested dyes were found to limit the detection of radicals, by inhibiting either their formation or their detection, at least at near-neutral pH.

After aqueous dyes, the oxidative system was analyzed in the presence of a solid substrate: cellulosic fibers.

V.4.2.4.ii With cellulosic fibers

The objective of this study was to evaluate whether fibers were able to accelerate HO• generation. If so, further trials would consist in representing our substrate with dyed fibers. Only strong alkaline pH was tested in this case, with the H₂O₂/Cu-Phen system. The results are shown in Figure V-47.

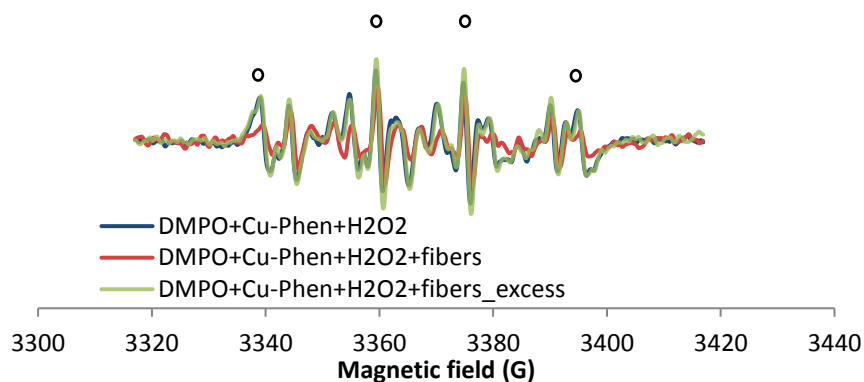


Figure V-47. X-band EPR signal of NaOH+DMPO+Cu-Phen+H₂O₂ with and without cellulosic fibers - Assignments: o=DMPO-OH

No clear effect was observed in the presence of fibers: neither acceleration nor slowing down. One idea was to increase the concentration of the cellulosic substrate by replacing it with Avicel. However, Avicel was shown earlier to bind strongly to copper. It would thus be very difficult to conclude. This is why further analyses were not conducted.

V.4.2.5 Conclusions

In conclusion, these EPR/spin-trapping investigations at ambient temperature confirmed the generation of hydroxyl radicals with copper(II)-activated hydrogen peroxide, whatever the pH. Yet, two systems were distinguished:

- at near-neutral pH, an intense HO• production was found, and the H₂O₂/Cu-Phen system seemed to produce more radicals than H₂O₂/CuSO₄ and a similar amount as the Fenton reactant (H₂O₂/FeSO₄ at pH 3),
- at strong alkaline pH, a rather low but more continuous flow of HO• was observed, with H₂O₂/Cu-Phen only.

The addition of substrate such as the dyes or fibers was found to complicate the understanding of the activated H₂O₂ oxidative system, since both substrates interacted with the spin-trap. Consequently, it was impossible to study the influence of the substrate on HO• formation, as well as the selectivity of these radicals towards the dyes and cellulose fibers.

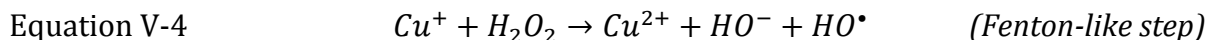
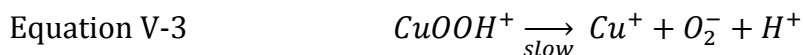
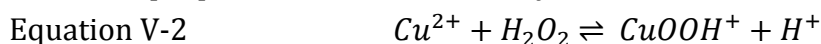
V.5 PROPOSITION OF A FENTON-LIKE MECHANISM

In the first part of this chapter, the possibility of a catalytic mechanism was investigated. The idea was that Cu²⁺ may oxidize the dye or cellulose and thus be reduced into Cu⁺, which would be reconverted into Cu²⁺ by reacting with H₂O₂. The complexation of Cu by Phen would be in favor of the oxidation of the substrate (more adequate potential of Cu-Phen complexes), and, most importantly, Phen would stabilize Cu²⁺, since without Phen, CuSO₄ tends to precipitate.

Such a catalytic cycle (reduction of Cu^{II} by a “substrate” into Cu^I, followed by reoxidation of Cu^I into Cu^{II} by H₂O₂) may work at both near-neutral and strong alkaline pHs. It is inspired by the mechanism proposed by Halma and coworkers [3] at alkaline pH, with the dye or cellulose as a new substrate instead of lignin (Figure V-1). The main feature is that when Cu^I is reoxidized back to Cu^{II}, it participates to a Fenton-like step, thus generating hydroxyl radicals by decomposition of H₂O₂.

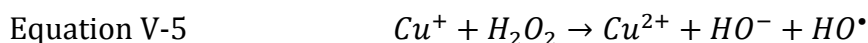
Other catalytic routes involving the reduction of Cu^{II} were explored by Perez-Benito at near-neutral pH. In a kinetic study based on the “initial-rate method”, the author found three routes for the decomposition of H₂O₂ by Cu^{II}. All these routes involved free radicals.

The route proposed in the case of catalytic amounts of Cu²⁺ was the following [53]:

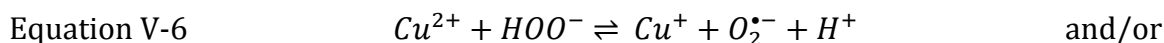


In this reaction path, Cu²⁺ would react with H₂O₂ to form a Cu^{II}-hydroperoxide complex, which would be further reduced into Cu^I after unimolecular decomposition via homolytic cleavage of the Cu-O bond. The last step is again a Fenton-like reaction between Cu⁺ and H₂O₂.

In this chapter, the radical way was thoroughly explored using EPR/spin-trapping. Note that the study was conducted at room temperature. Therefore, slight differences at high temperature probably resulted in significant differences at room temperature, thus providing more clues on the reaction mechanisms under different conditions. At near-neutral pH, H₂O₂ was proved to decompose into hydroxyl radicals in the presence of Cu^{II}: at room temperature, strong decomposition was observed with H₂O₂/Cu-Phen and some (but much less) with H₂O₂/CuSO₄. A sudden and intense HO[•] flow was generated in that case. At strong alkaline pH, the decomposition only appeared with H₂O₂/Cu-Phen and it was a more regular and slow HO[•] generation. Two different mechanisms are thus probably responsible for the dye degradation, but both may involve the production of HO[•]. A Fenton-like mechanism could explain the efficacy of such systems. Cu^I would be converted into Cu^{II}, as proposed by the above cited authors, but also by Gierer and coworkers for the decomposition of H₂O₂ into hydroxyl radicals in the presence of metal ions, under alkaline conditions [23]. Once again, a preliminary step reducing Cu^{II} would be necessary. The mechanism starts with Cu^I.



To reconvert Cu^{II} into Cu^I, two reactions are possible under alkaline conditions:



The best pH for this pathway would be 11.6, as it is H₂O₂'s pK_a, so H₂O₂ has its minimum stability at that pH [23].

The HO• radicals formed via this Fenton-like mechanism would then react with organic substrates (dyes or cellulose here) via two ways:

- 1) Electrophilic addition to double bonds or aromatic nuclei of dyes
- 2) H-abstraction from aliphatic groups of cellulose, leading to peeling

Knowing that 1) is 10 times faster than 2) [23], the reaction should be selective towards the dye. However, the quantity of dye impregnated on fibers after pulp dyeing being very low compared to cellulose (314.5 μmol/kg of pulp in the main study, see II.1.4), h

droxyl radicals may act unpreferably on both cellulose and dyes as observed in the present study.

Finally, even though the formation of Cu^I was not proved, the results seem to be in favor of a catalytic mechanism involving H₂O₂ decomposition into hydroxyl radicals. The initiating step should be the reduction of Cu^{II}, either by the dye or cellulosic substrate, or by H₂O₂ itself, HOO• or O₂•⁻.

In all the activated color-stripping results (with and without fibers), both coordination and hydroxylation of Cu^{II} appeared to have a key importance in its ability to activate color-stripping. Detoni et al. [54] discussed the Lewis acidity of the Cu center in a study on the catalysis of H₂O₂ by Cu^{II}-Phen complexes with 1, 2 or 3 Phen. The Lewis acidity of Cu varies depending on its coordination. The most easily reduced complex was the most acid one, and the most active complex was indeed found to be (CuPhen₂Cl)Cl, over CuPhenCl₂ and (CuPhen₃)Cl₂. The latter, with 3 phenanthroline ligands, stabilized the oxidation state of Cu^{II} so much that it prevented electron transfer: no catalysis was observed. Therefore, it is likely that a compromise is necessary to modulate the activity of the complex so that it decomposes hydrogen peroxide sufficiently but not too strongly and rapidly. Indeed, this would allow good decolorization while avoiding strong cellulose depolymerization. According to the color-stripping trials presented in Chapter IV, this compromise was found at strong alkaline pH, with the 1:2 Cu-Phen complex, i.e. with a majority of CuPhen(OH)₂ in the medium.

In conclusion, two mechanisms are proposed, one at alkaline pH and the other one at near-neutral or weak alkaline pH. Both mechanisms involve a catalytic cycle.

Mechanism proposal at alkaline pH

The CuPhen(OH)₂ complex, predominant in alkaline medium for a Cu:Phen ratio of 1:2, would be the active species in the alkaline H₂O₂/Cu-Phen system. CuPhen(OH)₂ is fully soluble in the medium, whereas without Phen, CuSO₄ tends to precipitate as hydroxylates and limits the activation of H₂O₂. Phen probably acts as a stabilizer or solubilizer of Cu^{II}. In addition, the coordination of copper with Phen also modifies the redox potential of the Cu^{II}/Cu^I couple, which may enhance the oxidation of the substrate at a given pH. The following mechanism, similar to that suggested by Korpi *et al.* for activated oxygen delignification, is thus proposed in alkaline medium (Figure V-48).

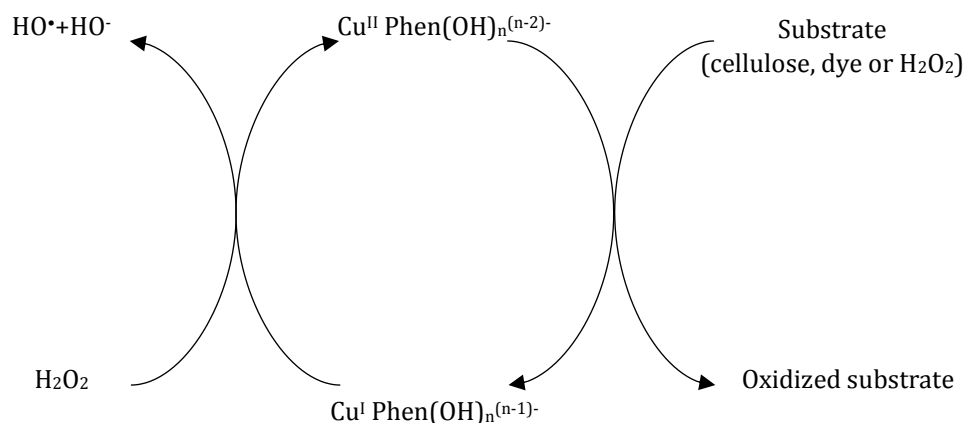


Figure V-48. Proposed mechanism for the $\text{H}_2\text{O}_2/\text{Cu-Phen}$ color-stripping system in alkaline medium

Assuming that $n = 2$, $\text{Cu}^{\text{II}}\text{Phen}(\text{OH})_2$ coordinates with the substrate: dye and cellulose. The phenanthroline ligand is then ejected from copper's environment: copper is probably linked only with the substrate and hydroxyls. Then, this Cu^{II} complex probably oxidizes the substrate, leading to partial cellulose and dye degradation. In parallel, the Cu^{II} complex is reduced into Cu^{I} , which is finally re-oxidized into Cu^{II} by H_2O_2 via a Fenton-like mechanism. During this step, H_2O_2 is reduced, generating hydroxyl radicals that strongly degrade the substrate. In such a catalytic system, the hydroxyl radicals are produced in a continuous way, maintaining a color-stripping activity until complete H_2O_2 consumption.

Mechanism proposal at near neutral pH

At near-neutral pH, both $\text{H}_2\text{O}_2/\text{Cu-Phen}$ and $\text{H}_2\text{O}_2/\text{CuSO}_4$ systems were efficient for the color-stripping of dyed pulps. $\text{H}_2\text{O}_2/\text{CuSO}_4$ had a similar color-stripping efficiency as $\text{H}_2\text{O}_2/\text{Cu-Phen}$ at alkaline pH but oxidized cellulose extensively, and $\text{H}_2\text{O}_2/\text{Cu-Phen}$ was less efficient than in alkaline medium.

In neutral medium, EPR analyses at 100 K clearly showed that CuSO_4 was reduced by H_2O_2 into Cu^{I} species, in the absence of any substrate. After phenanthroline addition, the reduction of Cu^{II} was not detected, but it probably occurred as well. The presence of Phen does not seem necessary to activate H_2O_2 , however it avoids strong cellulose degradation. EPR/spin-trapping revealed a major difference between hydrogen peroxide decomposition at near-neutral and alkaline pH: at near-neutral pH, the system generated an intense and short-duration hydroxyl radical flow, similar to the Fenton system.

Cu^{II} should not oxidize the dye nor cellulose at neutral pH. A possible reaction on cellulose would be the oxidation of terminating aldehydes or carbonyl groups on the cellulose chain, which are present in very low amount (few millimoles per mol of anhydroglucose unit). This absence of cellulose oxidation, along with the observation of copper reduction in the absence of substrate (whereas no reduction was observed at alkaline pH), suggests that the only possible substrate for the catalytic mechanism is H_2O_2 . The reacting species would thus be either $(\text{Cu}^{\text{II}} + \text{H}_2\text{O}_2)$, or $(\text{Cu}^{\text{II}}\text{-Phen}_n + \text{H}_2\text{O}_2)$. The proposed mechanism is given in Figure V-49.

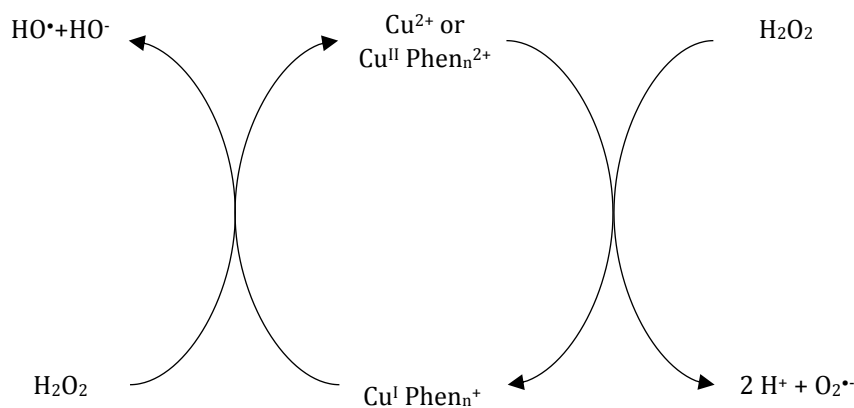


Figure V-49. Proposed mechanism for the H₂O₂/Cu-Phen or H₂O₂/CuSO₄ color-stripping system in near-neutral medium

Since without Phen, the HO[•] production was weak, the active species in that case is rather the copper complex Cu(Phen)₂²⁺ (given by the predicted speciation for a Cu:Phen ratio of 1:2). In the presence of H₂O₂, this complex would lead to a Cu-H₂O₂ coordinate, namely Cu^{II}-OOH⁺ according to Perez-Benito (or possibly Cu^{II}-Phen_n-OOH⁺, if one assumes a peroxide coordinate stabilized by Phen), which is further reduced into Cu^I. Then, Cu^I is re-oxidized into Cu^{II} and H₂O₂ is reduced, leading to hydroxyl radical generation.

In conclusion, in alkaline medium, the catalytic cycle would be initiated by the oxidation of the dye and/or cellulose by Cu^{II} species, whereas in neutral medium, the dye substrate would not participate to the catalytic cycle: the decomposition of H₂O₂ by Cu^{II} species would be the only reaction responsible for substrate (dye and cellulose) degradation.

The variation in HO[•] radical flows with pH may be explained by such mechanistic differences between neutral and alkaline medium. Under neutral conditions, an intense and short-duration HO[•] flow is produced as in conventional Fenton reaction with Fe^{II}/Fe^{III} in acidic medium, contrarily to the alkaline case for which the HO[•] flow is lower. In alkaline medium, the presence of hydroxyl groups in the copper environment modulates the decomposition of H₂O₂ by Cu^{II} species, and enables to activate substrate oxidation by hydroxylated Cu^{II}-Phen complexes. Nevertheless, since the major part of color-stripping and cellulose depolymerization originates from HO[•] radical production, significant substrate degradation prevails whatever the pH.

V.6 REFERENCES

- [1] C. Coucharriere, "Mise au point et étude d'un système d'activation du peroxyde d'hydrogène en délignification et blanchiment des pâtes chimiques," PhD thesis, University of Grenoble, France, 2000.
- [2] N. Marlin, C. Coucharriere, G. Mortha, D. Lachenal, P. Larnicol, and J. C. Hostachy, "Use of o-phenanthroline as a catalyst in hydrogen peroxide stages," in *Proceedings of the 13th International Symposium on Wood Fibre and Pulping Chemistry*, Auckland, New Zealand, 2005, pp. 29–34.

- [3] M. Halma, D. Lachenal, N. Marlin, A. Deronzier, M. C. Brochier, and M. Zarubin, "H₂O₂ oxidation of lignin model dimers catalyzed by copper(II)-phenanthroline," *Industrial Crops and Products*, vol. 74, pp. 514–522, Nov. 2015.
- [4] N. I. Vladut, V. Durrieu, J. Albet, J. Blanc, C. Calais, and G. Mortha, "Novel investigations on hydrogen peroxide bleaching catalysis by copper-phenanthroline complex," in *Proceedings*, Tianjin, China, 2011, vol. 2, pp. 715–720.
- [5] S. Das, "Pure cellulose production from wood by an environmentally friendly process using catalysed hydrogen peroxide," PhD thesis, University of Grenoble, 2012.
- [6] S. Das, D. Lachenal, and N. Marlin, "Production of pure cellulose from Kraft pulp by a totally chlorine-free process using catalyzed hydrogen peroxide," *Industrial Crops and Products*, vol. 49, pp. 844–850, Aug. 2013.
- [7] H. Korpi, P. J. Figiel, E. Lankinen, P. Ryan, M. Leskelä, and T. Repo, "On in situ prepared Cu-Phenanthroline complexes in aqueous alkaline solutions and their use in the catalytic oxidation of veratryl alcohol," *European Journal of Inorganic Chemistry*, vol. 2007, no. 17, pp. 2465–2471, Jun. 2007.
- [8] N. Terinte, R. Ibbett, and K. C. Schuster, "Overview on native cellulose and microcrystalline cellulose I structure studied by X-ray diffraction (WAXD): Comparison between measurement techniques," *Lenzinger Berichte*, vol. 89, pp. 118–131, 2011.
- [9] C. Pearce, "The removal of colour from textile wastewater using whole bacterial cells: a review," *Dyes and Pigments*, vol. 58, no. 3, pp. 179–196, Sep. 2003.
- [10] A. Srinivasan and T. Viraraghavan, "Decolorization of dye wastewaters by biosorbents: A review," *Journal of Environmental Management*, vol. 91, no. 10, pp. 1915–1929, Oct. 2010.
- [11] M.-S. Chiou, P.-Y. Ho, and H.-Y. Li, "Adsorption of anionic dyes in acid solutions using chemically cross-linked chitosan beads," *Dyes and Pigments*, vol. 60, no. 1, pp. 69–84, Jan. 2004.
- [12] J. Oakes and P. Gratton, "Kinetic investigations of azo dye oxidation in aqueous media," *Journal of the Chemical Society, Perkin Transactions 2*, no. 9, pp. 1857–1864, 1998.
- [13] C. Galindo and A. Kalt, "UV-H₂O₂ oxidation of monoazo dyes in aqueous media: a kinetic study," *Dyes and Pigments*, vol. 40, no. 1, pp. 27–35, Jan. 1999.
- [14] C. Hachem, F. Bocquillon, O. Zahraa, and M. Bouchy, "Decolourization of textile industry wastewater by the photocatalytic degradation process," *Dyes and Pigments*, vol. 49, no. 2, pp. 117–125, May 2001.
- [15] Z. Li, J. Sheng, Y. Wang, and Y. Xu, "Enhanced photocatalytic activity and stability of alumina supported hematite for azo-dye degradation in aerated aqueous suspension," *Journal of Hazardous Materials*.
- [16] M. Muruganandham and M. Swaminathan, "Solar driven decolourisation of Reactive Yellow 14 by advanced oxidation processes in heterogeneous and homogeneous media," *Dyes and Pigments*, vol. 72, no. 2, pp. 137–143, Jan. 2007.
- [17] W. Zhu, Z. Yang, and L. Wang, "Application of ferrous-hydrogen peroxide for the treatment of H-acid manufacturing process wastewater," *Water Research*, vol. 30, no. 12, pp. 2949–2954, Dec. 1996.

- [18] K. Swaminathan, S. Sandhya, A. Carmalin Sophia, K. Pachhade, and Y. . Subrahmanyam, "Decolorization and degradation of H-acid and other dyes using ferrous–hydrogen peroxide system," *Chemosphere*, vol. 50, no. 5, pp. 619–625, Feb. 2003.
- [19] P. Ghosh, L. K. Thakur, A. N. Samanta, and S. Ray, "Electro-Fenton treatment of synthetic organic dyes: Influence of operational parameters and kinetic study," *Korean Journal of Chemical Engineering*, vol. 29, no. 9, pp. 1203–1210, Sep. 2012.
- [20] L. Cheng, M. Wei, L. Huang, F. Pan, D. Xia, X. Li, and A. Xu, "Efficient H₂O₂ oxidation of organic dyes catalyzed by simple copper(II) ions in bicarbonate aqueous solution," *Industrial & Engineering Chemistry Research*, vol. 53, no. 9, pp. 3478–3485, Mar. 2014.
- [21] T. Reitberger and J. Gierer, "Chemiluminescence as a means to study the role of hydroxyl radicals in oxidative processes," *Holzforschung*, vol. 42, no. 6, pp. 351–356, 1988.
- [22] J. Gierer and T. Reitberger, "The Reactions of Hydroxyl Radicals with Aromatic Rings in Lignins, Studied with Creosol and 4-Methylveratrol," *Holzforschung*, vol. 46, no. 6, pp. 495–504, Jan. 1992.
- [23] J. Gierer, K. Jansbo, and T. Reitberger, "Formation of hydroxyl radicals from hydrogen peroxide and their effect on bleaching of mechanical pulps," *Journal of Wood Chemistry and Technology*, vol. 13, no. 4, pp. 561–581, Dec. 1993.
- [24] G. C. Hobbs and J. Abbot, "The role of radical species in peroxide bleaching processes.," *Appita J.*, vol. 45, no. Copyright (C) 2016 American Chemical Society (ACS). All Rights Reserved., pp. 344–8, 1992.
- [25] G. C. Hobbs and J. Abbot, "The role of the hydroxyl radical in peroxide bleaching processes," *Journal of Wood Chemistry and Technology*, vol. 14, no. 2, pp. 195–225, May 1994.
- [26] J. Bouchard, J. Wang, and R. Berry, "The role of hydroxyl and oxyl anion radicals in selectivity of oxygen delignification," *Holzforschung*, vol. 64, no. 2, pp. 153–159, Feb. 2010.
- [27] K. R. Naqvi, J. M. Marsh, S. Godfrey, M. G. Davis, M. J. Flagler, J. Hao, and V. Chechik, "The role of chelants in controlling Cu(II)-induced radical chemistry in oxidative hair colouring products," *International Journal of Cosmetic Science*, p. n/a–n/a, 2012.
- [28] S. Singh and R. C. Hider, "Colorimetric detection of the hydroxyl radical: Comparison of the hydroxyl-radical-generating ability of various iron complexes," *Analytical Biochemistry*, vol. 171, no. 1, pp. 47–54, May 1988.
- [29] C. Chirat and D. Lachenal, "Effect of hydroxyl radicals on cellulose and pulp and their occurrence during ozone bleaching," *Holzforschung*, vol. 51, no. 2, pp. 147–154, Jan. 1997.
- [30] F. Pouyet, C. Chirat, and D. Lachenal, "On the Origin of Cellulose Depolymerization During Ozone Treatment of Hardwood Kraft Pulp," *BioResources*, vol. 8, no. 4, Aug. 2013.
- [31] C. Lagercrantz and S. Forshult, "Trapping of Free Radicals formed by γ -Irradiation of Organic Compounds," *Nature*, vol. 218, no. 5148, pp. 1247–1248, Jun. 1968.
- [32] E. G. Janzen and B. J. Blackburn, "Detection and identification of short-lived free radicals by an electron spin resonance trapping technique," *Journal of the American Chemical Society*, vol. 90, no. 21, pp. 5909–5910, Oct. 1968.

- [33] S. Bhattacharjee, L. J. Deterding, S. Chatterjee, J. Jiang, M. Ehrenshaft, O. Lardinois, D. C. Ramirez, K. B. Tomer, and R. P. Mason, "Site-specific radical formation in DNA induced by Cu(II)-H₂O₂ oxidizing system, using ESR, immuno-spin trapping, LC-MS, and MS/MS," *Free Radical Biology and Medicine*, vol. 50, no. 11, pp. 1536–1545, Jun. 2011.
- [34] S. Backa, K. Jansbo, and T. Reitberger, "Detection of Hydroxyl Radicals by a Chemiluminescence Method - A Critical Review," *Holzforschung*, vol. 51, no. 6, pp. 557–564, Jan. 1997.
- [35] I. Kraljić and C. N. Trumbore, "p-nitrosodimethylaniline as an OH radical scavenger in radiation chemistry," *Journal of the American Chemical Society*, vol. 87, no. 12, pp. 2547–2550, Jun. 1965.
- [36] P. M. Hanna and R. P. Mason, "Direct evidence for inhibition of free radical formation from Cu(I) and hydrogen peroxide by glutathione and other potential ligands using the EPR spin-trapping technique," *Archives of Biochemistry and Biophysics*, vol. 295, no. 1, pp. 205–213, May 1992.
- [37] G. R. Buettner, "Spin Trapping: ESR parameters of spin adducts 1474 1528V," *Free Radical Biology and Medicine*, vol. 3, no. 4, pp. 259–303, 1987.
- [38] E. Finkelstein, G. M. Rosen, and E. J. Rauckman, "Spin trapping of superoxide and hydroxyl radical: Practical aspects," *Archives of Biochemistry and Biophysics*, vol. 200, no. 1, pp. 1–16, Mar. 1980.
- [39] R. L. Legge, J. E. Thompson, and J. E. Baker, "Free radical-mediated formation of ethylene from 1-aminocyclopropane-1-carboxylic acid: a spin-trap study," *Plant Cell Physiol*, vol. 23, no. 2, pp. 171–177, Jan. 1982.
- [40] M. M. Mossoba, K. Makino, P. Riesz, and R. C. Perkins, "Long-range proton hyperfine coupling in alicyclic nitroxide radicals by electron paramagnetic resonance," *J. Phys. Chem.*, vol. 88, no. 20, pp. 4717–4723, Sep. 1984.
- [41] E. Finkelstein, G. M. Rosen, and E. J. Rauckman, "Spin trapping. Kinetics of the reaction of superoxide and hydroxyl radicals with nitrones," *Journal of the American Chemical Society*, vol. 102, no. 15, pp. 4994–4999, Jul. 1980.
- [42] B. C. Gilbert, S. Silvester, and P. H. Walton, "Spectroscopic, kinetic and mechanistic studies of the influence of ligand and substrate concentration on the activation by peroxides of CuI-thiolate and other CuI complexes," *Journal of the Chemical Society, Perkin Transactions 2*, no. 6, pp. 1115–1122, 1999.
- [43] A. J. Carmichael, M. M. Mossoba, P. Riesz, and I. Rosenthal, "Food dye-sensitized photoreactions in aqueous media," *Photobiochemistry and photobiophysics*, vol. 10, pp. 13–21, 1985.
- [44] P. M. Hanna, W. Chamulitrat, and R. P. Mason, "When are metal ion-dependent hydroxyl and alkoxyl radical adducts of 5,5-dimethyl-1-pyrroline N-oxide artifacts?," *Archives of Biochemistry and Biophysics*, vol. 296, no. 2, pp. 640–644, Aug. 1992.
- [45] M. J. Burkitt, S. Ying Tsang, S. Ching Tam, and I. Bremner, "Generation of 5,5-Dimethyl-1-pyrroline N-Oxide Hydroxyl and Scavenger Radical Adducts from Copper/H₂O₂Mixtures: Effects of Metal Ion Chelation and the Search for High-Valent Metal-Oxygen Intermediates," *Archives of Biochemistry and Biophysics*, vol. 323, no. 1, pp. 63–70, Oct. 1995.

- [46] K. Makino, T. Hagiwara, and A. Murakami, "A mini review: Fundamental aspects of spin trapping with DMPO," *International Journal of Radiation Applications and Instrumentation. Part C. Radiation Physics and Chemistry*, vol. 37, no. 5–6, pp. 657–665, 1991.
- [47] F. Nerud, P. Baldrian, J. Gabriel, and D. Ogbeifun, "Decolorization of synthetic dyes by the Fenton reagent and the Cu/pyridine/H₂O₂ system," *Chemosphere*, vol. 44, no. 5, pp. 957–961, Aug. 2001.
- [48] F. A. Villamena, E. J. Locigno, A. Rockenbauer, C. M. Hadad, and J. L. Zweier, "Theoretical and Experimental Studies of the Spin Trapping of Inorganic Radicals by 5,5-Dimethyl-1-Pyrroline N-Oxide (DMPO). 1. Carbon Dioxide Radical Anion," *J. Phys. Chem. A*, vol. 110, no. 49, pp. 13253–13258, Dec. 2006.
- [49] R. D. Willett and K. 'un Chang, "The crystal structure of copper(II) chloride bis(dimethylsulphoxide)," *Inorganica Chimica Acta*, vol. 4, pp. 447–451, 1970.
- [50] V. O. Sippola and A. O. I. Krause, "Bis(o-phenanthroline)copper-catalysed oxidation of lignin model compounds for oxygen bleaching of pulp," *Catalysis Today*, vol. 100, no. 3–4, pp. 237–242, Feb. 2005.
- [51] B. Gueneau, N. Marlin, A. Deronzier, and D. Lachenal, "Pulp delignification with oxygen and copper(II)-polyimine complexes," *Holzforschung*, vol. 68, no. 4, Jan. 2014.
- [52] J. F. Kadla and C. R. Cornman, "An EPR investigation into the reactions of alkaline hydrogen peroxide with cyanamide," *Journal of the Chemical Society, Perkin Transactions 2*, no. 10, pp. 2309–2314, 1998.
- [53] J. F. Perez-Benito, "Reaction pathways in the decomposition of hydrogen peroxide catalyzed by copper(II)," *Journal of Inorganic Biochemistry*, vol. 98, no. 3, pp. 430–438, Mar. 2004.
- [54] C. Detoni, N. M. F. Carvalho, D. A. G. Aranda, B. Louis, and O. A. C. Antunes, "Cyclohexane and toluene oxidation catalyzed by 1,10-phenantroline Cu(II) complexes," *Applied Catalysis A: General*, vol. 365, no. 2, pp. 281–286, Aug. 2009.

CONCLUSION

Conclusion

With the goal to encourage the reuse of high quality recovered cellulosic fibers to produce printing and writing paper or market deinked pulp, our approach was to improve the bleaching of these recovered fibers by reducing its cost and environmental impact.

The main purpose of this thesis was to assess whether copper-phenanthroline could improve the color-stripping of dyed cellulosic fibers by hydrogen peroxide, and how. Indeed, answering these questions was considered as a first step towards the enhancement of hydrogen peroxide in the bleaching of high quality recovered fibers. Three main issues were investigated to solve this problem:

- (1) Does copper-phenanthroline alone have an effect on the dye?
- (2) Does copper-phenanthroline improve the color-stripping of a dyed pulp by hydrogen peroxide?
- (3) How does the hydrogen peroxide/copper-phenanthroline system improve dye color-stripping?

The study of the copper-phenanthroline/dye system with the DR81L red dye provided information on the interactions between copper, phenanthroline, and the dye. Copper-phenanthroline was found to be coordinated to the dye, with more or less replacement of the phenanthroline ligand depending on the pH conditions and quantity of phenanthroline. The complexation of copper with the dye was found to result in apparent decolorization of the dye solution, which was not expected.

After this interesting finding in the absence of oxidant and fibers, the second part of our work consisted in applying color-stripping treatments on dyed pulps. Again in the absence of oxidant, trials with copper-phenanthroline and copper sulfate alone were found to have a slight decolorizing effect. This effect was limited due to the heterogeneity of the medium and to the attachment of dyes to cellulosic fibers. Hence, it is only when introducing hydrogen peroxide that significant color-stripping was observed. Both copper sulfate and copper-phenanthroline enhanced the decolorization, copper-phenanthroline being more efficient at strong alkaline pH. In all these oxidative treatments, dye removal was accompanied with severe cellulose degradation, especially at near-neutral pH. This result was in accordance with the hypothesis of a radical reaction, which was investigated in the third part of this work.

In the third part, we examined the possible mechanism responsible for the improvement of dye color-stripping by activated hydrogen peroxide. For this purpose, only aqueous analyses were carried out. The possibility of a catalytic cycle was first investigated by analyzing the state of Cu by EPR spectroscopy, assuming that the mechanism would involve the redox properties of copper. Copper(II) would be reduced into copper(I) and reoxidized into copper(II) to complete a cyclic pathway. Copper(I) was not detected, yet this hypothesis was not rejected. Then, the formation of radicals was followed using several techniques including EPR/spin-trapping, and strong decomposition of hydrogen peroxide into hydroxyl radicals was found, evidencing that copper activated the generation of hydroxyl radicals, probably via a Fenton-like mechanism. The variation of radical flow depending on pH and coordination of copper suggested that the decomposition of hydrogen peroxide was related to the redox properties of copper, since these are modified with the above cited parameters (pH, coordination). Consequently, it seems that the two approaches – catalysis and radical way – met, and that the most probable mechanism is a catalytic cycle involving hydrogen peroxide decomposition into hydroxyl radicals.

Finally, all these findings converge to answer our main research question. Indeed, copper-phenanthroline was proved to improve the color-stripping of dyed cellulosic fibers. The mechanism probably involves interactions between copper and the dye, as evidenced in the first part, and a catalytic cycle leading to the decomposition of hydrogen peroxide into hydroxyl radicals.

A mechanism was proposed for this catalytic cycle. Its first step would be the reduction of the Cu(II) species into Cu(I) by reaction with a substrate. At alkaline pH, the substrate would be the dye and cellulose, whereas at neutral pH, it would be H₂O₂ itself. Then, the generated Cu(I) would react with H₂O₂, thus producing hydroxyl radicals that are able to degrade the dye. However, hydroxyl radicals are not selective and also impair the degree of polymerization of cellulose. Yet, according to the dyed-pulp color-stripping results, the physical properties of the pulp should not be significantly affected. Another major difference observed between neutral and alkaline conditions was the nature of the hydroxyl radical flow. In neutral medium, an intense and short-duration flow was produced as in the Fenton reactant, whereas in alkaline medium, the radical flow was less intense and more even. The pH could thus be used to regulate the radical flow.

Overall, the conclusions of our investigations tend to confirm the hypothesis of Vladut et al. that the main oxidant in the hydrogen peroxide/copper-phenanthroline system is the hydroxyl radical. However, this is not incompatible with a catalytic route similar to that proposed by Coucharrière and Halma et al. In the present case, the scheme is applied on an almost lignin-free substrate, so that the first step, i.e. the reduction of copper(II), should involve a substrate other than lignin. In our study, this may occur not only at alkaline pH as commonly used in the pulp bleaching studies mentioned above, but also at near-neutral pH. Therefore, hydrogen peroxide could be enhanced not only during the strong alkaline bleaching of deinked pulp, but also during the weak alkaline pulping of deinked pulp. During bleaching, the activator should not prevent the action of hydrogen peroxide on lignin, since it was already shown to improve it in numerous delignification studies. In addition, the detection of interactions between the dye and copper-phenanthroline opened various means of application of copper sulfate or copper-phenanthroline in the absence of any oxidant. Dyes in paper or textile effluents could coordinate to copper (with or without phenanthroline) and, depending on the pH and concentrations, either (1) be apparently decolorized thanks to the hypochromic effect of the complexation, or (2) be precipitated and further removed, allowing the recovery of solid dye, copper, and phenanthroline.

For future research, it would be interesting to carry out further trials to propose an effluent treatment process based on the dye/copper-phenanthroline interactions. Regarding the color-stripping of pulp, the process parameters should be optimized, then trials could be conducted in the presence of other chromophores (native and kraft lignin), and finally on deinked pulp, to confirm the feasibility of our project to improve deinked pulp bleaching and reduce the use of reductive bleaching agents. Another promising research goal would be to confirm the catalytic route by a comprehensive mechanistic study, at least involving the detection of copper(I) compounds. Indeed, this would be useful for the improvement of both deinked pulp bleaching and delignification.

As a result of our material choices and methodology, the study encountered some limitations, which need to be considered for future research. First, the DY11L and DR81L dyes were commercial paper dyes. These paper dye solutions were useful to obtain representative results in the pulp bleaching trials, but their unknown formulations complicated the understanding of the

Conclusion

chemical behavior of the studied system. Therefore, theoretical investigations should first be conducted with pure dyes, and commercial dyes should be tested in a second step. Secondly, the EPR studies were difficult to conduct in the conditions of our trials (heterogeneous medium, high temperature) and the interactions between copper and the spin-trap also limited further discussion. Yet, the results found at room temperature allowed to discriminate the influence of different parameters such as coordination with phenanthroline, pH, etc., whereas high temperature trials actually displayed lower differences, which were thus more difficult to discuss.

To conclude, this work proved that the copper-phenanthroline complex enhances hydrogen peroxide for the color-stripping of azo dyes and dyed pulp. It also provided evidence that phenanthroline acts as a stabilizer to adjust the solubility, stability and redox potential of copper(II), but may not be indispensable. The results of our mechanistic study supported the hypothesis of substrate oxidation by radical formation rather than by hydrogen peroxide itself, this mechanism being probably part of a catalytic cycle. The high "screening effect" of cellulose capturing the major part of the radical flow was unavoidable, probably explaining the partial (and not full) decolorization of the dyed pulp. Therefore, along with further research proposed based on our conclusions, this work should contribute to the improvement of deinked pulp bleaching as well as wastewater treatment in the pulp and textile industries.

Beyond the original context of recovered cellulosic fiber color-stripping, this thesis revealed the great potential of hydrogen peroxide/copper-phenanthroline as a hydroxyl radical generating system. Various fields of application arise, such as advanced oxidation processes (AOPs), polymer science, chemical synthesis (oxidative coupling reactions), or biomass deconstruction.

ANNEXES

TABLE OF CONTENTS

LIST OF FIGURES	266
LIST OF TABLES	266
ANNEX 1.....	268
ANNEX 2.....	271

LIST OF FIGURES

Figure 1. Experimental X-band EPR spectra recorded at 100 K in frozen aqueous solutions of (a) CuSO ₄ and CuSO ₄ +DY11L (b) Cu-Phen and Cu-Phen+DY11L (c) CuSO ₄ +DY11L and Cu-Phen+DY11L, at pH 6.5, with Cu:Phen = 1:2, DY11L:Cu = 10:1.5 and [Cu] = 1.5 mM.....	268
Figure 2. Experimental X-band EPR spectra recorded at 100 K in frozen aqueous solutions of (a) CuSO ₄ and CuSO ₄ +DY11L (b) Cu-Phen and Cu-Phen+DY11L (c) CuSO ₄ +DY11L and Cu-Phen+DY11L, at pH 12.3, with Cu:Phen = 1:2, DY11L:Cu = 10:1.5 and [Cu] = 1.5 mM	269
Figure 3. Experimental X-band EPR spectra recorded at 100 K in frozen aqueous solutions of (a) CuSO ₄ +DY11L and CuSO ₄ +DY11L+H ₂ O ₂ , (b) Cu-Phen+DY11L and Cu-Phen+DY11L+H ₂ O ₂ , at pH 12.3, with Cu:Phen = 1:2, DY11L:Cu = 10:1.5, Cu:H ₂ O ₂ = 1:1 and [Cu] = 1.5 mM.....	270
Figure 4. Comparison between the experimental and simulated spectra of DMPO+Cu-Phen	271
Figure 5. Comparison between the experimental and simulated spectra of DMSO+DMPO+Cu-Phen+H ₂ O ₂	272
Figure 6. Comparison between the experimental and simulated spectra of HCOO ⁻ +DMPO+Cu-Phen+H ₂ O ₂	273

LIST OF TABLES

Table 1. DMPO+Cu-Phen – Simulation results.....	271
Table 2. DMSO+DMPO+Cu-Phen+H ₂ O ₂ – Simulation results	272
Table 3. HCOO ⁻ +DMPO+Cu-Phen+H ₂ O ₂ – Simulation results	272
Table 5. DMPO+CuSO ₄ – Simulation results	273

Table 6. HCOO ⁻ +DMPO+Cu-Phen+H ₂ O ₂ t=5 min – Simulation results	273
Table 7. HCOO ⁻ +DMPO+Cu-Phen+H ₂ O ₂ after heating – Simulation results	273
Table 8. DMPO+CuSO ₄ +H ₂ O ₂ – Simulation results.....	274
Table 9. DMSO+DMPO+CuSO ₄ +H ₂ O ₂ – Simulation results.....	274
Table 10. HCOO ⁻ +DMPO+CuSO ₄ +H ₂ O ₂ – Simulation results	274
Table 11. DMPO+FeSO ₄ +H ₂ O ₂ at pH 3 – Simulation results.....	274
Table 12. DMSO+DMPO+CuSO ₄ – Simulation results.....	275
Table 13. DMSO+DMPO+Cu-Phen – Simulation results	275
Table 14. HCOO ⁻ +DMPO+Cu-Phen – Simulation results	275
Table 15. HCOO ⁻ +DMPO+Cu-Phen after heating – Simulation results	275
Table 16. DMPO+H ₂ O ₂ after heating – Simulation results	276
Table 17. NaOH+DMPO+CuSO ₄ – Simulation results	276
Table 18. NaOH+DMPO+Cu-Phen – Simulation results.....	276
Table 19. NaOH+HCOO ⁻ +DMPO+Cu-Phen t=8 min – Simulation results.....	276
Table 20. NaOH+DMPO+Cu-Phen+H ₂ O ₂ – Simulation results	277
Table 21. NaOH+DMSO+DMPO+Cu-Phen+H ₂ O ₂ – Simulation results.....	277
Table 22. NaOH+HCOO ⁻ +DMPO+Cu-Phen+H ₂ O ₂ – Simulation results	277
Table 23. Integration and simulation results: total peak area, and distribution of DMPO adducts and degradation products for some experiments, as relative areas of each radical, in percents.	278

ANNEX 1

The supplementary material presented here provides information on the analysis of DY11L in the presence of CuSO_4 or Cu-Phen at both near-neutral and strong alkaline pH, plus some tests at alkaline pH with hydrogen peroxide. The exact same trials performed on DR81L were presented in V.2.2.2.

The analyses on DY11L were performed with an excess of dye compared to copper, i.e. with $[\text{DY11L}] = 10 \text{ mM}$, since the same system with DR81L was found to display strong coordination at that concentration. The results are shown in Figure 1. for near-neutral conditions and Figure 2 for strong alkaline conditions.

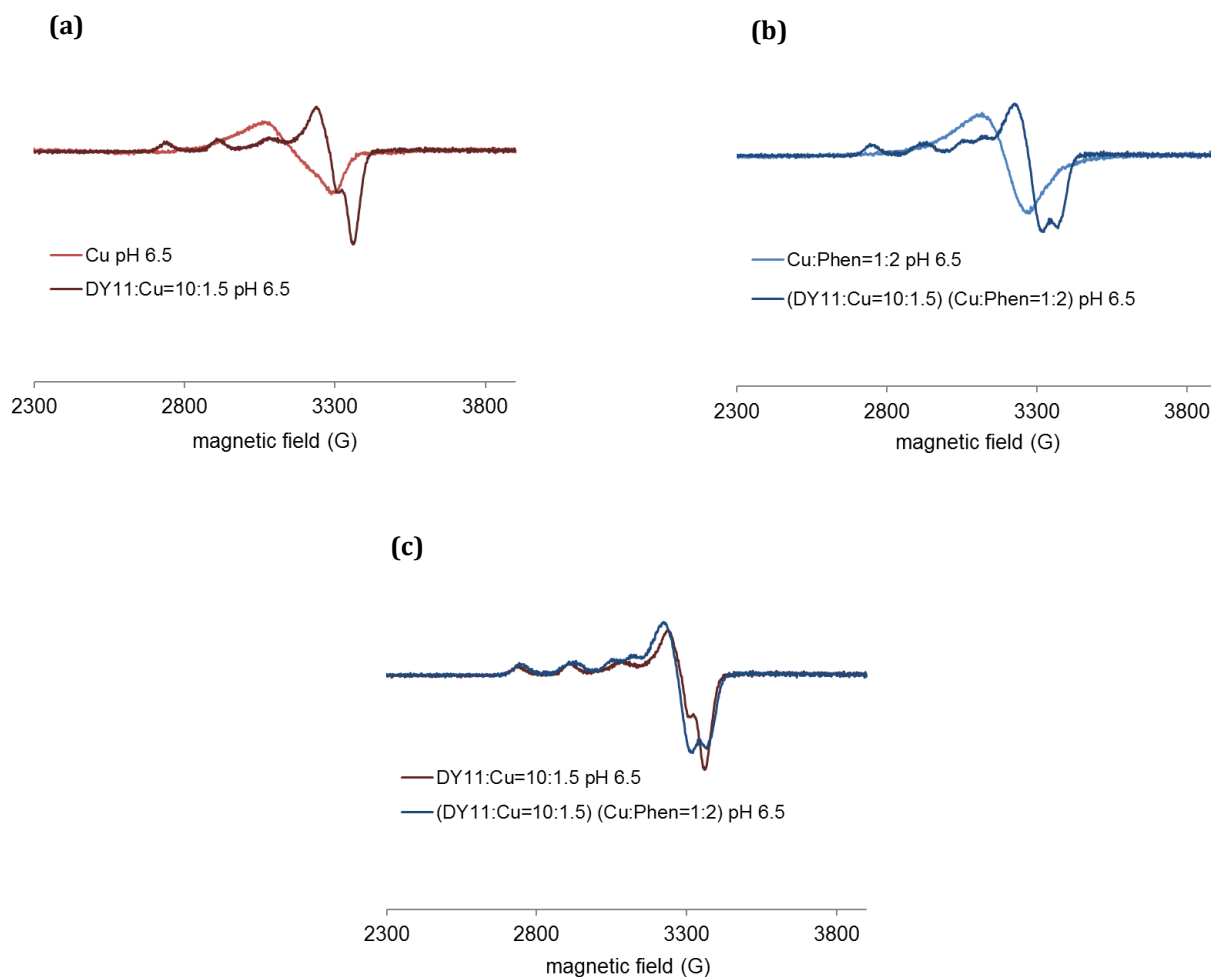


Figure 1. Experimental X-band EPR spectra recorded at 100 K in frozen aqueous solutions of (a) CuSO_4 and CuSO_4 +DY11L (b) Cu-Phen and Cu-Phen+DY11L (c) CuSO_4 +DY11L and Cu-Phen+DY11L, at pH 6.5, with Cu:Phen = 1:2, DY11L:Cu = 10:1.5 and $[\text{Cu}] = 1.5 \text{ mM}$

At neutral pH, the addition of DY11L to CuSO_4 led to a signal with a hyperfine structure, evidencing some coordination between DY11L and copper. The peaks were sharper than in the case of DR81L (Chapter III), which indicates a stronger structuration of Cu^{II} or fewer different complexes, the structure of DY11L being more simple than that of DR81L. The complex mixture was slightly

different with CuSO_4 and with Cu-Phen, as suggested by slightly different hyperfine coupling constants.

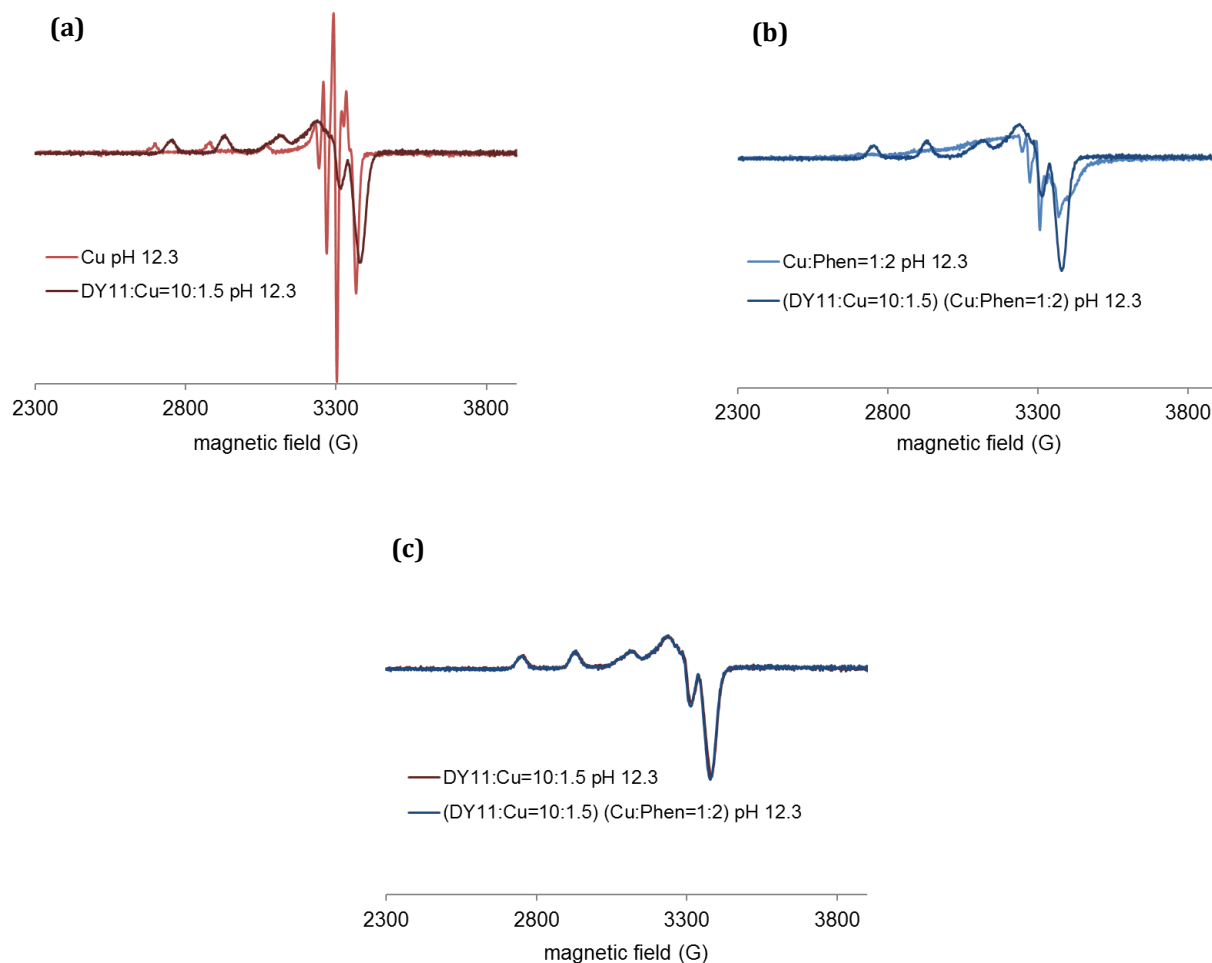


Figure 2. Experimental X-band EPR spectra recorded at 100 K in frozen aqueous solutions of (a) CuSO_4 and CuSO_4 +DY11L (b) Cu-Phen and Cu-Phen+DY11L (c) CuSO_4 +DY11L and Cu-Phen+DY11L, at pH 12.3, with Cu:Phen = 1:2, DY11L:Cu = 10:1.5 and $[\text{Cu}] = 1.5 \text{ mM}$

At alkaline pH, the signals of CuSO_4 and Cu-Phen alone were different from those at near-neutral pH, due to the presence of hydroxyl groups in the environment of Cu^{II} (see Chapter III). The signals of DY11L+ CuSO_4 and DY11L+Cu-Phen were even more structured than at neutral pH. Interestingly, these spectra were actually identical, evidencing that Phen was ejected in the case of DY11L+Cu-Phen. The same phenomenon was observed in Chapter III with DR81L. Consequently, at alkaline pH, Phen seems to be totally replaced by the dye (either DR81L or DY11L) around Cu^{II} .

Finally, at both pHs, no reduction was observed in the absence of H_2O_2 , and the dye substrate, as well as cellulose, was shown to interact with Cu by coordination only.

The addition of H_2O_2 was then tested at alkaline pH with both CuSO_4 and Cu-Phen, see Figure 3.

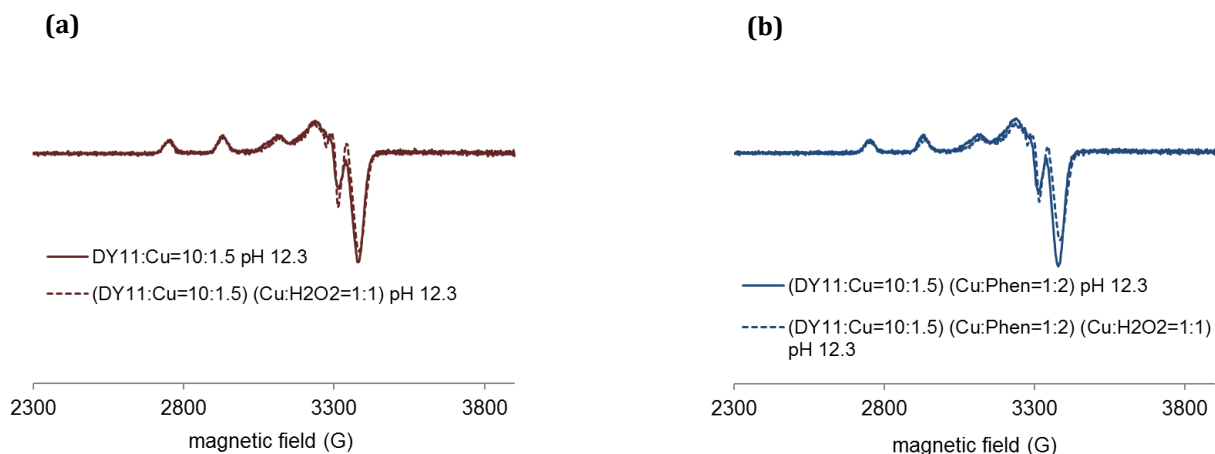


Figure 3. Experimental X-band EPR spectra recorded at 100 K in frozen aqueous solutions of (a) CuSO₄+DY11L and CuSO₄+DY11L+H₂O₂, (b) Cu-Phen+DY11L and Cu-Phen+DY11L+H₂O₂, at pH 12.3, with Cu:Phen = 1:2, DY11L:Cu = 10:1.5, Cu:H₂O₂ = 1:1 and [Cu] = 1.5 mM

As in the case of DR81L, the spectra were unchanged after the introduction of hydrogen peroxide at room temperature.

ANNEX 2

The supplementary material presented here illustrates the EPR simulations performed to find the relative amounts of different DMPO adducts during the spin-trapping experiments presented in V.4.2.2.

The details of the simulation results for DMPO+Cu-Phen are given in Table 1 and the simulated spectrum is compared to the experimental spectrum in Figure 4. Similar Tables and Figures are given for DMSO+DMPO+Cu-Phen+H₂O₂ (Table 2 and Figure 5) and HCOO⁻+DMPO+Cu-Phen+H₂O₂ (Table 3 and Figure 6), as presented for DMPO+Cu-Phen+H₂O₂ in Table V-7 and Figure V-36. Table 2 to Table 21 show all the other simulation results from spectra presented in Chapter V. Finally, Table 22 gathers all the radical species distributions found by simulation. The first 12 rows correspond to the distributions already presented in Table V-8.

Table 1. DMPO+Cu-Phen – Simulation results

	DMPO-OH	DMPO-R	Triplet
a_N (G)	15.088	15.781	14.354
a_H (G)	14.943	23.27	/
L_w (G)	0.500/0.449/0.458	0.902/0.846/0.952	0.756/0.756/0.805
Lorentzian (%)		18	
Relative area (%)	6	77	17

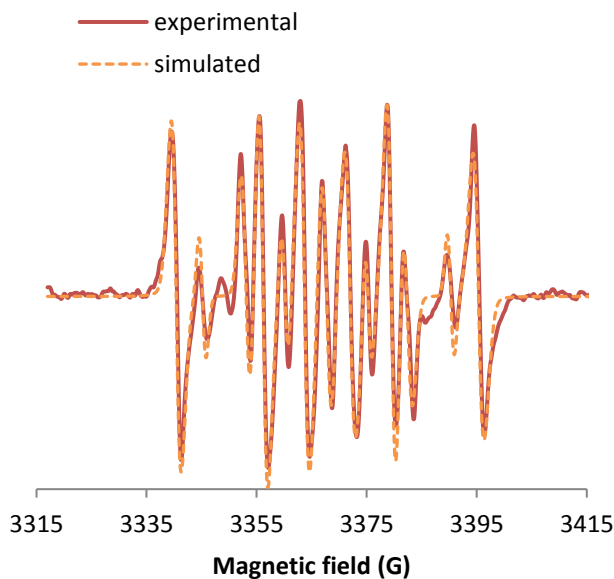
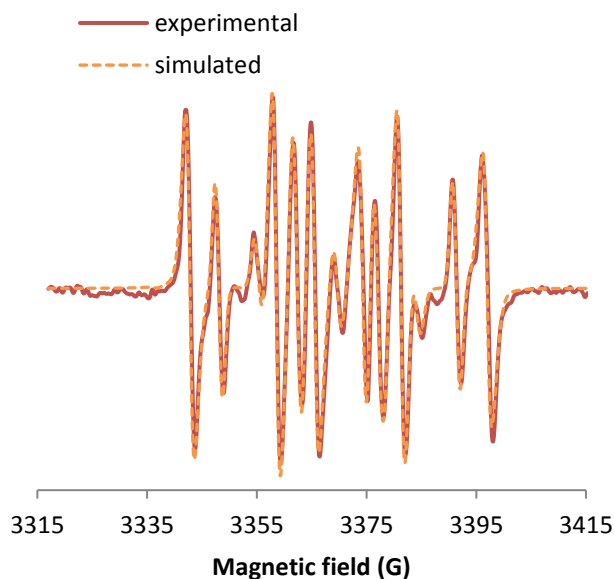


Figure 4. Comparison between the experimental and simulated spectra of DMPO+Cu-Phen

Table 2. DMSO+DMPO+Cu-Phen+H₂O₂ – Simulation results

	DMPO-OH	DMPO-CH ₃	Triplet	DMPO-R
a _N (G)	14.7	15.7	14.349	15.786
a _H (G)	13.851	22.651	/	20.11
L _w (G)	0.658/0.659/0.658	1.086/0.951/1.098	0.805/0.756/0.854	0.852/0.754/1.974
relative area (%)	18	73	5	5

**Figure 5. Comparison between the experimental and simulated spectra of DMSO+DMPO+Cu-Phen+H₂O₂****Table 3. HCOO⁻+DMPO+Cu-Phen+H₂O₂ – Simulation results**

	DMPO-OH	DMPO-R	Triplet	DMPO-COO ⁻
a _N (G)	14.902	15.64	14.593	15.749
a _H (G)	15.233	23.266	/	19.098
L _w (G)	0.649/0.561/0.609	1.047/1.047/1.193	0.708/0.708/0.898	0.551/0.551/0.551
Relative area (%)	18	28	5	49

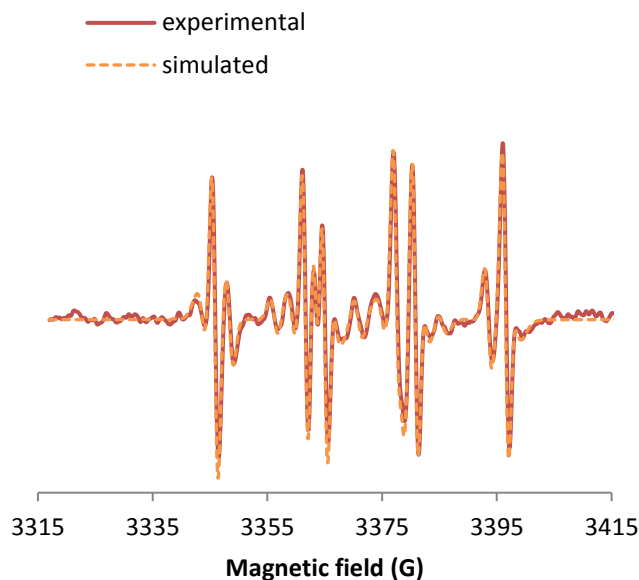


Figure 6. Comparison between the experimental and simulated spectra of HCOO⁻+DMPO+Cu-Phen+H₂O₂

Table 4. DMPO+CuSO₄ – Simulation results

	DMPO-OH	DMPO-R	Triplet	Other
a _N (G)	15.798	15.798	14.609	16.323
a _H (G)	14.928	23.237		26.653
L _w (G)	0.6/0.659/0.658	1/1.049/1.098	0.702/0.654/0.751	1.291/2.463/1.632
Relative area (%)	5	74	8	13

Table 5. HCOO⁻+DMPO+Cu-Phen+H₂O₂ t=5 min – Simulation results

	DMPO-OH	DMPO-R	Triplet	DMPO-COO ⁻
a _N (G)	15.049	15.651	14.463	15.781
a _H (G)	14.976	23.872		19.098
L _w (G)	0.649/0.610/0.658	1/1/1.098	0.897/1.191/1.093	0.6/0.6/0.6
Relative area (%)	14	12	4	70

Table 6. HCOO⁻+DMPO+Cu-Phen+H₂O₂ after heating – Simulation results

	DMPO-OH	DMPO-R	Triplet	DMPO-COO ⁻
a _N (G)	15	15.602	14.512	15.781
a _H (G)	15.074	23.607		19.049
L _w (G)	0.649/0.561/0.6	0.902/0.805/0.951	0.854/0.854/1.049	0.551/0.551/0.551

Relative area (%)	10	8	3	79
-------------------	----	---	---	----

Table 7. DMPO+CuSO₄+H₂O₂ – Simulation results

	DMPO-OH	DMPO-R	Triplet	Other	Other
a _N (G)	15.244	15.7	14.598	13.975	12.195
a _H (G)	14.83	23.51		21.435	11.463 (3H)
L _w (G)	0.6/0.561/0.6 49	1.049/1.049/1.1 95	0.805/0.903/0.9 51	1/0.805/1.4 88	0.751/6.855/0.8 98
Relative area (%)	7	57	16	10	9

Table 8. DMSO+DMPO+CuSO₄+H₂O₂ – Simulation results

	DMPO-OH	DMPO-R	Triplet
a _N (G)	14.707	15.651	14.354
a _H (G)	13.951	22.658	
L _w (G)	0.651/0.708/0.697	1/1.049/1.244	0.756/0.756/0.805
Relative area (%)	16	76	8

Table 9. HCOO⁻+DMPO+CuSO₄+H₂O₂ – Simulation results

	DMPO-OH	DMPO-R	Triplet	DMPO-COO ⁻	Other
a _N (G)	15.269	15.749	14.695	15.793	13.709
a _H (G)	14.951	23.559		18.97	7.508 (3H)
L _w (G)	0.651/0.561/0. 648	1.244/1.1049/1. 293	0.805/0.854/0. 951	0.556/0.556/0. 556	1.288/1.484/1. 142
Relative area (%)	15	34	10	23	18

Table 10. DMPO+FeSO₄+H₂O₂ at pH 3 – Simulation results

	DMPO-OH	DMPO-R	Triplet
a _N (G)	15	14.675	14.793
a _H (G)	14.732	21.703	
L _w (G)	0.651/0.708/0.697	1/1.098/1.586	0.952/0.854/0.854
Relative area (%)	86	7	7

Table 11. DMSO+DMPO+CuSO₄ – Simulation results

	DMPO-OH	DMPO-R	Triplet
a _N (G)	14.697	15.439	14.354
a _H (G)	14.015	22.586	
L _w (G)	0.597/0.644/0.644	1/0.944/1.049	0.707/0.658/0.756
Lorentzian (%)		85	
Relative area (%)	14	78	8

Table 12. DMSO+DMPO+Cu-Phen – Simulation results

	DMPO-OH	DMPO-R	Triplet
a _N (G)	14.697	15.488	14.305
a _H (G)	13.82	22.635	
L _w (G)	0.597/0.595/0.595	1/0.944/1.049	0.707/0.658/0.756
Lorentzian (%)		76	
Relative area (%)	22	72	6

Table 13. HCOO⁻+DMPO+Cu-Phen – Simulation results

	DMPO-OH	DMPO-R	DMPO-COO ⁻	Triplet
a _N (G)	14.843	15.644	15.683	14.593
a _H (G)	15.428	23.244	19.293	
L _w (G)	0.499/0.4/0.498	0.902/0.902/1.000	0.463/0.651/0.500	0.756/0.756/0.854
Lorentzian (%)		42	98	
Relative area (%)	19	58	11	12

Table 14. HCOO⁻+DMPO+Cu-Phen after heating – Simulation results

	DMPO-OH	DMPO-R	DMPO-COO ⁻	Triplet
a _N (G)	14.746	15.644	15.781	14.788
a _H (G)	15.428	23.342	19	
L _w (G)	0.548/0.302/0.546	0.902/0.902/1.098	0.463/0.546/0.463	0.805/0.756/1.195
Lorentzian (%)			28	
Relative area (%)	11	13	72	4

Table 15. DMPO+H₂O₂ after heating – Simulation results

	DMPO-OH	DMPO-R	Triplet
a _N (G)	14.756	14.813	14.842
a _H (G)	15.391	21.535	
L _w (G)	0.549/0.451/0.500	1.045/2/1.830	0.903/0.893/0.996
Lorentzian (%)	36	42	9
Relative area (%)	38	38	24

Table 16. NaOH+DMPO+CuSO₄ – Simulation results

	DMPO-OH	DMPO-R	Triplet	Other
a _N (G)	15.195	15.741	14.549	
a _H (G)	15.294	23.488		17.975 (2H)
L _w (G)	0.402/0.402/0.305	0.800/0.995/1.288	0.610/0.800/0.654	3.3/0.7/9.6
Lorentzian (%)	8	76		
Relative area (%)	2	72	6	20

Table 17. NaOH+DMPO+Cu-Phen – Simulation results

	DMPO-OH	DMPO-R	Triplet	Other
a _N (G)	15.234	15.742	14.398	14.999
a _H (G)	15.623	23.83		21.246
L _w (G)	0.597/0.400/0.595	1/0.902/1.195	0.756/0.756/0.756	0.800/0.749/1.000
Lorentzian (%)		10		
Relative area (%)	17	58	10	14

Table 18. NaOH+HCOO⁻+DMPO+Cu-Phen t=8 min – Simulation results

	DMPO-R	DMPO-COO ⁻
a _N (G)	15.595	15.805
a _H (G)	22.756	19
L _w (G)	0.658/0.658/0.658	0.507/0.451/0.451
Lorentzian (%)		37
Relative area (%)	8	92

Table 19. NaOH+DMPO+Cu-Phen+H₂O₂ - Simulation results

	DMPO-OH	DMPO-R	Triplet
a _N (G)	15.439	15.79	14.646
a _H (G)	15.049	23.488	
L _w (G)	0.5/0.5/0.549	1.049/1.146/1.293	0.659/0.751/0.800
Lorentzian (%)		33	
Relative area (%)	21	69	11

Table 20. NaOH+DMSO+DMPO+Cu-Phen+H₂O₂ - Simulation results

	DMPO-OH	DMPO-CH ₃	Triplet
a _N (G)	13.926	15.937	14.788
a _H (G)	14.072	22.658	
L _w (G)	0.743/0.839/0.986	0.658/0.658/0.609	0.658/0.658/1.293
Lorentzian (%)	34	9	
Relative area (%)	16	80	5

Table 21. NaOH+HCOO⁻+DMPO+Cu-Phen+H₂O₂ - Simulation results

	DMPO-OH	DMPO-R	DMPO-COO ⁻	Triplet
a _N (G)	15.342	15.742	15.805	14.691
a _H (G)	15.537	24.123	19.049	
L _w (G)	0.499/0.351/0.498	0.804/1.097/1.049	0.507/0.5/0.451	0.561/0.609/0.451
Lorentzian (%)	42		16	
Relative area (%)	17	28	47	8

Table 22. Integration and simulation results: total peak area, and distribution of DMPO adducts and degradation products for some experiments, as relative areas of each radical, in percents

NaOH	HCOO ⁻	DMSO	H ₂ O ₂	Additive	Details	Total peak area (a.u.)	DMPO-OH (%)	DMPO-CH ₃ (%)	DMPO-COO ⁻ (%)	DMPO-R (%)	Triplet (%)	Other(s) (%)
				CuSO ₄		1.12	5			74	8	13
				Cu-Phen		1.46	6			77	17	
			x	Cu-Phen		1.29	38			54	8	
		x	x	Cu-Phen		n/a	18	73		4.5	4.5	
	x		x	Cu-Phen		0.65	18		49	28	5	
	x		x	Cu-Phen	+10min	0.54	14		70	12	4	
	x		x	Cu-Phen	heating	0.79	10		79	8	3	
			x	CuSO ₄		0.89	7			57	16	19
		x	x	CuSO ₄		n/a	16			76	8	
	x		x	CuSO ₄		0.21	15		23	34	10	18
			x	FeSO ₄	pH 3	0.43	86			7	7	
		x		CuSO ₄		n/a	14			78	8	
		x		Cu-Phen		n/a	22			72	6	
	x			Cu-Phen		n/a	19		11	58	12	
	x			Cu-Phen	heating	n/a	11		72	13	4	
			x	/	heating	n/a	38			38	24	
x				CuSO ₄		n/a	2			72	6	20
x				Cu-Phen		n/a	17			58	10	14
x	x			Cu-Phen	+8min	n/a			92	8		
x			x	Cu-Phen		n/a	21			69	11	
x		x	x	Cu-Phen		n/a	16	80			5	
x	x		x	Cu-Phen		n/a	17		47	28	8	

Résumé de la thèse en français :

Titre : Étude de l'activation du peroxyde d'hydrogène par le complexe cuivre(II)-phénanthroline pour la décoloration de fibres cellulosiques récupérées

Les papiers récupérés sont de plus en plus utilisés pour fabriquer du papier recyclé de haute blancheur. La ligne de recyclage inclut entre autres les opérations de désencrage et de blanchiment, le peroxyde d'hydrogène (H_2O_2) étant le réactif blanchissant le plus utilisé en milieu alcalin (stade P). Son efficacité est toutefois limitée car il est peu ou moyennement réactif sur les fonctions azoïques des colorants papetiers. L'objectif de cette étude était donc d'améliorer l'élimination des colorants azoïques lors d'un stade P.

L'amélioration du stade P utilisé en délignification des pâtes chimiques a fait l'objet de nombreuses études. En particulier, l'activation ou la catalyse de H_2O_2 par des complexes cuivre(II)-phénanthroline (Cu-Phen) présentant des résultats très intéressants, des essais de blanchiment de pâtes désencrées et colorées ont été entrepris. Le système H_2O_2 /Cu-Phen s'est également révélé efficace en décoloration, mais le mécanisme n'avait alors pas été étudié.

L'objectif de ce travail était donc de déterminer dans quel cas et pourquoi le complexe cuivre(II)-phénanthroline était capable d'améliorer la décoloration de fibres cellulosiques colorées. Trois questions intermédiaires se sont posées : (1) quel effet Cu-Phen a-t-il sur le colorant isolé ? (2) la décoloration d'une pâte de fibres colorées par H_2O_2 est-elle améliorée par Cu-Phen ? (3) par quel mécanisme la décoloration est-elle rendue plus efficace ?

Le travail a donc été organisé en trois études : (1) caractérisation des colorants sélectionnés et du complexe en l'absence d'oxydant et examen des interactions entre les deux, (2) étude et optimisation paramétrique de H_2O_2 /Cu-Phen pour la décoloration de pâtes colorées, (3) étude du mécanisme d'oxydation en milieu aqueux, en l'absence et en présence de cellulose.

Ce travail s'est appuyé sur de nombreuses techniques analytiques (spectroscopies RMN, FTIR, UV-vis et RPE ; ESI-MS) et des calculs de spéciation. Il a prouvé que le complexe Cu-Phen en présence de H_2O_2 améliorait la décoloration de colorants azoïques, avec ou sans fibres cellulosiques. Il a été mis en évidence que la phénanthroline agissait comme un stabilisant permettant d'ajuster la solubilité, la stabilité et le potentiel d'oxydo-réduction du cuivre(II), mais qu'elle n'était pas indispensable. De plus, le pH du milieu est également un paramètre clé, jouant à la fois sur l'activité du complexe et sur ses interactions avec le substrat. Le substrat (colorant mais aussi cellulose) s'est trouvé fortement dégradé par ce système H_2O_2 /Cu-Phen. Les résultats corroborent l'hypothèse de l'oxydation du substrat par les radicaux hydroxyles issus de la décomposition de H_2O_2 , plutôt que par H_2O_2 lui-même, ce mécanisme étant l'une des étapes d'un cycle catalytique.

La recherche menée et les résultats obtenus sont applicables non seulement à l'amélioration du blanchiment des pâtes désencrées, mais aussi au traitement d'effluents colorés dans les industries du papier et du textile.

Mots clés : Fibres cellulosiques récupérées, décoloration, oxydation avancée, peroxyde d'hydrogène, cuivre-phénanthroline, mécanisme réactionnel

Résumé de la thèse en anglais :

Title: Study of the activation of hydrogen peroxide by the copper(II)-phenanthroline complex for the color-stripping of recovered cellulosic fibers

Today, recovered papers are reused for the manufacture of bright paper after deinking and fiber bleaching, which generally starts with an alkaline hydrogen peroxide stage (H_2O_2). However, the efficiency of H_2O_2 is often limited due to its low reactivity on the azo groups of paper dyes contained in recovered papers. The goal of this study was to improve the removal of these azo dyes by H_2O_2 .

The improvement of H_2O_2 bleaching has been studied thoroughly in the context of chemical pulp delignification. In particular, the activation or catalysis of H_2O_2 by copper(II)-phenanthroline complexes (Cu-Phen) was found to be very effective. This inspired a preliminary bleaching study on deinked pulp and dyed pulp, and resulted in significant improvement of dye removal, which gave birth to our project.

The purpose of this work was to determine to what extent copper(II)-phenanthroline could improve the hydrogen peroxide color-stripping of dyed cellulosic fibers, and how. To answer this question, three intermediate issues were addressed: (1) does Cu-Phen alone have an effect on the dye? (2) does Cu-Phen improve the color-stripping of a dyed pulp by H_2O_2 ? (3) how does the H_2O_2 /Cu-Phen system enhance the dye-color-stripping efficiency?

This work was thus divided into three studies: (1) the selected dyes and the complex were characterized in the absence of any oxidant and the interactions between the two were examined, (2) the H_2O_2 /Cu-Phen system was applied on two dyed pulps to assess their color-stripping potential and to attempt to optimize it, and (3) the oxidation mechanism was investigated via trials in aqueous solution, with and without cellulose.

Using several analytical techniques (NMR, FTIR, UV-vis and EPR spectroscopy; ESI-MS) and speciation calculations, this work proved that the Cu-Phen complex enhanced H_2O_2 for the color-stripping of azo dyes, with and without fibers. It also provided evidence that phenanthroline acted as a stabilizer to adjust the solubility, stability and redox potential of copper(II), but may not be indispensable. The substrate (dyes but also cellulose) was strongly degraded by the H_2O_2 /Cu-Phen system. The results of the mechanistic study supported the hypothesis of substrate oxidation by radicals produced via decomposition of H_2O_2 rather than by hydrogen peroxide itself. This mechanism, strongly dependent on the pH, is probably part of a catalytic cycle.

Finally, along with further research proposed based on our conclusions, this thesis should contribute to the improvement of deinked pulp bleaching as well as wastewater treatment in the pulp and textile industries.

Keywords: Recovered cellulosic fibers, color-stripping, advanced oxidation, hydrogen peroxide, copper-phenanthroline, reaction mechanism